
NUCLEAR POWER - OPERATION, SAFETY AND ENVIRONMENT

Edited by **Pavel V. Tsvetkov**

INTECHWEB.ORG

Nuclear Power - Operation, Safety and Environment

Edited by Pavel V. Tsvetkov

Published by InTech

Janeza Trdine 9, 51000 Rijeka, Croatia

Copyright © 2011 InTech

All chapters are Open Access articles distributed under the Creative Commons Non Commercial Share Alike Attribution 3.0 license, which permits to copy, distribute, transmit, and adapt the work in any medium, so long as the original work is properly cited. After this work has been published by InTech, authors have the right to republish it, in whole or part, in any publication of which they are the author, and to make other personal use of the work. Any republication, referencing or personal use of the work must explicitly identify the original source.

Statements and opinions expressed in the chapters are these of the individual contributors and not necessarily those of the editors or publisher. No responsibility is accepted for the accuracy of information contained in the published articles. The publisher assumes no responsibility for any damage or injury to persons or property arising out of the use of any materials, instructions, methods or ideas contained in the book.

Publishing Process Manager Petra Zobic

Technical Editor Teodora Smiljanic

Cover Designer Jan Hyrat

Image Copyright Andrea Danti, 2010. Used under license from Shutterstock.com

First published July, 2011

Printed in Croatia

A free online edition of this book is available at www.intechopen.com
Additional hard copies can be obtained from orders@intechweb.org

Nuclear Power - Operation, Safety and Environment, Edited by Pavel V. Tsvetkov

p. cm.

ISBN 978-953-307-507-5

INTECH OPEN ACCESS
PUBLISHER

INTECH open

free online editions of InTech
Books and Journals can be found at
www.intechopen.com

Contents

Preface IX

Part 1 Operation and Safety 1

- Chapter 1 **World Experience in Nuclear Steam Reheat 3**
Eugene Saltanov and Igor Pioro
- Chapter 2 **Integrated Approach for Actual Safety Analysis 29**
Francesco D'Auria, Walter Giannotti and Marco Cherubini
- Chapter 3 **LWR Safety Analysis and Licensing
and Implications for Advanced Reactors 47**
P. F. Frutuoso e Melo, I. M. S. Oliveira and P. L. Saldanha
- Chapter 4 **Geodetic Terrestrial Observations for the
Determination of the Stability in the
Krško Nuclear Power Plant Region 71**
S. Savšek, T. Ambrožič and D. Kogoj
- Chapter 5 **Low Power and Shutdown PSA for the Nuclear
Power Plants with WWER440 Type Reactors 89**
Zoltan Kovacs
- Chapter 6 **A Study on the Actuator
Efficiency Behavior of Safety-Related
Motor Operated Gate and Globe Valves 111**
Shin Cheul Kang, SungKeun Park, DoHwan Lee,
YangSeok Kim and DaeWoong Kim
- Chapter 7 **Investigation of High Energy Arcing
Fault Events in Nuclear Power Plants 127**
Heinz Peter Berg and Marina Röwekamp
- Chapter 8 **Research on Severe Accidents
in Nuclear Power Plants 155**
Jean-Pierre Van Dorsselaere, Thierry Albiol
and Jean-Claude Micaelli

- Chapter 9 **Imaging of Radiation Accidents and Radioactive Contamination Using Scintillators 183**
 Tomoya Ogawa, Nobuhiko Sarukura, Masahito Watanabe, Tsuguo Fukuda, Nobuhito Nango, Yasunobu Arikawa, Kohei Yamanoi, Tomoharu Nakazato, Marilou Cadatal-Raduban, Toshihiko Shimizu, Mitsuo Nakai, Takayoshi Norimatsu, Hiroshi Azechi, Takahiro Murata, Shigeru Fujino, Hideki Yoshida, Kei Kamada, Yoshiyuki Usuki, Toshihisa Suyama, Akira Yoshikawa, Nakahiro Sato, Hirofumi Kan, Hiroaki Nishimura, Kunioki Mima, Masahito Hosaka, Masahiro Katoh, Nobuhiro Kosugi, Kentaro Fukuda, Takayuki Yanagida, Yuui Yokota, Fumio Saito, Kouhei Sakai, Dirk Ehrentraut, Mitsuru Nagasono, Tadashi Togashi, Atsushi Higashiya, Makina Yabashi, Tetsuya Ishikawa, Haruhiko Ohashi and Hiroaki Kimura
- Chapter 10 **Simulation of Ex-Vessel Steam Explosion 207**
 Matjaž Leskovar
- Part 2 Environmental Effects 235**
- Chapter 11 **Radiological Releases and Environmental Monitoring at Commercial Nuclear Power Plants 237**
 Jason T. Harris
- Chapter 12 **Radiological and Environmental Effects in Ignalina Nuclear Power Plant Cooling Pond – Lake Druksiai: From Plant put in Operation to Shut Down Period of Time 261**
 Tatjana Nedveckaitė, Danute Marciulionienė, Jonas Mazeika and Ricardas Paskauskas
- Chapter 13 **Power Uprate Effect on Thermal Effluent of Nuclear Power Plants in Taiwan 287**
 Jinn-Jer Peir
- Part 3 Radiation Effects 303**
- Chapter 14 **Long-Term Effects of Exposure to Low-Levels of Radioactivity: a Retrospective Study of ²³⁹Pu and ⁹⁰Sr from Nuclear Bomb Tests on the Swiss Population 305**
 Pascal Froidevaux, Max Haldimann and François Bochud
- Chapter 15 **The Biliprotein C-Phycocyanin Modulates the DNA Damage Response in Lymphocytes from Nuclear Power Plant Workers 327**
 K. Stankova, K. Ivanova, V. Nikolov, K. Minkova, L. Gigova, R. Georgieva and R. Boteva
- Chapter 16 **Effects of Gamma-Ray Irradiation on Tracking Failure of Polymer Insulating Materials 341**
 Boxue Du, Yu Gao and Yong Liu

Preface

Energy demands due to economic growth and increasing population must be satisfied in a sustainable manner assuring inherent safety, efficiency and no or minimized environmental impact. New energy sources and systems must be inherently safe and environmentally benign. These considerations are among the reasons that lead to serious interest in deploying nuclear power as a sustainable energy source. Today's nuclear reactors are safe and highly efficient energy systems that offer electricity and a multitude of co-generation energy products ranging from potable water to heat for industrial applications. At the same time, catastrophic earthquake and tsunami events in Japan resulted in the nuclear accident that forced us to rethink our approach to nuclear safety, design requirements and facilitated growing interests in advanced nuclear energy systems, next generation nuclear reactors, which are inherently capable to withstand natural disasters and avoid catastrophic consequences without any environmental impact.

This book is one in a series of books on nuclear power published by InTech. Under the single-volume cover, we put together such topics as operation, safety, environment, and radiation effects. The book is not offering a comprehensive coverage of the material in each area. Instead, selected themes are highlighted by authors of individual chapters representing contemporary interests worldwide. Our book consists of three major sections housing sixteen chapters:

Part 1. Operation and Safety

1. World Experience in Nuclear Steam Reheat
2. Integrated Approach for Actual Safety Analysis
3. LWR Safety Analysis and Licensing and Implications for Advanced Reactors
4. Geodetic Terrestrial Observations for the Determination of the Stability in the Krško Nuclear Power Plant Region
5. Low Power and Shutdown PSA for the Nuclear Power Plants with WWER440 Type Reactors
6. A Study on the Actuator Efficiency Behavior of Safety-Related Motor Operated Gate and Globe Valves
7. Investigation of High Energy Arcing Fault Events in Nuclear Power Plants
8. Research on Severe Accidents in Nuclear Power Plants

9. Imaging of Radiation Accidents and Radioactive Contamination Using Scintillators
10. Simulation of Ex-Vessel Steam Explosion

Part 2. Environmental Effects

11. Radiological Releases and Environmental Monitoring at Commercial Nuclear Power Plants
12. Radiological and Environmental Effects in Ignalina Nuclear Power Plant Cooling Pond – Lake Druksiai: From Plant put in Operation to Shut Down Period of Time
13. Power Uprate Effect on Thermal Effluent of Nuclear Power Plants in Taiwan

Part 3. Radiation Effects

14. Long-Term Effects of Exposure to Low-Levels of Radioactivity: a Retrospective Study of ^{239}Pu and ^{90}Sr from Nuclear Bomb Tests on the Swiss Population
15. The Biliprotein C-Phycocyanin Modulates the DNA Damage Response in Lymphocytes from Nuclear Power Plant Workers
16. Effects of Gamma-Ray Irradiation on Tracking Failure of Polymer Insulating Materials

Our opening section is devoted to nuclear power operation and safety. The discussion begins with an overview of nuclear steam supply systems that focuses on steam reheat. The second chapter introduces the integrated safety analysis approach. Further chapters introduce readers to licensing, probabilistic safety analysis, component operation and safety. The section closes with chapters surveying approaches and topics related to severe accident studies.

The second section is dedicated to environmental effects of nuclear power. Included chapters address radiological release monitoring and consequences as well as thermal pollution.

The third and final section discusses radiation effects on general population, plant workers and materials.

With all diversity of topics in 16 chapters, the integrated system analysis approach of nuclear power operation, safety and environment is the common thread. The “system-thinking” approach allows synthesizing the entire body of provided information into a consistent integrated picture of the real-life complex engineering system – nuclear power system – where everything is working together.

The goal of the book is to bring nuclear power to our readers as one of the promising energy sources that has a unique potential to meet energy demands with minimized environmental impact, near-zero carbon footprint, and competitive economics via robust potential applications. The book targets everyone as its potential readership

groups - students, researchers and practitioners - who are interested to learn about nuclear power. The idea is to facilitate intellectual cross-fertilization between field experts and non-field experts taking advantage of methods and tools developed by both groups. The book will hopefully inspire future research and development efforts, innovation by stimulating ideas.

We hope our readers will enjoy the book and will find it both interesting and useful.

Pavel V. Tsvetkov
Department of Nuclear Engineering
Texas A&M University
United States of America

Part 1

Operation and Safety

World Experience in Nuclear Steam Reheat

Eugene Saltanov and Igor Pioro
University of Ontario Institute of Technology (UOIT)
Faculty of Energy Systems and Nuclear Science
Canada

1. Introduction

Concepts of nuclear reactors cooled with water at supercritical pressures were studied as early as the 1950s and 1960s in the USA and Russia. After a 30-year break, the idea of developing nuclear reactors cooled with SuperCritical Water (SCW) became attractive again as the ultimate development path for water cooling. This statement is based on the known history of the thermal power industry, which made a “revolutionary” step forward from the level of subcritical pressures (15 – 16 MPa) to the level of supercritical pressures (23.5 – 35 MPa) more than fifty years ago with the same major objective as that of SuperCritical Water-cooled Reactors (SCWRs) – to increase thermal efficiency of power plants by 10 – 15%. The main objectives of using SCW in nuclear reactors are: 1) to increase the thermal efficiency of modern Nuclear Power Plants (NPPs) from 30 – 35% to about 45 – 50%, and 2) to decrease capital and operational costs and hence, decrease electrical-energy costs.

To achieve higher thermal efficiency a nuclear steam reheat has to be introduced inside a reactor. Currently, all supercritical turbines at thermal power plants have a steam-reheat option. In the 60’s and 70’s, Russia, USA and some other countries have developed and implemented the nuclear steam reheat at a subcritical pressure in experimental boiling reactors. Therefore, it is important to summarize the experience of implementing nuclear steam reheat at several experimental Boiling Water Reactors (BWRs) worldwide and utilize it in the context of development of SCWRs with the steam-reheat option.

2. USA experience in nuclear steam reheat

An active program for the development and demonstration of BWRs with nuclear steam reheat was implemented and directed by the United States Atomic Energy Commission (USAEC). Two general types of the reactors were demonstrated:

1. Reactors in which steam was generated and reheated in the same core (integral reheating design); and
2. Reactors, which only used reheated steam that was supplied from another source (separate reheating design);

Under the USAEC program, the following reactors were constructed: BOiling Reactor Experiment V (BORAX-V, started operation in December of 1962), BOiling NUclear Superheater (BONUS, started operation in December of 1964), and Pathfinder (started operation in July of 1966). Main parameters of these reactors are listed in Tables 1 and 2 (Novick et al. 1965).

At the design stage of these reactors a certain number of problems arising with the implementation of steam reheat were encountered and addressed. Among them were:

1. Fuel-element sheath performance and corrosion resistance at high temperatures;
2. Corrosion, erosion, and deposits on fuel-element surfaces due to ineffective steam separation prior to the reheating-zone inlet;
3. Maintenance of the desired power split in the evaporating and reheating zones during extended reactor operation;
4. Fission products carry-over in direct-cycle systems; And
5. Reactivity changes as a result of inadvertent flooding of the reheating zone.

In search of the solutions to these problems USAEC also instituted a number of programs to determine long-term integrity and behavior of the fuel-element sheath. Since May of 1959, the Superheat Advance Demonstration Experiment (SADE) and the subsequent Expanded SADE (ESADE) loops had been utilized to irradiate a total of 21 fuel elements in the Vallecitos BWR. Saturated steam at about 6.9 MPa from the Vallecitos BWR was supplied to the fuel-element section where it was superheated to temperatures of 418 – 480°C. The results of those irradiation tests combined with out-of-core corrosion tests led to the following conclusions (Novick et al. 1965):

1. Commercial 18-8 stainless steel (18-8 SS) was not satisfactory for fuel-sheath material in the SuperHeated Steam (SHS) environment it was subjected to in the SADE and ESADE experiments;
2. Materials with higher nickel-alloy content, such as Inconels and Incolloys, appeared to perform satisfactorily as a sheath material in the SHS environment; And
3. Strain cycling coupled with environmental chemistry were significant in the failure rate of sheath materials for reactors with the steam reheat.

Additional information on design of these reactors constructed under the USAEC program can be found in USAEC reports 1959, 1961, and 1962 and in Ross (1961).

Parameters	BORAX-V		BONUS		Pathfinder	
	Zone		Zone		Zone	
	Boiling	SHS	Boiling	SHS	Boiling	SHS
Structural material (core)	A1(X8001)	SS	Zr-2	SS-248	Zr-2	SS
Fuel type	Rod	Plate	Rod	Rod	Rod	Annular
Fuel material	UO ₂	UO ₂ -SS cermet	UO ₂	UO ₂	UO ₂	UO ₂ -SS cermet
Fuel enrichment, %	4.95	93	2.4	3.25	2.2	93
Sheath material	SS-304	SS-304L	Zr-2	Inconel	Zr-2	SS-316L
Control rod shape	Cruciform and "T"	Cruciform and "T"	Cruciform	Slab	Cruciform	Round rod
Control rod material	Boral	Boral	1.0% wt ¹⁰ B in SS	1.0% wt ¹⁰ B in SS	2% wt ¹⁰ B in SS	2% wt ¹⁰ B in SS
Average power density, MW _{th} /m ³	42.5	40.5	33.6	11.5	45.2	46.5

Table 1. Main general parameters of BWR NPPs with integral reheat design (Novick et al. 1965).

Parameters	BORAX-V	BONUS	Pathfinder
Electric power, MW _{el} (gross)	3.5	17.5	66
Electric power, MW _{el} (net)	3.5	16.5	62.5
Thermal power, MW _{th}	20	50	200
Reheat loop to evaporating loop power ratio	0.21	0.35	0.22
Gross cycle thermal efficiency, %	-	35	33
Net cycle thermal efficiency, %	-	33	31
NPP steam cycle	Direct	Direct	Direct
Reheating-zone location	Central or Peripheral	Peripheral	Central
Nominal operating pressure, MPa	4.1	6.7	4.1

Table 2. Main thermal parameters of BWR NPPs with integral reheat design (Novick et al. 1965).

The major conclusion, which is based on the USA experience with the nuclear steam reheat, is that the nuclear steam reheat is possible, and higher thermal efficiencies can be achieved, but this feature requires more complicated reactor-core design and better materials.

3. Russian experience in nuclear steam reheat

This section presents a unique compilation of materials that overviews all major aspects of operating experience of the first in the world industrial NPP with implemented nuclear steam reheat.

3.1 General information

Reactors with the nuclear steam reheat were also developed in the former Soviet Union. Beloyarsk Nuclear Power Plant (BNPP) was the first NPP in the world where the nuclear steam reheat was implemented. Two reactors (100 MW_e and 200 MW_e) were installed with identical steam parameters at the turbine inlet ($P_{in} = 8.8$ MPa and $T_{in} = 500 - 510^{\circ}\text{C}$). The first reactor (Unit 1) was put into operation on April 26, 1964, and the second reactor (Unit 2) – on December 29, 1967. Both reactors have similar dimensions and design. However, the flow diagram and the core arrangement were significantly simplified in Unit 2, compared to that of Unit 1. Schematics and simplified layouts of the BNPP Units 1 and 2 are shown in Figures 1 and 2.

Operation of BNPP has proved the feasibility of steam-reheat implementation on an industrial scale. Major results of the BNPP operation are listed below (Petrostyants 1969):

1. Reactor start-up from the cold state was achieved without external heat sources. The reactor heat-up was carried out at 10% power until the water temperature in the separators reached 285 – 300°C at 8.8 MPa. Levels in the separators were formed during heat-up. Transition from water to steam cooling in the SHS channels did not cause significant reactivity changes.
2. The radial neutron flux flattening achieved was one of the best among operating reactors. The radial neutron flux irregularity coefficient, K_{ir} , for both units was 1.28 – 1.30, while the design values were: $K_{ir} = 1.46$ for Unit 1 and $K_{ir} = 1.24$ for Unit 2.
3. Radioactivity in the turbine and technological equipment of the plant is an important indicator for NPP. Radiation rates at the high-pressure cylinders were not higher than 10 $\mu\text{R/s}$ and not higher than 8 $\mu\text{R/s}$ at the low-pressure cylinders. Such low dose rates

were attained by implementation of fuel elements that eliminated the possibility of fission-fragment activity transported via the coolant loop. BNPP operation experience showed that radiation levels near Unit 1 equipment were significantly lower than that of other operating reactors, and releases of radioactive products into the atmosphere were 5 - 10 times lower than allowed by codes.

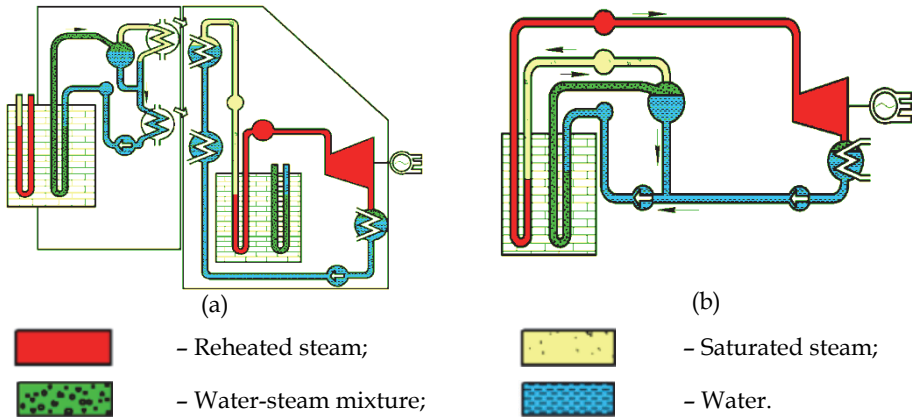


Fig. 1. BNPP Unit 1 (a) and Unit 2 (b) general schematics of thermodynamic cycle (Yurmanov et al. 2009a):

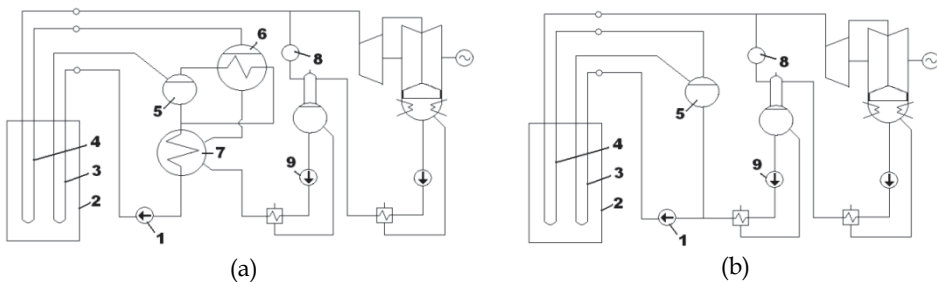
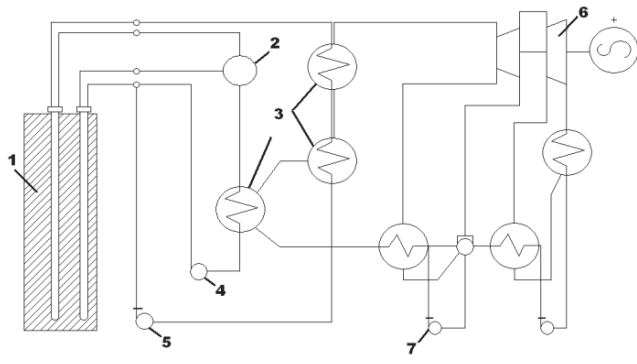


Fig. 2. Simplified layout of BNPP Unit 1 (a) and Unit 2 (b) (Petrosyants 1969): 1 - circulation pump; 2 - reactor; 3 - Boiling Water (BW) channels; 4 - SHS channels; 5 - steam separator; 6 - Steam Generator (SG); 7 - economizer; 8 - bubbler; and 9 - Feed Water Pump (FWP).

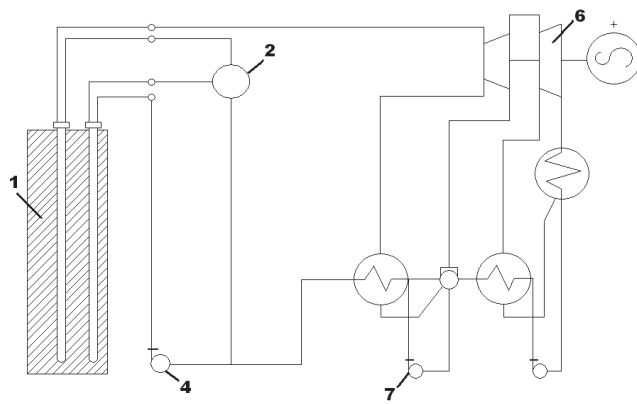
3.2 Cycle development

Reliability, simple design, and efficiency are the main criteria when choosing the flow diagram for both the fossil and nuclear power plants. Special requirements for impermeability and water regime are specified for NPPs. Additionally, the reasonable development of temperature regimes for fuel channels allows safe power increase for the a reactor size.

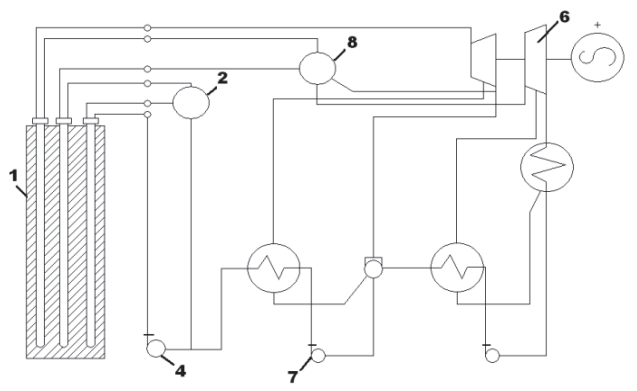
Several layouts of thermodynamic cycles for a NPP with a uranium-graphite reactor were considered for the BNPP (see Figure 3). In the considered layouts the coolant was either boiling water or superheated steam. Feasibility of the NPP designs was also taken into account (Dollezhal et al. 1958).



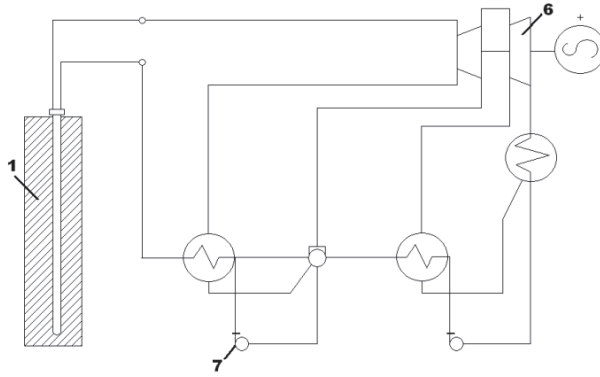
(a)



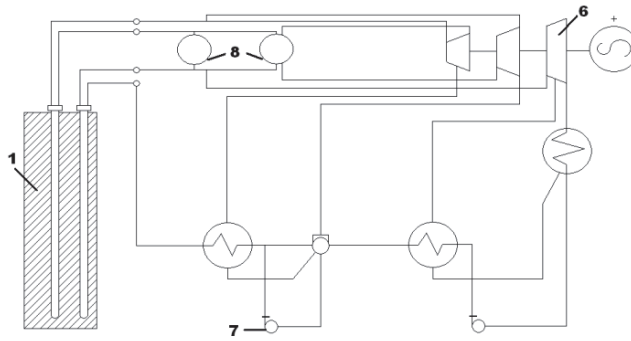
(b)



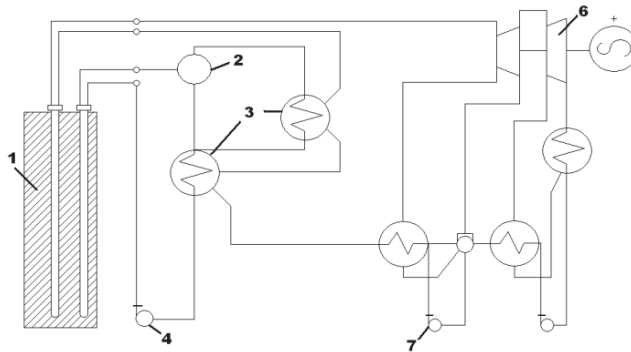
(c)



(d)



(e)



(f)

Fig. 3. Possible layouts of NPPs with steam reheat (Dollezhal et al. 1958): 1 – reactor; 2 – steam separator; 3 – SG; 4 – Main Circulation Pump (MCP); 5 – circulation pump; 6 – turbine with electrical generator; 7 – FWP; and 8 – intermediate-steam reheat.

Layout (a). A steam separator, steam generator (consisting of preheating, boiling and steam-superheating sections), and two circulation pumps are included in the primary coolant loop. Water and very high-pressure steam are the primary coolants. High- and intermediate-pressure steam is generated in the secondary loop and directed to the turbine.

Layout (b). Direct-cycle layout. Steam from a reactor flows directly to a turbine. The turbine does not require an intermediate-steam reheat.

Layout (c). Steam from a reactor flows directly to a turbine. The turbine requires the intermediate-steam reheat. The reactor has three types of operating fuel channels: 1) water preheating, 2) evaporating-boiling, and 3) steam-superheating.

Layout (d). Direct-cycle layout. The evaporation and reheat are achieved inside a reactor. The turbine does not require the intermediate-steam reheat.

Layout (e). Direct-cycle layout. One or two intermediate-steam reheats are required.

Layout (f). Water circulates in the closed loop consisting of a reactor, steam separator, preheater, and circulation pump. Partial evaporation is achieved in the first group of channels. Steam exiting the steam separator is directed to the boiling section of the steam generator and condenses there. Condensate from the boiler is mixed with water from the separator. The cooled water is fed to a preheater and then directed to circulation pumps. The generated steam on the secondary side is superheated in the second group of channels and then directed to the turbine.

Layouts (b–e) were not recommended due to unpredictable water-chemistry regimes at various locations throughout the thermodynamic cycle. Layout (a) with the secondary-steam reheat required high pressures and temperatures in the primary loop. Circulation pumps with different parameters (power and pressure) were used to feed common header upstream of the channels of the primary group. In this respect, Layout (a) was considerably more complex and expensive than Layout (f). Activation of SHS, which could occur in Layout (f), was not considered to be posing any significant complications to the turbine operation, and hence remained a viable option (Dollezhal et al. 1958).

From the considerations above, Layout (f) was chosen to be developed at the BNPP Unit 1. Surface-corrosion products in the secondary loop and salts in condenser coolant were trapped in the steam generator and removed from it during purging. Additionally, modern separators provided steam of high quality, which resulted in very low salt deposits in the turbine.

3.3 Beloyarsk NPP reactor design

The reactor was placed in a cylindrical concrete cavity, where a 3-m thick wall served as a part of the biological shield. A cooled ferro-concrete base of the reactor with six base jacks was implemented on the bottom of the cavity. The bottom bedplate attached to the bottom supporting ring was held by jacks. Cooling coils were placed on the bottom of the bedplate to provide its cooling.

The cylindrical graphite stack (3 m in diameter and 4.5 m in height) of the reactor was installed on the bottom bedplate. The stack was made of columns, assembled of hexagonal blocks (0.12-m width across corners) in the center and of sectors in the periphery. The central part of the stack was penetrated by vertical operating channels (long graphite cylinders containing inner thin steel tubes with fuel elements). The reactor core (7.2-m diameter and 6-m height) was surrounded with a 0.8-m thick graphite reflector. An additional 1-m thick graphite layer and an approximately 0.5-m cast-iron layer over the upper reflector formed the principal part of the biological shield. A 0.6-m thick graphite layer serving as the lower neutron shield was located below the lower reflector.

The graphite stack (9.6-m overall diameter and 9.0-m height) was enclosed in a gas-tight cylindrical carbon-steel shell filled with nitrogen to prevent graphite deterioration. The outer graphite blocks were penetrated by steel uprights with horizontal lateral braces in several places along their height. The entire stack rested on the bottom bedplate. The graphite stack was covered on the top with a plate carrying standpipes with openings for the insertion of operating channels. The piping for feeding the coolant to the fuel bundles and for removing the coolant water from control rods was located between the standpipes. The piping of the operating channels and protective coating failure-detection system was also located between the standpipes. The plate rested on supports installed on the tank of the side water shield. The plate was connected with the graphite stack shell by means of a compensator, which allowed both for vertical elongations of the shell and horizontal elongations of the plate, which occurred during heating (Emelyanov et al. 1982).

As shown in Figure 4, the reactor had 1134 operating channels and contained 998 fuel channels, 6 automatic control rods, 78 channels for reactivity compensating rods, 16 shut-down rods, and 36 channels for ionization chambers and counters. The fuel channels were represented with 730 BW channels, also referred to as evaporating channels, and 268 SHS channels, also referred to as steam-reheat channels.

The main parameters of the BNPP reactors are listed in Table 3.

3.4 Physical parameters of Beloyarsk NPP reactors

Flattening of a power distribution was achieved at the BNPP with physical profiling: appropriate distribution of control rods and fuel channels of different uranium enrichment (for fresh load) and profiling of burn-up fuel along the reactor radius. The reactor load consisted of SHS channels of 2% and 3% uranium enrichments (SHS-2 and SHS-3, respectively) and BW channels. The BW channels were located in rings in alternate locations with SHS-2. SHS-3 were located along the circumference and had lower pressure losses in the steam circuit (Dollezhal et al. 1964).

Neutronics calculations were made to choose optimal distribution of channels to achieve required power shape. Most of the calculations for the core-reactor physics were performed in the 2-group approximation. In accordance with the fuel-channels distribution the core was represented by four cylindrical regions with the radii: $R_1 = 175$ cm (234 fuel channels), $R_2 = 268$ cm (324 fuel channels), $R_3 = 316$ cm (220 fuel channels), and $R_4 = 358$ cm (220 fuel channels). The previous calculations and operating experience of large uranium-graphite reactors with relatively small neutron leakage showed that a simplified schematic could be used when neutron distribution in the reactor is determined by the multiplication characteristics of the reactor regions. The multiplication constants obtained for the 4 regions ($k_{inf,1} = 1.013$, $k_{inf,2} = 1.021$, $k_{inf,3} = 1.043$, and $k_{inf,4} = 1.045$) allowed flattening of the neutron distribution along the reactor radius with $K_{ir} = 1.20 - 1.25$. The increase in the multiplication constants values to the periphery of the reactor was attained by placing fuel channels with 3% uranium enrichment. Refuelling schemes and, therefore, fuel burn-up at different regions were chosen such as to allow designed power flattening in the end of the campaign, with corresponding values of $k_{inf,i}$. Control rods insertion in the core maintained $k_{inf,i}$ values in the necessary limits during normal operation (Vikulov et al. 1971).

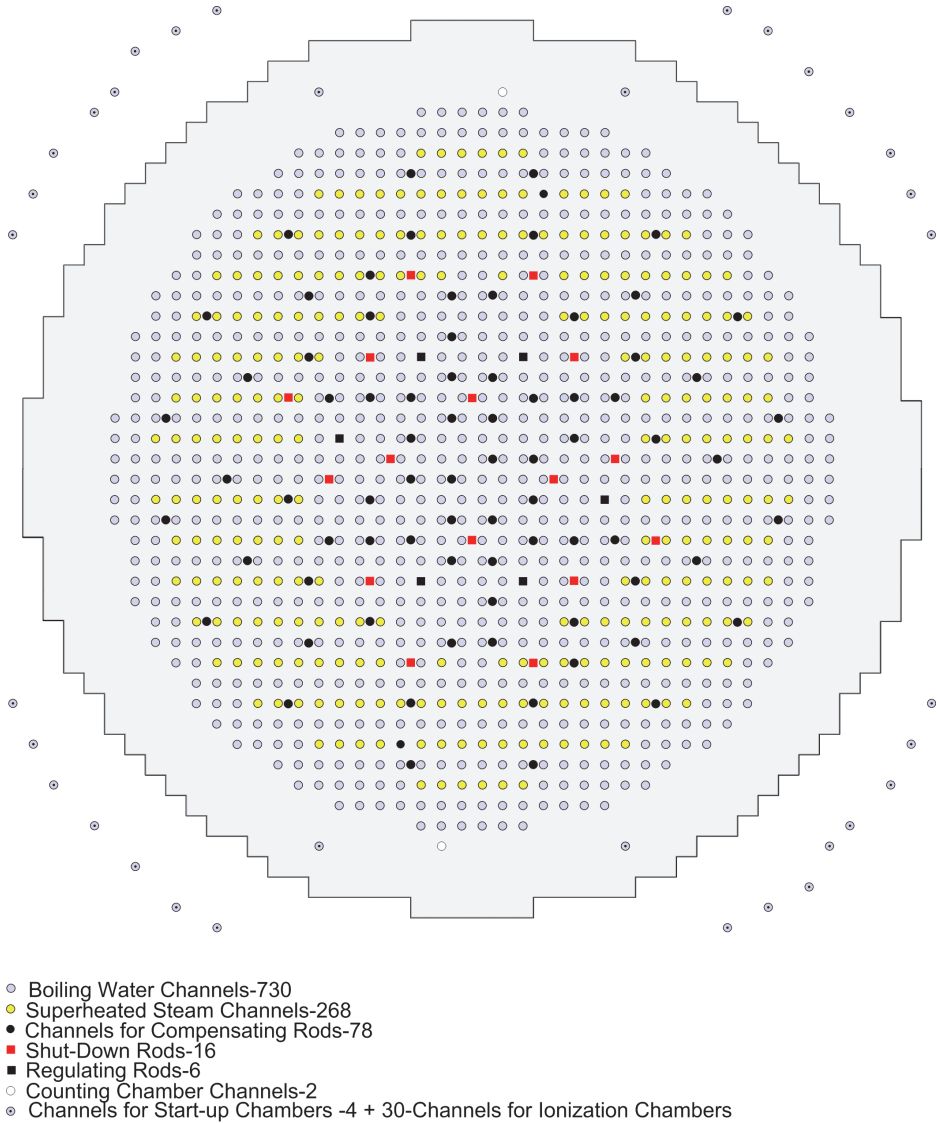


Fig. 4. BNPP Unit 1 channels layout (Pioro et al. 2010, this figure is based on the paper by Dollezhal et al. 1958).

Parameters	BNPP Unit 1 (730 BWs & 268 SHSs)	BNPP Unit 2 (732 BWs & 266 SHSs)
Electrical power, MW_{el}	100	200
Number of K-100-90-type turbines	1	2
Inlet-steam pressure, MPa	8.5	7.3
Inlet-steam temperature, °C	500	501
Gross thermal efficiency, %	36.5	36.6
Total metal content (top & bottom plates, vessel, biological shielding tank, etc.), t	1800	1800
Weight of separator drums, t	94	156
Weight of circulation loop, t	110	110
Weight of graphite stacking, t	810	810
Uranium load, t	67	50
Specific load, MW_{th}/t	4.3	11.2
Uranium enrichment, %	1.8	3.0
Specific electrical-energy production, $MW_{el}\cdot\text{days}/t$	4000	10000
Square lattice pitch, mm	200	200
Core dimensions, m: Diameter	7.2	7.2
Height	6	6

Table 3. Main parameters of BNPP reactors (Aleshchenkov et al. 1964; Dollezhal et al. 1969, 1971).

One of the requirements to be met when implementing nuclear steam reheat is to maintain a constant specified power split (π) between SHS and BW channels during the operating period. The SHS channel temperature up to 520°C at the BNPP was obtained by setting $\pi = 0.41$ at the optimum parameters of the thermodynamic cycle. The number of SHS channels was chosen to provide a π -value of 0.41 at the partial refuelling scheme where the $K_{ir} \approx 1.25$. The steady-state regime was characterized with small fluctuations of approximately 1% in the π -value between the refuellings. Circular arrangement of SHS channels (Unit 1) had an advantage of small π -sensitivity to the changes in radial neutron flux distributions, while for central arrangement of SHS channels (Unit 2) π values were more sensitive (see Table 4).

π	0.408	0.429	0.452	0.494
K_{eff}	1.20	1.36	1.53	1.78

Table 4. Steam-superheating-zone power to boiling-zone power ratio (π) dependence on neutron flux K_{eff} for BNPP Unit 2 (Vikulov et al. 1971).

However, preference was given to the central arrangement of SHS channels, because this allowed attaining a higher π -value (around 12% higher) with the same number of SHS channels. Additionally, central arrangement of SHS channels provided better multiplication characteristics than BW channels. SHS channels were placed in the central region to increase average fuel burn-up by 10%. It should be noted, that during the initial operation period the burn-up rates were different for BW and SHS channels of fresh load, which led to an unbalance of power between superheating and boiling zones. Figure 5 shows the calculated

dependence of π -values and power variations for different types of fuel channels on the power generated by the reactor (Vikulov et al. 1971).

Calculations were performed assuming $K_{ir} \approx 1.25$. A fast decrease in the superheating-zone power relative to that of the boiling zone in the initial period was accounted for by a lower power change in SHS channels due to slightly higher fuel conversion in the low enriched SHS-2. Practically achieved values of K_{ir} were approximately 1.4 for Unit 1 and 1.3 for Unit 2.

One of the features of the uranium-graphite reactors cooled with water is the possibility of reactivity change with water-content change in the reactor. Substitution of boiling water with steam in the operating channels leads to the rapid change of coolant average density. Failure of a fuel-element sheath is another possibility of water-content change that was considered while designing the BNPP reactors. The chosen core lattice with respect to reactivity change turned out to be weakly dependent on water-content changes. It was explained by the compensation of effects of increased resonance neutrons captured by increased water content and an increase at the same time of non-productive neutrons absorption (Dollezhal et al. 1964). Normalized thermal-neutrons distribution along the operating channel cell was studied experimentally for the reactor lattice as shown in Figure 6

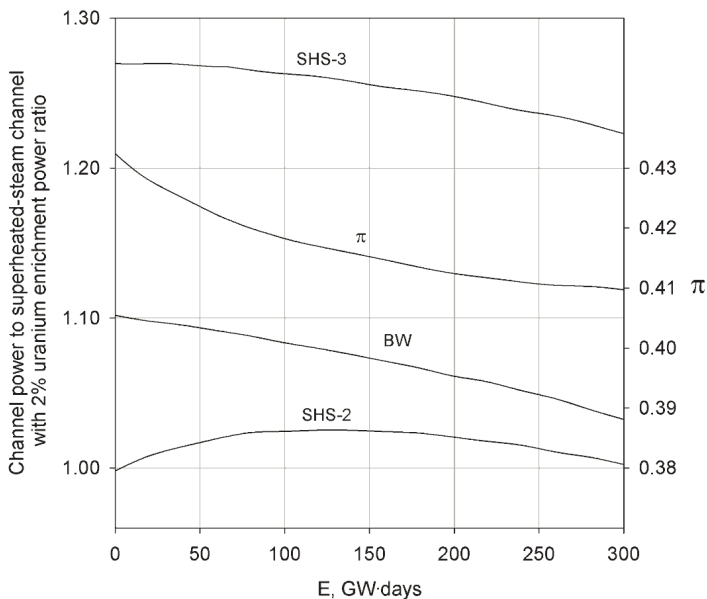


Fig. 5. Channel power ratios and power split between SHS and BW channels (π) dependences on burnup produced by BNPP Unit 2 during the first operating period (Vikulov et al. 1971); SHS-3 - superheated steam channel with 3% uranium enrichment and SHS-2 - superheated steam channel with 2% uranium enrichment.

The gradients in the normalized thermal-neutrons distributions along the reactor radius and height for both units indicated a significant disturbance in the normalized thermal-neutron flux near the outer edge of the reactor likely where the steam-reheat channels end affecting the power distribution. The results indicate a more stable distribution for the BNPP Unit 2. Distribution deformation near the end of operating period was explained by non-uniform fuel burn-up. The results proved a possibility of elementary diffusion-theory application for determining neutron distributions and showed the impact of the arrangement of the superheated-steam channels on power distribution.

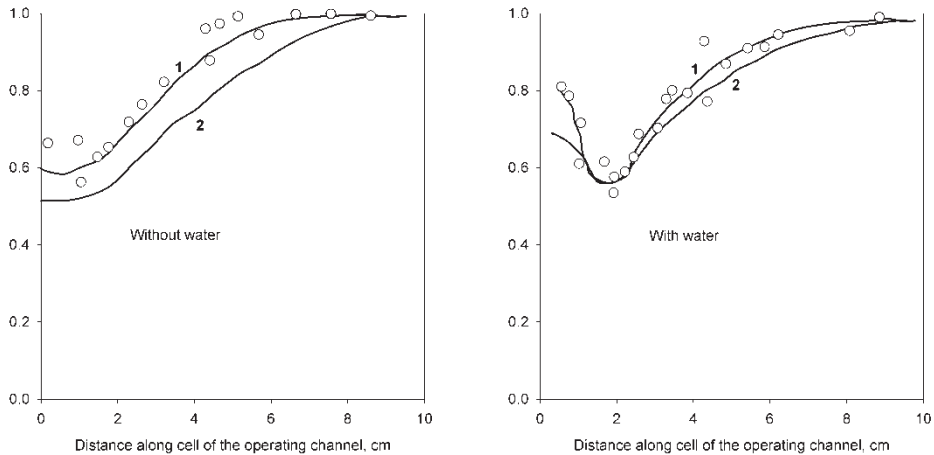


Fig. 6. Normalized thermal-neutrons-density distribution along cell of the operating channel (Dollezhal et al. 1958): 1 – experimental curve and 2 – design curve.

3.5 Boiling-water channels

Fault-free operation of BW channels was achieved with reliable crisis-free cooling of bundles and avoiding interchannel and subchannel pulsations of the coolant-flow rate. The appropriate experiments were performed during design of the BNPP. As the result of increased power, the inner diameter of the fuel element was increased from 8.2 mm for Unit 1 to 10.8 mm for Unit 2. Note that an annular-fuel design is used and increasing the inner diameter results in thinner fuel and lower-centerline temperatures. Coolant is on the inside of the annular fuel and graphite is on the outside of the fuel.

Experiments were performed at different pressures and equal heat flux, steam content and coolant mass fluxes and showed that wall temperature increases at the boiling crisis was higher when coolant pressure was lowered. At the same time, with the lowered coolant pressure the critical steam content increased. The experiments on hydrodynamic stability showed that mass-flux pulsations within the region of high steam content did not introduce danger for the BNPP reactors, because nominal pressure in the evaporating loop was 8.8 MPa and steam content at the channels outlet was not higher than 35%. Wall-temperature oscillations were in the phase with the subchannel flow-rate pulsations. With the increased pressure both the amplitude of temperature oscillations and coolant flow rate decreased.

The same effect occurred at the decreased heat flux and increased flow rate per channel. Wall-temperature oscillations were within the range of 65°C at 1000 kg/h flow rate and 30°C at 1500 kg/h flow rate at constant pressure of 4.9 MPa and 0.2 MW power (Dollezhal et al. 1964).

Fuel elements of larger inner diameter used at Unit 2 compared to that of Unit 1 allowed to lower heat flux and hydraulic resistance. With the equal outer diameter (20 mm), fuel elements inner diameter of the BWs at Unit 1 were 9.4×0.6 mm while that of Unit 2 – 12×0.6 mm. Diameter of the central tube for feeding the coolant was also increased. There were no other differences in the BWs construction used at BNPP Units 1 and 2. Uranium-molybdenum alloy with magnesium filler was used as fuel in the BWs.

3.6 Superheated-steam channels

At the BNPP, SHS channels were operated at higher temperatures compared to those in the BW channels and, therefore, limited the choice of fuel composite and materials. The development of fuel elements for SHS channels underwent several stages. Preliminary tests on the manufacturing technology and performance of fuel elements of various designs were made. As the result, a tubular fuel element with a stainless-steel sheath and a uranium-dioxide fuel composite was chosen for further development (Samoylov et al. 1976). Fuel elements in the initial modification had a tubular design formed by two coaxial stainless-steel sheaths (9.4×0.6 mm and 20×0.3 mm, respectively). Thus, SHS channels with such fuel elements did not differ significantly from BW channels (Figure 7), consisting of 6 fuel elements arranged in a graphite collar with a central steam feeding tube. Steam entered the central tube and was superheated while passing along the fuel bundles.

Later, a U-shape design was developed. The central tube (9.4×0.6 mm) was replaced with an absorbing soft-control rod (12×0.6 mm). The decreased width of the active material decreased non-productive neutron absorption and allowed some power flattening. The steam was reheated first passing downward along three fuel bundles and then passing upwards along another three fuel bundles. Such construction reduced temperature conditions for SHS channels and allowed usage of simpler and cheaper materials. Also, reactor-graphite-stack temperature was lowered by 100°C at a channel power of 0.36 MW. This was achieved with the transfer of heat released in the graphite stack to the downward flow fuel elements that operated at intermediate temperatures (Dollezhal et al. 1964).

Efforts for further improvement of heat and physical parameters were made. They led to another modification of channels and fuel elements. One upward flowing fuel element was eliminated, inner fuel-element sheath was increased to the size of 16×0.7 mm, and outer-sheath size was increased to 23×0.3 mm.

Physical and thermal parameters improved sharply after such a modification due to decreased matrix material in the fuel elements and increased flow cross-section. 6-elements channels were gradually replaced by 5-elements channels during refuelling of the operating reactor. The reduction of one of the elements increases the steam velocity in the upward flowing fuel elements (Samoylov et al. 1976). Stainless steel was used as the outer-sheath material. Uranium-dioxide dispersed in matrix alloy was used as fuel elements in SHS channels. Improvements in the performance of various BNPP parameters are listed in Table 5.

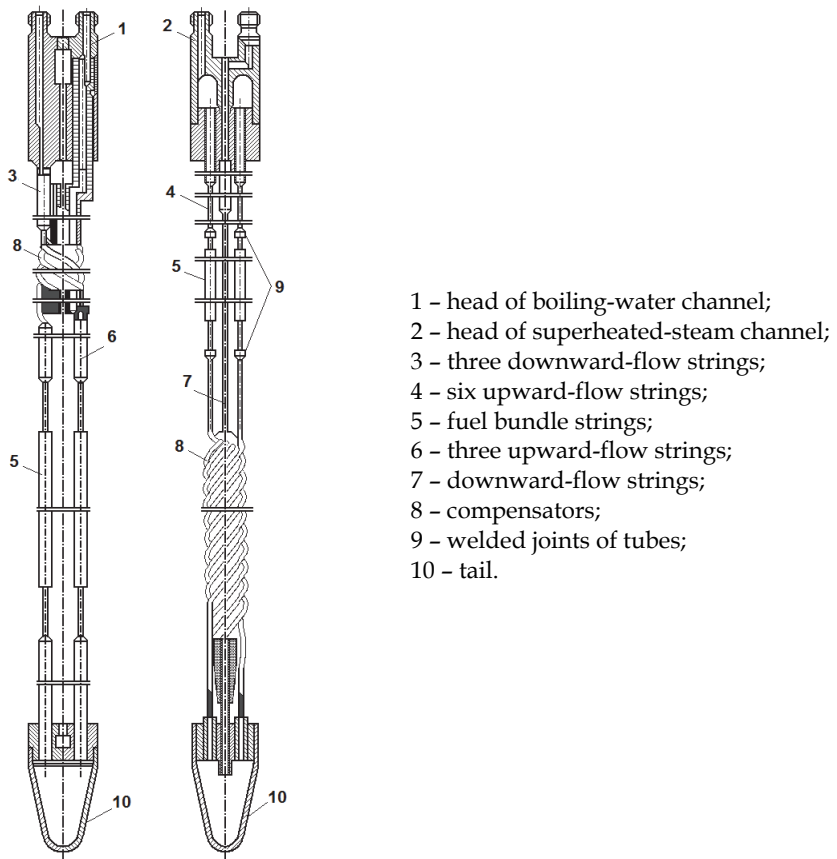


Fig. 7. Principal design scheme of boiling-water and superheated-steam channels (Emelyanov et al. 1972)

Parameters	Before SHSs installation	After SHSs installation
Electrical power, MW_{el}	60-70	100-105
Steam P_{in} , MPa	5.9-6.3	7.8-8.3
Steam T_{in} , °C	395-405	490-505
Exhaust steam P , kPa	9-11	3.4-4.0
Mass flowrate of water in 1 st loop, kg/h	1400	2300-2400
P in separators, MPa	9.3-9.8	11.8-12.7
Gross thermal efficiency, %	29-32	35-36
Electrical power for internal needs, %	10-12	7-9

Table 5. Average parameters of BNPP Unit 1 before and after installation of superheated-steam channels (Dollezhall et al. 1969).

Parameters	BNPP Unit 1	BNPP Unit 2 (U-shaped channel with 6 fuel elements)	
		Downward-flow fuel elements	Upward-flow fuel elements
Max channel power, kW	368	767	
Min channel power, kW	202	548	
Steam mass-flow rate through max. power channel, kg/h	1900	3600	
Steam mass flow rate through channel operating at minimal power, kg/h	1040	2570	
Steam P_{in}/P_{out} , MPa	10.8/9.81	12.9/12.3	12.2/10.8
Steam T_{in}/T_{out} , °C	316/510	328/399	397/508
Max heat flux, MW/m ²	0.56	0.95	0.79
Max steam velocity, m/s	57	76	112
Max T , °C:			
sheath	530	426	531
fuel	550	482	565
graphite	725	735	735

Table 6. Design parameters and operating conditions of superheated-steam channels (Dollezhal et al. 1964).

3.7 Hydrodynamic stability of the Beloyarsk NPP channels during reactors start-up

During start-up and nominal operating conditions it is necessary to provide reliable cooling of fuel bundles (crisis-free heat transfer and hydrodynamic stability). Experiments on set-up simulating Units 1 and 2 were performed for determining safe operating conditions for coolant flow rate with no pulsations during the start-up.

Both SHS and BW channels of the BNPP were filled with water in the initial state. During reactor start-up, the water in the SHS channels was to be discharged and transfer to cooling by steam was to be performed. Additionally, the units were preheated and started without external heat sources.

The coolant flow rate stability in the BW channels was studied for wide ranges of pressures, flow rates and powers (Smolin et al. 1965). Special attention was paid to determination of the pressure, flow rate, steam content and power. Different combinations of these parameters created conditions leading to pulsations. When occurred, flow rate pulsations took place when coolant reached saturation temperature at the outlet of the BWs. Pulsations were in the form of coolant flow rate periodical oscillations in peripheral tubes. Oscillations were phase-shifted in different tubes while the total flow rate was constant.

Two pulsation regions were determined as the result of the experiments: small steam content region ($x = 0 - 15\%$, 3 - 6 oscillations per min) and high steam content region ($x = 25 - 80\%$, 15 - 20 oscillations per min). Flow rate pulsations in tubes were accompanied by wall

tube temperature oscillations along its length with the frequency being equal to that of flow rate oscillations. Wall temperature oscillations in the top cross-sections of the heating zone within the small steam content region occurred with a shift to the smaller values in the surface or volumetric boiling zones and to both the smaller and higher values in the economizer zone. Wall temperature oscillations in the top cross-sections of the heating zone within the high steam content shifted only to the higher values causing boiling crisis (Smolin et al. 1965).

The curves distinguishing stability zones (above the curves) from pulsation zones (below the curves) for the BW and SHS channels of the BNPP Unit 2 are shown in Figure 8.

As seen in Figure 8 the range of stable operation of channels broadens with the increase in pressure or increase in flow rate. The stable operation range contracts with the increase in power. The operating conditions that provide stable flow rate and reliable cooling of the BW and SHS channels at the start-up and nominal operating conditions were chosen based on the performed research. The method of replacing water coolant by steam coolant in SHS channels using accumulated heat was accepted for experimental testing of start-up conditions on Unit 1. The method of gradual replacement of water in the SHS channels first by a water-steam mixture and then by steam was accepted for experimental tests of start-up regime on Unit 2 (Smolin et al. 1965). The experimentally obtained data are presented in Figures 9 – 10.

Both methods were elaborately tested and proved to provide reliable cooling of the BW and SHS channels during the start-up. They were adapted for the development of the BNPP start-up conditions.

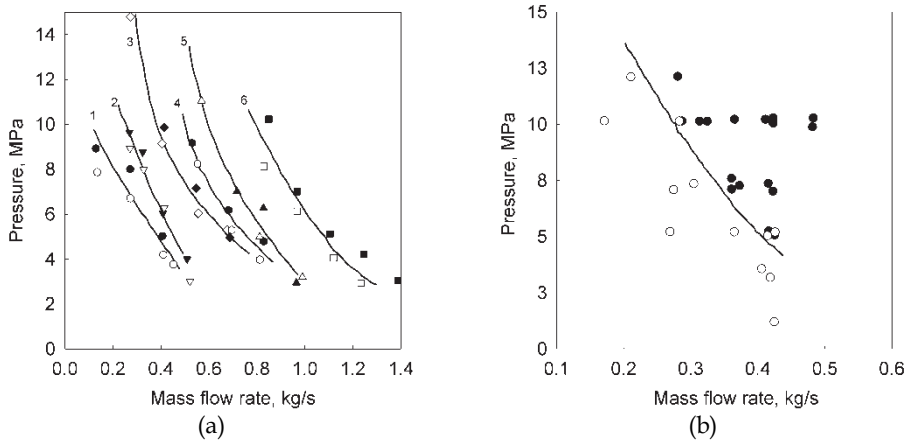


Fig. 8. Ranges of hydrodynamic stability in BW (a) and SHS (b) channels of BNPP Unit 2 at different channel power (regions of channels stable operation are above curves, closed symbols) (Smolin et al. 1965): 1 - 50 kW; 2 - 100 kW; 3 - 200 kW; 4 - 300 kW; 5 - 400 kW; and 6 - 800 kW.

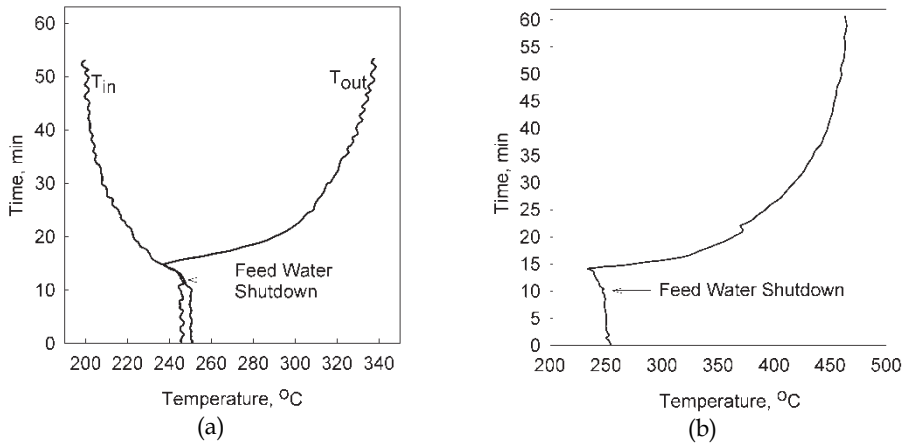


Fig. 9. Temperature variations at BNPP Unit 1 SHS channels at transitional regime (Smolin et al. 1965): (a) – coolant inlet (T_{in}) and outlet temperatures (T_{out}) and (b) –sheath temperature.

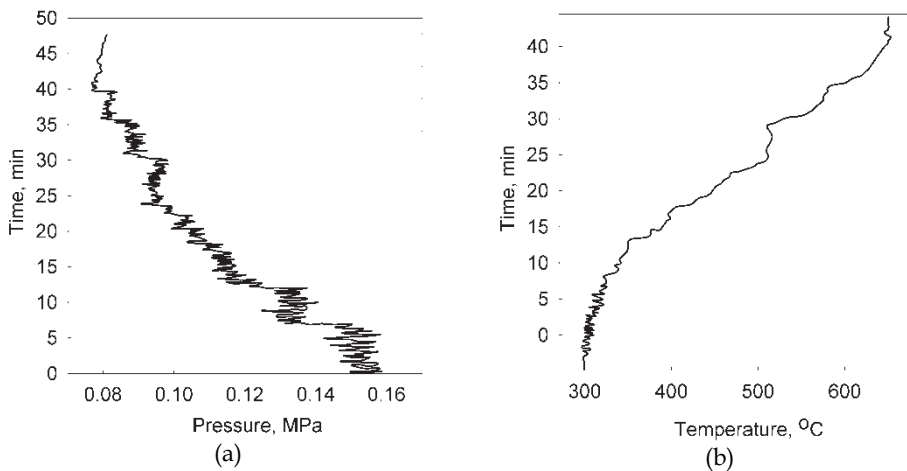


Fig. 10. Variations of pressure drop (a) and sheath temperature (b) at BNPP Unit 2 during high-power start-up (Smolin et al. 1965).

3.8 Start-up of Beloyarsk NPP reactors

The start-up testing of the Unit 1 and Unit 2 reactors of the BNPP are described in this section. During the Unit 1 start-up, both loops were filled with deaerated water, water circulation was established, air was removed, and the pressure was raised up to 10 MPa and 3 MPa in the primary and secondary loops, respectively (Aleshchenkov et al. 1971).

Equipment was heated up at 10 – 14% of reactor power. Average heat-up rate was kept at 30°C/h as measured at the separators. This value was chosen based on experience of drum

boilers operation, though reactor equipment allowed significantly higher heat-up rate. No heat removal was provided during the heat-up to the 160°C coolant temperature at the reactor outlet. The water level was formed at 160°C in the bubbler and the excess heat started being released to the turbine condenser. When water temperature at the outlet of the SHS channels reached 230°C the heat-up was terminated. Total heat-up time was about 9 h.

At the next step, water was purged from SHS channels. The transient processes took place in the second loop while constant pressure and boiling-free cooling of BWs were provided in the primary loop. Reactor power was rapidly reduced to ~2% of its nominal level and feedwater flow rate was reduced to provide water level in the SGs to purge SHS channels. Water-steam mixture from evaporators and steam from the steam loop were directed to the bubbler and then to the deaerator and the turbine condenser.

The purging of SHS channels started after the level in the SGs had been formed. The purging regime was monitored by the pressure drop between the reactor inlet and outlet steam headers and the coolant temperature at the outlet of each SHS channel. Additional steam discharge by increased pressure drop rate was achieved and thus the purging was accelerated by opening gate valves in front of the bubbler for 1 – 2 min. The pressure drop rate was chosen based upon the allowed temperature condition and was set to ~0.15 MPa/min. Overall time for the level formation in the evaporators was ~8 – 10 min, the time of purging ~6 – 10 min. The gate valves in front of bubblers were closed and reactor power was increased after the purging had finished. Thus, the pressure and the temperature in SHS channels were increase. After 2 hours the SHS channels purging had been finished and the reactor achieved a stable operation at 10% power level. The heating of steam pipes and the turbine was initiated and the turbine connection to the power line was prepared. Further power increase was made once the turbine had been connected to the power line.

The first loop was transferred to the boiling flow regime and the separators levels were formed at 35% reactor power and ~6 MPa pressure. During the transient to the boiling regime, the operating conditions of the MCPs were continuously monitored. Water temperature was maintained 5 – 6°C below the boiling margin for intake pipes of the main circulation pumps. Level formation in the separators was accompanied by smooth pressure change. It took about 3 h for the water to reach controlled level in the separators, the time being dependent only on the separator bleed lines throughput.

The specific features of a single-circuit flow diagram made the sequence of the BNPP Unit 2 start-up operations somewhat different. SHS channels purging and transition to boiling regime in the BW channels took place simultaneously. Filling of the circuits and equipment heat-up were the same as in Unit 1. The terminal heat-up parameters were higher ($P \approx 9.3$ MPa and $T \approx 290^\circ\text{C}$). Two main circulation pumps were used to drive coolant circulation in the evaporating loop. After heat-up the reactor power was reduced to 2 – 3% of nominal level. SHS channels purging, and transition to boiling regime in the BW channels took place after the heat-up. The feedwater flow rate was considerably reduced, water was purged out of the separators, and the flow rate to the bubblers was increased to form levels in the separators. As a result, the water in the fuel channels and separators boiled causing the purging of water and water-steam mixture from SHS channels. The monitoring of the purging process was the same as at the Unit 1. After SHS channels purging had been completed, the reactor power was increased and steam flow into the bubbler was reduced at the reheated steam temperature rise rate of about 1°C/min with the pressure drop between the steam headers at least ~50 – 60 kPa. The automatic level control system was put into operation as soon as the water in the separators reached the rated level. The subsequent

reactor power increase, turbine preparation, and connection of the turbine to the power line were the same as for Unit 1 (Aleshchenkov et al. 1971).

3.9 Pumps

All pumps at the BNPP were high-speed type (3000 rpm). Serial high-power feeding pumps were used. Other pumps were special canned type, in which the motor spindle and pump spindle were revolved in a pumped medium and were separated from the motor stator by a thin hermetic nichrome plate. Bearing pairs of the pumps were lubricated and cooled by pumped water. The revolving details of bearings were made of advanced hard alloys and bearing bushes were made of special plastics. Some minor failures were observed in operation of MCP (Emelyanov et al. 1972). Those were due to cracks in nichrome jacket, to malfunctioning of fan of the stator front parts, to pilot-valve distribution system imperfections, and to failures of the fasteners in the pump interior. Modernizations of some individual elements of the MCP and reconstruction of independent pump cooling loops improved optimal on-stream time between maintenance and repairing (16,000 h). As a result, the failure probability of the MCP was reduced to minimum. Operating experience of the MCP showed that serial pumps could be used instead of specially designed canned pumps under no fragment activity in the loops conditions that were achieved at BNPP.

3.10 Water chemistry

The experiments on effectiveness of water and steam radiolysis suppression by hydrogen in BW and SHS channels respectively were performed after 16 months of Unit 1 operation. Water and steam samples were taken at the drum-separator, MCPs, inlet and outlet of SHS channels. Ammonia dosing was terminated before the test for determination of the required amount of hydrogen that was necessary to suppress water and steam radiolysis that was partially caused by ammonia decomposition (Yurmanov et al. 2009b). Hydrogen concentration in saturated steam at the separator was found to be 45 – 88 nml/kg and in circulation water at the main circulation pump was found to be 2.75 – 12.8 nml/kg. Despite some hydrogen excess, oxygen concentration decreased from 2.28 mg/dm³ to 0.1 mg/dm³. Dissolved oxygen concentration in the circulating water at the main circulation pump did not exceed 0.01 – 0.03 mg/dm³. At the next stage of experiments, steam radiolysis in SHS channels and the possibility of suppressing it by hydrogen concentration levels were studied. Hydrogen concentration was set to 1.2 – 6.2 nml/kg in steam and 1.2 – 1.8 nml/kg in circulating water. Oxygen concentration was below 0.15 mg/kg in steam and about 0.02 mg/dm³ in the circulating water. The obtained results demonstrated effective suppression of water radiolysis.

Additional research was carried out at 60% reactor power. The results showed that the oxygen concentration was decreased to 0.03 mg/kg at the SHS channels outlet only at 45 nml/kg hydrogen concentration. The water-steam mixture at the turbine ejector consisted of hydrogen (62 – 65%) and oxygen (8 – 10%) at a hydrogen concentration of 40 – 45 nml/kg. The water-steam mixture was needed to be diluted with air to a non-explosive state, i.e., hydrogen volume fraction was to be decreased below 2 – 3% (Shitzman 1983).

The equipment for Unit 2 was made from the following constructional materials: stainless steel (5500 m², 900 m² of which were used for the core); carbon steel (5600 m²); brass and cupronickel (14,000 m²); stellite (4.8 m²). The studies showed that radiolytic gases production rate was approximately 5 times lower than that of a BWR of the same power.

Water radiolysis at the BW channels of the BNPP Unit 1 was suppressed by ammonia dosing. This kept radiolytic oxygen content in water at several hundredths of a milligram per liter. Ammonia dosing wasn't used at Unit 2 due to the danger of corrosion of the condenser tubes and low-pressure heaters. Radiolytic fixation of oxygen in the steam that was bled to high-pressure heaters was achieved by hydrazine hydrate dosing. The operation norms and the actual quality of coolant at the BNPP Unit 2 are listed in the Table 7. Additional information on water flow regime may be found in paper by Konovalova et al. (1971).

All the indicators of coolant quality were in the range set by the water regime regulations during normal operating period.

Parameters	Feed water	Reactor circulating water	Reactor bleed water	Saturated / Reheated steam	Turbine condensate
SiO ₂₋₃ , µg/kg	-	-	100-300	5-15 / 5-15	-
Chlorides, µg/kg	25	25	25	- / -	-
Iron oxides, µg/kg	20-60	20-60	30-60	20-30 / 20-30	0
Copper, µg/kg	-	-	7-30	0.4 / -	0.8
Specific activity, Ci/l	-	-	10 ⁻⁵	- / 10 ⁻⁷	-
Oxygen, µg/kg	10-15	30	30	(5-6) · 10 ³ / (5-6) · 10 ³	40-50
Ammonia, mg/kg	1-25	0.6-1.4	0.6-1.4	0.8-2 / 0.8-2	1-2
pH	9.2-9.5	8-9	9-9.5	9-9.5 / 9-9.5	9-9.5

Table 7. Actual parameters of BNPP Unit 2 coolant quality during period of normal operation (Konovalova et al. 1971).

In August 1972 (after 4.5 years of operation) neutral no-correction water was implemented at Unit 2 (Dollezhai et al. 1974). Operation in the new conditions revealed the following advantages over the ammonia treated state:

1. The cease of feedwater ammonia treatment led to the zero nitrate content in the reactor circulation water. This allowed an increase of the pH from 4.8 to the neutral level at the 300°C operating temperature.
2. Balance of the corrosion products content in the circulation water and chemical flushing of the BW channels showed that the rate of metallic oxide deposits formation on the fuel-bundles surfaces in the evaporating zone of the reactor was three times lower using no-correction water.
3. The Co-60 deposition rate outside the core was 7 – 10 times lower using no-correction water.
4. Condensate purification experience using no-correction water allowed an increasing filter service cycle by 6 times.

3.11 Section-unit reactor with steam-reheat

The BNPP became the first in the world industrial NPP with a uranium-graphite power reactor. Examination of the main characteristics of the BNPP reactors (for example, see Table 3) shows that that performance of such type of reactors could be improved. BNPP used slightly enriched uranium and the calculations showed that increasing enrichment to 5% would increase fuel burn-up 4 – 10 times (up to 40,000 MW·days/t).

All channel reactors were constructed with traditional cylindrical shape of core. Therefore, power increase in such a reactor could be attained by increasing the number of working channels in the core and a proportional increase in diameter size. However, increase in power per reactor would then be limited by the maximum size of the reactor upper plate that could be built and withstand a high load. A way out of this situation was found in section-unit design of the channel reactor with a rectangular core. Such a shape would allow separating not only the core, but also reactor as a whole, into equal geometry sections. Then the reactor of a specified capacity can be constructed of the required number of sections. Each section would stay the same for reactors of different power outputs, and, consequently, core width and maximum size of the upper metalwork would stay the same too. Therefore, the power of a section-unit reactor power would not be limited by the size of the upper plate (Emelyanov et al. 1982).

Section-unit type reactors with coolant at supercritical fluid conditions (see Figure 11) was developed at Research and Development Institute of Power Engineering (RDIPE, Moscow, Russia) as an improvement to the existing RBMK (Russian acronym for Channel Reactor of High-Power).

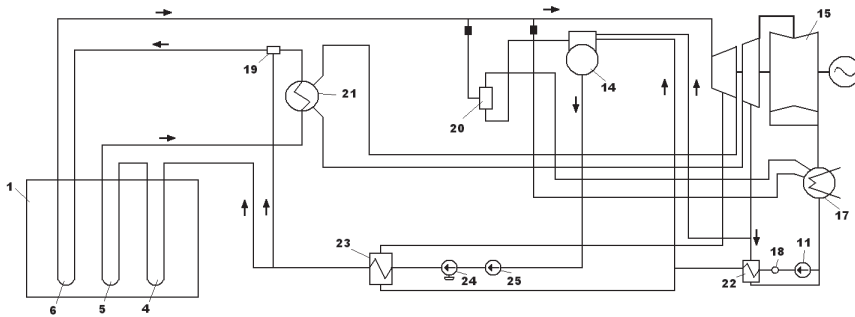
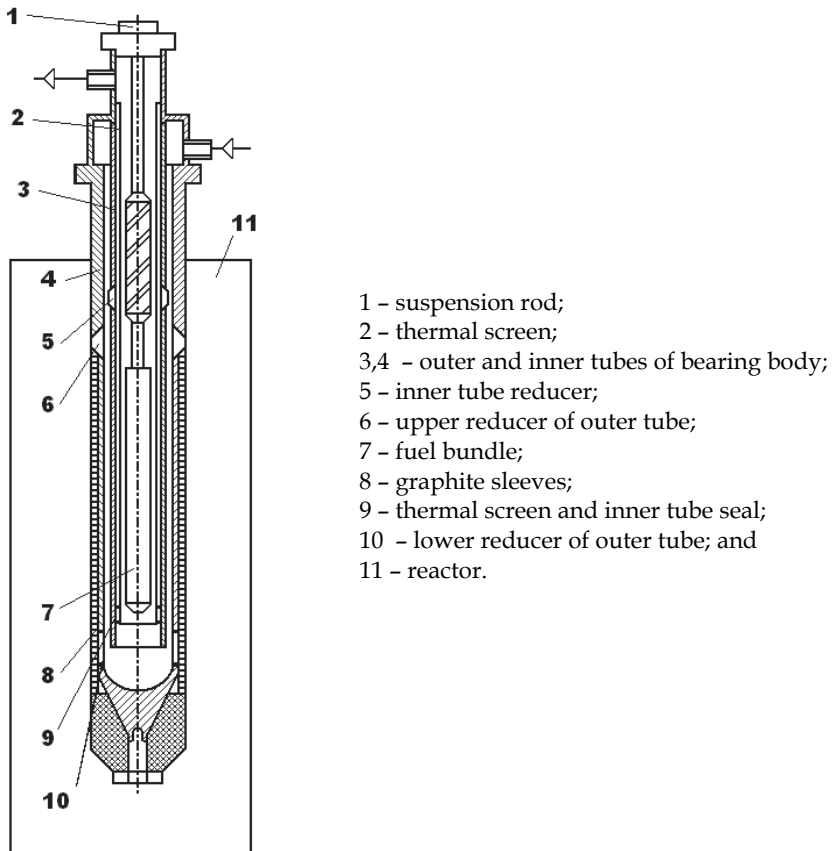


Fig. 11. Schematic of RDIPE SCW NPP (Aleshchenkov et al. 1971): 1 - reactor; 4 - preheating channel; 5 - first SHS; 6 - second SHS; 11 - Condensate Extraction Pump (CEP); 14 - deaerator; 15 - turbo-generator; 17 - condenser; 18 - condenser purifier; 19 - mixer; 20 - start-up separator; 21 - intermediate steam reheat; 22 - low-pressure regenerative preheater; 23 - high-pressure regenerative preheater; 24 - feed turbo-pump; and 25 - booster pump.

Rod fuel bundles were inserted into Zirconium SHS (SHS-Z) channels (see Figure 12) on the core level. UO_2 fuel elements with steel sheath were designed. Fuel bundles were covered by a sheath to hold SHS-Z channel wall below 360°C (Grigoryants et al. 1979). Therefore, saturated steam entering the channel was split into two streams. About 25% of the steam flowed through the annular gap cooling the SHS-Z channel wall. Both streams mixed at the core exit. Steam mixture was at about 455°C . Tests with SHS-Z channels were performed in BNPP Unit 1 to check design decisions. SHS-Z channels were tested in 23 - 24 start-ups - shutdowns, including 11 emergency shutdowns of the reactor when the steam temperature change rate was $20 - 40^\circ\text{C}/\text{min}$ during the first 3 minutes of an automatic control system operation, and $5^\circ\text{C}/\text{min}$ after that. SHS-Z channel wall temperature reached $400 - 700^\circ\text{C}$ and that of the fuel bundles sheath reached $650 - 740^\circ\text{C}$ during start-up operation at a steam

pressure of 2.45 – 4.9 MPa. Channels were operated about 140 h at high temperature conditions. Studies showed that fuel element seal failures were mainly due to short-duration overheating (Mikhan et al. 1988).



- 1 - suspension rod;
- 2 - thermal screen;
- 3,4 - outer and inner tubes of bearing body;
- 5 - inner tube reducer;
- 6 - upper reducer of outer tube;
- 7 - fuel bundle;
- 8 - graphite sleeves;
- 9 - thermal screen and inner tube seal;
- 10 - lower reducer of outer tube; and
- 11 - reactor.

Fig. 12. Principal scheme of SHS-Z (Mikhan et al. 1988)

Additional information on SHS-Z-channel tests in BNPP Unit 1 may be found in the papers by Grigoryants et al. (1979) and by Mikhan et al. (1988).

4. Conclusions

The operating experience of the reactors with nuclear steam reheat worldwide provides vital information on physical and engineering challenges associated with implementation of steam reheat in conceptual SuperCritical Water-cooled Reactors (SCWRs). Major advancements in implementation of steam reheat inside the reactor core were made in the USA and Russia in 1960s – 1970s. Three experimental reactors were designed and tested in the 1960s – 1970s in the USA. In the former Soviet Union, nuclear steam reheat was implemented at two units at the Beloyarsk NPP. Operating experience of the units showed a

possibility of reliable and safe industrial application of nuclear steam reheat right up to outlet temperatures of 510 – 540°C after over a decade of operation. Thermal efficiency of the Beloyarsk NPP units was increased by 5% as the result of implementing nuclear steam reheat. The introduction of nuclear steam reheat was economically justified in cases where the steam was superheated up to 500°C and higher with the use of stainless-steel-sheath fuel elements.

The experiments and operating experience obtained to date also indicate that further improvements in SHS channel design and in reactor design are possible.

5. Acknowledgements

Financial supports from the NSERC/NRCan/AECL Generation IV Energy Technologies Program and NSERC Discovery Grant are gratefully acknowledged.

The authors would like to acknowledge contributions of Wargha Peiman, Amjad Farah and Krysten King.

6. Nomenclature

K_{eff}	effective multiplication constant
K_{ir}	neutron flux irregularity coefficient
P	pressure, MPa
R	radius, m
T	temperature, °C
x	steam quality

Greek letters

π	power split between superheated-steam and boiling-water and channels
-------	--

Subscripts

el	electrical
in	inlet
out	outlet
th	thermal

Abbreviations and Acronyms

AECL	Atomic Energy of Canada Limited
BNPP	Beloyarsk Nuclear Power Plant
BONUS	BOiling NUclear Superheater
BORAX	BOiling Reactor Experiment
BW	Boling-Water (channel)
BWR	Boiling Water Reactor
CEP	Condenser-Extraction Pump
ESADE	Superheat Advance Demonstration Experiment
FWP	FeedWater Pump
MCP	Main Circulation Pump
NSERC	Natural Sciences and Engineering Research Council (Canada)
NPP	Nuclear Power Plant

NRCan	Natural Resources of Canada
RBMK	Russian Acronym for Channel Reactor of High-Power
RDIFE	Research and Development Institute of Power Engineering (Moscow, Russia)
SADE	Superheat Advance Demonstration Experiment
SCW	Supercritical Water
SCWR	SuperCritical Water-cooled Reactor
SG	Steam Generator
SHS	SuperHeated Steam (channel)
SS	Stainless Steel
USAEC	United States Atomic Energy Commission
Z	Zirconium

7. References

- Aleshchenkov, P.I., Zvereva, G.A., Kireev, G.A., Knyazeva, G.D., Kononov, V.I., Lunina, L.I., Mityaev, Yu.I., Nevskii, V.P., and Polyakov, V.K., 1971. Start-up and Operation of Channel-Type Uranium-Graphite Reactor with Tubular Fuel Elements and Nuclear Steam Reheating, *Atomic Energy (Атомная Энергия, стр. 137-144)*, 30 (2), pp. 163–170.
- Aleshchenkov, P.I., Mityaev, Yu.I., Knyazeva, G.D., Lunina, L.I., Zhirnov, A.D., and Shuvalov, V.M., 1964. The Kurchatov's Beloyarsk Nuclear Power Plant, (In Russian) *Atomic Energy*, 16 (6), pp. 489–496.
- Dollezhal, N.A., Malyshev, V.M., Shirokov, S.V., Emel'yanov, I.Ya., Saraev, Yu.P., Aleshchenkov, P.I., Mityaev, Yu.I., and Snitko, E.I., 1974. Some Results of Operation of the I.V. Kurchatov Nuclear Power Station at Belyi Yar, *Atomic Energy (Атомная Энергия, стр. 432-438)*, 36 (6), pp. 556–564.
- Dollezhal, N.A., Aleshchenkov, P.I., Bulankov, Yu.V., and Knyazeva, G.D., 1971. Construction of Uranium-Graphite Channel-Type Reactors with Tubular Fuel Elements and Nuclear-Reheated Steam, *Atomic Energy (Атомная Энергия, стр. 149-155)*, 30 (2), pp. 177–182.
- Dollezhal, I.Ya., Aleshchenkov, P.I., Evdokimov, Yu.V., Emel'yanov, I.Ya., Ivanov, B.G., Kochetkov, L.A., Minashin, M.E., Mityaev, Yu.I., Nevskiy, V.P., Shasharin, G.A., Sharapov, V.N., and Orlov, K.K., 1969. BNPP Operating Experience, (In Russian), *Atomic Energy*, 27 (5), pp. 379–386.
- Dollezhal, N.A., Emel'yanov, I.Ya., Aleshchenkov, P.I., Zhirnov, A.D., Zvereva, G.A., Morgunov, N.G., Mityaev, Yu.I., Knyazeva, G.D., Kryukov, K.A., Smolin, V.N., Lunina, L.I., Kononov, V.I., and Petrov, V.A., 1964. Development of Power Reactors of BNPP-Type with Nuclear Steam Reheat, (In Russian), *Atomic Energy*, (11), pp. 335–344 (Report No. 309, 3rd International Conference on Peaceful Uses of Nuclear Energy, Geneva, 1964).
- Dollezhal, N.A., Krasin, A.K., Aleshchenkov, P.I., Galanin, A.N., Grigoryants, A.N., Emel'yanov, I.Ya., Kugushev, N.M., Minashin, M.E., Mityaev, Yu.I., Florinsky, B.V., and Sharapov, B.N., 1958. Uranium-Graphite Reactor with Reheated High Pressure Steam, Proceedings of the 2nd International Conference on the Peaceful Uses of Atomic Energy, United Nations, Vol. 8, Session G-7, P/2139, pp. 398–414.

- Emelyanov, I.Ya. , Mikhan, V.I., Solonin, V.I., Demeshev, R.S., Reکشnya, N.F., 1982. *Nuclear Reactor Design*, (In Russian). *Energoizdat Publishing House*, Moscow, Russia, 400 pages.
- Emelyanov, I.Ya., Shasharin, G.A., Kyreev, G.A., Klemin, A.I., Polyakov, E.F., Strigulin, M.M., Shiverskiy, E.A., 1972. Assessment of the Pumps Reliability of the Beloyarsk NPP from Operation Data, (In Russian). *Atomic Energy*, 33 (3), pp. 729–733.
- Grigoryants, A.N., Baturov, B.B., Malyshev, V.M., Shirokov, S.V., and Mikhan, V.I., 1979. Tests on Zirconium SRCh in the First Unit at the Kurchatov Beloyarsk Nuclear Power Station, *Atomic Energy (Атомная Энергия, стр. 55–56)*, 46 (1), pp. 58–60.
- Konovalova, O.T., Kosheleva, T.I., Gerasimov, V.V., Zhuravlev, L.S., and Shchapov, G.A., 1971. Water-Chemical Mode at the NPP with Channel Reactor and Nuclear Steam Reheat, (In Russian), *Atomic Energy*, 30 (2), pp. 155–158.
- Mikhan, V.I., Glazkov, O.M., Zvereva, G.A., Mihaylov, V.I., Stobetskaya, G.N., Mityaev, Yu.I., Yarmolenko, O.A., Kozhevnikov, Yu.N., Evdokimov, Yu.V., Sheynkman, A.G., Zakharov, V.G., Postnikov, V.N., Gladkov, N.G., and Saraev, O.M., 1988. Reactor Testing of Zirconium Steam-Reheat Channels with Rod Fuel Elements in Reactors of the First Stage of BNPP, (In Russian), *BNPP Operating Experience: Information Materials* (in 4 volumes), USSR Academy of Sciences, Ural Branch, 207 pages.
- Novick, M., Rice, R.E., Graham, C.B., Imhoff, D.H., and West, J.M., 1965. Developments in Nuclear Reheat, *Proceedings of the 3rd International Conference, Geneva, Vol. 6*, pp. 225–233.
- Petrosyants, A.M., 1969. Power Reactors for Nuclear Power Plants (from the First in the World to the 2-GW Electrical Power NPP) , (In Russian). *Atomic Energy*, 27 (4), pp. 263–274.
- Piolo, I., Saltanov, Eu., Naidin, M., King, K., Farah, A., Peiman, W., Mokry, S., Grande, L., Thind, H., Samuel, J. and Harvel, G., 2010. Steam-Reheat Option in SCWRs and Experimental BWRs, Report for NSERC/NRCan/AECL Generation IV Energy Technologies Program (NNAPJ) entitled “Alternative Fuel-Channel Design for SCWR” with Atomic Energy of Canada Ltd., Version 1, UOIT, Oshawa, ON, Canada, March, 128 pages.
- Ross, W.B., 1961. Pathfinder Atomic Power Plant, Superheater Temperature Evaluation Routine, An IBM-704 Computer Program. United States Atomic Energy Commission, Office of Technical Information, Oak Ridge, TN, 49 pages.
- Samoilov, A.G., Pozdnyakova, A.V., and Volkov, V.S., 1976. Steam-Reheating Fuel Elements of the Reactors in the I.V. Kurchatov Beloyarsk Nuclear Power Station, *Atomic Energy (Атомная Энергия, стр. 371–377)*, 40 (5), pp. 451–457.
- Shitzman, M.E., 1983. *Neutral-Oxygen Water Regime at Supercritical-Pressure Power Units*, (in Russian), *Energoatomizdat Publishing House*, Moscow, Russia.
- Smolin, V.N., Polyakov, V.K., Esikov, V.I., and Shuyinov, Yu.N., 1965. Test Stand Study of the Start-up Modes of the Kurchatov’s Beloyarsk Nuclear Power Plant, (In Russian). *Atomic Energy*, 19 (3), pp. 261–269.
- USAEC Report ACNP-5910, 1959. Allis-Chalmers Manufacturing Co., Pathfinder Atomic Power Plant, Final Safeguards Report, May.
- USAEC Report (MaANL-6302), 1961. Design and Hazards Summary Report—Boiling Reactor Experiment V (Borax-V), Argonne National Laboratory.

- USAEC Report PRWRA-GNEC 5, 1962. General Nuclear Engineering Corp., BONUS, Final Hazards Summary Report, February.
- Vikulov, V.K., Mityaev, Yu.I., Shuvalov, V.M. , 1971. Some Issues on Beloyarsk NPP Reactor Physics, (In Russian), *Atomic Energy*, 30 (2), pp. 132-137.
- Yurmanov, V.A., Belous, V. N., Vasina, V. N., and Yurmanov, E.V., 2009a. Chemistry and Corrosion Issues in Supercritical Water Reactors, Proceedings of the IAEA International Conference on Opportunities and Challenges for Water Cooled Reactors in the 21st Century, Vienna, Austria, October 26–30.
- Yurmanov, V.A., Vasina, V. N., Yurmanov, E.V and Belous, V. N., 2009b. Water Regime Features and Corrosion Protection Issues in NPP with Reactors at Supercritical Parameters", (In Russian), Proceedings of the IAEA International Conference on Opportunities and Challenges for Water Cooled Reactors in the 21st Century, Vienna, Austria, October 26–30.

Integrated Approach for Actual Safety Analysis

Francesco D'Auria, Walter Giannotti and Marco Cherubini
GRNSPG - University of Pisa
Italy

1. Introduction

Actual trend in reactor safety deterministic analysis are evolving toward best estimate approach. Best estimate analyses imply use of best estimate codes and input data. The best estimate concept is not limited to thermal-hydraulics rather in general terms it covers many fields, likewise three dimensional neutron kinetics, structural analysis and containment performance evaluation.

The general frame is to put efforts in avoiding conservative assumptions performing analysis adopting the best tool available for each specific topic, all contributing to give an integrated evaluation of the plant response.

The needs to adopt an integrated approach in performing safety analysis come from the inherent complexity of a Nuclear Power Plant and from the tight interactions among the subsystems constituting the plant itself. These interactions directly involve the necessity to consider a broad spectrum of disciplines typically coming into play in different not interacting analyses.

An example of the integral approach is given in the present document. The integral approach has been pursued for the safety analyses of the 'post-Chernobyl modernized' Reactor Bolshoy Moshchnosty Kipyashiy (RBMK) specifically for Smolensk 3. These analyses were performed at the University of Pisa within the framework of a European Commission sponsored activity.

The mentioned analyses deal with events occurring in the primary circuit, as well as excluding those events originated from plant status different from the nominal operating conditions. Following the evaluation of the current state of the art in the safety analysis area, targets for the analysis were established together with suitable chains of computational tools. The availability of computational tools, including codes, nodalizations and boundary and initial conditions for the Smolensk 3 Nuclear Power Plant, brought to their application to the prediction of the selected transient evolutions that, however, are not classified as licensing studies.

The integrated approach for safety analysis yields to the evaluation of complex scenarios not predictable adopting just a single computational tool. Example is given considering the Multiple Pressure Tube Rupture (MPTR) event which constitute one of the main concern of this kind of plant.

The content of this document includes an introduction to the critical issues to be accounted for in the frame of an integral safety analysis approach; the selection of suitable computational tools to proper deal with the scenario subject of the investigation; an

approach on how to link (coupling issues) the selected tools; the use of intermediate code outcomes and interpretation of the global predicted plant behaviour. All the aspects presented in general terms are applied in the case study of a Multiple Pressure Tube Rupture having as reference plant the Smolensk 3 Nuclear Power Plant. The selected event may occur as a consequence of a fuel channel blockage which (if not detected) brought to the rupture of the affected pressure tube. The dynamic loads generated by its breach may lead to the rupture of the surrounding pressure tubes. Direct consequence of the pressure tube rupture is the pressurization of the reactor cavity which envelopes all the core. In the case of Multiple Pressure Tube Rupture event, involving a large number of pressure tubes, the lifting of the reactor cavity top may occur, putting in direct connection the core with the environment. The present example is a kind of analysis that cannot be performed if an integrated approach is not adopted.

2. Framework

The best estimate approach is the actual trend of the NPP deterministic analysis (International Atomic Energy Agency [IAEA], 2008). The concept of best estimate is generally applied to the software codes used in the analysis. However the best estimate approach concept has a broader meaning. It applies to the general framework of the analysis, and it involves not only the codes, but the kind of analyses to be performed, the approach to realize the models to be realized for the analyses, the input data including boundary and initial conditions also. The best estimate approach is not only connected with a calculation performed with a best estimate code. The result of the analysis is a best estimate evaluation, if all the aspects of the analysis (input data, systems models, results) are best estimate, in addition to the codes. As a consequence the use of a best estimate code, assuming not best estimate data or systems model cannot be considered a best estimate analysis.

A calculation of a complex system like a NPP, poses a lot of issues to perform a best estimate analysis. The main relevant aspect is constituted by the many areas involved in the analysis of a NPP. Knowledge in many technical areas are necessary. The solution can be obtained by “linking” in a single instrument of investigation the different tools developed for investigation in each of the different areas.

2.1 Complexity of the approach

The scope is the safety of nuclear power plants, is demonstration of the capability to keep the radiation exposure of personal and population within specified limits. It is ensured by maintaining the integrity of safety barriers, which are part of the plant defence in depth concept.

A series of barriers prevents the release of radioactive fission products from their source beyond the reactor containment and into the environment. In analyzing the NPP safety, it is essential to assess the integrity of these barriers and to decide to what degree the response of the whole NPP and its systems to a certain initiating event is acceptable from the viewpoint of the plant safety. The integrity of the safety barriers is related to certain threshold values, which are referred to as acceptance criteria. Design limits are adopted with a conservative margin so that the safety barrier integrity is guaranteed as long as the parameters do not exceed the relevant criteria. In the case of not efficacy of the barriers a radioactive release occurs and an evaluation of the dose to the workers and population is done (IAEA, 1996 and IAEA, 2000).

The complexity of the analysis is due to the involvement of a number of different technological areas requests a detailed identification of topics and targets together with a suitable connection with adopted codes and activities.

The nuclear technology sectors or computational areas relevant for NPP safety and design include the following areas: the system thermal-hydraulics, the computational fluid-dynamics, the structural mechanics, the neutron kinetics with the cross section generation and the fission product release and transport.

The interconnections among individual Technological Areas identify a chains of codes. Figure 1 gives an idea of the complexity of the activities and related technological areas necessary for a such analysis.

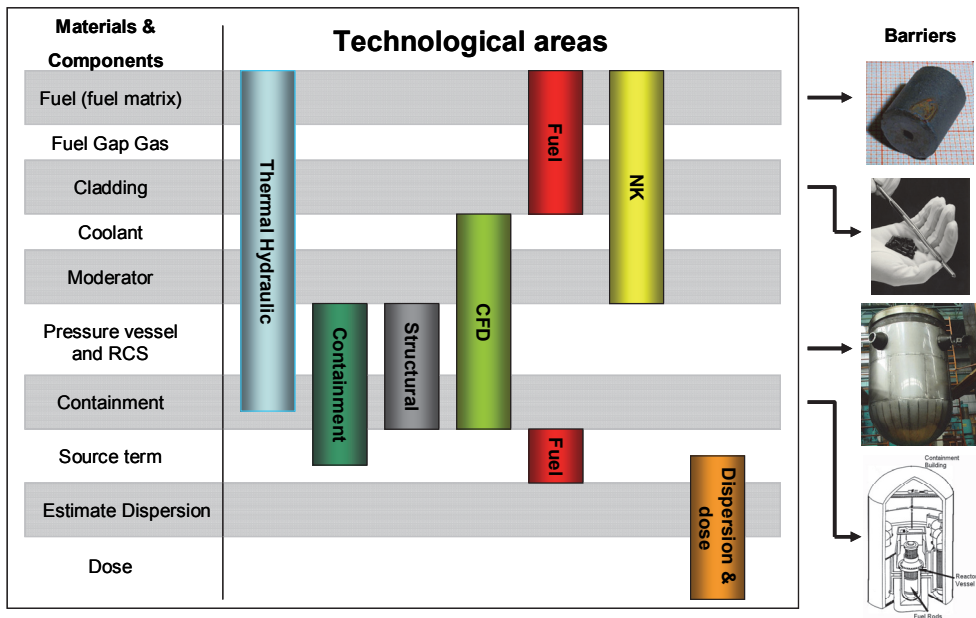


Fig. 1. Technological areas for the integrated an analysis

The effort to perform a such analysis is aimed to establish a connection with the regulatory or licensing environment. This connection must take into account the evolution of safety concepts following improvements of the technical knowledge, including the availability of powerful computational tools and of experimental evidences.

The framework constitutes by the development & qualification of computational tools is also related to relevant points like “physical phenomena understanding”, and “analysis of complex scenarios expected during accident conditions” considering the current licensing practices.

The strategic objective is the set-up of a suitable chain of codes to deal with accident scenarios. The motivation for the selection of individual accidents is given by expecting challenging phenomena for the concerned safety barrier. The concerned phenomena shall also be connected with the existing code typologies and capabilities. These codes are

supposed to be qualified for the prediction of individual accidents whose relevant and detailed boundary and initial conditions have been defined.

The list of phenomena, which are taking place during progression of an accident shall be analyzed, discussed and selected. Relevant information can be taken from international literature (e.g. IAEA, 2002) or from experimental tests. The operative objective is to demonstrate the capability of computational tools to reproduce relevant transient phenomena and to show that the same tools can be linked together.

Generally speaking, best estimate is associated to the TH SYS codes. About this kind of codes is clear the meaning of best estimate approach. Descriptions of this concept are largely diffused in international literature. The concept of best estimate is less clear about the codes related to the other technological areas. The general concept of best estimate approach is in avoiding any intentional conservatism. This concept is applied in all the aspects of the calculation: input data, conditions of the calculation, model of the systems and of course the code. From this point of view the aspects to be considered for each individual codes are:

- The physical modelling.
- The approximations that are made and their limitations.
- The used correlations.
- An assessment of uncertainties due to the physical models.
- The practice of application associated to these codes
- and their level of validation and/or certification.
- the associated impact on the drawing of safety analyses.

In such a complex analysis, requiring different codes, the data used as input for a code are derived from the result of another previous code calculation. So a relevant role is also played by the evaluation and selection (as input data in next calculations) of the results obtained by code application. The figure. 2 gives an idea of the links between the different technical areas.

Referring to the figure 2, some links are hereafter exemplified.

- Path a) the TH codes results are used to supply boundary data to the code for fuel evaluation.
- Path b) the TH codes supply the thermal hydraulic boundary conditions to the NK codes. The results of the NK codes are supplied to the TH code core component.
- Path c) the TH codes supply the thermal hydraulic boundary conditions to the CFD codes. The results of the CFD codes are supplied to the TH for evaluation of specific areas of the systems.
- Path d) the CFD codes supply the boundary conditions to the Structural code for evaluation of mechanical resistance of systems components.
- Path e) the results from the Containment code are supplied to the TH codes for calculation of the evolution of the accident in the reactor coolant system and containment.
- Path f) the results of the Structural code about the integrity of the systems (e.g. containment systems) are supplied to the containment codes.
- Path g) the results of the Containment code about possible failure and source terms are supplied to the codes for dispersion and dove evaluation.
- Path h) the results of the Fuel code about source terms are supplied to the codes for dispersion and dove evaluation.

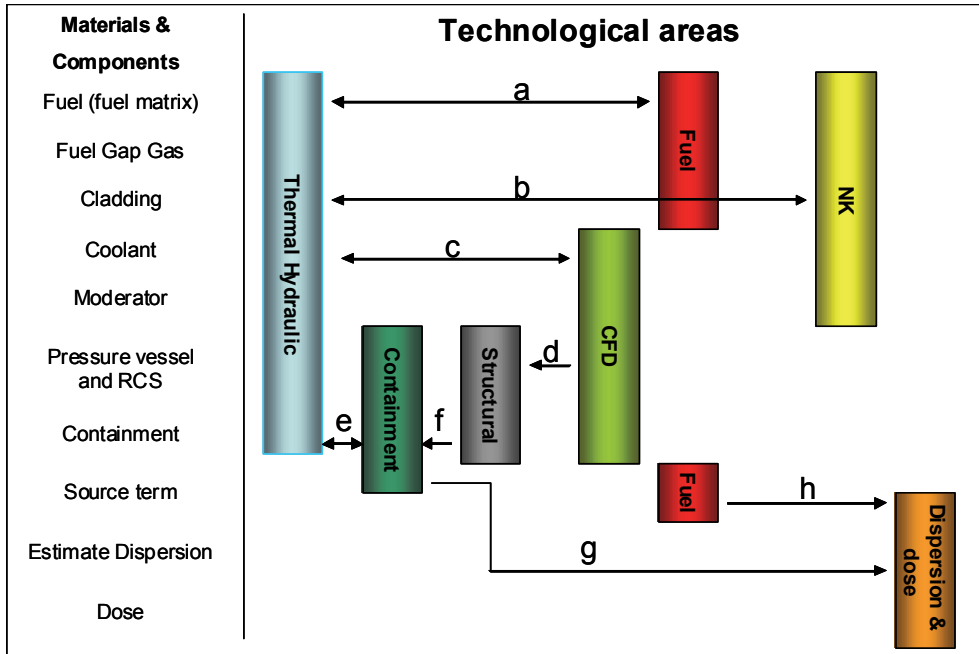


Fig. 2. Links between the different technical areas

2.2 Qualification and uncertainty

A relevant aspect in best estimate application is the qualification of the process of code application:

The following specific topics must be covered:

- Development process of generic codes and their capabilities;
- Developmental Assessment;
- Structure of specific codes
- Numerical methods;
- Description of input decks;
- Description of fundamental analytical problems;
- Analysis of fundamental problems;
- International Standard Problem Activity and benchmarks;
- Example of code results from applications to ITF;
- Plant accident and transient analyses application;
- Modalities for developing the nodalization;
- Description and use of nodalization qualification criteria;
- Qualitative and quantitative accuracy evaluation;
- Use of thresholds for the acceptability of results for the reference case;
- Description of the available uncertainty methodologies;
- Coupling methodologies.

A specific aspect of best estimate application is constitute by uncertainty evaluation (Wickett et al., 1998). For the TH codes specific methodologies were developed and applied.

International literature offers a spread documentation about this uncertainty methodologies for TH codes.

Concerning the codes not connected with the TH area the following items must be evaluated to derive the evaluation of the uncertainty.

- Description of the numerical methods. Generally the codes are validated versus some reference calculations and the related uncertainty is also given.
- International Standard Problem Activity and benchmarks. From the comparison with the result of other qualified codes can be estimated the uncertainty of the code.
- Code application to experimental tests.
- Code application to experimental tests in Plant accident and transient analyses.

Additional and relevant aspects to be also considered are:

- Procedure for developing the nodalization developed by the user or in the code manual.
- Description and use of nodalization qualification criteria.
- User experience

2.3 Computational tools needed in the analysis

The computational tools include:

- the best estimate computer codes;
- the nodalization including the procedures for the development and the qualification;
- the uncertainty methodology including the procedure for the qualification;
- the computational platforms for coupling and interfacing inputs and outputs from the concerned codes and nodalization.

An outline of the codes listed in the table below is provided in the table 1.

No	Field of application	Example of applications
1.	System Thermal-Hydraulics	All transients
2.	I&C Modelling	All transients (where I & C, i.e. control, limitation and protection systems, play a role).
3.	Computation Fluid Dynamics	Special detailed analyses of specific components and/or systems
4.	Structural Mechanics	PTS and structural mechanics integrity of the vessel wall.
5.	Fuel (mechanics)	All transients in relation to which the number of failed rods is calculated
6.	Neutron Physics (and supporting)	Transients analyzed by 3D coupled neutron kinetics - thermal-hydraulics: spatial or local neutron flux effects are relevant – transient conditions.
	Confinement	Severe accident
7.	Radiological Consequences (and supporting)	Environment diffusion and dose tot the population

Table 1. Outline of the codes needed in the analysis

All considered codes should be well established within the international community and some referenced document per each code should be provided that gives access to the peculiarities of the code.

Key issues for the application of the codes are represented by:

- a. the demonstration of the code qualification level;
- b. the demonstration of the current user capabilities in the use of the codes.

The quality demonstration of individual codes, item a), can be derived by several hundred worldwide available documents. In addition to such documents, per each code there are specific-additional qualification documents issued. The reference document provided per each code, gives one access to international qualification documents.

Connected with the above item a), the quality of the code application results is increased by a systematic and comprehensive application of independent codes for deriving the same result. All the codes should be applied by the users, item b), having experience (years) in the code application and results analysis. Code qualification cases shall be considered in order to prove the user capabilities in the application of the codes.

2.3.1 System Thermal-Hydraulics

The quantitative characterization of a system transient scenario constitutes the main role for the System Thermal-hydraulic (SYS-TH) code, consistently with the main objective for its development. The SYS-TH code gives the results connected with the thermal hydraulic parameters evolution of the NPP during a transient. The application of the SYS-TH code, because of the capability to represent all the systems in a quit compact and fast calculations, is typically also used to derive the initial conditions for the application of other more specific codes/tools.

These kinds of codes generally have embedded some additional capabilities:

- The multi-dimensional component in SYS-TH code developed to allow the user to more accurately model the multi-dimensional flow behaviour that can be exhibited in any component or region of a system.
- Neutron kinetic modules: the NK module can have from zero to three dimensions representation capabilities.
- Severe accident module: a limited capability can be included in simulating core damage occurrence and fission fragment distribution in the systems.

2.3.2 I&C modeling

The aim is to simulate the performance of the control, the limitation and the protection systems of the NPP. The simplified representation of the protection system only could be not sufficient for a detailed analysis. The Instrumentation and Control (I&C) can be modelled in the SYS-TH code. But the complexity of the control (also including limitation) systems request a more capable end flexible tool. Some applications have been done just realizing software (e.g. Fortran based software) coupled with the SYS-TH code.

In the I&C software the equations are solved to simulate the transient behaviour of the various transducers, actuators and logic of operation of each individual component that constitutes the control, the limitation and the protection systems of the NPP. The code receives the system information at each time step from the SYS-TH code related to any requested thermal-hydraulic variable (e.g. pressure, level, pressure drop, fluid temperature). The related information is processed, e.g. considering the inertia of the transducer or the

delay of the signal transmission, and commands for components (typically pumps, valves, control rods, heaters, etc.) modelled in SYS-TH are generated. With the new system configuration a new time step is calculated and the above process starts again.

2.3.3 Computational Fluid Dynamics

The main role of CFD is to support and validate the application of the SYS-TH in relation to the mixing phenomena and in calculating pressure drop coefficients at geometric discontinuities where information from experimental data is not adequate. The latter role is also relevant to the PTS study.

CFD features the following modelling capabilities:

- Steady-state and transient flows.
- Laminar and turbulent flows.
- Subsonic, transonic and supersonic flows.
- Heat transfer and thermal radiation.
- Buoyancy.
- Non-Newtonian flows.
- Transport of non-reacting scalar components.
- Multiphase flows.
- Combustion.
- Flows in multiple frames of reference.
- Particle tracking.

2.3.4 Structural mechanics

The structural mechanics code is used to calculate stress and strains in components other than the fuel rods. Two main uses are exemplified in order to summarize the role of the code:

- a. demonstration that dynamic loads, following transient scenarios, do not cause rupture/collapse of or the substantial deformation of the relevant component potentially affecting the coolability of the core;
- b. calculation of stresses in the components relevant to prevent radioactive releases. Typical application is constituted by PTS analysis.

These tools are adopted to perform static and dynamic analyses of linear and non-linear problems (due to materials properties, geometry, contact between surface, etc.) in many fields of application (structural, thermal, electromagnetic, fluid-dynamic, etc.). It is possible to solve coupled problems as well as fluid-structure interaction, thermal-mechanical calculation. In addition several special purpose features are available, namely: fracture mechanics, composites, fatigue, beam analyses.

2.3.5 Fuel mechanics

The key goal for the use of the code is the evaluation of the integrity of the fuel claddings. The number of nuclear fuel rod claddings that are damaged following each transient constitutes the typical output from the code. The code is a computer program for the thermal and mechanical analysis of fuel rods in nuclear reactors. The code was specifically designed for the analysis of a whole rod. Code incorporates physical models of thermal and radiation densification of the fuel, models of fuel swelling, fuel cracking and relocation, a model of generation of fission gases, a model of redistribution of oxygen and plutonium,

and some other physical models. The code has the capabilities of analysis of all fuel rod types under normal, off-normal and accident conditions (deterministic and probabilistic).

2.3.6 Neutron physics

The transient (time dependent) three-dimensional calculation of the neutron flux following global or local perturbations constitutes the main goal from the use of the code. The neutron kinetics subroutines require as input the neutron cross-sections in the computational nodes of the kinetics mesh. A neutron cross-section model has been implemented that allows the neutron cross-sections to be parameterized as functions of SYS-TH code heat structure temperatures, fluid void fraction or fluid density, poison concentration, and fluid temperatures. Additional codes are necessary to (not exhaustive list):

- to derive macroscopic cross sections thus supporting the application of the Nestle code;
- to support and to validate calculation results (fluxes and several reaction rates in each point of the calculation domain and to perform criticality analyses);
- to calculate fuel cell calculation versus burn-up;
- to calculate the build up, decay, and processing of radioactive materials;
- to convert evaluated nuclear data file in continuous-energy or multi-group microscopic cross sections libraries.

2.3.7 Radiological consequences

The purpose is to simulate the impact of severe accidents at nuclear power plants on the surrounding environment. The principal phenomena considered are atmospheric transport, mitigation actions based on dose projections, dose accumulation by a number of pathways including food and water ingestion, early and latent health effects, and economic costs.

Several aspects must be considered:

- Calculation of the radioactivity inventory in the fuel elements.
- Tracking the transport of radioactivity products inside the primary system and the containment.
- Calculating the offsite radioactivity dispersion and the dose to the population.
- Calculating the onsite dispersion and the dose to the control room personnel

2.3.8 Nodalizations

The nodalizations are the result of a brainstorming process by the code-users, which connect each code with the physical system to be simulated. The process for developing a nodalization especially for a best estimate code does not necessarily require less effort than the process of development of the code itself. The same is true in relation to the qualification. Expert users develop the nodalization for an assigned purpose, provided that Best Practice Guidelines are followed whenever available. Sensitivity tests can be performed to demonstrate the nodalization quality and the achievement of mesh-independence of the results, which means that varying the node density (or the number of nodes) does not make the results change to a large extent. All nodalizations shall be developed according to suitable quality assurance procedures and criteria. The procedures are linked with the code characteristics and with the expertise of the users.

All nodalizations developed to apply the BE codes must be qualified according to current standards that are specific for each code. Plant nodalization should be developed according to predefined qualitative and quantitative acceptance criteria.

Three major steps in the process must be distinguished each one characterized by a number of sub-steps, by procedures and by acceptability thresholds:

1. Nodalization development: the nodalization must be characterized by ‘geometric fidelity’ with the modelled physical systems that are part of the NPP.
2. Acceptance of steady state.
3. The transient capability: the capability of the code-nodalization in simulating the phenomena of interest must be demonstrated

Qualitative and quantitative acceptability thresholds and criteria are adopted at step 1). Quantitative acceptability thresholds are adopted at step 2). Qualitative and quantitative accuracy evaluation is performed for step 3) with quantitative thresholds.

A simplified scheme of a procedure for the qualification of the nodalization is depicted in the figure 3. It is assumed that the code has fulfilled the validation and qualification process and a “frozen” version of the code has been made available to the final user. The steps of the diagram are described below.

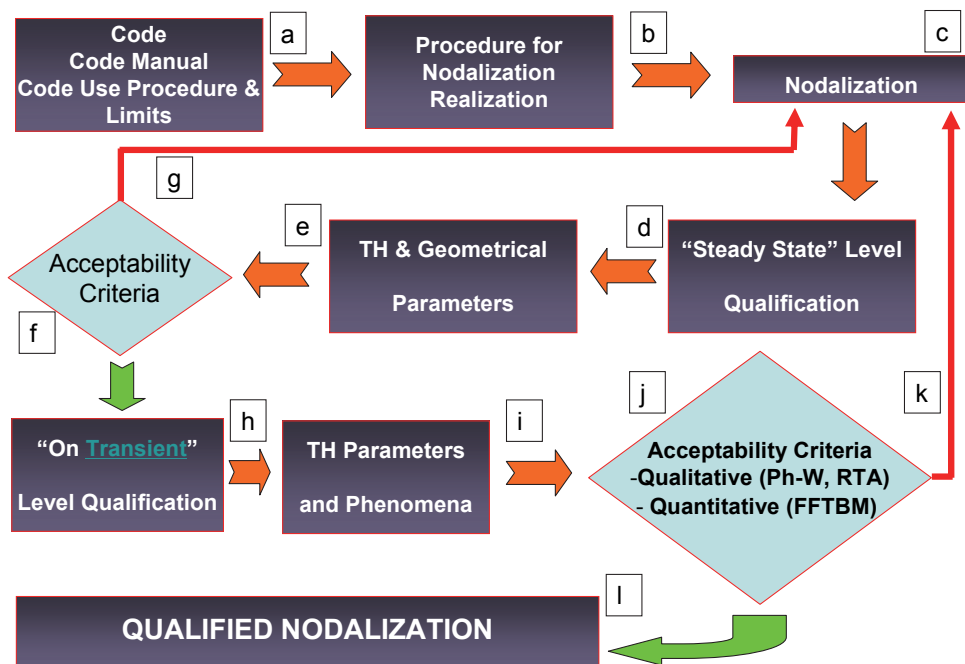


Fig. 3. Simplified scheme for nodalization qualification

Step “a”: this step is related to the information available by the user manual and by the guidelines for the use of the code.

Step “b”: user experience and developers recommendations are listed and considered.

Step “c”: the nodalization must reproduce all the relevant parts of the reference plant; this includes geometrical and materials fidelity and consideration of components and logics.

Step “d”: different checks are performed under this step mostly geometry related (does not require running the code-nodalization).

Step “e”: different checks are performed under this step.

Step "f": this is the step where the adopted acceptability criteria are applied to evaluate the comparison between hardware and implemented geometrical values in the nodalization and between the experimental and calculated steady-state parameters.

Step "g": if one of the criteria in the step "f" are not fulfilled, a review of the nodalization (step "c") must be performed. The path "g" must be repeated till all acceptability criteria are satisfied.

Step "h": this step constitutes the "On Transient" level qualification and allows the verification of selected data that are relevant only during transient.

Step "i": in this step the thermal-hydraulic parameters that are at the basis of the qualitative or quantitative accuracy evaluations are characterized.

Step "j": checks are performed to evaluate the acceptability of the calculation, e.g. of the 'Kv-scaled' calculation both from qualitative and from quantitative points of view.

Step "k": this path is actuated if any of the checks (qualitative and quantitative) is not fulfilled.

Step "l": the obtained nodalization is used for the selected transient and the selected facility or plant. Any subsequent modification of the nodalization requires a new qualification process both at "steady state" and at "on transient" level.

3. Example of application: introduction to the analysis of the MPTR

The RBMK core is constituted by more than one-thousand pressurized channels housed into stacked graphite blocks and connected at the bottom and at the top by small diameter (D) and long length (L) pipes (less than 0.01 and more than 10 m, respectively) that end up into headers and drum separators. Control valves are installed in the bottom lines. Due to the large L/D value and to the presence of valves and other geometric discontinuities along the lines connecting with the pressure channels, the Fuel Channel Blockage (FCB) event is possible and already occurred in two documented NPP events. Previous investigations, have shown the relevance of these events for the safety technology, and the availability of proper computational technique for the analysis (NIKIET, 1983 and 1992).

The occurrence of the FCB event remains undetected for a few tens of seconds because of the lack of full monitoring for the individual channels. Therefore, fission power continues to be produced in the absence of cooling. This brings in subsequent times to fuel rod overheating, pressure tube failure, damage of the neighbouring graphite brick and ejection of damaged fuel. Following the pressure tube rupture, reactor cavity pressurization, radioactivity release into the same area and change of fluid properties occur that allow the detection of the event and cause the reactor scram at a time of a few tens of seconds depending upon the channel working conditions and the severity of the blockage.

Notwithstanding the scram and the full capability of the reactor designed safety features to keep cooled the core, the multiple pressure tube rupture (MPTR) issue is raised. The question to be answered is whether the 'explosion' of the blocked pressure tube damages not only the neighbour graphite bricks but propagates to other channels causing the potential for several channel failure.

In order to address the MPTR issue fuel channel thermal-hydraulics and three-dimensional (3D) neutron kinetics analyses have been performed, as well structural mechanics calculations for the graphite bricks and rings (graphite rings surround the pressure tube to accommodate for thermal and radiation induced expansions).

The bases for the analysis and the results of the study are presented. The conclusion, not reported within a licensing based format, is that the MPTR consequences are not expected to be relevant for the safety of the RBMK installations.

3.1 Execution of the analysis

The detailed knowledge of the RBMK system configuration was not spread in the Western world till the 1986 event. Afterwards, “information batches” of RBMK technology became available and were unavoidably evaluated in the light of the Chernobyl event. The results of recently completed project sponsored by European Commission (EC), with the participation of RBMK designers in Russia and the supervision of the national utility and the regulatory authority, allow to give an idea of RBMK current safety characteristics. The project has been made possible owing to the availability of sophisticate computational tools developed and qualified in the last decade. These include powerful computers, advanced numerical solution methods, techniques for developing input decks and for proving the qualification level. Following the identification and the characterization of bounding scenarios assuming to envelope all accident conditions relevant to RBMK safety technology, two main chains of codes have been set-up and utilized to perform safety analyses.

3.2 The computational tools

The computational tools include the numerical codes, the nodalizations and the relevant boundary and initial conditions related to the Smolensk 3 NPP in the present case. The application of computational tools requires systematic demonstration of quality and suitable documentation detail. However, within the scope of the performed activity, there is the ‘as-far-as-possible’ demonstration of quality for codes, the development of nodalizations, the implementation of boundary and initial conditions as available and the achievement of results from computer calculations. Furthermore, terms like ‘capable code’ and ‘suitable code’ have been introduced. A code is ‘capable’ when it is able to simulate the phenomena and the physical scenarios expected during the assigned NPP accident. A code is ‘suitable’ when a user can run the code addressing (or calculating) the expected phenomena within a reasonable time with reasonable resources. It should be noted that the term ‘capable’ is less binding for a code than the term ‘qualified’ and a quantification is provided for the items ‘reasonable resources’ and ‘reasonable time’.

3.3 The numerical codes

The numerical codes adopted are those listed in the third column of Table 2.

Identification		Codes adopted	Reasons for the selection
No.	ACRONYM explanation		
A1	LOCA-PH-FIGDH: LOCA in Pressure Header with failure to isolate GDH	Relap5	Largest primary system break with single failure. Challenging core cooling and the ECCS design
A2	LOCA-SL: LOCA originated by a break in Steam Line		Highest depressurization rate. Challenging core cooling and the ECCS design

Identification		Codes adopted	Reasons for the selection
A3	LOOP-ATWS: Loss of on Site Power with the ATWS condition		Challenging core cooling and the neutron kinetics model of the thermal-hydraulic system codes
A4	GDH-BLOCKAGE: Full blockage of the GDH		Check of the capability of the 'ECCS bypass' to cool the core
B1	GDH-BLOCKAGE-SA: Full blockage of the GDH with the 'Severe Accident' assumption of no bypass line available	Cocosys and Relap5	Challenging the venting capability of the reactor cavity (part of the confinement)
B2	LOCA-PH-FIGDH: See A1	Contain and Relap5	Challenging the ALS (part of the confinement) structural resistance (same as A1)
B3	LOCA-SL: See A2	Contain	Challenging the reactor building (part of the confinement) venting capability (same as A2)
C1	FC-BLOCKAGE: Full blockage of one fuel channel	Relap5-3D©/Nestle	Challenging the calculation of the local fission power generation (same as D1)
C2	GDH-BLOCKAGE: See A4		To assess and to understand the local core response (same as A4)
C3	CR-G-WITHDRAWAL: Continued withdrawal of a CR bank (or group)	Korsar-Bars	Challenging RIA (Reactivity Initiating Event)
C4	CPS-LOCA: Voiding (or LOCA) of the CPS	Relap5-3D©/Nestle	
D1	FC-BLOCKAGE: See C1	Relap5-Ansys Katran-U-Stack	Driving accident for the study. Challenging various areas and codes
D2	FC-LOCA: Rupture of one FC	Contain & Relap5 Fluent-Ansys Korsar-Rapta	To assess the ballooning model in the fuel pin mechanics area
E1	FC-BLOCKAGE: See C1	Cocosys Melcor	To assess the hydrogen and the fission products source term and transport (same as B1)
E2	GDH-BLOCKAGE-SA: See B1		To assess the hydrogen and the fission products source term and transport in one extreme conditions (same as B1)
F1	FC-BLOCKAGE: See C1	Relap5	To formulate the ICM proposal (same as D1)

Table 2. Adopted numerical codes

The area for the application of the codes can be deduced from the second column in the same table and from the diagrams in figure. 4 and figure 5 that are applicable for the Russian and the Western codes, respectively. Topological subjects relevant to the deterministic safety analysis of RBMK are identified in Figs. 4 and 5 and the correspondence with the range of application of numerical codes is established.

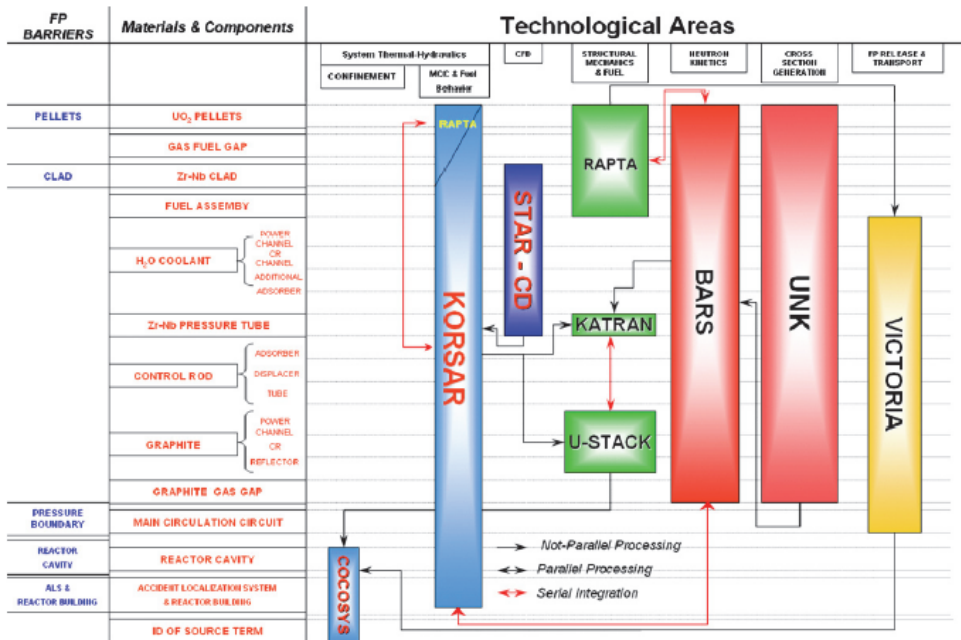


Fig. 4. Codes adopted by Russian group

The topological subjects include:

- Five fission product barriers: the fuel pellet, the clad, the pressure boundary of the primary cooling system and the confinement regions corresponding to the reactor cavity, the (ALS) and the reactor building.
- The materials and components constituting the NPP hardware: the coolant, the fuel and the moderator are examples of 'materials'; the control rods, the pressure tube and the zones of the confinement are examples of 'components'.

The technological areas (for deterministic safety analysis) include the system thermal-hydraulics, the computational fluid-dynamics, the structural mechanics, the neutron kinetics with the cross section generation and the fission product release and transport.

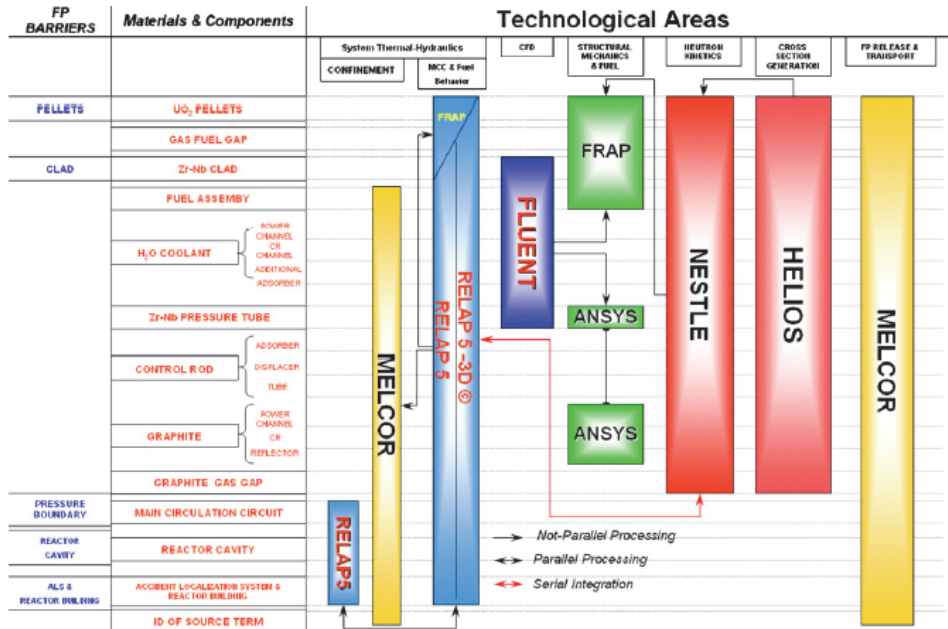


Fig. 5. Codes adopted by western group

3.4 The nodalizations

Nodalizations were developed for both Western and Russian codes by modelling the materials and components, by making reference to the technological areas and by considering the features of codes with the target of demonstrating codes capability and suitability, but also to assess the integrity of the fission product barriers. Nodalizations are typically the result of wide range brainstorming processes whose outcome depends upon the code features, the available computer power, the expertise of the user and the target for the analyses. An example of the realized nodalizations is reported in the table 3.

3.5 The boundary and the initial conditions

Boundary conditions for NPP accident analyses are constituted by huge amount of data ranging from in the present case the mass of water in the steam drum, to the individual fuel bundle burn-up, to the material properties of irradiated graphite, to the thickness and the Young module for the tank that encompasses the graphite stacks, to the free volume of the reactor cavity, to the net flow areas of the valves/openings connecting various zones of the confinement with the environment.

The boundary conditions for the MPTR issue is the accident scenario originated by the fuel channel blockage (FC-BLOCKAGE making reference to boundary conditions in the Smolensk-3 NPP unit.

3.6 The multidisciplinary problem associated with the FC-BLOCKAGE scenario

The background for addressing the multidisciplinary problem arising from the FC-BLOCKAGE and the MPTR include the presentation of following aspects:

No.	System or component	Code	Total number of nodes	Target for the nodalization
1	Main coolant circuit	Relap5	6491/52735*	Thermal-hydraulic performance of the RBMK primary loop in case of DBA and BDBA
2		Korsar	829/5256*	
3	Confinement system	Relap5	621/2625*	Thermal-hydraulic performance of the RBMK confinement in case of DBA and BDBA
4		Cocosys	37	
5	Reactor core	Nestle	29856	Three-dimensional calculation of fission power in the core
6		Bars	17416	
7	Part of a FC	Fluent	$\sim 10^6$	Calculation of fluid-dynamic forces acting upon fuel rods following FC break
8	FC Inlet Zone	Star-cd	$3.7 \cdot 10^5$	Calculation of pressure and velocity fields to assess the appearance of steam cavitation in control valve
9	Broken Single Channel and neighboring FC	Relap5	167/2810*	Calculation of break area and position and 'local' hydraulic parameters for primary system and confinement
10	Individual Pressure Tube and connected Graphite Stack	Ansys	4700	Stresses in pressure tube and in graphite stack consequent to the creep deformation of pressure tube
11	Fuel moderator and coolant	Helios	$14 \times 4 + 30 \times 4$ (zones)	To derive macroscopic cross section sets suitable for the use of three-dimensional neutron kinetics codes
12		MCNP	Not applicable	
13	Graphite stack as a whole	U_Stack	–	To address the MPTR issue by the deformation method

* Number of hydraulic nodes and number of mesh points for conduction heat transfer are distinguished.

Table 3. Realized nodalizations

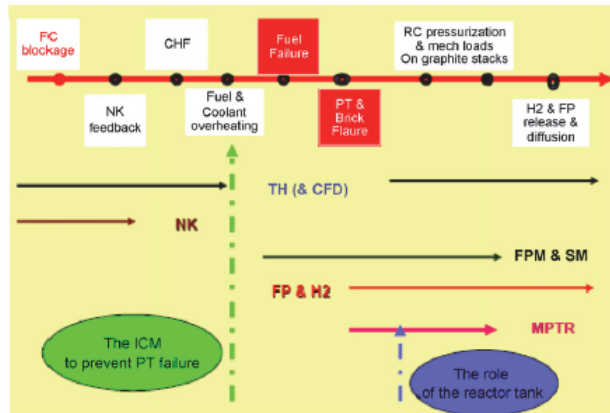
- study of the components and zones of the RBMK core region to make clear the concerned accident scenario,
- the characterization of the steady state operation of the reference RBMK boiling channel,
- the experience from the pressure tube (PT) rupture events in RBMK NPP,
- the phenomenological evolution of the transient.

An overview of the multidisciplinary problem associated with the blockage of one fuel channel scenario is given by the phenomenological aspects associated with the scenario originated by the blockage of one fuel channel in the RBMK NPP (i.e. FC-BLOCKAGE event). To this aim, phenomena are identified that characterize the progression of the event, the failure map for RBMK pressure tubes and the probable position for break elevation following FCBLOCKAGE.

The multidisciplinary nature and the demonstration of complexity for the concerned scenario is shortly highlighted in the figure 6 e table 4 and can be summarized in the following list:

- System Thermal-Hydraulics related to reactor coolant system
- Fuel pin mechanics to evaluate the fuel performance parameters including rod deformation following the FC-BLOCKAGE event in the RBMK fuel bundle.
- System Thermal-Hydraulics related to confinement
- Computational fluid dynamics to calculate the hydraulic loads acting upon the fuel rods following the rupture of the pressure tube occurring during the FC-BLOCKAGE event.
- Neutron kinetics for generation of average parameters for microscopic cross-sections as a functions of energy
- Neutron kinetics: 3D transient neutron flux to calculate the neutron kinetics parameters in the individual fuel channel and associated graphite stack following the FC-BLOCKAGE event.
- Structural mechanics to calculate stresses and strains in the pressure tube and in the graphite blocks following the rupture of the pressure tube occurring during the FC-BLOCKAGE event.

- Fission products generation to calculate the source term associated with the operation of a fuel channel of the RBMK, i.e. the amount of radioactivity that is released during the progression of the FC-BLOCKAGE event.
- Fission products transport to calculate the transport of the fission products generated as a consequence of the melting and the damage of a RBMK fuel bundle during the progression of the FC-BLOCKAGE event.



Nomenclature: CFD= Computational Fluid Dynamics, CHF = Critical Heat Flux, FC = Fuel Channel, FP = Fission Products, FPM = Fuel Pin Mechanics, ICM = Individual Channel Monitoring (see D’Auria et al. 2007e), MPTR = Multiple Pressure Tube Rupture, NK = Neutron Kinetics, PT = Pressure Tube, RC = Reactor Cavity, SM = Structural Mechanics, TH = Thermal-hydraulics.

Fig. 6. Scheme of the multidisciplinary approach

No.	Technological safety area		Codes	Notes
1	System Thermal-Hydraulics	Primary System	Relap5, Korsur	Also includes H2 generation and transport
2		Fuel	Frap, Rapta	
3		Confinement	Cocosys, Relap5	
4	Computational Fluid Dynamics		Fluent	The MPTR issue is addressed by the U.Stack code and by a procedure (given in chapter 6)
5		Structural Mechanics	Katran, Ansys (U.Stack) ^a	
6	Neutron Kinetics	Generation of average parameters (e.g., macroscopic cross-sections or 'λ-functions')	Njoy, Unk, Helios	
7		3D transient neutron flux	Bars, Nestle	
8	Fission Products	Generation	Refp, Melcor	
9		Transport	Cocosys, Melcor	

^a U.Stack code has capabilities to handle technological safety areas 1, 2, 3 and 5.

Table 4. Technical areas involved in the analysis

3.7 Results of the analysis

The scenario puts an enormous challenge to the codes: all key technological areas relevant to the deterministic reactor safety are involved. About 40 phenomena have been identified as characterizing the scenario and related computational tools have been evaluated.

However the possibility for the occurrence of the multiple pressure tube rupture (MPTR) was excluded.

4. Conclusions

The best estimate concept is defined as the efforts in avoiding conservative assumptions in performing analysis. It implies to adopt the best suitable tool available for each specific topic relevant for an analysis. In the case of an analysis related to a like NPP complex system it is necessary to “enlarge” the investigation in many technological areas. A direct consequence is constituted by the adoption of an integrated approach in performing safety analysis. A further relevant consequence is that the best estimate concept must be applied to a broad spectrum of disciplines.

This integrated best estimate approach for safety analysis means the availability of qualified tools and qualified users in many technical areas. The qualification has to be also applied to the coupling of the codes typically organized in a sort of “chain” including not only the code itself but also the input of the codes and the input and output data.

It is also relevant the availability of a suitable computational power necessary to perform the calculation with the different codes. The importance of this aspect is connected with the capability to include in the calculations all the details necessary to obtain a result to be considered as best estimate input for other linked codes.

The uncertainty is another relevant aspect. Best estimate application always requests uncertainty evaluation. The uncertainty evaluation is rather well developed for TH SYS code, but requires a focused and special effort in the case of all the other technical areas.

Summarizing, the best estimate concept applied in analysis for complex systems should be applied as an integrated approach in the meaning of application covering many technological areas and it requests a large effort in terms of technical competences, capability in qualified use of tools and user, and computational power.

5. References

- International Atomic Energy Agency (2008) *Best Estimate Safety Analysis for Nuclear Power Plants: Uncertainty Evaluation*, Safety Reports Series No. 52, IAEA ISBN 978-92-0-108907-6, Vienna
- International Atomic Energy Agency (1996) *Defense in Depth in Nuclear Safety*, INSAG-10, IAEA ISBN 92-0-102596-3, Vienna
- International Atomic Energy Agency (2000) *Safety of Nuclear Power Plants: Design*, Safety Standard Series No. NS-R-1, IAEA ISBN 92-0-101900-9, Vienna
- International Atomic Energy Agency (2002) *Accident Analysis for Nuclear Power Plants*, Safety Reports Series No. 23, IAEA ISBN 92-0-115602-2, Vienna
- NIKIET 1992 *Accident Analysis of rupture of fuel channel 52-16 at Leningrad NPP Unit 3* (in Russian). Internal Report 040-116-4101, Moscow (Ru)
- NIKIET, 1983. *Accident Analysis of 62-44 Fuel Channel Rupture at Chernobyl-1: Reasons and Consequences* (in Russian). Internal Report 040-103-1571d, Moscow (Ru).
- Wickett T. (Editor), D’Auria F., Glaeser H., Chojnacki E., Lage C. (Lead Authors), D. Sweet, A. Neil, G.M. Galassi, S. Belsito, M. Ingegneri, P. Gatta, T. Skorek, E. Hofer, M. Kloos, M. Ounsy and J.I. Sanchez 1998, *Report of the Uncertainty Method Study for Advanced Best Estimate Thermal-hydraulic Code Applications – Vols. I and II* OECD/CSNI Report NEA/CSNI R (97) 35, Paris (F)

LWR Safety Analysis and Licensing and Implications for Advanced Reactors

P. F. Frutuoso e Melo¹, I. M. S. Oliveira¹ and P. L. Saldanha²

¹COPPE/UFRJ – Programa de Engenharia Nuclear

²Associação Brasileira de Ensino Universitário, UNIABEU

²Comissão Nacional de Energia Nuclear, CNEN-CGRC
Brazil

1. Introduction

Most reactors under operation nowadays are light water reactors (LWR). The licensing and safety basis for them has been mainly deterministic. This approach has been under use since the beginning of commercial nuclear power in the 1950s. The purpose of this chapter is to discuss what this deterministic basis is, and how it has been used with emphasis on the US and German experience. This emphasis is because the first Brazilian reactor is of Westinghouse design, while the second one is of KWU (Kraftwerk Union)/Siemens/Areva design. Both designs are pressurized water reactors (PWR).

This chapter starts with the discussion of safety criteria, consideration of the defense in depth approach and deterministic criteria (safety margins), and the discussion of design basis accidents, including plant safety systems for meeting safety design criteria (IAEA, 2009a), Ahn et al (2010).

The approaches used thus far for safety analyses of LWRs have been essentially deterministic, where engineering judgment and conservatism have been used to face uncertainties. An example of this approach is the consideration of design basis accidents (such as large loss of coolant accidents - LOCA). They have been defined by arbitrarily combining initiating events with single failures (for example, loss of an injection pump), Kim et al (2010).

The inception of risk-informed decision making was in the 1970s, with the publication of the Reactor Safety Study NRC (1975), although it was initially named probabilistic risk assessment in the US. Since then, many improvements have been achieved but risk criteria have not as yet been established.

The risk-informed approach has been adopted by the US Nuclear Regulatory Commission (NRC) as an aid in the licensing and safety basis of US nuclear power plants. This means that the formal licensing process is to be approached by deterministic and probabilistic methods. The risk-informed approach may represent the formal presentation of a level 3 probabilistic safety assessment (PSA), so that plant risk curves are available. However, regulators do not as yet have risk criteria for this purpose, so that PSAs are recommended but their results are not compared to any criteria. Instead, there is a criterion concerning level 1 PSAs (in this case, the reactor core degradation frequency is estimated), and this is the central feature of risk-informed decision making nowadays, NRC (2002).

The risk-informed approach will be discussed in the light of US plants experience. Approaches in other countries will also be presented and the gained experience will be commented, Kadak & Matsuo (2007).

2. Basic definitions

Safety analysis is the study, examination and description of a nuclear installation expected behavior throughout its life, under normal and transient conditions, and also under postulated events, in order to determine: a) safety margins provided in normal operation and in transient regimes; b) the adequacy of items to prevent the consequences of accidents that may occur.

Safety assessment is the systematic and independent evaluation carried out by the regulator on the submitted safety analysis. It is used to support and subsidize the licensing decision on the plant acceptability, once the risk associated with its operation is known.

Inspection is the core activity performed by the regulator to verify compliance with its regulatory requirements or expressed in terms of licenses and permits and to implement them through coercive actions.

Regulatory inspection is the examination, observation, measuring, testing and verification of documentation executed by the regulator during any stage of the licensing process, to ensure compliance of materials, components, systems, structures, operational activities, processes, procedures and qualification of personnel with pre-established requirements or determined by the regulatory body.

Figure 1 displays the general Brazilian licensing process, where the definitions discussed herein play an important role.

The Preliminary Safety Analysis Report (PSAR) is one of the reports of the application for a building permit. It aims at demonstrating that the applicant is qualified to manage the construction application by providing design-related technical information to the regulator.

The Final Safety Analysis Report (FSAR) presents the final analysis and evaluation of plant design, as constructed, and the behavior of items in order to assess the risk to health and safety of the population as a whole, resulting from the installation and considering the information provided since the presentation of the PSAR.

A discussion on PSA meaning will be presented in Section 7 in the context of risk-informed decision making.

3. Defense in depth

The basic philosophy of nuclear power plant design has been described as defense in depth expressed in terms of three safety levels (NRC). These levels cover a variety of considerations that often intertwine, so that the allocation of certain aspects of the project to one level or another is somewhat arbitrary. However, these levels are useful to indicate the various stages in the safety design of a nuclear power plant. NRC defines each safety level through ordinances or rules. The basic purpose of reactor safety is to maintain the integrity of multiple barriers against the release of fission products. This integrity is supported by a defense in depth approach on three safety levels: a) prevention; b) protection; c) mitigation.

However, it has been more convenient to subdivide the second safety level (protection) into three new levels. Therefore, the implementation of the defense in depth concept is made through five levels whose objectives and essential means are displayed in Table 1, IAEA

(1996). The role of each safety level can be clearly seen in the table. One desirable effect of the defense in depth concept is that the plant that adopts it tends to be more resilient to failures.

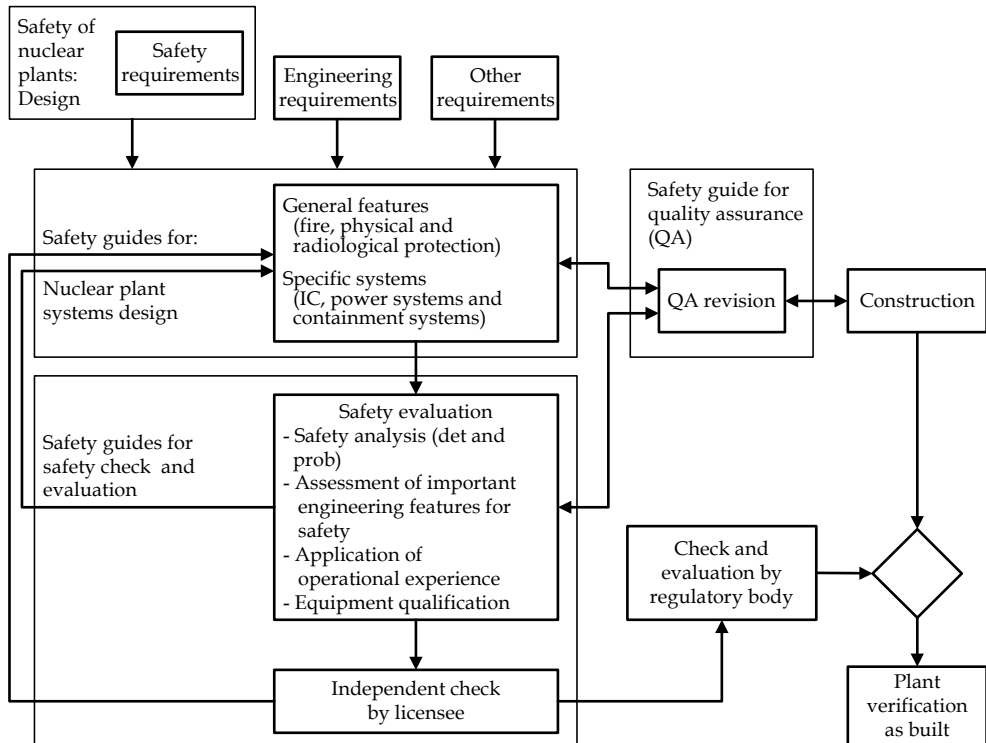


Fig. 1. General Brazilian licensing process

Level	Objective	Essential means
1	Prevention of abnormal operation and/or failures	Conservative design High quality in construction & operation
2	Control of abnormal operation and detection of failures (protection)	Control systems Limiting systems Protection systems
3	Accident control within design basis (protection)	Engineered safety features Accident procedures
4	Control of severe plant conditions (protection)	Complementary measures Accident management
5	Mitigation of radiological consequences of significant radioactive releases	Off-site emergency response

Table 1. Objectives and essential means of the defense in depth approach, IAEA (1996)

4. Accident analysis

The construction and operation of nuclear power plants requires the submission of a safety analysis report which must contain an analysis of a wide range of conceivable abnormal events. The purpose is to demonstrate that the project provides a means to control these events or otherwise accommodate their consequences without undue risk to health and safety of the public.

Analyzed conditions include: a) small transients that occur with moderate frequency and represent minor hazards; b) unlikely accident situations that can have serious consequences and therefore require different measures to protect the public.

Safety analysis is concerned with the potential effects of every conceivable (or anticipated) transient that may occur as a result of: a) operational malfunctions, e.g., human errors or small instrumentation or other equipment failures, or b) serious mechanical failures of different types.

Transients of moderate frequency can result from operational occurrences (or other), which create an imbalance between heat generation in the fuel and its removal: a) thermal power increase, caused by: a.1) decrease of coolant temperature; or a.2) removal of control material (burnable poisons); b) decrease in cooling efficiency.

As to low frequency events, there can be: a) small pipe ruptures; b) loss of flow accidents (LOFA); and c) design basis accidents (DBA).

Small pipe ruptures are more serious when they occur in an input line of the pressure vessel of a PWR primary system circuit. The reactor is shut down by the reactor protection system (RPS) but there is loss of water to the containment (vapor flashing also occurs). In general, for breaches of equivalent diameter smaller than 0.5", the chemical and volume control systems (CVCS) compensates for inventory losses of the reactor cooling system (RCS).

Should a loss of off-site and on-site power occur, all pumps eventually stop and the result is a loss of flow accident (LOFA). However, in 10s, in general, power will be available through emergency diesel generators. Meanwhile, the reactor is shut down when receiving a loss of flow signal, and steam is removed automatically from the turbine (steam dump). As there is some energy production during steam withdrawal, recirculation pumps typically remain connected to the main generator bus for about 10 seconds. Recirculation during pump shutdown and some natural circulation of coolant is usually sufficient to prevent the condition of critical heat flux after reactor trip.

Design basis accidents involve the postulated failure of one or more major systems and an analysis based on conservative assumptions (e.g., pessimistic estimates of fission product releases). It must be shown that the radiological consequences are within preset limits. These accidents serve as a basis for assessing the general acceptability of a particular reactor design. Design basis accidents are classified as Knief (1993): a) overcooling - heat removal increasing on the secondary side; b) subcooling - reduced heat removal on the secondary side; c) overfilling - increased inventory of reactor coolant; d) loss of flow - RCS (reactor coolant system) decreased flow; e) coolant loss - loss of reactor coolant inventory; f) Reactivity - reactivity and power distribution anomalies in reactor core; g) ATWS - anticipated transients without scram; h) Spent fuel and waste system - radioactivity release from spent fuel element or a subsystem or reactor component; i) external events - natural or man-made events that can affect plant operation and safety systems.

A major break in a steam line results in a reactivity insertion of cold water (overcooling) systems in several loop systems. This event causes liquid flashing in the secondary side of

steam generators. The secondary fluid cools by removing heat from the primary (overcooling), with important implications for the reactivity balance.

In accidents related to overcooling, or others that require rapid reduction in temperature in support of depressurization, the pressurized thermal shock (PTS) phenomenon is a concern of great importance. It is a boundary condition of reactor vessel integrity. It may occur during a system transient that primarily causes severe overcooling of the vessel wall inner surface and then results in high repressurization. If there is significant degradation due to radiation embrittlement and if there are defects of critical sizes in the vessel wall, this may fail. PTS is prevented by operating within boundary curves of temperature-pressure which are periodically revised to reflect the vessel current condition, particularly in terms of radiation embrittlement. This approach tends to lead to increasing restrictions on the operation window for plant heating (heatup) and cooling (cooldown) as the plant ages.

The anticipated transient without scram (ATWS) has two general characteristics: a) it starts through a transient whose occurrence is anticipated one or more times in reactor life; b) posterior reactor trip does not occur (that is, a failure occurs). This failure, especially a reactivity insertion (control rod removal) is solved by negative reactivity feedbacks that diminish the reactor power level, or at least diminish its growth. Adequate reliability of control rods and the reactor protection system are important to prevent such events.

A large rupture or leak in one or more steam generator (SG) tubes of a PWR results in a particular loss of coolant accident (LOCA) scenario because primary coolant passes directly to the secondary side. In addition to being radioactive, the coolant also represents an irretrievable loss of inventory in the containment building. The response to this accident includes isolation of damaged generators and rapid cooling and depressurization, to reduce the coolant loss, where care must be taken to avoid other accidents (e.g., PTS).

A loss of coolant accident (LOCA) occurs in general when there is loss of inventory in the primary system through a rupture of equivalent diameter larger than 0.5" (for ruptures with equivalent diameter less than 0.5", the chemical and volume control systems (CVCS) compensates for inventory losses. Three types of LOCA are typically considered: a) small LOCAs: for equivalent rupture diameters between 0.5" and 3"; b) medium LOCAs: for equivalent rupture diameters between 3" and 6"; c) large LOCAs; for equivalent rupture diameters between 6" up to the double-ended or guillotine break in a reactor coolant system (RCS) cold leg, being this rupture considered as one of the design basis accidents.

The events that occur within the first 2 min following a design basis LOCA in a PWR are: a) blowdown: in which the reactor coolant is expelled from reactor vessel; b) refill: when emergency cooling water begins to fill the reactor vessel starting from the core bottom; c) reflood: when the water level raises enough to cool all reactor core.

In general, the emergency core cooling system (ECCS), one of the engineered safety features, should be designed to fit the following criteria under a postulated design basis LOCA in a PWR: a) the calculated maximum cladding temperature after the accident should not exceed 2200 °F (1204 °C); b) the calculated total cladding oxidation due to interaction of zircaloy with hot steam should not exceed 17% of the total cladding thickness before oxidation; c) the total amount of H₂ generated shall not exceed 1% of the hypothetical amount generated if all cladding material around pellets reacted; d) calculated changes in geometry, e.g., diameter of fuel rods and spacing should be such that the core can still be cooled; e) the calculated core temperature, after successful ECCS starting, must be maintained appropriately low for the time necessary for the decay of long half-life fission products in reactor core. More details on LOCA analysis may be found in Glasstone & Sesonske (1994).

Companies that sell reactors must provide analysis tools through which one can establish that the proposed reactor is designed to meet the criteria for emergency core cooling. These tools are generally complex computer programs that use thermal hydraulic models for calculating fuel and cladding temperatures, and other relevant situations and reactor characteristics. These tools should include means for calculating: a) energy sources; b) hydraulic parameters; c) heat transfer mechanisms of various hypothetical accident stages.

Different calculation programs have been developed and are being refined in order to calculate characteristic parameters, such as: a) coolant flow rates; b) enthalpy; c) coolant, fuel, and cladding temperatures; d) system pressure, under steady state and transient conditions.

Central to the above calculations is the notion of nodalization. Real reactor circuits must be nodalized, that is, a set of nodal volumes and junctions are defined and inserted into calculation programs to perform the desired safety calculations. An example of these nodalization procedures may be found in Borges et al (2001) concerning Angra 2 power plant.

5. Severe accidents and accident management

Severe accidents are those which are characterized by at least an initial core damage, typically specified as the overcoming of regulatory fuel limits, as, for example, 1200°C in the fuel cladding, as discussed in Section 4.

The need for considering severe accidents became apparent upon the issuance of the Reactor Safety Study (which will be briefly discussed in Section 7), NRC (1975), where a probability per year of the order of 1 in 20,000 reactor-years was estimated for core melt. This value was apparently higher than the one implicitly estimated for the reactors operating at that time (Petrangeli, 2009). This calculated figure meant an expected core melt each 40 years, although the Reactor Safety Study itself estimated that only one in about 100 core melt events could cause severe health consequences (up to 10 causalities). It is noteworthy that the Three Mile Island event reinforced and confirmed the need initially arisen for progress in nuclear safety by considering possible events beyond design basis.

IAEA (2000a) defines a severe accident as a very low probability plant state beyond design basis accident condition (like those discussed in Section 4), which may arise due to multiple failures of safety systems leading to significant core degradation. These failures may jeopardize the integrity of many or all of the barriers to the release of radioactive material.

IAEA (2000a) also mentions that the consideration of severe accidents shall not be performed as design basis accidents are, that is, by assuming conservative assumptions. Rather, realistic or best estimate assumptions, methods and analytical criteria should be employed.

In this sense, important event sequences that may lead to severe accidents shall be identified using a combination of probabilistic and deterministic methods and engineering judgement. Next, these event sequences are to be reviewed against a set of criteria aimed at determining which severe accidents shall be addressed in safety analysis.

Accident management has arisen to cope with severe accidents. IAEA (2000b) establishes some requirements on severe accident management and accident management in the operation of nuclear power plants. According to this, plant staff shall receive instructions in the management of accidents beyond design basis.

Examples of event sequences for PWRs in this context have been considered in the Reactor Safety Study (NRC, 1975), as a large-break LOCA with loss of all ac power and a transient-induced accident. This latter is caused by an event that requires reactor trip combined with a station blackout, i.e, the loss of all power, as well as the loss of capability of the secondary system to remove heat from the primary circuit.

External events might also play an important role in severe accident management since they are an importance source of energy for the reactor (Knief, 1992).

IAEA (2009b) discusses severe accident management programs for nuclear power plants. D'Auria & Galassi (2010) discuss important features on scaling in nuclear reactors that might be relevant for severe accident management. As mentioned earlier, as best estimates are to be used in severe accident management rather than conservative estimates, uncertainty analysis plays a dominant role in this field. Na et al (2004) present an approach for the prediction of major transient scenarios for severe accidents in nuclear power plants by using artificial intelligence.

6. Licensing of nuclear power plants

6.1 Introduction

The licensing of nuclear power reactors is a formal activity that constitutes a permanent process of decision making, involving the issuance of licenses, permits, amendments or their cancellations, covering issues involving the safety of nuclear reactors, and the radiological protection of operators, the general population and the environment.

Decision making is performed based on the results of two complementary activities: a) safety assessment; and b) inspection.

The decision should consider whether there is sufficient assurance that the facility operation will not result in undue risk to: a) population, b) operators and c) the environment.

The licensing process of nuclear facilities is regulated by standard CNEN-NE-1.04 (CNEN, 1984), in force since 1984. The issuance of licenses or permits shall be preceded by the applicant request together with information, data, plans and reports, whose content is described in the standard.

6.2 Applicable standards

There are over 40 standards in force in CNEN (Brazilian Nuclear Energy Commission), and 20 apply to nuclear power reactors. In the absence of appropriate standardization, codes and guidelines of the International Atomic Energy Agency (IAEA), are preferably used, where necessary. Table 2 displays the most important nuclear standards concerning nuclear power reactors issued by CNEN. These standards may be found in cnen.gov.br.

6.3 The licensing process

The licensing process requires the issuance by CNEN of the following acts: a) Site Approval (AL); b) Construction License (LC); c) Authorization for Nuclear Material Use (AuMN); d) Authorization for Initial Operation; e) Authorization for Permanent Operation (AOP).

The various reports and programs per act required during the licensing process are presented below.

For site approval: a) Site Report; and b) Preliminary Program of Pre-Operational Monitoring.

Number	Title
NE-1.01	Reactor Operator Licensing
NE-1.04	Licensing of Nuclear Installations
NN-1.12	Qualification of Technical Independent Oversight Bodies in Nuclear Facilities
NE-1.14	Report of Nuclear Plants Operating
NN-1.15	Independent Technical Supervision in Quality Assurance Activities
NE-1.16	Quality Assurance for nuclear-power plants
NE-1.17	Personnel Qualification and Certification for Non-Destructive Testing Items in Nuclear Facilities
NE-1.22	Meteorological Programs in Support of nuclear-power plants
NE-1.26	Safety in Operation of nuclear-power plants
NE-2.01	Physical Protection of Nuclear Operating Units of Area
NN-2.03	Fire Protection in nuclear-power plants
NE-3.01	Basic Guidelines for Radiation Protection

Table 2. Typical CNEN standards for nuclear power reactors

For the Construction License (LC): a) Preliminary Safety Analysis Report (PSAR); b) Preliminary Plan of Physical Protection (PPPF); c) Quality Assurance Program (QAP); and d) Preliminary Plan for Personnel Training.

The following activities do not depend on a previous license: a) site excavation; b) infrastructure preparation; c) buildings not intended for safety-important items; and d) system components manufacturing.

Obligations during plant construction: a) report of deficiencies in the executive project, construction and pre-operational phase with impact on safety; b) progress report of activities; c) results of the programs of research and development (R & D) designed to solve safety problems; d) reports on equipment storage; e) audit programs on contractors; f) procedure for pre-operational tests, and g) submit to resident construction inspection.

Authorization for Initial Operation (AOI): a) Final Safety Analysis Report (FSAR); b) answers to LC constraints; c) authorization for nuclear material use; d) final plan for physical protection (FPF); e) radiation protection plan; f) fire protection plan; g) commissioning program; h) test procedures; i) Quality Assurance Program (PGQ); j) operating procedures manual; k) local emergency plan (PEL); l) operator team licensed by CNEN; m) civil responsibility insurance against damages; and n) submit to resident inspection.

Authorization for Permanent Operation (AOP): a) initial report of operations; b) commissioning report, and c) responses to AOI requirements.

During Operation: a) periodic reports; b) operational event reports; c) report to CNEN in Emergencies; d) shutdown planning; e) technical specification changing requests; f) technical modification requests; g) operator licenses reassessment; h) safety periodic review (each 10 years); i) response to CNEN requirements; j) submit to periodical inspections; and k) submit to resident inspection.

For safety review and assessment activities, four basic procedures are used: a) comparison with other facility used as a reference; b) verification of requirement, standard, and

specification adherence; c) design verification through independent calculations; and d) incorporation of requirements arising from international experience in nuclear technology. The verification of compliance requirements is made through a detailed examination of normative and support documents, identifying clearly the criteria that support the regulator assessment.

The analysis of the document or activity being evaluated is performed by comparing it with the regulator assessment criteria and/or previous requirements issued, following proper procedures for each type of task, such as: a) operational event; b) modification project; c) technical specification changes; d) Accident Analysis; e) periodical reports; and f) system and component design.

Next, a balance of deficiencies and nonconformities is performed.

The final product of the safety assessment is a technical advice. This document must contain the basis of judgement and conclude in a clear and concise way on the acceptability of the document or the activity under review. If there are deficiencies or nonconformities requirements for the implementation of corrective actions should be issued.

The objectives of independent calculations are: a) verify the completeness and adequacy of the analysis performed by the designer; and b) provide the regulator technical staff with experience and knowledge about phenomena and modeling techniques associated with the facility operation in normal or accident conditions.

Lessons learned through international operating experience and nuclear accidents are permanent sources of improvement of licensing requirements adopted by CNEN.

An inspection activity is made throughout all licensing phases, through testimonies, inspections and audits. Inspections may be reactive or routine. Reactive inspections (advised or not) are dependent on the project phase or on the occurrence of a significant event that requires verification. For reactors in permanent operation routine checks follow a regular program, which is established on an annual basis.

Regulatory Inspections are formal activities conducted by a team of inspectors which follows a previously prepared checklist, considering: a) inspection requirements (standards, license or permit terms, etc); b) examination of documents that regulate the inspected activity, such as: b.1) quality assurance program; b.2) operation manual; b.3) technical codes or standards; b.4) design specifications; b.5) FSAR applicable sections; b.6) checking of requirements not fulfilled in previous inspections.

During plant construction and operation phases, CNEN keeps a team of resident inspectors, which makes a plant daily monitoring and issues periodical audit reports. These reports describe inspection activities, identify non-compliances and formulate proper requirements for the licensed facility to deploy appropriate corrective actions, when necessary. Figure 2 display CNEN's inspection approach.

Tasks of power reactor licensing are performed through acts. These acts are related to the different steps during the licensing process: a) pre-licensing; b) site approval; c) construction issuance; d) during construction; e) AOP Issuance; f) operation monitoring. Acts related to pre-licensing involve: a) management contacts; b) verification of project objectives and preliminary schedules; and c) team meetings on licensing, quality systems and safety analysis.

Acts related to site approval involve: a) site report assessment (demographics, seismology, hydrology, meteorology, geography, and external events); b) emergency plan viability; and c) interaction with the environmental licensing (through the Brazilian environmental agency, IBAMA).

Acts related to construction issuance involve: a) PSAR examination and evaluation to check the safety concept acceptability of the plant design (design basis accidents, philosophy, design approach, experimental support, safety research, reference plant, standards adopted in the design and fabrication, program quality assurance and development of major providers, training program for human resources) ; and b) assessment of the pre-operational environmental monitoring program.

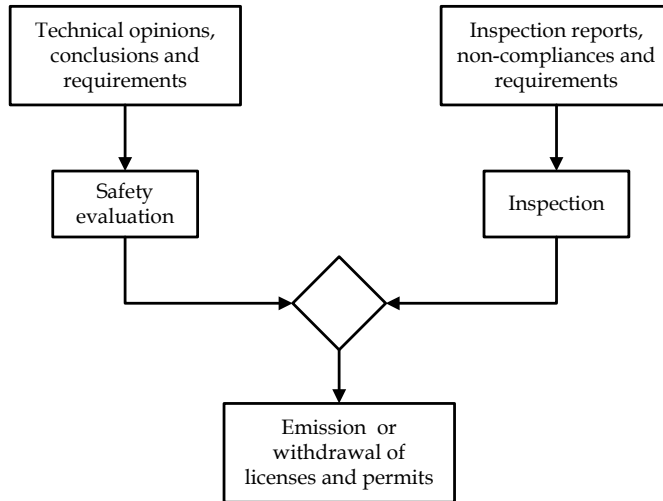


Fig. 2. Brazilian nuclear regulator (CNEN)'s inspection approach

Acts during construction: a) assessment of safety deficiencies identified during the execute design, construction, assembly or pre-operational tests, from non-conformities recorded in the context of the Quality Assurance Program, or from deviations from the criteria and design basis as stated in PSAR, or arising from significant damage during construction, assembly or testing; b) PSAR review to check whether the design final specification confirms safety analysis findings; c) implementation inspection of procedures established in QAP, facility compliance as constructed in relation to licensed design, test adequacy on structure and system integrity as well as functional tests of components and systems; d) monitoring of international experience, with emphasis on the reference installation, to identify any additional measures that need to be required to improve safety of the facility under construction.

Acts during AOP issuance: a) assessment of compliance with all LC and AOI conditions; b) assessment of compliance with all CNEN safety significant requirements in earlier stages; c) beginning of resident inspection; d) procedure analysis and witness of integrated tests including loading tests; e) initial criticality; f) low power physical tests and other tests; g) initial operation report (ROI) evaluation to determine the adequacy of commissioning program to demonstrate foundations of safety analysis; h) survey of international safety standard and licensing evolution since the last license or permit issued.

Acts related to operation monitoring: a) resident inspection to verify compliance with terms set out in the AOP, particularly in relation to technical specifications; b) safety assessment on requirement and restriction compliance expressed in AOP; c) conduction of periodic

inspection and audit program on activities that affect quality and are safety significant; d) assessment of operational safety by examining periodic operation reports, of consolidation of CNEN issued requirements and the examination of significant event reports; e) control and daily record of operational activities; f) assessment of technical change applications to be introduced in the licensed project or technical specifications changes; and g) monitoring of international operating nuclear reactors experience.

6.4 PSAR and FSAR

The minimum content of PSAR comprises: *a)* Description and safety analysis of the site for the facility; *b)* Facility description and analysis with special attention to design features and operation; *c)* Preliminary design of the facility, with emphasis on: *c.1)* the main criteria; *c.2)* the design bases and their relationship with the main criteria, and *c.3)* information related to building materials, arrangement and approximate dimensions; *d)* Preliminary analysis and evaluation of project performance and installation of items in order to assess the risk to health and safety of people (safety margins for normal operation and transient conditions and adequacy of the items designed for accident prevention); *e)* Description and justification of the choice of variables based on the analysis and preliminary assessment that will be subject to technical specifications, and *f)* description of control systems for release of effluents and radioactive waste.

FSAR must include information that: *a)* describes the facility; *b)* provides the basis for the project; *c)* defines the limits of operation, and *d)* allows a safety analysis of the installation as a whole.

FSAR should allow for *a)* perfect understanding of the system design; and *b)* clear display of the relationships between the system design and safety assessments.

FSAR should also contain information relating to plant operation, like: *a)* quality assurance; *b)* program of pre-operational tests and initial operation; *c)* program for the conduct of operation, including: *c.1)* maintenance; *c.2)* periodic tests of items, and *d)* proposed technical specifications (TS).

Table 3 displays the FSAR contents.

Chapter 17 of FSAR is the only one written in Portuguese for Brazilian power plants, because all FSAR chapters except this one are prepared by the vendor. The chapter on quality assurance is prepared by the licensee itself.

A chapter 19 on probabilistic safety assessment (to assess core melt frequency, the so called Level 1 PSA as will be discussed in Section 7) is to be added to FSAR for Brazilian power plants.

6.5 Licensing of Angra 1 nuclear plant

Angra 1 has had its license covered by CNEN NE 1.04 and has been based on the American model of the Nuclear Regulatory Commission (NRC).

The operation time of 40 years was used in the project and considered in the safety assessment review for issuance of the Provisional Authorization of Operation (APO) in 1984, and later in the Authorization for Initial Operation (AOI) in 1987, and Authorization for Permanent Operation (AOP) in 1994.

In AOP, the time of 40 years was considered as a basis for 1984 and a review of the authorization to ratify or amend its terms is scheduled every 10 years. This ensures a periodical safety assessment review, keeping the licensing bases of CNEN-NE-1.26 standard.

Chapter	Contents
01	Introduction and General Description
02	Site Characteristics
03	Design of Structures, Components, Equipments & Systems
04	Reactor
05	Reactor Coolant Systems and Connected Systems
06	Engineered Safety Features
07	Instrumentation and Control
08	Electric Power
09	Auxiliary Systems
10	Steam and Power Conversion System
11	Radioactive Waste Management
12	Radiation Protection
13	Conduct of Operations
14	Initial Test Program
15	Accident Analysis
16	Technical Specifications
17	Garantia de Qualidade (Quality Assurance)
18	Human Factors Engineering

Table 3. FSAR contents

General Design Criteria adopted are described in Appendix A of 10 CFR 50, and were the minimum requirements for Angra 1 main criteria. The establishment of a defined accident spectrum that has been postulated for the project, whose consequences could not exceed the maximum dose limits on the borders of the "exclusion area", according to 10 CFR 100, characterized the deterministic licensing model.

The exclusion area is defined as the area in which an individual located at any point on its edge for 2 hours immediately after the release of fission products, would not receive a whole body radiation dose greater than 25 rem or a total thyroid radiation dose greater than 300 rem due to iodine exposure (Lamarsh & Baratta, 2000).

The verification of requirements established pursuant to 10 CFR 50 was driven by regulatory guides that consolidate the positions adopted and accepted by NRC technical assessment teams. FSAR standard model, as provided in standard NE-1.04, was the Regulatory Guide RG 1.70, Standard Format and Content of Safety Analysis Report for NPPs (1978). NUREG 0800, Standard Review Plan for Review Safety Analysis Report for NPP, is employed by CNEN for safety assessment.

6.6 Licensing of Angra 2 nuclear plant

Just as Angra 1's, Angra 2's licensing is subject to standards CNEN-NN-1.04 and 1.26. There is a direct correspondence between the American and German licensing models. To maintain uniformity between both Angra 1 and Angra 2 licensing, the FSAR contents, as provided in standard CNEN-NE-1.04 (CNEN, 1984) is in accordance with RG-1.70 (NRC, 1978), as amended to incorporate the developments in NUREG 0800 (NRC, 1996).

As will be discussed in Sec. 6.7, a noteworthy feature of Angra 2 licensing is the inclusion of human factors.

The safety criteria document presents the German Interior Ministry requirements that can be understood as minimum criteria in relation to the plant main design criteria. Guidelines for PWR reactors have recommendations for different design, divided into 25 chapters and, where applicable, they take into account technical standards from others, like ASME.

6.7 Human factors and human reliability

A point worth mentioning is the incorporation into FSAR of the so called human factors engineering (Chapter 18). NUREG 0711 (NRC, 2004) has been adopted as a reference for the safety evaluations, taking into account the technological differences between Westinghouse and Siemens/KWU (AREVA) designs.

The human factors engineering approach to be presented in FSAR is composed by the following topics: a) Human factors engineering program management; b) Operating experience review; c) Functional Requirements Analysis and Function Allocations; d) Task Analysis; e) Personnel Qualification and Quantification; f) Human Reliability Analysis; g) Human - System Interface Design; h) Procedures Development; i) Development of the Training Programs; j) Human Factors Verification and Validation.

Figure 3 displays the NRC human factors engineering approach that has been adopted by CNEN.

6.8 Licensing in US

The Brazilian nuclear regulation was strongly influenced by the model used in the U.S., particularly with regard to stages of the licensing process. The basic law to regulate nuclear power is the Atomic Energy Act, 1954. In 1974, through the Energy Reorganization Act, an exclusive agency was created to regulate the use of nuclear energy, called the Nuclear Regulatory Commission (NRC).

The Code of Federal Regulations (CFR) is the collection of US technical documents. It has several titles, and Title 10 refers to energy. Titles are divided into parts. NRC's regulations are in Title 10 (Parts 0-199). Appendix A to 10 CFR 50 sets out general design criteria (GDC) for nuclear power plants, which set out requirements for the design, manufacture, construction, testing and performance of systems and structures, NRC (1999).

There are 45 GDCs, divided into six categories: 1 - General Requirements; 2 - Protection Against Multiple Barriers for Fission Product Release; 3 - System Protection and Reactivity Control; 4 - Systems Containing Fluids; 5 - Reactor Containment, and 6 - Control of Fuel and Radioactivity.

Appendix B of 10 CFR - Part 50 presents the program requirements for quality assurance. The FSAR contents are established in 10 CFR-Part 50.34 (Contents of Applications; Technical Information). NRC publishes documents called regulatory guides, which, although not mandatory (but strongly recommended), describe methods, standards and acceptable ways to meet the requirements of 10 CFR. These documents are broken down into 10 divisions, where division 1 concerns power reactors.

RG 1.70 (NRC, 1978) establishes the content and format for the FSAR. The Reg Guides mention standards and industry standards that NRC recognizes as safe engineering practices e.g., IEEE Std-323 for electrical and mechanical equipment qualification, IEEE (2004). Some codes and industry standards are considered mandatory and are explicitly

mentioned in paragraphs of 10 CFR - Part 50 (eg 10 CFR 50.55a - ASME Code for Pressure Vessels and boilers). See the NRC site (nrc.gov) for details on CFR

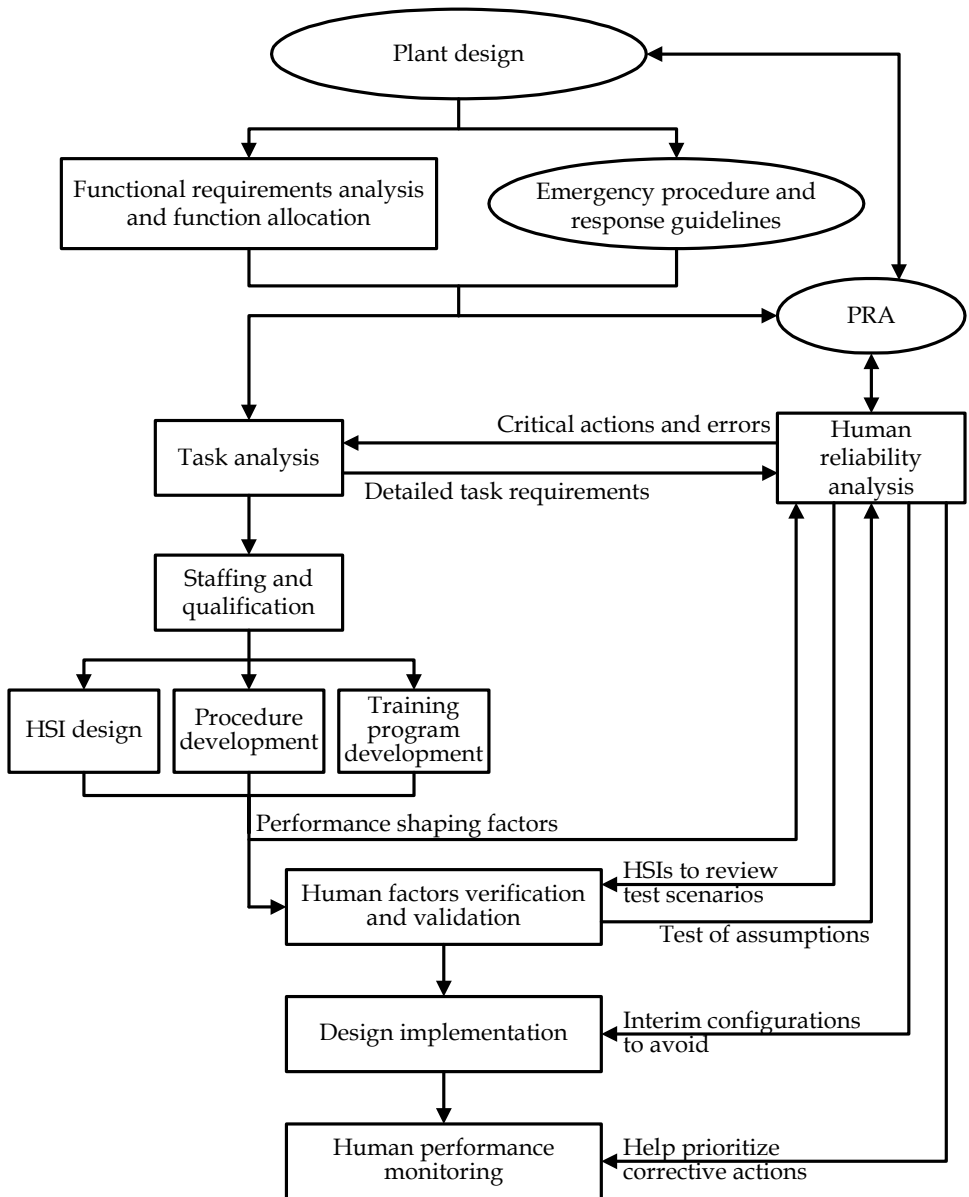


Fig. 3. NRC human factor engineering approach (NRC, 2004).

Industry standards are prepared by institutions which have began to produce special rules for application in the nuclear area, the main ones being: American Society for Mechanical Engineers (ASME), asme.org; Institute of Electrical and Electronics Engineers (IEEE), ieee.org; American Society for Testing Materials (ASTM), astm.org; Health Physics Society (HPS), hps.org; American Institute of Chemical Engineers (AIChE), aiche.org; Institute of Nuclear Materials Management (INMM), inmm.org.

Technical documents referred as NUREGs are used by NRC in its regulatory action. These reports are diverse in nature and support decision-making. They can result of technical studies, record of experience, training programs, etc. NUREG-0800, Standard Review Plan for Review of Safety Analysis Reports of Nuclear Power Plants is an example. It is used by NRC technical staff for guidance on the assessment of safety analysis reports. Figure 4 displays the general US licensing procedure.

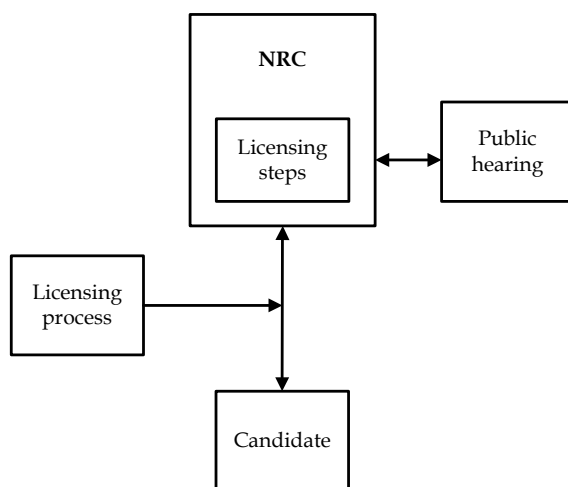


Fig. 4. Licensing in US

6.9 Licensing in Germany

The Atomic Energy Act (AtG in German) of 1960 provides the legal basis for the peaceful use of nuclear energy in Germany. By the German constitution, states (*Länder*) are responsible for implementing AtG on behalf of the German federal government. To ensure uniform application of AtG, the Federal Government oversees the states. Section 7 of ATG refers to nuclear installations and their licensing.

AtG provisions are supplemented by other laws and regulations of acts in the following areas: radiation protection; environmental impact; emissions control; and service water.

The various acts include the following areas: radiological protection; nuclear licensing procedures; financial insurance; cost of the atomic act; nuclear safety authority; and payment of disposal.

Safety requirements are of general characteristics, providing an environment for different technical solutions, but these solutions must have the same goal of protection. Licensing and supervision authorities have to examine whether this goal is achieved through a variety of safety regulations.

Safety regulations include: a) safety criteria for nuclear power plants, approved by the state committee for nuclear energy; b) BMI (former Ministry of Interior) and BMU (present-day Ministry of Interior and the Environment) guides for qualification of personnel for nuclear power plants; c) safety criteria for final storage; d) safety guidelines of the Committee on Reactor Safety; e) safety standards of the Nuclear Standards Committee; f) standards of the German Institute for Standardization.

The licensee applies for a license to build and operate the plant to the Licensing Authority of the state, preparing the safety report in accordance with the legislation requirements. The state licensing authority examines whether the prerequisites for ensuring the permit were met, assisted by the Organization of Independent Inspection. At the same time, BMU is involved in the process. BMU is assisted by a radiation protection committee. After project evaluation, this committee shall present its recommendations to BMU.

BMU evaluates the recommendations and submit its comments to licensing authorities, which are considered in the decision making process of the state authority. The state authorities, communities near the plant, other authorities and institutions whose areas of responsibility may be affected (nature protection, fire protection, disaster control, etc.) take part in the examination process.

Licensing authorities may request opinions from experts about nuclear safety and radiological protection requirements. However, experts only give technical support to the authorities, having no power of decision in licensing. A step in licensing are public hearings, which may contest the licensing authority, based on current legislation, and consequently taking action to an administrative court.

7. Risk-informed decision making

PSA is a methodology that can be applied to provide a structured analysis process to evaluate the frequency and consequences of accidents scenarios in nuclear power plants. NRC first applied PSA in the Reactor Safety Study (NRC, 1975). An important initiative taken by NRC in 1988 was the issuance of Generic Letter GL-88-20, which originated the program known as IPE (Individual Plant Examination). This is because the Reactor Safety Study did not consider each plant individually in the risk assessment.

Since that time, NRC has been using risk assessment and directing the issuance of decisions on complex items associated with or related to safety such as: a) total loss of power (station blackout); b) anticipated transients without reactor shutdown (ATWS); c) pressurized thermal shock events (PTS); and e) Maintenance Rule.

NRC issued the Probabilistic Safety Assessment Policy Statement (NRC, 1995), which incorporated risk assessment as a tool in the regulatory process. It consists of elements that have originated the Risk-informed Decision Making (RIDM) and the Performance Based Regulation (PB).

The following PSA-based RIDM regulatory guides were issued: a) changes in the bases of the specific plant licensing, RG-1.174 (NRC, 2002) ; b) assessment of changes and implementation of technical specifications, RG-1.177 (NRC, 1998c); c) in-service inspections in pipes, RG-1.175 (NRC, 1998a); d) quality assurance, RG 1.176 (NRC, 1998b); e) an approach to determine the technical quality of APS results for RIDM, RG 1.200 (NRC, 2002). Many of the current regulations, based on deterministic requirements, can not be quickly replaced. In January 2001, Paragraph 69 of the 10 CFR 50 (see nrc.gov), which regulates RIDM, was issued.

'Risk insights' is used to refer to the results and decisions that are made after probabilistic safety assessments are performed. It is necessary to distinguish three approaches or treatments in the decision making process: a) Risk Based (RB); b) Risk Informed (RI); and c) Performance Based (PB).

The risk-based approach to decision making is the one where only the numerical results of a probabilistic safety assessment are taken into consideration. This causes a strong dependence on the results of risk assessment, due to uncertainties associated with PSA (such as completeness and use of data). NRC does not endorse the risk-based approach, however does not invalidate the use of probabilistic calculations to demonstrate compliance with some criteria.

The risk-informed approach to the process of regulatory decision-making represents a philosophy according to which the outcomes and decisions arising from risk assessment are considered along with other factors to establish requirements that will best target on issues related to the design and operation that impact safety and health of the public.

The RI approach extends and improves the deterministic treatment because it: a) allows explicit consideration of a wide range of changes for safety; b) provides rationale for prioritizing these changes based on risk, operational experience and/or engineering judgment; c) facilitates the consideration of a broad range of resources to support these changes; d) identifies and describes uncertainty sources in the analysis; and e) leads to proper decision making, providing a mechanism to test the results' sensitivity to a set of assumptions.

Where appropriate, a regulatory approach with information on risk can be used to reduce unnecessary conservatism in deterministic treatment, or can be used to identify areas with insufficient conservatism in deterministic analysis and provide the foundation and additional requirements or regulatory actions.

The RI approach lies between the risk-based approach and the purely deterministic treatment. The details of the regulatory approach to be used will determine where the RI-based decision will fall in this spectrum. The concept of defense in depth remains the principle of regulatory practice. The findings and decisions arising from risk assessment can make the elements of defense in depth clearer due to the PSA quantitative approach.

Rules can be either prescriptive or performance based (PB). Prescriptive requirements specify particular aspects, activities or program elements to be included in the project or process, as a means of achieving the desired goal. A performance-based requirement depends on results (measured or calculated, i.e., performance data) to be found. It provides greater flexibility to the licensee to achieve these results.

RIDM philosophy is the reconciliation of the results of PSA insights with the traditional deterministic analysis. Often, PSA results conflict with deterministic insights (defense in depth and safety margin, for example). It is noteworthy that the use of RIDM by the licensee is voluntary.

As a result of policy implementation methodologies for the use of risk information, NRC expected the regulatory process would improve in three aspects: a) by PSA incorporation into regulatory decisions; b) preserving agency's resources; and c) reducing unnecessary effort on licensing.

RIDM follows principles for implementation and evaluation of changes proposed by the licensee, and to evaluate these changes a series of assumptions is adopted by the regulator. It is expected that the proposed changes meet the set of principles described below. PSA techniques can be used to ensure and show compliance with these principles, which are displayed in Table 4.

Principle	Description
1	Change meets the existing law and is explicitly related to the requested exception or rule change
2	The proposed change is consistent with the philosophy of defense in depth
3	The proposed change has sufficient margins
4	When the proposed change results in an increased frequency of core damage and/or risk, this increase should be small and consistent with the regulations laid down in (51FR30028, 4/8/86)
5	The impact of the proposed change should be monitored using performance measures

Table 4. Principles to be followed by RIDM

The evaluation of proposals and licensing acceptance guides adopt these same five principles, according to the eight assumptions detailed next.

Assumption # 1: All safety impact of the proposed change has been assessed in an integrated manner as part of the general approach of risk management, in which the licensee uses risk analysis to improve operational and engineering decisions in the identification of actions to reduce risks, and not to justify the elimination of licensing requirements perceived as undesirable. For those cases where risk increases are proposed, the benefits should be consistent with the increased risk proposal. The approach used to identify changes in requirements must also be used to identify areas where the requirements should be increased or reduced.

Assumption # 2: The content (scope and quality) of engineering analysis (deterministic and probabilistic) performed to conduct and justify the proposed changes have been appropriate to the change nature and scope and should be based on the plant as built and operated, reflecting its operational experience.

Assumption # 3: The plant-specific PSA that supports all licensee proposals has been subject to quality control and an independent evaluation or certification.

Assumption # 4: Consideration of appropriate uncertainties has been provided and decision interpretations supplied, using a monitoring, feedback and corrective actions program to consider significant uncertainties.

Assumption # 5: The use of core damage frequency (CDF) and large early release frequency (LERF) as a basis for PSA acceptance is an acceptable approach to Principle 4.

Assumption # 6: Variations in estimates of CDF and LERF arising from proposed changes to licensing bases will be limited to small increments. Cumulative effects of these changes will be monitored and considered in decision making.

Assumption # 7: Proposal acceptance will be evaluated by licensee in order to ensure that all principles are met.

Assumption # 8: Data, methods and evaluation criteria used to support regulatory decisions should be documented and available for public scrutiny.

Figure 5 displays NRC approach for RIDM.

Regulatory Guide 1.174 (NRC, 2002) describes the approach accepted by NRC to assess the nature and impact of licensing basis conditions (LBC) by considering engineering aspects and application of risk insights.

Regulatory Guide 1.200 describes the approach accepted by NRC to determine that PSA quality, in part or in whole is sufficient to assure its results so that they can be used in

regulatory decision making. Figure 6 illustrate the role of the above discussed regulatory guides.

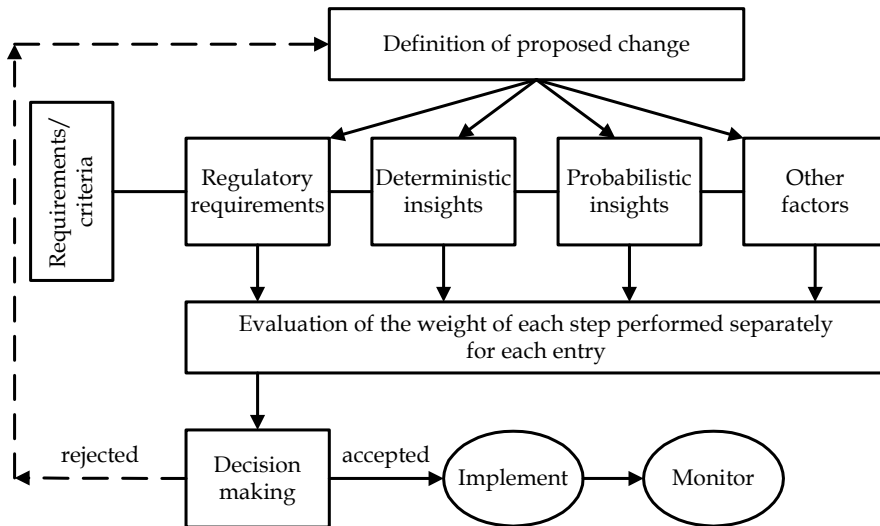


Fig. 5. NRC approach for RIDM (NRC, 2002)

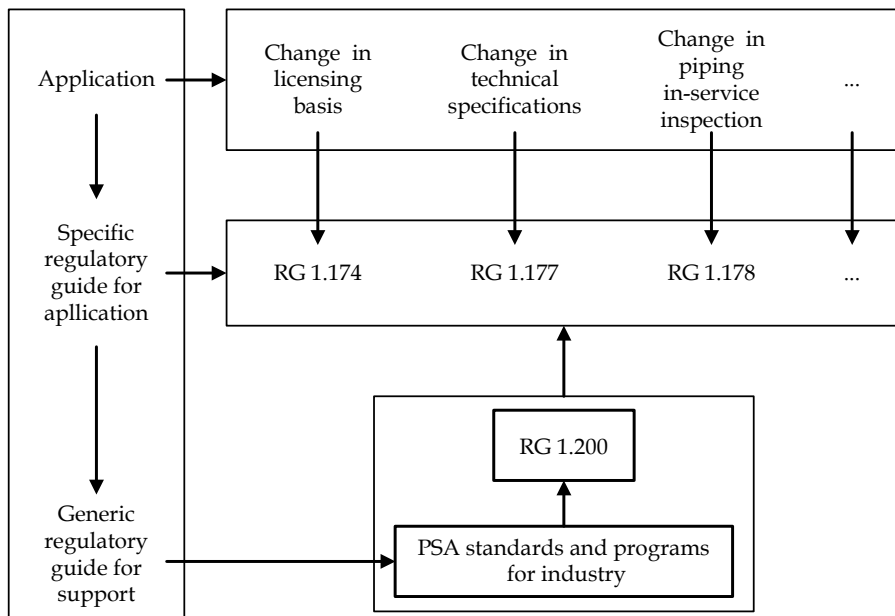


Fig. 6. Role of NRC regulatory guides in RIDM.

In what concerns PSA role in decision making, the key is to provide an assessment of change impacts on risk. It has been necessary to develop a quantitative criterion to serve as a guideline and meet NRC principles. These guidelines have been created to allow comparisons of risk variation evaluations (including internal and external events, full load, low load and shutdown). This criterion uses the core damage frequency obtained from a Level 1 PSA and also the Large Early Release Frequency and is presented in Figure 7.

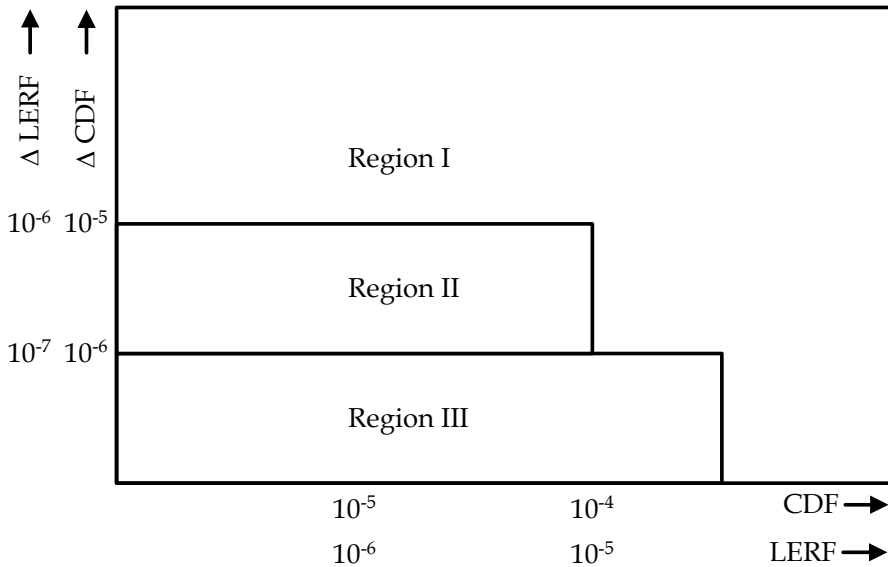


Fig. 7. Criteria for the results of a Level 1 PSA (NRC, 2000)

Kadak & Matsuo (2007) present a discussion about US experience on RIDM usage, where 35 nuclear plants have effectively implemented RIDM. By comparing INPO performance indices with NRC indices for these 35 plants with those of another 19 plants that have not implemented RIDM it is clearly seen that RIDM implementation has significantly improved performance indices. The performance indicators considered in the analysis were: a) Unit capacity factor; b) Automatic unplanned shutdowns (7,000 hr of criticality); c) Safety systems performance; d) Safety injection system actuation; e) Auxiliary feedwater system actuation; f) Power system actuation; g) Fuel element reliability; h) Collective radiation exposure; and i) Water chemistry performance.

Table 5 summarizes RIDM status in different European countries (NRC, 2001).

8. Final considerations

It is noted that licensing is characterized by decision making in various fields and disciplines and its steps can influence the course of evolution of the enterprise. The relationship between the licensing agency and applicants for licenses and permits must be honest, keeping the formalism and the independence of the institutions themselves that are recognized with distinct responsibilities. Controversial topics should be discussed openly

and the decision making process formalized in writing (technical advice, inspection reports and minutes of meetings).

The demonstration that the facility presents no undue risk to the public and the environment may require engineering activities, analytical or experimental, that may significantly affect the initial schedules and preliminary costs estimates. Design features significantly innovative or new reactor concepts require extensive research and testing of prototypes at all levels, such as components, systems, and small-scale facilities.

Country	Status
Spain	Recommends PSA use to define changes in requirements
France	The methodology Optimisation de la Maintenance par la Fiabilité (OMF - Maintenance Optimization for Reliability) has been developed to apply criteria for use of risk information for the optimization of plant maintenance including in-service inspection
Sweden	An update of rules considers in-service inspection use with risk information through qualitative and quantitative approaches
Finland	Expects to rationalize in-service inspection by a combination of deterministic and probabilistic methods under regulator initiative.
UK	Proposals for adoption of methodologies that use risk information in nuclear power plant management represent an evolution.
Switzerland	Expects to produce guidelines for implementation of a risk-informed in-service inspection quantitative method within a few years.
Czech Republic	Believes it is too complicated to introduce a risk-informed approach for in-service inspection, yet its interest on the matter is significant.

Table 5. RIDM efforts in some countries (NRC, 2000)

The physical and mathematical models used in engineering projects are validated by experimental data or calculations. Realistic models of best estimate are preferable to conservative models, but their use requires an adequate treatment of the uncertainties involved, determined from extensively developed databases.

The identification of areas of specialty where the technical staff of the regulatory body lacks experience must occur in a timely manner to enable this qualification or the necessary arrangements to hire consultants or consulting teams.

The timing of any nuclear development should provide the time intervals prior to the granting of licenses and permits for the analysis and evaluation of the regulatory body.

The licensing model in Brazil, in the aspects of safety analysis is deterministic in nature, that is, the plant behavior, after assuming an initiating event or malfunction, is studied with calculation models that describe the physical process of systems reactor.

The objective of this type of analysis is to check whether the allowed values of key plant variables are exceeded. The probabilistic safety analysis (PSA) focuses on the identification of sequences of events that can lead to meltdown of the reactor, and studies of reliability of safety systems. The objective of this analysis is to indicate potential weaknesses in the design of systems and provide the basis for improving safety.

CNEN has introduced in Standard NE-1.26 (CNEN, 1997) the requirement for risk management, where the operating organization should develop, implement and continuously refine a model for managing the risk associated with various operational configurations. Thus, a probabilistic safety analysis complements the deterministic safety analysis, and it is incorporated into the licensing procedure, because during plant operation, the impact on total risk measured by the model for risk management should be considered. This encompasses decision making involving activities like: a) design modifications and specifications changes or exceptions; b) system configuration management; c) maintenance and testing planning; and d) analysis of operational events.

The responsibility for nuclear safety in all phases of the enterprise belongs to the licensed organization. The licensing activity decides whether the licensee has the technical and organizational competence to fulfill this responsibility.

A very important point in this context concerns the licensing of advanced reactors, like the AP-1000. The risk-informed approach has brought into light the conciliation of deterministic and probabilistic methods for safety analysis. Accident scenarios both in the design basis and also beyond the design basis are being approached much more precisely and many advances in safety philosophy are proving to be effective in this way.

9. References

- Ahn, S. K.; Kim, I. S. & Oh, K. M. (2010). Deterministic and risk-informed approaches for safety analysis of advanced reactors: Part I, Deterministic approaches. *Reliability Engineering and System Safety*, pp. 451-458
- Borges, R. C.; D'Auria, F. & Alvim, A. C. (2001). Independent qualification of the CIAU tool based on the uncertainty estimate in the prediction of the LOBI test A1-93. *Kerntechnik*, Vol. 66, no. 4, (August 2001), pp. 161-170
- CNEN (1984). *Licensing of Nuclear Installations*, Standard CNEN-NN-1.04, National Nuclear Energy Commission, Rio de Janeiro, RJ, Brazil
- CNEN (1997). *Safety in Operation of Nuclear Power Plants*, Standard CNEN-NN-1.26, National Nuclear Energy Commission, Rio de Janeiro, RJ, Brazil
- D'Auria, F. & Galassi, G. M (2010). Scaling in Nuclear Reactor System Thermal-hydraulics. *Nuclear Engineering and Design*, Vol. 240, pp. 3267-3293
- Glasstone, S. & Sesonske, A. (1994). *Nuclear Reactor Engineering, Reactor Systems Engineering*, Vol. 2, Chapman & Hall, New York
- IAEA (1996). *Defense in Depth in Nuclear Safety, a Report by the International Nuclear Safety Advisory Group*. INSAG-10. International Atomic Energy Agency, Vienna, Austria.
- IAEA (2000a). *Safety of Nuclear Power Plants: Design*. IAEA Safety Standard Series No. NS-R-1, International Atomic Energy Agency, Vienna, Austria
- IAEA (2000b). *Safety of Nuclear Power Plants: Operation*. IAEA Safety Standard Series No. NS-R-2, International Atomic Energy Agency, Vienna, Austria
- IAEA (2009a). *Deterministic Safety Analysis for Nuclear Power Plants*. IAEA Safety Standards, Specific Safety Guide No. SSG-2, International Atomic Energy Agency, Vienna, Austria

- IAEA (2009b). *Severe Accident Management Programmes for Nuclear Power Plants*. IAEA Safety Guide Series No. NS-G-2.15, International Atomic Energy Agency, Vienna, Austria
- IEEE (2003) *Qualifying Class 1E Equipment for Nuclear Power Generating Stations*. IEEE Std-323. Institute of Electrical and Electronics Engineers, Piscataway, NJ, USA
- Kadak, A. C & Matsuo, T. (2007). The Nuclear Industry's Transition to Risk-informed Regulation and Operation in the United States. *Reliability Engineering and System Safety*, Vol. 92, pp. 609-618
- Kim, I. S.; Ahn, S. K. & Oh, K. M. (2010). Deterministic and Risk-informed Approaches for Safety Analysis of Advanced Reactors: Part II, Risk-informed Approaches. *Reliability Engineering and System Safety*, Vol. 95, pp. 459-468
- Knief, R. A. (1993). *Nuclear Engineering, Theory and Technology of Commercial Nuclear Power*, Taylor & Francis, Washington, DC, USA
- Lamarsh, J. & Baratta, A. (2000). *Introduction to Nuclear Engineering*, Prentice Hall, Upper Saddle River, NJ, USA
- Na, M. G.; Shin, S. H.; Lee, S. M.; Jung, D. W.; Kim, S. P.; Jeong, J. H. & Lee, B. C. (2004). Prediction of Major Transient Scenarios for Severe Accidents of Nuclear Power Plants. *IEEE Transactions on Nuclear Science*, Vol. 51, no. 2 (April 2004), pp. 313-321
- NRC (1975). *Reactor Safety Study – An Assessment of Accident Risks in US Commercial Nuclear Power Plants*. WASH-1400, NUREG-75/014, Nuclear Regulatory Commission, Washington, DC, USA
- NRC (1978). *Standard Format and Content of Safety Analysis Reports for Nuclear Power Plants*. RG-1.70, Nuclear Regulatory Commission, Washington, DC, USA
- NRC (1995). Use of Probabilistic Risk Assessment Methods in Nuclear Regulatory Activities, Final Policy Statement. Federal Regulation-60FR 42622, Nuclear Regulatory Commission, Washington, DC, USA
- NRC (1996). *Standard Review Plan for the Review of Safety Analysis Reports for Nuclear Power Plants*, LWR Edition. NUREG-0800, Nuclear Regulatory Commission, Washington, DC, USA.
- NRC (1998a). *An Approach for Plant-Specific, Risk-Informed Decision Making: Inservice Testing Assurance*. RG-1.175, Nuclear Regulatory Commission, Washington, DC, USA
- NRC (1998b). *An Approach for Plant-Specific, Risk-Informed Decision Making: Graded Quality Assurance*. RG-1.176, Nuclear Regulatory Commission, Washington, DC, USA
- NRC (1998c). *An Approach for Plant-Specific, Risk-Informed Decision Making: Technical Specifications*. RG-1.177, Nuclear Regulatory Commission, Washington, DC, USA
- NRC (1999). General Design Criteria for Nuclear Power Plants. Appendix A of 10 CFR 50. Nuclear Regulatory Commission, Washington, DC, USA
- NRC (2001). *Technical Committee Meeting on Risk Informed Decision Making (RIDM)*. Nuclear Regulatory Commission, Washington, DC, USA
- NRC (2002). *An Approach for Using PRA in Risk-Informed Decisions on Plant-Specific Changes to the Licensing Basis*. RG-1.174, Nuclear Regulatory Commission, Washington, DC, USA
- NRC (2004). *Human Factors Engineering Review Program*. NUREG-0711, Nuclear Regulatory Commission, Washington, DC, USA

- NRC (2007). *An Approach for Determining the Technical Adequacy of Probabilistic Risk Assessment Results for Risk-Informed Activities*. RG-1.200, Nuclear Regulatory Commission, Washington, DC, USA
- Petrangeli, G. (2006). *Nuclear Safety*. Butterworth-Heinemann/Elsevier, Amsterdam, The Netherlands

Geodetic Terrestrial Observations for the Determination of the Stability in the Krško Nuclear Power Plant Region

S. Savšek, T. Ambrožič and D. Kogoj
*University of Ljubljana, Faculty of Civil and Geodetic Engineering
Slovenia*

1. Introduction

The first research of the stability in the Krško plain was carried out in the period 1964–1969, when the area was chosen as the potential location for a nuclear power plant. The foundation stone for the Krško Nuclear Power Plant (NEK) was laid on December 1, 1974. In January 1984 NEK acquired the full operation permit. NEK has been in commercial operation for more than 20 years. Regarding the standards of nuclear safety and stability, NEK is today in the top 25% of operational nuclear power plants in the world. The Krško Nuclear Power Plant is of strategic importance for the Republic of Slovenia, producing electricity for users in Slovenia and Croatia. High level of security is of high importance; therefore, a comprehensive supervision of structures is carried out. A special attention is paid to the security systems, including the measurements of vertical displacements of benchmarks and measurements of horizontal displacements of the dam on the Sava River. Periodic geodetic observations are carried out on important technological structures comprising the nuclear island, the Sava River dam and the nuclear waste storage.

Since local stability of the Krško nuclear power plant is very important, several research works were conducted to test the stability of the Krško region. Based on the Project of permanent observations of tectonic movements in the surroundings of the Nuclear Power Plant Krško and geological researches of crustal movements along the Orlica fault in Krško region the micro network Libna was established. The intention of the network was to determine the horizontal crustal movements along the Orlica fault. The points of the net were stabilized in 1998, when also the zero measurement was realised.

Several epochs of measurements in both micro networks Krško and Libna were made. After a careful analysis and quality estimation of single epochs, the displacements were estimated and the accuracy of estimating the two-epoch displacements was calculated. We proposed original method, where simulations of an actual probability distribution function are determined, providing the basis for calculating the right critical value at a chosen significance level. In this way, statistically significant point displacements can be determined far more accurately. When assessing point displacements, the information on the actual risk of making an error when rejecting the true null hypothesis is very useful and the calculation of this value is advisable. Based on the assumption that the distribution function is established in detail, the suggested test statistic is simple and fits for day-to-day use as well as refers to the first estimation of the geodetic network.

2. Determination of point displacements in the geodetic network

2.1 Single epoch processing

For the identification of point displacement by geodetic observations, the reference points need to be chosen. Characteristic points on the object are tested for displacements. According to the required accuracy of point displacement determination, the observations must be carried out carefully with proper tools while following standard observational rules. The observations in the geodetic network are adjusted and the network quality estimated.

Importantly, in networks for displacement identification network quality estimation is carried out prior to the measurements examining the accuracy, reliability and sensitivity of setting up a network. More details about network quality estimation can be found in Caspary (2000). For the identification of displacements, network reliability and sensitivity are of primary importance. Thus, great effort must be made in detecting the presence of undisclosed gross errors. In the planning and optimization phase, the sensitivity of observations needs to be enabled, thereby increasing the probability of detecting outliers.

2.1.1 Free network adjustment

In deformation analysis single epochs are usually adjusted as free networks. In this way the best linear unbiased estimation of the unknowns and independence of test statistic regarding the chosen network datum is enabled.

Observations of each epoch measurement individually have to be adjusted as free network with minimum trace of the matrix of coordinate point correction factors, as it is valid for other procedures of deformation analysis. This means that not only the sum of the squares of the weighted residuals $\mathbf{v}_i^T \mathbf{P}_i \mathbf{v}_i = \min.$ has to be minimal, but also the sum of the squares of unknowns $\hat{\mathbf{x}}_i^T \hat{\mathbf{x}}_i = \min..$ Index i defines the epoch measurement. Previous epoch measurement is carried out in time t_1 , and the current in time t_2 . Of course, the orientation unknowns have to be removed by reducing the unknowns in the observation equations. Also any possible unknown due to the factor of network scale has to be reduced (Van Mierlo, 1978). If the number of network points in epoch measurement t_1 differs from those in epoch measurement t_2 , the coordinate unknowns of non-identical points are eliminated by the S-transformation (Van Mierlo, 1978).

2.1.2 Detection and elimination of outliers

A well projected network for displacement detection should enable a high degree of detection and elimination of gross errors in observations as well as minimize the effect of potentially undetected outliers influencing the unknowns. Testing the relation between the a posteriori variance $\hat{\sigma}_0^2$ and the a priori reference variance σ_0^2 is called the *global model hypothesis testing*. At the same time, the presence of gross error observations in the network is tested, which is in turn possible only by having a reliable knowledge of the a priori reference variance. In case of incongruence between the observations and the model in the course of the global testing, the Baarda's Data Snooping method for examination, detection and elimination of outliers in observations is introduced. The Pope's Data Screening approach or the Danish approach is used when the a priori reference variance is not reliably known.

2.1.3 S-transformation

In the deformation analysis based on geodetic measurements conducted in different epoch moments the occurring point displacements and deformations of the physical surface of the earth are detected and defined using methods of statistical analysis. Of course, the point displacements can only be detected and defined at identical points. If not all points in the epoch measurements are identical, the non-identical points shall be eliminated. This can be done by the S-transformation of an individual epoch measurement into the datum of identical points. The S-transformation can also be used if the transformation of the results of adjustment from one datum to another is required.

In order to transform the vector of unknowns and the cofactor matrix from datum A to a newly selected datum B, the vector of unknowns and the cofactor matrix are calculated using the following equations (without derivation; for derivation see Caspary, 2000, Mierlo, 1978):

$$\hat{\mathbf{x}}_B = \mathbf{S}_B \hat{\mathbf{x}}_A \quad (1)$$

$$\mathbf{Q}_{\hat{\mathbf{x}}\hat{\mathbf{x}}_B} = \mathbf{S}_B \mathbf{Q}_{\hat{\mathbf{x}}\hat{\mathbf{x}}_A} \mathbf{S}_B^T, \quad (2)$$

where:

$\hat{\mathbf{x}}_A$, $\mathbf{Q}_{\hat{\mathbf{x}}\hat{\mathbf{x}}_A}$ are the vector of unknowns and the cofactor matrix in datum A,

$\hat{\mathbf{x}}_B$, $\mathbf{Q}_{\hat{\mathbf{x}}\hat{\mathbf{x}}_B}$ are the vector of unknowns and the cofactor matrix in datum B,

$\mathbf{S}_B = (\mathbf{N} + \mathbf{G}_B^T \mathbf{G}_B)^{-1} \mathbf{N}$ is the S-transformation matrix, with the weakness that the inverse matrix $(\mathbf{N} + \mathbf{G}_B^T \mathbf{G}_B)^{-1}$ of the order $u \times u$ has to be calculated, which is why it is more appropriate to use the form $\mathbf{S}_B = \mathbf{E} - \mathbf{B}^T (\mathbf{G}_B \mathbf{B}^T)^{-1} \mathbf{G}_B$, where only the inverse matrix of the order $d \times d$ has to be calculated, which is a significant advantage,

$\mathbf{N} = \mathbf{N} \mathbf{Q}_{\hat{\mathbf{x}}\hat{\mathbf{x}}_B} \mathbf{N}$ is the matrix of normal equations,

$$\mathbf{G}_B = \mathbf{B} \mathbf{E}_B, \quad (3)$$

$$\mathbf{B}_{(2D)} = \begin{bmatrix} \hat{x}_1 & \hat{y}_1 & \hat{x}_2 & \hat{y}_2 & \dots & \hat{x}_m & \hat{y}_m \\ 1/\sqrt{m} & 0 & 1/\sqrt{m} & 0 & \dots & 1/\sqrt{m} & 0 \\ 0 & 1/\sqrt{m} & 0 & 1/\sqrt{m} & \dots & 0 & 1/\sqrt{m} \\ -\eta_1 & \xi_1 & -\eta_2 & \xi_2 & \dots & -\eta_m & \xi_m \\ \xi_1 & \eta_1 & \xi_2 & \eta_2 & \dots & \xi_m & \eta_m \end{bmatrix} \quad (4)$$

$$x_s = \frac{1}{m} \sum_{k=1}^m x_k \quad \text{and} \quad y_s = \frac{1}{m} \sum_{k=1}^m y_k \quad (5)$$

$$\bar{x}_k = x_k - x_s \quad \text{and} \quad \bar{y}_k = y_k - y_s, \quad k = 1, \dots, m \quad (6)$$

$$c^2 = \frac{1}{\sum_{k=1}^m (\bar{x}_k^2 + \bar{y}_k^2)} \quad (7)$$

$$\xi_k = c\bar{x}_k \text{ and } \eta_k = c\bar{y}_k, \quad k = 1, \dots, m, \quad (8)$$

where:

m is the number of all points,

E_B is the datum matrix of datum B.

In order to transform the results of the free network adjustment to a network defined with the newly selected points, these networks have to be entered into the datum matrix at the

places where the unknowns of the selected points, ones ($E_B = \begin{bmatrix} 0 & 0 & 0 \\ 0 & I_k & 0 \\ 0 & 0 & 0 \end{bmatrix}$), are located. The

transformation yields the solution (vector of unknowns), which minimizes the partial norm $\|\hat{x}_k\|_2$ of k unknowns of the newly selected points. The sum of adequate k variances also reaches the minimum, i.e. the partial trace of the cofactor matrix of coordinate difference of the newly selected points $Q_{\hat{x}\hat{x}_k}$ is minimal.

2.2 Testing statistical significance of displacements

The basis for displacement determination of a man-made object or any given object on the surface of the earth is to identify the displacements of characteristic points of an object. The points comprise networks, which are monitored in time intervals called *epochs*, set out in advance. The point displacements between two epochs can be inferred only from *identical points*, measured in two epochs. However the points are often damaged or they have to be included into the network due to changes of circumstances. Non-identical points are eliminated in the adjustment procedure or with S-transformation. More details about the procedure can be found in Mierlo (1978). After the two-epoch adjustment the point displacements and their standard deviations are estimated.

2.3 Displacement estimation and displacement accuracy estimation

In geodetic networks it is essential that both displacement and its standard deviation are determined. If the estimated displacements are several times the size of the displacement standard deviations, the most probable displacements can be inferred from the differences in point positions. In addition to determining the magnitude and direction of the displacements, the hypothesis testing for the displacement is also necessary. Consequently, these corresponding calculations must be performed.

Point displacements are determined on the basis of comparing point coordinates in two epochs. Let us assume the point coordinates $T(y, x)$ in a plane and time t and $t + \Delta t$. We assume that the coordinates in time t are not correlated with the coordinates in time $t + \Delta t$.

In order to calculate the estimation accuracy of point displacements, the covariance matrix of point coordinates for respective epochs must be known. $T_i(y_t, x_t)$ represents the position of point T in time t , Σ_t is the corresponding covariance matrix, and $T_{t+\Delta t}(y_{t+\Delta t}, x_{t+\Delta t})$ represents the coordinates of point T in time $t + \Delta t$ with the corresponding covariance matrix $\Sigma_{t+\Delta t}$. This can be expressed as

$$\Sigma_{T_t} = \begin{bmatrix} \sigma_{y_t}^2 & \sigma_{y_t x_t} \\ \sigma_{y_t x_t} & \sigma_{x_t}^2 \end{bmatrix} \quad \Sigma_{T_{t+\Delta t}} = \begin{bmatrix} \sigma_{y_{t+\Delta t}}^2 & \sigma_{y_{t+\Delta t} x_{t+\Delta t}} \\ \sigma_{y_{t+\Delta t} x_{t+\Delta t}} & \sigma_{x_{t+\Delta t}}^2 \end{bmatrix}. \quad (9)$$

The covariance matrix of coordinates of identical points $y_t, x_t, y_{t+\Delta t}, x_{t+\Delta t}$ can be written as

$$\Sigma_{T_t T_{t+\Delta t}} = \begin{bmatrix} \sigma_{y_t}^2 & \sigma_{y_t x_t} & 0 & 0 \\ \sigma_{y_t x_t} & \sigma_{x_t}^2 & 0 & 0 \\ 0 & 0 & \sigma_{y_{t+\Delta t}}^2 & \sigma_{y_{t+\Delta t} x_{t+\Delta t}} \\ 0 & 0 & \sigma_{y_{t+\Delta t} x_{t+\Delta t}} & \sigma_{x_{t+\Delta t}}^2 \end{bmatrix}. \quad (10)$$

The displacement of point T may be evaluated as

$$d = \sqrt{\Delta y^2 + \Delta x^2} = \sqrt{(y_{t+\Delta t} - y_t)^2 + (x_{t+\Delta t} - x_t)^2}. \quad (11)$$

Further on, the displacement variance is determined by

$$\sigma_d^2 = \mathbf{J}_d \Sigma_{T_t T_{t+\Delta t}} \mathbf{J}_d^T, \quad (12)$$

where the Jacobi matrix \mathbf{J}_d equals:

$$\mathbf{J}_d = \begin{bmatrix} \frac{\partial d}{\partial y_t} & \frac{\partial d}{\partial x_t} & \frac{\partial d}{\partial y_{t+\Delta t}} & \frac{\partial d}{\partial x_{t+\Delta t}} \end{bmatrix} = \begin{bmatrix} -\frac{\Delta y}{d} & -\frac{\Delta x}{d} & \frac{\Delta y}{d} & \frac{\Delta x}{d} \end{bmatrix}. \quad (13)$$

By inserting Equations (10) and (13) into Equation (12) we get the representation for displacement variance of point T

$$\sigma_d^2 = \left(\frac{\Delta y}{d}\right)^2 (\sigma_{y_t}^2 + \sigma_{y_{t+\Delta t}}^2) + 2 \frac{\Delta y}{d} \frac{\Delta x}{d} (\sigma_{y_t x_t} + \sigma_{y_{t+\Delta t} x_{t+\Delta t}}) + \left(\frac{\Delta x}{d}\right)^2 (\sigma_{x_t}^2 + \sigma_{x_{t+\Delta t}}^2), \quad (14)$$

that is used for testing displacements by a test statistics given in Equation (15) and described in the next section.

2.4 Distribution function of test statistic by simulations

After adjusting at least two epochs it is possible to determine the displacement of point d according to Equation (11) and standard deviation of displacement σ_d according to Equation (14). Since these two parameters can be calculated prior to a detailed deformation analysis, they are rightly used in the statistical testing.

When estimating displacements, the test statistic is often calculated as:

$$T = \frac{d}{\sigma_d} \quad (15)$$

and compared to the critical value according to the chosen significance level α . Point displacements are established with an appropriate probability only when the displacements are significantly larger than the estimation accuracy of displacements.

Assuming that the errors of observations are distributed normally $\varepsilon \sim N(0, \sigma^2)$, then the parameters being the linear functions of the observations $\hat{x} \sim N(\mu_x, \sigma_x^2)$ are distributed normally as well. The point displacement is calculated with Equation (11). Since Δy and Δx are calculated as the difference of two normally distributed random unknowns, Δy and Δx

are distributed normally, too. This, however, is not the case for the point displacement d , which is a nonlinear function of Δy and Δx . Consequently, it is difficult to analytically determine the form and the type of the distribution of the test statistic (15). The distribution function for the discussed test statistic is therefore determined by simulations, see Rubinstein (1981).

The coordinate differences Δy and Δx are normally distributed random variables with variance-covariance matrix as follows:

$$\Sigma = \begin{bmatrix} \sigma_{\Delta y}^2 & \sigma_{\Delta y \Delta x} \\ \sigma_{\Delta y \Delta x} & \sigma_{\Delta x}^2 \end{bmatrix}. \quad (16)$$

The standard deviations of coordinate differences in two epochs are calculated as

$$\sigma_{\Delta y} = \sqrt{\sigma_{y_t}^2 + \sigma_{y_{t+\Delta t}}^2}, \quad \sigma_{\Delta x} = \sqrt{\sigma_{x_t}^2 + \sigma_{x_{t+\Delta t}}^2}, \quad (17)$$

where $\sigma_{y_t}^2, \sigma_{y_{t+\Delta t}}^2, \sigma_{x_t}^2, \sigma_{x_{t+\Delta t}}^2$ are coordinate variances of $y_t, y_{t+\Delta t}, x_t, x_{t+\Delta t}$. The covariance is calculated as:

$$\sigma_{\Delta y \Delta x} = \sigma_{y_t x_t} + \sigma_{y_{t+\Delta t} x_{t+\Delta t}}, \quad (18)$$

where $\sigma_{y_t x_t}$ and $\sigma_{y_{t+\Delta t} x_{t+\Delta t}}$ are covariances of the coordinates in both epochs.

To generate the sample of the normally distributed random variables, the Box and Müller approach was applied (Box & Müller, 1985; Press et al., 1992). The basic idea of generating a sample of dependent normally distributed random variables is to generate a sample of *independent* normally distributed random variables and then use a linear transformation to obtain a sample of *dependent* random variables. Let us assume that u_{1i} and u_{2i} , $i=1, \dots, n$ are samples of two independent and uniformly distributed random variables U_1 and U_2 , and n is the number of simulations. The sample of two independent normally distributed random variables Z_1 and Z_2 is calculated as follows:

$$\mathbf{z}_i = \begin{bmatrix} z_{1i} \\ z_{2i} \end{bmatrix} = \begin{bmatrix} \sqrt{-2 \ln u_{1i}} \sin(2\pi u_{2i}) \\ \sqrt{-2 \ln u_{1i}} \cos(2\pi u_{2i}) \end{bmatrix}, \quad i = 1, \dots, n. \quad (19)$$

To generate a sample of dependent normally distributed random variables, a linear transformation is needed. The variance-covariance matrix Σ is decomposed by Cholesky decomposition

$$\Sigma = \mathbf{U}^T \mathbf{U}. \quad (20)$$

In our case \mathbf{U} takes the following form

$$\mathbf{U} = \begin{bmatrix} \sigma_{\Delta y} & \frac{\sigma_{\Delta y \Delta x}}{\sigma_{\Delta y}} \\ 0 & \sigma_{\Delta x} \sqrt{1 - \left(\frac{\sigma_{\Delta y \Delta x}}{\sigma_{\Delta y} \sigma_{\Delta x}} \right)^2} \end{bmatrix}. \quad (21)$$

For the transformation of a sample of independent normally distributed random variables to a sample of dependent random variables the linear transformation

$$\mathbf{y}_i = \mathbf{U}^T \mathbf{z}_i, \quad i = 1, \dots, n \quad (22)$$

is used.

In our case the coordinate differences are generated by the following equations

$$\begin{aligned} \Delta y_i &= z_{1i} \sigma_{\Delta y}, \\ \Delta x_i &= z_{1i} \frac{\sigma_{\Delta y \Delta x}}{\sigma_{\Delta y}} + z_{2i} \sigma_{\Delta x} \sqrt{1 - \left(\frac{\sigma_{\Delta y \Delta x}}{\sigma_{\Delta y} \sigma_{\Delta x}} \right)^2}, \end{aligned} \quad (23)$$

where it is assumed that the means of Δy and Δx are zero ($\mu_{\Delta y} = \mu_{\Delta x} = 0$) and $i = 1, \dots, n$. The standard deviations of point coordinates in respective epochs vary from point to point. Therefore, the distribution function of the test statistic (15) takes on a different form for each point in each of the two epochs. By using the simulated normally distributed random variables (23), d is calculated using equation (11) and σ_d using equation (14). Consequently, in n simulations this procedure allows us to determine the empirical cumulative probability distribution function of the test statistic (15) for individual points.

2.4.1 Critical value T_{crit} and actual risk α_T

Critical value T_{crit} and actual risk α_T are determined from the obtained empirical cumulative distribution function by the following procedure (Savšek-Safić et al., 2006):

1. generate coordinate differences $\Delta y_i, \Delta x_i; i = 1, \dots, n$; Equation (23)
2. calculate displacement d_i ; Equation (11), its standard deviation σ_{d_i} ; Equation (14) and test statistic $T_i; i = 1, \dots, n$; Equation (15)
3. form empirical cumulative probability distribution function F_T^* by sorting T_i ; $F_T^*(T_i) = \frac{i}{n}; T_i \leq T_{i+1}$
4. determine critical value T_{crit} from $F_T^*: T_{crit} = T_{i=[(1-\alpha)n]}$ or
5. determine actual risk α_T from $F_T^*: \alpha_T = 1 - \frac{i}{n}$ for such i that $\min T_i > T$.

The test statistic is then tested according to the given null hypothesis and its alternative hypothesis:

$H_0 : d = 0$; the point is stable between two epochs, and

$H_a : d \neq 0$; the point has changed its position.

The test statistic (15) is compared to the critical value acquired from empirical cumulative distribution function. If the test statistic value is smaller than the critical value at a chosen significance level α , then the risk of rejecting the true null hypothesis is too high. Accordingly, it is established that the displacement is not statistically significant. If the test statistic value exceeds the critical value, the risk of rejecting the true null hypothesis is lower than the chosen significance level α . Therefore, the null hypothesis is rightly rejected and the statistical significance of the displacement is thereby confirmed.

This decision is supported by calculating the actual risk α_T of rejecting the true null hypothesis (the probability of committing *Type I Error*). Two possibilities are examined:

- $T > T_{crit}$ i.e. $\alpha_T < \alpha$: the null hypothesis is rejected; the point displacement is statistically significant and
- $T < T_{crit}$ i.e. $\alpha_T > \alpha$: the null hypothesis is not rejected; the point displacement is statistically insignificant.

Regarding the actual risk and the consequences of making a wrong decision, it is up to the user to decide upon the risk level of acceptability. As a consequence, a point is considered as stable or displaced.

3. Significant displacement testing in a test network

3.1 The network shape

3.1.1 The Krško network

The Sava River dam was built to ensure the minimum Sava River water level and thus enable the water pumping for cooling. The dam has six 15 m wide spillways. To ensure earthquake stability the dam is split into two large concrete frame structures. The structure height is 15.5 m and is therefore considered as large dam according to international standards, and needs to be technically monitored. 7 control points have been stabilised on the dam to determine horizontal displacements. Along the outlet, there were 5 reference observation points stabilised with concrete pillars (Figure 4).

3.1.2 The Libna network

The Libna network is classical terrestrial trigonometric net applied for the determination of local horizontal stability along the Orlica fault. The network's shape is that of an irregular pentangle with five circumferential points, where point 6 is a linking point amplifying the network reliability (Figure 6). The points represent the geometrical basis for determining the positions of four ground points defined on the basis of geologic situation. Basically, the ground points are ex-centre points of four points of the net.

The network size is described by indicating the area of the circumferential points of a polygon, amounting to approx. 4.27 ha. The longest length in the network is 385 m, the shortest length is less than 40 m. The network of the town of Libna in the vicinity of Krško was set up to determine point stability at the Orlica fault.

3.2 Stabilization of the ground points

3.2.1 The Krško network

The reference points of the base network for the performance of measurements are stabilised with concrete pillars, representing the conventional stabilisation of geodetic points for deformation measurements. The chosen stabilisation enables forced centring of the instrument and the reflector – *Leica Wild* system.

The stabilisation of control points on the dam also enables forced centring of the reflector – *Leica Wild* system. The control points were screwed into the concrete base, where the footplate can be fitted with the prism mount, which, in turn, enables horizontal alignment. Figure 1 shows the stabilisation and signalisation of the reference and control points.



Fig. 1. Stabilisation and signalisation of the reference and control points

3.2.2 The Libna network

The measuring points were determined by a set of two physically stabilised points. The measuring points, onto which the reflector was forced-centred, presented the points monitored for displacements. In all measurement epochs we used the same reflectors - Kern ME 5000. All the measurements were carried out on the points that were - according to the reference measuring points - set up ex-centrally. The term ex-central stand was introduced. The distance from the ex-centre to the centre point was 10 - 20 m (Figure 2).

The reference points were stabilised by combining the methods described above (Figure 3). However, the implementation was simplified and the costs were lower. A mass-produced concrete tube with $\Phi = 0.25$ m in diameter and 1 m length was used. A hole of the same diameter was drilled into the pillar, and a concrete tube was put into the hole. The tube was filled in with concrete and a device for forced-centring was built in. The cylinder top was covered with a mass-produced cover for full protection.

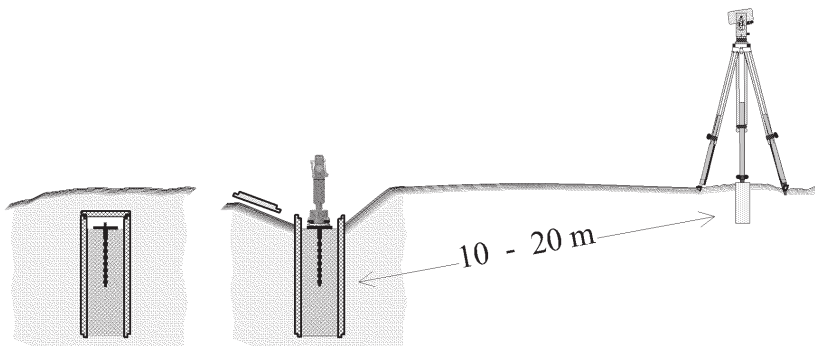


Fig. 2. Ground stabilisation of the centre and the ex-central stand



Fig. 3. Signalisation of the centre and the ex-central stand

The instrument stand was stabilised with the usual ground stabilisation by means of a concrete square stone with a built-in plug. Above the instrument stand, a tripod was set-up, centred and levelled. The centring accuracy did not influence the end results, since the coordinates of the measuring point onto which the reflector was forced-centred were of crucial importance, not the co-ordinates of the instrument stand. However, the tripod's stability during the measurements was essential.

The procedure of ensuring the appropriate network geometry and required precision for the determination of the horizontal coordinates of points in this way is theoretically and practically described in the article (Kogoj, 2004).

3.3 History of measurements and measuring accuracy

3.3.1 The Krško network

Due to the changed measuring instrument, in 2004 also the method of measurements based on simulation of observations was changed in the combined Krško micro network. We chose a combination of triangulation and trilateration, which provides a larger number of redundant observations. Since periodic measurements of the dam are foreseen twice a year (in spring and in autumn), so far 14 independent measurements have been conducted.

In the Krško micro trigonometric network the classic terrestrial surveying was chosen. The measurements were performed with the precision of electronic total station *Leica Geosystems TC2003* intended for precise angle and distance measurements in precision terrestrial geodetic networks (Savšek-Safić et al., 2007). Measuring accuracy for angle measurements is $\sigma_{DIN18723-Theo (Hz-V)} = 0.5''$ and for distance measurements $\sigma_S : 1 \text{ mm}; 1 \text{ ppm}$. Forced centring of the instrument, signalisation of measuring points and measurement of meteorological parameters were performed by tested and calibrated supplementary equipment (reflectors, footplate with reflector mounts, psychrometer, barometer). The first measurement in 2009 was due to changed instrument performed by precise electronic tachymeter *Leica Geosystems TCRP 1201*. Measuring accuracy for angle measurements is $\sigma_{DIN18723-Theo (Hz-V)} = 1.0''$ and for distance measurements $\sigma_S : 2 \text{ mm}; 2 \text{ ppm}$. In the same year we bought the most advanced electronic tachymeter by the manufacturer *Leica Geosystems TS30*, with which we performed

the last three measurements. The measuring accuracy for angle measurements is $\sigma_{DIN18723-Theo (Hz-V)} = 0.5''$ and for distance measurements $\sigma_s : 0,6 \text{ mm}; 1 \text{ ppm}$.

The measuring accuracy was determined on the basis of *Ebner'* s method of the a-posteriori weight determination (Vodopivec & Kogoj, 1997). The results included position accuracy and are given in Table 1.

<i>Epoch</i>	$\sigma_a ['']$	$\sigma_s [\text{mm}]$
August 2004	1.51	0.33
December 2004	1.89	0.23
August 2005	1.35	0.32
November 2005	2.96	0.37
July 2006	2.34	0.40
November 2006	1.23	0.15
May 2007	1.71	0.23
October 2007	2.05	0.32
April 2008	1.88	0.43
September 2008	1.60	0.37
May 2009	0.53	0.21
September 2009	0.80	0.27
May 2010	0.48	0.27
October 2010	0.53	0.10

Table 1. Measuring accuracy achieved in the Krško network

3.3.2 The Libna network

The Libna network was stabilised in 1998. So far, we have realised seven measurement epochs.

To determine horizontal coordinates of the net points, we used the combination of angle and distance measurements. The measuring method was a combination of triangulation and trilateration. In each epoch we realised measurements on all ecetrical stands.

We used the best instrumentation available. For the first six measuring epochs Electronic theodolite *Kern E2* was used for angle measurements. The instrument is one of the first most precise electronic theodolites of the first generation. Its construction and accuracy stability is excellent. The measuring accuracy defined on DIN standard procedure is $\sigma_{DIN18723-Theo (Hz-V)} = 0.5''$ For distance measurements we used precise distancemeter *Kern Mekometer ME 5000*. This instrument was constructed in the 1980's but it has been so far considered as the most precise geodetic electrooptical distance meter in series production. Measuring accuracy is $\sigma_s : 0.2 \text{ mm}; 0.2 \text{ ppm}$.

In last two measuring epochs electronic total station *Leica Geosystems TC2003* was used. This instrument is designed for the most precise angle and distance measurements. With the selected additional accessories the highest accuracy can be achieved. The measuring accuracy for angle measurements is $\sigma_{DIN18723-Theo (Hz-V)} = 0.5''$ and for distance measurements $\sigma_s : 1 \text{ mm}; 1 \text{ ppm}$.

For temperature and humidity measurements we used 2 *precise psychrometers*, and for air pressure measurements we used *digital barometer Paroscientific*, model 760-16B.

Similar as in the Krško network, the measuring accuracy was determined on the basis of *Ebner's* method of the a-posteriori weight determination (Vodopivec & Kogoj, 1997). The results included position accuracy and are given in Table 2.

<i>Epoch</i>	σ_a ["]	σ_s [mm]
November 1998	1.03	0.45
December 1999	0.53	0.23
December 2000	0.62	0.52
November 2001	1.81	0.60
March 2003	0.94	0.72
April 2005	1.09	0.31
February 2008	3.30	0.62

Table 2. Measuring accuracy achieved in the Libna network

3.4 Determination of point displacements

3.4.1 The Krško network

3.4.1.1 The adjustment

The geodetic datum of the horizontal network was determined by two given assumingly stable points – reference points O1 and O5. To preserve the identical network geometry, as well as measurement and observation methods, the reference points were first tested for stability. The comparison of changes in coordinates between the last campaigns indicated that pillars O1 and O5 were statistically stable. In this way, the determination of the datum in the network enabled us to determine the statistically significant displacements of control points with a higher probability (Savšek-Safić et al., 2007).

The horizontal coordinates were calculated into the existing local co-ordinate system of the network to the level of the lowest point (reference point O4). The observations were tested for the potential presence of gross error, following the Danish method. The input data for the horizontal adjustment were the reduced averages of three sets of angles and the slope distances reduced to the chosen level. The reduction of distances took into account the instrumental, meteorological, geometric and projection corrections (Kogoj, 2005). The zenith angles were observed to establish the height stability of the reference and control points. The observations in the horizontal network were adjusted following the method of indirect observations. First, the adjustment of the free network was performed, which gave us an unbiased estimate of observations (Figure 4). Then the S-transformation was used, where the geodetic datum was determined by two statistically stable reference points O1 and O5. The results of the horizontal adjustment are the most probable values of horizontal coordinates of measuring points in the local system with the corresponding accuracy estimates.

3.4.1.2 The displacements

In the area of NEK the horizontal stability of the Sava River dam was investigated based on fourteen consecutive epochs. In December 2003, the transition to a new way of measurements (measurement method, instrument, network geometry) and the determination of a new geodetic datum in the micro network of Krško enabled a higher reliability of the determination of statistically significant displacements. Based on an expert

geological opinion we decided that the geodetic datum in the Krško network would be represented by two assumingly most stable reference points O1 and O5.

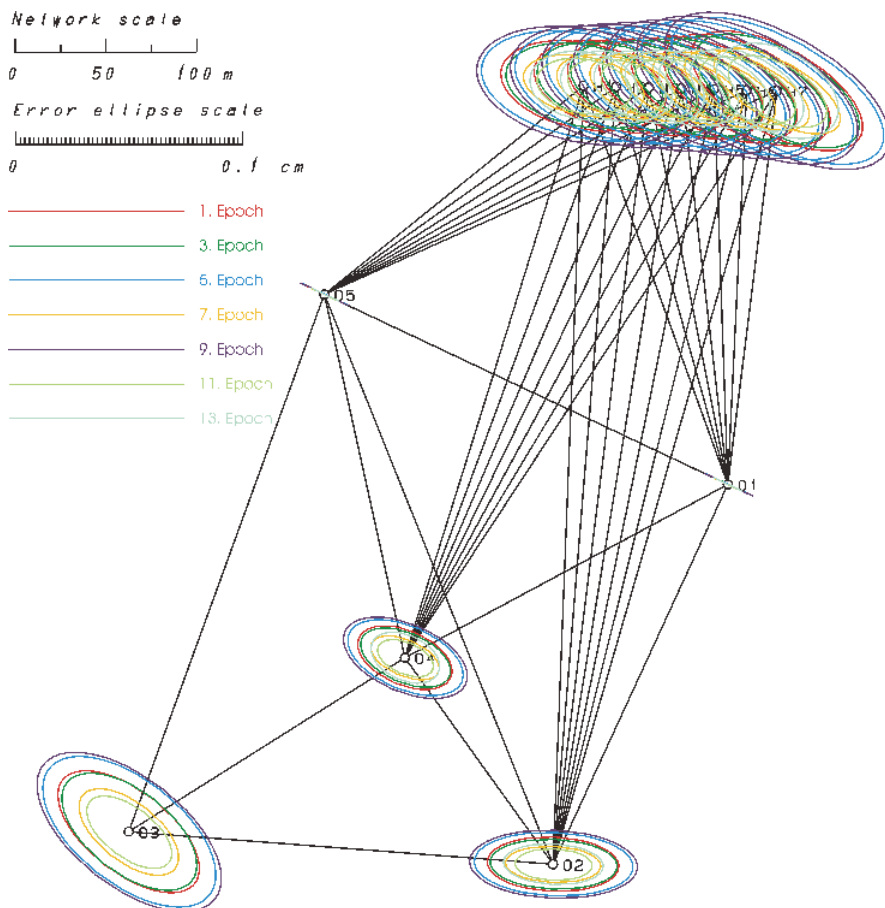


Fig. 4. Position accuracy for single epochs - Helmerts error ellipses - free net adjustment of the Krško network

After the adjustment of at least two epochs, it was possible to determine the displacement of point d and displacement variance σ_d^2 . The probability function for the test statistic (15) was determined empirically with simulations, and then compared to the critical value considering the chosen significance level α . Displacements could be identified as statistically significant according to the distribution of test statistic and chosen significance level α . If the test statistic was smaller than the critical value at the chosen significance level α , we assumed that the displacement was statistically insignificant. If the test statistic is higher than the critical value, the hypothesis was justifiably rejected and we could confirm the statistical significance of the displacement. In Figure 5 the regression coefficient defines the displacement velocity in meters per day with transformation S on points O1 and O5.

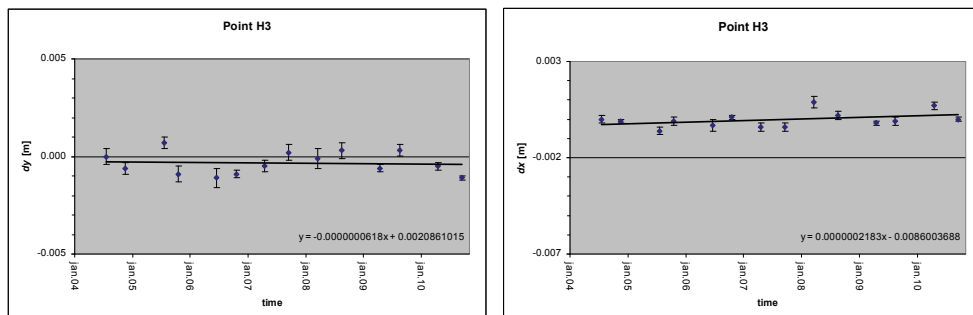


Fig. 5. The displacements of control point H3 in the directions of coordinate axes with the belonging standard deviations in time.

The time line of horizontal displacements of points on the Sava River dam was represented with the displacements of control points and the corresponding relative displacement ellipsoids referring to the two-epoch displacements. The relative displacement ellipsoids are calculated from the point determination accuracy in a single epoch.

3.4.2 The Libna network

3.4.2.1 The adjustment

For the adjustment we need mean values of six sets measured in horizontal directions. In each epoch a priori statistical analyses was made for the elimination of gross errors and for the computation of measuring accuracy.

The horizontal coordinates of net points are determined on the local level. We considered meteorological, geometrical and projectional reductions of measured distances (Kogoj, 2005). On the basis of measuring differences in both directions we also estimated the accuracy of the distances.

In zero epoch measurement the local datum of the net was determined. The orientation of the coordinate axes is nearly parallel with the Slovenian national Gauß-Krüger coordinate system.

The adjusted coordinates of ground points A, B, C and D of zero epoch in 1998 are approximate coordinates for all other epochs. The definitive coordinates of points A, B, C and D for each epoch were determined on the basis of the adjustment process. We supposed that the accuracy of horizontal directions was the same for each instrumental standing point. The distances in the net were short. Based on this, we should determine the weights of the distances on the basis of only the constant part of the error. We always used the software GEM4 for simultaneous angle and distances network adjustment. The final results were the horizontal coordinates of the net points and the accuracy estimation (elements of error ellipses).

First we adjusted the net as a free network for all epochs. Based on the results we analysed the measuring accuracy and the position accuracy of the net points. The reason for this is that free network adjustment gives the most objective results of measuring accuracy because there is no influence of the datum parameter.

The following Figure 6 shows the size of the semi-major axis of the error ellipses (worst case), obtained in each epoch. Comparison of the absolute values of the ellipses is due to

high precision level questionable. The increase in value from 0.2 mm to 0.3 mm means a loss of numerical precision of about 50%. From geodetic point of view we know that between these values there are practically no differences!

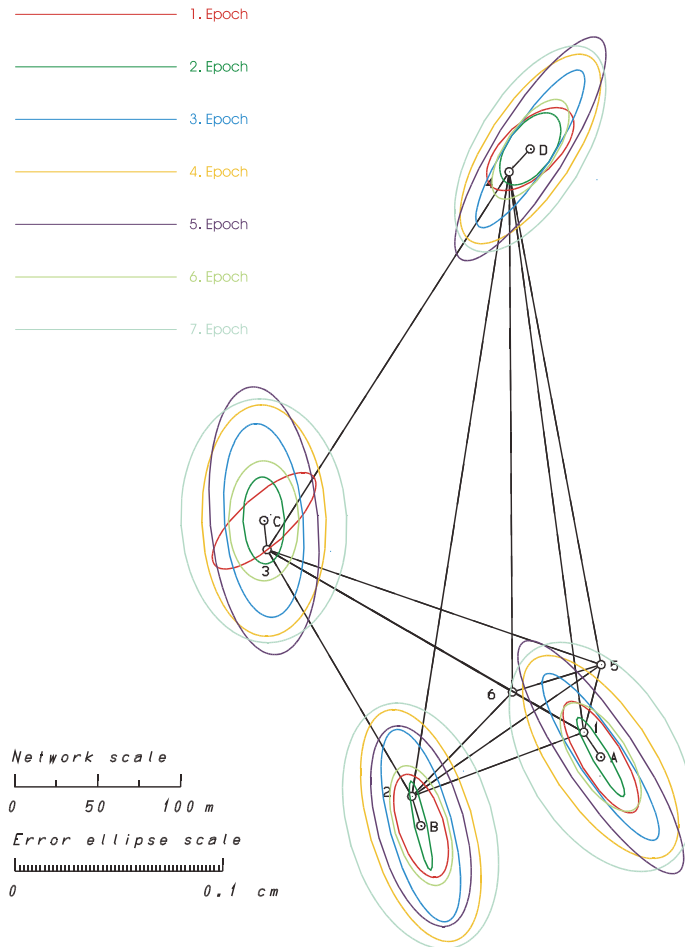


Fig. 6. Position accuracy for single epochs - Helmerts error ellipses - free net adjustment of the Libna network

3.4.2.2 The displacements

The main problem in the displacement determination process is the choice of stable points. The defect of the geodetic datum was 3, so we needed at least one and a half given points. On the basis of geological situation there were two logical possibilities. We could choose points A and B or C and D.

The differences of the coordinate values of points A and B between single epochs were minimal. We once again adjusted each epoch on four different datums of the net. The main conclusions, based on the results, are:

- the size of proven displacements on points C and D are practical invariants on the datum of the net based on points A and B,
- from the aspect of minimal influence of the accuracy of given points on the final parameters of displacement vectors the best choice is the determination of the datum based on the S-transformation.

We used our own software Premik. The elements of the displacement vectors for all epochs combinations were calculated.

In further analyses we computed the displacement velocity. The displacement velocities of points C and D in y and x directions with standard deviations determined on the basis of the S-transformation on points A and B are computed on the basis of linear regression analyses. We used the same procedure also for the determination of the datum on the basis of points C and D. In Figure 7 the regression coefficient defines the displacement velocity in meters per day with the S-transformation on points C and D.

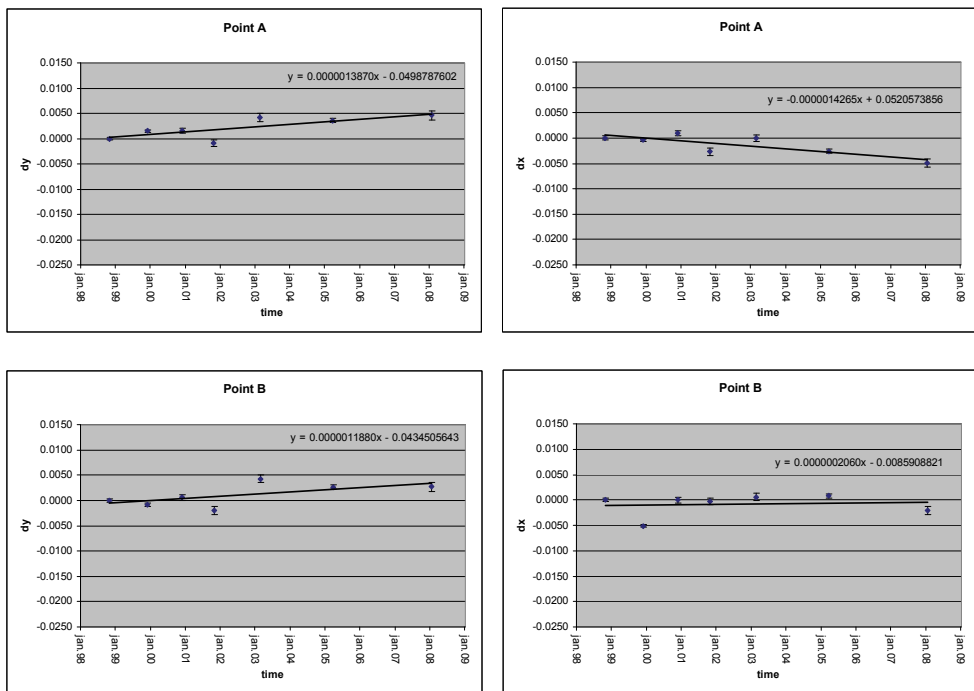


Fig. 7. The displacements of points A and B in the directions of coordinate axes with the belonging standard deviations in time.

4. Conclusion

A contractor of geodetic works is expected to present not only data on point displacements, but also to provide assurance in terms of the quality of displacement estimation. In addition to the assumed null hypothesis $H_0: d=0$ and the chosen significance level α , the actual risk of rejecting the true null hypothesis is crucial. The participation of the commissioning

party in the process of evaluating the estimated displacements is highly recommended. The decision upon risk acceptability is then in the hands of the commissioner.

The Sava River dam has a specific place among the NEK buildings, since it is subjected to the great force of the Sava River flow and to the differences in filling and emptying of the reservoir, i.e. the difference between high flow and low flow. Periodically larger displacements of the entire dam are to be expected.

The Libna network was stabilised in such way that two points are located on one and two points on the other side of the fault. The purpose of several years of continuous measurements was to determine tectonic activities of the fault in question.

Due to expected small displacements in both networks we were mainly focused on:

- precise ground stabilisation (example Libna) or concrete observation pillars (example Krško), which allows forced centering of the instrument or reflector;
- use of precise measuring instruments and additional measuring equipment;
- meeting the condition of as large number of redundant observations as possible to assure quality measurements and results;
- consideration of all influences on the measured quantities;
- analysis of the precision of measurements and detection of any major errors (outliers) in the measurements;
- transformation of adjusted coordinate points into geodetic datum of assumingly stable points, where the displacement of other points can be measured.

As shown, test statistic (15) along with the empirical cumulative distribution function is appropriate tools for testing the significance of point displacements in a geodetic network. Since the displacement and its respective accuracy are acquired by a simple method, the suggested procedure is appropriate and provides good results that furnish a good first estimate of the situation in the discussed network. The test example illustrates that the estimation of displacement significance is directly dependent upon the critical value at a chosen significance level α . Accurate displacement estimation is achieved only if the critical value is determined according to the actual distribution function of the test statistic. Having in mind the difficulty level of the assignment and its consequences, the decision must be made whether there is the need for a detailed deformation analysis to be carried out using one of the known approaches.

5. Acknowledgment

We gratefully acknowledge the help of the company IBE d.o.o., specifically Mr. Božo Kogovšek, the expert responsible for the NEK technical monitoring.

6. References

- Box, G.E.P. & Müller, M.E. (1985). A note on the generation of random normal deviates. *Annals of Mathematical Statistics*, Vol. 29, pp. 610-611, ISSN 0003-4851
- Casparly, W.F. (2000). *Concepts of Network and Deformation Analysis*, Kensington, School of Surveying, The University of New South Wales, ISBN 0-85839-044-2, Kensington, N.S.W., Australia
- Kogoj, D. (2004). New methods of precision stabilization of geodetic points for displacement observation. *Allgemeine Vermessungs-Nachrichten*, Vol.111, No.8/9, pp. 288-292, ISSN 0002-5968

- Kogoj, D. (2005). *Merjenje dolžin z elektronskimi razdaljemerji*, UL-FGG, ISBN 961-6167-47-2, Ljubljana, Slovenia (in Slovene)
- Mierlo, J. van (1978). A testing Procedure for Analysing Geodetic Deformation Measurements, *Proceedings of the 2nd FIG Symposium on Deformation Measurements by Geodetic Methods*, pp. 321-353, Bonn, Germany
- Press, W.H.; Teukolsky, S.A.; Vetterling, W.T. & Flannery, B.P. (1992). *Numerical recipes in Fortran 77: the art of scientific computing* (Second Edition), Cambridge University Press, ISBN 0-521-43064-X, Cambridge, USA
- Rubinstein, R.Y. (1981). *Simulation and the Monte Carlo Method*, John Wiley & Sons, ISBN 0-471-08917-6, New York, USA
- Savšek-Safić, S.; Ambrožič, T.; Stopar, B. & Turk, G. (2006). Determination of point displacements in the geodetic network. *Journal Of Surveying Engineering-ASCE*, Vol.132, No.2, pp.58-63, (May 2006), ISSN 0733-9453
- Savšek-Safić, S.; Kogoj, D.; Marjetič, A. & Jaklič, S. (2007). 49. *geodetska izmera horizontalnih premikov geodetskih točk NEK*, UL-FGG, Ljubljana, Slovenia (in Slovene)
- Vodopivec, F. & Kogoj, D. (1997). Ausgleichung nach der Methode der kleinsten Quadrate mit der a posteriori Schätzung der Gewichte. *Österreichische Zeitschrift für Vermessungswesen und Geoinformation*, Vol.85, No.3, pp. 202-207, ISSN 0029-9650

Low Power and Shutdown PSA for the Nuclear Power Plants with WWER440 Type Reactors

Zoltan Kovacs

*RELKO Ltd, Engineering and Consulting Services
Slovakia*

1. Introduction

Two nuclear power plants (NPPs) are in operation in Slovakia equipped with WWER440/V213 type reactors. The Jaslovské Bohunice V2 NPP has two reactors in operation, the Mochovce NPP has also two reactors in operation and another two reactor units are under construction which will be given into operation in 2013. Full power and shutdown level 1 and level 2 probabilistic safety assessment (PSA) as part of the plant safety report were performed for these plants by the RELKO PSA team.

The role of PSA for NPPs is an estimation of the risks in absolute terms and in comparison with other risks of the technical and the natural world. Plant-specific PSAs are being prepared for the NPPs and being applied for detection of weaknesses, design improvement and backfitting, incident analysis, accident management, emergency preparedness, prioritization of Research & Development and support of regulatory activities.

There are three levels of PSA, being performed for full power operation and shutdown operating modes of the plant:

- Level 1 PSA: The dominant accident sequences leading to the core damage are identified and the core damage frequency is calculated. The strengths and weaknesses of the safety systems and procedures to prevent the core damage are also provided as results.
- Level 2 PSA: The ways in which radioactive releases from the plant can occur are identified and the magnitudes and frequency of release are calculated. Detailed analyses of the containment are performed. Safety measures are proposed to minimize the release of radioactive materials into the environment after a severe accident.
- Level 3 PSA: The public health and other societal risks such as contamination of land or food are estimated. Damage to people (number of fatalities, the number of injured, reduction of life expectancy) and damage to property (loss of agricultural products and of natural resources, destruction, the cost of relocating the population and decontaminating effected areas, etc.) are identified and safety measures are proposed to be implemented to minimize the risk. The Nuclear Regulatory Authority does not require the level 3 PSA for NPPs in Slovakia, however, the performance of analyses is strongly recommended.

There are two basic types of the plant outage: unplanned maintenance outages due to the repair of the components and planned refuelling outages. The differences are in:

- Safety systems availability,
- Duration of outage,
- Neutron and thermal-hydraulic conditions,
- Reactor coolant system (RCS) and containment configuration.

For the unplanned shutdowns, the operation can continue after several hours. In general, for these shutdown modes it is not necessary to achieve the cold shutdown state or to open the reactor vessel. Preparing of the action schedule is required for each shutdown of the unit, where the individual actions done by the personnel are indicated.

During these outages the reactor subcriticality is achieved by the insertion of all control rods into the core. Operational records of the WWER440 type reactors have shown us, that there are several events during the year where it is necessary to decrease the power for urgent repairs. The unplanned unit trip also occurred.

The outage of the reactor is planned once per year for the refuelling. These are the planned yearly outages for the refuelling of the reactor and the general plant maintenance. The reactor is cooled down to cold state and the reactor vessel is open. Only a fraction of the fuel is replaced by the new fuel (typically about 25% of the total number) in the short refuelling outage. The rest of the fuel elements remains in the reactor vessel during the outage. The refuelling is performed according to the approved refuelling program. These are the planned outages for the refuelling of the reactor and extended plant maintenance.

Long refuelling outage is performed every fourth year, and involves in-service inspection of the reactor vessel. The difference between the short and the long outage is mostly in the scheduled inspection of the reactor vessel. However, the whole reactor core is transferred to the spent fuel pool.

The risk from nuclear power plants was assumed for many years to be dominated by the risk during full-power operation. The deterministic licensing process, the PSA focused on full power. It seemed clear that shutdown was the safe condition.

After all, the reactor is shutdown, the decay heat is low, substantial time is available for recovery, and many recovery options are possible. On the other hand, a growing number of incidents during shutdown, some of them leading to substantial loss of reactor coolant through draining, began to focus attention on the possibility of significant risk during shutdown conditions. In fact, although decay heat is low, it can still be substantial and must be removed.

In addition, much equipment is unavailable due to maintenance, there may be unusual plant configurations, automatic safety features may be disabled, and manual response is required (often with little guidance from procedures and training). Also, knowledge of timing and success criteria is limited.

During last few years, operational experience and performance of the low power and shutdown PSA highlighted the magnitude of the risk contribution from those, previously considered safe operating modes. This risk was found to be significant. Many studies such as the shutdown PSA for PWR in Western Europe (France and Switzerland) and WWER plants in Central Europe (Slovak, Hungary and Czech Republic) as well as latest industry events, such as Paks NPP shutdown fuel damage accident, demonstrated that the core damage frequency (CDF) from an accident occurring during shutdown or low power operation modes was higher (up to 100% of CDF for some plants) than the one at power.

This risk is not related to the plant design. It is rather related to the unavailability of equipment due to maintenance activities undertaken during an outage, presence of

additional (contractor) personnel who may not be fully aware of the safety issues, presence of additional heavy loads and flammable materials, etc. All of these items increase the risk during plant outage.

Adequate planning and preparation of activities during outages can reduce both the probability and the consequences of possible events. In other words, there are a lot of possibilities for safety improvements in those operating modes. To decide what kind of improvements are the best on safety and cost beneficial grounds, a variety of analytical approaches could be used.

One of these is administrative control based on the experience of individuals involved in the outage planning. While any careful analysis will find ways to improve safety during outages, it is felt that this approach would not be best suited to very well handle a more complex interface, since critical configurations may not always be recognised.

Another approach is a PSA-type modelling, which considers a variety of interactions and dependencies of important systems. Performance of PSA for shutdown and low power operating modes (SPSA), may support the enhancement of the safety during plant outage, and may contribute to reduction of the outage duration. Thus a detailed analysis of shutdown operation may:

- contribute to a more economical plant operation,
- improve plant safety and
- decrease the consequences of incidents.

The full power PSA is no longer representative of the actual plant risk profile during the operational condition when the configuration of safety and support systems has changed extensively. This usually happens when the reactor power is below a certain level and automatic actuation of safety systems is being interlocked. Therefore, contribution of the risk during plant outage deserves a special attention and a shutdown PSA appears to be an ideal tool to improve safety during plant outage.

This chapter gives the view of level 1 and 2 SPSA modelling issues and results for the Slovak NPPs. The lessons learned in this area are presented and the PSA applications are described. The PSA models were developed in the RISK SPECTRUM PSA code.

2. Modelling issues related to Level 1 SPSA

The level 1 PSA study of the plant calculates the CDF and identifies the dominant initiating events (IE) and accident sequences that contribute to the core damage. The main modelling issues related to SPSA are described in this part of the chapter:

- Plant operating modes and plant operational states,
- Initiating events,
- Screening analysis,
- Modelling of accident sequences (fault trees and event trees),
- Human reliability analysis (HRA),
- Quantification of accident sequences and
- Application of SPSA.

2.1 Plant operating modes and plant operational states

The definition of the plant operating mode varies from country to country. The Slovak plants have adopted the USA definitions. There are seven operating modes, numbered 1 to 7. These are:

1. Full power operation,
2. Reactor criticality,
3. Hot shutdown,
4. Semi-hot shutdown,
5. Cold shutdown – reactor vessel is closed,
6. Cold shutdown – reactor vessel is open and
7. Empty reactor vessel (the fuel is removed from the reactor vessel and located to the spent fuel pool).

Understanding of plant operating modes and its characteristics in terms of systems available and the general plant conditions is essential for the development of the low power and shutdown PSA model. Operating modes are also highly important for defining the interface between power PSA and low power and shutdown PSA. For an integrated PSA model of a plant, it is significant to adequately define the interface between power PSA and low power and shutdown PSA. This interface does not necessarily coincide with the definition of the operating modes. Typically, the full power PSA considers 100% nominal power.

In terms of the thermal hydraulic response to an initiating event, there is not much difference between 100% power and lower power levels, expect that at lower power levels the time available for selected corrective actions may be somewhat greater. The 100% power case is therefore conservatively a representative of the whole spectrum of power levels.

When the reactor power reaches a certain power level, the automatic actuation of the safety systems is disabled. Depending on the reactor design, and in some cases on operating practice, this could be between 0-10% nominal power. This point is the natural interface between the full power PSA and SPSA (see Fig. 1).

While the reactor is on low power, even without automatic actuation of safety systems, the power PSA models (with appropriate modifications) could be used to determine the risk level. This is generally true also for the hot stand-by mode.

Once the reactor is in the shutdown mode, and especially when the decay heat is removed via residual heat removal system (RHR), the state of the plant is such that most of the power PSA models are not applicable without major modifications.

Plant operating modes are important from the standpoint of the conduct of the plant operation. For a SPSA the plant operating modes do not mean much. Due to extensive changes in plant configuration during a shutdown period, it is necessary to define plant operational states (POSs) which will properly reflect the plant configuration during an outage evolution.

The POS is used to define boundary conditions within which there would be no changes in major characteristics which are important for PSA modelling.

The POS is defined as a period during a plant operating mode when important characteristics are distinctively different from another plant operating state. The important characteristics describing a plant operating state are:

- RCS temperature and pressure,
- RCS water level (inventory),
- Decay heat removal,
- Availability of safety and support systems,
- Containment integrity,
- System alignments and
- Reactivity margins.

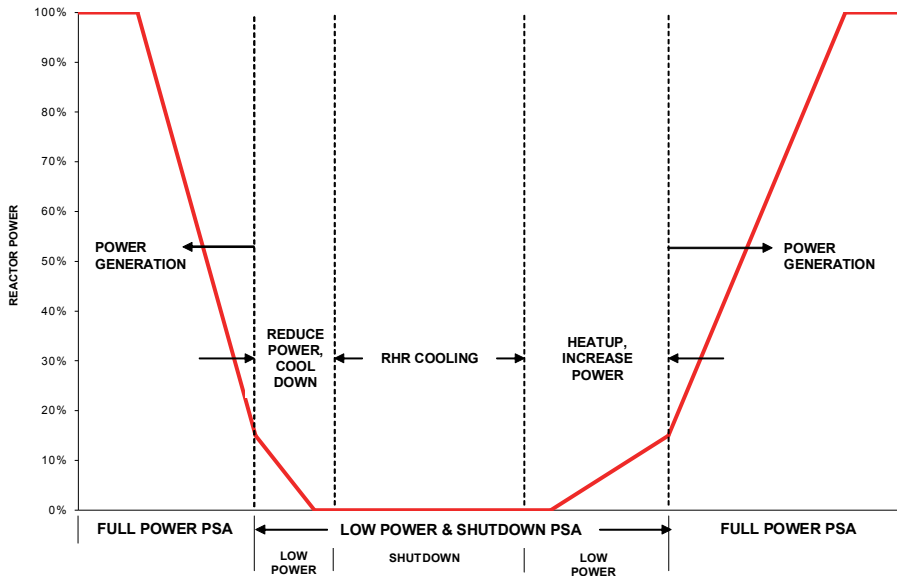


Fig. 1. Full power, low power and shutdown PSA

Some or all characteristics indicated above should be considered in defining the plant operational states. It is obvious that defining the POSs for every possible plant condition may result in a very large number of POSs. The attempt to define all the POSs which are relevant for SPSA could result in several hundreds POSs. One of the initial activities related to defining the POSs is their grouping to reduce the number of POSs to a manageable level. The grouping process shall consider issues like specific success criteria, typical IEs and system availability. The actual practice varies among PSA practitioners, but the general guidance is always to distinct POS in their main characteristic. A typical number of POSs considered in SPSA varies from 10 to 15. Newer studies tend to have more POSs than the early ones. It should be noted that the scope and objectives of a SPSA have a dominant effect on the selection of the POSs.

Examples of POSs for a WWER440 type reactor are shortly described below:

1. POS1. The reactor is sub-critical. The RCS pressure is between the nominal pressure and 4 MPa. The RCS temperature is between nominal and 180°C. All trains of the safety systems are available (exceptions are allowed by the limiting conditions of operation). All SGs are connected to the reactor vessel. The primary to secondary side heat removal operates in the steam-water regime using the auxiliary feedwater system and steam removal via the steam dump station to the condenser initially and via the technological condenser at the end of POS. In this POS the containment is closed.
2. POS2. RCS temperature is below 180°C but above 100°C. The RCS pressure is 1-4 MPa. All trains of the safety systems are available (exceptions are allowed by the limiting conditions of operation). Some ESFAS signals are disconnected when the RCS temperature is below 180°C. All SGs are connected to the reactor vessel. In the first part of this POS the secondary side heat removal is in the steam-water regime. At the end of

- POS the RHR is working in the water-water regime, RHR pump is running and the heat removal is performed via the technological condenser. At the end of this POS the containment is open.
3. POS3. The RCS temperature is between $T_{\text{brittle fracture}}$ and 40°C. The HPSI pumps are disconnected. These pumps are available in this POS for the accident mitigation only under the conditions defined in the limiting conditions of operation. However, exceptions are possible in case of the severe accidents (for example if primary bleed and feed is needed). One train of the safety systems is unavailable due to preventive maintenance. Two SGs are connected to the reactor vessel for residual heat removal in natural circulation, one loop is in reserve mode of operation (with one main isolation valve (MIV) fully closed and one MIV fully open). The RHR is working in the water-water regime and the heat is removed via the technological condenser.
 4. POS4. The RCS temperature is 40°C. The RCS pressure is the atmospheric pressure. The reactor vessel is being open (drainage of vessel level is needed). One train of the safety systems is in the planned maintenance. Two SGs are connected to the reactor vessel; one SG is in the reserve mode. The RHR is working in the water-water regime and the heat is removed via the technological condenser. The water level is increased in the refuelling cavity in the end of POS.
 5. POS5S. The RCS temperature is 40°C. The RCS pressure is the atmospheric pressure. The reactor vessel is open and the refuelling cavity is filled to the refuelling level. One train of the safety systems is unavailable due to the planned maintenance. Two SGs are connected to the reactor vessel; one SG is in the reserve mode. The RHR is working in the water-water regime and the heat is removed via the technological condenser.
 6. POS5L. RCS temperature is 40°C. RCS pressure is the atmospheric pressure. The reactor vessel is open and the refuelling cavity is filled to the refuelling level. All fuel elements are located into the spent fuel pool. One train of the safety systems is unavailable due to the planned maintenance. This POS occurs only once per four years during the long refuelling outage. This POS contains all steps of POS5S. In addition, the reactor vessel inspection is being performed.
 7. POS6. The RCS temperature is 40°C. The RCS pressure is the atmospheric pressure. In this POS the reactor vessel is being closed (drainage of the reactor vessel level is needed). One train of the safety systems is in the planned maintenance. Two SGs are connected to the reactor vessel; one SG is in the reserve mode. The RHR is working in the water-water regime and the heat is removed via the technological condenser.
 8. POS7. The RCS temperature is between $T_{\text{brittle fracture}}$ and 40°C. The RCS pressure is between the atmospheric pressure and 2 MPa. There is a peak pressure of 3.5 MPa during a pressure test. The HPSI pumps are disconnected. These pumps are available for the accident mitigation only under the conditions defined in the limiting conditions of operation. Exception is possible during the severe accident (for example if primary bleed and feed is needed). Initially two SGs are connected to the reactor vessel; one SG is in the reserve mode. The RHR is working in the water-water regime and the heat is removed via the technological condenser. At the end of POS the RCS is heated by five main coolant pumps and the containment is closed.
 9. POS8. The RCS pressure test is performed at the pressure of 13.7 MPa. Also the high pressure dynamic test at the pressure of 17.2 MPa is being performed (once per four years or if new welding is performed in the RCS). The RHR is stopped. If the pressure

test is not successful the plant is returned to POS7. Given the test successful the plant goes to POS9 and the containment is closed.

10. POS9. RCS temperature and pressure is gradually increasing to 200°C and to 12.26 MPa. The RCS coolant is heated by the main coolant pumps. At 180°C the interlocked ESFAS signals are becoming available. All trains of the safety systems are available (exceptions are based on the limiting conditions of operation). The primary to secondary side heat removal is performed in the steam-water regime by the AFW system. All SGs are connected to the reactor vessel.
11. POS10. The reactor is on the power. The RCS pressure is nominal. The temperature is increasing from 200°C to 260°C. All trains of the safety systems are available (exceptions are based on the limiting conditions of operation). At the RCS temperature of 245°C another ESFAS signals are becoming available. At the end of POS the reactor power is 2% of the nominal power.

Examples of POS duration in hours per year are presented in Table 1. Power 1 and 2 is duration of low power operation.

POS	Planned refuelling outages	Unplanned outages +	Planned and unplanned outages
Power 1	18.47	2.91	21.38
POS 1	13.71	3.68	17.39
POS 2	8.96	3.75	12.71
POS 3	34.58	23.61	58.19
POS 4	206.91		206.91
POS 5S	224.66		224.66
POS 5L	1 094.29		1 094.29
POS 6	259.77		259.77
POS 7	107.51	1.89	109.40
POS 8	19.05	0.40	19.45
POS 9	29.41	3.19	32.60
POS 10	79.82	6.61	86.43
Power 2	123.88	7.69	131.57
POS 1-10	$\sum_j = 984.38/1854.01^*$	$\sum_j = 43.13$	$\sum_j = 1027.51/1897.14^*$
Power 1-2	$\sum_j = 142.35$	$\sum_j = 10.60$	$\sum_j = 152.95$

*) Unplanned outages caused by component/system failures and initiated reactor shutdown to corresponding POS.

*) The first number is applicable for short refuelling outage; the second number is applicable for long refuelling outage.

Table 1. Duration of POS

2.2 The initiating events

Defining a list of initiating events is the major step, which influence the whole SPSA development process. While the main aim is similar to power PSA, actual initiators considered in a SPSA are different from those of the power PSA. The profile of initiators also

highly depends on the actual outage considered (lengths and type; forced, refuelling, etc.). Three broad categories of internal initiators are typically considered in a SPSA, and they are as follows:

- Loss of cooling,
- Loss of coolant (LOCA) and
- Reactivity events.

LOCA represents a group of events which result in loss of heat removal from the core. When the core is cooled by the RHR system, its failure is the main initiator in that group.

Loss of coolant events are a challenge to the RCS integrity in the same way as during full power operation. However, the profile and the causes of LOCAs are significantly different in the shutdown mode. In the shutdown mode breaks of pipes and reactor vessel rupture are still possible, but the dominant sources for LOCAs are the drain-down events, including inadvertent opening of valve and similar, both drain-downs to the plant rooms inside the containment or to another system (intersystem LOCA outside the containment) should be considered in a SPSA. Cold over-pressurisation events which are challenging the integrity of primary circuit may be broadly grouped with this category.

Reactivity events are a specific category due to their specific issues and consequences. Reactivity accidents can lead to a local or a full core criticality. Examples like boron dilution, unintentional withdrawal of control rods or refuelling errors are considered in the SPSA. Experience has shown that many such events occurred at NPPs, and their frequencies are high, though the consequences are low (recoveries are possible in many of those events). Some phenomena, like unborated slug of water entering the core and its consequences, are still being analysed.

Like in a full power PSA, hazards can be divided into two groups, internal hazards and external hazards. Internal events include fires, floods and events like drop of heavy loads. These events in comparison to power state are differently treated in a SPSA due to their specific attributes. Internal fire can have higher frequencies in comparison to the power operation. The possible fire locations increase during an outage due to maintenance activities. A fire during an outage is usually initiated by some repair work like welding, while fires during the power operation are usually initiated by electric circuits. Flooding has increased frequency due to maintenance activities where floods would be caused by opening isolation valves and similar activities. Drop of heavy load is an event which is seldom considered in the power PSA but it could have significant impact on the SPSA results. Numerous operations with overhead cranes has actually been analysed in several studies, although the results were not found to dominate the risk profile.

In addition, the external hazards must be taken into consideration: aircraft crash, external meteorological conditions, seismic events and impact of the neighbouring industry.

2.2.1 Grouping of the IE

The initiating event grouping was performed based on the qualitative criteria. Some modifications in grouping are possible later when the frequency of the initiating events is calculated and accident sequence modelling and fault tree modelling is performed.

The qualitative criteria applied for grouping at this stage are the following:

- In order to take benefit from the existing event trees and fault trees, the initiating event groups were selected as much as possible consistently with the list of the initiating event groups for the full power PSA.

- Plant response and core cooling requirements associated with each of the LOCA categories are conservatively assumed to be the same as for the full power conditions. However, this assumption was revised within the system analysis task as one train of the safety systems is unavailable in some POSs. Core cooling requirements can also be relaxed taking into account that at the shutdown conditions the residual heat rate of the core is lower than at the full power conditions.
- Frequency of the initiating events was not taken into account in the first step of grouping. Some of the groups can be screened out due to an extremely low frequency of the events (provided that they do not lead to a severe plant degradation, i.e. they are not expected to have a high risk impact).
- Some of the events with different consequences (risk impact) were assigned to the same group when the consequences did not differ very much. In this case the group is defined based on the event with the highest consequences.
- When the consequences of the events (groups) are expected to be different at least in one POS, such events (groups) are listed separately. However, for some POS these differences may be negligible and many events can be grouped together.
- All events grouped together are not necessarily applicable to the same POS.

Special cases of the event defined as a group representative may have a slightly different consequences. Bounded events have also different consequences than the event defined as a group representative as well as a different origin (contrary to the special cases). List of the events provided as examples is not necessarily exhaustive. Other events that are not indicated as a special cases or examples are expected to be exhaustive.

Further grouping was possible based on the result of data quantification and system analysis tasks. Initiating event frequency was one of the aspects on which further grouping could depend. Generally, it was assumed that the initiating events or IE group could be conservatively included into another group with similar but worse consequences if its frequency was not higher than the frequency of the main event representative for the group. This assumption was verified and the grouping confirmed when the initiating event frequency was finally determined.

Combination of the individual groups was also possible when the plant response and mitigation system requirements were defined more precisely.

2.2.2 Assignment of IE to POS

The first stage of POS assignment was done mostly on the basis of possibility of an occurrence. For instance, the breaks were not considered unless there was an overpressure in the circuit, the human errors associated with a maintenance were not considered unless some maintenance activities were conducted in the specific POS, etc.

In general, the assignment of an applicable POS to the initiating event group was carried out by the considering each event included into the group. In many cases the applicability of POS was dependent on the particular scenario either through a particular plant configuration or through specific maintenance activities associated with a certain POS.

In general, the frequency of IE was not taken into account in the POS assignment process. However, in some cases the frequency was considered in a qualitative way.

For some POS the risk impact of the event was expected to be very low either due to a low frequency or small consequences or both. However, only a qualitative and subjective judgement could be provided to justify such observations. Therefore, the event credibility level is not indicated in the POS assignment results.

However, a credit was given to the fact that during a specific POS the conditions for IE may change (e.g. the pressure is decreasing to atmospheric, so the credibility of a LOCA is diminished). Another aspect that was addressed explicitly was the case when an event was applicable to a part of POS only (but not a negligible part). This aspect was also subsequently considered in an estimating of IE frequency.

Since the selection of POS for IE calculation also depends on the expected frequencies and consequences, another stage of grouping was needed in a co-operation with other PSA tasks. In this stage a consideration was given to the assumptions taken during the accident sequence modelling and to the frequency estimation.

For some POS to which an initiating event was applicable the consequence of this event was considered negligible. The accident sequence task revealed such cases and these events were screened out for these POS. Typical examples of such screening include: events related to loss of the reactor core cooling in POS5S (because of a large inventory of the water in the reactor refuelling pool) and in POS8 (because the system does not need any cooling and the RHR is switched off) or the loss of working cooling pump in any POS (because of a relatively low decay heat generation in the spent fuel pool (exception is POS5S).

Initiating events were considered for the deletion if they lead to the core damage in a time period greater than 24 h. However, it should be noted that simply exceeding this 24 h window was not, by itself, considered to be sufficient reason for deleting initiating events.

Frequency of the events during particular POS was not taken into account in the initial stage of the grouping and POS assignment tasks. For some assigned POS an initiating event (or even a whole group of events) was screened out later due to a low frequency (provided that it was not expected to have a very high risk impact).

The duration of some POS is very short comparing with other POS, so an initiator or even the whole group can be screened out on that basis as well (see Table 1). Example for IE assignment to POS is provided in Table 2.

IE group	Event description	POS number										
		1	2	3	4	5S	5L	6	7	8	9	10
RT(RBD)	Rapid boron dilution											
RT(SBD)	Slow boron dilution											
RAT	Uncontrolled reactivity addition											



Applicable to the POS



Non-applicable to the POS

Table 2. IE assignment to POS – reactivity events

2.2.3 IE frequency calculation

The basic principles for calculation the IE frequencies are the same as for the full power PSA. However, the determination of the IE frequencies for shutdown events is much more plant specific due to configuration, maintenance practices and other issues. In SPSA the frequency of an IE is dependent on POS, and it must be determined for every POS individually.

There are three basic approaches to calculate the IE frequency in a given POS:

- calculation of frequency based on plant specific data,
- calculation of frequency by quantifying a logical model of an initiator and
- considering the full power PSA frequencies of IE with additional recalculation.

Determination of the IE frequencies based on actual operating experience (plant specific data) could be the most accurate approach but in the same time it is the most difficult one. A thorough evaluation of the records on various occurrences during outages is essential in determining the IEs frequencies. It is very important that the evaluation of experience is performed together with the plant personnel who could correctly interpret the information contained in the historical records. The outage schedule as well as POS defined in the previous step should be evaluated to identify the possibility of the occurrences of each specific IE in every POS.

The SPSA studies found that human interactions are a high contributor to the frequencies of many IEs. HRA is used for IE frequency calculation. The IE frequencies considered in the full power PSA may be only the starting point in defining the IE frequencies for SPSA. Many of the full power IEs are not directly applicable and the frequencies may be significantly different during an outage.

In many SPSA studies the frequencies for LOCAs are just adopted from the full power PSA. Such approach causes some controversy as whether:

- LOCAs frequencies should be modified to reflect that the systems are operating at much lower pressure (some analysts argue that non-pressurised primary piping will have the reduced pipe ruptures failure rate).
- LOCAs frequencies should not be modified to be conservative.
- In fact, the contribution to CDF from LOCAs caused by pipe rupture is found to be negligible in the SPSAs. LOCA caused by human errors is much more important.

The following approaches were applied for initiating event frequency calculation:

1. For the initiators that were quantified based on the plant operational history the applicable events are uniformly distributed across all applicable POS. For the time dependent events uniform distribution of the events is assumed within the applicable time period. The following formula is applied for the annual frequency calculation:

$$f_{i,k} = (N_i/T) \times (t_k/\Sigma t_j)$$

where

$f_{i,k}$ - frequency of initiating event „i“ per reactor year per POS „k“,

N_i - number of the applicable operating events reported during exposure time period

T ,

T - exposure time in reactor years,

t_k - duration of POS „k“, hours,

Σt_j - total duration of applicable POS, hours.

2. For the events that were quantified based on full power data it is assumed that the initiating event frequency per hour of the full power operational states is the same for the applicable shutdown states. The following formula is applied for the annual frequency calculation:

$$f_{i,k} = f_{i,FP} \times t_k/T_{FP}$$

where

$f_{i,k}$ - frequency of initiating event „i“ per reactor year per POS „k“,
 $f_{i,FP}$ - frequency of initiating event „i“ per reactor year for full power operational states (generic or based on full power operational statistics),
 t_k - duration of POS „k“, hours,
 T_{FP} - exposure time for full power operation in hours per reactor year.

- Human reliability analysis is applied for several initiators that involve human actions and never occurred in the plant. These included the initiating events related to the cold over-pressurization, man induced LOCA and boron dilution. In the most cases there is the inadvertent actuation leading to the initiating events. The frequency is calculated based on HRA. In general, the probability of the inadvertent actuation is calculated from the following formula:

$$P_{IC} = P_I \times P_C$$

where P_{IC} is the probability of not corrected inadvertent actuation, P_I is the probability of the inadvertent actuation and P_C is the conditional probability that the error is not corrected. The commission error probability or probability of the inadvertent actuation (opening) is $P_I = 3.0E-3$, the conditional probability that the error is not corrected $P_C = 0.1$. The probability of the inadvertent actuation is $P_{IC} = 3.0E-4$.

- Bayesian approach is applied to calculate the initiating event frequency for the events which never occurred in the plant and the IE frequency can not be calculated using HRA. After updating the prior frequency by the plant specific frequency the posterior frequency is received.

2.3 The screening process

IE with available recovery times longer than 24 hours could be screened out without much danger of leaving out important results. IE with very short recovery times, which are those earlier in an outage and which involve very specific system availability, shall not be screened-out because of their generally high importance.

Screening process can be performed in two phases:

- After screening-out the clearly unimportant events, the draft event trees can be developed for remaining sequences.
- The remaining sequences then could be analyses qualitatively or/and quantitatively.

The main idea of the whole process is to select events of higher safety significance and to reduce the level of details in modelling work for sequences with lower safety impact. The final step in the screening process is re-grouping of POSs and initiators. The result of the whole process is a list of safety important POSs and IE groups. The SPSA requires iterative processing for re-defining and re-grouping POSs and IEs several times during the process. Development of detailed accident sequences (including supporting TH analysis, HRA, etc.) is the most labour intensive part of the SPSA. Its aim is to focus on essential issues only. Establishment of a systematic screening procedure is the best way of removing unimportant accident sequences.

2.4 The accident sequences

2.4.1 The fault trees

The fault tree models developed for the full power PSA could be used, with exceptions, as a basis for SPSAs as well. Revision of the models is necessary due to the following reasons:

- system is operational in shutdown (it is in the standby mode during power operation),

- system actuation is manual (it is automatic during power operation),
- mission time is different,
- system success criteria changes with POS,
- redundancies are different in different POSs,
- recovery possibilities are different and
- system alignment is different for individual POSs.

2.4.2 The event trees

The accident sequence modelling is usually performed using event trees. The event trees developed for full power PSA may be modified for use in SPSA. The modification will typically include removal of some headings (i.e. reactor trip) and relaxation of the others due to lower decay heat levels. Some new headings may be added to reflect operator actions which may not be possible during power operation.

Shutdown state also has some specific characteristics which are not modelled in the full power PSA. Operation of the RHR system and related operator responses often requires development of new sequence models. A longer time is available to operators to recover from initial failures. Possibilities to establish non-conventional accident mitigation (as an example, supplying water into the open reactor vessel) require from the PSA analysts to consider options which have not been addressed in the full power PSA.

2.5 The human reliability analysis

Human reliability analysis is the most important issue in a SPSA. Both the plant outage and the start-up activities involve a large number of operator actions, functional tests and maintenance activities. All of those have to be correctly introduced in a SPSA.

In a SPSA different types of human actions are considered:

- human actions before initiating event, affecting availability of equipment,
- human actions as an IE,
- procedure based post-accident human interactions to terminate an IE,
- human recovery actions to recover the failed equipment or to terminate an event.

Compared to the full power PSA, human interaction analysis in a SPSA is much more complex since they require identification of actual ways the work is being done and consideration of interactions which are not obvious.

The following issues needed to be addressed when evaluating the human interactions during outage safety analysis:

- operating procedures,
- supervision on maintenance activities,
- appreciation of risk during shutdown and
- comprehensive and appropriate training.

The following steps are important for considering human interactions:

- identify all possibly important human interactions during plant outage,
- screen these human interactions and prioritise them from the risk perspective, and
- collect information from plant experience during shutdown operating mode, and establish human error data base.

During an outage, the dependencies between human errors tend to be much more complex than during power operation. Testing and maintenance activities during shutdown operation create new dependencies which need to be identified and documented. Cross-

connections and support system status may cause hidden dependencies which need to be taken into account.

2.6 Quantification of accident sequences

Quantification of accident sequences is performed for all POSs. First, the total CDF is presented for an average refuelling outage, short refuelling outage and long refuelling outage. Then, the dominant initiating events, accident sequences, minimal cut sets and dominant categories of the basic events are identified. Results of the importance and sensitivity analyses are also summarized.

The task is similar to quantification in the power PSA. However, the sources of data as well as the procedure to develop a data base may be different. Data for component unavailability for SPSA have significantly different emphases than for the power PSA. While in the power PSA the unavailability of safety components are (often) dominated by the failures in stand-by, in SPSA they are clearly dominated by maintenance unavailability. Maintenance schedules and actual duration of various tests and maintenance actions are carefully evaluated to determine the actual equipment availability. Quantification of accident sequences, uncertainty and sensitivity analysis follow the same methodological approach as for the full power PSA. Due to various influences, it was shown that the SPSA results typically have higher uncertainties.

The dominant initiating events identified for all POSs are presented in Table 3. This is graphically depicted in the pie chart in Fig. 2. Instantaneous CDF for each POSs is presented in Fig. 3. The dominant contributions to the total CDF are from POS6, POS4, POS7, POS5S, POS3 and POS5L. The combined contribution of these POSs is 98.1% of total CDF.

No.	Initiating event	Description	CDF [1/y] mean value	Contribution to total CDF (%)
1	LOSW(OP)	Loss of service water	1.14E-5	20.5
2	LNC(GP)	Loss of natural circulation - gas penetration	1.12E-5	20.3
3	L(MI-SL)	Man-induced small LOCA	9.81E-6	18.0
4	LOP	Loss of offsite power	7.77E-6	14.1
5	LRHR	Loss of residual heat removal	5.95E-6	10.8
6	COVPR	Cold over-pressurisation	1.87E-6	3.4
7	LVBB	Loss of vital 6 kV bus bar	1.43E-6	2.6
8	LNC(OD)	Loss of natural circulation - over-draining	1.32E-6	2.4
9	LBA(B)	Leakage in the spent fuel pool	1.32E-6	2.4
10	LNVBB	Loss of non-vital bus bar	1.27E-6	2.3

Table 3. The dominant IE for all POSs

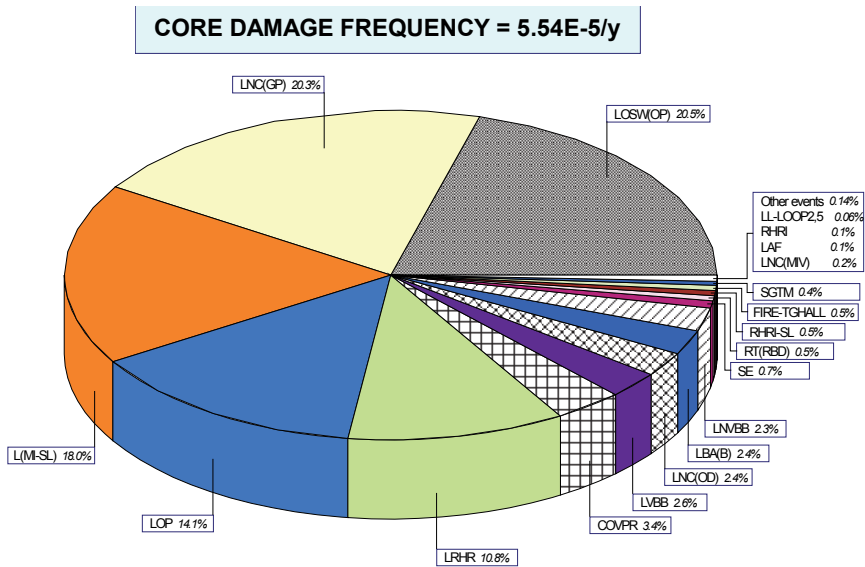


Fig. 2. The average core damage frequency with dominant IE for a WWER440 plant for all POSs

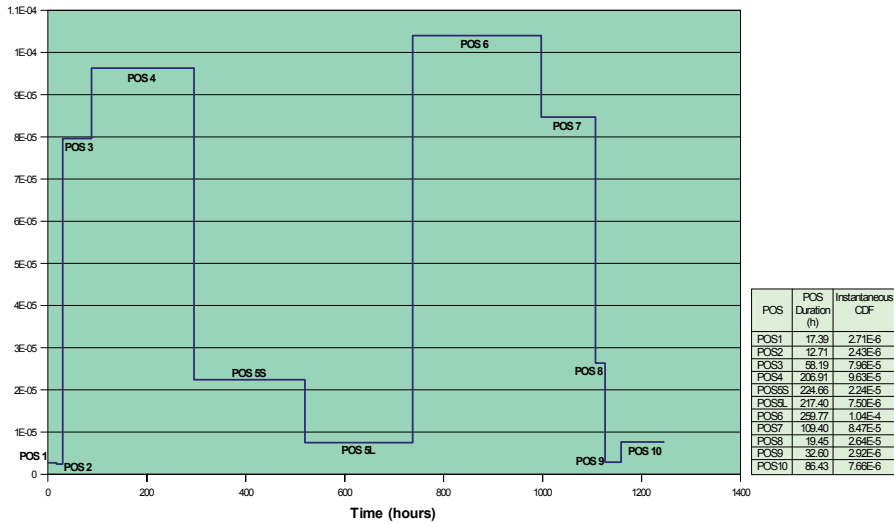


Fig. 3. Instantaneous CDF for each POS

2.7 Application of SPSA

The following applications of SPSA model and results are considered:

- outage planning and scheduling,
- optimization of operating and maintenance procedures,

- optimization of limiting conditions of operation,
- accident procedures, emergency planning and
- making decision on hardware modification.

The Equipment Out Of Service (EOOS) risk monitor is developed for the J.Bohunice V2 plant in Slovakia. The monitor is used by operator and schedulers of maintenance (see Fig. 4, 5 and 6).

An example for SPSA application is described for the preventive maintenance strategy of the safety systems in the plant: 1) the maintenance activities are performed in operating mode 5 (reactor cavity not flooded) and 6 (the reactor cavity is flooded), 2) only a single train is under preventive maintenance, 3) the second safety train is available based on limiting condition of operation, 4) the third safety train can be or can not be available, the availability is not required by limiting condition of operation, 5) the systems that could be used for decay heat removal and accident mitigation should be available to the maximum extent possible but this is not the case in the plant. Recommendation for changes from SPSA: 1) planned maintenance activities will begin when the reactor cavity is flooded, 2) availability of all three safety trains will be required by limiting conditions of operations, 3) one train out of three is allowed to be unavailable due to preventive maintenance.

3. Modelling issues related to Level 2 SPSA

3.1 The plant damage states

The level 1 PSA sequences are terminated and the level 2 PSA sequences are started with the core damage. The interface between the level 1 and level 2 PSA is accomplished through the definition of plant damage states (PDS). The PDS defines the plant state at the beginning of the core damage and defines the conditions necessary for conducting severe accident progression analysis. PDS are developed as an initial step to a level 2 PSA. The status of some safety systems may not be identifiable from the level 1 PSA models. So, their availability during various core damage sequences must be addressed by means of an extension to the level 1 system models. In the level 2 PSA, post core damage recovery actions (using the existing system in automatic or manual mode) are also identified.

The criteria for binning the level 1 sequences into the plant damage states are based on the following five characteristics of each sequence:

- IE,
- Time to core damage,
- Status of high pressure and low pressure safety injection system,
- Status of containment spray system and
- Status of containment isolation.

The PDS are further grouped based on POS of the plant at power operation and during refuelling outage. Several POS groups (G0 - G4) were introduced to facilitate the PDS grouping process:

G0: Full power operation

G1: POS1, 9 and 10, which are essentially similar to the full power operation. Both the RCS and the containment are normally closed.

G2: POS2, 3, 7 and 8 in which the RCS is closed but the containment is open.

G3: POS4, 5S and 6, in which both the RCS and containment are open. The fuel is located in the reactor vessel.

G4: POS5L, which is a special case because the fuel is relocated to the spent fuel pool.

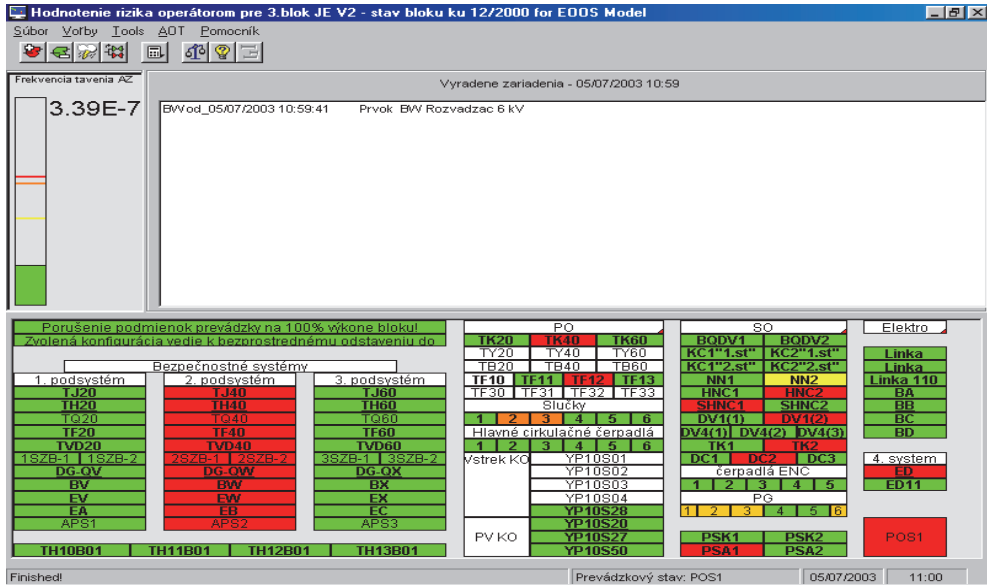


Fig. 4. Risk monitor for the operator (components in red colour are unavailable, CDF = 3.39E-7/y)

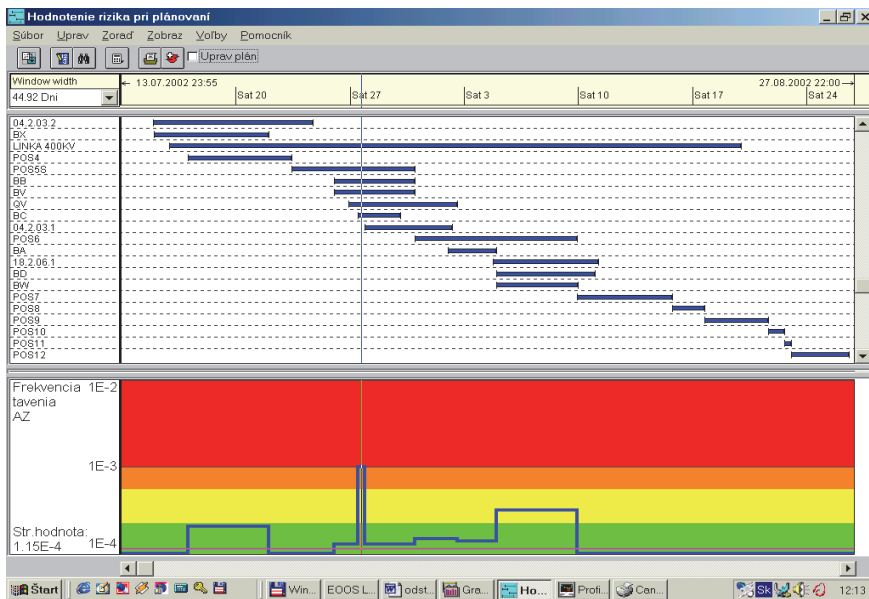


Fig. 5. Risk monitor for planning of maintenance activities (high risk profile)

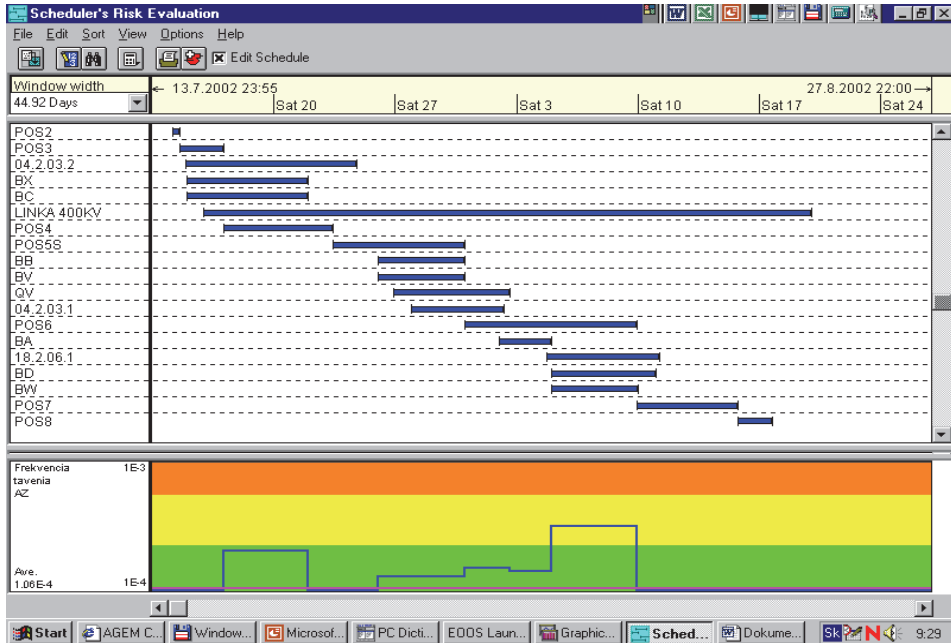


Fig. 6. Risk monitor for planning of maintenance activities (low risk profile)

3.2 Accident progression analysis

The MELCOR code is used to model all aspects of the severe accident progression, including:

- reactor coolant system thermal-hydraulic response to the initiating event prior to the core damage,
- core heat up, fuel degradation and material relocation within the reactor vessel,
- possible failure of the reactor vessel pressure boundary, and subsequent release of molten fuel and core debris to the containment,
- thermal and chemical interactions between the core debris and containment structures, such as concrete floors, and the containment atmosphere, and
- containment behaviour (including its pressure and temperature history, hydrogen mixing and combustion, and the effect of the operation of containment safeguard systems).

This code provides an integrated framework for the evaluating the timing of key accident events, thermodynamic histories of the reactor coolant system, core and containment, and corresponding estimates of fission product release.

3.3 Containment performance analysis

Deterministic calculations of severe accident progression generate pressure and temperature histories within the containment during the various accident sequences. To determine whether the containment pressure boundary will be able to withstand the loads, quantitative estimates of its structural performance limits must be generated.

Challenges to the containment integrity can take many forms. Therefore, the analysis of containment performance limits must address several topics. Typically, the following containment challenges are considered:

- internal, rapid and slow pressurization transients greater than nominal design conditions,
- high temperatures,
- thermal-mechanical erosion of concrete and steel structures (if contact with ejected core debris is possible),
- impact from internally-generated missiles and
- localised dynamic loads, such as shock waves, hydrogen detonation, etc.

In some instances, these challenges may exist simultaneously. For example, high temperatures often accompany high pressures.

Engineering calculations of structural response to these types of challenges are performed as part of the level 2 PSA. Quantitative failure criteria are developed as the primary reference for estimating the likelihood of containment failure for a wide spectrum of accident sequences. These criteria are based on plant specific design and construction data and represent realistic material response properties.

3.4 Construction of the containment event trees

Probabilistic model in the form of containment event trees (CET) is constructed for the evaluating the containment performance. The model is displaying the alternative accident progressions that may evolve from a given core damage sequence or a plant damage state.

The initiating event of the containment event tree is the PDS. During the construction of CET the following issues are taken into consideration:

1. Important time phases of severe accident progression. Different phenomena may control the nature and intensity of challenges to the containment integrity and the release of radionuclides as an accident proceeds in time. The following time frames are identified:
 - After the core damage begins, but prior to failure of the reactor vessel lower head. This period is characterised by the core damage and radionuclide release from the fuel while core material is confined within the reactor vessel. Hydrogen detonation is possible.
 - Immediately following reactor vessel failure. The level 2 PSA analysis concludes that many of the important challenges to the containment integrity occur just following reactor vessel failure. They often occur as a direct consequence of the release of molten core materials from the reactor vessel to the reactor cavity.
 - Long term accident behaviour. In the absence of the heat removal to the environment, the loads may steadily increase to the point of containment failure in a long term.
 - It must be noted that release is possible also from the containment which remains intact via the normal leakage.
2. Probabilities associated with events in the CETs are of different types: failure probability of safety system, probability that a human will not perform specific activity or probability of accident phenomena (for example hydrogen burn). Probabilities in the first two cases are developed in similar manner as in the level 1 PSA. The last one represents uncertainty in the occurrence or effects of severe accident phenomena. In this case, the split fraction associated with this event is not based on reliability data. Rather,

it is a reflection of the uncertainties in the engineering analyses required to characterise hydrogen generation, release, distribution and combustion. The probabilities are obtained using decomposition event trees.

3. Recognition of the interdependencies of phenomena. Most severe accident phenomena and associated events require certain initial or boundary conditions to be relevant. For example, a steam explosion can only occur if molten core debris comes in contact with the water. Therefore, it may not be meaningful to consider ex-vessel steam explosions during accident scenarios in which the reactor cavity is dry at the time of vessel breach. Logic models for evaluating containment performance capture these and many other such interdependencies among severe accident events and phenomena.

3.5 Source terms

Estimation of the magnitude of fission product release to the environment (i.e. source terms) are a major product of a level 2 PSA. Plant specific source terms were evaluated for the Slovak plants.

The following source terms categories are defined:

1. STC1 - containment intact, containment spray available, no vessel failure,
2. STC2 - containment intact, containment spray unavailable, no vessel failure,
3. STC3 - containment intact, containment spray available, core cooling recovery after vessel failure,
4. STC4 - containment intact, containment spray unavailable, core cooling recovery after vessel failure,
5. STC5 - containment intact, containment spray available, no core cooling recovery after vessel failure,
6. STC6 - containment intact, containment spray unavailable, no core cooling recovery after vessel failure,
7. STC7 - very early containment failure before vessel failure,
8. STC8 - release from the spent fuel pool,
9. STC9 - early containment failure at vessel failure, no core cooling recover after vessel failure,
10. STC10 - late containment failure after vessel failure, core cooling recover after vessel failure,
11. STC11 - late containment failure after vessel failure, no core cooling recover after vessel failure,
12. STC12 - late containment failure without vessel failure,
13. STC13 - containment not isolated, containment spray unavailable, vessel failure
14. STC14 - containment not isolated, containment spray unavailable, open reactor vessel, no vessel failure,
15. STC15 - containment not isolated, containment spray unavailable, open reactor vessel, vessel failure,
16. STC16 - containment bypassed after SGTR,
17. STC17 - containment bypassed after interfacing LOCA.

3.6 Large early release

The effective doses are identified from the source term for the public. Based on the effective doses the countermeasures are implemented, as for example evacuation. Based on an

estimate of the effective dose that could be avoided by implementing a particular countermeasure, the lower and upper emergency reference levels are defined. Below the lower level, introduction of the countermeasure would not be justified because of the harm that it would cause. The upper level is the dose level at which every effort should be done to introduce the countermeasure, except in exceptional circumstances. It is set at ten times the dose of the lower level.

The lower and upper levels for sheltering are a dose of 5 mSv and 50 mSv respectively. For evacuation, they are 50 mSv and 500 mSv. These are higher than the recommended dose limit for routine exposure, which is 1 mSv per year for the public. This is because the dose levels are not intended to represent the boundary between what is 'safe' and what is 'unsafe', but to represent an acceptable balance between the harms and benefits of an action. In case of fission product release the release is large if more than 1% caesium is released to the environment from the core inventory. It can correspond to the dose of 50 mSv/y for the public. Large early release is a release to the environment before implementation of required countermeasure (before evacuation). For the purpose of the WWER440 units it is considered that the evacuation can not be performed until 10 h from the beginning of the accident. The release until 10 h is the early release.

For the groups G0, G1 a G2 the Large early release frequency (LERF) is given as sum of frequencies of the following source term categories: STC7 + STC9 + STC13 + STC16 + STC17. For group G3 the LERF is given by STC14 and STC15 (the reactor vessel is open, the containment is open). For group G4 the LERF is given by STC8 (the spent fuel pool is outside the containment).

3.7 Results

The source term category 14 for group G3 is presented in Table 4 for illustration of the results. The fission product groups Xe, I and Cs are presented in table with the corresponding frequency.

Source term category	Frequency 1/y	Beginning of the release	Xe [%]	I [%]	Cs [%]
14	4.08E-6	Early	94.8307	86.0377	83.8331

Table 4. The source term categories for group G3

The risk of fission product release from the spent fuel pool is very small in operating mode 7. The source term category frequency is 3.0E-9/y. However, the quantity of fission products in the source term is extremely high because the pool is located outside the containment and the spray system has no impact on the fission products which can be released into the environment. The fuel inventory is also higher in comparison with the core inventory.

The LERF for each group G0-G4 is less than 1.0E-5/y. The requirement of the Nuclear Regulatory Authority is met.

4. Conclusion

The level 1 shutdown risk of the WWER440/V213 plants presented in the form of CDF was higher than the risk coming from the full power operation. Safety measure were implemented which significantly decreased the CDF. After implementation of the proposed

changes the same level of risk is achieved for shutdown operating modes as for the full power operation.

The changes in the limiting condition of operation are the most important from the shutdown risk reduction point of view. In operating mode 5 and 6 only one train of safety system was required to be available. Now the limiting conditions of operation require the availability of safety system trains to the maximum extent possible. It was also recommended that the preventive maintenance for all three trains of safety systems should be done only in operating mode 6, when there is high water level in the reactor refuelling cavity and more than 30 h are required to core uncover after loss of residual heat removal. Symptom-based emergency operating procedures (SB EOPs) for shutdown operating modes, developed by Westinghouse and implemented in the Slovak NPPs, also significantly reduce the risk.

In addition, risk reduction factor of automatic operation of low pressure safety injection pumps during shutdown operating modes is also high.

The level 2 shutdown risk in POSs with open reactor vessel and open containment was also higher than the full power risk. The reason was in high core damage frequency in plant operational state during shutdown (groups G2 and G3). The proposed safety measures decreased the risk arising from the high core damage frequency. So, also the level 2 risk is decreased. Further decrease of the level 2 risk can be achieved after planned implementation of Severe accident management guidelines (SAMGs) for shutdown operating modes, being developed by Westinghouse.

The risk of fission product release from the spent fuel pool is very small in operating mode 7. The source term category frequency is $3.0E-9/y$. However, the quantity of fission products in the source term is extremely high because the pool is located outside the containment and the spray system has no impact on the fission products which can be released into the environment. The fuel inventory is also higher in comparison with the core inventory.

The full power, low power and shutdown PSA models of the Slovak NPPs are periodically updated. Risk monitors are used to generate the risk profiles and to maintain the risk on the acceptable level for all operating modes. SB EOPs and SAMGs from Westinghouse guarantee high reliability of operators in post-accident situations.

5. References

- US NUCLEAR REGULATORY COMMISSION (1989): Severe accident risks: an assessment for five U.S. Nuclear Power Plants - NUREG-1150, USNRC
- Kovacs, Z. et al. (2002): Post-reconstruction Shutdown Level 1 PSA Study for Unit 1 of J. Bohunice V1 NPP, Summary Report, RELKO Report, No. 0R0400, Bratislava
- Kovacs, Z. et al. (2008): Full Power and Shutdown Level 2 PSA Study for Unit 1 of Mochovce NPP, Main Report, RELKO Report, No. 5R0506, Bratislava
- OECD (2007): Recent Developments in Level 2 PSA and Severe Accident Management, NEA/CSNI/R
- IAEA SAFETY STANDARD SERIES (2008): Development and Application of Level 1 Probabilistic Safety Assessment for Nuclear, DS349, Vienna
- IAEA SAFETY STANDARD SERIES (2002): Probabilistic Safety Assessment of NPPs for Low Power and Shutdown Modes, TECDOC-1144, IAEA, Vienna

A Study on the Actuator Efficiency Behavior of Safety-Related Motor Operated Gate and Globe Valves

Shin Cheul Kang, SungKeun Park, DoHwan Lee,
YangSeok Kim and DaeWoong Kim
*Nuclear Power Laboratory, KEPRI
Korea*

1. Introduction

A motor operated valve (MOV) consists of a motor, an actuator, and a valve. Fig. 1 shows a schematic diagram of an MOV. A motor that is bolted to the actuator housing drives the actuator. Attached to the motor shaft is the pinion gear, which drives a gear train. The gear train drives a worm that is splined onto the opposite end of the worm shaft. This worm assembly is capable of moving axially as it revolves with the worm shaft. The axial movement is a means of controlling the output torque of the actuator. The worm drives a worm gear that rotates the drive assembly. As the drive sleeve rotates, the stem nut raises or lowers a valve stem. When the valve is seated or obstructed, then the worm gear can no longer rotate, and the worm slides axially along its splined shaft compressing a spring pack. This axial movement operates a torque switch, causing the motor to be de-energized.

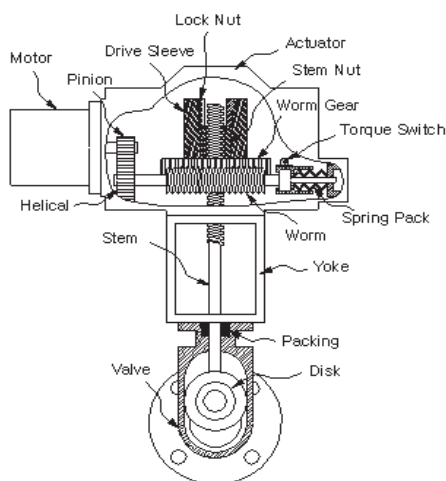


Fig. 1. Schematic diagram of MOV

An MOV with such operational principles is an essential element to control the piping flow in nuclear power plant or other facilities. In fact, the operational failure of a safety-related MOV in a nuclear power plant can have catastrophic results. Therefore, it is necessary that the operability of the safety-related MOVs should be integral and required in the design basis conditions. The US Nuclear Regulatory Commission (NRC) issued Generic Letter (GL) 89-10 regarding safety-related MOV testing and surveillance (USNRC, 1989). Subsequently, in South Korea, the Korea Institute of Nuclear Safety (KINS) required similar testing and verification, as follows:

- Reviewing and documenting the design basis for the operation of each MOV
- Establishing the correct switch settings
- Demonstrating the MOV to be operable at the design basis differential pressure and/or flow

Once the operability of each MOV was proven, the need arose to preserve the operability of every tested MOV to maintain the safety of nuclear power plants. The USNRC and KINS issued regulatory requirements, which specify periodic verification (PV) of the operability of MOVs. The requirements recommend utilities to develop an effective PV program of MOV design capability, considering the fact that aging can decrease the thrust/torque output of motor actuators (USNRC, 1996). To address the two types of requirements described above, at least in part, Korean nuclear power plants have implemented static diagnostic tests that can provide information on the thrust/torque output of the motor actuator, and any changes to the motor-actuator output as a result of aging effects. The first static test for each MOV had been conducted from 1999 to 2004, in order to guarantee its operability and design basis conditions. The second static test has been conducted from 2005, ongoing to the present, in order to implement PV requirements. Up until 2009, it had been assumed that the actuator efficiency, one of the most important factors in evaluating the motor actuator output, does not degrade over time. In other words, the design efficiency provided by manufacture had been used in the calculation of motor actuator output. In addition, in the event that the design efficiency had not been provided by the manufacturer, the design efficiency of other manufacture with similar motor speed and actuator size had been used.

Therefore, the purpose of this chapter is to confirm the validation of the design efficiency by analyzing the efficiency behavior over time for motor operated gate and globe valves with rising stem, and comparing the design efficiency with the efficiency calculated from a method that is introduced in this chapter.

It is presented herein that most actuators of gate and globe valves have minor variations in efficiency from test-to-test, but no increasing or decreasing trend over time, as well as demonstrating higher efficiency than the design efficiency. The efficiency variations for some actuators with lower motor speed, lower actuator size, and lower gear ratio also were not increased or decreased over time, but their design efficiency was susceptible to decrease below the their original value. For those actuators, the threshold efficiency was calculated for the purpose of replacing their design efficiency.

From 2010, those results with two other evaluation studies over time on stem/stem nut friction coefficient and valve disk/seat friction coefficient have been applied for the PV program of safety-related MOVs in Korean nuclear power plants. The three studies including the contents introduced in this chapter have helped us to develop optimized PV program that can enhance the operability of the valves. Furthermore, they have made key roles in extending the maximum test frequency from 5 years to 10 years.

2. Calculation of actuator efficiency

2.1 Data acquisition

As described in Section 1, the diagnostic static tests have been conducted to ensure the motor actuator output of safety-related MOVs for 20 units of nuclear power plants from 1999 to the present in Korea. For each valve, more than two tests have been conducted. The first test was the design basis test from 1999 to 2004, and the second was the periodic test from 2005 to 2009. Each test was composed of one 'as-found' and two 'as-left' tests to compare and analyze conditions before and after maintenance jobs, according to the field test procedures. The comprehensive static test data for each valve were used in this study.

In the tests, the actuator torque and the three phases of currents and voltages were measured from the strain gage type sensor attached on the stem, and current and voltage probes installed at the power lines toward the actuator, respectively. Fig. 2 shows the sensors installed to measure currents and voltages at the valve. The measured values for gate and globe valves were used in analyzing their respective actuator efficiency behavior.



Fig. 2. A picture of installed sensors at a valve test

2.2 Efficiency calculation process

The actuator efficiency is a factor transferring motor torque produced by an electric motor into actuator torque, necessary in rotating actuator inner gears. The typical efficiency can be calculated using the following expression:

$$\eta = \frac{Tq}{MTq \times OVR} \quad (1)$$

Where η is the actuator efficiency, $Tq[ft-lb]$ is the actuator torque, $MTq[ft-lb]$ is the motor torque, and, OVR is the overall gear ratio provided by the manufacturer. In this study, the equation (1) was used to calculate the efficiency.

2.2.1 Data preparation

As shown in equation (1), the values of actuator torque and motor torque can be used to calculate the efficiency. The measured actuator torque in the static tests was applied directly for the equation (1). The motor torque was not measured directly in the static tests. Accordingly, in order to calculate actuator efficiency, a method to estimate motor torque

was introduced. In this chapter, the motor torque was estimated by a motor torque estimator, NEET (S.C. Kang et al., 2006), which can estimate the motor torque using the three phases of currents and voltages, and resistance values between phases measured in the static tests. The NEET was developed on the basis of several assumptions. First, the stator windings are assumed to be sinusoidally wound to couple only to the fundamental-space-harmonic component of air-gap flux. Second, the self-inductances of the rotor are assumed not to vary with rotor angular position. Finally, linear magnetics are assumed. Under these assumptions, the air-gap torque produced by a two-phase induction motor, which can be transformed from the three-phase induction motor is given by

$$T = P(\lambda_{s\alpha}i_{s\beta} - \lambda_{s\beta}i_{s\alpha}) \quad (2)$$

Where, $\lambda_{s\alpha}$ and $\lambda_{s\beta}$ are the flux linkages of the two stator phases. $i_{s\alpha}$ and $i_{s\beta}$ are the currents of the two stator phases and P is the number of pole pairs. The currents $i_{s\alpha}$ and $i_{s\beta}$ can be directly measured at the stator terminals. The flux linkages can also be determined from terminal measurements. For a two-phase machine,

$$\begin{bmatrix} v_{s\alpha} \\ v_{s\beta} \end{bmatrix} = R_s \begin{bmatrix} i_{s\alpha} \\ i_{s\beta} \end{bmatrix} + \frac{d}{dt} \begin{bmatrix} \lambda_{s\alpha} \\ \lambda_{s\beta} \end{bmatrix} \quad (3)$$

Where, $v_{s\alpha}$ and $v_{s\beta}$ are the two stator voltages and R_s is the stator phase resistance. Thus, the motor torque is expressed only in terms of stator variables, which can be measured in field test. Except for the NEET, other motor torque estimators can be used in the estimation of motor torque. Fig. 3 shows an example of motor torque signal estimated by NEET using the electrical data acquired from a field test.

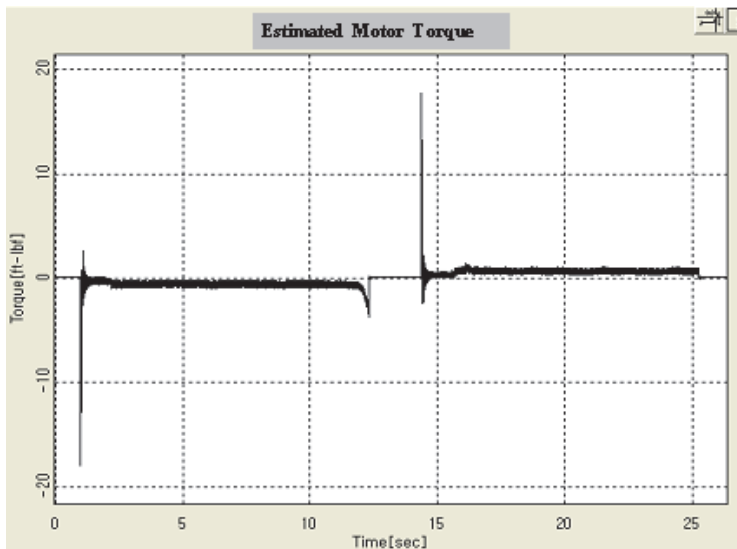


Fig. 3. An example of motor torque signal estimated by NEET

2.2.2 Efficiency calculation

By substituting the estimated motor torque, the measured actuator torque, and the overall gear ratio provided by manufacturer into the equation (1) the efficiency can be calculated easily.

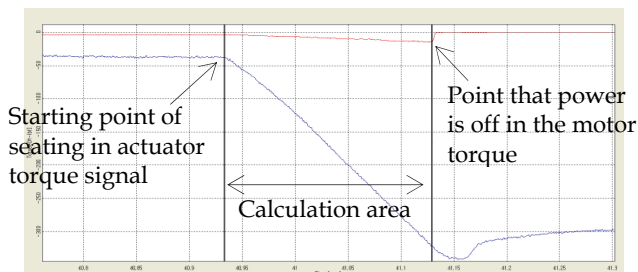


Fig. 4. An example of efficiency calculation area

In this study, the added algorithm into the NEET for the calculation of efficiency was used, and the efficiency calculation procedures from the algorithm are as follows:

- a. Read the estimated motor torque signal.
- b. Read the measured actuator torque signal.
- c. Input the overall gear ratio.
- d. Establish the area to be analyzed from the two signals above (Fig. 4): the left and right reference points of the area were set up based on the starting point of seating in the actuator torque signal, and the point in the motor torque signal where power is turned off, respectively.
- e. Calculate the actuator efficiency of each point within the established area, including the reference points by using the equation (1) (Fig. 5).
- f. Calculate the average actuator efficiency by dividing the total sum of efficiency of each point by the total number of points in the area. As a matter of convenience, the average actuator efficiency is referred to as the actuator efficiency henceforth.
- g. Calculate the two 'as-left' actuator efficiencies of the design basis test, and 'as-found' efficiency of the periodic test for each valve by applying the procedures from (a) to (f).
- h. Calculate the average value of the two 'as-left' actuator efficiency (avg. 'as-left' efficiency), the difference between avg. 'as-left' efficiency and the 'as-found' efficiency (Δ efficiency), and the time interval between design basis test and periodic test needed to analyze the efficiency behavior over time.

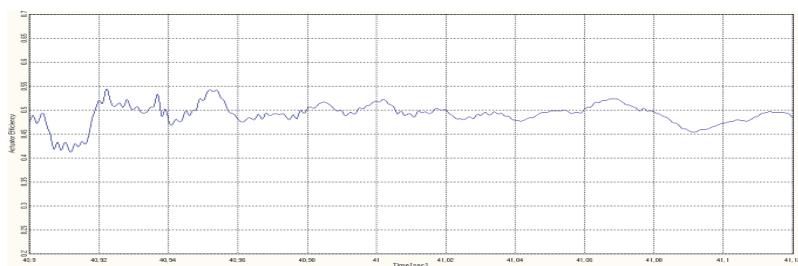


Fig. 5. An example of calculated actuator efficiency for each point

2.3 Efficiency behavior analysis process

As the known equation (1), actuator efficiency is dependent on motor torque, actuator torque, and the overall gear ratio. One of the important parameters in determining the motor torque output is motor speed. In addition, one of the important parameters in determining the actuator torque output is maximum motor torque rating. Accordingly, the motor speed, maximum motor torque rating, and overall gear ratio were selected as major factors in analyzing the efficiency behavior for gate and globe valves. The design information about these factors included in this study is described in Table 1.

The efficiency behavior by the three factors described above was analyzed according to the following process:

- Analyze the distribution of the avg. 'as-left' and 'as-found' efficiencies based on the test-to-test time interval in order to address the potential degradations with the passage of time. The time interval covers the efficiency variations over a period of several years.
- Compare the avg. 'as-left' and 'as-found' efficiency with the design efficiency. In this study, the pullout efficiency, which is the lowest efficiency among the starting, stall and pullout efficiencies usually provided by manufacturers, was selected as the design efficiency because most nuclear power plants use the efficiency in the calculation of the actuator output torque.
- Modify the design efficiency based on the analysis results of item (b), if necessary.

Motor Manufacturer	Motor Speed (RPM)	Actuator Manufacturer	Actuator Model	Overall Gear Ratio	Max. Torque Rating	Design Efficiency
Reliance	1800	Limitorque	SMB-000	33.5~62.5	120	0.4
			SMB-00	23~81.1	260	0.4
			SMB-0	34.9~54.8	700	0.4
			SMB-1	50.4~60.1	1100	0.4
				103.2		0.35
			SMB-2	26.4~67.4	1950	0.4
			SMB-3	53.7~70.9	4200	0.4
				98.6		0.38
			3600	AMB-000	SMB-000	36.5
	SMB-00	34.1~41			260	0.45
		67.5				0.4
	SMB-0	31.3~39.1			700	0.45
	SMB-1	27.2~35.9			1100	0.45
	SMB-2	46.6~82.5			1950	0.4
	SMB-3	66.1~70.9	4200	0.4		

Table 1. Design information of tested valves

3. Efficiency behavior

Fig. 6 to 8 depict the actuator efficiency distribution for the avg. 'as-left' efficiency (\diamond blue), 'as-found' efficiency (\square red), and Δ efficiency (\triangle green) by motor speed, maximum motor torque rating, and overall gear ratio, respectively. In the figures, the x-axis is the time interval between the design basis test and the periodic test. The y-axis includes the actuator efficiency and Δ efficiency (-0.2 to +0.2). The figures also include the design efficiency provided by manufacturer. Based on the results displayed in the figures, the efficiency behaviors over time were analyzed.

3.1 Motor speed

The efficiency distribution of the actuators with design efficiency, 0.4 was shown in Fig. 6 by the motor speed 1800 RPM (Fig. 6a) and 3600 RPM (Fig. 6b). In both figures, Δ efficiency was distributed in the positive and negative areas evenly over time. The actuator efficiencies have variations in efficiency from test-to-test, but no increasing or decreasing trend over time. However, from the distribution of the avg. 'as-left' efficiency and 'as-found' efficiency, most of the actuators with 3600 RPM are observed to possess greater efficiency than the design efficiency, 0.4, while some actuators with 1800 RPM have lower efficiency than the design efficiency. From those observations, we concluded that motor speed does not affect the age-related or service-related degradation, while the efficiency of actuators with 1800 RPM can be susceptible to a decrease below the design efficiency.

3.2 Overall gear ratio

In order to analyze if the OVR affects the potential degradation in efficiency, the various OVRs were grouped by 20~40, 40~60, and 60~80 (Fig. 7a, 7b, 7c). The design efficiency of the groups is 0.4. In the three figures, Δ efficiency was distributed in the positive and negative areas evenly over time. The actuator efficiencies have variations in efficiency from test-to-test, but no increasing or decreasing trend over time.

However, the greater number of actuators was distributed in the area below design efficiency as the OVR increased. From those observations, we concluded that OVR does not affect the age-related or service-related degradation, while the efficiency of actuators with more OVR can be susceptible to a decrease below the design efficiency.

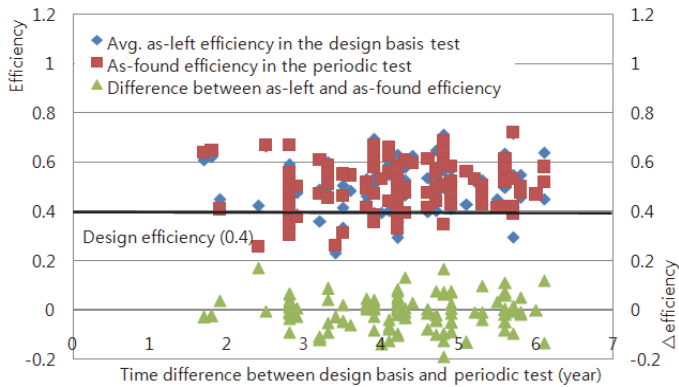
3.3 Maximum motor torque rating

The efficiency distribution of the various actuators was shown in Fig. 8 by the maximum motor torque rating (Fig. 8a to Fig. 8n). In the figures, Δ efficiency was distributed in the positive and negative areas evenly over time. The actuator efficiencies have variations in efficiency from test-to-test, but no increasing or decreasing trend over time.

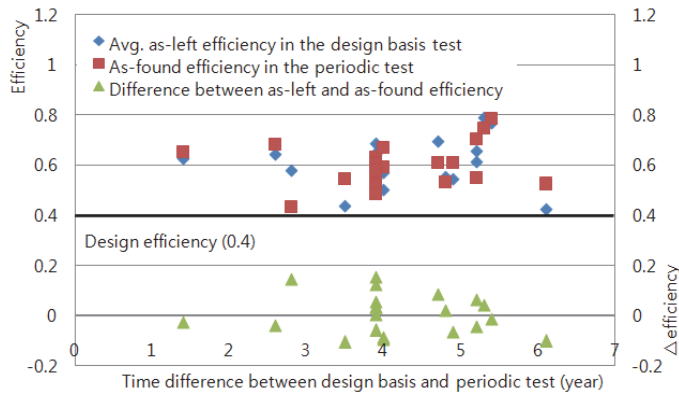
Some valve's efficiencies of 120 and 260 of maximum motor torque rating with an 1800 RPM motor (Fig. 8a, 8b) were showing up in the region below the design efficiency line. However, such trends appeared in the other actuators only with the 1800 RPM motor. The design efficiencies for those actuators were considered still available because data points showing such behavior are less than two at most for an actuator, and the deterioration from the design efficiency is small and can be explained based on the following engineering judgments. First, one avg. 'as-left' efficiency of 700 of maximum motor torque rating is lower than the design efficiency (Fig. 8c) but the behavior was considered temporary because the

'as-found' efficiency was recovered up to the design efficiency. The same behavior was also observed for 1950 of maximum motor torque rating (Fig. 8e). In the Fig. 8e, both avg. 'as-left' and 'as-found' efficiency were lower than the design efficiency, but the maximum deviation from the design efficiency was less than 11% approximately, which is an approximation of the sum of 8% for uncertainty of sensors for stem torque and 3% uncertainty of motor torque estimator based on NEET.

From these observations, maximum motor torque rating does not affect the efficiency degradation over time, but lower motor torque rating could have lower efficiency than the design only, for 120 and 260 of maximum motor torque rating with the 1800 RPM motor.

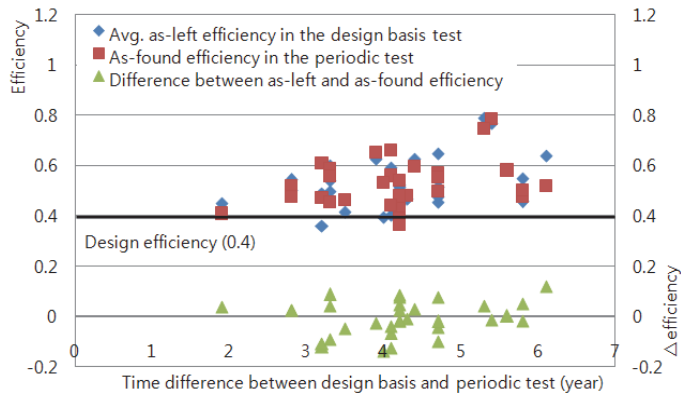


(a) 1800 RPM

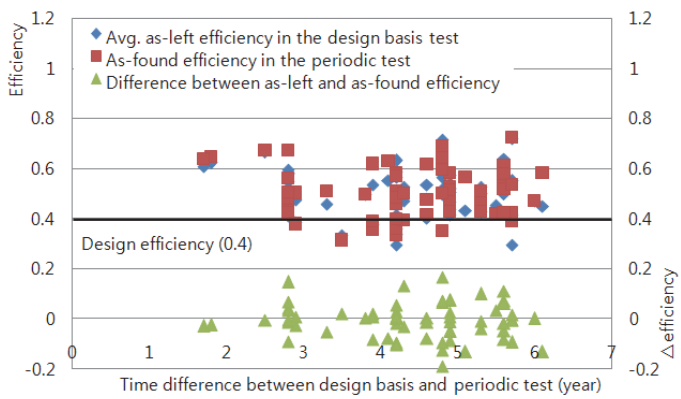


(b) 3600 RPM

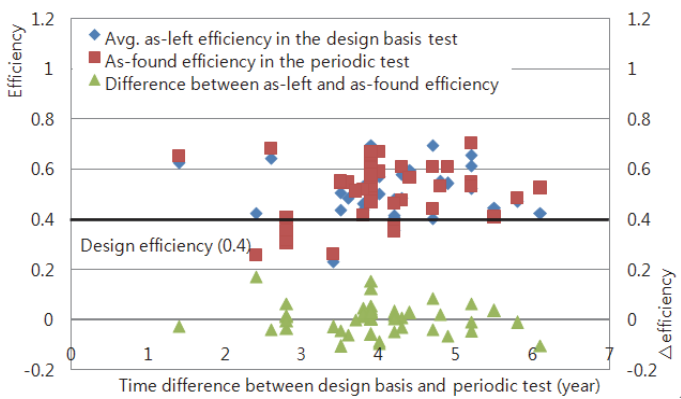
Fig. 6. Efficiency distribution by motor speed



(a) OVR 20~40

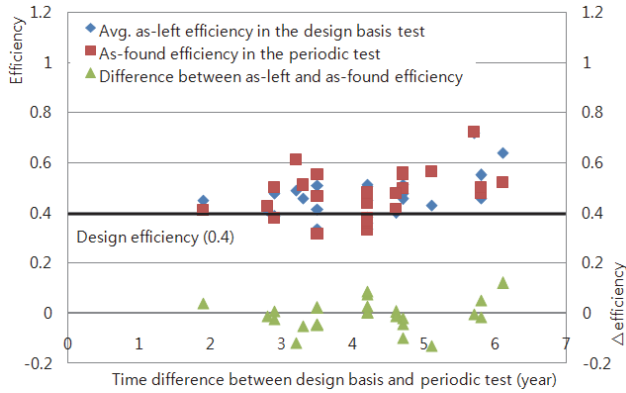


(b) OVR 40~60

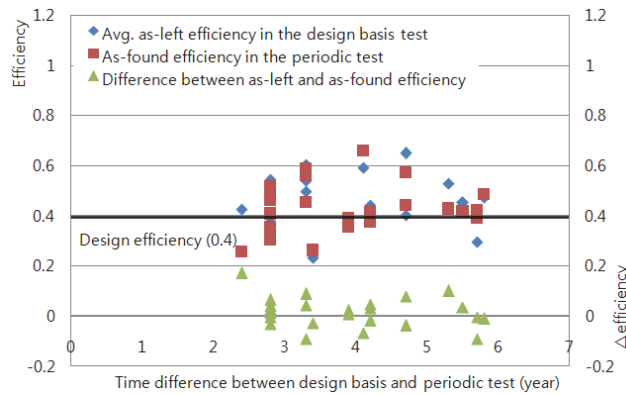


(c) OVR 60~80

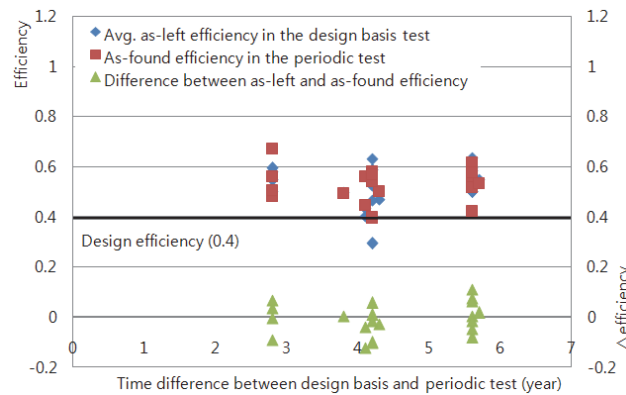
Fig. 7. Efficiency distribution by OVR



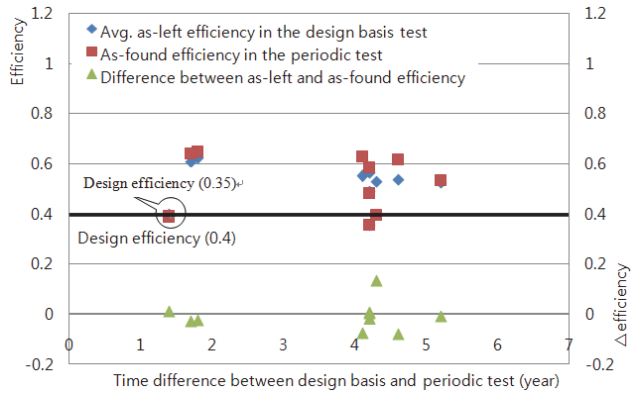
(a) 120 of max. motor torque rating (1800 RPM)



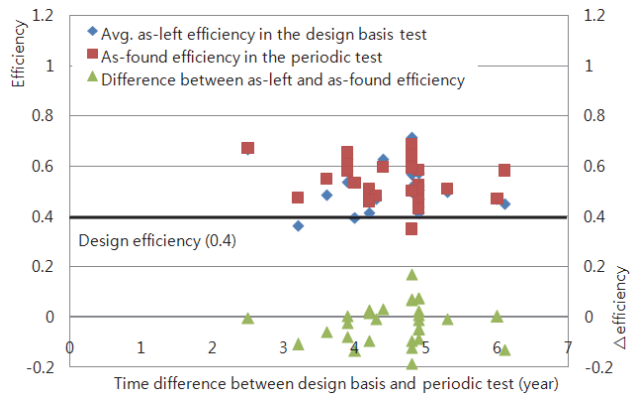
(b) 260 of max. motor torque rating (1800 RPM)



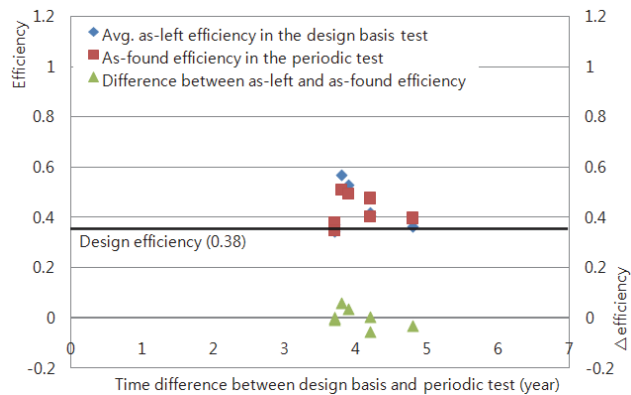
(c) 700 of max. motor torque rating (1800 RPM)



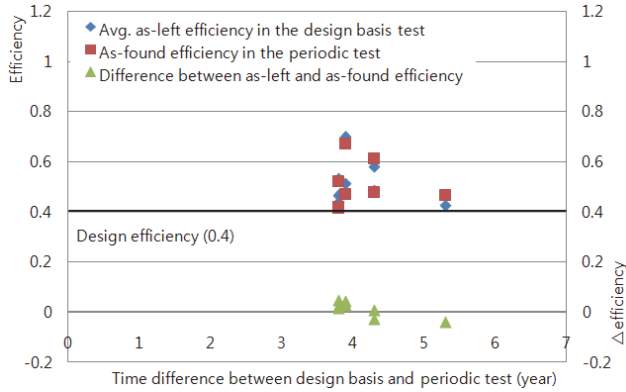
(d) 1100 of max. motor torque rating (1800 RPM)



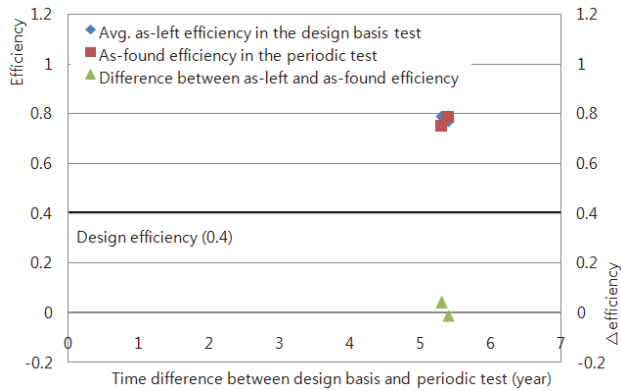
(e) 1950 of max. motor torque rating (1800 RPM)



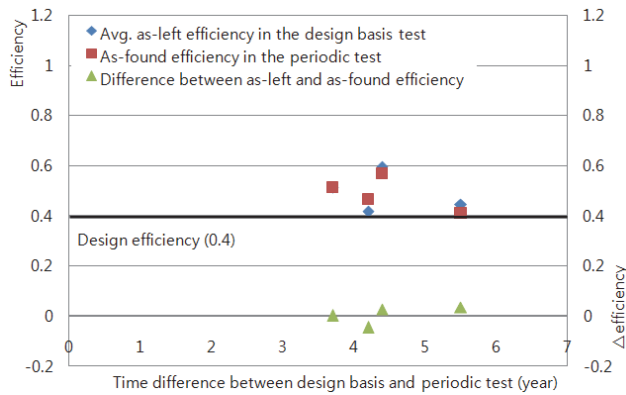
(f) 4200 of max. motor torque rating (1800 RPM, 53.7~70.9 OVR)



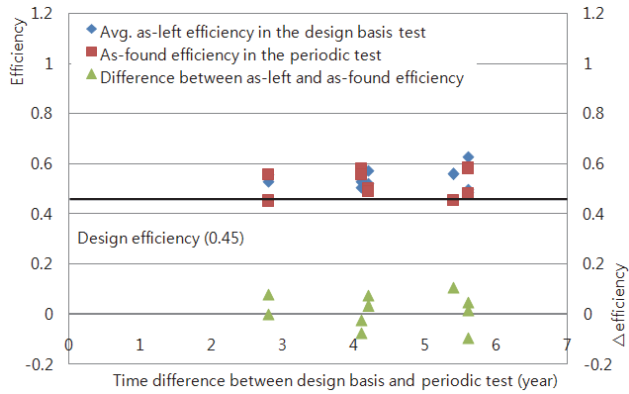
(g) 4200 of max. motor torque rating (1800 RPM, 98.6 OVR)



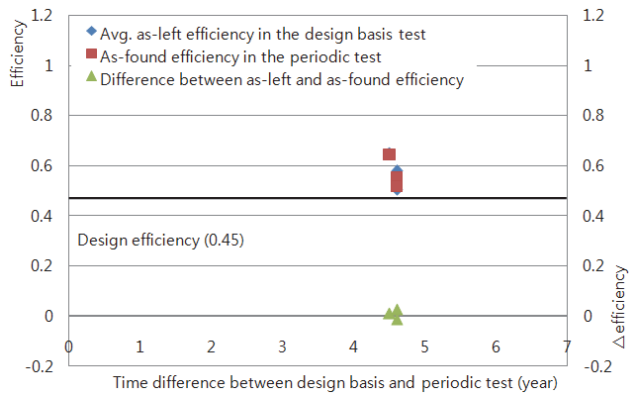
(h) 120 of max. motor torque rating (3600 RPM)



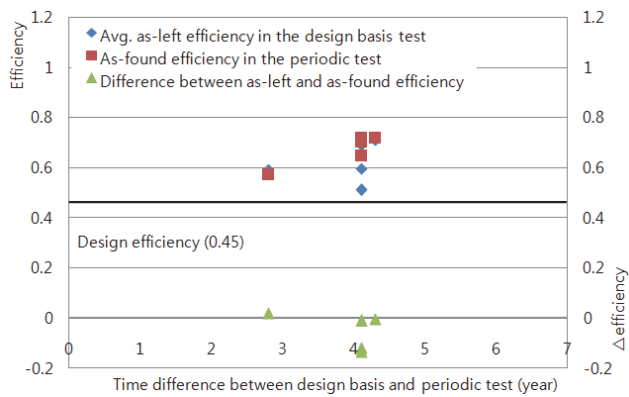
(i) 260 of max. motor torque rating (3600 RPM, 34.1~41 OVR)



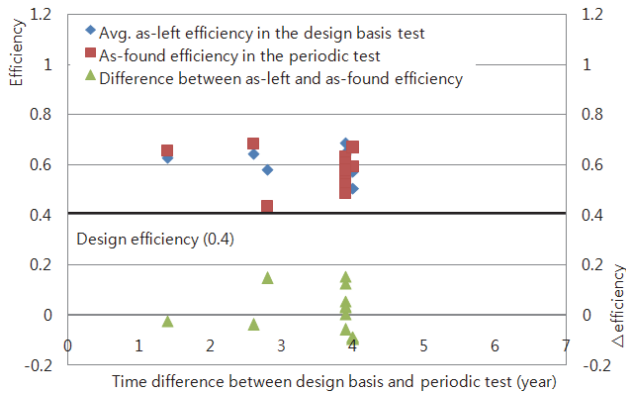
(j) 260 of max. motor torque rating (3600 RPM, 67.5 OVR)



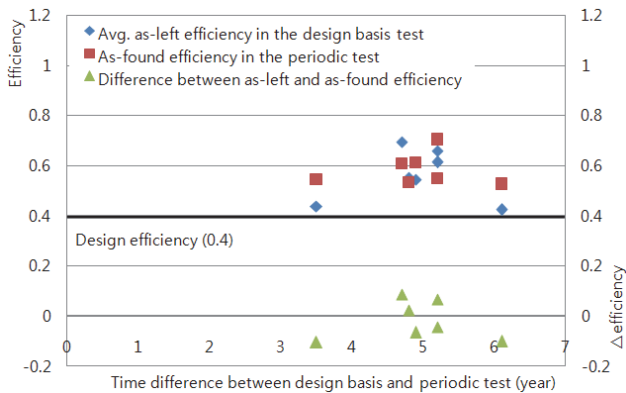
(k) 700 of max. motor torque rating (3600 RPM)



(l) 1100 of max. motor torque rating (3600 RPM)



(m) 1950 of max. motor torque rating (3600 RPM)



(n) 4200 of max. motor torque rating (3600 RPM)

Fig. 8. Efficiency distribution by max. motor torque rating

4. Threshold value calculation

As described in Section 3, the actuator efficiency of gate and globe valves have variations in efficiency from test-to-test, but no increasing or decreasing trend over time. Some of the variation is due to, for example, uncertainty in test measurements or in the estimation of motor torque. Some of the variation can be due to random variation in efficiency. Although the efficiencies of the two actuators, 120 and 260 of motor torque rating with an 1800 RPM motor, also were not increased or decreased over time, where their values are susceptible to be lower than design values. The decrease can be due to the various combinations of causes such as lower motor speed, lower maximum motor torque rating, overall gear ratio, operational environment, maintenance history after installation of those valves. For those actuators, change of design efficiency is needed to verify proper MOV setup and to quantify operational margin, as well as to provide any needed information on potential actuator degradation. Therefore, the threshold efficiencies for the two actuators are established using a deterministic approach (JOG, 1994), based on engineering judgment, which bounds 95% of

the efficiency data. This is shown by the dashed lines in Fig. 9 and Fig. 10 of the labeled threshold boundary. The intersection of a +45° line and a horizontal line at $\Delta\text{efficiency} = 0$ creates a wedge-shaped boundary. For points on the +45° line, design efficiency + $\Delta\text{efficiency} = 0$ constant. In other words, all data points on such a line will end up at the same final efficiency after a change in efficiency occurs. Points to the right of the line will end up at a higher efficiency and points to the left of the line will end up at a lower efficiency. The $\Delta\text{efficiency} = 0$ line is also used as a discriminator because points with negative $\Delta\text{efficiency}$ (below the line) are not a concern regarding potential decrease in efficiency. This threshold boundary can be positioned until a place is found where 5% of the data lie to the left of the +45 line and above the $\Delta\text{efficiency} = 0$ line (i.e., within the 135° wedge). In this position, the intercept of the +45° line with the x-axis is the threshold efficiency. For 95% of the data, efficiency decreases will not result in a final efficiency exceeding the threshold. Using this approach, a threshold value that bounds 95% (1 out of the 25 data points in Fig. 9 and 1 out of the 26 data points in Fig. 10) of the data for maximum torque rating 120 and 260 with 1800 RPM motor is determined as 0.332 and 0.335, respectively.

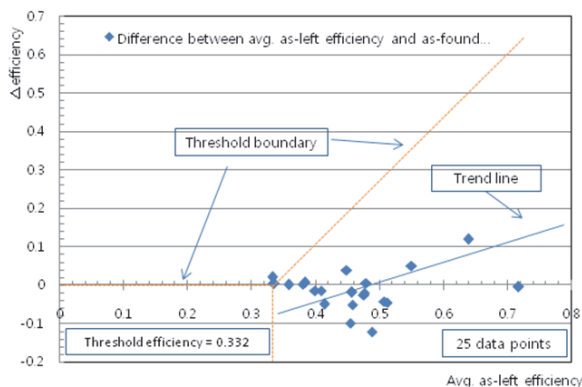


Fig. 9. Threshold efficiency for motor torque rating, 120 with 1800 RPM

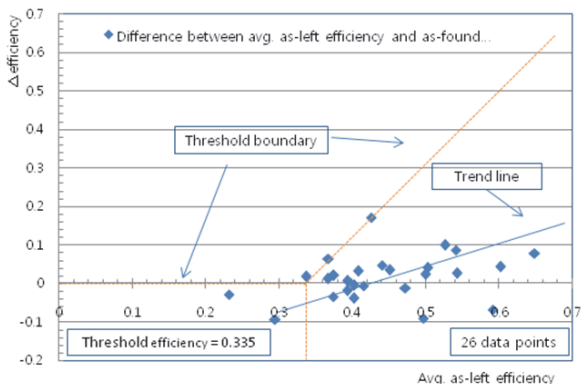


Fig. 10. Threshold efficiency for motor torque rating, 260 with 1800 RPM

5. Conclusion

The actuator efficiency has variations in efficiency from test-to-test, but no increasing or decreasing trend over time. In other words, there is no potential degradation in efficiency due only to the passage of time. Under certain conditions, however, decreases in efficiency to below the design efficiency were observed. Specifically, the actuators with low speed, low actuator size, and high gear ratio are susceptible to decrease in efficiency. However, these decreases tend to occur progressively down to a plateau level because those actuators have variations in efficiency from test-to-test, but no increasing or decreasing trend over time.

In this chapter, the two actuators that have 120 and 160 of motor torque rating with an 1800 RPM motor appeared to possess those behaviors. For the two actuators, change of design efficiency is needed to verify proper MOV setup and to quantify operational margin, as well as to provide any needed information on potential actuator degradation. Accordingly, the threshold efficiencies for the 120 and 160 of motor torque rating which bounds 95% of the efficiency data were determined as 0.332 and 0.335, respectively. The threshold values and efficiency behaviors over time can be applied only for the actuators described in the Table 1, because the design efficiencies and features of actuators depend on manufacturers. However, when it is assumed that design efficiencies are pertinent for some actuators, it can be possible to evaluate the potential degradation in design efficiencies only for the actuators with lower speed motor, lower actuator size, and higher gear ratios based on the results of this chapter.

6. Acknowledgment

The authors express their sincere appreciation to KHNP (Korea Hydro & Nuclear Power Company) for its support in the behavior analysis of the actuator efficiency.

7. References

- USNRC, Generic Letter 89-10 (1989). Safety Related Motor Operated Valve Testing and Surveillance, USA
- USNRC, Generic Letter 96-05 (1996). Periodic Verification of Design-Basis Capability of Safety-Related Motor-Operated Valves, USA
- S.C. Kang, S.K. Park, D.H. Lee, Y.S. Kim (2006). Motor Control Center (MCC) Based Technology Study for Safety-Related Motor Operated Valves, Nuclear Engineering and Technology, Vol. 38, No. 2, 155-162.
- JOG, (2004). Joint Owners' Group (JOG) Motor Operated Valve Periodic Verification Program Summary, pp. E1-E2, USA.

Investigation of High Energy Arcing Fault Events in Nuclear Power Plants

Heinz Peter Berg¹ and Marina Röwekamp²

¹*Bundesamt für Strahlenschutz*

²*Gesellschaft für Anlagen - und Reaktorsicherheit (GRS) mbH
Germany*

1. Introduction

Operating experience from different industries has shown a considerable number of reportable events with non-chemical explosions and rapid fires resulting from high energy arcing faults (HEAF) in high voltage equipment such as circuit breakers and switchgears.

High energy arcing faults can occur in an electrical system or component through an arc path to ground or lower voltage, if sufficiently high voltage is present at a conductor with the capacity to release a high amount of energy in an extremely short time. High energy arcing faults may lead to the sudden release of electrical energy through the air.

The significant energy released in the arcing fault of a high voltage component rapidly vaporizes the metal conductors involved and can destroy the equipment involved. The intense radiant heat produced by the arc can cause significant damage or even destructions of equipment and can injure people. However, this problem has been underestimated in the past (Owen, 2011a and 2011b).

Arcing events are not limited to the nuclear industry. Examples for such events could be found, among others, in chemical plants, waste incineration plants, and in conventional as well as in nuclear power plants underlining that high-energetic arcing faults are one of the main root causes of fires in rooms with electrical equipment (HDI-Gerling, 2009).

An evaluation of several loss incidents in different types of industrial plants has shown that causes for the generation of arcing faults are mainly due to (HDI-Gerling, 2009):

- contact faults at the screw-type or clamp connections of contactors, switches and other components due to, e.g., material fatigue, metal flow at pressure points, faulty or soiled clamp connections,
- Creeping current due to humidity, dust, oil, coalification (creeping distances, arcing spots),
- Mechanical damage due to shocks, vibration stress and rodent attack,
- Insulation faults due to ageing (brittleness), introduction of foreign matter and external influences.

Investigations of HEAF events have also indicated failures of fire barriers and their elements as well as of fire protection features due to pressure build-up in electric cabinets, transformers and/or compartments, which could lead to physical explosions and fire. These events often occur during routine maintenance.

HEAF have been noted to occur from poor physical connections between the equipment and the bus bars, environmental conditions and failure of the internal insulation (Brown et al., 2009).

The interest in fire events initiated by high energy arcing faults has grown in nuclear industry due to more recent events having occurred at several nuclear installations.

In the ongoing discussion on an international level it appeared necessary to find a common understanding about the definition of high energy arcing faults.

Currently, high energy arcing faults are seen as high energy, energetic or explosive electrical equipment faults resulting in a rapid release of electrical energy in the form of heat, vaporized metal (e.g. copper), and pressure increase due to high current arcs created between energized electrical conductors or between an energized electrical conductor and neutral or ground.

Components that may be affected include specific high-energy electrical devices, such as switchgears, load centres, bus bars/ducts, transformers, cables, etc., operating mainly on voltage levels of more than 380 V (OECD/NEA, 2009a).

The energetic fault scenario consists of two distinct phases, each with its own damage characteristics and detection/suppression response and effectiveness:

1. First phase: Short, rapid release of electrical energy which may result in projectiles (from damaged electrical components or housing) and/or fire(s) involving the electrical device itself, as well as any external exposed combustibles, such as overhead exposed cable trays or nearby panels, that may be ignited during the energetic phase.
2. Second phase, i.e., the ensuing fire(s): this fire is treated similar to other postulated fires within the zone of influence.

However, a common definition of high energy arcing faults is expected as one result of a comprehensive international activity of the OECD on high energy arcing faults in the member states of the Nuclear Energy Agency (NEA) (see below).

A variety of fire protection features may be affected in case of high energy arcing faults events by the rapid pressure increase and/or pressure waves (e.g. fire barriers such as walls and ceilings and their active elements, e.g. fire doors, fire dampers, penetration seals, etc.).

The safety significance of such events with high energy arcing faults is non-negligible. Furthermore, these events may have the potential of event sequences strongly affecting the core damage frequency calculated in the frame of a probabilistic fire risk assessment.

2. High energy arcing faults and work safety

Although only the technical consequences for nuclear power plants and other nuclear installations in case of a HEAF event are discussed in the following in detail, another important hazard resulting from arcing faults should not be ignored. This is the possible injury of workers.

Based on previous statistics it is expected that solely in the U.S. more than 2,000 workers will be seriously burnt by the explosive energy released during arcing faults within one year (Lang, 2005). The magnitude of this problem is far reaching, and the following statistics are staggering (Burkhart, 2009):

- 44,363 electricity-related injuries occurred between 1992 and 2001,
- 27,262 nonfatal electrical shock injuries,
- 17,101 burn injuries,

- 2,000 workers admitted annually to burn centres for extended arc flash injury treatment.

Three main consequences for workers result from a high energy arcing fault: blinding light, intense heat and thermo-acoustic effects.

1. Blinding light:

As the arc is first established, an extremely bright flash of light occurs. Although it diminishes as the arcing continues, the intensity of the light can cause immediate vision damage and increases the probability for future vision problems.

2. Intense heat:

The electrical current flowing through the ionized air creates tremendously high levels of heat energy. This heat is transferred to the developing plasma, which rapidly expands away from the source of supply. Tests have shown that heat densities at typical working distances can exceed 40 cal/cm². Even at much lower levels, conventional clothing ignites, causing severe, often fatal, burns. At typical arc fault durations a heat density of only 1.2 cal/cm² on exposed flash is enough to cause the onset of a second-degree burn.

3. Thermo-acoustic effects:

As the conductive element that caused the arc is vaporized, the power delivered to the arc fault rises rapidly. Rapid heating of the arc and surrounding air corresponds to a rapid rise in surrounding pressure. The resultant shock wave can create impulse very high sound levels. Forces from the pressure wave can rupture eardrums, collapse lungs and cause fatal injuries.

Most of these people will neither have been properly warned of the hazards associated with arc flash nor will they have been adequately trained in how to protect themselves.

While the potential for arc flash does exist for as long as plants have been powered by electricity several factors have pushed arc flash prevention and protection to the forefront.

The first is a greater understanding of arc flash hazards and the risk they pose to personnel. Research has started since a few years for quantifying energy and forces unleashed by arc flash events. This has resulted in the development of standards to better protect workers.

Arc-flash hazard analysis is important in determining the personal protective equipment required to keep personnel safe when working with energized equipment. Contact with energized equipment is a commonly known risk; however exposure to incident energy from an electrical arc is sometimes overlooked. On that background approach boundaries have been determined to improve the arc flash hazard protection (Lane, 2004)

There is much discussion regarding how thorough an arc-flash hazard assessment must be. A complete examination of the system would require assessment at each and every possible work location, a task that is unrealistic to complete. Even if this task was undertaken, some of the accepted analysis methods pose some concerns as to whether the assessment considers the 'most likely' fault scenarios.

The fundamentals of arc-flash hazard analysis are discussed in (Aventd, 2008 and Lane, 2004). The methodology used in the arc-flash hazard analysis is recommended in (IEEE, 2002) where techniques for designers and facility operators are provided to determine the arc flash boundary and arc flash incident energy. How to use this IEEE standard is described in (Lippert et al., 2005).

First and foremost, when considering arc-flash hazards four primary factors have to be mentioned which determine the hazard category:

1. System voltage.

2. Bolted fault current – calculated at the location/equipment to be assessed and subsequently used to calculate the theoretical arcing fault current.
3. Working distance – as measured from the personnel’s head/torso to the location of the arc source.
4. Fault clearing time.

Two of the four primary factors determining the arc-flash hazard category have a larger impact than the others: working distance and fault clearing time.

In (Avendt, 2008) it is underlined that fault clearing time plays the largest role in the arc-flash hazard category. A time-current curve is frequently used to show the relationship between current (amps) and response time (seconds). Most protective devices have an inverse characteristic: as current increase, time decreases. Examples of such curves are given in (Avendt, 2008).

In order to fulfil the obligation to protect workers, several standards and guidelines are currently updated or under development.

For example, the Electricity Engineers Association has developed a discussion paper on the issue of arc flash (EEA, 2010) that will enable the subsequent preparation of a guide which will provide best practice advice for employers and asset owners needing to determine the probability of an arc flash occurring, its severity, means of mitigation and relevant personnel protection equipment.

An overview of various arc flash standards for arc flash protection and arc flash hazard incident energy calculations are presented in (Prasad, 2010).

3. Systematic query of international and national databases

In order to confirm these indications by feedback from national and world-wide operating experience, the national German database on reportable events occurring at nuclear power plants as well as international databases, such as IRS (Incident Reporting System) and INES (International Nuclear Event Scale), both provided by the International Atomic Energy Agency (IAEA), or the OECD FIRE Database (cf. OECD/NEA, 2009) have been analysed with respect to high energy arcing faults events which resulted in a fire and high energy arcing faults events with only the potential of deteriorating fire safety.

That systematic query underlined that a non-negligible number of reportable events with electrically induced explosions and extremely fast fire sequences resulting from high energy arcing faults partly lead to significant consequences to the environment of impacted components exceeding typical fire effects.

All results of the international and national databases are presented in Tables 1, 2 and 3 in the same manner, containing in particular the current plant operational state in case of the event, the information in which component the cause of the event was identified, the voltage level, if only the impacted component was damaged, and information if fire barriers being available had been deteriorated.

3.1 International OECD HEAF activity

Due to the high safety significance and importance to nuclear regulators OECD/NEA/CSNI (Committee on the Safety of Nuclear Installations) has initiated an international activity on “High Energy Arcing Faults (HEAF)” in 2009 (OECD/NEA, 2009a) to investigate these phenomena in nuclear power plants in more detail as an important part of better understanding fire risk at a nuclear power plants which is better accomplished by an

international group to pool international knowledge and research means. In this task it is stated:

“The main objectives of this common international activity are to define in technical terms a HEAF event which is likely to occur on components such as breakers, transformers, etc., to share between experts from OECD/NEA member states HEAF events, experiences, research and potential mitigation strategies. In addition, the physical and chemical phenomena of a HEAF event shall be investigated and characterized from a fire dynamics perspective. In this context, a simple model and/or deterministic correlation is intended to be developed to reasonably and quickly predict the potential damage areas associated with a HEAF.

Furthermore, generally acceptable input criteria and boundary conditions for CFD (computerized fluid dynamics) models shall be defined being likely to be accepted by industry and regulatory agencies. In a last step, the needs for possible experiments and testing to develop input data and boundary conditions for HEAF events to support the development of HEAF models shall be identified and the correlations and models developed be validated and verified.”

The working group with members e.g. from Canada, France, Germany, Korea, and the United States decided during the Kick-Off Meeting at OECD/NEA in Paris in May 2009 that the goals of the task are to develop deterministic correlations to predict damage and establish a set of input data and boundary conditions for more detailed modelling which can be agreed to by the international community.

The output of the OECD activity may directly support development of improved methods in fire probabilistic risk assessment for nuclear power plant applications. The task may also result in the definition of experimental needs to be addressed later in a project structure (OECD/NEA, 2009a).

3.2 Information from of international databases

First information from the international operating experience collected within the IRS database - for more severe reportable incidents at nuclear power plants - and INES, both provided by IAEA, is given in Table 1.

In addition, applications of the OECD FIRE Database (cf. OECD/NEA, 2009) have indicated that a non-negligible contribution of approx. 6 % of the in total 343 fire events collected in the database up to the end of 2008 (cf. Berg & Forell et al., 2009) are high energy arcing faults induced fire events. Details can be found in Table 2.

At the time being, the existing data base on high energy arcing faults events in nuclear installations is still too small for a meaningful statistical evaluation.

However, the first rough analysis of the available international operating experience gives some indications on the safety significance of this type of events, which potentially will also result in relevant contributions to the overall core damage frequency.

Up to the end of 2009, thirty-eight high energy arcing faults events have been identified in the OECD FIRE Database. Details on these events are provided in the following paragraphs.

The database query was started in Germany. One application of the OECD FIRE Database selected by the German experts was an analysis of events associated with explosions. A query in this database on the potential combinations of fire and explosion events (cf. Berg & Forell et al., 2009) indicated a significant number of explosion induced fires. Most of such event combinations occurred at transformers on-site, but outside of the nuclear power plant buildings or in compartments with electrical equipment.

Year of Occurrence	Reactor Type	Plant State	Component	Voltage Level	Damage Limited to Component	Barrier Deteriorated	Fire / Explosion
2006	PWR	FP	transformer busbar	20 kV	yes	no	F
2006	BWR	FP	switchgear station	400 kV	yes	no	-
2001	PHWR	LP/SD	circuit breaker cables	not indicated	no	no	F
2001	PWR	FP	power switch	not indicated	no	no	E / F
2001	PWR	FP	circuit breaker	not indicated	no	yes	F
2000	PWR	FP	circuit breaker	6 kV	yes	yes	F
2000	PWR	FP	circuit breaker	12 kV	yes	no	F
1996	PWR	FP	power switch	not indicated	no	yes	E / F
1996	PWR	FP	lightning arrester	not indicated	no	no	F
1995	PWR	FP	circuit breaker	6 kV	no	no	E / F
1992	PWR	FP	switchgear room	6 kV	yes	no	F
1991	PWR	FP	control cabinet	6 kV	yes	no	F
1991	PWR	FP	busbar	0.4 kV	yes	no	F
1990	PWR	LP/SD	switchgear station	400 V	yes	no	-
1990	PWR	FP	busbar	6 kV	yes	no	-
1990	LGR	FP	busbar	6 kV	no	no	F
1989	PWR	FP	distribution	6.9 kV	no	no	E / F
1988	PWR	FP	distribution	13.8 kV	yes	no	E / F
1984	BWR	FP	main transformer	not indicated	no	yes	E / F
1983	GCR	LP/SD	control panel	5.5 kV	no	yes	E / F

Table 1. Operating experience from HEAF events reported to INES and IRS (from Berg & Forell et al., 2009)

Year of Occurrence	Reactor Type	Plant State	Component	Voltage Level	Damage Limited to Component	Barrier Deteriorated	Fire / Explosion
2007	PWR	FP	high voltage transformer	not indicated / 345 kV	yes	no	E / F
2006	PWR	FP	electrically driven pump	12 kV	yes	no	E / F
2006	PWR	FP	high voltage transformer	6 kV / 20 kV	no	yes	E / F
2006	PWR	LP/SD	medium and low voltage transformer - oil filled	not indicated / 400 kV	no	no	E / F
2005	BWR	FP	high voltage transformer	not indicated	yes	no	E / F
2005	PHWR	FP	high voltage transformer	not indicated / 500 kV	yes	no	E / F
2003	GCR	FP	high voltage transformer	6.6 kV / 400 kV	no	no	E / F
2002	BWR	LP/SD	high voltage transformer	not indicated	yes	no	E / F
2002	PWR	FP	high voltage breaker	34.5 kV	yes	no	E / F
2001	PWR	LP/SD	high or medium voltage electrical cabinet	6.6 kV	no	yes	E / F
2001	PWR	not indicated	high or medium voltage electrical cabinet	6.6 kV	no	no	E / F
1999	PWR	FP	high voltage transformer	20 kV / 161 kV	yes	no	E / F
1995	PWR	FP	medium and low voltage transformer - dry	not indicated / 130 kV	yes	no	E / F
1994	PWR	FP	high voltage transformer	not indicated / 400 kV	yes	no	E / F
1990	PWR	FP	high or medium voltage electrical cabinet	6.6 kV	yes	no	E / F
1988	PWR	LP/SD	high voltage transformer	20 kV / 400 kV	yes	no	E / F
1988	PWR	FP	high voltage transformer	20 kV / 400 kV	yes	no	E / F
1988	PWR	FP	high voltage transformer	20 kV / 400 kV	yes	no	E / F

Table 2. Operating experience from fire events with HEAF included in the OECD FIRE Database (from Berg & Forell et al., 2009)

Approximately 50 % of the fires in the database were extinguished in the early (incipient) fire phase before the fire had fully developed.

As there is no specific coded field in the database to indicate explosions, the main source of information is provided by the event description field. The following terms were used as search filters:

- search for *explo* (explosion, exploded, etc.): 26 events
- search for *defla* (deflagration, deflagrated, etc.): no events
- search for *deto* (detonation, detonated, etc.): no events

In three of the in total 26 cases no explosion occurred according to the event description but the term “explo” was used in another meaning.

In case of one event, the explosive release of ‘INERGEN’ gas from a gas cylinder occurred. The 22 reported explosions amount to 6.4 % of the 373 events reported up to date. Some details of the explosions are listed in (Berg & Forell et. al., 2009).

Concerning the process of explosion distinction should be made between an explosion as a process of rapid combustion (chemical explosion) and an explosion as a physical process resulting from a sudden gas pressure rise by a high energy arcing fault.

A chemical explosion was found for only three events (solvent vapour, diesel fuel, hydrogen). In the other 18 cases, high energy arcing faults events obviously took place at the same time indicating a physical explosion.

In some of these cases the electric fault might have caused a fuel pyrolysis/spread and acted as an ignition source for a chemical explosion, thus a high energy arcing fault event and a chemical explosion may have taken place simultaneously. In one event, a fire led to the explosion of diesel fuel vapour while in another event a fire and an explosion occurred independently from each other in parallel. In all other cases explosions induced the fire.

The buildings/locations where the events took place are also listed in (Berg et al., 2009). It was found that 13 (59 %) events took place outside buildings, 3 inside electrical buildings. A majority of 59 % of the reported explosions (again 13 events) started at transformers.

The other nine events took place at electrical cabinets, other electrical equipment, or process equipment (three each representing 14 %).

External fire brigades were needed in 4 of 22 cases (18 %). The 22 events were also evaluated concerning the fire duration with the following results:

- Fire duration between 0 and less than 15 min: 11 events
- Fire duration between 15 and less than 30 min: 3 events
- Fire duration between 30 and 60 min: 3 events
- Fire duration longer than 60 min: 3 events

For the remaining two events no information on the fire duration is provided. This result is in good agreement with the fire durations recorded in the database for all events, where for approx. 55 % of the events (i.e. 128 out of 233 events with fire duration provided) a fire duration of less than 15 min could be found.

3.3 Information from of the German database

The German national operating experience from reportable events at nuclear power plants is summarized in Table 3. As one can see from this table different components were impacted, in particular – as expected – switchgears. In many cases the voltage level could not be identified. The damage was in most cases limited to the component where the HEAF occurred, only in one case a barrier was deteriorated. One third of these events were correlated with a fire.

Year of Occurrence	Reactor Type	Plant State	Component	Voltage Level	Damage Limited to Component	Barrier Deteriorated	Fire / Explosion
2007	BWR	FP	transformer	380 kV	yes	no	E / F
2007	PWR	FP	transformer	380 kV	yes	no	-
2006	BWR	LP/SD	auxiliary service pump	not indicated	yes	no	-
2006	PWR	FP	switchgear drawer	not indicated	yes	no	-
2006	BWR	FP	switchgear drawer	not indicated	yes	no	-
2005	BWR	FP	Switch	not indicated	yes	no	-
2004	PWR	LP/SD	emergency power feed line	not indicated	yes	no	-
2004	BWR	FP	diesel generator	6 kV	no	no	F
2004	BWR	FP	cable connection	not indicated	yes	no	F
2004	PWR	LP/SD	diesel generator. exciter	6 kV	yes	no	-
2003	BWR	FP	diesel generator. exciter	6 kV	yes	no	-
2003	PWR	FP	emergency power feed line	500 V	yes	no	F
2002	BWR	FP	emergency power busbar	500 V	no	no	F
2001	PWR	FP	generator transformer switch	not indicated	yes	no	-
2001	BWR	FP	emergency power distribution	660 V	yes	no	-
1999	PWR	FP	ventilation exhaust	not indicated	yes	yes	-
1998	PWR	FP	emergency power distribution	660 V	no	no	-
1996	BWR	FP	switch drawer	500 V	yes	no	F
1995	BWR	FP	switchgear drawer	not indicated	yes	no	-
1993	PWR	FP	currency converter	380 V	yes	no	-
1992	PWR	LP/SD	emergency power generator	not indicated	yes	no	F
1991	BWR	FP	emergency power busbar	10 kV	yes	no	-
1989	PWR	FP	switchgear feed cell	10 kV	no	no	F
1989	PWR	LP/SD	switchgear feed area	380 V?	no	no	F
1988	PWR	LP/SD	switchgear	220 kV	no	no	E / F
1987	BWR	FP	emergency diesel generator	not indicated	yes	no	-

Year of Occurrence	Reactor Type	Plant State	Component	Voltage Level	Damage Limited to Component	Barrier Deteriorated	Fire / Explosion
1987	PWR	FP	auxiliary service water system	not indicated	yes	no	-
1986	PWR	LP/SD	busbar	380 V	no	no	F
1984	BWR	LP/SD	auxiliary power supply	not indicated	yes	no	-
1981	PWR	FP	safety injection pump motor	not indicated	yes	no	-
1979	BWR	LP/SD	switchgear	400 V	yes	no	-
1979	PWR	LP/SD	control rod distribution	not indicated	yes	no	F
1978	PWR	FP	switchgear	220 kV	yes	no	-
1977	PWR	LP/SD	switchgear	350 V	yes	no	-
1977	BWR	LP/SD	emergency switchgear	not indicated	yes	no	-

Table 3. Operating experience concerning reportable HEAF events from German NPP (from Berg & Forell et al., 2009)

In all three tables the following abbreviations are used:

PWR:	pressurized water reactor	BWR:	boiling water reactor
PHWR:	pressurized heavy water reactor	GCR:	gas cooled reactor
FP:	full power	LP/SD:	low power / shutdown
E:	explosion	F:	fire

4. Questionnaire to gain further insights on HEAF

As a result of the evaluation of the above mentioned international databases IRS and INES, a questionnaire has been developed by German experts providing a list of questions, which mainly shall be answered by the licensees (see Röwekamp & Klindt, 2007 and Röwekamp et al., 2007).

The answers to this questionnaire shall provide further insights on the basic phenomena regarding high energy arcing faults and may allow the evaluation of such events as well as the identification of effective preventive measures to be taken in nuclear installations in the future.

This questionnaire has been discussed nationally and in an international experts group. The results of the international discussions as well as a first pilot completion of this questionnaire in a German nuclear power plant resulted in enhancing the questionnaire and its sub-division into two parts depending on the availability of experiences with this type of events in the plants under consideration.

The questions concerning events which occurred at the nuclear power plant cover the operating experience in the respective plant, consequences and effects of the events, fire suppression measures (if needed), event causes and resulting corrective actions.

Questions without plant-specific observations from events deal with preventive measures in the plant and assessment activities performed without direct observations from the events (Röwekamp & Berg, 2008 and Röwekamp et al., 2009). The complete list of elaborated questions is provided in the following.

Part I: Questions concerning events occurred at nuclear power plants

- Operating experience
 1. Does the operating experience of the nuclear power plant (including grid connection) reveal either reportable or minor, non-reportable events interconnected to a high energy electric (i.e. arcing) failure of electric components and equipment with ≥ 6 kV?
 2. What was the damage? What was the damage zone? Was there damage by the high energy release (explosion pressure wave, etc.), or by fire or by both?
 3. In which buildings / compartments / plant areas did the event occur?
 4. At what type of component was the fault initiated (e.g., switchgear, motor control centre, transformer (oil filled or dry ones), breakers, cables etc.)?
 5. What voltage level did the component operate at? What was the nominal current load available to the component?
 6. If known, what was the estimated overload current observed during the arcing fault?
 7. How was the HEAF observed or detected? Directly by fire detectors, visual or auditory detection in the location where the fault occurred or indirectly by faulty/spurious signals indirect fire alarms, etc.? (An as far as feasible detailed and exhaustive description of the event is needed.) What were the observations and findings?
 8. What was the arcing duration in case of arcing being the cause? How did the arcing stop? (Note: Due to expert judgment from international experts there may be a correlation between arcing duration and damage consequences/extent)
- Consequences / Effects
 9. Which consequences/effects including secondary ones (e.g. pressure waves, impact by missiles, i.e. induced high frequent voltage, etc.) to adjacent/nearby components (including cables) and compartments / plant areas have been observed besides the typical fire effects? Did, as a consequence, protective equipment fail or become ineffective?
 10. Was the damage limited to one fire compartment and or one redundant safety train or were further compartments / trains affected?
 11. Which functions of fire protection features (fire barriers and their elements as well as active means) have been impaired by the effects of high energy arcing faults, in particular by pressure waves and missiles?
- Fire suppression (if needed)
 12. Was fire extinguishing performed?
 13. If yes, which extinguishing means were applied? Which were successful?
 14. What was (rough estimate) the total fire duration?
- Event causes
 15. Was it possible to find out the causes of the high energy impacts observed? If yes, what were the potential causes?
 16. Were the initial causes (root causes) man-induced (mal-operation, errors), or purely technical ones, administrative causes, or combinations of different causes? Have the root causes been found? (Please list all the root causes.)
- Corrective actions
 17. What are the corrective actions after the event for prevention of recurrence?

Part II: Questions without observations from events at nuclear power plants

- Preventive measures
 18. In which compartments / plant areas are components and equipment with the potential of HEAF installed? Are there safety significant / safety related components available in these compartments / plant areas and/or adjacent ones? If yes, which ones? What are the preventive (structural) measures there against such events?
 19. Which measures are foreseen (originally in the design as well as improved ones after the event) to limit the consequences of such high energy arcing faults failures?
 20. Is it possible to practically exclude by the preventive measures that safety significant equipment is impaired?
 21. Are further measures intended for prevention of these faults (continuous controls, in-service inspections, etc.), and if yes, which ones?
- Assessment without direct observations from the events
 22. In how far are such high energy arcing fault events and their potential effects considered in the frame of periodic safety reviews (deterministic safety status analysis as well as probabilistic safety assessment)?

This German questionnaire could be the basis for gaining plant-specific information also from nuclear power plants in other countries.

5. Some examples of HEAF events in nuclear power plants

In the following, typical examples of high energy arcing fault events which occurred in different nuclear power plants in the last thirty years are provided.

5.1 HEAF in a 10 kV cable with a spontaneous short circuit

A high energy arcing faults event from a spontaneous short circuit with a longer time duration took place in a German nuclear power plant.

This event, which occurred in a 10 kV cable at a BWR type plant, has been analyzed in detail by the responsible expert organization on behalf of the regulator in charge (Berg & Katzer et al., 2009). Details on the electric circuit are provided in Figure 1.

The affected cable was routed from the station service transformer together with various other cables through an underground cable channel to the switchgear building.

Due to the conditions in the ground, cables were partly imbedded in so-called 'cable cylinder blocks' manufactured from concrete (see Figure 2).

The short circuit with a duration of some seconds occurred in a single 10 kV cable inside one of the cylinder blocks. Neighboring cables were not affected. During this time period, the PVC insulated cable including the copper conductor evaporated completely on a length of approx. 1 m (see photos in Figure 3).

The pyrolysis and/or evaporation of the PVC cable insulations caused a strong smoke release inside the cable channel.

The automatic fire detectors directly gave an alarm. Due to the typically high air humidity inside the channel, a smoke exhaust system was installed for the cable channel, which removed the smoke rapidly after actuation by the fire detectors.

The overpressure arising from the high voltage short circuit was relieved via open cable conduits to the transformer and leakages.

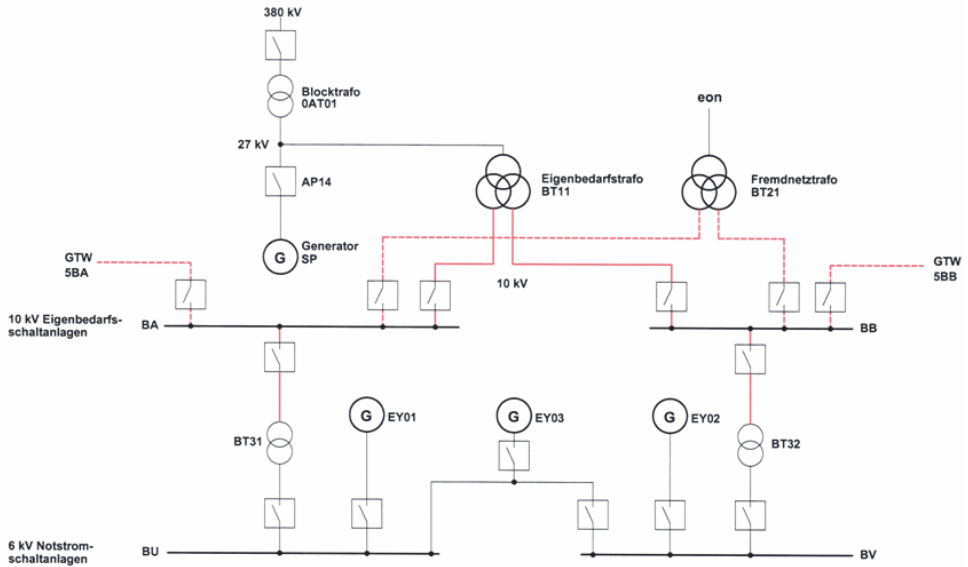


Fig. 1. Scheme of the electric circuit affected

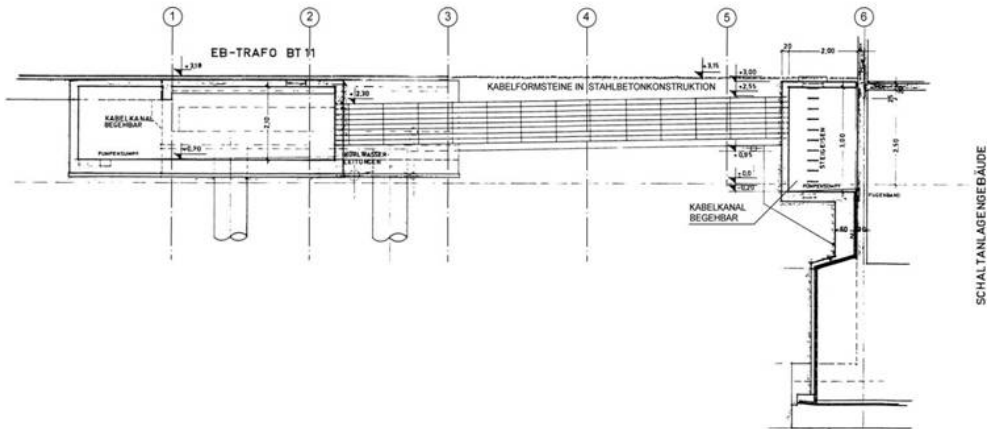


Fig. 2. Cross section of the cable tray inside the cable cylinder blocks inside ground between the buildings



Fig. 3. Photos of the cable damage; left: location of the damaged cable, right: damage by the cable fire/evaporation



Fig. 4. Cables with protection by intumescent coating; left: photo of the cable channel, right: photo of the coating

Unfortunately, the pressure value having really occurred during the event could not be determined. Damage to fire doors, dampers, or fire stop seals were not observed. The high energy short circuit did not result in any fire propagation; the combustion was limited to the location where the short circuit occurred. The fire self-extinguished directly after the electric current had been switched off. The fire duration was only a few seconds, however, the smoke release was high.

It has to be mentioned that all cables inside the cable channel were protected by intumescent coating (see Figure 4 above). This coating ensured the prevention of fire spreading on the cables.

The detailed analysis led to the definite result that the event was mainly caused by ageing of the 10 kV cables. The ageing process was accelerated by the insufficient heat release inside the cable cylinder blocks.

As a corrective action, all high voltage (mainly 10 kV) cables with PVC shielding being older than 30 years were replaced by new ones.

Another effect of the event was the smoke propagation to an adjacent cable channels via a drainage sump. As a preventive measure, after the event each cable channel was supplied

by its own drainage system. Moreover, all the channels were separated by fire barriers with a resistance rating of 90 min.

5.2 Arcing fault in an electrical cabinet of the exciter system of an emergency diesel generator

This event occurred at a German nuclear power plant in 1987.



Fig. 5. Photographs: a) view into the exciter cabinet, in the foreground location where the screw loosened and b) view into the cabinet



Fig. 6. Photographs of the damaged fire door from outside the room

Performing a load test during a regular in-service inspection (usually at an interval of four weeks) of the emergency diesel generator, an arcing fault with a short-to-ground took place in the electrical cabinet of the exciter system of the emergency diesel generator (cf. Figure 5 above).

The ground fault is assumed to be caused by a loose screw. The ionization of air by the arc developed to a short circuit within approximately four seconds.

The coupler breakers between the emergency power bus bar and the auxiliary bus bar opened 0.1 s after the occurrence of the short circuit, due to the signal “overload during parallel operation”.

1.5 s later the diesel generator breaker opened due to the signal “voltage < min” at the emergency power bus bar. Another 0.5 s later the emergency power bus bar was connected automatically to the offsite power bus bar.

The smouldering fire is believed to be caused by the short circuit of the emergency diesel generator.

Due to the high energy electric arcing fault a sudden pressure rise occurred in the room (room dimensions are approximately 3.6 m x 5.5 m x 5 m) that damaged the double-winged fire door.

Photographs of the damaged fire door from outside the room are shown in Figure 6 above.

5.3 Short circuit leading to a transformer fire

This event occurred at a German nuclear power plant in June 2007. A short circuit resulted in a fire in one of the two main transformers. The short circuit was recognized by the differential protection of the main transformer. Due to this, the circuit breaker between the 380 kV grid connection and the affected generator transformer (AC01) as well as the 27 kV generator circuit breaker of the unaffected transformer (AC02) were opened.

At the same time, de-excitation of the generator was actuated. The short circuit was thereby isolated. In addition, two of the four station service supply bus bars (3BC and 4BD) were switched to the 110 kV standby grid (VE). A simplified diagram is given in Figure 7 (Berg & Fritze, 2011).

Within 0.5 s, the generator protection system (initiating 'generator distance relay' by remaining current during de-excitation of the generator which still feeds the shot circuit) caused the second circuit breaker between the 380 kV grid connection and the intact generator transformer (AC02) to open. Subsequently the two other station service supply bus bars (2BB and 1BA) were also switched to the standby grid. After approx. 1.7 s, station service supply was re-established by the standby grid.

Due to the short low voltage signalization on station service supply bus bars the reactor protection system triggered a reactor trip.

As soon as the switch to the standby grid had taken place, feed water pump 2 was started automatically. After about 4 s the pump stopped injecting into the reactor pressure vessel and subsequently was switched off again. This caused the coolant level in the reactor pressure vessel to drop so that after about 10 min the reactor protection system actuated steam line isolation as well as the start-up of the reactor core isolation cooling system. About 4 min after the actuation of steam line isolation, two safety and relief valves were opened manually for about 4 min. This caused the pressure in the reactor to drop from 65 bar to approx.. 20 bar. As a result of the flow of steam into the pressure suppression pool, the coolant level in the reactor pressure vessel dropped further.

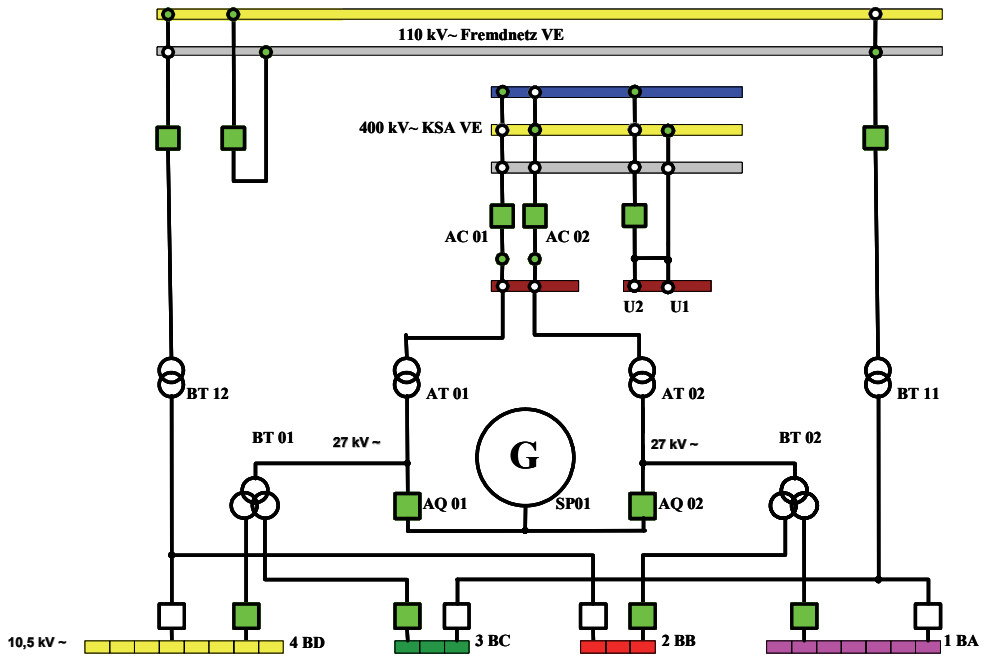


Fig. 7. Simplified diagram of the station service supply and the grid connection of the nuclear power plant

After closing the safety and relief valves the level of reactor coolant decreased further because of the collapse of steam bubbles inside the reactor pressure vessel. Thereby the limit for starting the high-pressure coolant injection system with 50 % feed rate was reached and the system was started up by the reactor protection system. Subsequently, the coolant level in the reactor pressure vessel increases to 14.07 m within 6 min. The reactor core isolation cooling system was then automatically switched off, followed by the automatic switch-over of the high-pressure coolant injection system to minimum flow operation. Subsequent reactor pressure vessel feeding was carried out by means of the control rod flushing water and the seal water.

Due to the damage caused by the fire in the transformer, the plant was shut down. The fire of the transformer showed the normal behaviour of a big oil-filled transformer housing, the fire lacks combustion air and produces a large amount of smoke (see Figure 8).

A detailed root cause analysis regarding the different deviations from the expected event sequence was carried out. The cause of the fire was a short circuit in the windings of the generator transformer. Due to the damages to the transformer it was not possible to resolve the failure mechanisms in all details.

To end the short circuit, the differential protection system of the generator transformer caused to open the circuit breaker between the 380 kV grid connection and the affected generator transformer as well as the generator circuit breaker to the unaffected transformer.

The generator circuit breaker to the affected transformer did not open since the generator circuit breakers are not able to interrupt the currents flowing during a short circuit. The

opening of the circuit breaker between the second 380 kV grid connection and the remaining intact generator transformer is caused by the remaining current after de-exciting the generator which initiates the distance relay of the generator protection system.

The loss of the operational feed water supply was caused by the time margins in between the opening of the two 380 kV circuit breakers. The logical sequence in the re-starting program of the feed water pumps could not cope with the specific situation of the delayed low voltage signals during the incident.

The further drop in the reactor pressure vessel level following the actuation of steam line isolation and the reactor core isolation cooling system was caused by the manual opening of the two safety and relief valves for 4 min. The manual opening of safety and relief valves was not needed in the case of this event sequence and at that point in time. The reason for the manual opening of two safety and relief valves will be part of a detailed human factor analysis which is not completed.

As a consequence of these indications, improvements concerning the fire protection of transformers are intended in Germany (Berg et al., 2010).



Fig. 8. Flame and smoke occurring at the generator transformer; the photo on the right hand shows the fire extinguishing activities

5.4 Phase-to-phase electrical fault in an electrical bus duct

A phase-to-phase electrical fault, that lasted four to eight seconds, occurred in a 12 kV electrical bus duct at the Diablo Canyon nuclear power plant in May 2000 (Brown et al., 2009). This bus supplied the reactor coolant and water circulating pumps, thus resulting in a turbine trip and consequently in a reactor trip.

The fault in the 12 kV bus occurred below a separate 4 kV bus from the start-up transformer, and smoke resulting from the HEAF caused an additional failure.

When the circuit breaker tripped, there was a loss of power to all 4 kV vital and non-vital buses and a 480 V power supply to a switchyard control building, which caused a loss of power to the charger for the switchyard batteries. After 33 hours, plant personnel were able to energize the 4 kV and 480 V non-vital buses.

This event was initiated due to the centre bus overheating causing the polyvinyl chloride (PVC) insulation to smoke, which led to a failure of the adjacent bus insulation. Having only a thin layer of silver plating on the electrodes, noticeably flaking off in areas not directly affected by the arc, contributed to the high-energetic arcing fault event.

Other factors that caused the failure were heavy bus loading and splice joint configurations, torque relaxation, and undetected damage from a 1995 transformer explosion. Two photos of this failure are shown in Figure 9. More photos are provided in (Brown et al, 2009).



Fig. 9. Photographs of the damages at the Diablo Canyon nuclear power plant (from Brown et al., 2009)

5.5 Short circuit due to fall of a crane onto cable trays

This event occurs at a Ukrainian plant which was at that time under construction when work on dismounting of the lifting crane was fulfilled (IAEA, 2004).

The crane was located near the 330/6 kV emergency auxiliary transformers TP4 and TP5 which are designed for transformation 330 kV voltage to 6 kV for power supply of the 6kV AC house distribution system of the unit 4 and the emergency power supply system 6 kV for unit 3. They are located outside at a distance 50 m from the turbine hall of the unit 4. There are two metal clad switchgear rooms (with 26 cabinets and 8 switchers) about four meters from the emergency auxiliary transformers.

The supply of the sub-distribution buses building from the power centre rooms (see Figure 10), was ensured by a trestle with cable trays consisting of power, control and instrumentation cables for the units 3 and 4.

All trays were provided with the cut-off fire barriers. The transformer rooms were supplied by an automatic fire extinguishing system, which actuated when the gas and differential protection actuated.

The event started when the jib of the crane fell on the trestle with the cables passed from 330/6 kV transformer TP 4 and TP 5 to unit 4 and broke them. The cables fell on the ground. The diagram of the situation after the event is provided in Figure 10 (IAEA, 2004).

Damages of all cable trays lead to loss of instrumentation cables for relay protection of the transformers and the trunk line 6 kV.

As a result the earth fault of the cables 6kV could not be disconnected rapidly. The emergency relay protection of the transformers during earth fault 6 kV from the side 330 kV with the executive current from the storage battery for open-type distribution substation 330 kV was not designed.

To remove this earth fault the plant was cut off from outside high-voltage transmission lines 330 kV by electrical protection actuation and the voltage on the power supply bus was decreased.

There was a loss of normal and emergency auxiliary power supply which resulted in a decrease of the frequency of the power supply buses of the main coolant pumps. The emergency protection was actuated and the reactors of units 2 and 3 were scrammed. The long-term exposure of this earth fault (1 min and 36 sec.) caused a high earth fault currents which burn the cables. This led to a fire spread to the 6 kV supply distribution buses and 6 kV metal clad switchgear rooms resulting inside these rooms in high temperature and release of the toxic substance. Also the equipment of the transformers TP 4 and TP 5 was damaged.

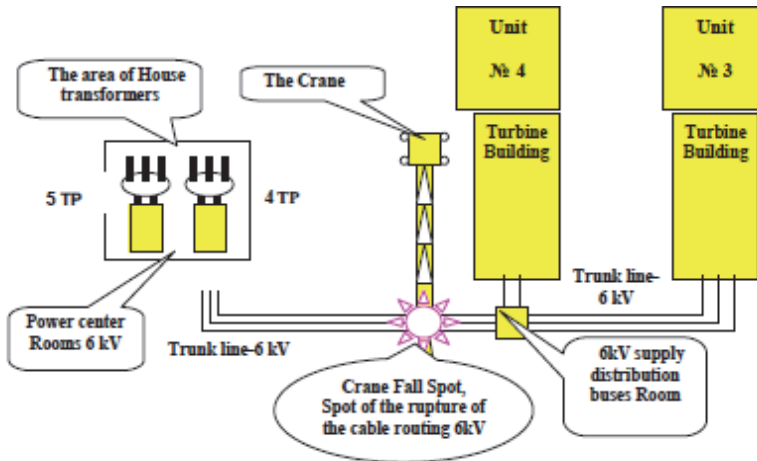


Fig. 10. Diagram of the situation after the event (from IAEA, 2004)

The earth fault has to be disconnected with differential protection of the line 330 kV but it was actuated with the output relays of the TP 4 and TP 5 which was damaged.

The fire was detected by the security guard, the on-site fire brigade was informed, including the outside agency. The automatic fire extinguishing system was activated but stopped working right away because of fire pump's power supply loss. There was no water in the fire mains.

Then the fire brigade laid fire-fighting hoses and provided water with a mobile pump unit. Then the fire brigade waited for the permission from the shift leader.

In compliance with a written procedure, after elimination of the short circuit and restoration of the house distribution power supply the fire brigades could start fire fighting and extinguished the fire about one hour and thirty minutes after detection.

5.6 A triple-pole short circuit at the grounding switch caused by an electrician

In December 1975, a safety significant fire occurred in unit 1 of a nuclear power plant in the former Eastern Germany (see, e.g., Röwekamp & Liemersdorf, 1993 and NEA, 2000). At that time, two units were under operation. Unit 1 was a PWR of the VVER-440-V230 type. The reactor had 6 loops and 2 turbine generators of 220 MWe each.

An electrician caused a triple-pole short-circuit at the grounding switch between one of the exits of the stand-by transformer and the 6 kV bus bar of the 6 kV back-up distribution that

was not required during power operation. The circuit-breaker on the 220 kV side was defective at that time. Therefore, a short circuit current occurred for about 7.5 minutes until the circuit-breaker was actuated manually. The over current heated the 6 kV cable which caught fire over a long stretch in the main cable duct in the turbine building.

The reactor building is connected to the turbine building via an intermediate building, as typical in the VVER plants. The 6 kV distribution is located in this building and the main feed water and emergency feed water pumps all are located in the adjacent turbine building. In the main cable routes nearly all types of cables for power supply, instrumentation and control were located near each other without any spatial separations or fire resistant coatings. In the cable route that caught fire there were, e.g., control cables of the three diesel generators.

Due to the fire in the 6 kV cable, most of those cables failed. The cable failures caused a trip of the main coolant pumps leading to a reactor scram and the unavailability of all feed water and emergency feed water pumps. The heat removal from the reactor was only possible via the secondary side by steam release. Due to the total loss of feed water, the temperature and pressure in the primary circuit increased until the pressuriser safety valves opened. This heating was slow, about 5 h, due to the large water volumes of the six steam generators, 45 m³ in each. In this situation one of the pressuriser safety valves was stuck open. Then the primary pressure decreased and a medium pressure level was obtained so that it was possible to feed the reactor by boron injection pumps. Due to cable faults, the instrumentation for the primary circuit was defective (temperature, pressuriser level). Only one emergency diesel could be started due to the burned control cables. The primary circuit could be filled up again with the aid of this one emergency diesel and one of six big boron injection pumps. With this extraordinary method it was possible to ensure the residual heat removal for hours.

The Soviet construction team personnel incidentally at the site then installed temporarily a cable leading to unit 2. With this cable one of the emergency feed water pumps could be started and it was possible to fill the steam generator secondary side to cool down the primary circuit to cold shutdown conditions. Fortunately, no core damages occurred.

Regarding the weak points with respect to fire safety, first of all, the cause for the fire has to be mentioned. This fire could only occur because there was no selective fusing of power cables.

Another very important reason for the wide fire spreading concerning all kinds of cables was the cable installation. Nearly all cables for the emergency power supply of the different redundancies as well as auxiliary cables were installed in the same cable duct, some of them on the same cable tray.

All the fire barriers were not efficient because the ignition was not locally limited but there were several locations of fire along the cable.

In the common turbine building for the units 1 to 4 of the Greifswald plant with its total length of about 1.000 m there were no fire detectors nor automatic fire fighting systems installed. Therefore, the stationary fire fighting system which could only be actuated manually was not efficient. The design as well as the capacity of the fire fighting system were not sufficient.

Although there were enough well trained fire fighting people, the fire-brigade had problems with manual fire fighting due to the high smoke density as there were no possibilities for an efficient smoke removal in the turbine hall.

5.7 Explosion in a switchgear room due to a failure of a circuit breaker

In December 1996, in a PWR in Belgium the following event occurred. The operator starts a circulating pump (used for cooling of a condenser with river water). This is the first start-up of the pump since the unit was shut down.

About eight seconds later, an explosion occurs in a non safety related circuit breaker room (located two floors below the control room), followed by a limited fire in the PVC control cables inside the cubicles. Due to some delay in the reaction time of the protection relays, normal (380 kV) and auxiliary (150 kV) power supply of train 1 are made unavailable. Safety related equipment of train 1 are supplied by the diesel generating set 1. Normal power supply of train 2 is still available.

The internal emergency plan is activated and the internal fire brigade is constituted. The fire is rapidly extinguished by the internal fire brigade.

As a direct consequence of the explosion five people were injured during the accident, one of them died ten days later.

The fire door at the room entrance was open at the moment of the explosion; this door opens on a small hall giving access to the stairs and to other rooms (containing safety and non safety related supply boards) at the same level; all the fire doors of these rooms were closed at the moment of the explosion and were burst in by the explosion blast. Three other fire doors were damaged (one of these is located on the lower floor); some smoke exhaust dampers did not open due to the explosion (direct destruction of the dampers, bending of the actuating mechanism). One wall collapsed, another one was displaced.

The explosion did not destroy the cubicle of the circulating pump circuit breaker; the supply board and the bus bar were not damaged, except for the effects of the small fire on the control cables; other supply boards located in the same room were not damaged. In the room situated in front of the room where the explosion occurred, the fire door fell down on a safety related supply board, causing slight damages to one cubicle (but this supply board remained available except for the voltage measurement).

A comprehensive root cause analysis has been performed and has shown that the explosion occurred due to the failure of the circuit breaker. The failure occurred probably when the protection relay was spuriously actuated 0.12 seconds after the start up of the pump (over current protection) and led to an inadvertently opening of the circuit.

Based on an investigation of the failing circuit breaker, it was concluded that two phases of a low oil content 6 kV circuit breaker did not open correctly and the next upstream protection device did not interrupt the faulting device. This has led to the formation of long duration high energy arcing faults inside the housing and to the production of intense heat release. This resulted in an overpressure with subsequent opening of the relief valve located at the upper part of the circuit breaker presumably introducing ionised gases and dispersed oil into the air of the cubicle/room. This mixture in combination with the arcs is supposed to be at the origin of the explosion. Indications of arcing between the three phases of the circuit breaker have been observed, resulting in a breach of the housing on two phases. Many investigations were conducted to identify the root cause of the circuit breaker failure (dielectric oil analyses, normal and penalising conditions tests, mechanical control valuations) but no clear explanation could be found. Moreover, the circuit breaker maintenance procedure was compared with the constructor recommendations and the practice in France. No significant difference was noticed.

Although the explosion occurred in a non safety related supply boards room, the event was of general importance, because the same types of circuit breakers were also installed in

safety related areas. Therefore, this event was reported to IAEA and included in the IRS database.

6. First insights

Due to the safety significance of this type of events and the potential relevance for long-term operation of nuclear power stations there is a strong interest in these phenomena in various countries with nuclear energy. Investigations on high energy arcing faults are ongoing in several OECD/NEA member states.

The licensees of German nuclear power plants are principally willing and able to answer the questionnaire concerning HEAF events as far as possible and information being available. In particular, experts from nuclear power plants in Northern Germany have already answered this questionnaire. The licensees intend to use the feedback from the operational experience provided by the answers to the survey and by conclusions and recommendations from the analysis for potential improvements of fire protection features in this respect in their nuclear power plants.

The evaluation of the answers of the remaining licensees to the questionnaire is ongoing and is planned to be completed by the end of 2011.

Due to the most recent experience from German nuclear power plants, it is necessary from the regulatory point of view to investigate high energy arcing fault events. Moreover, it might be helpful to investigate precursors to such events in more detail.

Table 3 gives indications that more than 40 % of the reportable events in Germany related to high energy arcing faults have been reported since 2001. This underlines the increasing relevance of this type of events.

Moreover, nearly half of those events, for which information regarding voltage level is not available, are among the most recent events whereas usually specific information is more difficult to collect for events in the far past. All these different activities and explanations of the current state-of-the-art should be supported by the evaluation of the answers to the German questionnaire.

Concerning high energy arcing fault events, short circuit failure of high voltage cables (typically 10 kV) in cable rooms and cable ducts (channels, tunnels, etc.) is not assumed for German nuclear power plants at the time being. Moreover, a failure of high voltage switchgears (10 kV or more) and the resulting pressure increase are presumed to occur and to be controlled.

Specific investigations with respect to such scenarios have resulted in additional measures for pressure relief inside switchgear buildings of German nuclear power plants.

According to international fire testing standards (EN, 2009) fire barrier elements are designed predominantly against the thermal impact of fires given by the standard fire curve according ISO 834. The pressure build-up due to a HEAF is not considered as fire barrier design load. In the course of several events fire barrier elements such as fire doors were opened or deformed by a HEAF. One example is described in 5.7.

7. Concluding remarks and outlook

7.1 Improvement of the basic knowledge on HEAF

As soon as the questionnaire has been answered by the German nuclear power station licensees, the answers will be statistically examined and interpreted. In particular, potential

consequences of events with this failure mechanism on equipment adjacent to that where the high-energetic arcing faults occurred (particularly safety related equipment including cables, fire protection features) as well as HEAF events in plant areas exceeding the typical fire effects (smoke, soot, heat, etc.) shall be identified. The major goal of this task is to provide first, still rough estimates on the contribution of high energy arcing faults events to the core damage frequency.

The results of the German survey may reveal additional findings on the event causes, possible measures either for event prevention or for limiting the consequences of such faults such that nuclear safety is not impaired. In this context, additional generic results from the OECD HEAF activity are expected.

A review of secondary effects of fires in nuclear power plants (Forell & Einarsson, 2010) based to the OECD FIRE database showed that HEAFs did not only initiated fire event but were also secondary effect of a fire. In two events included in the database, fire generated smoke propagated to an adjacent electrical cabinet, which was ignited by a HEAF. This can be interpreted as a special phenomenon of fire spread. In one case smoke from an intended brush fire spread between the near 230 kV lines and caused a phase-to-phase arc.

As soon as the answers to the questionnaire have been analyzed in detail and the results from the operation feedback are known, a discussion between licensees, reviewers and regulators can be started on the general conclusions and potential back fitting measures and improvements inside the nuclear installations.

Based on the international operating experience, state-of-the-art information and data on high energy arcing faults of electric components and equipment shall be collected and assessed with respect to the phenomena involved. In particular, potential consequences of events with this failure mechanism on adjacent equipment (particularly safety related equipment, fire protection features) and high energy arcing faults events in plant areas exceeding the typical fire effects (smoke, soot, heat, etc.) shall be identified. Based on the collected information and data a more comprehensive and traceable assessment can be performed.

7.2 HEAF assessment

The high energy arcing fault assessment approach developed in (USNRC, 2005) primarily represents an empirical model. As such, it depicts observations mainly based on a single event and characterizes a damaging zone affected this event. To capture variations in current and voltage level, insulation type and cabinet design a mechanistic model has been developed (Hyslop et al., 2008).

Some recent studies have further developed the understanding of the high energy arcing faults phenomena through experimentation and re-evaluation of previous theories.

Damage to cables and equipment by high energy impulses from arcing faults has been shown to be different from that caused by fires alone. Specific components, such as transformers, overhead power lines, and switchgears, have been identified as vulnerable to arc events. However, when looking at the dynamic nature of high energy arcing faults, there are still many factors being not well understood.

Computational fluid dynamics models have also been used to measure the pressure and temperature increase (e.g. in switchgear rooms) and present reasonable results on arc events (Friberg & Pietsch, 1999). However, fires were not evaluated.

The existing research is mainly limited in scope and has not yet addressed all factors important to perform a full-scope probabilistic fire risk assessment including high energy

arcing faults. In general, high energy arcing faults events have been minimally explored but improvements in the early quantitative results have been made. In particular, fire PSA needs to assess the event behaviour beyond the initial arc-fault event itself (as past research has focussed) so as to encompass the issues related to the enduring fire. Issues that go beyond the initial arc fault event include the characterization of the potential for ignition of secondary combustibles, characterization of the fire growth and intensity following the enduring fire, and the effectiveness and timing of fire suppression efforts.

In order to improve the probabilistic fire safety assessment approach, further research including experimental studies with respect to the arc mechanisms and phenomena as well as to the damage criteria of the relevant equipment affected by high energy arcing faults is needed. To better address the needs of probabilistic fire safety assessment, the scope of the testing will need to be expanded as compared to past studies. These research activities will be started in the U.S. in the near future (Hyslop et al., 2008), partially together with other countries interested in high energy arcing faults and their significance.

7.3 Strategies for reducing arc flash hazards

An arc flash fault typically results in an enormous and nearly instantaneous increase in light intensity in the vicinity of the fault. Light intensity levels often rise to several thousand times normal ambient lighting levels. For this reason most, if not all, arc flash detecting relays rely on optical sensors to detect this rapid increase in light intensity. For security reasons, the optical sensing logic is typically further supervised by instantaneous over current elements operating as a fault detector. Arc flash detection relays are capable of issuing a trip signal in as little as 2.5 ms after initiation of the arcing fault (Inshaw & Wilson, 2004).

Arc flash relaying compliments existing conventional relaying. The arc flash detection relay requires a rapid increase in light intensity to operate and is designed with the single purpose of detecting very dangerous explosive-like conditions resulting from an arc flash fault. It operates independently and does not need to be coordinated with existing relaying schemes.

Once the arc flash fault has been detected, there are at least two design options. One option involves directly tripping the upstream bus breakers. Since the arc flash detection time is so short, overall clearing time is essentially reduced to the operating time of the upstream breaker. A second option involves creating an intentional three-phase bus fault by energizing a high speed grounding switch. This approach shunts the arcing energy through the high-speed grounding switch and both faults are then cleared by conventional upstream bus protection. Because the grounding switch typically closes faster than the upstream breaker opens, this approach will result in lower incident energy levels than the first approach. However, it also introduces a second three-phase bolted fault on the system and it requires that a separate high speed grounding switch be installed and operational (Inshaw & Wilson, 2004).

To prevent or alleviate HEAF effects, manufacturers have been working to develop arc arrestors and arc detection methods and to improve composite materials in the switchgear interior. The experiments conducted (see e.g. Jones et al., 2000) indicated that research and testing are required to determine the voltage level, insulation type, and construction where bus insulation may help extinguish or sustain arc once established. The use of such devices would likely impact estimates of fire ignition frequency for such events, but no methods currently exist to account for the presence, or absence, of such equipment.

8. References

- Avendt, J.M. (2008). *A time-current curve approach to flash-arc hazard analysis*, United Service Group, July 9, 2008
- Berg, H. P.; Forell, B.; Fritze, N. & Röwekamp, M. (2009). First National Applications of the OECD FIRE Database. *Proceedings of SMiRT 20, 11th International Seminar on Fire Safety in Nuclear Power Plants and Installations*, August 17-19, 2009, Helsinki, Finland, GRS-A-3496, paper 3.19
- Berg, H.P.; Katzer, S.; Klindt, J. & Röwekamp, M. (2009). Regulatory and experts position on HEAF and resulting actions in Germany, *Proceedings of SMiRT 20, 11th International Seminar on Fire Safety in Nuclear Power Plants and Installations*, August 17-19, 2009, Helsinki, Finland, GRS-A-3496, paper 3.12
- Berg, H. P.; Fritze, N.; Forell, B. & Röwekamp, M. (2010). Risk oriented insights in transformer fires at nuclear installations, *Proceedings of the ESREL Conference 2010, Rhodes*, Taylor & Francis Group, London, pp. 354-361
- Berg, H.P. & Fritze, N. (2011). Reliability of main transformers, *Reliability and Risk Analysis: Theory and Applications*, in press
- Brown, J.W., Nowlen, S.P. & Wyant, F.J. (2009). *High energy arcing fault fires in switchgear equipment, a literature review*, Report SAND2008-4820, Sandia National Laboratories, February 2009
- Burkhart, E.F. (2009). The danger of arc flash, *Fire Engineering*, Vol. 162, Issue 7, July 1, 2009
- Electricity Engineers' Association - EEA (2010). *Discussion paper on arc flash hazards*, December 2010
- EN (2009). Fire classification of construction products and building elements - Part 2: *Classification using data from fire resistance tests, excluding ventilation services*, EN13501-2, September 2009
- Forell, B. & Einarsson, S. (2010). A Survey of Secondary Effects from Fires in Nuclear Power Plants, *Proceedings of the ESREL Conference 2010, Rhodes*, Taylor & Francis Group, London, 1204-1209
- Friberg, G. & Pietsch, G.J. (1999). Calculation of pressure rise due to arcing faults, *IEEE Transactions on Power Delivery*, Vol. 14, No. 2, 365-370
- HDI-Gerling (2009). *Risk engineering guideline, fire protection in electrical equipment rooms*, 04.09
- Hyslop, J.S., Brown, J.W. & Nowlen, S.P. (2008). Considerations for improving fire PRA treatment of high energy arcing faults, *Proceedings of the ANS PSA 2008 Topical Meeting, Knoxville, Tennessee, September 2008*, on CD-ROM
- Inshaw, C. & Wilson, R.A. (2004). Arc flash hazard analysis and mitigation, *Western Protective Conference*, Spokane, WA, October 20th, 2004
- Institute of Electronics and Electrical Engineers (IEEE). (2002). *Guide for performing arc flash hazard calculations*, IEEE 1584, September 2002
- International Atomic Energy Agency (IAEA). (2004). *Experience gained from fires in nuclear power plants: Lessons learned*, IAEA-TECDOC-1421, November 2004
- Jones, R.A., Liggett, D.P., Capelli-Schellpfeffer, M., Macalady, T. Saunders, L.F., Downey, R.E., McClung, L.B., Smith, A., Jamil, S. & Saporita, V.J. (2000). Staged tests increase awareness of arc-flash hazards in electrical equipment, *IEEE Transactions on Industry Applications*, Vol. 36, No. 2, 659-667

- Lane, J. (2004). *Arc-flash hazard analysis, "Putting the pieces of the puzzle together"*, November 8, 2004
- Lang, M.J. (2005). Multiple hazards of arcing faults, *Tech Topics: Arc Flash Note 1, Issue 1*, Ferraz Shawmut
- Lippert K.J., Colaberardino, D.M. & Kimblin, C.W. (2005). Understanding IEEE 1584 arc flash calculations, *IEEE Industry Applications Magazine*, 69 -75, May/June 2005
- National Fire Protection Association (2009). *NFPA 70E: Standard for Electrical Safety in the Workplace*
- Nuclear Energy Agency (NEA), Committee on the Safety of Nuclear Installations. (2000). *Fire Risk Analysis, Fire Simulations, Fire Spreading and Impact of Smoke and Heat on Instrumentation Electronics*, NEA/CSNI/R(99)27, March 10, 2000
- OECD/Nuclear Energy Agency (NEA), Committee on the Safety of Nuclear Installations (CSNI). (2009). *FIRE Project Report, "Collection and Analysis of Fire Events (2002-2008) - First Applications and Expected Further Developments"*, NEA/CSNI/R6 (2009), May 2009
- OECD/Nuclear Energy Agency (NEA), Committee on the Safety of Nuclear Installations (CSNI). (2009a), *"Task on High Energy Arcing Events (HEAF)"*, CAPS submitted to CSNI / IAGE and to CSNI/PRG, Version 9 October 2008 - revised with PRG Chair 27 April 2009, Paris, 2009
- Owen, E.D. (2011a). Arc flash: how extensive is this problem? Part I, *Electrical Source Magazine*, January/February 2011, 33-35
- Owen, E.D. (2011b). Arc flash: how extensive is this problem? Part II, *Electrical Source Magazine*, March/April 2011, in press
- Prasad, S. (2009). Arc flash hazard standards - the burning question, *IDC Electrical Arc Flash Forum, Melbourne*, April 14 -15, 2010
- Röwekamp, M. & Berg, H.P. (2008). PSA significance of events with electrically induced high energy arcing faults, *Proceedings of the International Conference on Probabilistic Safety Assessment and Management (PSAM 9)*, Hong Kong May 18 - 23, 2008 (CD ROM)
- Roewekamp, M. & Liemersdorf, H. (1993). Analysis of fire events in nuclear power plants and conclusions with respect to fundamental requirements concerning fire safety, *Proceedings of 3rd International Seminar on Fire Safety of Nuclear Power Plants, Held in Conjunction with 12th International Conference on Structural Mechanics in Reactor Technology (SMIRT 12)*, 23-24 August 1993, Heidelberg, Germany. Kernforschungszentrum Karlsruhe, 103-126
- Röwekamp, M., & Klindt, J. (2007). *Questionnaire on High Energy Electric Arc Faults HEAF*, Draft including international comments, January 2007
- Röwekamp, M., Frey, W., Klindt, J. & Katzer, S. (2009). *Hochenergetisches elektrisches Versagen von Schaltanlagen*, Gesellschaft für Anlagen- und Reaktorsicherheit (GRS) mbH, GRS-A-3485, Köln; August 2009
- Röwekamp, M., Klindt, J. & Katzer, S. (2007). *Internationaler Fragenkatalog zum hochenergetischen elektrischen Versagen (High Energy Electric (Arc) Faults, HEEF*, December 2007

U.S. Nuclear Regulatory Commission and Electric Power Research Institute (2005).
EPRI/NRC-RES Fire PRA methodology for nuclear power facilities, Report NUREG/CR-6850 and EPRI TR-1011989, September 2005

Research on Severe Accidents in Nuclear Power Plants

Jean-Pierre Van Dorsselaere, Thierry Albiol and Jean-Claude Micaelli
Institut de Radioprotection et de Sûreté Nucléaire (IRSN)
France

1. Introduction

Severe accidents (SA) in nuclear power plants (NPPs) are unlikely events but with serious consequences, as recently shown by the accident that occurred in April 2011 in the Fukushima Japanese NPPs. SA research started originally in the seventies with initial risk assessment studies and later on with experimental programs, development of numerical simulation codes, and Level 2 Probabilistic Safety Assessments (PSA2). A huge amount of research and development (R&D) was performed in the last thirty years in the international frame. This was pushed forward by the two core meltdown accidents that occurred: first in the Unit N°2 of the Three Mile Island (TMI-2) Pressurized Water Reactor (PWR) near Harrisburg (Pennsylvania, USA) on March 28, 1979; then in the Chernobyl RBMK (Water-cooled channel-type reactors with graphite as moderator, designed by Soviet Union) reactor in Ukraine. Large progress has been reached in recent years on the understanding of SA but several issues still need research activities to reduce uncertainties and consolidate the accident management plans.

Along with the progress of understanding and the limited amount of the national budgets on SA R&D, the high complexity of the physical phenomena and the high cost of experiments made necessary to better rank the R&D needs. In 2004 the European Commission judged necessary to better coordinate the national efforts to optimise the use of the available expertise and the experimental facilities in order to resolve the remaining issues for enhancing the safety of existing and future NPPs. This led to launch SARNET (Severe Accident Research NETwork of Excellence) (Albiol et al., 2008; Micaelli et al., 2005), in the framework of the 6th Framework Programme (FP6) of the European Commission, gathering most worldwide actors on R&D SA. One of the main outcomes was the identification of the highest priority SA issues still to be solved. A second phase of the network (SARNET2 project) has started in April 2009, again supported by EC in the FP7 for four years, again coordinated by IRSN.

Section 2 describes shortly what a severe accident is (most of the material described in this section is issued from the reference IRSN-CEA, 2007). Section 3 presents the general approach on SA R&D. Section 4 explains in details the approach that was adopted in SARNET to rank the R&D priorities. Section 5 describes the current SARNET2 FP7 project and the common research programmes, and finally Section 6 focuses, for the sake of illustration, on the important issue of coolability of a degraded core during reflooding.

2. Severe accidents in nuclear power plants

2.1 Case of present nuclear power plants

The “severe accident” refers to an event with an extremely low probability of occurrence (such as 10^{-5} per reactor per year¹ for internal events), thanks to the preventive measures implemented by NPP operators, but causing significant damage to the reactor core, with more or less complete core meltdown and finally possible serious consequences in case of release of radioactive products into the environment.

SAs are generally caused by a cooling failure within the reactor cooling system (RCS), which prevents proper evacuation of residual power from the core, and by multiple dysfunctions, arising from equipment and/or human error, including the failure of safety procedures. A series of complex phenomena then occur, according to various scenarios and depending on the initial conditions of the accident and on the operator actions. For the purpose of this document, “early releases” are those liable to occur before all the measures aiming at protecting the general public can be implemented. Figure 1 schematically presents the major physical phenomena that may occur during a SA, as well as a few safety systems involved.

If the reactor core remains uncovered by water for an extended period of time (typically a few hours), nuclear fuel progressively overheats due to residual power. Steam initiates an exothermic oxidation of zircaloy fuel cladding, resulting in substantial production of hydrogen and thermal power. Additionally, chemical reactions between fuel and its cladding produce low-melting-point eutectics, resulting in relocation of molten materials (called “corium”) in the core. The fuel first releases the most volatile fission products, then the semi-volatile products.

Progressively, a corium pool forms in the core and progresses towards the lower head of the vessel. When it reaches water remaining there, water is vaporized, corium is fragmented and forms a debris bed. During core degradation, standby supplies of water can be delivered to the RCS or the secondary cooling system. Reflooding a degraded core is a complex phenomenon which may enable the accident progression to be slowed down or halted under certain conditions. In contrast, reflooding may also increase hydrogen production and cause further release of fission products.

Corium melts and debris accumulate in the vessel lower head and may cause its rupture, either by thermal erosion, creep or plastic failure, depending on pressure conditions in the RCS. After vessel rupture in case of high-pressure conditions within the vessel, part of the ejected corium is fragmented and may be dispersed into the containment. This may provoke a pressure spike, resulting in substantial heat exchange with the air, oxidation of the corium metallic components and, in some cases, simultaneous combustion of the hydrogen present in the containment building. This phenomenon is called “direct containment heating” (DCH).

Following vessel rupture, corium slumps and accumulates in the reactor pit. A corium-water interaction (called Fuel-Coolant Interaction or FCI) may occur if the pit contains some water, which may be followed by a more violent phenomenon called steam explosion. This explosion may create projectiles that could threaten the leak-tightness of the containment buildings. Without initial presence of water in the pit, corium will thermally erode the concrete basemat, which could cause the loss of containment: this is the Molten-Corium-Concrete-Interaction or MCCI. During this phase, a substantial quantity of incondensable gas (H_2 , CO , CO_2) is released, resulting in a progressive increase in pressure within the containment building. To avoid a potential break in this structure, a ventilation-filtration

¹ This figure could be updated in the future, following the recent Fukushima accident.

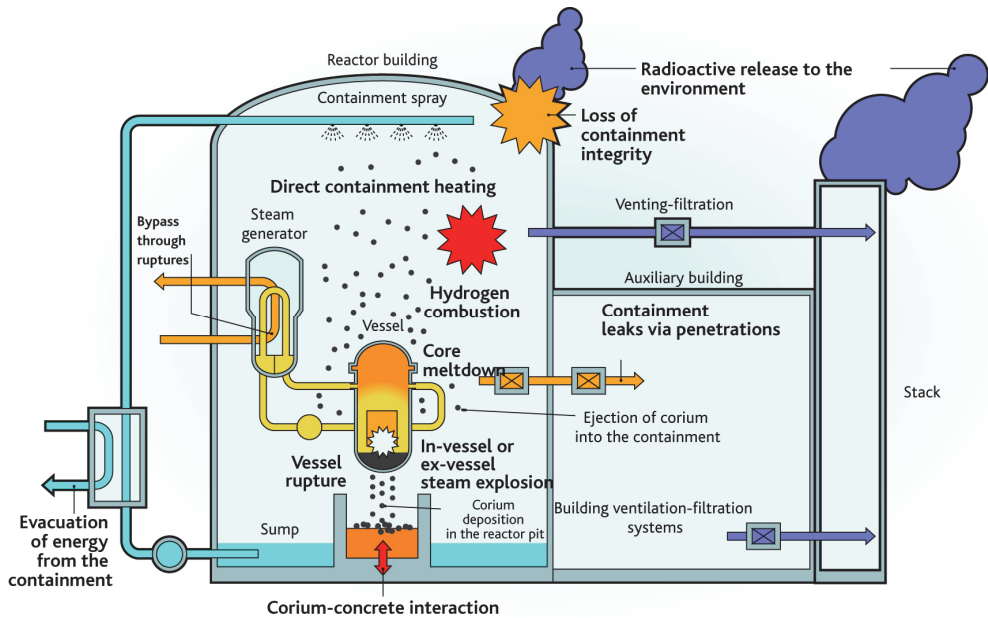


Fig. 1. Main physical phenomena during a severe accident

system has been installed in all Light Water Reactors (LWR): it can be activated in general 24 hours after an accident begins, if the containment heat removal system fails.

Hydrogen produced by core degradation is released into the containment, where it burns on contact with oxygen, provoking a pressure and temperature spike which may damage the containment building. This combustion can either be slow acting (slow deflagration) or more rapid (rapid deflagration) and, in some cases, explosive (detonation). Hydrogen combustion may lead to the loss of the containment barrier: a commitment to making this risk residual has been demonstrated by the progressive implementation of hydrogen Passive Autocatalytic Recombiners (PAR) in many NPPs.

For all modes of containment rupture, the release of fission products into the environment depends on the conditions affecting their transfer within the reactor. The transfer of fission products depends primarily on their physical and chemical properties, i.e. whether they are gases or aerosols and their chemical form. Iodine and ruthenium behaviour requires particular attention, given their complexity and their significant short-term radiological impact. Regarding longer-term accident consequences, particular attention must be paid to caesium releases.

In the event of a SA, operating personnel are called upon to follow the recommendations in the Severe Accident Management Guidelines (SAMG). Actions recommended in the SAMG serve primarily to maintain containment, aiming to:

- Avoid or minimise airborne radioactive releases outside the containment building,
- Provide sufficient time before potential containment loss to allow implementation of the public protection measures described in emergency plans.

2.2 Case of future nuclear power plants

For all new NPPs of any type under construction or planned today, named “Generation III” (noted Gen.III in the following), the provisions aim to significantly enhance accident prevention and the SAs are addressed from the design phase.

For the EPR (European Pressurized Reactor), the technical directives specified that:

- Core meltdown accidents, particularly under pressurised conditions, postulated to cause large early releases must be “practically eliminated”. While such accidents remain physically possible, design measures must be implemented to prevent them. For instance a dedicated pressurisation valve, coupled with an isolation valve, was integrated in the RCS, in addition to the standard safety mechanisms protecting this system from overpressure. PARs have also been installed in the containment.
- Low-pressure core meltdown sequences must proceed in such a way that the maximum conceivable releases only require measures very limited in duration and scope to protect the public. Thus a system was implemented to collect corium and stabilise it on the long-term: this “core-catcher” is built in the containment building and linked to the reactor pit. Besides, the containment has a double concrete wall, with filtration, to increase the containment tightness with respect to radioactive release.

In other Gen.III NPPs, different designs have been elaborated for stopping corium progression or limiting its consequences. Some NPPs aim at maintaining corium within the vessel (In-Vessel-Retention or IVR) by cooling the external surface of the vessel lower head through water injection into the pit. Others have designed core-catchers differently from the EPR one that is based on corium spreading. Advanced VVERs² adopt a core-catcher underneath the vessel (like the one at Tian Wan in China or being built in Belene in Bulgaria): this core-catcher makes use of sacrificial materials consisting mainly of steel, iron oxide ceramic and alumina.

3. Research and development on severe accidents

3.1 General approach

The general approach for SA R&D (Figure 2) is based on one hand on experiments and on the other hand on computer codes for simulation of physical phenomena.

The SA R&D presents some specific features that imply very high costs:

- Complexity of the physical phenomena,
- High number of phenomena, with the need of considering them together due to their mutual interactions (“coupling”),
- Extreme conditions: very high temperatures (above 3000°C), high pressure (up to 200 bars), irradiation effects,
- Need of tests with real materials (importance of the “material effect”),
- Difficulty to extrapolate to the reactor scale.

It has involved in the past very substantial human and financial resources as well as collaboration between nuclear stakeholders, industry groups, research centres and safety authorities, at both the national and international levels. The international programmes concerned mainly the Framework Programmes of Research and Development of the European Commission (see <http://cordis.europa.eu>) and the projects conducted under the

² VVER: water-cooled water-moderated power reactors (PWR type) that were developed in the ex-Soviet Union.

auspices of the CSNI (Committee on the Safety of Nuclear Installations) of NEA (Nuclear Energy Agency) in the OECD (Organisation for Economic Cooperation and Development) (CSNI, 2000; OECD, 2007).

The research in this area thus aims to further understand the physical phenomena and reduce the uncertainties on their quantification, with the ultimate goal of physical developing models that can be applied to reactors. These models, implemented in computer codes, allow predicting SA progression and consequences.

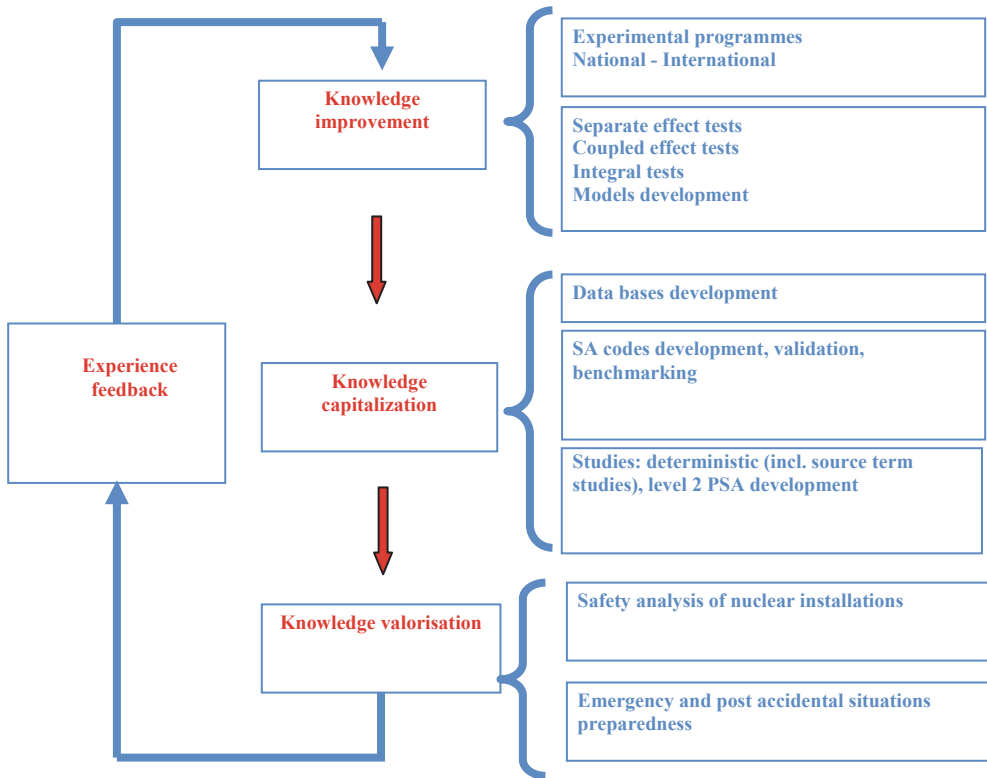


Fig. 2. General R&D approach

For Gen.III NPPs, this research allowed to design specific devices for SA prevention and for mitigation of consequences, as described in Section 2.2. However, for existing plants (called Generation II and noted Gen.II in the following), SAs were not a design consideration. Consequently, modifications of their design are limited and the research in this area is primarily aimed at limiting the potential impact of SAs. Specifically, there are two complementary research orientations: a) characterising releases and studying modes of containment failure, and b) developing methods to limit the consequences of the SA scenarios.

3.2 Experimental R&D programmes

Different categories of experiments are usually defined:

- *Separate effect tests (SET)* investigate a single phenomenon and yield data for development of a model which describes its effect and which is to be integrated as a sub-routine into a computer code. The corresponding facilities are typically single-purpose, small-scale channels, loops or vessels equipped with specialised, sophisticated, high-accuracy instrumentation.
- *Coupled effect tests (CET)* investigate the coupling of two or more phenomena previously explored in SETs, and provide data for the appropriate integration of the corresponding models into a code. The corresponding facilities are typically of small to intermediate-scale, using a test loop or a test vessel with comprehensive instrumentation adapted to the effects to be investigated.
- *Integral Experiments* represent all or part of a reactor accident sequence. They examine the interactions of several phenomena previously studied in SETs and/or CETs. The data obtained are needed for confirmatory validation of a code and its application, i.e. adequate problem set-up by the code user, correct and complete modelling of the relevant phenomena and their interactions within the code. The corresponding facilities are typically intermediate to large-scale models of full size bundle or containment, in the latter case with variable infrastructure for investigating many aspects of containment behaviour.

3.3 Development of computer codes for SA numerical simulation

3.3.1 Types of codes

Three classes of SA codes can be defined, depending on their scope of application: integral codes, detailed codes and dedicated codes.

- *Integral codes* (also called “system” codes or, in the past “engineering-level” codes): these codes simulate the overall NPP response, i.e. the response of the RCS, the containment, and the source term to the environment, using “integrated” models for a self-consistent thorough analysis of the accident. They include a well-balanced combination of phenomenological and user-defined parametric models for the simulation of the relevant phenomena. They must be (relatively) fast running to enable sufficient number of simulations of different scenarios to be performed, accompanied by parameter studies to address uncertainties: the computing time should be roughly around the accident real time. These codes are primarily not designed to perform Best-Estimate simulations, but rather to allow the user to bound important processes or phenomena by numerous user-defined parameters. Integral codes are usually used to support PSA2 analyses and for the development and validation of Severe Accident Management (SAM) programmes. In the last years, the rapid increase of the computer performance enabled more and more the replacement of parametric models by mechanistically based ones in the integral codes. The main internationally used codes are today ASTEC (see Section 5.6), jointly developed by IRSN and GRS (Van Dorsselaere et al., 2009), MAAP, developed by Fauske & Associates Inc. (USA), and MELCOR, developed by Sandia National Laboratories (USA).
- *Detailed codes* (also called mechanistic codes): they are characterised by best-estimate phenomenological models, consistent with the state of the art, to enable as far as possible an accurate simulation of the behaviour of a NPP in case of SA. In order to better illustrate the differences with the approach of integral codes, in most cases, a numerical solution is found for integral-differential equations while in integral codes

some correlations may be used. Basic requirements are that the modelling uncertainties are comparable with the uncertainties on the experimental data used to validate the code and that user-defined parameters are only necessary for phenomena that are not understood due to insufficient experimental data (including scaling problems). Since, as a basic principle, these codes should have as few as possible user options, existing uncertainties in the simulation of the different phenomena must be specified to enable the definition of the uncertainties of the key results. The main advantages of these codes are to give a more detailed insight into the progression of a SA and to design and optimise mitigation measures. They can also be used for benchmarking the integral codes. Due to the high computation time, they simulate only a part of the plant, e.g. RCS or containment. Their computation time depends on the scope of the application but it can span over days and weeks. The main internationally used codes are today: for the RCS behaviour and the core degradation ATHLET-CD (GRS), SCDAP/RELAP5 (INL in the USA), RELAP/SCDAPSIM (ISS in the USA) and ICARE/CATHARE (IRSN) and for containment CONTAIN (ANL in the USA) and COCOSYS (GRS).

- *Dedicated codes*: these codes that deal with a few phenomena have become important in context with the requirements of the regulatory authorities to take into account SAs in the design of new NPPs and to reduce uncertainties of risk-relevant phenomena. In general they have to be very complex with the drawback of large calculation time. Typical issues for which dedicated codes are required include: steam explosion and melt dispersal (e.g. MC3D at IRSN), structure mechanics (e.g. CAST3M at CEA in France, or ABAQUS in the USA). This family of codes includes the CFD (Computational Fluid Dynamics) codes that solve Navier-Stokes thermal-hydraulics equations in 3D geometry, such as GASFLOW in KIT (Germany), TONUS in IRSN, CFX as commercial tool, etc....

3.3.2 Process of code development and validation

The general process of code development is composed of the following steps, with possible iterations between them:

- Code requirements (scope of application, computing time, etc...),
- General specifications (structure, programming language, level of details of modelling, numerical schemes, etc...),
- Detailed specifications, possibly with prototyping to check a model or a numerical scheme,
- Physical model development,
- Implementation into a computer code,
- Code verification (tests on analytic solutions of equations, laws of conservation of mass, energy, and momentum, portability on diverse computers types, numerical coupling between models, etc..).

The code validation process aims at providing a sufficiently accurate representation of the reality of the SA phenomena. But this SA field presents some very peculiar features due to the continuous evolution of knowledge and to the extreme conditions that occur in a SA, notably the geometry scale that is difficult to achieve in laboratory experiments. The VASA project (Allelein et al., 2001) took place in the FP4 of the European Commission to analyse this SA validation process in details. Two stages can be defined:

- Comparing the code results with results of experimental programmes, which leads to define a “validation matrix”.
- Verifying the code capability to adequately simulate real SA scenarios at full-scale, which may be done through several types of work:
 - Benchmarking the code results of plant applications with results of other codes, either integral codes or detailed ones,
 - Applying the code to real plant SA scenarios, which is very scarce except for the TMI-2 and Chernobyl accidents (and in addition the Fukushima accident in the future when reliable data become available),
 - Performing uncertainty analyses in order to show the consistency and the reliability of code results, including the analysis of the influence of nodalisation and of numerical time-steps.

The CSNI International Standard Problems (ISP) provide a particularly valuable source of information for code validation: they are comparative exercises in which predictions of different computer codes for a given physical problem are compared with each other and with the results of a carefully controlled and well documented experiment. Over the last thirty years, forty-nine ISPs have been sponsored (CSNI, 2000).

The qualification of the code user is an important part of the code validation process. The user may have an impact on the quality of the SA analysis. It is considered essential that users have a good knowledge of the modelling inside the code and that the codes should not be run as “black boxes”.

4. SARNET approach on severe accident R&D ranking

Most of the material described in the Section 4 is issued from the SARNET reference (Schwinges et al., 2008).

4.1 Objectives and work scope of the SARP group

The EURSAFE thematic network (Magallon, 2005) yielded a list of 21 areas of needed research in the SA domain, which included recommendations for experimental programmes and code development. To further develop this list as a living document, the work package “Severe Accident Research Priorities” (SARP) was established in the SARNET FP6 project.

The activities in SARP focused on the identification of areas where the knowledge has been considerably improved and where further experimental research and/or model development seemed not to be of high priority. Furthermore it had to identify research areas which needed reorientation and, last but not least, the needed research not yet being covered. The outcome of the SARP work was an up-dated ranking, giving different priorities to the research issues, and helping (thus linking the last sentence to the previous one..) decision to perform the different research programmes.

The working scope was outlined as:

- Agree on methodology,
- Identify issues resulting from EURSAFE not appropriately covered and review them,
- Analyse R&D recent progress,
- Analyse results from PSA2 studies,
- Reassess the ranking of research issues and reorient the priorities,
- Review potential experimental and theoretical programmes to address these issues,
- Make recommendations for revision of R&D programmes.

4.2 EURSAFE methodology and results

The objectives of EURSAFE were to establish a large consensus on the SA issues, where large uncertainties still subsist, and to propose a structure to address these uncertainties by appropriate R&D programmes making the best use of the European resources. It incorporated issues related to existing plants (PWR, BWR³ and VVER), lifetime extension of these plants, evolutionary concepts (higher burn-up and mixed oxide –MOX– fuels), and safety and efficiency of future systems. Twenty partners representing R&D governmental institutions, regulatory bodies, nuclear industry, utilities and universities from nine European countries and Canada worked together in a network structure, which was supposed to be a starting point of SARNET.

To achieve the objectives, sufficient convergence on issues and phenomena and on their importance in terms of safety and knowledge was required among all actors. The final objective was a consensual approach to resolve the remaining uncertainties and open issues. Establishing Phenomena Identification and Ranking Tables (PIRT) has been proved in other areas (e.g. Loss of Coolant Accidents or LOCA) to be an efficient and unbiased way to reach such a consensus (NUREG, 2000). In EURSAFE the PIRT integrated all the SA issues from core degradation up to release of fission products from the containment, taking into account any possible counter-measures and the evolution of fuel management.

As a basis, a comprehensive list of 1016 SA phenomena was established. The phenomena were classified in five groups:

- In-vessel (162 phenomena),
- Ex-vessel (149 phenomena),
- Dynamic loading of the containment (461 phenomena),
- Long-term loading of the containment (116 phenomena),
- Fission products (128 phenomena).

Three safety-oriented groups of experts scrutinized these phenomena of the five lists and ranked them in accordance to their safety importance for primary circuit, containment and source term. Two evaluations were established: the safety importance ratio and the knowledge ratio. Starting with 1016 identified phenomena, the list was reduced to 239 items, important for safety, of which 106 were found with significant lack of knowledge.

After completion of the two ranking phases, this procedure clearly emphasized the phenomena being simultaneously highly important for safety and significantly lacking of knowledge. The remaining 106 phenomena were obviously candidates for further R&D work:

- 24 phenomena for In-vessel,
- 28 phenomena for Ex-vessel,
- 26 phenomena for Dynamic loading of the containment,
- 10 phenomena for Long-term loading of the containment,
- 18 phenomena for Fission products.

As a further step, the research needs and programmes to address each selected phenomenon of the PIRT list were identified and established in a list. According to the similarities in terms of research needs and physical processes, with the scope of being able to set up a limited number of coherent R&D programmes, several phenomena were merged into research issues without further elimination or selection. A rationale for these research needs

³ Boiling Water Reactors

was established based on safety relevance and lack of knowledge. The outcomes of this process are summarised in Table 1, which gives the 21 items of needed research (EURSAFE Research Issues or ERI) and corresponding rationales drawn from the 106 phenomena selected in the PIRT.

ERI	EURSAFE Research Issue	Rationale for selection
1,1	Hydrogen generation during reflooding or melt relocation into water	Rapid generation of hydrogen which may not be accommodated by recombiners and the risk of early containment failure. Improve knowledge about the magnitude of hydrogen generation.
1,2	Core coolability during re-flooding and thermal-hydraulics within particulate debris	Termination of the accident by re-flooding of the core while maintaining the integrity of the RCS. Increase predictability of core cooling during reflooding.
1,3	Corium coolability in lower head and external corium catcher device	Improve predictability of the thermal loading on Reactor Pressure Vessel (RPV) lower head or corium catcher devices to maintain their integrity.
1,4	Integrity of RPV due to external vessel cooling	Improve data base for critical heat flux and external cooling conditions to evaluate and design Accident Management (AM) strategies of external vessel cooling for in-vessel melt retention.
1,5	Integrity of RCS	Improve predictability of heat distribution in the RCS to quantify the risk of RCS failure and possible containment bypass.
1,6	Corium release following vessel failure	Improve predictability of mode and location of RPV failure to characterise the corium release into the containment.
2,1	MCCI: molten pool configuration and concrete ablation	Improve predictability of axial versus radial ablation up to late phase MCCI to determine basement material failure time and loss of containment integrity.
2,2	Ex-Vessel corium coolability, top flooding	Increase the knowledge of cooling mechanisms by top flooding the corium pool to demonstrate termination of accident progression and maintenance of containment integrity.
2,3	Ex-Vessel corium catcher: corium ceramics interaction and properties	Demonstrate the efficiency of specific corium catcher designs by improving the predictability of the corium interaction with corium catcher materials.
2,4	Ex-Vessel corium catcher: coolability and water bottom injection	Demonstrate the efficiency of water bottom injection to cool corium pool and its impact on containment pressurisation.

ERI	EURSAFE Research Issue	Rationale for selection
3,1	Melt relocation into water and particulate formation	Determine characteristics of jet fragmentation, debris bed formation and debris coolability towards maintenance of vessel and respectively containment integrity.
3,2	FCI incl. steam explosion: melt into water, in-vessel and ex-vessel	Increase the knowledge of parameters affecting steam explosion energetic during corium relocation into water and determine the risk of vessel or containment failure.
3,3	FCI incl. steam explosion in stratified situation	Investigate the risk of weakened vessel failure during reflooding of a molten pool in the lower head.
3,4	Containment atmosphere mixing and hydrogen combustion / detonation	Identify the risk of early containment failure due to hydrogen accumulation leading to deflagration or detonation and to identify counter-measures.
3,5	Dynamic and static behaviour of containment, crack formation and leakage at penetrations	Estimate the leakage of fission products to the environment.
4,1	Direct containment heating	Increase the knowledge of parameters affecting the pressure build-up due to DCH and determine the risk of containment failure.
5,1	Oxidising environment impact on source term	Quantify the source term, in particular for ruthenium, under oxidation conditions / air ingress for high burn-up and MOX fuels.
5,2	RCS high temperature chemistry impact on source term	Improve predictability of iodine species exiting RCS to provide the best estimate of the source into the containment.
5,3	Aerosol behaviour impact on source term	Quantify the source term for aerosol retention in the secondary side of steam generator (SG) and leakage through cracks in the containment wall as well as the source in containment due to revolatilization in RCS.
5,4	Containment chemistry impact on source term	Improve the predictability of iodine chemistry in containment to reduce the uncertainty in iodine source term.
5,5	Core reflooding impact on source term	Characterise and quantify the fission product release during core reflooding.

Table 1. EURSAFE Research Issue and rationale for selection

4.3 Decision procedure followed in SARP

In the SARNET FP6 project, the SARP work, lead by GRS, was performed in close collaboration with eight organizations, representing diverse types of organizations (IRSN, CEA, EDF, FZK now KIT, GRS, KTH, TUS, VTT). The collaboration between those who perform research and those who use its results was essential to correctly address the problem.

One requirement was that all steps of the decision process must be documented to allow a well-funded judgement for the SARNET community and for the end-users of SARNET products. For this reason a template (Trambauer, 2005) was constructed and updated as a living document during the whole process. The template was used for the three possible “Decisions”:

- a. “To be closed” meaning that the issue is closed by sufficiently improved knowledge
- b. “Reorientation” meaning that the work should be reoriented to fulfil the objectives
- c. “New Item” meaning that a new research item should be set up.

The structure of the template reflected the strategy of the intended decision process, with 10 successive “Actions” with a clear indication of responsibility and the time of execution. A comprehensive description of the “Rationale for the decision to be taken” was included, as well as a step of comments from the SARNET community and the end-users.

4.4 SARP results

The methodology applied in EURSAFE to establish an internationally agreed list of needed research items was proven as adequate. It started with a comprehensive list of phenomena and finished by using a bottom-up approach with 21 items of needed research areas. Investigations showed that a well balanced top-down approach gives very similar results. Therefore the EURSAFE methodology was applied in SARP too.

In a first step seven possible new or reoriented research items were identified. The assessment of the following items was performed (for most of them, only a reorientation or a small extension of experimental and/or analytical work planned in SARNET was necessary):

- Investigation of high burn-up cladding materials at high temperature and under reflooding conditions,
- Spreading of corium into cavity nearby compartments possibly filled with water,
- Effect of hydrogen mitigation systems (esp. PAR) on hydrogen distribution,
- Combustion of hydrogen jets in atmosphere with different hydrogen concentrations (in relation to DCH),
- Retention of aerosols in RCS, SG tubes or concrete cracks under consideration of mechanical resuspension,
- Decomposition of iodides by heat-up in PARs and its impact on source term,
- Ruthenium volatility and behaviour in containment.

Then all ERI issues from Table 1 were reassessed in a top-down approach with respect to gain of knowledge and further necessary activities in SARNET. This last step resulted in the merging of some issues and in the following ranking:

- Six issues were regarded to be investigated further with **high** priority:
 - Core coolability during reflooding and debris cooling of a not totally degraded core,
 - Ex-vessel melt pool configuration during MCCI, ex-vessel corium coolability, by top flooding,
 - Melt relocation into water, ex-vessel FCI,

- Hydrogen mixing and combustion in containment,
- Oxidising impact (ruthenium oxidising conditions/air ingress for high burn-up and MOX fuel elements) on source term,
- Iodine chemistry in RCS and in containment.
- Four issues were reassessed with **medium** priority; these items should be investigated further as planned in the different research programs. The risk significance was reduced due to significant progress of knowledge, but some questions were still open:
 - Hydrogen generation during reflooding and during melt relocation in vessel,
 - Corium coolability in vessel lower head,
 - Integrity of reactor pressure vessel due to external vessel cooling,
 - Direct containment heating.
- Five issues were assessed with **low priority**; the current knowledge was considered as sufficient according to the state and progress of knowledge and the risk and safety relevance and taking into account ongoing activities outside SARNET frame, and they could be closed after the end of the related activities:
 - Corium coolability in external core-catcher,
 - Corium release following vessel rupture,
 - Crack formation and leakages in concrete containment,
 - Aerosol behaviour impact on source term (SG tubes and containment cracks);
 - Core reflooding impact on source term.
- Three issues were marked as “issue **could be closed**”. This means that the current issue knowledge was considered as sufficient assessing both the state and progress of knowledge and the risk and safety relevance and taking into account ongoing activities:
 - Heat distribution in RCS and RCS integrity,
 - Ex-vessel core-catcher and corium-ceramics interaction, cooling with water bottom injection,
 - FCI including steam explosion in weakened vessel.

Concerning the end-users' opinion, the utilities and vendors are mainly interested in the practical value of research results which can be used for developing plant-specific solutions for SAM measures. Risk-informed ranking seems not to be a straightforward approach for assessment because the results of PSA2 are plant-specific. Anyhow the aspect of risk must be taken into account during the assessment discussions by reflecting the risk relevance of each phenomenon with respect to the source term (large releases or not) as threat to the environment. The discussions on each issue should definitely include the applicability of the expected research results to possible SAM measures (planned, envisaged or under development). The approach adopted in the SARP group is an attempt to come within a reasonable time with consideration of all pertinent factors to an agreed decision considering all aspects of innovation and economic efficiency. The outcomes of the final SARP report already served as a proposal to provide the orientations for joint activities for research of common interest and high priority in the SARNET2 FP7 project. An important aspect has also been the total traceability for possible future updates.

5. The SARNET2 project

5.1 General description of the network

Forty-two partners (Table 2) from Europe, Canada, Korea and the USA, participate in the SARNET2 FP7 project (Van Dorsseleare et al., 2011) that started in April 2009 for a period of

Partner	Short name	Country
Institut de Radioprotection et de Sûreté Nucléaire	IRSN	France
KFKI Atomic Energy Research Institute	AEKI	Hungary
AREVA NP GmbH	AREVA GmbH	Germany
AREVA NP SAS	AREVA NP SAS	France
Budapest University of Technology and Economics	BME	Hungary
Commissariat à l'Energie Atomique et aux Energies Alternatives	CEA	France
ENEA - Ricerca Sul Sistema Elettrico SpA	RSE	Italy
Chalmers tekniska högskola AB	CHALMERS	Sweden
Centro de Investigaciones Energeticas Medio Ambientales y Tecnologicas	CIEMAT	Spain
National Centre for Scientific Research "DEMOKRITOS"	DEMOKRITOS	Greece
Electricité de France SA	EDF	France
Energy Institute JSC Sofia	EI	Bulgaria
Ente per le Nuove Tecnologie, l'Energia e l'Ambiente	ENEA	Italy
Forschungszentrum Juelich GmbH	JÜLICH	Germany
Karlsruhe Institute of Technology	KIT	Germany
Gesellschaft für Anlagen- und Reaktorsicherheit mbH	GRS	Germany
National Autonomous Company for Nuclear Activities - Nuclear Research Subsidiary Pitesti	INR	Romania
Institute for Nuclear Research and Nuclear Energy	INRNE	Bulgaria
Inzinierska Vypoctova Spolocnost Trnava s.r.o.	IVS	Slovakia
Jozef Stefan Institute	JSI	Slovenia
Kungl Tekniska Högskolan	KTH	Sweden
Lithuanian Energy Institute	LEI	Lithuania
National Nuclear Laboratory	NNL	United Kingdom
Nuclear Research & Consultancy Group v.o.f.	NRG	Netherlands
Paul Scherrer Institut	PSI	Switzerland
Ruhr-Universität Bochum	RUB	Germany
Tractebel Engineering SA	TRACTEBEL	Belgium
Thermodata	THERMODATA	France
Technical University of Sofia	TUS	Bulgaria
Urad Jadroveho Dozoru Slovenskej Republiky	UJD SR	Slovakia
Ustav Jaderneho Vyzkumu Rez a.s.	UJV	Czech Rep.
University of Newcastle upon Tyne	UNEW	United Kingdom
Dipartimento di Ingegneria Meccanica, Nucleare e della Produzione - Università di Pisa	UNIPI	Italy
Universität Stuttgart	USTUTT	Germany
NUBIKI Nuclear Safety Research Institute	NUBIKI	Hungary
VTT Technical Research Centre of Finland	VTT	Finland

Partner	Short name	Country
VUJE Trnava, a.s. – Inzinierska, Projektova a Vyskumna Organizacia	VUJE	Slovakia
Commission of the European Communities – Joint Research Centres	JRCs	European Union
Atomic Energy Canada Limited	AECL	Canada
Korea Atomic Energy Research Institute	KAERI	Korea
United States Nuclear Regulatory Commission	USNRC	USA
Korea Institute of Nuclear Safety	KINS	Korea

Table 2. List of SARNET2 partners

four years. They represent a large majority of the European actors involved in SA research plus a few non-European important ones. Diverse types of organizations are represented: research organizations, universities, industry, utilities, safety authorities and Technical Safety Organisations (TSO). A new partner, BARC (India), is joining the network in October 2011.

The network is organised with a Steering Committee of ten members in charge of strategy and decisions, advised by an Advisory Committee of end-user organisations. A General Assembly, composed of one representative of each SARNET Consortium member, plus the EC representative, is called periodically for information and consultation on the progress of the network activities, the work orientations and the decisions taken by the Steering Committee. A Management Team, composed of the network coordinator and of seven Work-Packages (WP) leaders, is entrusted with the day-to-day management of the network. In the continuity of the SARNET FP6 project, the SARNET2 FP7 project has been defined in order to optimize the use of the available means and to constitute a sustainable consortium in which common research programmes and a common computer code on SA, ASTEC, are developed. ASTEC capitalizes the whole knowledge produced in the network through new or improved physical models. The Joint Programme of Activities can be divided into several elements:

- Ranking periodically the priorities of the research programmes, harmonizing and re-orienting existing ones and jointly defining new ones when necessary,
- Performing small and large-scale experiments on the highest priority issues as defined in the SARNET FP6 project and jointly analysing their results in order to elaborate a common understanding of the concerned physical phenomena,
- Developing physical models, integrating them into ASTEC, and validating this code versus experiments and through benchmarks on plant applications with other codes,
- Storing all the experimental results in a scientific database, based on the STRESA tool,
- Disseminating the knowledge to students or young researchers, as well to new nuclear emergent countries, through educational courses, textbooks, mobility of personnel between the network partners, and international conferences that become the major SA event in the world.

On the basis of the outcomes of the SARP work, the research programmes focus on the six high-priority issues that were presented in Section 4.4. They are analyzed in the WP N°5 to 8. The experimental efforts are mainly devoted to two of these issues for which real progress toward the closure of the issue is expected: corium/debris coolability and MCCI. For all these 6 issues, the same method is being adopted: review and selection of available relevant

experiments, contribution to the definition of test matrices, synthesis of the interpretation of experimental data, benchmark exercises between codes, review of models, synthesis and proposals of new or improved models for ASTEC. Indeed a key integration aspect is the set-up of the technical circles, each covering a specific detailed topic. They bring experimenters and modellers closer together, concerning test definition, interpretation, model development etc... In each of the domains, additional studies are being performed in order to bring research results into reactor applications. Calculations of SA scenarios in reactor conditions are being performed using various computer codes, including ASTEC, in order to evaluate the importance of the involved phenomena, in particular through uncertainty studies.

Sections 5.2 to 5.6 summarize the work that is performed in the WP5 to 8 and on the ASTEC code assessment. Section 5.7 summarizes all activities related to dissemination of knowledge.

5.2 Activities on corium and debris coolability

The major motivation is to reduce or possibly solve the remaining uncertainties on the possibility of cooling structures and materials during SA, either in the core or the vessel lower head or in the reactor cavity, in order to limit the progression of the accident. This could be achieved by water injection, either by ensuring corium retention within the vessel or at least slowing down corium progression and limiting the flow rates of corium release into the cavity. These issues are covered within SAM for current reactors, and also within the scope of the design and safety evaluation of future reactors. The current PSA2 studies still show very large uncertainties in the results of the core reflooding phase. For the issue of in-vessel retention in principle two different aspects have to be considered, the probability for reflooding systems to begin operation in due time, and the status or degree of core damage. If core damage occurs at high pressure, low pressure reflooding systems cannot inject against that pressure. But they may be available with a high degree of reliability. In such conditions it is crucial to evaluate if and when depressurisation of the reactor coolant system occurs which would lead to immediate reflooding. In the bottom of BWRs vessel there is a continuous injection through the control rod and pump seal flushing water. Depending on the reliability and capacity of these systems and the pressure in the RCS, the core degradation may be inhibited.

The following three key situations and processes for the investigation of corium and debris coolability are considered.

Reflooding and coolability of a degraded core

The focus is on the accident phase after water boil-off in the core. Heating and melting may produce a severely damaged, partly molten core with relocated material and partly broken parts. Quenching of such a hot and partly degraded core is the main issue here. The specific case of reflooding of a debris bed is detailed in Section 6.

The experimental database on degraded core reflooding was analysed to derive the crucial information about success of reflooding. The QUENCH experiments in KIT constitute the main part of this database. The behaviour of fuel rod bundles can be outlined in a “reflooding map” with respect to the reflooding mass flow rate and the core damage state to deduce the limits up to which final bundle cooling can be expected to be successful and hydrogen production may be tolerated.

The analyses show that even at the onset of severe core degradation at temperatures up to app. 2200 K, the accident progression can be stopped with a sufficiently high flowrate for

core reflooding of ~ 1 g/s per rod. The reflooding map on core degradation and hydrogen release is still under development and is considered as a tool to summarize the existing knowledge and to identify blank areas for efficient future experimental work.

Remelting of debris, melt pool formation and coolability

If core cooling fails, a melt pool will form in the core and melt might flow down into remaining water in the lower head. The TMI-2 accident indicated that even though coolability of the core is not attained, a coolable configuration may result from break-up of the melt in the water of the lower head. If cooling in the core and in the lower head is not possible, the development of a melt pool in the lower head has to be analysed and it has to be established whether a melt pool can be kept in-vessel due to external vessel cooling; if it is not possible, the timing and modes of vessel failure have to be considered. This is the general objective of the LIVE programme (KIT). These phenomena resulting from core melting are studied experimentally in large-scale 3D geometry and in supporting separate-effects tests, with emphasis on the transient behaviour. One experimental result is e.g. that melt pouring near the vessel wall at the beginning of the test results in considerable asymmetric heat flux distribution even during the steady state. The time period of the solidification ranges from 50 minutes to several hours, depending on the cooling conditions and the position of the melt/crust interface.

The external cooling conditions, which are the second important aspect for achieving in-vessel coolability, are investigated by the CNU experimental programme (CEA) which is a unique experimental set-up, large scale, dedicated to the study of two-phase flow with steam production around a heated RPV geometry.

If all the attempts to cool down the vessel fail, the location and size of the vessel breach are of concern. Up to now the following main conclusions can be drawn for large PWRs: when the vessel fails, the liquid corium is mainly oxidic with potentially some metal. The mass of corium that can be ejected into the reactor pit at vessel failure is estimated between 2 and 20 tonnes. The breach is most probably located on the lateral surface of the vessel. Only local breaches are expected and not vessel unzipping.

Ex-vessel debris formation and coolability

A porous debris bed can be formed in a water pool of the reactor cavity due to the fragmentation of the molten corium jet ejected from the lower head of the vessel. The water pool is available through cavity flooding (e.g. SAMs in Swedish and Finnish BWRs) or water accumulation in the sump of a PWR due to Loss of Coolant conditions or containment spray. This is a similar process to the in-vessel situation, when melt relocates from the core to a water filled lower head. The large depth of water pools in BWRs yields additional effects.

The first issue concerns the debris bed formation by break-up of melt, with the DEFOR (KTH) and FARO (JRC/IE-Ispra) experiments. The second issue concerns the investigations on coolability of debris beds, with the STYX (VTT) and DEBRIS (IKE) experiments (for the latter, see more details in Section 6).

Bringing research results into reactor application

As an example of research results for reactor applications, the IVR via external reactor vessel cooling (ERV) has been recognised as a feasible and promising SAM strategy for VVER-440/V213 reactors. The most important design features of these reactors, favourable for

adoption of the IVR concept, are low thermal power, RPV without penetrations in lower head, massive stainless steel vessel internals, large volume of residual water in lower head and high driving head for natural circulation in ERVC loop.

Recent activities devoted to IVR concept via ERVC for standard VVER-440/V213 reactors are performed in the frame of SARNET as well as within national programmes performed in the countries operating this type of reactors. From the results obtained so far it follows that there should be sufficient gap width (~ 1 cm) between RPV wall and thermal/biological shield for the coolant flow in natural circulation regime alongside the outer surface of RPV wall. Further research should be focused on confirmation of the estimated heat flux values. Here the outcomes of the SARNET2 project and results of ASTEC analysis will be of high importance.

In order to evaluate the ability of current advanced codes to predict in-vessel core melt progression and coolability of the degraded core, a benchmark is being organized in close collaboration with the OECD/NEA/CSNI. It addresses an alternative scenario of the TMI-2 accident.

5.3 Activities on MCCI

In the postulated case of a SA with vessel melt-through, the containment is the ultimate barrier between the corium and the environment. The addressed situation is the reactor pit initially dry but with the possibility of water injection later during MCCI. The work programme has been designed to be complementary with the MCCI project of the OECD/NEA that finished in 2010.

Recent 2D experiments like VULCANO (CEA) in prototypical materials have provided new results that questioned the reliability of the available models and their extrapolation to reactor conditions. As an example, it becomes clear that new effects have to be taken into account to be able to describe the ablation anisotropy observed in case of silica-rich concrete and the different behaviour of limestone concrete. This anisotropy was also present in the ablation of Chernobyl silica-rich concrete. The intention is thus to gain sufficient experimental data in order to determine which phenomena are responsible for the observed isotropy/anisotropy of the concrete ablation.

Concerning the oxide/metal configuration, only few experimental programmes were conducted with stratified pools using simulant melts, for instance in KIT the large-scale 2D BETA test series with a large test matrix, and the series of COMET experiments, which were performed in alumina thermite within the LACOMERA EC project. They provided a valuable database on long-term MCCI for various initial and boundary conditions. The VULCANO experiments with oxide and metal pools have the unique characteristics of providing heat to the oxide layer, like in the reactor case. Several experiments were performed (VULCANO, MCCI-OECD, HECLA in VTT) but more data are required to improve knowledge in these configurations. The following question remains open: does a stratified configuration exist in the reality? The other need is to improve in the modelling the stratification criteria for onset and termination of stratification.

The other current experiments are MOCKA (KIT) at a large-scale in simulant materials, COMETA (UJV) for thermochemistry tests on real corium samples, the Laser melting facility (JRC/ITU), and CLARA and ABI (CEA) SETs in simulant materials.

Water-cooling is the main available way to terminate the concrete ablation. It was mainly studied within the OECD/NEA MCCI project. Recently, interest has been shown to pursue R&D on concepts that could be used to provide bottom-cooling in the cavity of current reactors.

5.4 Activities on containment issues

The considered issue is the threat to the containment integrity, due to two types of highly energetic phenomena: steam explosion and hydrogen combustion. Steam explosion may be caused by ex-vessel FCI due to a RPV failure and pouring of the reactor core melt in the flooded reactor cavity. Hydrogen combustion (deflagration and detonation) may be caused by ignition of a gas mixture with high local hydrogen concentrations, which may be due to the imperfect mixing of the containment atmosphere. Phenomena linked to these threats are considered as well. Essential insights and results from this research should be applicable to actual NPPs.

Ex-vessel FCI may lead to steam explosion. The corium ejected in the reactor cavity after vessel failure may lead to high-pressure loads on the containment or vital components in case of FCI. The work performed in the frame of SARNET and SERENA-1 (OECD/NEA project) allowed the identification of the major uncertainties that make difficult to quantify containment safety margins for an ex-vessel steam explosion. These uncertainties mainly concern the level of void in the pre-mixing phase and the role of material properties on explosion energetics. A new OECD/NEA project (SERENA-2) has been launched in October 2007 to resolve these uncertainties by performing a limited number of well-designed tests with advanced instrumentation reflecting a large spectrum of ex-vessel melt compositions and conditions in the KROTOS (CEA) and TROI (KAERI) facilities, and the required analytical work to bring the code predictive capabilities to a sufficient level for use in reactor analyses. The main objective in SARNET is to further review and debate the progress made in the SERENA-2 programme, and to propose and perform any activity that might be needed to complement (and possibly have positive feedback on) the work performed in SERENA-2, with the help of data produced in SARNET such as MISTEE, DEFOR and DROP experiments in KTH.

Phenomena that are linked to the hydrogen-in-containment issue, which is still today of highest priority, are addressed. This issue covers the containment thermal-hydraulics, including the hydrogen distribution, the different hydrogen combustion regimes, their impact on containment structures and measures to prevent (severe) combustion processes or at least to mitigate their consequences with specific devices like PARs or with accident management measures, like containment sprays. The involved experiments are: TOSQAN and ENACEFF (IRSN and CNRS/Orléans), MISTRA (CEA), HyKA and DISCO (KIT), CONAN (Univ. of Pisa), THAI (Becker Technologies, Germany). Benchmarks between codes are performed on most of these experiments.

5.5 Activities on source term

The overall objective is to reduce the uncertainties associated with calculating the potential release of radiotoxic fission products to the environment that may occur during a severe accident in water-cooled nuclear reactors. It concentrates on iodine and ruthenium, given their high radio-toxicity, noting that the release of ruthenium is enhanced in oxidising atmospheres, such as those that may follow air ingress into the RCS. The research treats the transport of these elements through the primary circuit, including consideration of the SG, and their behaviour in the containment. The prediction of volatile iodine and ruthenium species in the containment atmosphere of particular importance, because they are hard to remove by containment sprays or by filtration while venting the containment. For ruthenium, the enhanced release from the fuel in oxidising conditions is also studied.

Full advantage is taken of cooperation with international programmes such as Phébus FP (Clément et al., 2005), the International Source Term Programme (ISTP) (Clément et al., 2005), and the projects of the OECD/NEA/CSNI, to avoid duplication of experiments, to help consistency of the programmes and to identify remaining needs.

As concerns the oxidising influence on source term, the technical work concentrates in particular on ruthenium source term from the fuel up to its behaviour in-containment:

- Release of fission products from fuel (FIPRED experiments in INR, RUSSET ones in AEKI, VERCORS past RUSSET and VERDON future ones in CEA, Phébus FP past experiments in IRSN): release from high burn-up and MOX fuels; role of fuel cladding, i.e. the competition between cladding oxidation, UO₂ oxidation and fission products release; fission products release under mixed steam-air conditions, which are more realistic than 100% air conditions in accident situations;
- Ruthenium transport in RCS (experiments in Chalmers University): thermodynamic behaviour of ruthenium oxides; reactivity with surfaces and other chemical compounds such as caesium;
- Ruthenium behaviour in containment (EPICUR experiments in IRSN, VTT ones, THAI ones in Becker Technologies): behaviour of ruthenium oxides as aerosols, and their potential conversion to volatile forms; thermodynamic behaviour of ruthenium species in liquid phase and potential volatilization.

As concerns the iodine chemistry in the RCS and containment, two main situations are addressed:

- Iodine transport in circuits (CHIP experiments in IRSN, EXSI ones in VTT): kinetics of gaseous phase reactions; speciation of revaporised iodine and of other fission products; development of a databank from plant iodine spiking data and associated development of a correlation-type model covering some steam generator tube rupture (SGTR) events, volatile iodine mass transfers and adsorption/deposition in SG secondary side in case of a SGTR event;
- Iodine behaviour in containment (EPICUR experiments, RTF ones in AECL): mechanisms of iodine association with painted surfaces (adsorption of iodine from particulate iodides deposited on “wetted” surfaces); subsequent volatile iodine formation from iodine-loaded paint; radiolytic destruction of gaseous iodine species to form nucleate particles and subsequent behaviour of these particulate iodine oxides; iodine binding on sump materials and in sump screen blockages; effect of PARs on iodine source term.

5.6 ASTEC code assessment and improvements

IRSN and GRS jointly develop the ASTEC code to describe the complete evolution of a SA in a nuclear water-cooled reactor, including the behaviour of engineered safety systems and procedures used in SAM (Van Dorselaere et al., 2009). The new series of versions V2 (Figure 3) can simulate the EPR, especially its external core-catcher, and it includes the advanced core degradation models of the ICARE2 IRSN mechanistic code.

IRSN and GRS deliver the successive code versions and the corresponding documentation to the code users: ASTEC V2.0 in July 2009; V2.0rev1 in mid-2010 and V2.1 foreseen in 2013. They also assure the code maintenance and the support to the code users, notably through Users Club meetings that are organized about every eighteen months (the next one in spring 2012).

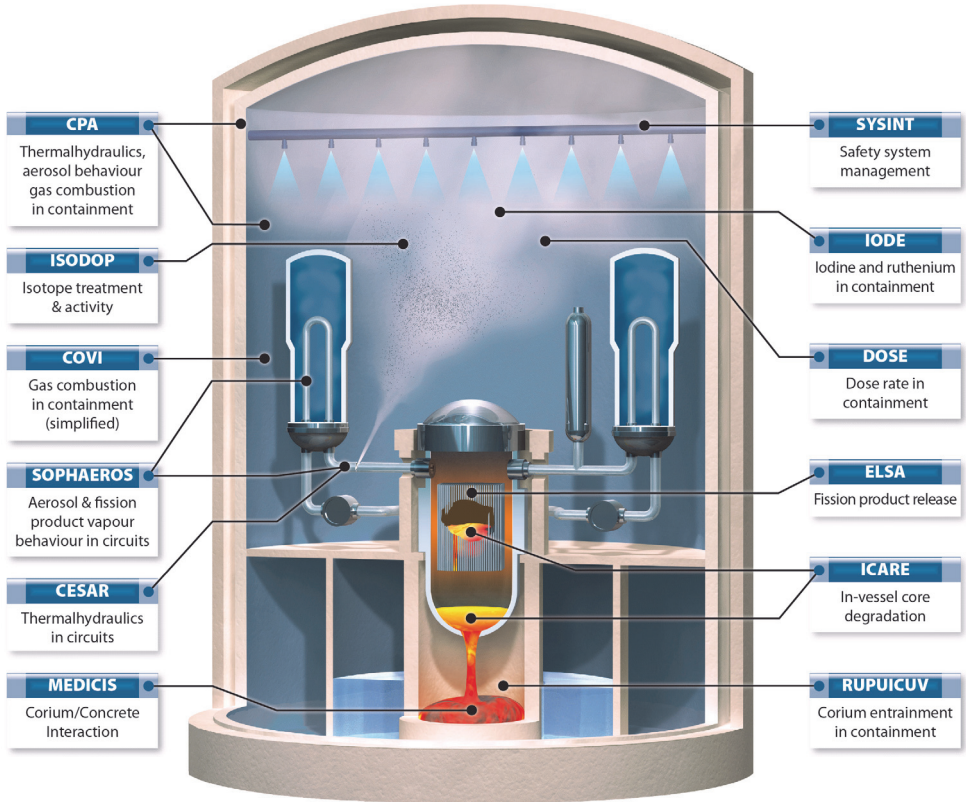


Fig. 3. Structure of the ASTEC integral code for SA simulation

Twenty-nine organizations collaborate on the development and assessment of the successive ASTEC versions. The developments will account for the model improvements proposed by the joint research activities of the JPA. Besides, four partners work on the model adaptations to simulate SA sequences in BWR and PHWR⁴ reactors: IKE and KTH for BWR, INR and AECL for PHWR. They write model specifications, and validate the code against adequate experiments and benchmarking with other codes. Most ASTEC models are already applicable to these two types of NPPs except for core degradation. The BARC Indian partner is developing new PHWR core degradation models and validating them against Indian experiments.

The assessment activity mainly consists:

- On one hand in validating the code against experiments of diverse types (SETs, CETs, and integral tests). The comparison of code results with integral experiments such as Phébus FP and with real plant accidents such as TMI-2 is an essential task;

⁴ PHWR : pressurized heavy water reactors (including the CANDU type that is designed by Canada)

- On the other hand in covering a broad matrix of ASTEC reactor applications, aiming at the most important SA scenarios for the diverse types of reactors (PWR including VVER, BWR and PHWR). Sensitivity and uncertainty calculations are being performed in order to demonstrate the reliability and consistency of the ASTEC calculations. Although not the prime objective, partners may benchmark ASTEC with other reference codes that they master, such as the integral codes MELCOR and MAAP and the detailed codes such as ICARE/CATHARE, ATHLET-CD, SCDAP/RELAP5, COCOSYS, CONTAIN, TONUS...

5.7 Spreading of excellence

The objective of the DATANET database, developed in the frame of SARNET, is to collect the available SA experimental data in a common format in order to ensure their preservation, exchange and processing, including all related documentation. The data are both previous experimental data that SARNET partners are willing to share within the network and all new data produced within SARNET. DATANET is based on the STRESA tool (Zeyen, 2009) developed by the Joint Research Centre (JRC) in Ispra (Italy) and now managed by JRC-IE in Petten (The Netherlands). It consists of a network with several local databases. All access rights are managed in accordance with the rules adopted in the SARNET consortium. The protection of confidential data is an important feature that is taken into account as the information security of the database. Six STRESA nodes are open and the results of about 250 experiments from 35 facilities have been implemented. JRC-IE can create new local STRESA nodes for partners and support the users through training sessions when necessary.

The public web site (www.sar-net.eu) aims at providing general information on the SA research field to the general public. For the communication between all network members, the e-collaborative Internet Advanced Communication Tool is used. About 300 papers related to SARNET work in the last 5 years have been presented in conferences or published in scientific journals. The dissemination of information is also done through periodic newsletters or participation to public events.

Four ERMSAR conferences (European Review Meetings on Severe Accident Research) have been organized in the last five years successively in France, Germany, Bulgaria and Italy as a forum to the SA community. They are becoming the major event in the world on this topic. The 4th one, hosted by ENEA (Italy) on May 11-12, 2010 in Bologna (Italy), gathered 100 participants.

The Education and Training programme is focusing on raising the competence level of the university students (Master and PhD) and researchers engaged in SA research. Towards this purpose, education courses are elaborated on the phenomenology of the SA various areas. The teaching is not a survey but an in-depth treatment in order to allow the students and researchers to understand the methodology in the topics further and use analysis computer codes, mainly ASTEC, more effectively for any type of NPP. The description of the scenarios with event trees and fault trees is performed, with indication of the probabilities of the various events occurring. Best-estimate analyses are provided with uncertainty analyses. Close links exist with the European ENEN association (European Nuclear Education Network). Four one-week educational courses were organised during the last five years, gathering from 40 to 100 persons: the latter was organised in the University of Pisa in January 2011, with a special focus on Gen.III NPPs. Another training course will be

proposed in the future for staff of plant operators or regulatory authorities, with emphasis on identifying what the SAM procedures are based on, and why they are effective.

The textbook on SA phenomenology was drafted during the SARNET FP6 project. It covers historical aspects of water-cooled reactors safety principles and phenomena concerning in-vessel accident progression, early and late containment failure, fission product release and transport. It contains also a description of analysis tools or codes, of management and termination of SA, as well as environmental management. It gives elements also on Gen.III reactors. The final review was performed in 2010, and the publication is planned in the second part of 2011.

Finally, a programme enables university students and researchers to go into different laboratories for education and training in the SA area. Some stages for master thesis may be organised in the ENEN framework to obtain the 20 credits necessary for the achievement of the European EMSNE (European Master of Science in Nuclear Engineering) certification. The staff deputation programme has involved for the last five years about 40 secondments with an average duration of 3 months: a researcher from one laboratory can spend several months in another European Laboratory where he/she would participate in an area of the SA research ongoing there.

6. Illustration on a specific R&D issue: Reflooding of debris beds

One of the high-priority issues concerns the core and debris coolability and thermal-hydraulics within particulate debris during core reflooding. PSA results do not give a unanimous answer for the ranking of the issue. While in German PSA studies the possibility of reflooding is classified with low probability, French PSA on 900 MWe reactors give a higher probability. Finally because reflooding of a degraded core can potentially terminate the core degradation and stop the accident, corresponding SAM measures are intended and consequently the investigation of conditions for successful reflooding is important.

New QUENCH-Debris experiments (KIT) and CODEX experiments (AEKI) are foreseen in bundle configurations, analysing the relocation of cladding and fuel and the formation and cooling of in-core debris beds to gain information on the characteristics of the created particles. The main objective of these tests is the investigation of these processes under prototypical boundary conditions for a whole bundle. The QUENCH-Debris facility consists in modifications of the QUENCH existing facility to study debris formation and coolability within a rod bundle. Two tests are planned during the SARNET2 timeframe.

The DEBRIS facility (IKE) concerns model-oriented experiments for improvement of constitutive laws for friction and heat transfer as well as study of specific two dimensional effects under top and bottom flooding conditions at different system pressures. New POMECO test facilities (KTH) are designed and constructed to perform isothermal and boiling two-phase flow tests with better instrumentation and flexibility to accommodate various prototypical conditions: they aim at analyses under boil-off conditions with emphasis on basic laws and specific 2D effects (downcomers) more oriented at lower head or ex-vessel situations but also addressing basically the situation in the degraded core. Both DEBRIS and POMECO programmes deal with irregular particles aiming at realistic debris.

IRSN is preparing larger quenching experiments with 2D porous media allowing multi-dimensional progression of the quench front. This PEARL programme (Figure 4) (Stenne et

al., 2009) will simulate the reflooding of a debris bed, characteristic of an in-core debris bed, surrounded by a more permeable medium (such as intact structures and rods). PEARL goes beyond DEBRIS quenching analyses by the larger size (60 cm diameter vs. 15 cm in DEBRIS) and thus the possibility to perform extended analyses on multidimensional effects. It will also provide a general basis for the assessment of the overall behaviour described in the codes (both in- and ex-vessel phenomena).

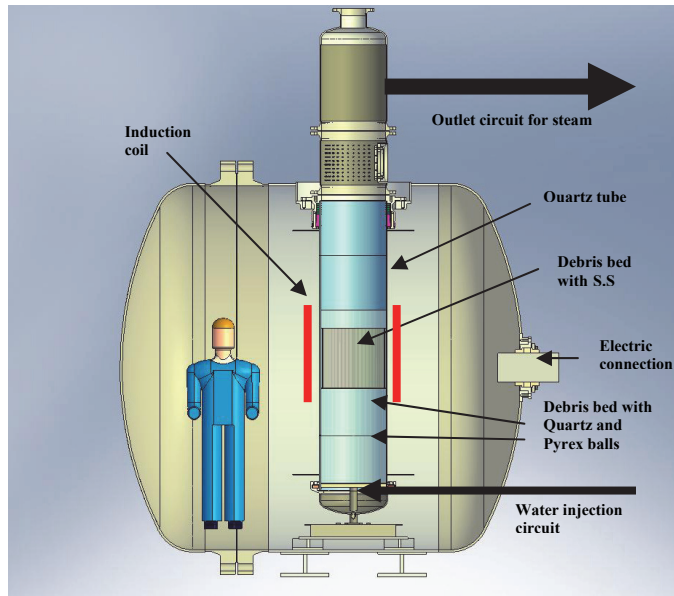


Fig. 4. PEARL facility (©2010 IRSN)

The PRELUDE preliminary program is ongoing in IRSN to test the performance of the induction heating system on stainless steel particles, in order to optimize the instrumentation in a two-phase flow. The debris bed is one-dimensional, with a smaller size than PEARL, at atmospheric pressure and up to temperatures of 1000°C. The investigated parameters are:

- Stainless amagnetic steel particles, 2 and 4 mm in diameter,
- Inlet water velocity between 1 and 8 mm/s (4 to 30 m³/h/m²), in the range foreseen in PEARL test matrix,
- Power at 300 W/kg (maintained or not during the reflooding phase),
- Initial temperature before reflooding at 420 K, 500 K, 600 K and 1000 K.

Additional PRELUDE experiments were performed to evaluate the power distribution inside a larger debris bed diameter (from 110 to 280 mm). This campaign ended with two experiments with a heating sequence of a debris bed (test section diameter 180 mm, particles 4 mm) up to 1000 K at about 140 and 200 W/kg before the water injection. Those

experiments were well instrumented with many thermocouples inside the debris bed (different radial and axial positions) to follow the water front propagation along time (Figure 5, shows the thermocouples measurements at different axial levels).

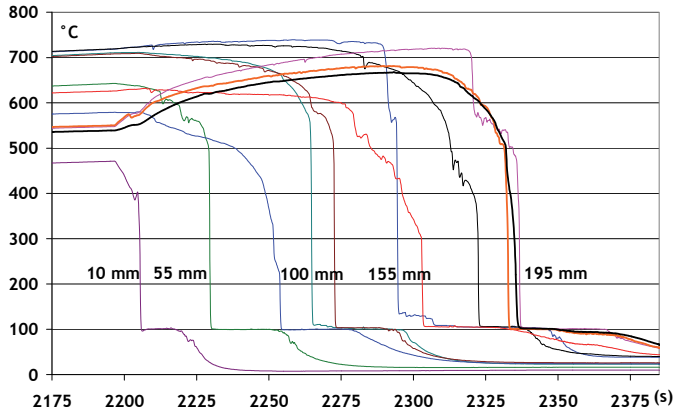


Fig. 5. PRELUDE measurements of the water front evolution along time

The objective is to assure the consistency between the PEARL, DEBRIS and QUENCH-DEBRIS experimental programmes.

Concerning the coolability of porous media, theoretical analyses have indicated the importance of multi-dimensional effects. Quenching analyses performed in SARNET showed agreement concerning a strongly favoured coolability by inflow of water from lateral water-filled regions of the core with higher porosities. Since lateral water inflow, especially via lower regions, strongly improves coolability, in general the coolability is much better than concluded from 1D analyses with top flooding. 2D/3D computer codes including adequate descriptions of constitutive laws are thus required to analyse the real coolability situation. Also, it is necessary to improve the modelling of the formation of porous media in the core.

In parallel, plant applications must be performed, along with uncertainty studies, on different in-vessel geometrical configurations, taking into account water supply, in order to reveal major trends (cooling vs. melt pool formation). The modelling work is being done in the detailed codes ICARE/CATHARE (IRSN) and ATHLET-CD (work by IKE on the MEWA module of the German GRS code). These codes aim at a detailed understanding and simulation of the physical phenomena. Their validation on above experiments will allow improving their models. The final objective is to derive simplified models from these codes and to implement them into the ASTEC code.

7. Conclusion

For severe accidents in Generation II-III nuclear power plants, R&D is progressing on the remaining open issues that have been ranked in the SARNET network of excellence. The

work concerns new experiments and new physical modelling, in particular in the ASTEC integral code that is considered as the European reference SA code. For Gen.II NPPs, the objective is to reduce the remaining uncertainties on SA and consolidate the accident management plans in order to lead their safety level closer to the level of the new Gen.III plants under construction.

The accident in the Fukushima plant occurred when this chapter was written. It is very likely that the accident will imply some reorientations of the planned R&D but it is too early to get a clear view on that aspect. Nevertheless it can be already observed that the highest-priority issues that were selected in the SARNET work programme have clearly conditioned the evolution of the accident: for instance reflooding of a degraded core, hydrogen explosion in the containment, and degradation of fuel bundles and release of fission products in an air atmosphere (in the case of spent fuel pools). The SARNET work programme is being reviewed in order to get as soon as possible a feedback of this accident on the needs of further R&D. In particular, it seems likely that the aspects of mitigation of the SA consequences will have to be emphasized in the near future.

A first step towards a sustainable integration of the European SA research capacities has been reached. A strong link must be kept between the “SARNET community” and the “PSA2 community”, in continuation of the ASAMPSA2 FP7 project on PSA2 best-practice guidelines (ASAMPSA2, 2011). The European SNETP (Sustainable Nuclear Energy Technology Platform), that gathers all nuclear fission actors and aims at providing the stakeholders and the public with a 2020–2050 vision on R&D, has delegated to SARNET the coordination of R&D on SA for Gen.II-III NPPs. Such a living and unique pool of experts should periodically assess the remaining issues on SA, notably using the results of all international programmes (OECD/NEA, EC FP7-8, ISTP,...), update the research priorities and propose relevant R&D programmes to address them. Their scope of investigations could extend in the future to the new Generation IV plant designs.

Efforts will continue in parallel on the transfer of knowledge to younger generations through the ERMSAR periodic international conferences, educational courses and delegations in laboratories.

8. Acknowledgements

The authors wish to thank in particular all the authors of the reference (IRSN-CEA, 2007) and all the members of the SARNET network, as well as the European Commission for its support to the SARNET network of excellence.

9. References

- Albiol, T., Van Dorsselaere, J.-P., & Reinke, N. (2008). SARNET: a success story. Survey of major achievements on severe accidents and of knowledge capitalization within the ASTEC code, *Proceedings of EUROSAFE Forum*, Paris (France), November 2008. Available from www.eurosafe-forum.org
- Allelein, H.-J. et al. (2001). Validation Strategy for Severe Accident codes (VASA), *FISA 2001: EU research in reactor safety*, Official Publication of European Communities, Luxembourg

- ASAMPSA2 FP7 project. Advanced safety Assessment Methodologies: level 2 Probabilistic Safety Assessment. Available from www.asampsa2.eu
- Birchley, J., Clément, B., Löffler, H., Tromm, W., & Amri, A. (2010). Outcome of the OECD/SARNET Workshop on In-vessel Coolability. *4th European Review Meeting on Severe Accident Research (ERMSAR-2010)*, Bologna (Italy), May 2010. Available from www.sar-net.eu
- Clément, B., Zeyen R. (2005). The Phébus FP and International Source Term Programmes. *Proceedings of International Conference on Nuclear Energy for New Europe*, Bled (Slovenia), Sept. 2005
- CSNI. (2000). CSNI International Standard Problems, Brief description (1975-1999), *NEA/CSNI/R (2000)5*
- IRSN-CEA. (January 2007). Research and development with regard to severe accidents in pressurised water reactors: Summary and outlook. Available from www.irsn.fr/EN/news/Documents/R_and_D_severe_accident_report.pdf
- Magallon, D., et al. (2005). European Expert Network for the Reduction of Uncertainties in Severe Accident Safety Issues (EURSAFE). *Nuclear Engineering and Design*, N°235 (2005), pp.309-346
- Micaelli, J.-C., et al. (2005). SARNET: A European Cooperative Effort on LWR Severe Accident Research. *Proceedings of the European Nuclear Conference*, Versailles (France)
- NUREG. Phenomena Identification and Ranking Tables (PIRT's) for Loss-of-Coolant Accidents in Pressurized and Boiling Water Reactors Containing High Burn up Fuel. *NUREG/CR-6744, LA-UR-00-5079*
- OECD. (2007). Nuclear Safety Research in OECD Countries Support Facilities for Existing and Advanced Reactors (SFEAR). *NEA/CSNI/R (2007)6*, ISBN 978-92-64-99005-0
- Schwinges, B., et al. (2008). Ranking of Severe Accident Research Priorities. *3rd European Review Meeting on Severe Accident Research (ERMSAR-2008)*, Nesseber (Bulgaria), September 2008. Available from www.sar-net.eu
- Stenne, N., Fichot, F., Van Dorsselaere, J.-P., Tromm, W., Steinbrueck, M., Stuckert, J., & Buck, M. (2009). R&D on reflooding of degraded cores in SARNET - Focus on PEARL new IRSN facility. *EUROSAFE Forum*, Brussels (Belgium), November 2009
- Trambauer, K. (2005). Research Needs in the Domain of Severe Accidents. *1st European Review Meeting on Severe Accident Research (ERMSAR-2005)*, Aix-en-Provence (France), Nov. 2005. Available from www.sar-net.eu
- Van Dorsselaere, J.-P., Seropian, C., Chatelard, P., Jacq, F., Fleurot, J., Giordano, P., Reinke, N., Schwinges, B., Allelein, H.-J., & Luther, W. (2009). The ASTEC integral code for severe accident simulation. *Nuclear Technology*, Vol.165, March 2009
- Van Dorsselaere, J.-P., Auvinen, A., Beraha, D., Chatelard, P., Journeau, C., Kljenak, I., Sehgal, B.R., Tromm, W., & Zeyen R. (2010). Status of the SARNET network on severe accidents. *International Congress on Advances in Nuclear Power Plants (ICAPP '10)*, San Diego, CA (USA), June 2010

Zeyen, R. (2009). European approach for a perennial storage of Severe Accident Research experimental data, as resulting from EU projects like SARNET, Phébus FP and ISTP. *ANS winter meeting*, Washington (USA), November 2009

Imaging of Radiation Accidents and Radioactive Contamination Using Scintillators

Tomoya Ogawa et al.*

*Laboratory of Crystal Physics and Technology
Japan*

1. Introduction

An accident in a nuclear power plant, which can be caused by an unpredictable event such as an explosion, fire, and earthquake, has severe and far-reaching consequences. Therefore, it is crucial to carefully and constantly monitor the plant and precisely detect any radiation source. Radiation contamination in laboratories and in the environment due to nuclear fallout is among the issues that require an immediate solution. Radiation detection has become increasingly important because of the increasing number of nuclear power plants that have been established to replace conventional power plants, as part of the effort to suppress carbon dioxide emission. For these purposes, this chapter will discuss the principle and method of mapping flying radiations. Visual mapping of intensity and direction of

* Nobuhiko Sarukura², Masahito Watanabe³, Tsuguo Fukuda⁴, Nobuhito Nango⁵, Yasunobu Arikawa², Kohei Yamanoi², Tomoharu Nakazato², Marilou Cadatal-Raduban², Toshihiko Shimizu², Mitsuo Nakai², Takayoshi Norimatsu², Hiroshi Azechi², Takahiro Murata⁶, Shigeru Fujino⁷, Hideki Yoshida⁸, Kei Kamada⁹, Yoshiyuki Usuki⁹, Toshihisa Suyama¹⁰, Akira Yoshikawa¹¹, Nakahiro Sato¹², Hirofumi Kan¹², Hiroaki Nishimura², Kunioki Mima², Masahito Hosaka¹³, Masahiro Katoh¹⁴, Nobuhiro Kosugi¹⁴, Kentaro Fukuda¹⁰, Takayuki Yanagida¹¹, Yuui Yokota¹¹, Fumio Saito¹¹, Kouhei Sakai², Dirk Ehrentraut¹¹, Mitsuru Nagasono¹⁵, Tadashi Togashi¹⁵, Atsushi Higashiya¹⁵, Makina Yabashi¹⁵, Tetsuya Ishikawa¹⁵, Haruhiko Ohashi^{15,16}, and Hiroaki Kimura^{15,16}

²*Institute of Laser Engineering, Osaka University, Japan*

³*Department of Physics, Gakushuin University, Japan*

⁴*Fukuda Crystal Laboratory, Japan*

⁵*Ratoc System Engineering Co., Japan*

⁶*Department of Chemistry, School of Science, Tokai University, Japan*

⁷*Department of Materials Process Engineering, Graduate School of Engineering, Kyushu University, Japan*

⁸*Ceramic Research Center of Nagasaki, Japan*

⁹*Furukawa Co., Ltd., Japan*

¹⁰*Tokuyama Corporation, Japan*

¹¹*Institute of Multidisciplinary Research for Advanced Materials, Tohoku University, Japan*

¹²*Central Research Laboratory, Hamamatsu Photonics K.K., Japan*

¹³*Graduate School of Engineering, Nagoya University, Japan*

¹⁴*UVSOR Facility Institute for Molecular Science, Japan*

¹⁵*RIKEN XFEL Project Head Office, Japan*

¹⁶*Japan Synchrotron Radiation Research Institute, Japan*

incident radiations is necessary to detect any radiation accident and/or invisible radiation contamination. Discussion will focus on directional detection of radiation sources, being the minimum requirement for identifying and characterizing unpredictable accidents and contamination.

Specifically, this chapter will discuss two-dimensional imaging of radiation accidents and radioactive contamination. It will also detail the development of a “panchromatic” detector that is suitable for use against radiation from different types of sources. This detector combines several types of scintillating elements into a bundle, which is composed of well-designed and regularly arranged scintillation fiber-segments or thin cylinders to detect and display the radiation sources as a map, using the directional sensitivity of the segments or cylinders for locating sources of incident radiation. In addition, this chapter will discuss the numerical designs and the characteristics of two detector configurations. These are the telescope configuration, wherein all the extended lines of the scintillator fiber segments or thin cylinders composing the bundle are focused to a point; and the magnifier configuration, wherein all the extended lines of the segments within the bundle are diverging from the focus.

An integral part of the radiation detector is the scintillator. Scintillators are created and developed to correctly detect and count incident radiations. In this regard, part of this chapter will also be devoted to the discussion of the properties of scintillators that are ideal for use in radiation detectors. In particular, the effect of scintillator shape and decay time will be outlined, leading to the attributes of an ideal imaging scintillator. For instance, one of the size effects is the directional sensitivity to incident radiations. This can be realized by using a thin cylinder-type or a fiber segment-type scintillator. The output signals from the thin cylinder are proportional to the number of radiations that passed through it, if its length is good enough to absorb the incident radiations.

To complete the chapter, the performance of various scintillators will be discussed. Among the scintillators that will be discussed is the praseodymium-doped lithium glass (APLF80+3Pr), cerium-doped lutetium lithium fluoride ($Ce^{3+}:\text{LuLiF}_4$), zinc oxide (ZnO), and neodymium-doped lanthanum fluoride ($\text{Nd}^{3+}:\text{LaF}_3$).

2. Scintillators

Scintillators are fluorescent materials that mediate the detection of high energy (ionizing) electromagnetic or charged particle radiation. A scintillator absorbing high-energy radiation fluoresces at a characteristic Stokes-shifted (longer) wavelength that can be detected by conventional detectors like photodiodes or photomultiplier tubes. If the properties of the scintillator are known, then the high-energy radiation that it absorbed can in turn be characterized. Radiation detectors are typically useful for imaging by utilizing high-penetration power radiation and for spectroscopy by utilizing characteristic radiation from each atom. As part of a detection unit, the broad application of scintillators comprises various scientific disciplines such as high-energy physics, nuclear physics, astronomy, and mineral exploration. It has also found applications in product quality control, airport security, nuclear safeguards verification, cargo container inspection, toxic dumpsite monitor, and environmental monitoring. Moreover, Positron Emission Tomography (PET) for medical imaging has gained popularity as a common clinical tool for detection of tumors.

2.1 Shape of scintillators

Scintillation is caused by collision between a high-energy radiation and an electron belonging to a heavy dopant atom. This collision is considered as one of the ideal stochastic processes. As such, a scintillation detector is usually prepared as a very large block to correctly count incident radiations while excluding its size effects.

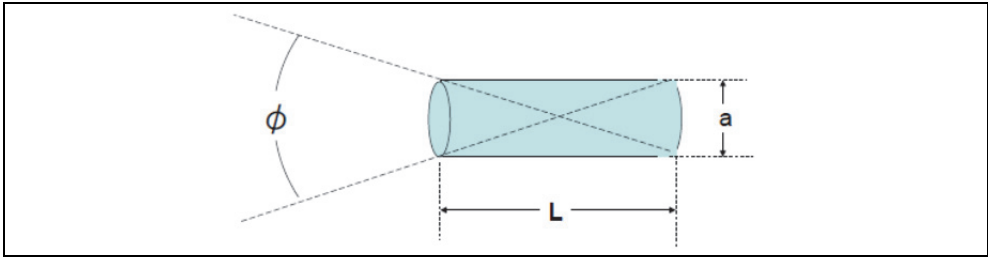


Fig. 1. A thin cylinder or fiber segment scintillator and its incident radiation acceptance angle, where a is its diameter, L is its length, and Φ is the divergence of its sensitivity against incoming radiation.

One of the size effects is the directional sensitivity to incident radiations. This can be realized by using a thin cylinder-type or a fiber segment-type scintillator. The output signals from the thin cylinder are proportional to the number of radiations that passed through it if its length is good enough to absorb the incident radiations. On the other hand, radiations crossing obliquely through a segment may or may not generate scintillation even if every radiation were moving along an identical line. This can, therefore, constitute random noise. The signals arising from radiation passing directly through the scintillator can be separated from the random noise generated by radiation crossing the scintillator obliquely through the well-known noise reduction technique using multi-integration.

In most materials, the refractive index for high energy radiations is nearly equal to unity. Therefore, the aperture, Φ , of the cylinder for which incident radiations is detected is

$$2\tan^{-1}(a/L) \quad (1)$$

where L and a are the cylinder length and diameter, respectively, as illustrated in Fig. 1. Surface smoothness of the cylinder is very important since multiple scattering of the scintillation light at its surface is detrimental to the imaging of output light signals.

2.2 The decay time of scintillation

Since scintillators are created and developed to correctly detect and count incident radiations, a very short scintillation decay time is desirable for precise time-resolved radiation measurement. Decay time of well-known scintillators is much less than one microsecond. For the case of scintillators developed mainly for imaging, measurement is limited by the refresh rate of the television or monitor. The refresh rate of monitors and televisions is typically 30 frames per second. It is therefore acceptable that the decay time of imaging scintillators is in the millisecond range. This decay time is longer than the requirement for scintillators used in radiation counting. For this purpose, development of brighter scintillators without regard to decay times would be of primary importance when developing an imaging device.

2.3 Scintillation crystals

A comparison of the performance of different scintillator materials is shown in Table 1 (Ishii & Kobayashi, 1991, 2007). One of the best candidates for imaging will be thin scintillation cylinders made from CsI:Tl crystals. This material is ideal as an imaging scintillator because among the materials in Table 1, it has the largest photoluminescence output per radiation energy of 59,000 photons/MeV. It also has a relatively long decay time of 1 μ s. Moreover, it has a high melting point of 621°C and is only slightly hygroscopic.

Material	Density (g/cm ³)	Radiation length, X ₀ (cm)	PL output (Photons/MeV)	Decay (ns)	Application
NaI:Tl	3.67	2.59	38000	230	General purpose
CsF	4.11	2.23	2000	2.8	
CsI:Tl ⁺	4.53	1.86	59000	1050	X-CT
CsI	4.51	1.85	30*	6, 35	
Bi ₄ Ge ₃ O ₁₂	7.13	1.12	8200	300	PCT, NP, HE
CdWO ₄	7.68	1.06	15000	5000	X-CT
Gd ₂ SiO ₅ :Ce	6.71	1.38	10000	60	PET
Lu ₂ SiO ₅ :Ce	7.4	1.14	30000	40	PET
PbWO ₄	8.2	0.92	490	10	HE

NP: Nuclear physics experiment

* Faster decay component

HE: High energy physics experiment

+ Slight hygroscopicity

Table 1. Characteristic features of scintillation crystals

3. Configuration and compilation of the scintillation thin cylinders

Visual mapping of intensity and direction of incident radiations is necessary to detect any radiation accident and/or invisible radiation contamination. For this purpose, thin cylinder scintillators or fiber segments are compiled to form a bundle where every extended line of the cylinder is either focused into a point, as shown in Fig. 2 or diverging from a point, as shown in Fig. 3. The former is referred to as the telescope configuration while the latter is referred to as the magnifier configuration (Ogawa, 2007, 2010).

3.1 Telescope configuration

Figure 2 demonstrates a typical telescope configuration. The terminal end of the scintillation cylinder bundle where the focus side is located is optically connected to a two dimensional photodetector, such as a charge coupled device (CCD). An image intensifier or a micro-imaging plate is used to amplify the signals before reaching the CCD.

The field angle or aperture of this telescope is determined by R and F , where R is the diameter of the circle circumscribed by the terminal ends and F is the distance between the focus and the terminal plane. With this configuration, the intensity and direction of incident radiations will be indicated as a map on the computer, after image processing.

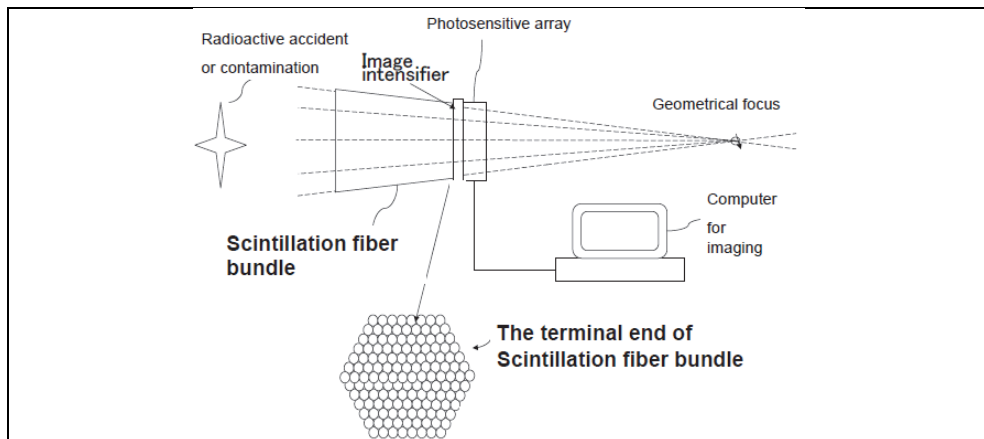


Fig. 2. The telescopic configuration. All the extended lines of the scintillator fiber segments or thin cylinders composing the bundle are focused to a point.

3.2 Magnifier configuration

For the magnifier configuration, the size of the focal point is nearly equal to or a little larger than the diameter of the fiber. In this configuration, a radiation source such as an X-ray tube or a small block of ^{60}Co is continuously emitting its radiation at the focal point. On the other hand, the specimen being studied is placed at a plane between the focus and the front of the bundle. This way, the transparency of this specimen against the radiation will be observed as its magnified image. This is similar to an optical magnifier. If radiation substances or radioactive isotopes are scattered on a plane, a map of this contamination will be observed when the focus of the magnifier either approaches or departs from that plane, as shown in Fig. 3.

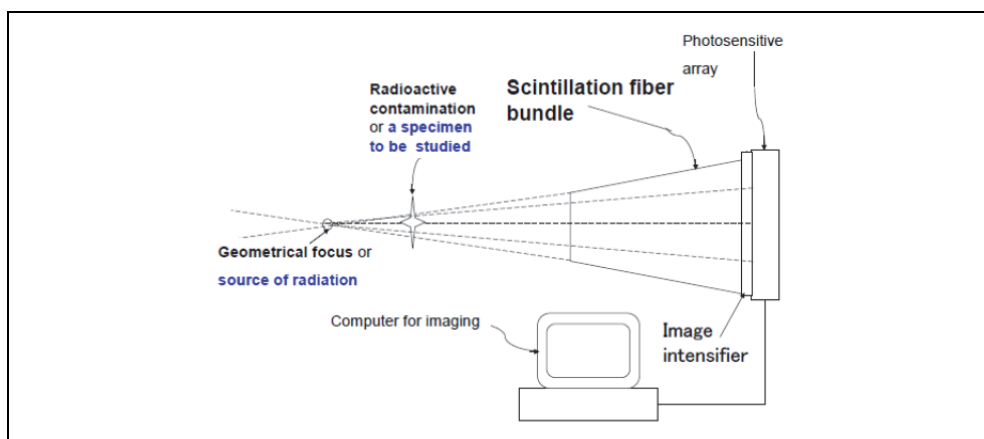


Fig. 3. The magnifier configuration. All the extended lines of the segments within the bundle are diverging from the focus.

4. Numerical designs

In this section, we discuss the numerical considerations for designing the telescope and magnifier configurations. In particular, the characteristic features of the cylinders to be used in the telescope configuration as well as the diameter of the fiber segments for the magnifier configuration are discussed.

4.1 Numerical designs of cylinders for the telescope configuration

The sensitivity divergence, Φ , of a thin scintillation cylinder and the aperture for imaging, Θ , of the cylinder bundle are defined as follows:

$$\Phi = 2 \tan^{-1}(a/L) \quad (2)$$

$$\Theta = 2 \tan^{-1}(R/F) \quad (3)$$

On the other hand, the total number of the cylinders, N , is given by

$$N = 3n(n+1) + 1 \quad (4)$$

where n is number of cylinders along the radius of the circle circumscribed by the terminal ends. Thus Θ , Φ and n are related as follows:

$$\Phi = (\Theta/2n)p \quad (5)$$

In this equation, p is an overlapping or tolerance factor of the scintillation cylinder or fiber segment. In our calculations, we chose Θ as 47° , 24° , 8° , and 2.5° because these apertures correspond to the 50 mm, 100 mm, 300 mm and 1000 mm focal length lens of the 35 mm camera system, respectively.

The length of a cylinder, L , is such that the incident radiation is enough to be absorbed for scintillation but the light generated within it will be perfectly received at the terminal end. In our calculations, L was assumed to be

$$L = 5X_0 \quad (6)$$

where X_0 is the radiation length of the scintillation material. In this case, the incident radiation will be attenuated to $1/e$, which is equal to 0.0067 times (Fukuda et al., 2004). This attenuation value is acceptable for the present purpose. The radiation length of various scintillators is summarized in Table 1. As an example, by using a CsI:Tl crystal having an X_0 of 18.6 mm, the suitable crystal length, L , would be 93 mm. Correspondingly, the diameter, a , of the CsI:Tl cylinders can be obtained using equations (2) and (5) with $p = 2$. Calculation results of the diameter of CsI:Tl cylinders for different apertures (Θ) and number of cylinders (n) are shown in Table 2. It is worth mentioning that the diameter of the commercially available $\text{Bi}_4\text{Ge}_3\text{O}_{12}$ (BGO) cylinders is 0.6 times compared to that of CsI:Tl because the radiation length of BGO is 0.60 times shorter than that of CsI:Tl.

4.2 Numerical designs of fiber segments for the magnifier configuration

The size of the focal point is nearly equal to or a little larger than the diameter of the fiber segment, as indicated in Fig.3. It is, therefore, more desirable to make thinner fiber segments. Today, the diameter of commercially available scintillation fibers, for example the BGO fiber is about $30 \mu\text{m}$ (Fukuda & Chani, 2007; Fukuda et al., 2004). This is very similar in size to the focus of a commercial microfocus X-ray tube. If fibers with a $1 \mu\text{m}$ diameter were

available, the resolution of the transparent image against radiation will clearly be improved because the half shadow of the image will be dramatically diminished.

(The case when $p = 2$)

$\frac{n}{N}$	10	20	50	100
$\frac{N}{n}$	331	1261	7651	30.301
47° ($f = 50$)	3.82 mm	1907 μm	763 μm	381 μm
24° ($f = 100$)	1.95 mm	970 μm	380 μm	195 μm
8° ($f = 300$)	0.65 mm	325 μm	130 μm	65 μm
2.5° ($f = 1000$)	0.20 mm	101 μm	41 μm	20 μm

The value of f in the parentheses indicates focal length of the lens with the same aperture under the film size: 35-mm camera system.

Table 2. The diameter of CsI:Tl scintillation cylinders

5. Scintillators for time-resolved measurement

As mentioned in Section 2.2, a very short scintillation decay time is desirable for precise time-resolved radiation measurement. Over the past years, several scintillators have been studied for this purpose, wherein several schemes have been considered in order to improve the response time of fluoride, oxide, and glass scintillators. In this section, the characteristics of fluoride, oxide, and glass scintillators will be discussed. Emphasis will be given to the improvement in the fluorescence decay time. In particular, the scintillation properties of cerium-doped lutetium lithium fluoride ($\text{Ce}^{3+}:\text{LuLiF}_4$), praseodymium-doped lithium glass (APLF80 + 3Pr), neodymium-doped lanthanum fluoride ($\text{Nd}^{3+}:\text{LaF}_3$), and zinc oxide (ZnO) will be discussed.

5.1 Pr-doped glass

In the field of fusion research, understanding the plasma dynamics could very well be the key in feasibly attaining controlled fusion. Moreover, studying the scattered neutrons is currently the most viable way of probing the fusion plasma. For this reason, neutron diagnostics is an indispensable tool for both inertial confinement fusion (ICF) and magnetic confinement fusion research (Cheon et al., 2008; Glebov et al., 2006; K.A. Tanaka et al., 2004; Lerche et al., 1995; Petrizzi et al., 2007; Ress et al, 1988). In particular, the observation of scattered neutrons from the high-density imploded deuterium plasma in laser fusion experiments is desired (Izumi et al., 2003). At the center of the imploded deuterium fuel plasma, deuterium-deuterium (DD) neutrons having energy of 2.45 MeV and scattered neutrons from the fuel deuterium are generated. The scattering probability depends only on the plasma areal density, which is the radial integral of density ρR , in units of g/cm^2 . In addition, a wide observable range of up to 3 g/cm^2 is required for future fusion reactors. These factors make the scattered neutron diagnostics method, highly expected to be further developed as an invaluable tool in ICF research. For this purpose, a fast-response neutron scintillator with a high cross section for scattered neutrons is strongly required.

The nuclear reaction,



has a large cross section resonant peak, well-fit to the back scattered neutron spectrum peak around 0.27 MeV, and a large Q value producing enough photons for lower energy scattered neutrons. Thus, a ${}^6\text{Li}$ scintillator with a high lithium density is an ideal detector for this method (Izumi et al., 2003). Since scattered neutrons having energy around 0.27 MeV must be discriminated from the overwhelming majority of the 2.45 MeV primary neutrons or x-rays via time-of-flight experiments, a sufficiently fast time response is required. Moreover we must also discriminate the neutrons scattered by the experimental setup itself such as the vacuum chamber wall. Thus, the detector has to be placed at close proximity to the fusion plasma; necessitating a scintillator with a time decay of less than 20 ns. In this work, results are presented on the fast response time of a custom-developed Pr^{3+} (Praseodymium)-doped lithium glass as a scintillator material (Arikawa et al., 2009).

The Pr^{3+} ion with a higher emission cross section in the deep ultraviolet region (~ 270 nm) is preferred as a dopant (Yoshikawa et al., 2008) over the slower, albeit more widely-used Ce^{3+} (Cerium) ion with its smaller emission cross section at longer wavelengths (Ehrlich et al., 1979; Fairley & Spowart, 1978; Suzuki et al., 2002). Additionally, high Li-density fluoro-lithium glass is chosen as the host material over UV-transparent, Li-doped fluoride crystals such as LiCaAlF_6 , primarily due to its ease-of-preparation and design flexibility.

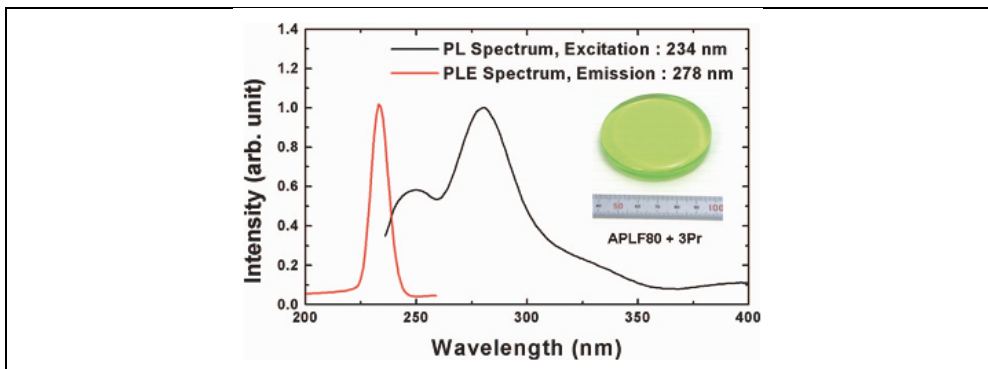


Fig. 4. Photoluminescence (PL) and photoluminescence excitation (PLE) spectrum of the APLF80+3Pr. The PL peak is observed at 279 nm while the PLE maximum occurs at 234 nm. The photograph shows the glass scintillator sample. The diameter is 6cm with a thickness of 1 cm.

The APLF80 + 3Pr glass sample, having a composition of $20\text{Al}(\text{PO}_3)_3 - 80\text{LiF} + 3\text{PrF}_3$ (in mol) using 95.5% ${}^6\text{Li}$ enriched lithium fluoride, is shown in the inset of Fig. 4. It was prepared using the melt-quenching method, where PrF_3 -containing starting materials were melted in a glassy carbon crucible at 1100 degrees Celsius under nitrogen atmosphere. The glass melt was then cooled down to 400 degrees Celsius in the furnace, and subsequently annealed near the glass transition temperature. The lithium density was measured using an atomic absorption photometer to be 7.98 w%, 31.6 mmol/cc. This is the highest reported value for conventional ${}^6\text{Li}$ glass scintillators, thus far (Saint-Gobain Crystals, 2007-2008). Fluorescence increase upon ${}^{241}\text{Am}$ -alpha excitation was observed with higher doping of Pr^{3+} . The highest doping of Pr^{3+} was found to be 3% at the present manufacturing procedure. The preliminary characteristics were reported in (Murata et al., 2009).

Before the neutron observation experiments were conducted, the spectral- and temporal-optical characteristics of the sample were evaluated. From the peak of the pulse height distribution of the APLF80+3Pr sample, we estimated the fluorescence photons yield to be about 300 photons / 5.5 MeV-alpha, taking into consideration the limited acceptance angle of the photomultiplier window even though the emission can be regarded to be isotropic in all directions. Figure 4 shows the photoluminescence (PL) and photoluminescence excitation (PLE) spectra of the sample. Strong emission at around 278 nm due to the 5d-4f transition, which was the design wavelength, was seen. Furthermore, the host material was found to have good transmission in the vacuum ultraviolet region down to 180 nm, and no absorption at the luminescence region was observed.

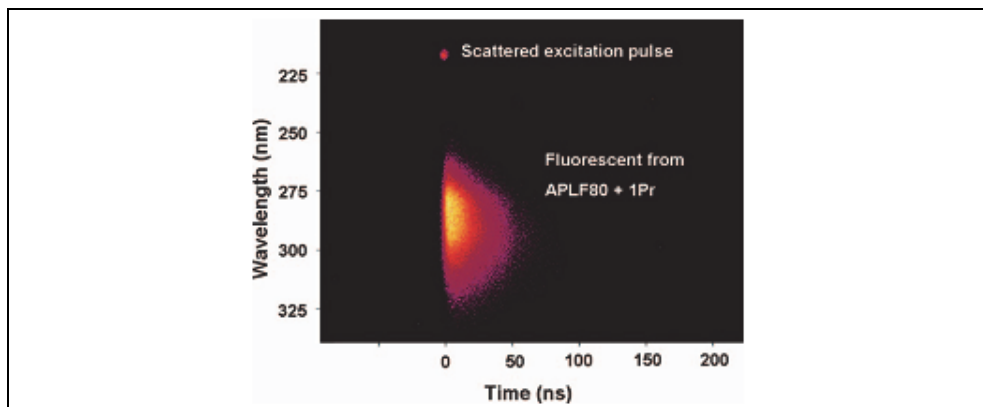


Fig. 5. Streak camera image of the spectral and time resolved luminescence of the APLF+1Pr. The excitation source is the 4th harmonics of a Ti: Sapphire laser.

The spectrally-resolved fluorescence lifetime of the APLF80+1Pr sample, excited with 217-nm 150, fs pulses using the 4th harmonics of a Ti:sapphire laser, was measured using a streak camera as shown in Fig. 5. The spectrally-integrated fluorescence decay profile, along with the other decay profiles for other excitation sources are shown in Fig. 6; where all the decay curves were fitted with a single exponential decay in the region from 50 % to 10 % of the peak value. For ultraviolet excitation, the fluorescence lifetime was determined to be 19.5 ± 0.80 ns. The decay from short x-ray excitation pulses from laser-produced plasma was measured to be 20.8 ± 0.85 ns. In this experiment, a 10- μ m thick aluminum plate target was irradiated by 4 ps/80 J Nd-glass laser pulses. The generated electron energy spectrum of a few MeV at the peak was also measured using an electron spectrometer. On the other hand, the fluorescence decay profile for 5.5 MeV ^{241}Am alpha-particle excitation was 6.7 ± 0.03 ns. Neutron excitation, having energy from 0.5 MeV to 10 MeV using ^{252}Cf , exhibited the fastest decay time of 5.9 ± 0.16 ns. This significant difference of decay times for neutrons and x-ray excitation is preferable for the time-of-flight measurements, although the mechanism of response time difference is not clear. A similar difference in the response time was also observed for conventional Ce^{3+} -doped Li glass scintillation (Fairley & Spowart, 1978). Based on these information, we show the feasibility of the custom-developed APLF80 + 3Pr scintillator material as a fast-response neutron detector for laser fusion diagnostics. The detection of ICF-originated neutrons was successfully carried out in laser fusion experiments at the GEKKO XII facility of the Institute of Laser Engineering, Osaka

University. In this study, a fusion target made from a deuterated plastic shell was irradiated by the 12 high-intensity Nd-glass lasers of the GEKKO XII facility. A detailed description of typical fusion experiment at GEKKO XII is described in (Azechi et al., 1991). As much as 5×10^5 DD-fusion neutrons were observed using conventional neutron detectors, based on plastic scintillators. The fluorescence from the APLF80 + 3Pr sample that was positioned at about 10 cm from the fusion target was transmitted using a bundle optical fiber and detected by an ultraviolet photomultiplier as shown in Fig. 7. Taking into account the distance between the target and the APLF80+3Pr glass scintillator, and the difference of the time-of-flight of X-ray (30 cm/ns) and neutrons (2.2 cm/ns), the signal at round 10 ns in Fig. 8 was identified to be that of DD primal neutron. With decay time of about 80 ns, such clear discrimination between x-rays and neutrons in this short interval is impossible with traditional cerium doped lithium glass scintillators.

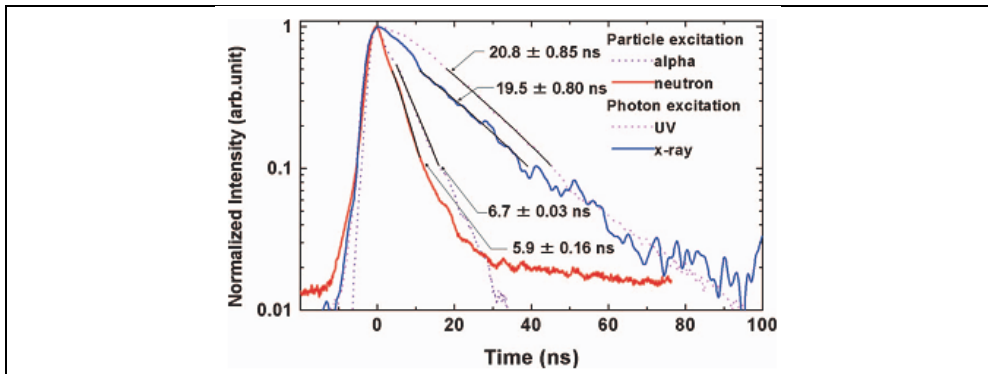


Fig. 6. The APLF+3Pr luminescence lifetime for alpha, neutron, x-ray, and UV pulse excitation. The lifetime varies from ~ 20 ns to under 7 ns, depending excitation source. This variation in the sample's decay time for different excitation energies suggests its capability to be used as detector in laser fusion time of flight experiments.

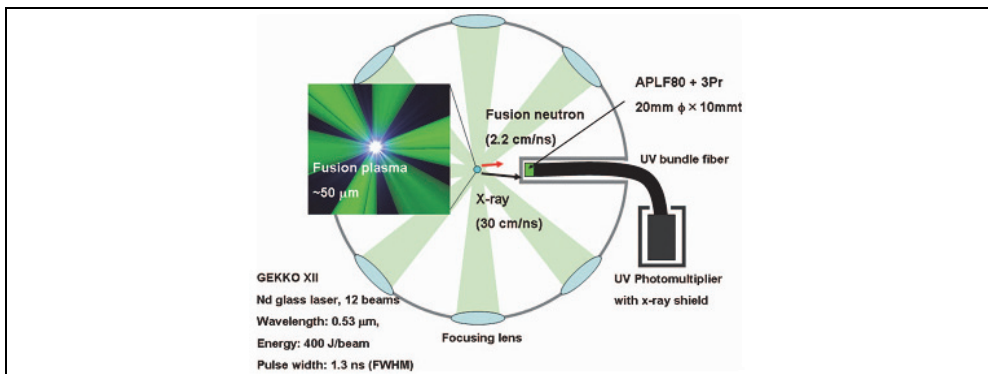


Fig. 7. Experimental set up of the time-of-flight experiment for the neutron detector. The detector is placed about 10 cm from the deuterated plastic target. The target is irradiated by 12 high energy beams of the GEKKO XII facility of the Institute of Laser Engineering, Osaka University.

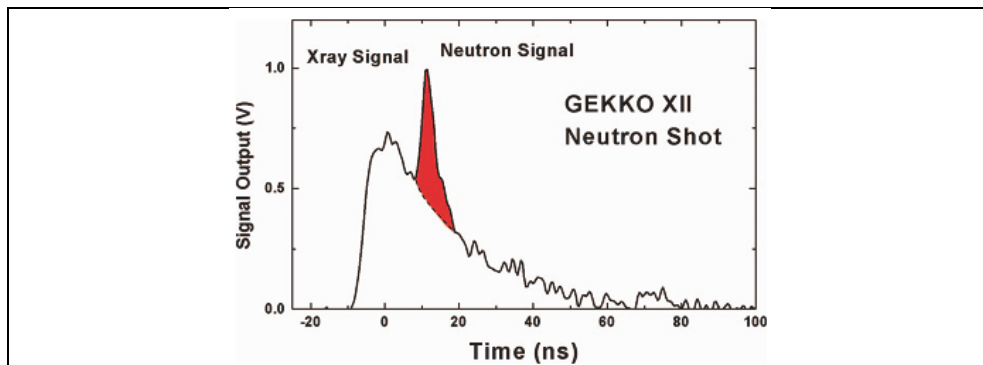


Fig. 8. The neutron signal at about 12 ns was successfully detected at the GEKKO XII facility fusion experiment.

5.2 Ce-doped fluoride

As mentioned in section 5.1, ${}^6\text{Li}$ is known to have a large cross section for high-energy neutrons. This makes lithium-rich compounds prominent candidates for a host, especially when doped with a high quantum efficiency light emitting ion. Particularly, Li-rich fluorides are important hosts for these applications because of their relatively wide bandgap, which make them transparent even down to the vacuum ultraviolet region (below 200 nm). On the other hand, three trivalent ions are being considered as dopants, namely, Cerium (Ce^{3+}), Praseodymium (Pr^{3+}), and Neodymium (Nd^{3+}) (van Eijk et al., 1994). Previously, $\text{Nd}^{3+}:\text{LaF}_3$ (Nakazato et al., 2010a) and $\text{Nd}^{3+}:\text{La}_x\text{Ba}_{(1-x)}\text{F}_{(3-x)}$ (Cadatal et al., 2007, 2008) have been reported as possible scintillator materials. However, of these three, Ce^{3+} has the smallest energy difference between the 4f and 5d levels, therefore resulting to a more efficient energy transfer to the dopant ion (van Eijk et al., 1994). The small energy difference also translates to a longer emission wavelength for Ce^{3+} -doped materials. A longer emission wavelength is advantageous because it can easily match the sensitivity of light sensors. For these reasons, $\text{Ce}^{3+}:\text{LuLiF}_4$ (Ce:LLF) is explored as a viable scintillator material (Nakazato et al., 2010b). This material has been extensively investigated as a tunable ultraviolet laser medium and amplifier (Dubinskii et al., 1992; Sarukura et al., 1995a, 1995b, 1998).

For the development of scintillators, specifically for nuclear fusion applications, material optimization and doping concentration are extremely important. Material screening is typically accomplished through characterization of the material's response time for different neutron or photon excitation energies (M. Tanaka et al., 2007). However, since the short-pulse and high-energy neutron generated by nuclear fusion is not available on a daily basis; the free electron laser (FEL) can be an alternative excitation source for material screening. Moreover, the FEL provides flexibility in tunability and operation, therefore making it an important aide in accelerating material development. Among such FELs, the storage ring free-electron laser (SRFEL) is an appropriate choice because of its adequately high repetition rate, which is needed for the suitable evaluation of fluorescence decay times that are typically in the order of tens of nanoseconds (Hosaka et al., 2002). These decay times have been characteristically observed from Ce^{3+} doped fluorides.

In this section, Ce:LLF is reported as a fast scintillator using a SRFEL operating in the deep ultraviolet region. The response time is comparable to that of commercially available

scintillators, KG2 and GS2 (Saint-Gobain Crystals, 2007-2008). Fluorescence spectral and temporal profiles also seem to have a flat spectral response at each of its three excitation channels. This report is the first systematic study on Ce:LLF as a scintillator where SRFEL is also shown to be a powerful tool for material survey.

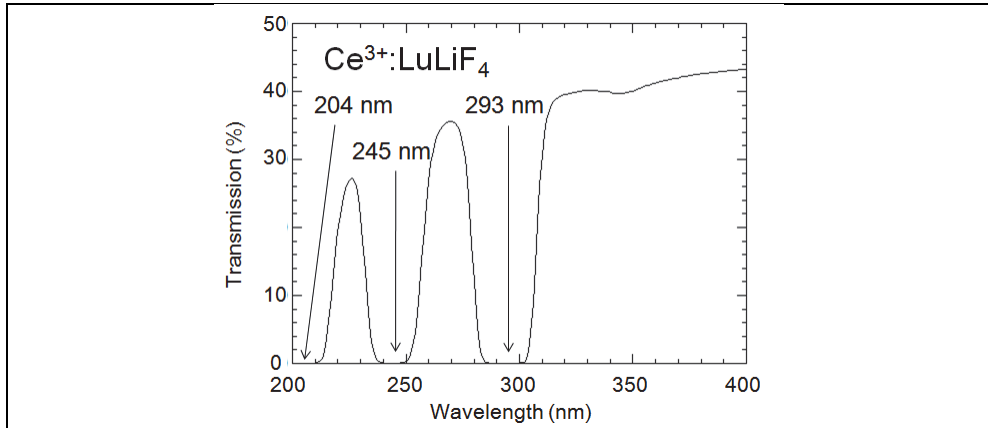


Fig. 9. Transmission spectrum of the 10 mm thick Ce:LLF.. Central wavelength of the absorption bands are situated at around 204 nm, 245 nm, and 293 nm. The doping concentration of this material is 1mol%.

The Ce:LLF crystal used in our experiments contained 1mol% Ce³⁺. The crystal, which was grown by the Czochralski technique, was cut into a half-cylinder with dimensions of 18mm for the diameter of the semi-circle and 10 mm for the length. The crystal's c-axis is along its length, such that it is parallel to the direction of the excitation beam. All of the three flat surfaces were polished. Detailed specification of the Ce:LLF crystal used in this experiment is referred to in (Ranieri et al., 2000; Liu et al., 2000).

The experiment was carried out at the UVSOR facility of the Institute for Molecular Science. The SRFEL, which is parasitically installed at the BL5U beam line, was used as the excitation source. Wavelengths from 199 nm to 800 nm with a repetition rate of 11 MHz and pulse duration of 15 ps were available for material characterization (Zen et al., 2009). This wide range of tunability is advantageous for material characterization because it allows one to choose the excitation wavelength to match the absorption band of the material. For the case of Ce:LLF, the wavelength was consecutively tuned to 216 nm and 243 nm. As shown in Fig. 9, these wavelengths exactly match the absorption band of CeLLF. These well-defined bands can be attributed to 4f-5d transitions in Ce³⁺. The beam from the SRFEL was focused to the sample almost along the c-axis. A streak camera coupled to a spectrograph and a CCD camera was used to measure the time-resolved fluorescence spectra. The system has a spectral resolution of ~1 nm and a temporal resolution of ~9.4 ns. The spectral and temporal profile of the fluorescence spectra was also measured using the third harmonic (290 nm) of a Ti:Sapphire regenerative amplifier, for reference. The 290-nm emission of this laser system operated at a repetition rate of 1 KHz, a pulse energy of ~40 μJ, and a pulse duration of ~100 fs. All experiments were done at room temperature.

Fluorescence image, as captured by the streak camera, for the 243-nm excitation wavelength is shown in Fig. 10. Two spectra can be observed in this streak camera image. These are

fluorescence emissions from two consecutive excitation pulses. The 11 MHz repetition rate of the SRFEL meant that the sample is irradiated by one pulse every ~ 90 ns. Therefore, two fluorescence emissions from two consecutive pulses were detected in one streak camera scan. This is also the case for the 216 nm excitation. We obtained the time-integrated fluorescence spectrum by integrating the signal over the time axis of the time-wavelength map of the streak camera data; and we found two fluorescence peaks, one at 308 nm and the other at 326 nm, as shown in Fig. 11 (blue line). These fluorescence peaks are consistent with previous reports (Sarukura et al., 1995; Ranieri et al., 2000; Rambaldi et al., 1998; Combes et al., 1997). The $4f^{25}d$ excited state configuration of Ce^{3+} in a LLF host is split into four energy levels as a result of the the S_4 point symmetry at the Ce^{3+} site (Sarukura et al., 1995; Combes et al., 1997). The three absorption bands in Fig. 9 correspond to the three lowest energy levels of this $4f^{25}d$ configuration with energies at $\sim 32.9 \times 10^3$ to $\sim 35.3 \times 10^3$ cm^{-1} (304 to 283 nm), $\sim 39.7 \times 10^3$ to $\sim 40.6 \times 10^3$ cm^{-1} (252 to 246 nm), and $\sim 46.7 \times 10^3$ to $\sim 50 \times 10^3$ cm^{-1} (214 to ~ 200 nm). The 308 nm ($\sim 32.5 \times 10^3$ cm^{-1}) and 329 nm ($\sim 30.4 \times 10^3$ cm^{-1}) emission peaks can therefore be attributed to radiative transitions from the lowest energy level of the $4f^{25}d$ excited state configuration to the $^2F_{5/2}$ (0 cm^{-1}) and $^2F_{7/2}$ ($\sim 2 \times 10^3$ cm^{-1}) energy levels of the $4f^3$ ground state configuration, respectively (Ehrlich et al., 1979). These energies are specified in the energy level diagram, shown in Fig. 12.

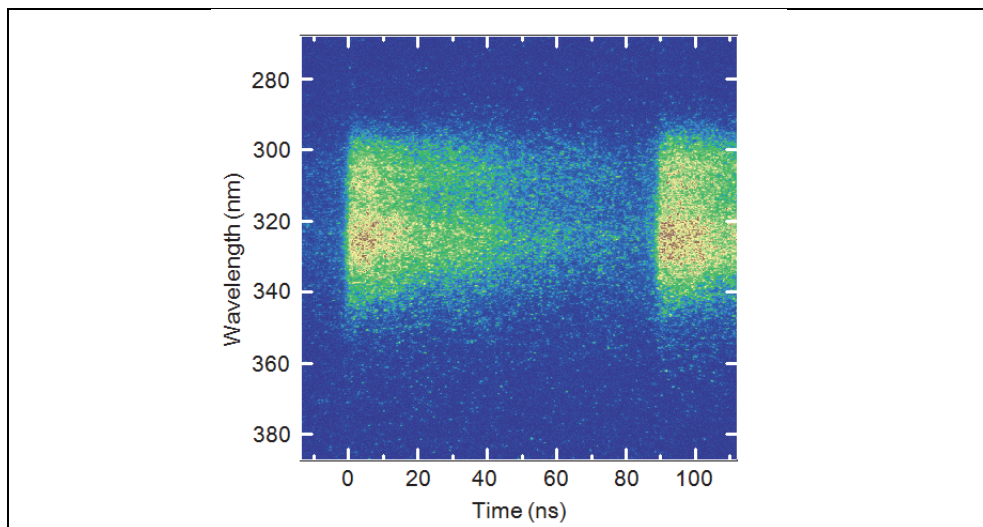


Fig. 10. Streak camera image of the Ce:LLF emission excited by the SRFEL tuned at 243 nm. The SRFEL had a repetition rate of 11 MHz, therefore two fluorescence images were captured by the 100-ns window of the streak camera.

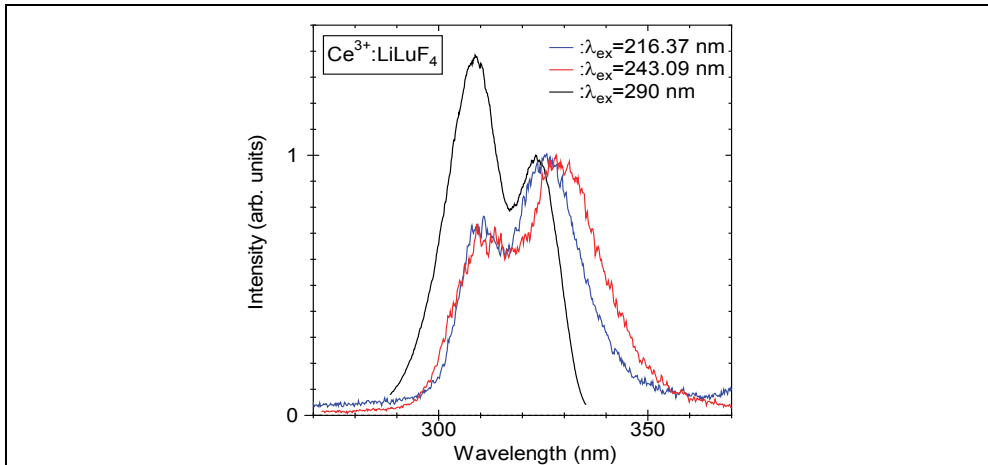


Fig. 11. Spectral profile of the fluorescence emission after consecutively exciting the three absorption channels of Ce:LLF with the SRFEL tuned at 243 nm and 216 nm and by the 290-nm emission of a Ti:sapphire laser. Transition from the $4f^25d$ excited state configuration to the $4f^3$ ground state configuration of Ce^{3+} resulted to two fluorescence peaks, one at 308 nm and the other at 329 nm.

Two peaks, 308 nm and 326 nm, were also observed for the 216 nm SRFEL excitation, as shown in Fig. 11 (blue line). Since the emission was also influenced by the Ce^{3+} doping, these fluorescence peaks were similar to the 243-nm excitation case wherein the fluorescence peaks were located at 308 nm and 329 nm where the transition was from the lowest energy level of the $4f^25d$ excited state configuration to the $^2F_{5/2}$ and $^2F_{7/2}$ energy levels of the $4f^3$ ground state configuration.

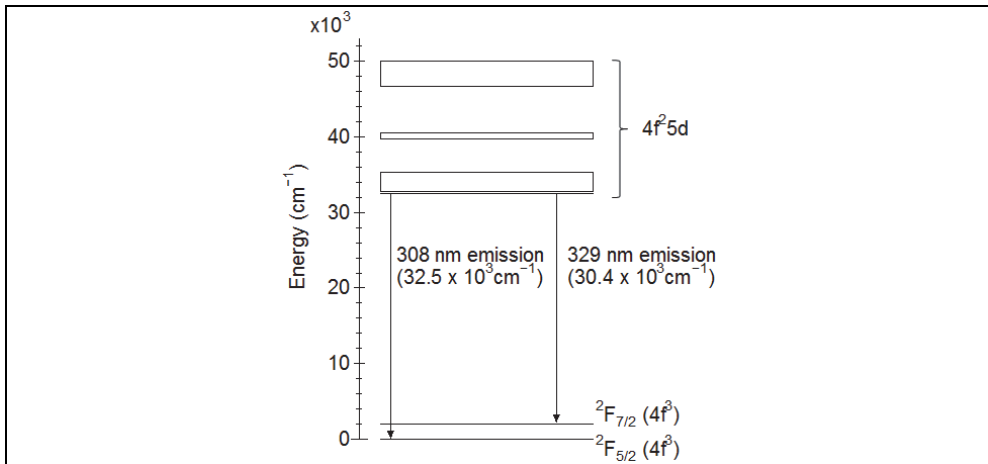


Fig. 12. Energy level diagram of Ce^{3+} in Ce:LLF. Two emission peaks originate from the transitions from the lowest $4f^25d$ excited states to the $^2F_{5/2}$ (308 nm emission) and $^2F_{7/2}$ (329 nm emission).

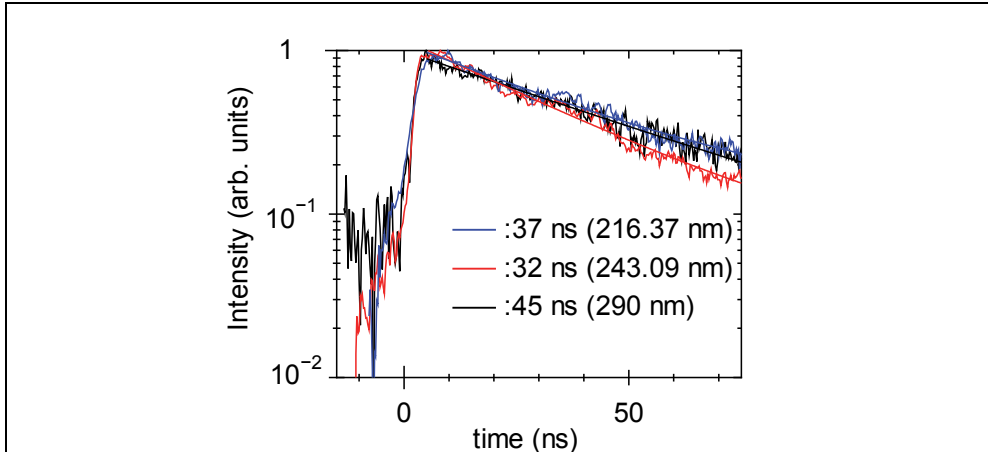


Fig. 13. Temporal profile showing fluorescence lifetimes for the 243 nm (SRFEL), 216 nm (SRFEL), and 290 nm (Ti:sapphire) excitation. These values are fast enough for ignition timing in fast-ignition, inertial confinement nuclear fusion using laser.

The fluorescence of the same sample was also measured when a 290-nm, fs excitation laser was used. The spectral profile is shown in Fig. 11 as well. Similar to the results of the SRFEL-excited fluorescence spectrum, peaks at 308 nm and 325 nm were observed. This similarity is indicative that the transitions brought about by the Ce^{3+} doping has a relatively flat spectral response across its absorption bands regardless of the excitation source, therefore making Ce:LLF as an attractive scintillator material for various excitation sources.

The fluorescence decay times for the three excitation wavelengths are shown in Fig. 13. The decay curves are single exponential with lifetimes of 32 ns, 37 ns, and 45 ns for the 243-nm, 216-nm, and 290-nm excitation wavelengths, respectively. The variation of these fluorescence decay times is less than the temporal resolution of the streak camera system, and thus within measurement uncertainty. The average value of the fluorescence decay time is ~ 40 ns. The relatively flat spectral response across its absorption bands makes Ce:LLF a viable scintillator material for various short-wavelength excitation sources. The fluorescence decay time of commercial scintillators, for example KG2 or GS2, is ~ 40 ns (Saint-Gobain Crystals, 2007-2008). Scintillation decay time of Ce:LLF might be a few ns slower, however, it is still acceptable for ignition timing in fast-ignition, inertial confinement nuclear fusion using laser.

5.3 Other scintillators

Fast scintillators, with response times in the nanosecond or even picosecond regime would play an important role in the advancement of radiation detection. For completeness, this section will discuss two solid-state materials that have been studied and have been shown to have potential as fast scintillators.

5.3.1 Zinc oxide (ZnO)

The feasibility of ZnO crystal as a fast scintillator in the ultraviolet (UV) and extreme ultraviolet (EUV) region is reported. Over the past decade, ZnO has been intensively

studied as a light emitting diode and as a nanostructured material with improved optical properties (Cao & Du, 2007; Hauschild et al., 2006; Ichimiya et al., 2006; Jen et al., 2005; Ohta et al., 2000; Qian et al., 2007; Xu et al., 2007; Yu & Cardona, 2001; Zhang et al., 2007). In relation to this, the hydrothermal method is a novel growth method suitable for growing various crystals, including oxides such as ZnO. This method is capable of producing high-crystalline quality and large-sized homogeneous samples (Ohshima et al., 2004). The efficacy of a hydrothermal-method-grown ZnO crystal as a scintillator for UV region has been previously demonstrated (Furukawa et al., 2008; M. Tanaka et al., 2007; Nakazato et al., 2009), wherein the reported decay time of the ZnO scintillator was 1ns for EUV excitation at 13nm using Ag-plasma EUV laser. However, a faster response time is needed. In this section, an intentionally iron (Fe)-doped, hydrothermal-method-grown, ZnO crystal, is demonstrated to exhibit a response time faster by over one order of magnitude for soft x-ray pulsed excitation from the actual XFEL prototype (SPring-8 compact self amplification of spontaneous emission source [SCSS] test accelerator) at the SPring-8 research facility in RIKEN (Shimizu et al., 2010; Yamanoi et al., 2010).

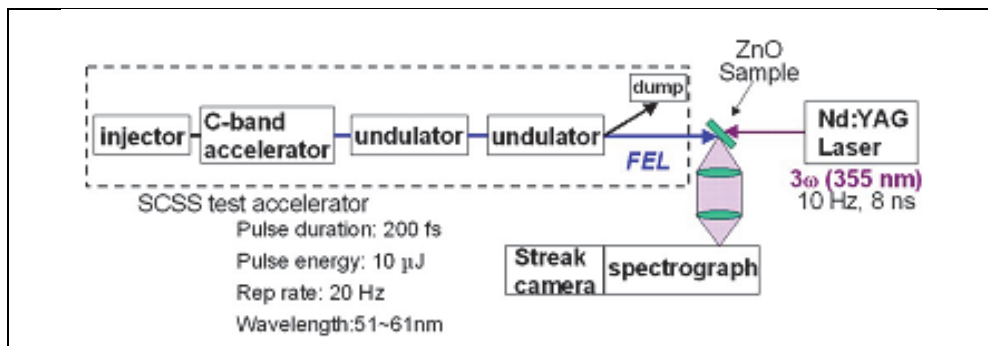


Fig. 14. Experimental setup for the measurement of the time resolved spectrum using the SCSS test accelerator (200-fs pulse duration, 10-μJ pulse energy, and 20-Hz repetition rate at 51-61nm). The sample was placed inside a vacuum chamber and excited by the EUV pulse from the SCSS test accelerator. The fluorescence was observed using a streak camera with the spectrograph.

The faster response time of the ZnO scintillator in this work was achieved by modifying the previously reported hydrothermal method ZnO crystal growth (Ohshima et al., 2004). The growth modification was aimed to introduce other fluorescence quenching channels by intentional doping during growth. To do this, the platinum lining of the crystal growth container was removed to facilitate the intentional doping of Fe-ion impurities. Three-dimensional-transition metals such as Fe in other semiconductor materials are known to play the role of lifetime-shortening impurity. The concentration of other impurities such as Li, K, and Al also increased, when the Pt lining was removed. However, the rate of increase in these metals is one order lower than that of Fe. Moreover, the contribution of these metals to the shortening of the lifetime is known to be smaller than that of transition metals. These results suggest that Fe is the main impurity. The sample was grown at a temperature of 300-400°C and at 80-100 MPa pressure and the crystal was cut at the (0001) surface orientation. The density of Fe-ion impurities in this sample was 0.61ppm, which is more than two orders of magnitude higher compared to previous ZnO samples grown with the Pt lining.

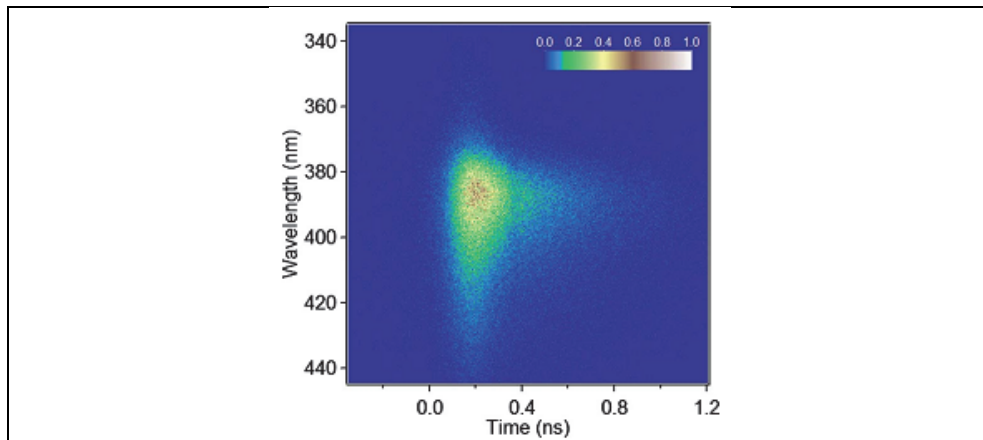


Fig. 15. Streak camera image of the fluorescence from ZnO. This is a 50000-shot integrated signal excited by 56 nm. The vertical axis is wavelength (nanometer) and the horizontal axis is time (nanosecond). The dominant fluorescence peak was centered at around 380 nm.

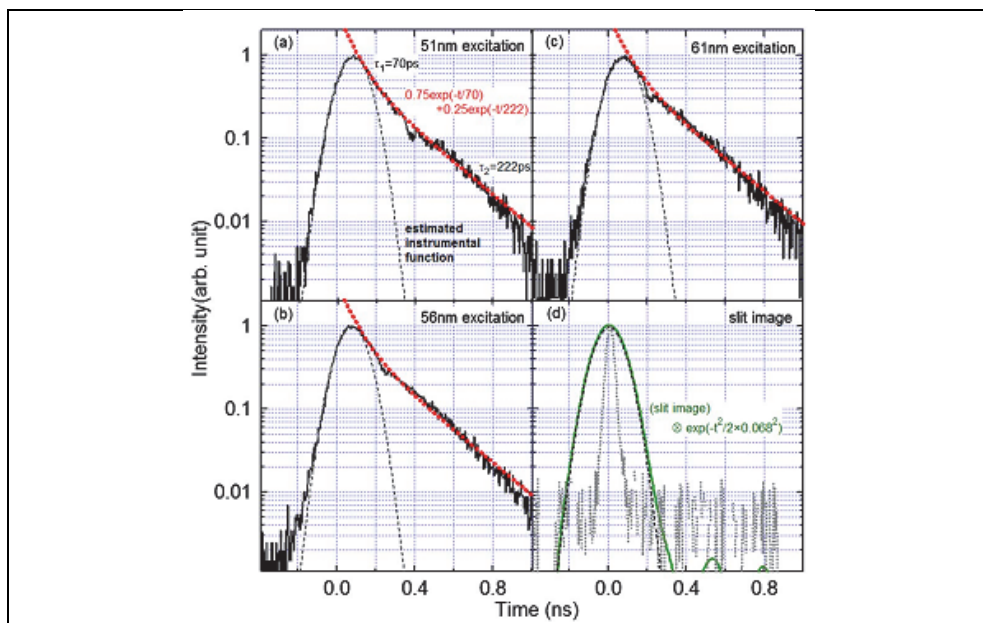


Fig. 16. Temporal profiles of the ZnO fluorescence excited by (a) 51nm, (b) 56nm, and (c) 61 nm. The observed profiles can be fitted by double exponential decays described as $I=A_1 \exp(-t/\tau_1)+A_2 \exp(-t/\tau_2)$ (dotted line). The fitting parameters are $A_1=0.75$, $A_2=0.25$, $\tau_1=70\text{ps}$, and $\tau_2=222\text{ps}$. The estimated instrumental function was plotted with a dot line in each graph. (d) Slit image (dotted line) and a calculated curve of a convolution of the slit image and a normal distribution function (solid line).

Initially, the response time of Fe-ion doped ZnO scintillator was evaluated using the third harmonics of a mode-locked Ti:sapphire femtosecond laser at 290nm. The typical band-to-band ultraviolet fluorescence at 380nm was successfully observed, with a decay time of ~80ps. This is significantly faster compared with the previously reported 1-ns decay time for the 380-nm fluorescence of undoped ZnO. The 1x1cm², 0.5-mm thick double-side polished ZnO crystal was mounted in a vacuum chamber, and the third harmonics of a neodymium-doped YAG (Nd:YAG) laser was initially used as excitation for alignment purposes. The sample was illuminated from the backside, in a counter propagation configuration with the beam path of the SCSS test accelerator, as shown in Fig. 14. The SCSS test accelerator having 200-fs pulse duration, 10-μJ pulse energy, and 20-Hz repetition rate, was focused by an oblique mirror (Mimura et al., 2008). With a mirror focal length of 1m, the spot size at the focus was about 20 μm. To minimize the risk of damage, however, the sample was placed 5 cm away from focus, and the radius of the beam at this location was estimated to be 500 μm. The emission wavelength of the SCSS test accelerator can be tuned from 51 to 61 nm. Fluorescence was collected and focused to the entrance slit of a spectrograph using quartz lenses. The fluorescence spectrum and the lifetime of the ZnO sample were measured using a 25-cm focal-length spectrograph (groovedensity600gr/mm) coupled to a streak camera unit (HAMAMATSUC1587) and a charge coupled device camera. The ZnO fluorescence, excited by light pulses of the SCSS test accelerator at 51, 56, and 61 nm with 50000 shots was measured using the spectrograph coupled to the streak camera system. Figure 15 shows the streak camera image of the fluorescence using 56-nm excitation from the SCSS test accelerator. The dominant fluorescence peak was centered at around 380 nm (Chen et al., 2000). The temporal profiles of this image at 51-, 56-, and 61-nm excitation are shown in Figs. 16(a)-10(c), respectively. The measured decay profiles can be well-fitted to a double exponential decay with time constants of 70 and 222 ps for the fast and slow decay-time constants, respectively. These two decay constants have been previously reported in several works involving UV-excited ZnO single crystals, where the fast decay time is attributed to the lifetime of free excitons, while the slower decay time is assigned to trapped carriers (Wilkinson et al., 2004). This measured response time is currently the fastest for a scintillator operating in the 50-60 nm region. In addition, the fluorescence intensity and time decay profile appears to be independent of the excitation wavelength within the 50-60 nm range. This flat response makes the Fe-doped ZnO scintillator ideal for operation both for UV and in soft x-ray excitation schemes.

5.3.2 Neodymium-doped lanthanum fluoride (Nd³⁺:LaF₃)

Scintillators in the vacuum ultraviolet (VUV) region are continuously being developed for various applications. In this section, the scintillation properties of Nd³⁺:LaF₃ is discussed. Characterization was performed by exciting the sample with the third harmonics of a Ti:sapphire regenerative amplifier having 1-KHz repetition rate, 10-μJ pulse energy, and 200-fs pulse duration. The excitation wavelength in this case is at 290 nm; while the reported fluorescence wavelength of Nd³⁺:LaF₃ is at 175 nm. With the unavailability of ultrashort-pulse EUV sources, we attempt to demonstrate the scintillation properties of this crystal for ultrafast excitation using possibly a multiphoton process. Spectroscopic studies have revealed that the absorption edge of this crystal is at ~168 nm (Nakazato et al., 2010a). Pulses were focused by a 20-cm lens onto the sample inside a vacuum chamber. A VUV spectrometer and streak camera system was used to evaluate fluorescence from this sample.

The streak camera image of fluorescence is shown in Fig. 17 (a). The streak camera image of the 290-nm, fs excitation is also shown in the same figure as Fig. 17 (b) for reference. On the other hand, the spectral and temporal profile obtained by sweeping across the vertical axis is shown in Fig. 18. The fluorescence peak is centered at around 175 nm with a decay time of about 7.1 ns.

The absorption spectrum of the sample from 200 to 400 nm revealed the presence of multiple absorption bands, particularly at 290 nm. Moreover, the slope of fluorescence intensity as a function of pump fluence was experimentally verified to be equal to unity. In this aspect, frequency up-conversion by energy transfer could have been the governing mechanism [3], owing to the absorption band at 290 nm. Since fluorides have low phonon energies, the lifetimes of intermediate levels are long enough (order of μs) for the accumulation of electrons in an intermediate excited state. Existing solid-state, inorganic scintillators in the ultraviolet region typically have decay times of a few tens of nanoseconds. As such, the $\text{Nd}^{3+}:\text{LaF}_3$ fluorescence decay time of about 7.1 ns would be among the fastest solid-state, inorganic scintillators.

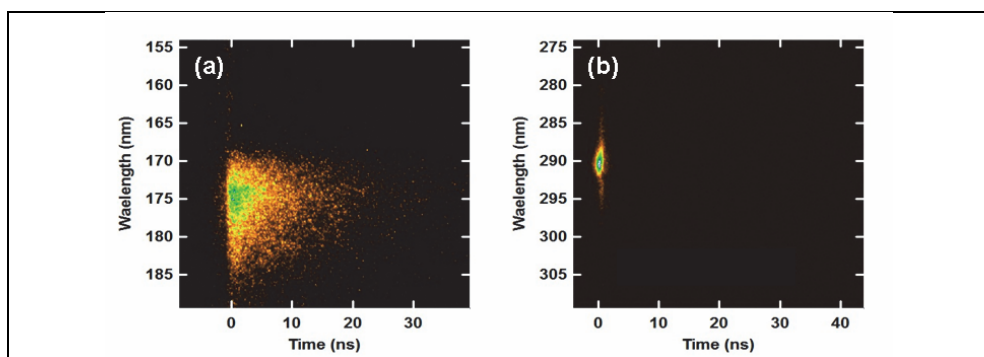


Fig. 17. (a) Streak camera image of fluorescence from a cuboid $\text{Nd}^{3+}:\text{LaF}_3$ excited by 290-nm femtosecond pulses shown in (b).

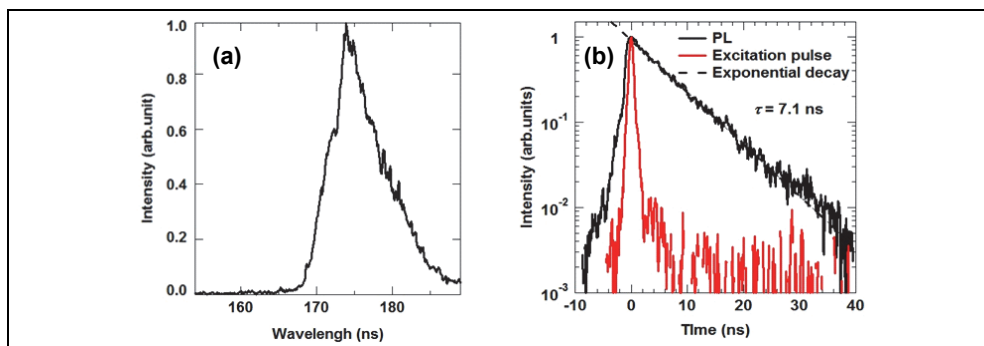


Fig. 18. (a) Spectral and (b) temporal profiles of the fluorescence shown in Fig. 17 (a).

6. Conclusion

In the field of fusion research, understanding the plasma dynamics could very well be the key in feasibly attaining controlled fusion. The time-resolved fluorescence spectra of Ce:LLF when excited by SRFEL tuned at 243 nm and 216 nm and by the 290-nm emission of a Ti:sapphire laser were measured to determine the feasibility of using this material as a scintillator for fast-ignition laser fusion. Two peaks were observed, one at 308 and another at 329 nm, which can be attributed to transitions from the lowest energy level of the $4f^25d$ excited state configuration to one of the two energy levels in the $4f^3$ ground state configuration of Ce^{3+} . The relatively flat spectral and temporal response across its absorption bands makes Ce:LLF an attractive scintillator material for various excitation sources. Scintillation decay time of Ce:LLF might be few ns slower, however, it is still acceptable for measurements of ignition timing in fast-ignition, inertial confinement nuclear fusion using laser.

In response to the need for a fast-response scintillator for precise time-resolved radiation measurement, we have succeeded in developing a fast-response 6Li glass scintillator material suitable for scattered neutron diagnostics of the ICF plasma, with a response time of about 20 ns. Using this custom-developed material, fusion-originated neutrons were successfully observed using the GEKKO XII laser at the Institute of Laser Engineering, Osaka University. These results could pave the way for a new class of scintillator devices, optimized for neutron detection. In particular, after proper growth and device design considerations are carried out, future discrimination between primary and low-energy scattered neutrons using this material could be realized.

Due to the increasing demand for scintillators with fast response time, several materials are currently being investigated. In this aspect, vacuum ultraviolet fluorescence from a $Nd^{3+}:LaF_3$ crystal excited by 290 nm femtosecond pulses from a Ti:sapphire laser is reported. Peak emission at 175 nm with 7 ns lifetime is observed. This decay time would be one of the fastest among fluoride scintillators. On the other hand, a hydrothermal-method grown ZnO scintillator exhibited an over one-order of magnitude faster response time by intentional Fe ion doping. The rise and decay time constants of the fluorescence are measured to be less than 10 ps and 100 ps, respectively. Its fluorescence is also sufficiently bright to be detected by a streak-camera system even in single shot mode without any accumulation.

Meanwhile, mapping of radiation sources is very useful to detect and characterize invisible radiation accidents and/or radioactive contamination. For this purpose, bundles composed of well-designed and regularly arranged scintillation fiber-segments or thin cylinders have been developed to detect and display the radiation sources as a map, using the directional sensitivity of the segments or cylinders for locating sources of incident radiation. In this case, the more important attribute would be scintillation intensity, regardless of decay time, since available moving picture systems are usually 30 frames per second. A bundle composed of several kinds of thin cylinder or fiber segment scintillators has appropriate sensitivity for several kinds of incident radiation and thus serves as a panchromatic detector; whereas a bundle made from a single type of scintillator functions as a monochromatic detector. By combining several types of scintillating elements into a bundle, we have developed a "panchromatic" detector that is suitable for use against radiation from different types of sources.

7. Acknowledgment

Work on Pr^{3+} -doped glass scintillator was supported by the Japan Society for the Promotion of Science under the contracts of Grant-in-Aid for Scientific Research (S) (GrantNo.18106016),

Grant-in-Aid on Priority Area (GrantNo.16082204), Open Advanced Research Facilities Initiative, and Research Fellowship for Young Scientists (GrantNo.3273).

Work on Ce:LLF was in part performed by auspice of MEXT Japanese Ministry of Education, Culture, Sports, Science, and Technology project on "Development of Growth Method of Semiconductor Crystals for Next Generation Solid-State Lighting" and "Mono-energetic quantum beam science with PW lasers" and Scientific Research Grant-in Aid (17656027) from the MEXT. The results were achieved under the joint research project of the Institute of Laser Engineering at Osaka University, Extreme Photonics project from the Institute for Molecular Science.

For the work on ZnO, we are also grateful to the SCSS Test Accelerator Operation Group at RIKEN for continuous support in the course of the studies and Fukuda Crystal Laboratory for support in sample preparation.

8. References

- Arikawa, Y., Yamanoi, K., Nakazato, T., Estacio, E. S., Shimizu, T., Sarukura, N., Nakai, M., Norimatsu, T., Azechi, H., Murata, T., Fujino, S., Yoshida, H., Kamada, K., Usuki, Y., Suyama, T., Yoshikawa, A., Sato, N., & Kan, H. (2009), Pr³⁺-doped fluoro-oxide lithium glass as scintillator for nuclear fusion diagnostics, *Review of Scientific Instruments*, Vol. 80, Issue 11, (November 2009), pp. 113504-113504-4, ISSN: 0034-6748
- Azechi, H., Jitsuno, T., Kanabe, T., Katayama, M., Mima, K., Miyanaga, N., Nakai, M., Nakai, S., Nakaishi, H., Nakatsuka, M., Nishiguchi, A., Norrays, P. A., Setsuhara, Y., Takagi, M., & Yamanaka, M. (1991). High-density compression experiments at ILE, Osaka, *Laser and Particle Beams*, Vol. 9, Issue 2, (June 1991), pp.193-207, ISSN: 0263-0346
- Cadatal, M., Seo, Y.S., Ono, S., Furukawa, Y., Estacio, E., Murakami, H., Fujimoto, Y., Sarukura, N., Nakatsuka, M., Suyama, T., Fukuda, K., Simura, R., & Yoshikawa, A. (2007), Nd³⁺:(La_{1-x}Ba_x)F_{3-x} Grown by Micro-Pulling Down Method as Vacuum Ultraviolet Scintillator and Potential Laser Material, *Japanese Journal of Applied Physics*, Vol. 46, No. 40, (October 2007), pp. L985-L987, ISSN: 0021-4922
- Cadatal, M., Furukawa, Y., Seo, Y. S., Ono, S., Estacio, E., Murakami, H., Fujimoto, Y., Sarukura, N., Nakatsuka, M., Fukuda, K., Simura, R., Suyama, T., Yoshikawa, A., & Saito, F. (2008), Vacuum ultraviolet optical properties of a micro pulling-down-method grown Nd³⁺:(La_{0.9}Ba_{0.1})F_{2.9}, *Journal of the Optical Society of America B*, Vol. 25, No. 7 (July 2008), pp. B27-B31, ISSN: 0740-3224
- Cheon, M. S., Pac, S., Lee, F. G., Bertalot, L., & Walker, C. (2008). In-vessel design of ITER diagnostic neutron activation system, *Review of Scientific Instruments*, Vol. 79, Issue 10, (October 2008), pp.10E505-10E505-3, ISSN: 0034-6748
- Combes, C. M., Dorenbos, P., van Eijk, C. W. E., Pedrini, C., DenHartog, H. W., Gesland, J. Y., & Rodnyi, P. A. (1997). Optical and scintillation properties of Ce³⁺ doped LiYF₄ and LiLuF₄ crystals, *Journal of Luminescence*, Vol. 71, Issue 1, (January 1997), pp. 65-70, ISSN: 0022-2313
- Dubinskii, M.A., Abdulsabirov, R.Y., Korableva, S.L., Naumov, A.K., & Semashko, V.V. (1992). New solid-state active medium for tunable ultraviolet lasers, *Proceedings of the 18th International Quantum Electronics Conference*, Moscow, Russia, June 1992

- Ehrlich, D., Moulton, P., & Osgood, R. (1979). Ultraviolet solid-state Ce:YLF laser at 325 nm, *Optics Letters*, Vol. 4, Issue 6, (Jun 1979), pp. 184-186, ISSN: 0146-9592
- Fairley, E. J. & Spowart, A. R. (1978). Neutron Scintillating Glasses Part Iii Pulse Decay Time Measurements At Room Temperature, *Nuclear Instruments and Methods*, Vol. 150, Issue 2, (April 1978), pp. 159-163, ISSN: 0168-9002
- Fukuda, T. & Chani, V. I. (2007). In: *Shaped Crystals*, Tsuguo Fukuda & Valery I.Chani, pp. , Springer-Verlag, ISBN: 978-3-540-71294-7, Berlin Heidelberg New York
- Fukuda, T., Rudolph, P. & Uda, S. (2004). In: *Fiber Crystal Growth from Melt*, Tsuguo Fukuda Peter Rudolph Satoshi Uda, pp. ,Springer-Verlag, ISBN: 3-540-40596-8, Berlin Heidelberg New York
- Glebov, V. Yu., Meyerhofer, D. D., Sangster, T. C., Stoeckl, C., Roberts, S., Barrera, C. A., Celeste, J. R., Cerjan, C. J., Dauffy, L. S., Eder, D. C., Griffith, R. L., Haan, S. W., Hammel, B. A., Hatchett, S. P., Izumi, N., Kimbrough, J. R., Koch, J. A., Landen, O. L., Lerche, R. A., MacGowan, B. J., Moran, M. J., Ng, E. W., Phillips, T. W., Song, P. M., Tommasini, R., Young, B. K., Caldwell, S. E., Grim, G. P., Evans, S. C., Mack, J. M., Sedillo, T. J., Wilke, M. D., Wilson, D. C., Young, C. S., Casey, D., Frenje, J. A., Li, C. K., Petrasso, R. D., Séguin, F. H., Bourgade, J. L., Disdier, L., Houry, M., Lantuejoul, I., Landoas, O., Chandler, G. A., Cooper, G. W., Leeper, R. J., Olson, R. E., Ruiz, C. L., Sweeney, M. A., Padalino, S. P., Horsfield, C., & Davis, B. A. (2006). Development of nuclear diagnostics for the National Ignition Facility (invited), *Review of Scientific Instruments*, Vol. 77, Issue 10, (October 2006), pp. 10E715-10E715-7, ISSN: 0034-6748
- Hosaka, M., Koda, S., Katoh, M., Yamazaki, J., Hayashi, K., Takashima, K., Gejo, T., & Hama, H. (2002). From the operation of an SRFEL to a user facility, *Nuclear Instruments and Methods in Physics Research Section A: Accelerators, Spectrometers, Detectors and Associated Equipment*, Vol. 483, Issues 1-2, (May 2002), pp. 146-151, ISSN: 0168-9002
- Ishii, M. & Kobayashi M. (1991). Single crystals for radiation detectors. *Progress in Crystal Growth and Characterization*, Vol. 23, (1992), pp. 245-311, ISSN: 0960-8974
- Izumi, N., Lerche, R. A., Phillips, T. W., Schmid, G. J., Moran, M. J., Koch, J. A., Azechi, H., & Sangster, T. C. (2002). Development of a gated scintillation fiber neutron detector for areal density measurements of inertial confinement fusion capsules, *Review of Scientific Instruments*, Vol. 74, Issue 3, (March 2003), pp. 1722–1725, ISSN: 0034-6748
- Kobayashi, M & Ishii, M. (2007). Chapter 7 Phosphors for X-ray and ionizing radiation, In: *Phosphor handbook*, William M. Yen , Shigeo Shionoya & Hajime Yamamoto, pp. 619-633, CRC Press, ISBN 978-084-9335-64-8, Florida, USA
- Lerche, R. A., Phillion, D. W., & Tietbohl, L. (1994). 25 ps neutron detector for measuring ICF-target burn history, *Review of Scientific Instruments*, Vol. 66, Issue 1, (January 1995), pp. 933 - 935, ISSN: 0034-6748
- Liu, Z., Shimamura, K., Nakano, K., Mujilatu, N., Fukuda, T., Kozeki, T., Ohtake, H., & Sarukura, N. (1999). Direct Generation of 27-mJ, 309-nm Pulses from a Ce³⁺:LiLuF₄ Oscillator Using a Large-Size Ce³⁺:LiLuF₄ Crystal, *Japanese Journal of Applied Physics*, Vol. 39, No. 2A, (February 2000), pp. L88-L89, ISSN: 0021-4922
- Murata, T., Fujino, S., Yoshida, H., Arikawa, Y., Nakazato, T., Shimizu, T., Sarukura, N., Nakai, M., Norimatsu, T., Azechi, H., Kamada, K., Usuki, Y., Suyama, T., Yoshikawa, A., Sato, N., & Kan, H. (2010). Custom-Designed Fast-Response Praseodymium-Doped Lithium 6 Fluoro-Oxide Glass Scintillator With Enhanced

- Cross-Section for Scattered Neutron Originated From Inertial Confinement Fusion, *IEEE Transactions on Nuclear Science*, Vol. 57, No. 3, (June 2010), pp. 1426-1429, ISSN: 0018-9499
- Nakazato, T., Cadatal-Raduban, M., Furukawa, Y., Pham, M., Estacio, E., Shimizu, T., Sarukura, N., Fukuda, K., Suyama, T., Yanagida, T., Yokota, Y., Yoshikawa, A., & Saito, F. (2010), Nd³⁺:LaF₃ as a Step-Wise Excited Scintillator for Femtosecond Ultraviolet Pulses, *IEEE Transactions On Nuclear Science*, Vol. 57, Issue 3, (June 2010), pp. 1208-1210, ISSN: 0018-9499
- Nakazato, T., Furukawa, Y., Cadatal-Raduban, M., Pham, M., Tatsumi, T., Saiki, A., Arikawa, Y., Sarukura, N., Nishimura, H., Azechi, H., Mima, K., Fukuda, T., Hosaka, M., Katoh, M., & Kosugi, N. (2010), Systematic Study on Ce:LuLiF₄ as a Fast Scintillator Using Storage Ring Free-Electron Lasers, *Japanese Journal of Applied Physics*, Vol. 49, No. 12, (December 2010), pp. 122602-122602-4, ISSN: 0021-4922
- Ogawa, T. (2007). Patent Application PCT/JP2007/062817
- Ogawa, T., Sarukura, N., Watanabe, M., Fukuda, T., Nango, N. (2010), Two dimensional imaging of radiation accidents and radioactive contamination, *Optical Materials*, Vol. 32, Issue 7, (May 2010), pp. 753-755, ISSN: 0925-3467
- Petrizzi, L., Barnsley, R., Ertalot, L., Esposito, B., Haskell, H., Mainardi, E., Marocco, D., Podda, S., Walker, C., & Villari, S. (2007). Neutronic design of the ITER radial neutron camera, *Fusion Engineering and Design*, Vol. 82, Issues 5-14, (October 2007), pp.1308-1314, ISSN: 0920-3796
- Rambaldi, P., Moncorge, R., Wolf, J. P., Pedrini, C., & Gesland, J. Y. (1998). Efficient and stable pulsed laser operation of Ce:LiLuF₄ around 308 nm, *Optics Communications*, Vol. 146, Issues 1-6, (January 1998), pp. 163-166, ISSN: 0030-4018
- Ranieri, I. M., Shimamura, K., Nakano, K., Fujita, T., Liu, Z., Sarukura, N., & Fukuda, T. (2000). Crystal growth of Ce : LiLuF₄ for optical applications, *Journal of Crystal Growth*, Vol. 217, Issue 1-2, (July 2000), pp. 151-156, ISSN: 0022-0248
- Ress, D., Lerche, R. A., Ellis, R. J., & Lane, S. M. (1988). Neutron imaging of inertial confinement fusion targets at Nova, *Review of Scientific Instruments*, Vol. 59, Issue 8, (August 1988), pp. 1694-1696, ISSN: 0034-6748
- Saint-Gobain Ceramics & Plastics, Inc. (2007-2008). Lithium glass scintillators, In: *Saint-Gobain Ceramics & Plastics, Inc.*, March 4, 2011, Available from: <<http://www.detectors.saint-gobain.com/Lithium-Glass-Scintillator.aspx>>
- Sarukura, N., Dubinskii, M.A., Liu, Z., Semashko, V.V., Naumov, A.K., Korableva, S.L., Yu Abdulsabirov, R., Edamatsu, K., Suzuki, Y., Itoh, T., & Segawa, Y. (1995). Ce³⁺-activated fluoride crystals as prospective active media for widely tunable ultraviolet ultrafast lasers with direct 10-ns pumping, *IEEE Journal of Selected Topics in Quantum Electronics*, Vol. 1, Issue 3, (September 1995), 792-804, ISSN: 1077-260X
- Sarukura, N., Liu, Z., Segawa, Y., Edamatsu, K., Suzuki, Y., Itoh, T., Semashko, V. V., Naumov, A. K., Korableva, S. L., Abdulsabirov, R. Yu., & Dubinskii, M. A. (1995), Ce³⁺:LuLiF₄ as a broadband ultraviolet amplification medium, *Optics Letters*, Vol. 20, No. 3 (February 1995), pp. 294-296, ISSN: 0146-9592
- Sarukura, N., Liu, Z., Izumida, S., Dubinskii, M.A., Abdulsabirov, R.Y., Korableva, A.K., & Stella, L. (1998) All-Solid-State Tunable Ultraviolet Subnanosecond Laser with Direct Pumping by the Fifth Harmonic of a Nd:YAG laser, *Applied Optics*, Vol. 37, Issue 27, (September 1998), pp. 6446-6448, ISSN: 1559-128X

- Shimizu, T., Yamamoi, K., Estacio, E., Nakazato, T., Sakai, K., Sarukura, N., Ehrentraut, D., Fukuda, T., Nagasono, M., Togashi, T., Higashiya, A., Yabashi, M., Ishikawa, T., Ohashi, H., & Kimura H. (2010), Response-time improved hydrothermal-method-grown ZnO scintillator for soft x-ray free-electron laser timing-observation, *Review of Scientific Instruments*, Vol. 81, Issue 3, (March 2010), pp. 033102-1- 033102-4, ISSN: 0034-6748
- Suzuki, Y., Kozeki, T., Ono, S., Murakami, H., Ohtake, H., Sarukura, N., Nakajyo, T., Sakai, F., & Aoki, Y. (2002). Hybrid time-resolved spectroscopic system for evaluating laser material using a table-top-sized, low-jitter, 3-MeV picosecond electron-beam source with a photocathode, *Applied Physics Letters*, Vol. 80, Issue.18, (May 2002), pp. 3280-3282, ISSN: 0003-6951
- Tanaka, K. A., Kodama, R., Kitagawa, Y., Kondo, K., Mima, K., Azechi, H., Chen, Z., Fujioka, S., Fujita, H., Johzaki, T., Lei, A., Matsuoka, T., Miyanaga, N., Nagai, K., Nagatomo, H., Nishimura, H., Norimatsu, T., Shigemori, K., Shiraga, H., Tanpo, M., Tohyama, Y., Yabuuchi, T. , Zheng, J., Izawa, Y., Norreys, P. A., Stephens, R., & Hatchett, S. (2004). Progress and perspectives of fast ignition, *Plasma Physics And Controlled Fusion*, Vol. 46, No. 12B, (December 2004), pp. B41-B49, ISSN: 0741-3335
- Van Eijk, C.W.E., Andriessen, J., Dorenbos, P., Visser, R. (1994). Ce³⁺ doped inorganic scintillators, *Nuclear Instruments and Methods in Physics Research Section A: Accelerators, Spectrometers, Detectors and Associated Equipment*, Vol. 348, Issues 2-3, (September 1994), pp. 546-550, ISSN: 0168-9002
- Yamanoi, K., Sakai, K., Nakazato, T., Estacio, E., Shimizu, T., Sarukura, N., Ehrentraut, D., Fukuda, T., Nagasono, M., Togashi, T., Matsubara, S., Tono, K., Yabashi, M., Kimura, H., Ohashi, H., Ishikawa, T. (2010), Response-time improved hydrothermal-method-grown ZnO scintillator for XFEL timing-observation, *Optical Materials*, Vol. 32, Issue 10, (August 2010), pp.1305-1308, ISSN: 0925-3467
- Yoshikawa, A., Kamada, K., Saito, F., Ogino, H., Itoh, M., Katagiri, T., Iri, D., & Fujita, M. (2008). Energy Transfer to Pr³⁺ Ions in Pr:Lu₃ Al₅O₁₂ (LuAG) Single Crystals, *IEEE Transactions on Nuclear Science*, Vol. 55, No. 3, (June 2008), pp.1372-1375, ISSN: 0018-9499
- Zen, H., Adachi, M., Hayashi, K., Katoh, M., Yamazaki, J., Tanikawa, T., Hosaka, M., Koike, M., Taira, Y., Uno, Y., & Yamamoto, N. (2009). Design Study of THz & VUV Coherent Source by Laser Seeding at UVSOR-II, *Proceedings of Free Electron Laser (FEL) Conference 2009, Liverpool, UK, August 2009*

Simulation of Ex-Vessel Steam Explosion

Matjaž Leskovar
Jožef Stefan Institute
Slovenia

1. Introduction

A steam explosion is a type of a fuel-coolant interaction (FCI), which results from the rapid and intense heat transfer that may follow the interaction between the molten material and the coolant (Berthoud, 2000; Corradini et al., 1988; Sehgal et al., 2008; Turland and Dobson, 1996). Such an interaction can occur when the melt is poured into the coolant, when the coolant is injected into the melt or when the melt and the coolant interact as stratified layers. As seen in Fig. 1, the steam explosion phenomenon is divided into the premixing and explosion phase. The explosion phase is further commonly divided into the triggering, propagation and expansion phases. The premixing phase covers the interaction of the melt with the coolant prior the steam explosion. At the interaction the coolant vaporizes around the melt-coolant interface, creating a vapour film (i.e. film boiling regime due to high melt temperature). The system may remain in the meta-stable state for a period ranging from a tenth of a second up to a few seconds. During this time the continuous melt (e.g. jet) is fragmented into melt droplets of the order of several mm in diameter, which may be further fragmented by the coarse break up process into melt droplets of the order of mm in diameter. If during the meta-stable state a local vapour film destabilization occurs, the steam explosion may be triggered due to the melt-coolant contact. A spontaneous destabilization could occur due to random processes or other reasons, e.g. when the melt contacts surrounding structures or if the water entrapped in the melt is rapidly vaporised. The destabilization can be induced artificially by applying an external trigger (e.g. chemical explosion, high pressure gas capsule). The destabilization causes the fine fragmentation of the melt droplets into fragments of the order of some 10 μm in diameter. The fine fragmentation process rapidly increases the melt surface area, vaporizing more coolant and increasing the local vapour pressure. This fast vapour formation due to the fine fragmentation spatially propagates throughout the melt-coolant mixture causing the whole region to become pressurized by the coolant vapour. If the concentration of the melt in the mixture is large enough and enough coolant is available, then the propagation velocity of the interaction front may rapidly escalate and the interaction may be sustained by energy released behind the interaction front. Subsequently, the high pressure region behind the interaction front expands and performs work on its surrounding. The time scale for the steam explosion phase itself is in the order of ms.

Major limitations of the steam explosion strength are due to:

- The limitation of the mass of the melt in the premixture. The mass of the melt in the premixture is limited due to the incomplete melt inflow and the incomplete melt fragmentation.

- The void production in the premixing phase. The presence of void hinders the steam explosion propagation and escalation due to the void compressibility and due to water depletion.
- The melt solidification during the premixing phase. The fine fragmentation during the explosion phase is limited due to the solidification of melt droplets.

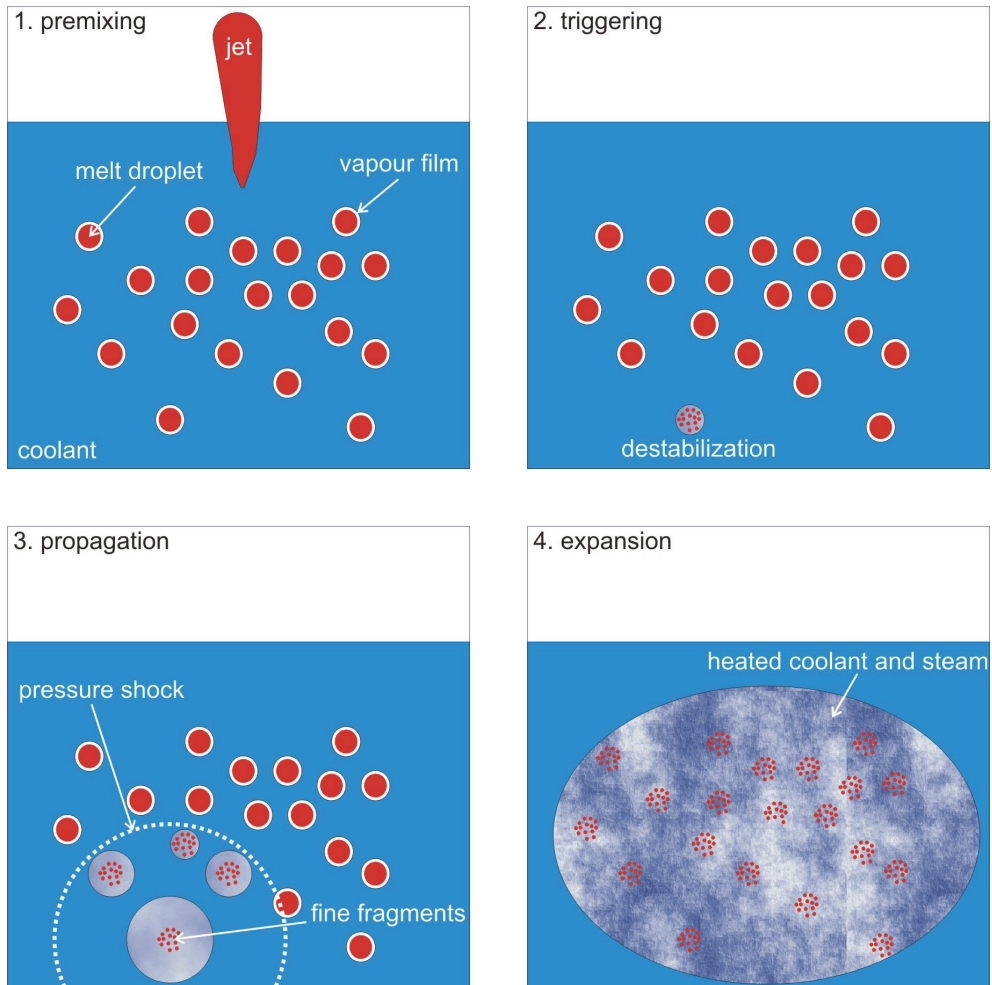


Fig. 1. Schematic illustration of the processes during the steam explosion phenomenon, starting with the melt pour into the coolant.

1.1 Steam explosion issue and nuclear safety

A steam explosion may occur during a hypothetical core melt accident in a light water reactor (LWR) nuclear power plant, when the molten corium interacts with the water (Corradini et al., 1988; Sehgal, 2006; Sehgal et al., 2008; Theofanous, 1995). Potentially severe

dynamic loadings on surrounding systems, structures and components could be induced by pressure peaks in the order of 100 MPa and duration in the order of ms. Steam explosions can therefore jeopardize the reactor vessel and the containment integrity (Esmaili and Khatib-Rahbar, 2005). Direct or by-passed loss of the containment integrity can lead to radioactive material release into the environment, threatening the safety of the general public. Consequently, the understanding of the steam explosion phenomenon is very important for nuclear safety.

As seen in Fig.2, several FCI situations in LWR were identified in which a steam explosion could occur (Sehgal et al., 2008). An in-vessel FCI could occur when the molten corium is poured into water in the lower head of the reactor pressure vessel (poured FCI) or when the relocated melt in the lower head is flooded (stratified FCI). In-vessel FCI may result in a steam explosion which causes the failure of the upper or lower head of the pressure vessel. When the molten corium melts through the vessel, the melt is poured into the cavity. An ex-vessel steam explosion can occur if the cavity is already filled with water (poured FCI) or if the cavity is flooded after the relocation of the melt in the cavity (stratified FCI).

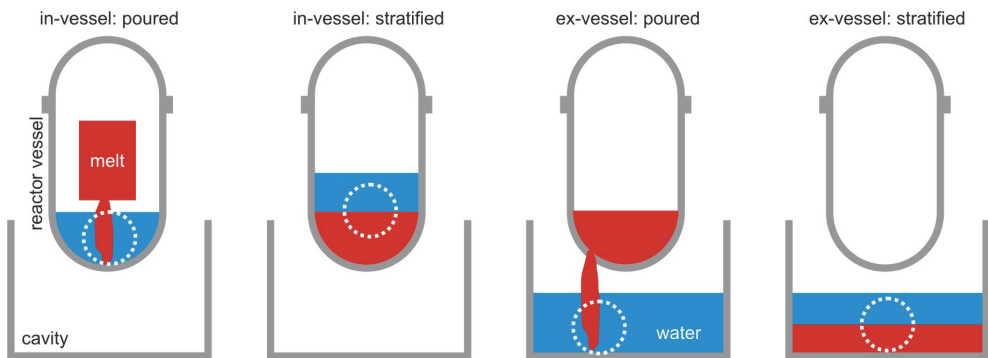


Fig. 2. Various FCI scenarios in LWR reactors.

In the past, the issue of in-vessel steam explosions causing the upper head failure of the reactor vessel was mainly concerned in LWR (WASH-1400, 1975). In this so called alpha mode containment failure it is considered that the ejected upper head could endanger the containment integrity. International reviews of the alpha mode failure probability and experimental investigations have indicated that the upper head and bolts can withstand the in-vessel steam explosion (Corradini et al., 1988; Krieg et al., 2003; Sehgal et al., 2008).

The importance of the poured in-vessel and ex-vessel steam explosions was recognized also by the OECD (Organisation for Economic Co-operation and Development), which started the SERENA (Steam Explosion Resolution for Nuclear Applications) Phase 1 research programme in the year 2002 (OECD/NEA, 2007). The objective of the SERENA programme was to evaluate the capabilities of FCI codes in predicting steam explosion induced loads, reaching consensus on the understanding of important FCI processes relevant to the reactor simulations, and to propose confirmatory research to bring the predictability of steam explosion energetics to required levels for risk management. Two main outcomes were obtained. First, the calculated loads are far below the capacity of a typical intact reactor vessel in case of an in-vessel steam explosion. However, for ex-vessel poured steam explosions the programme outcome was that the calculated loads are partly above the

capacity of typical reactor cavity walls. But due to the large scatter of the simulation results, which reflects the deficiency in the steam explosion phenomenon understanding and uncertainties on modelling and scaling, the safety margins for ex-vessel steam explosions could not be quantified reliably. To resolve the remaining open issues on the FCI processes and their effect on ex-vessel steam explosion energetics, the SERENA Phase 2 was launched at the end of the year 2007 (OECD/NEA, 2008). The main objective is to reduce the uncertainties on the coolant void and the material effect in FCI. The second phase comprises an experimental and an analytical program. The aim of the experimental program is to clarify the nature of prototypic material having mild steam explosion characteristics and to provide innovative experimental data for code validation, aiming to reduce the scatter of code predictions and to enhance the geometrical extrapolation capabilities of FCI codes to cover reactor situations. The aim of the comprehensive analytical program is to increase the capability of FCI models and codes for use in reactor analyses.

Due to the high risk significance of the steam explosion phenomenon for the containment integrity, the ex-vessel FCI issue is one of the six high priority safety issues, which were identified in the EU (European Union) network of excellence SARNET (Severe Accident Research NETwork of Excellence) Phase 1 (Albiol et al., 2008; Schwinges et al., 2010). The purpose of the SARNET network of excellence, which was founded in the year 2004, is to integrate European research capabilities on severe accidents in order to enhance the safety for the existing and future nuclear power plants. In the beginning of the year 2009 the follow-up SARNET Phase 2 was started. The purpose of the second phase is to focus on those safety issues, which were classified with high priority in the first phase. Beside the issue of ex-vessel FCI also the issues of the corium and debris coolability, the molten corium-concrete interaction, the hydrogen mixing and combustion in the containment and the source term are investigated.

The issue of stratified steam explosions is not considered being as important as steam explosions occurring after the pouring of the melt into water. Namely, the mass of the melt which can participate in the mixing process is limited in stratified cases if compared with the premixture melt mass in pouring cases (Sehgal et al., 2008).

The final goal of the FCI research related to nuclear safety is to bring the predictability of the steam explosion strength to required levels for the risk assessment in LWR. This is necessary for the risk management to be able to implement the optimal severe accident management approaches (e.g. flooding of reactor cavity, in-vessel retention, core catcher).

This chapter focuses on the simulation of poured ex-vessel steam explosions, which are of greatest interest. With the FCI code MC3D (Meignen and Picchi, 2005) different scenarios of ex-vessel steam explosions in a typical pressurized water reactor cavity were analyzed to get additional insight in the ex-vessel steam explosion behaviour and the resulting pressure loads. A parametric study was performed varying the location of the melt release (central, right and left side melt pour), the cavity water subcooling, the primary system overpressure at vessel failure and the triggering time for explosion calculations. The main purpose of the study was to establish the influence of the varied parameters on the FCI behaviour, to determine the most challenging cases and to estimate the expected pressure loadings on the cavity walls. For the most challenging central, right side and left side melt pour scenarios, according to the performed simulations, a detailed analysis of the explosion simulation results was performed. In addition, the influence of the jet breakup modelling and the melt droplets solidification on the FCI process was analyzed.

First, the applied FCI modelling approach is described and the analyzed ex-vessel FCI scenarios are given. Then the various premixing and explosion phase simulation results are presented and the most challenging cases established. For the most challenging cases a more detailed analysis is provided. Finally, for the most challenging central melt pour case the influence of the jet breakup modelling and the melt droplets solidification on the simulation results is analyzed and discussed.

2. Modelling

The simulations were performed with the MC3D computer code, which is being developed by IRSN, France (Meignen and Picchi, 2005). MC3D is a multidimensional Eulerian code devoted to study multiphase and multi-constituent flows in the field of nuclear safety. It has been built with the FCI calculations in mind. It is, however, able to calculate very different situations and has a rather wide field of potential applications. MC3D is a set of two FCI codes with a common numeric solver, one for the premixing phase and one for the explosion phase (i.e. triggering phase, propagation phase and initial stage of expansion phase). In general, the steam explosion simulation with MC3D is being carried out in two steps. In the first step, the distributions of the melt, water and vapour phases at steam explosion triggering are calculated with the premixing module. And in the succeeding second step, the escalation and propagation of the steam explosion through the premixture are calculated with the explosion module, using the premixing simulation results as initial conditions and applying a trigger.

The MC3D premixing module focuses on the modelling of the molten fuel jet, its fragmentation into large drops, the coarse fragmentation of these drops and the heat transfer between the melt and the coolant (Meignen, 2005). The fuel is described by two fields, the "continuous" fuel field (e.g. fuel jet or molten pool) and the "droplets" fuel field (melt droplets), considering the possible continuous or dispersed state of the fuel. The fuel is transferred between both fields during jet breakup and coalescence. In MC3D two jet breakup models are provided, a global model and a local model. In the global model the jet fragmentation rate is deduced from the comparison to a standard case (i.e. typical conditions in FARO experiments (Magallon and Huhtiniemi, 2001)) and the size of the created droplets is a user parameter. In the local model the jet fragmentation rate and the size of the created droplets are calculated based on local velocities applying the Kelvin Helmholtz instability model. Since the local model is very sensitive and in the process of being improved, the reference calculations were performed using the global jet breakup model. The diameter of the created droplets was set to 4 mm, what is the typical size of the melt droplets in the FARO experiments (Magallon and Huhtiniemi, 2001).

The explosion module focuses on the fine fragmentation of the melt droplets, generated during premixing, and the heat exchange between the produced fragments and the coolant (Meignen, 2005). In this module the "continuous" fuel field is not present, but there are two fields related to the dispersed fuel, i.e. the "droplets" fuel field and the "fragments" fuel field. During the fine fragmentation process the fuel is transferred from the "droplets" field to the "fragments" field. Both fine fragmentation processes, i.e. thermal fragmentation, resulting from the destabilization of the vapour film around the melt droplets, and hydrodynamic fragmentation, resulting from the velocity differences between the melt droplets and the surrounding medium, are considered. The diameter of the created fragments, which is a user parameter, was set to the code standard value 100 μm , which is

based on KROTOS experiments (Huhtiniemi et al., 1999). The explosion is triggered by applying a user defined initial local pressure pulse. The trigger pressure was set to 2 MPa and prescribed to a single mesh cell, as explained in Section 3.1. Simulations showed that the triggering strength has no significant influence on the explosion strength, once the trigger is strong enough that it can trigger the explosion.

In MC3D it is conservatively assumed that the melt droplets are completely molten if their bulk temperature is higher than the corium solidus temperature. This overpredicts the ability of corium droplets to efficiently participate in the explosion, since in reality, during premixing, a crust is formed on the corium droplets before the droplet bulk temperature drops below the solidus temperature (Huhtiniemi et al., 1999; Dinh, 2007). This crust inhibits the fine fragmentation process and if the crust is thick enough it completely prevents it.

To be able to perform a series of simulations of different ex-vessel steam explosion scenarios, the reactor cavity was modelled in a simplified 2D geometry, as is common practise (Meignen et al., 2003; Kawabata, 2004; Esmaili and Khatib-Rahbar, 2005; Moriyama et al., 2006; OECD/NEA, 2007). The 2D geometry has to be appropriately defined to assure that the 2D simulation results reflect qualitatively and quantitatively as closely as possible the conditions in a real 3D reactor cavity. Therefore, the simulations were performed with two different 2D representations of a typical pressurized water reactor cavity: the 2D axial symmetric model (Fig. 3) and the 2D slice model (Fig. 4). The 2D axial symmetric model is limited on the treatment of axial symmetric phenomena in the cylindrical part of the reactor cavity directly below the reactor pressure vessel and around it. Consequently, the venting through the instrument tunnel cannot be directly considered, and therefore conservatively was not considered. Contrary to the axial symmetric model, which treats only part of the

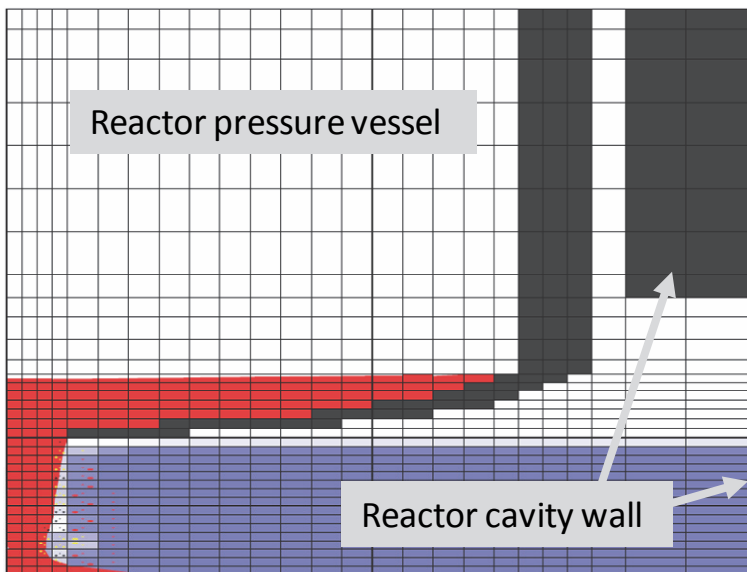


Fig. 3. Geometry and mesh of 2D axial symmetric model of reactor cavity for central melt pour. The scales in horizontal and vertical directions are different.

reactor cavity, the 2D slice model treats the whole reactor cavity. However it does not take into account the 3D geometry and the 3D nature of the phenomena. So the cylindrical part of the reactor cavity and the cylindrical reactor pressure vessel are not treated as cylinders but as planparallel infinite plates. A similar approach was applied by Esmaili and Khatib-Rahbar (2005). In the 2D slice model the height of the cavity opening on the left side (Fig. 4) was adjusted to match the opening area per reactor cavity width of the real 3D reactor cavity geometry.

The cavity geometry and dimensions were set in accordance with a typical pressurized water reactor cavity. In the models the dimensions of the cavity are: length $x \approx 10.5$ m, radius of cylindrical part $r \approx 2.5$ m, height $z \approx 13$ m, and the mesh sizes are: 2D axial symmetric model— 25×35 cells (Fig. 3), 2D slice model: right side melt pour— 62×39 cells and left side melt pour— 77×39 cells (Fig. 4). In regions, which are more important for the modelling of the FCI phenomena, the numerical mesh was adequately refined; therefore the meshes for the right and left side melt pour are not identical (Fig. 4). The initial pressure in the domain was set to the containment pressure and a constant pressure boundary condition at the cavity openings was applied.

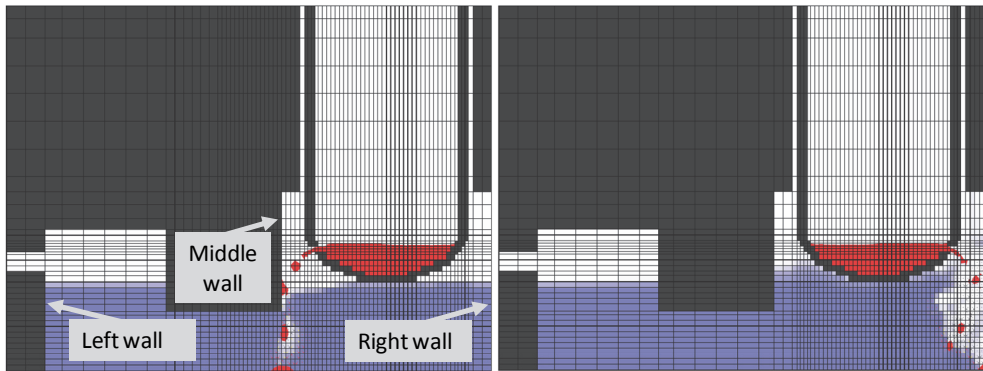


Fig. 4. Geometry and mesh of 2D slice model of reactor cavity for left and right side melt pour. The scales in horizontal and vertical directions are different.

3. Simulation

3.1 Simulated cases

In the performed ex-vessel steam explosion study, a spectrum of relevant scenarios has been analyzed to establish the influence and importance of different accident conditions on the FCI outcome and to eventually capture the most severe steam explosions. The simulations have been performed in two steps. In the first step, the premixing phase of the FCI process has been simulated for selected scenarios and then, in the succeeding second step, the explosion phase simulations have been performed by triggering the so established premixtures at different times.

As revealed in the MASCA experiments, the melt pool in the lower head may gradually stratify in three layers of different melt composition, i.e. a molten oxidic pool with a light metal layer on top and a heavy metal layer below (Seiler et al., 2007). Therefore the composition of the poured melt is expected to depend on the location of the reactor vessel

failure. The melt composition has an important influence on the triggerability and the energetics of the steam explosion (Huhtiniemi et al., 1999; Corradini, 1991). This material effect is still not understood in detail, and the uncertainties in its modelling and scaling are large. Therefore a conservative approach was applied, comprising artificial triggering and neglecting the inhibiting effects of the melt droplets crust formation on the fine fragmentation process, as explained in Section 2. Beside the melt composition, also the melt temperature is expected to depend on the vessel failure location. The temperature of the molten oxidic pool is estimated to be around 3000 K (OECD/NEA, 2007), whereas the temperature of the metal layer on top is estimated to be around 2100 K (Esmaili and Khatib-Rahbar, 2005). The melt temperature defines the thermal energy, which is potentially available to be partially transferred to mechanical work during the steam explosion. Due to modelling uncertainties and uncertainties in the composition and temperature of the poured melt it was however decided to perform all simulations with the same melt composition, i.e. the standard MC3D oxidic corium (Table 1), and the same initial melt temperature of 3000 K. By this the influence of the varied parameters may be established more directly. The premixing phase simulations have been performed for the cases presented in Table 2. The initial conditions were set reasonably according to expected conditions at vessel failure during a severe accident in a typical pressurized water reactor. They are comparable to the conditions used in the ex-vessel reactor simulations in the OECD programme SERENA phase 1, where a central melt pour was analyzed (OECD/NEA, 2007). Central and side melt pours were considered and a parametric analysis was performed varying the primary system overpressure (0 MPa, 0.2 MPa) and the water temperature (60–100 °C). The water saturation temperature at the assumed 0.15 MPa containment pressure is 111.4 °C, so the cavity water subcooling was in the range of 11.4–51.4 K. The simulated cases were denoted with three designators defined in Table 2 (e.g. case C2-60 is a central melt pour at 0.2 MPa primary system overpressure into cavity water with a temperature 60 °C).

Property	Value
Liquidus temperature	2800 K
Solidus temperature	2700 K
Latent heat	3.608×10^5 J/kg
Specific heat – liquid	520 J/kg/K
Specific heat – solid	380 J/kg/K
Density	8000 kg/m ³
Thermal conductivity	2.88 W/m/K
Dynamic viscosity	0.008 Pa/s

Table 1. Physical properties of applied standard MC3D oxidic corium.

The premixing phase was simulated 10 s after the start of the melt release. For each premixing simulation, a number of explosion simulations were performed triggering the explosion at different times. The explosion triggering times (Table 3) were selected so that the most important stages of the case specific melt releases were captured. In the central

melt pour cases with 0.2 MPa primary system overpressure (C2), when most melt was released from the reactor vessel, gas started to flow out of the vessel opening and dispersing the melt jet. To capture this phenomenon the explosion was triggered also at that time. The side melt pour cases with a depressurized primary system (R0, L0) were not triggered before 1.5 s, since about 1 s was needed for the melt to reach the water surface.

Parameter	Value	Designator
Melt composition	Standard MC3D oxidic corium (properties presented in Table 1)	/
Melt temperature	3000 K	/
Melt level	1.25 m	/
Melt mass	50 t	/
Free fall	0.44 m	/
Water level	3 m	/
Cavity radius	2.5 m	/
Annulus thickness	0.11 m	/
Containment pressure	0.15 MPa	/
Melt pour location	Central (Fig. 3) Right (Fig. 4) Left (Fig. 4)	C R L
Reactor vessel opening size	Central pour: radius 0.2 m Side pour: height 0.2 m	/
Primary system overpressure	0 MPa 0.2 MPa	0 2
Water temperature	100 °C (11.4 K subcooling) 80 °C (31.4 K subcooling) 60 °C (51.4 K subcooling)	100 80 60
Melt volume flow rate for central pour (estimated)	0.62 m ³ /s (0 bar overpressure) 1.08 m ³ /s (2 bar overpressure)	/
Melt velocity at water contact for central pour (estimated)	5.75 m/s (0 bar overpressure) 9.12 m/s (2 bar overpressure)	/

Table 2. Initial conditions for simulated premixing cases (also some estimations of the melt volume flow rate and the melt velocity at water contact are provided).

In addition to the triggering times listed in Table 3, for each simulated premixing case the explosions were triggered also at additional times when the calculated explosivity criteria were the highest. The explosivity criteria were based on the volume of liquid melt drops in contact with water as

$$\begin{aligned} \text{criterion 1: } V_1 &= \sum_{\text{cells}} \alpha_d \frac{\alpha_l}{\alpha_d + \alpha_l} C_m V_c, \\ \text{criterion 2: } V_2 &= \sum_{\text{cells with } \alpha_{lr} > 0.3} \alpha_d V_c, \\ C_m &= \min\left(1, \max\left(0, \frac{\alpha_{lr} - 0.3}{0.4}\right)\right), \quad \alpha_{lr} = \frac{\alpha_l}{\alpha_l + \alpha_g}, \end{aligned} \quad (1)$$

where the symbols α_l , α_g , α_d denote the liquid water, void and liquid melt droplets volume fractions, and V_c is the mesh cell volume. The explosivity criteria actually represent the volume of liquid melt drops in cells where the water content is high enough that the melt may efficiently participate in the steam explosion, and so are a good measure for the expected strength of the steam explosion. In this way it was tried to capture the strongest steam explosions. For the most explosive central melt pour case, e.g. case C2-60 (presented in the next section), a series of explosion simulations were performed triggering the explosion every 0.2 s during the whole simulated premixing duration in order to get a better insight in the influence of the triggering time on the steam explosion outcome. The explosion phase was simulated 0.1 s after triggering, capturing the significant loading events. The explosion was triggered in the cell, where the local cell explosivity criterion 2 (Eq. 1) was the highest (Meignen and Picchi, 2005).

Cases	Triggering times (s)							
C0	0.5	1	/	2	/	5	/	10
C2	0.5	1	/	2	/	5	6.5	10
R0, L0	/	/	1.5	2	3	5	/	10
R2, L2	0.5	1	/	2	3	5	/	10

Table 3. Triggering times for explosion phase simulations.

3.2 Simulation results

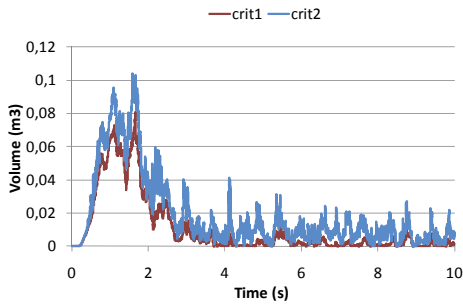
The premixing and explosion simulations were performed with the code MC3D version 3.5 with patch 1 on a network of PC computers with Windows operating system, having altogether about 30 processors, using the Condor distributed computing system. So a number of simulations could be performed simultaneously, each simulation running on its own processor. To establish the best model parameters enabling stable calculations, first a number of test simulations were performed. In Table 4 some computing information regarding stability and CPU times of simulations is provided. The water subcooling had the largest influence on the stability of the simulations. At a water

temperature of 50 °C (subcooling ~60 K), the premixing simulations diverged already shortly after melt-water contact. The stability of premixing simulations could be significantly increased by increasing the minimum bubble diameter from the default 0.5 mm to higher values, whereas this did not work for explosion simulations. So, if the premixing simulations did not converge, the minimum bubble diameter was increased gradually (to 1 mm, 2 mm) up to 5 mm, where most of the problematic simulations remained stable over the whole simulation time. By increasing the minimum bubble diameter, the surface area for condensation in subcooled conditions is reduced and so the heat transfer terms are less stiff, which has a benevolent influence on the numerical stability. Since the minimum bubble diameter influences the physics of the bubbly flow regime and the subsequent explosion phase, it was strived to perform the simulations with an as small as possible reasonable minimum bubble diameter.

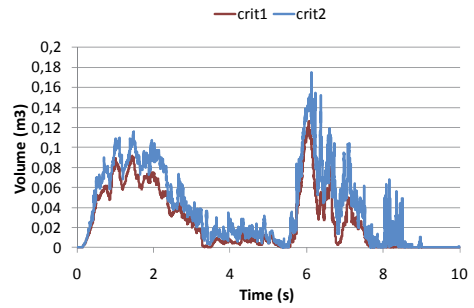
In Fig. 5, the calculated explosivity criteria (Eq. 1) during premixing are presented for some representative simulated cases. In general, the explosivity criteria are highest in the beginning of the simulation, when the melt jet enters the water and the void build up is still low (Figs. 3 and 4). The later evolution of the explosivity criteria however is case specific. In the depressurized central cases (C0, Fig. 5a) and the pressurized side cases (R2 and L2, Figs. 5d and 5f) the explosivity criteria remain low until the end of the simulation due to the void buildup. In the pressurized side cases the explosivity criteria at later stages are additionally reduced since after about 3 s the melt level in the reactor vessel is reduced to the lower boundary of the vessel opening and so only small amounts of melt are ejected from the vessel after that time. In the pressurized central cases (C2, Fig. 5b), after about 5 s when most of the melt is already released from the vessel, gas starts to flow with high velocity out of the reactor vessel and dispersing the melt jet. Due to the increased melt dispersal, more melt droplets are created, what results in an increase of the explosivity criteria (Fig. 5b). In the depressurized side cases (R0 and L0, Fig. 5c and 5e), more explosivity criteria peaks occur during the melt release since, due to the pressure buildup in the reactor cavity, the melt outflow from the reactor vessel is interrupted and so the melt release occurs in intervals. Each melt release interval produces one explosivity criteria peak.

Parameter	Stability (more stable to less stable)	CPU time (shorter time to longer time)
Melt pour location	Central > Right > Left	Central < Right < Left Premixing: C: ~day, L: ~week Explosion: C: ~hour, L: ~day
Primary system overpressure	0 bar > 2 bar	/
Water temperature	100 °C > 80 °C > 60 °C	/

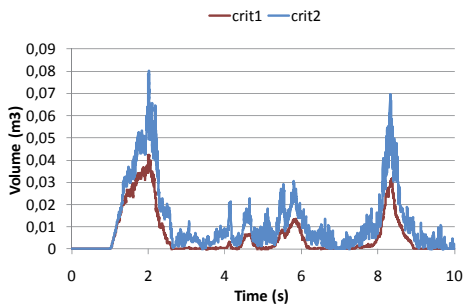
Table 4. Stability and CPU times of performed simulations.



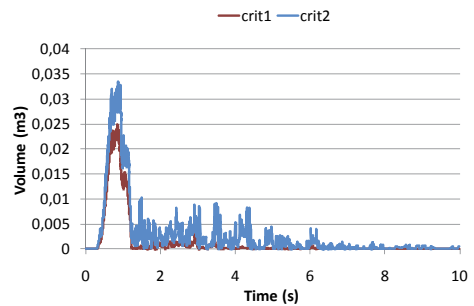
a) C0-60



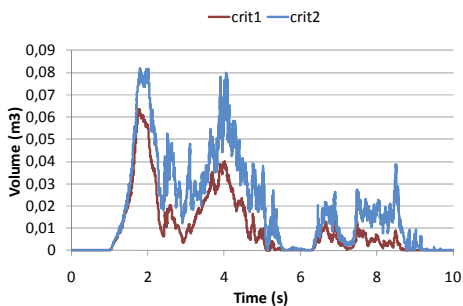
b) C2-60 (most explosive central case)



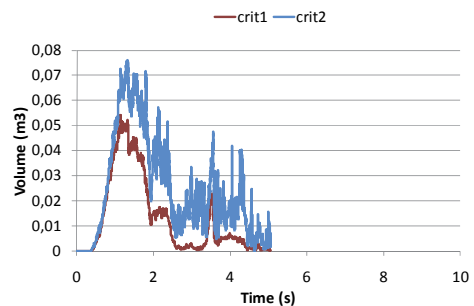
c) R0-80 (most explosive right side case)



d) R2-80



e) L0-60 (most explosive left side case)



f) L2-60 (diverged after 5.06 s)

Fig. 5. Explosivity criteria during premixing for representative central (top), right (middle) and left (bottom) pour cases at a depressurized (left) and pressurized (right) primary system.

In Fig. 6, the calculated maximum pressures in the cavity and maximum pressure impulses (integral of pressure over simulation time) at the cavity walls (cavity floor and vertical walls) are presented for the performed explosion phase simulations. The time axis denotes the explosion triggering times. In the calculation of the pressure impulses, the initial containment pressure was subtracted from the calculated absolute pressure since the dynamic pressure loads on the cavity walls are caused by the pressure difference. For some cases (e.g. case C0-60) more points are plotted at the same triggering time. This means that, in these cases, more premixing simulations were performed for the same conditions, using different minimum bubble diameters in the calculations, mostly due to convergence problems during premixing or later during the explosion simulation, and so on the figures the available explosion simulation results based on different premixing simulations are presented. By this an impression of the uncertainty of the calculation results may be obtained. The variation of the results for different minimum bubble diameters is quite large, e.g. in case C0-60 the variation of the maximum pressure and pressure impulse (Fig. 6a-b) for the triggering times around 1 s is up to a factor of two. It turns out that the influence of the minimum bubble diameter on the pressure loads is stochastic, what reveals the complexity of the FCI process. Some explosion simulations did not converge, and the results for these cases are consequently not presented in the graphs.

The strength of the steam explosion depends on the mass of melt droplets, which can efficiently participate in the steam explosion – that is the mass of liquid melt droplets in regions with high water content. In Fig. 7 the mass of liquid melt droplets in regions with different void fractions is presented for the most explosive cases during premixing. In the side melt pour cases, represented by 2D slice models (Fig. 4), in the mass calculation a slice of 1 m thickness was considered, what corresponds to a side melt pour through a fish mouth opening with a length of about 1 m. During the premixing phase some tons of melt droplets are formed in the considered scenarios (curve "Total"). A significant amount of these melt droplets are frozen (compare curves "Total" and "<100%") and so can not participate in the steam explosion since they are not able to undergo fine fragmentation. In addition, most of the liquid corium droplets are in regions with a high void content (compare curves "<100%" and "<60%"), whereas for the steam explosion development enough water has to be available for vaporization and for enabling the fine fragmentation process. It is estimated that the void fraction has to be at least below about 60% for a steam explosion escalation to develop. Despite these limiting factors, there are still (depending on scenario and triggering time) up to some hundreds of kilograms of liquid corium droplets available to participate in the energetic FCI process, resulting in severe pressure loads (Fig. 6).

The pressure curves and pressure impulse curves (Fig. 6) are reasonably correlated to the corresponding explosivity criteria curves (Fig. 5) and mass of liquid melt droplets curves (Fig. 7), as was expected. The results for the central melt pour cases show that, in the initial stage of the melt pour, stronger explosions mainly occur for higher cavity water subcooling and higher melt pour driving pressure. The reason for this could be that higher water subcooling results in less void build up and that higher driving pressure increases the melt fragmentation. On the contrary, at the later stage of the simulations, stronger explosions mainly occur for lower water subcooling, probably due to less droplet solidification with lower water subcooling. But the influence of the water subcooling on the explosion strength is not very clear, indicating that in the considered subcooling range the effects of void build up and melt droplets solidification nearly compensate. The results of the side melt pour cases reveal that stronger explosions may be expected with a

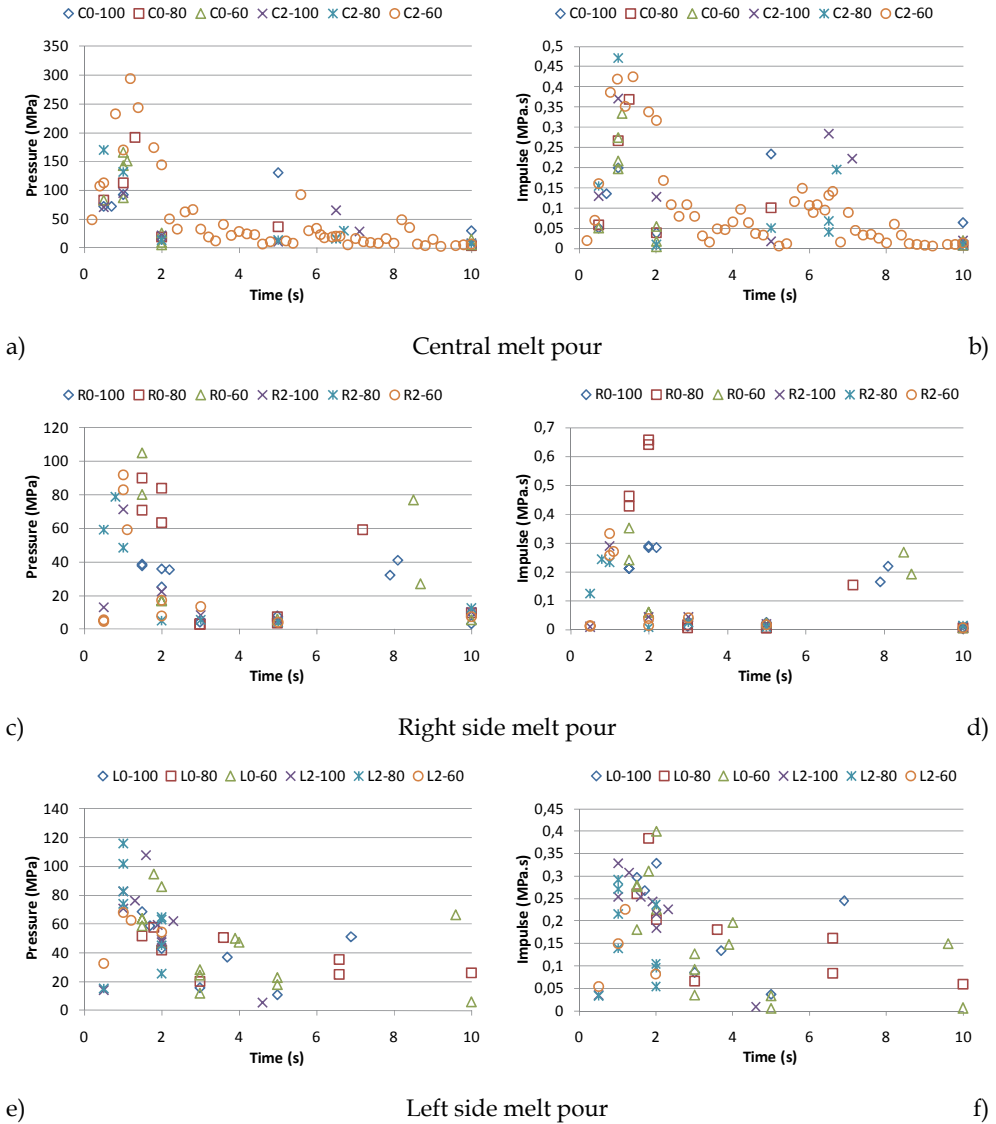


Fig. 6. Calculated maximum pressures in the cavity (left) and maximum pressure impulses at the cavity walls (right) for performed explosion phase simulations. The time axis denotes the explosion triggering times.

depressurized primary system. The reason for this could be that with a pressurized primary system the melt is ejected sideways on the cavity wall, sliding then into water at the wall, which hinders the formation of an extensive premixture. Moreover, with a pressurized system, already a tenth of a second after the start of the melt release gas starts to flow through the vessel opening into the cavity and pushes the water through the instrument tunnel out of the cavity, creating a highly voided region below the reactor vessel. For the side melt pour cases the influence of the water subcooling on the steam explosion strength seems to be somewhat stochastic, probably due to compensation effects of void buildup and melt droplets solidification in combination with the complex melt release dynamics.

In general, the highest pressures and pressure impulses were reached in the initial stage of the melt release (Fig. 6, Table 5). The highest pressure was obtained in case C2-60 (nearly 300 MPa) and the highest pressure impulse in case R0-80 (nearly 0.7 MPa-s). The maximum pressure and the maximum pressure impulse present only a rough measure of the steam explosion strength. To reveal the real damage potential of a steam explosion, the space and time development of the pressure field has to be analysed. Therefore for the most explosive central and side melt pour cases a detailed analysis was performed. As the criteria for establishing the most explosive cases, the maximum pressure impulse was taken (Table 5). For the central melt pour case the highest maximum pressure impulse was predicted for case C2-80, but since in case C2-60 the maximum pressure impulse is only slightly lower and remains high over a wide triggering time window (Fig. 6b), the latter was chosen for the detailed analysis.

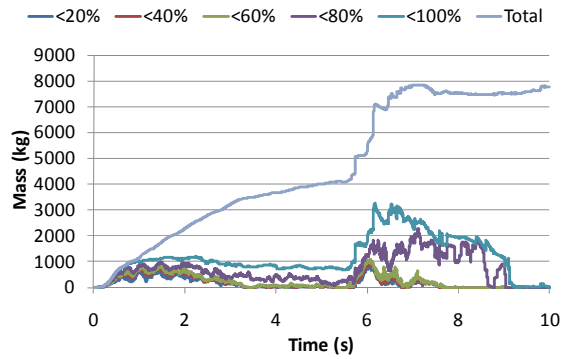
Pour location	Maximum pressure		Maximum impulse	
	p (MPa)	Case	I (MPa-s)	Case
C	293.7	C2-60	0.47	C2-80
R	105.1	R0-60	0.66	R0-80
L	116.1	L2-80	0.40	L0-60

Table 5. Maximum pressures in the cavity and maximum pressure impulses at the cavity walls (cavity floor included) for different melt pour locations.

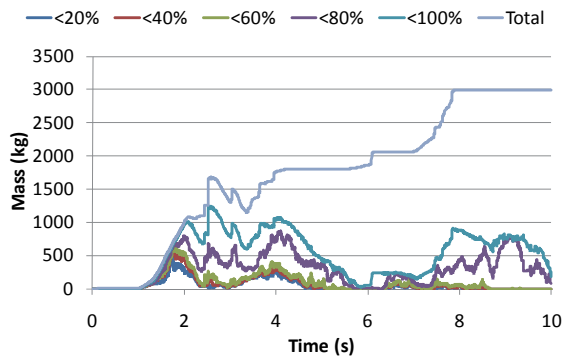
3.3 Detailed analysis

The detailed analysis of the explosion simulation results was performed for the most explosive central (C2-60), right side (R0-80) and left side (L0-60) melt pour cases. For each melt pour case the pressure field, the corium fraction and the liquid water fraction during the explosion were investigated in detail and the pressure development with corresponding pressure impulses at different wall locations was analyzed. Here only the main results are briefly presented.

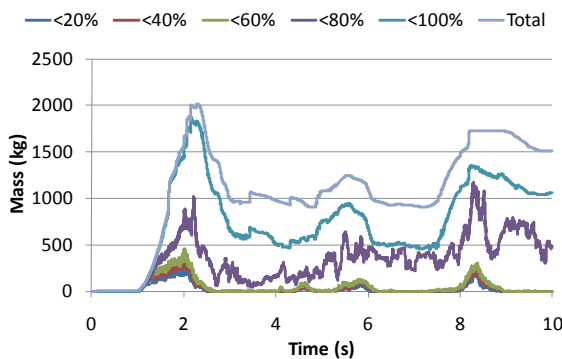
In the central melt pour case C2-60, soon after the triggering of the explosion a high pressure peak occurs in the centre of the cavity floor. This high pressure peak of short duration is created due to geometrical reasons, since the pressure field build up in the outer premixture region is focused in the central part of the cavity due to the applied 2D cylindrical geometry. Consequently this high pressure peak can not be considered as realistic for a 3D explosion.



a) Central melt pour: most explosive case C2-60



b) Left side pour: most explosive case L0-60



c) Right side pour: most explosive case R0-80

Fig. 7. Mass of liquid corium droplets in regions with different void fractions during premixing. The results are presented for regions with a void fraction below 20% (<20%) up to regions with a void fraction below 100% (<100%). In addition also the total (liquid and solid) corium droplets mass is presented (Total).

The highest calculated pressure on the vertical wall is much lower, only up to about 35 MPa. The maximum pressure impulse on the vertical wall (0.22 MPa·s) is about half of that calculated in the centre of the cavity floor (0.41 MPa·s). In the right side melt pour case R0-80 the highest pressure is reached at the bottom of the right wall (up to 46 MPa; see Fig. 4 for wall position), but it decreases quickly with height, so that at higher elevations the maximum pressure remains below 20 MPa. The whole cavity remains pressurized at around 5 MPa at the end of the explosion simulation, and there is no indication of a pressure decrease. Therefore, the pressure impulses at the walls are very high (0.66 MPa·s on the right wall) and rise at the end of the simulation. In the left side melt pour case L0-60 the highest pressure, nearly 90 MPa, is achieved on the cavity floor below the middle wall, where the premixture conditions are most favourable for the steam explosion escalation. The peak pressures on the cavity walls are much lower, only about 23 MPa. Similar to the right side melt pour case, the cavity remains pressurized at nearly 5 MPa at the end of the explosion simulation, and there is no indication of a pressure decrease. However the highest calculated pressure impulses on the walls are lower (0.34 MPa·s on the right wall; see Fig. 4 for wall position) due to the distance between the premixture, formed in the middle of the cavity, and the cavity walls.

In Table 6 the maximum calculated pressures and pressure impulses at the vertical cavity walls are given for the most explosive central (C2-60), right side (R0-80) and left side (L0-60) melt pour scenarios. As expected, the maximum calculated vertical wall pressures are significantly lower than the maximum calculated pressures in the cavity (Table 5) since the pressure is reduced during the propagation from the explosion region to the cavity walls. The maximum pressure impulses are predicted on the cavity walls, which are closest to the explosion. For the central and left side pours this is the cavity floor, and for the right side pour this is the right wall. Therefore for the central and left side pours the maximum pressure impulses in Table 6 are lower than those in Table 5, where also the cavity floor was considered. This reduction is more expressive for the central pour than for the left side pour since due to the cylindrical geometry of the central pour the pressure wave weakens faster and venting is more efficient.

The pressure impulses were calculated as the integral of the excess pressure (initial containment pressure subtracted) over the entire explosion simulation time. The planned explosion simulation time was 0.1 s, but due to stability problems some simulations stopped earlier, and in these cases consequently a shorter integration period had to be applied. The explosion simulation of the most explosive central pour case (C2-60, triggered at 1.4 s) was stable, but the most explosive right (R0-80, triggered at 2 s) and left (L0-60, triggered at 2 s) side pour calculations became unstable at about 0.08 s and 0.06 s, respectively, and so the corresponding pressure impulses consider this shorter periods.

The pressure impulse is a good measure to estimate the destructive consequences of a steam explosion if it considers the period with significant loading events. The lasting pressure load capacity of a typical pressurized water reactor cavity is estimated to be of the order of some MPa (based on Meignen (2004) and Hessheimer (2006) it was roughly estimated that lasting pressures of about 3 MPa could cause some damage to the cavity). The cavity may withstand also higher pressures if their duration is short enough. In this case the experienced pressure impulse is the decisive factor (Smith, 1994). It is estimated that a pressure impulse of the order of some tens of kPa·s may induce some damage to the cavity (OECD/NEA, 2007). However it should be stressed that for an accurate assessment of the damage caused by a steam explosion the real pressure history has to be taken into account.

For the mutual comparison of calculation results it is mainly important that for the calculation of the pressure impulse the same integration period is used. But for the assessment of the damage potential, the pressure impulse is only meaningful if it is calculated over the period, when the pressure exceeds the lasting pressure load capacity of the cavity. Therefore in Table 6 also the estimated maximum pressure impulses considering only the period of significant loading, when the pressure exceeds about 5 MPa (set arbitrarily) are given. By setting the cut-off pressure to ~5 MPa and reasonably applying it, the long lasting cavity pressurization in the side pour cases was not taken into account in the pressure impulse calculation. It may be observed that also the so determined pressure impulses are high. In the central pour case the maximum “significant loading” pressure impulse builds up in the bottom region of the cylindrical wall, when the pressure shock reaches the wall soon after explosion triggering. In the right side pour case the maximum “significant loading” pressure impulse builds up at the right wall in the region below the annulus, when the phases mixture is violently pushed through it, and in the left side pour it builds up at the right wall, when the water is pushed in the region between the reactor vessel and the cavity wall.

Pour location	Maximum pressure	Maximum impulse (MPa·s)	
	p (MPa)	Entire simulation	Significant loading
C	36.3	0.22 (0.1 s)	~0.16
R	45.7	0.66 (~0.08 s)	~0.56
L	23.0	0.34 (~0.06 s)	~0.19

Table 6. Maximum pressures and pressure impulses at the vertical cavity walls for different melt pour locations and different pressure integration periods.

4. Sensitivity study

For the most explosive central melt pour case C2-60 the influence of the jet breakup modelling and the melt droplets solidification on the FCI process was analyzed to get an impression about the uncertainty of the simulation results.

4.1 Influence of jet breakup modelling

In MC3D two jet breakup models are provided (Meignen and Picchi, 2005). The first model is a global model, which is based on the hypothesis that the fragmentation can be obtained through a correlation considering only the local physical properties of the fuel, liquid and vapour, whereas the local velocities have not to be calculated. The second model is a fully local model, which is based on the Kelvin-Helmholtz instability model considering also the local velocities.

The global model is, strictly speaking, applicable only for single large very hot jets in a water pool, so that the fragmentation is due to the friction of the vapour film, whose characteristics are governed mainly by buoyant forces. The model was validated on FARO steam explosion tests (Magallon and Huhtiniemi, 2001), so extrapolations to situations far from those of FARO are questionable. In the model, the volumetric jet fragmentation rate to droplets is deduced from the comparison to a standard case as

$$\Gamma_f = \Gamma_0 \left(\frac{T_0}{T_j} \right)^{0.75} \sqrt{\frac{\mu_g}{\mu_{g,0}} \bigg|_{p=1bar} \frac{\sigma_0}{\sigma_j} \left(\frac{\rho_0}{\rho_j} \right)^{0.5}}, \quad (2)$$

where for the standard case typical FARO conditions are chosen: reference fragmentation rate $\Gamma_0 = 0.1 \text{ m}^3/\text{m}^2/\text{s}$, jet temperature $T_0 = 3000 \text{ K}$, vapor viscosity $\mu_{g,0} = 10^{-3} \text{ kg/m/s}$, jet density $\rho_0 = 8000 \text{ kg/m}^3$ and jet surface tension $\sigma_0 = 0.5 \text{ N}\cdot\text{m}$. The diameter of the created drops is a user input parameter, with the default value of $d_d = 4 \text{ mm}$.

The local model is based on the Kelvin-Helmholtz instability model, which was modified to take into account the multiphase aspect. In the model the volumetric jet fragmentation rate is calculated with

$$\Gamma_f = N_f \frac{\sqrt{\rho_j \rho_{amb} (v_j - v_{amb})^2 - \sigma_j k_{\max} (\rho_j + \rho_{amb})}}{\rho_j + \rho_{amb}}, \quad (3)$$

$$k_{\max} = \frac{2}{3} \frac{\rho_j \rho_{amb}}{\rho_j + \rho_{amb}} \frac{(v_j - v_{amb})^2}{\sigma_j},$$

where subscript j stands for the jet and subscript amb for the ambient fluid, which properties are calculated by different ways of averaging. N_f is the jet fragmentation parameter with an expected value between 1 and 6. Direct comparisons with FARO experiments lead to use $N_f = 2$. In this model, the diameter of the created drops d_d is related to the wavelength λ of the instability, which is established from the wave number k_{\max} (Eq. 3)

$$d_d = N_d \lambda, \quad \lambda = \frac{2\pi}{k_{\max}}. \quad (4)$$

N_d is the droplet diameter parameter with an expected value between 0.1 and 0.5; the recommend value, based on comparisons with FARO experiments, is $N_d = 0.2$.

In the sensitivity study, performed for the most explosive central melt pour case C2-60, the global model with default parameters and the local model, using different values for the jet fragmentation and droplet diameter parameters, were applied. The performed simulation cases are presented in Table 7.

In Fig. 8a the time evolution of the jet and droplets mass during the jet breakup is presented for the simulated cases, applying different jet breakup models and model parameters. As expected, the jet fragmentation rate depends on the jet fragmentation parameter (Eq. 3). In case KH-2_02, in the beginning of the simulation the jet fragmentation rate is about two times larger than in the simulation using the global jet breakup model. In case KH-1_10, the jet fragmentation rate is about the same as with the global model. In case KH-2_02 after about 2.5 s a sort of runaway jet breakup reaction starts, voiding the premixture and expelling the droplets through the annulus and vessel out of the simulation domain.

Beside the mass of droplets in the premixture, an important FCI parameter is the size of droplets, since it determines the droplets surface area for heat transfer. In Fig. 8b the development of the droplets mean Sauter diameter is presented. The Sauter diameter is defined as the diameter of a sphere that has the same volume/surface area ratio as the

particle of interest. In the global model the size of the created droplets is a user parameter, and the default value of 4 mm was chosen in the simulation. So the initial mean Sauter diameter was 4 mm, and decreased to 3 mm during the simulation due to coarse drop breakup. The size of the droplets created with the local jet breakup model is in the initial stage of the jet penetration into water much smaller. Only about 0.3-0.5 mm in case KH-2_02. This is significantly lower than was measured in the FARO experiments, where the typical droplet size was in the range of 3-5 mm (Magallon and Huhtiniemi, 2001). But it should be stressed that in FARO experiments the conditions were different. In the analyzed reactor case the primary system is slightly pressurized, so the melt pour is pressure driven resulting in higher melt water penetration velocities than in FARO experiments. In case KH-1_10 the mean Sauter diameter is as expected larger (about 0.5-0.8 mm), but still much smaller than obtained with the global model.

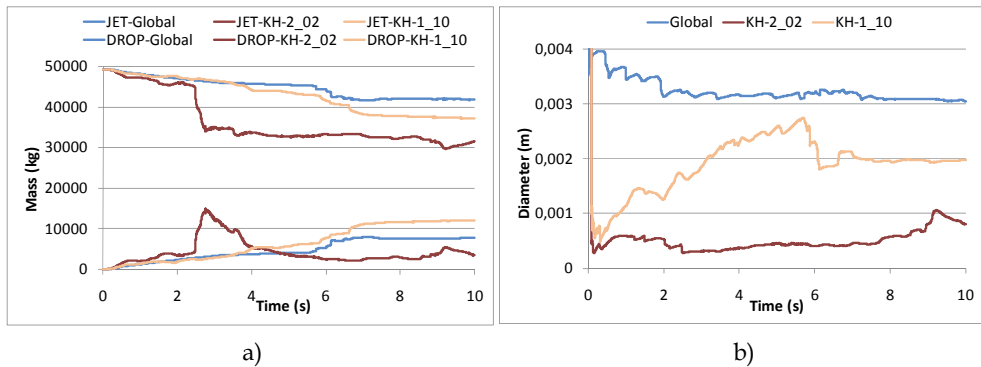


Fig. 8. Jet and droplets mass (left) and droplets mean Sauter diameter (right) during jet breakup for simulated cases (jet breakup model: Global, KH-2_02, KH-1_10).

Case	Model	Parameter
Global	Global	Default
		Fragmentation rate: $\Gamma_0 = 0.1 \text{ m}^3/\text{m}^2/\text{s}$ Droplets diameter: $d_d = 4 \text{ mm}$
KH-2_02	Local	Default
		Jet fragmentation parameter: $N_f = 2$ Droplet diameter parameter: $N_d = 0.2$
KH-1_10	Local	$N_f = 1, N_d = 1.0$

Table 7. Applied models and model parameters in sensitivity study.

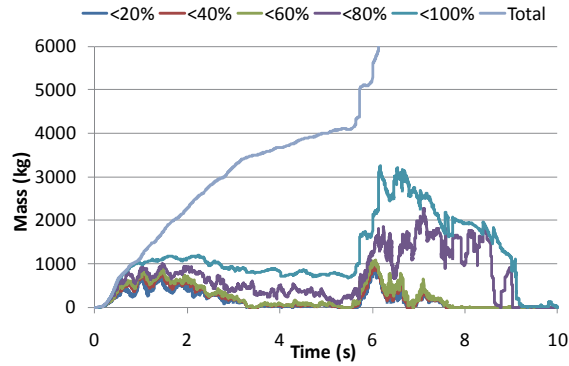
The strength of the steam explosion depends on the mass of droplets, which can efficiently participate in the steam explosion - that is the mass of liquid droplets in regions with high water content. In Fig. 9 the mass of liquid droplets in regions with different void fractions is presented during premixing. It may be observed that most of the melt drops are frozen and so can not participate in the steam explosion since they are not able to undergo fine fragmentation (compare curves "Total" and "<100%"). Most of the liquid droplets are in regions with a high void content (compare curves "<100%" and "<60%"). If it is assumed that the void fraction has to be at least below 60% that the melt drops can efficiently participate in the steam explosion process, the mass of melt which can participate in the explosion (active melt mass) is the following: for case Global up to ~1000 kg, for case KH-2_02 up to ~100 kg and for case KH-1_10 up to ~1000 kg. In case KH-2_02 during the jet breakup process very small droplets are created (Fig. 8b) resulting in a highly voided premixture (Fig. 9b) due to increased heat transfer. Therefore the active melt mass is so small. In case KH-1_10 larger droplets are formed (Fig. 8b) resulting in a less voided region (Fig. 9c) and consequently in a larger active melt mass.

In Fig. 10 the maximum calculated pressures in the cavity and the maximum calculated pressure impulses at the cavity walls are presented for the simulated cases. Some explosion simulations did not start, since no trigger location was found (too voided premixture in regions with liquid melt droplets), and some simulations did not converge. The results for these cases are consequently not presented in the graphs (e.g. case KH-2_02 between 3 and 9 seconds).

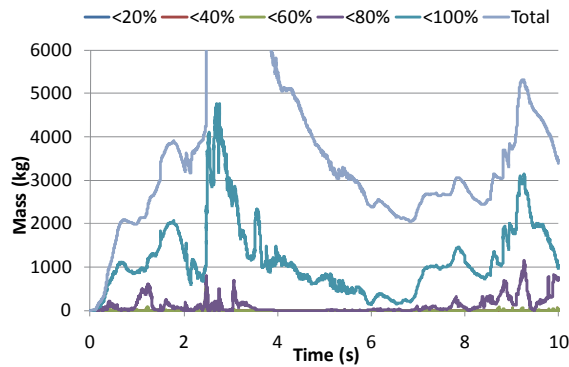
It may be observed that the selection of the jet breakup models and their parameters has a significant influence on the strength of the steam explosion. As expected, the pressure impulse curves (Fig. 10b) reasonably reflect the premixture conditions presented in Fig. 9. In general the largest pressure loads are obtained for explosions triggered at times when the mass of liquid melt in low voided regions is high. The highest maximum pressures were reached in case Global (nearly 300 MPa) since large droplets were created already in the beginning of the simulation (Fig. 8b) resulting in an initially less voided premixture, which is due to the low compressibility capable to build up so high pressures, when the pressure wave travels from the outer premixture region towards the centre of the 2D axial symmetric simulation domain. As expected, the lowest pressure impulses were obtained in case KH-2_02 (up to 0.11 MPa·s) due the smallest melt droplets (Fig. 8b) resulting in a highly voided premixture. The maximum calculated pressures and pressure impulses for the simulated cases are listed in Table 8.

Case	Maximum pressure (MPa)	Maximum impulse (MPa·s)
Global	293.7	0.42
KH-2_02	15.1	0.11
KH-1_10	78.3	0.23

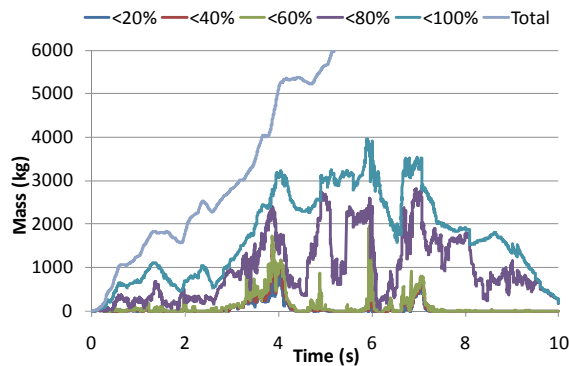
Table 8. Maximum pressures in the cavity and maximum pressure impulses at the cavity walls (cavity floor included) for different jet breakup models.



a) Global model: case Global



b) Local model: case KH-2_02



c) Local model: case KH-1_10

Fig. 9. Mass of liquid corium droplets in regions with different void fractions during premixing. The results are presented for regions with a void fraction below 20% (<20%) up to regions with a void fractions below 100% (<100%). In addition also the total (liquid and solid) corium droplets mass is presented (Total).

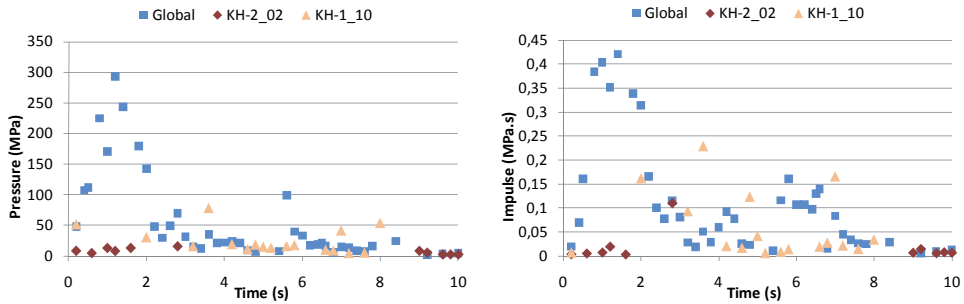


Fig. 10. Calculated maximum pressures in the cavity (left) and maximum pressure impulses at the cavity walls (right) for performed explosion phase simulations (jet breakup model: Global, KH-2_02, KH-1_10). The time axis denotes the explosion triggering times.

4.2 Influence of melt droplets solidification

In the explosion simulations it was assumed that the corium droplets in the premixture can potentially undergo fine fragmentation, and so contribute to the explosion escalation, if the droplets bulk temperature is higher than the corium solidus temperature. This overpredicts the ability of corium droplets to efficiently participate in the explosion, since in reality, during premixing, a crust is formed on the corium droplets much earlier than the droplets bulk temperature drops below the solidus temperature (Huhtiniemi et al., 1999; Dinh, 2007). This crust inhibits the fine fragmentation process and if the crust is thick enough it completely prevents it. To find out the impact of the melt droplets solidification on the explosion results, for the most explosive central melt pour case C2-60 additional explosion simulations were performed, considering different corium droplet bulk temperatures, below which the fine fragmentation process is suppressed. In this parametric study for the minimum fine fragmentation temperatures (MFFT) the corium solidus temperature 2700 K (default), the liquidus temperature 2800 K and the temperature 2750 K in-between were taken. The simulation results are presented in Fig. 11.

It may be observed that MFFT has a significant influence on the strength of the steam explosion. As is summarized in Table 9, both, the maximum pressure in the cavity and the maximum pressure impulse at the cavity walls, decrease with increasing MFFT. This was expected, since with a higher MFFT a smaller fraction of the corium in the premixture is hot enough to fulfil the strained temperature criterion for fine fragmentation, and consequently a smaller fraction of the corium in the premixture can potentially participate in the explosion process.

In Fig. 12 the time evolution of the mass of hot corium droplets, with the bulk temperature higher than MFFT, in regions with different void fractions is presented during premixing. During premixing nearly 8000 kg of corium droplets are formed (curve "Total"). The mass of hot corium droplets, which are potentially available to participate in the explosion (curves "<100%"), depends on the selected MFFT, and is up to ~3000 kg for MFFT 2700 K, up to ~2500 kg for MFFT 2750 K, and up to ~2000 kg for MFFT 2800 K. The hot corium droplets can efficiently participate in the explosion only in regions with enough water available for vaporization and for enabling the fine fragmentation process, which is essential for the steam explosion development. Therefore a better indicator for the expected strength of the resulting explosion is the available mass of hot droplets in regions, where the void fraction

is not too large, that is in regions, where the vapour fraction is below 60% (active melt mass). The so established corium droplet masses are much lower, up to ~900 kg for MFFT 2700 K, up to ~600 kg for MFFT 2750 K and up to ~300 kg for MFFT 2800 K. These differences in the active melt masses are reasonable reflected in the calculated pressure loads presented in Fig.11 and Table 9.

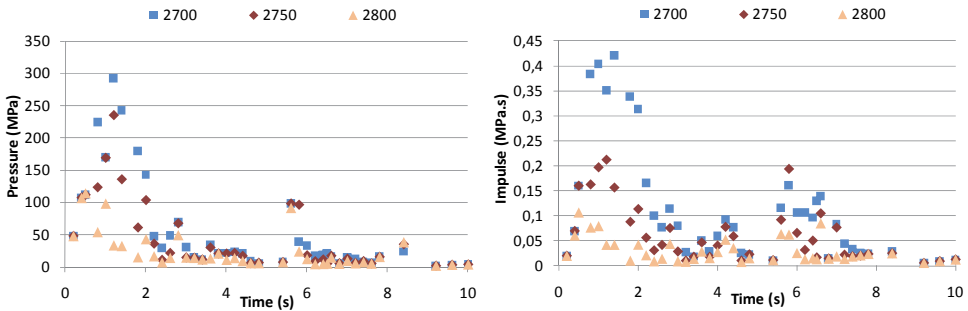


Fig. 11. Calculated maximum pressures in the cavity (left) and maximum pressure impulses at the cavity walls (right) for performed explosion phase simulations (minimum fine fragmentation temperature: 2700 K, 2750 K, 2800 K). The time axis denotes the explosion triggering times.

Minimum fine fragmentation temperature (K)	Maximum pressure (MPa)	Maximum impulse (MPa·s)
2700	293.7	0.42
2750	235.0	0.21
2800	114.7	0.11

Table 9. Maximum pressures in the cavity and maximum pressure impulses at the cavity walls (cavity floor included) for different minimum fine fragmentation temperatures.

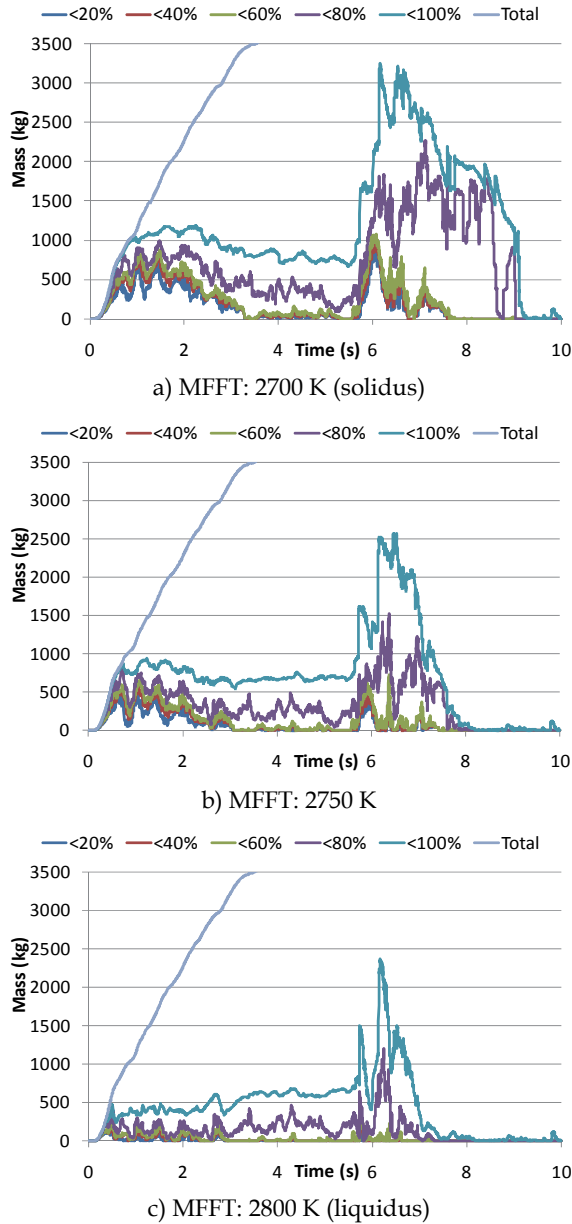


Fig. 12. Mass of corium droplets with the bulk temperature above the given minimum fine fragmentation temperature (MFFT) in regions with different void fractions during premixing. The results are presented for regions with a void fraction below 20% (<20%) up to regions with a void fractions below 100% (<100%). In addition also the total (liquid and solid) corium droplets mass is presented (Total).

5. Conclusions

An assessment of ex-vessel steam explosion pressure loads in a typical pressurized water reactor cavity was performed with the FCI code MC3D. To be able to perform a series of simulations, the reactor cavity was modelled in a simplified 2D geometry, trying to assure that the 2D simulation results reflect qualitatively and quantitatively as closely as possible the conditions in a real reactor cavity. A spectrum of relevant scenarios has been analyzed and a sensitivity study has been performed addressing the influence of the jet breakup modelling and the melt droplets solidification on the FCI process.

The simulation results revealed that the strongest steam explosions may be expected in the initial stage of the melt release, when the void build up is not so extensive. The results for the central melt pour cases showed that, in the initial stage of the melt pour, stronger explosions mainly occur for higher water subcooling and higher primary system overpressure. An explanation for this could be that higher water subcooling results in less void build up and that higher driving pressure increases the melt fragmentation. At the later stage of the simulations, stronger explosions mainly occur for lower subcooling, probably due to less droplet solidification with lower water subcooling. However the influence of the water subcooling on the explosion strength is not very clear, indicating that in the considered subcooling range the effects of void build up and melt droplets solidification nearly compensate. The results of the side melt pour cases revealed that stronger explosions may be expected with a depressurized primary system, since with a pressurized primary system the melt is ejected sideward on the cavity wall hindering the formation of an extensive premixture; moreover gas flows through the vessel opening into the cavity forming a highly voided region below the reactor vessel.

The high calculated pressure loads in the side pour cases could be attributed to the used 2D slice modelling of the reactor cavity, where the melt is released in the form of an infinite wide curtain and the explosion is triggered through the whole width of that curtain. This is quite conservative since, due to the 2D treatment, venting and pressure relief is underpredicted and the explosion development is overpredicted. So the performed side pour simulations should be regarded more as providing some basic qualitative insight in the FCI behaviour for side pour scenarios. For a more reliable estimation of the expected pressure loads in side pour scenarios a 3D modelling approach would be needed. The central pour cases are closer to the reality since for a central melt pour the 2D axial symmetric representation is quite suitable. So the reliability of central pour simulation results is higher than the reliability of side pour simulation results.

The sensitivity study revealed that the jet breakup and the melt droplets solidification have a significant influence on the strength of the steam explosion, and consequently have to be adequately modelled. Especially the correct establishment of the size of the created melt droplets during jet breakup is crucial, since the droplets size defines the melt surface area for heat transfer, which governs the melt droplets solidification and the void build. Both, the melt droplets solidification and the void build up may significantly reduce the strength of the steam explosion, as demonstrated by the preformed simulations.

The nature of FCI is very complex and already small modelling changes can have a significant influence on the simulation results. Therefore additional experimental and analytical work is needed, as being carried out in the OECD programme SERENA phase 2 and in the network of excellence SARNET-2 within the 7th EU framework program, to be able to reliably extrapolate the various experimental findings to reactor conditions and to perform reliable reactor simulations.

6. Acknowledgments

The author acknowledges the financial support of the Slovenian Research Agency within the research program P2-0026, the research project J2-2158, and the cooperative CEA-JSI research project (contract number 1000-0810-38400013). The Jožef Stefan Institute is a member of the Severe Accident Research Network of Excellence (SARNET2) within the 7th EU Framework Program.

7. References

- Albiol, T., Haste, T., van Dorsselaere, J.P., Journeau, C., Meyer, L., Chaumont, B., Sehgal, B.R., Schwinges, B., Beraha, D., Annunziato, A., Zeyen, R., (2008). Summary of SARNET achievements. ERMSAR conference, 23–25 September 2008, Nesseber, Bulgaria
- Berthoud, G. (2000). Vapor explosions. *Annu Rev Fluid Mech* 32, pp. 573-611, ISSN 0066-4189
- Corradini, M.L., Kim, B.J., Oh, M.D. (1988). Vapor Explosions in Light Water-Reactors – a Review of Theory and Modeling. *Prog Nucl Energ* 22, pp. 1-117, ISSN 0149-1970
- Corradini, M.L. (1991). Vapor explosions: a review of experiments for accident analysis. *Nuclear Safety* 32 (3), pp. 337–362, ISSN 0029-5604
- Dinh, T.N. (2007). Material Property Effect in Steam Explosion Energetics: Revisited, NURETH-12, Pittsburgh, Pennsylvania, USA, pp. 1–19
- Esmaili, H., Khatib-Rahbar, M. (2005). Analysis of likelihood of lower head failure and ex-vessel fuel coolant interaction energetics for AP1000. *Nucl Eng Des* 235, pp. 1583-1605, ISSN 0029-5493
- Hessheimer, M.F., Dameron, R.A. (2006). Containment Integrity Research at Sandia National Laboratories – An Overview. NUREG/CR-6906, SAND2006-2274P
- Huhtiniemi, I., Magallon, D., Hohmann, H. (1999). Results of recent KROTOS FCI tests: alumina versus corium melts. *Nucl Eng Des* 189, pp. 379–389, ISSN 0029-5493
- Kawabata, O. (2004). Analyses of Ex-Vessel Steam Explosion and its Structural Dynamic Response for a Typical PWR Plant. *ICONE-12*, Arlington, VA, USA, pp. 1–9
- Krieg, R., Dolensky, B., Goller, B., Hailfinger, G., Jordan, T., Messemer, G., Prothmann, N., Stratmanns, E. (2003). Load carrying capacity of a reactor vessel head under molten core slug impact - Final report including recent experimental findings. *Nucl Eng Des* 223, pp. 237-253, ISSN 0029-5493
- Magallon, D., Huhtiniemi, I. (2001). Corium melt quenching tests at low pressure and subcooled water in FARO. *Nucl Eng Des* 204, pp. 369–376, ISSN 0029-5493
- Meignen, R., Dupas, J., Chaumont, B. (2003). First evaluations of Ex-Vessel Fuel-Coolant Interaction with MC3D. *NURETH-10*, Seoul, Korea, pp. 1–18
- Meignen, R., Dupas, J. (2004). Analysis of Ex-Vessel Fuel Coolant Interaction Issue with MC3D. *CSARP 2004*, Arlington, VA, USA
- Meignen, R. (2005). Status of the Qualification Program of the Multiphase Flow Code MC3D, *Proceedings of ICAPP '05*, Seoul, Korea, pp. 1–12
- Meignen, R., Picchi, S. (2005). MC3D Version 3.5: User's Guide. IRSN Report, NT/DSR/SAGR/05-84
- Moriyama, K., Takagi, S., Muramatsu, K., Nakamura, H., Maruyama, Y. (2006). Evaluation of containment failure probability by ex-vessel steam explosion in Japanese LWR plants. *Journal of Nuclear Science and Technology* 43 (7), pp. 774–784, ISSN 0022-3131

- OECD/NEA (2007). OECD Research Programme on Fuel-Coolant Interaction; Steam Explosion Resolution for Nuclear Applications – SERENA; Final Report. NEA/CSNI/R(2007)11.
- OECD/NEA (2008). Agreement on the OECD/NEA SERENA Project – To address remaining issues on fuel-coolant interaction mechanisms and their effect on ex-vessel steam explosion energetics
- Sehgal, B.R. (2006). Stabilization and termination of severe accidents in LWRs. *Nucl Eng Des* 236, pp. 1941-1952, ISSN 0029-5493
- Sehgal, B.R., Piluso, P., Trambauer, K., Adroguer, B., Fichot, F., Müller, C., Meyer, L., Breitung, W., Magallon, D., Journeau, C., Alsmeyer, H., Housiadas, C., Clement, B., L., A.M., Chaumont, B., Ivanov, I., Marguet, S., Van Dorsselaere, J.P., Fleurot, J., Giordano, G., Cranga, M. (2008). *SARNET lecture notes on nuclear reactor severe accident phenomenology*. CEA, France, p. 415
- Seiler, J.M., Tourniaire, B., Defoort, F., Froment, K. (2007). Consequences of material effects on in-vessel retention. *Nucl Eng Des* 237, 1752–1758, ISSN 0029-5493
- Schwinges, B., Journeau, C., Haste, T., Meyer, L., Tromm, W., Trambauer, K., Members, S. (2010). Ranking of severe accident research priorities. *Prog Nucl Energ* 52, pp. 11-18, ISSN 0149-1970
- Smith, P.D., Hetherington, J.G. (1994). Blast and Ballistic Loadings of Structures. Butterworth-Heinemann Ltd., Oxford, ISBN 0 7506 2024 2
- Theofanous, T.G. (1995). The Study of Steam Explosions in Nuclear Systems. *Nucl Eng Des* 155, pp. 1-26, ISSN 0029-5493
- Turland, B.D., Dobson, G.P. (1996). *Nuclear science and technology, Molten fuel coolant interactions: a state of the art report*
- WASH-1400 (1975). Reactor safety study: An assessment of accident risks in U.S. commercial nuclear power plants. U.S. Nuclear Regulatory Commission

Part 2

Environmental Effects

Radiological Releases and Environmental Monitoring at Commercial Nuclear Power Plants

Jason T. Harris
Idaho State University
United States of America

1. Introduction

The generation of electricity from nuclear power has become increasingly important due to the growing concerns of global climate change. Nuclear energy has long been recognized as a leading energy source that produces minimal pollution to the environment that can contribute to this phenomenon. In addition, nuclear power offers an attractive option for countries looking for energy source diversification. Currently there are 442 commercial nuclear power reactors operating in the world (International Atomic Energy Agency [IAEA], 2010, 2011). These power plants contribute about 19% of the electricity production today. The United States of America (U.S.) has the largest commercial nuclear reactor fleet in the world with 104 operating reactors (U.S. Nuclear Regulatory Commission [USNRC], 2010). Of these reactors, 69 are pressurized water reactors (PWRs) and 35 are boiling water reactors (BWRs), located on 65 sites around the country. These power plants contribute about 20% of the U.S. electricity production.

Although it is known that commercial nuclear power plants release small amounts of radioactivity into the environment, there is still the potential for these releases to impact public health. This is especially important today as changes are occurring in nuclear power plant operations including: higher electric generating capacities, increased power levels due to mechanical uprates, and plant life extensions. Public health effects must be reexamined as new light water reactor designs are being considered for construction. In addition, recent events at multiple nuclear power plants in the U.S. involving unplanned releases, especially tritium (^3H), have led to increased scrutiny on monitoring and evaluating releases. Changes in radiation protection recommendations and regulations also warrant further and continued investigations in these matters. Although Harris (2007) and Harris & Miller (2008) have performed numerous studies of nuclear power effluent releases and environmental monitoring, data collection and analysis must continue to be performed for the entire nuclear industry.

This chapter focuses on recent research that has been conducted in the areas of commercial nuclear power radiological releases and environmental monitoring by the author. Although the emphasis will be on studies performed in the United States of America, international comparisons will be made where appropriate.

2. Background

Commercial nuclear power plants release small amounts of radiation into the environment under normal operating conditions. Many of the radioactive isotopes that are released are in the form of gaseous or liquid effluents and solid radioactive waste conditioned by the plant. These releases represent some of the by-products of electrical energy generation (Eisenbud & Gesell, 1997).

Three categories of radioactive by-products are produced during routine operation of a commercial light-water reactor: fission products, neutron activation products, and tritium (Glasstone & Jordan, 1980). Fission products are created as a result of the radioactive decay of the nuclear fuel. Approximately 300 different nuclides are formed in the operating reactor. Most of these nuclides are radioactive. Although there is a large quantity of fission products formed, many have little impact on the radioactive releases to the environment because of their extremely short half-lives (<1 day), small quantities, or biological insignificance. Gaseous fission products important to these releases include: ^3H , ^{85}Kr , and ^{133}Xe . Iodine, solid at room temperature, is also released as a gaseous effluent due to vaporization. Important dose significant iodine isotopes include: ^{131}I , ^{133}I , and ^{135}I . Other decay daughters of produced fission products may also appear in the gaseous effluents as particulate matter (USNRC, 1976a, 1976b).

Activation products are formed by neutron interactions with oxygen in water and air, with nitrogen and argon in air, and with impurity corrosion elements. Like fission products, many of the neutron activation products produced are insignificant in reactor effluents due to their short half-lives (<1 day) or small quantities. Relevant gaseous activation products include: ^{13}N , ^{14}C , ^{16}N , and ^{41}Ar (NCRP, 1985, 1987). Important liquid and solid waste activation products arising from interaction of neutrons with corrosion and erosion elements include: ^{51}Cr , ^{58}Co , ^{60}Co , and ^{59}Fe (Kahn, 1980; USNRC, 1976a, 1976b).

Tritium (^3H or T), is produced as a result of both nuclear fission (ternary fission) and neutron activation of deuterium (^2H). Tritium is typically treated separately because it is produced in such large quantities compared to any other effluent nuclide and because it arises from other nuclear reactions. One significant source of tritium is the interaction of high energy neutrons with boron. Boron is used in PWRs for shim control (as boric acid) and BWRs as a burnable poison (Glasstone & Jordan, 1980). Tritium is also formed from the interaction of neutrons with ^6Li (as lithium hydroxide in water treatment).

Typically, the radioactive emissions from operating nuclear power reactors result in insignificant doses to the general population. In 1988, when 110 nuclear power plants were operating at 70 sites in the United States, the mean collective effective dose commitment from all pathways ranged from a low of 1.1×10^{-5} person-Sv (0.0011 person-rem) to a high of 0.16 person-Sv (16 person-rem). The collective dose commitment for the 150 million persons living within the 2-80-km annuli was 0.75 person-Sv (75 person-rem) for that year (USNRC 1995). Other studies performed throughout the world have shown similar results for population doses around nuclear power plants (Walmsley et al., 1991; Ziqiang et al., 1996; Kim & Han, 1999; Nedveckaite et al., 2000; Liu et al., 2003; Quindos Poncela et al., 2003). Harris (2007) performed a study to look at the doses for maximally exposed individuals from all plants. A review of epidemiological studies of cancer in populations near nuclear facilities showed that in all scientific reports analyzing nuclear power plants, a cause and effect relationship between cancer risk and radiation exposure could not be found (Patrick, 1977; Jablon et al., 1990; Shleien et al., 1991; Lopez-Abente et al., 1999).

There has been a gradual reduction in both liquid and gaseous emissions from power reactors due to improvements in fuel performance and radioactive waste treatment system technology (Harris, 2002). However, the Electric Power Research Institute (EPRI) reports that although radioactive isotopes captured by these systems reduce effluent quantities, radioactive solid waste volumes increase (2003). Also, with longer operating times and license extensions, the accumulation of spent fuel is becoming more important. Many plants have begun storing spent fuel on-site in independent storage facilities. The ageing of existing nuclear power facilities and the increasing accumulation of radioactive wastes have led to an increased emphasis on solid radioactive waste disposal. However, at this time doses to the public have not increased during the handling or transportation of radioactive waste shipments. Worldwide estimates also show that nuclear power will continue to grow and thus remain a source of radioactivity exposure to the public.

2.1 Regulatory criteria of releases

The principles that apply to U.S. nuclear power plant radiological releases include consensus scientific recommendations, governmental regulations (Code of Federal Regulations [CFR]), and specific criteria in each plant's operating license. Dose limits, concepts and models based on scientific agreement about radiation effects are recommended by the International Commission on Radiological Protection (ICRP) and the NCRP. Government radiation protection guidance is developed by the U.S. Environmental Protection Agency (USEPA) and approved by the President to assist federal agencies, such as the U.S. Nuclear Regulatory Commission (USNRC), in developing radiation protection regulations. This guidance is usually in agreement with the ICRP or the NCRP. The regulatory standards developed are then required to be incorporated into each nuclear power plant as radiological effluent technical specifications (RETS) that are to be followed through procedures and programs (Andersen, 1995).

Since the inception of nuclear power, federal radiation protection regulations have been based upon the recommendations of the ICRP. The initial ICRP recommendations, published as ICRP Publication 1 and ICRP Publication 2, provided dose limits, models, and radiation concepts. Subsequent to these initial recommendations, the ICRP issued three major revisions, ICRP Publication 26, ICRP Publication 60, and ICRP Publication 103. These recommendations lowered the annual dose limits for members of the public and revised dose models and concepts. ICRP Publication 26 (1977) recommended an annual dose limit of 5 mSv y^{-1} (0.5 rem y^{-1}) to critical members of the general population (pregnant women and children). Critical members of the general population are those that are more susceptible to radiation effects. ICRP Publication 60 (1991) lowered recommended annual dose limits further to 1 mSv y^{-1} (0.1 rem y^{-1}) for members of the general population. ICRP Publication 103 (2007) continues with this dose limit. Another important recommendation in terms of reactor releases is given in ICRP Publication 29. This document provides the Committee's recommendations for evaluating pathways between radioactive materials released into the environment and man (ICRP, 1978).

One important recommendation made by the NCRP, published as NCRP Report 92, is specifically concerned with public radiation exposure resulting from nuclear power (NCRP, 1987). The report outlines dose concepts, risks, and technical information regarding the nuclear fuel cycle. In 2011, NCRP will release another recommendation (Report 169) on effluent and environmental monitoring design. Other organizations, including the United Nations Scientific Committee on the Effects of Atomic Radiation (UNSCEAR), have had a

tremendous influence on the understanding of radiation concepts. The UNSCEAR reports yearly to the General Assembly and periodically issues (every four to five years) the important publication, Sources and Effects of Ionizing Radiation (2000). Another United Nations organization, the International Atomic Energy Agency (IAEA), also influences the practice of radiation protection and issues radiation related reports.

The updated regulations important to nuclear power plant radiological effluents are found in 40 CFR 190 (USEPA 1977). These regulations include limits on radiation doses received by members of the public off-site of the nuclear power plant. During normal operation, the annual dose to any member of the public shall be limited to: 0.025 mSv y⁻¹ (25 mrem y⁻¹) to the whole (total) body; 0.075 mSv y⁻¹ (75 mrem y⁻¹) to the thyroid; and 0.025 mSv y⁻¹ (25 mrem y⁻¹) to any other organ. The USEPA has also set forth guidelines for the maximum amount of radioactivity released into the environment (e.g. 5 mCi of ¹²⁹I per gigawatt-year of electrical energy produced).

The USNRC issues standards and regulations for radiation protection and nuclear plant operations. Standards for radiation protection are contained in 10 CFR 20 (USNRC, 1991). These standards incorporate the dose concepts and models from the older ICRP Publication 26 and 40 CFR 190. The criteria in 10 CFR 20 regarding dose limitations include: a public dose limit of 1 mSv y⁻¹ (0.1 rem y⁻¹), compliance with USEPA's 40 CFR 190 standards, and a requirement for a licensee survey of radiation levels in unrestricted areas, in controlled areas, and in effluent releases. Appendix B to 10 CFR 20 includes limits on effluent concentrations for radiological releases in air and water. These concentration limits are derived from occupational inhalation and ingestion annual limits on intake (ALIs) adjusted to reflect the dose limits set forth by the standards.

USNRC standards for nuclear power plant operations are contained in 10 CFR 50. These standards include criteria for radiological effluent technical specifications, effluent release design objectives and limits, and notification and reporting for events involving the release of radioactive materials. Technical specifications on effluents from nuclear power plants are listed in 10 CFR 50.36a (USNRC, 1996). The specifications require that the licensee comply with 10 CFR 20; that procedures be established and followed regarding the control of effluents; that a radioactive waste treatment system be installed, maintained, and used; that a report be submitted annually to the USNRC regarding effluent releases and the attributed estimated doses to the public; and that procedures be developed that comply with the principle of achieving radiation levels ALARA. Appendix I to 10 CFR 50 gives numerical guides for design objectives and limiting conditions for operation to meet the ALARA criterion for radiological effluents. Doses to members of the general public from radioactive material in liquid effluents released to unrestricted areas shall be limited to 0.003 mSv y⁻¹ (3 mrem y⁻¹) to the whole (total) body, and 0.010 mSv y⁻¹ (10 mrem y⁻¹) to any other organ. The air dose due to the release of noble gases in gaseous effluents is restricted to 0.010 mGy y⁻¹ (10 mrad y⁻¹) for gamma radiation, and 0.020 mGy y⁻¹ (20 mrad y⁻¹) for beta radiation. The public dose from ¹³¹I, ³H, and all particulate radionuclides with half-lives greater than eight days in gaseous effluents is limited to 0.015 mSv y⁻¹ (15 mrem y⁻¹) to any organ. Standards in 10 CFR 50 also cover notification in the event of an abnormal radiological release.

Criteria for nuclear power plant effluents are contained in the radiological effluent technical specifications (RETS), which are part of the nuclear power plant operating license. The RETS include the Limiting Condition for Operation (LCO). The LCO is a description of the criteria that are to be met, the conditions under which the criteria apply, the actions to be taken if criteria are not met, and surveillance requirements to demonstrate that the criteria have

been met. The RETS must also contain a site specific Offsite Dose Calculation Manual (ODCM). The ODCM contains both the methodology and parameters used in calculating offsite doses resulting from radiological effluents and the REMP. The USNRC Regulatory Guide 4.1 outlines the programs for monitoring radioactivity in the environs of nuclear power plants (USNRC, 1975). The RETS and ODCM must be approved by the USNRC as part of the license application and approval process. Radiological effluent technical specifications guidelines are contained in NUREG-0133 (USNRC, 1978). The annual effluent report covers plant operations from the previous calendar year. The report includes a summary of the quantities of radiological effluents and solids discharged by the plant. USNRC Regulatory Guide 1.112 aids nuclear power plants in calculating effluent releases.

2.2 Environmental monitoring

Prior to the issuance of a construction permit or an operating license for a nuclear power station, federal agencies (i.e. USNRC) are required to assess the potential environmental effects of that facility to ensure that issuance of the permit or license will be consistent with the national environmental goals prescribed by the National Environmental Policy Act (NEPA) of 1969 and the Federal Water Pollution Control Act. In order to obtain information needed for this assessment, applicants are required to submit a report on the potential environmental impacts of the station and associated facilities. After the station becomes operational, an annual environmental report must be submitted to ensure continued compliance of the requirements set forth in the facility's license and of the Acts stated previously.

Radiological environmental monitoring programs at nuclear power plants are required in accordance with the Code of Federal Regulations. Development and maintenance of these programs are under the guidance of several federal documents. These radiological environmental monitoring programs are established to monitor the radiological impact of reactor operations on the environment. Objectives of these programs include: identification, measurement and evaluation of existing radionuclides in the environs of the facility and fluctuations in radioactivity levels which may occur; evaluation of the measurements to determine the impact of operations on the local radiation environment; collection of data to refine radiation transport models; verification that radioactive material containment systems are functioning to minimize environmental releases to levels that are as low as reasonably achievable (ALARA) and; demonstration of compliance with regulations. Implicit in these objectives are the requirements to trend and assess radiation exposure rates and radioactivity concentrations in the environment that may contribute to radiation exposures to the public. The results of the REMP are submitted as part of the plant's annual environmental report.

Each plant establishes their own, unique REMP program to reflect site-specific conditions and surrounding population characteristics. The program consists of preoperational and operational components. The preoperational program is conducted in part to measure background levels and their variations in environmental media in the area surrounding the plant. Environmental media include: milk produced from cows or goats, broadleaf vegetation, fish, fruits and vegetables, edible aquatic invertebrates, surface water, drinking water and ground water.

Each plant is to also make changes to its REMP program as conditions change. But, it has been reported recently that many plants are decreasing their programs due to budget constraints and lack of positive radioactivity measurements. This reduction can lead to

decreased litigation protection, decreased public confidence, and potential unreported or undetected releases. Reduced REMP programs have led to recent public opinion and regulatory problems for several facilities due to unexpected and/or undetected tritium releases. Decreased lower limits of detection (LLDs) and minimal detectable activities (MDAs) reportedly have led to newly quantifiable low levels of many radionuclides in the environs around nuclear power stations. Changes in operating conditions may also lead to new radionuclide transport pathways being developed, as has been seen with precipitation scavenging and concentration in ice.

Ultimately, a nuclear power plant's REMP program is designed to assess the impact of radiological releases on the environment and the public. Public opinion of the nuclear power industry has traditionally been very troubled, especially with the accidents at Three-Mile Island and Chernobyl. Positive public opinion to nuclear power can only be achieved through truthfulness by the nuclear power company regarding operations and radiological releases and accurate and comprehensive monitoring of these releases.

3. Effluent release study

As commercial nuclear power electrical generation steadily increases in the U.S. and the rest of the world, it has become even more important to evaluate the release of radioactive materials into the environment. An easy way to track industry wide effluent releases is by performing trend analyses. Accumulated data may also be used for analysing reactor power up-rate consequences, protecting the nuclear power industry against litigation, and for assisting in new power plant siting. Most importantly, collecting and maintaining an effluent database is necessary in maintaining a favourable public perception regarding the low environmental and biological impact of nuclear power. This is especially important now as several recent, inadvertent releases of radioactive materials from nuclear power plants have occurred. Because of these circumstances, the author has compiled and analysed the effluent data for all U.S. commercial nuclear power plants since 1995. Presented here is also an update of the comprehensive study performed by Harris & Miller (2008).

The classification and monitoring of liquid and gaseous radiological releases is fairly uniform around the world. The classification is based on the nuclide, chemical or physical form, and dose or activity significance. In the U.S., gaseous effluents are divided into fission and activation gases, iodines, particulates (with half-lives greater than eight days), and tritium. Liquid effluents are divided into fission and activation products, dissolved and entrained gases, tritium, and gross alpha activity. International organizations and other nations use the same categories, but combine the fission and activation products and the dissolved and entrained gases in liquid effluents (UNSCEAR, 2000; Harris, 2002).

The classification of radioactive releases is important because dose calculations are based upon them. For example, the collective effective doses calculated by UNSCEAR (2000) use these effluent categories. The groupings also allow plants and nations to compare and benchmark with another. Unlike the simplified general UNSCEAR model, the USNRC model requires specific nuclide, meteorological, and site specific conditions. Hence, this model provides more accurate estimates of dose.

Other studies have been performed to assess the doses from nuclear power radiological releases. Vold (1984) determined the ratio of the collective effective dose equivalent (CEDE) via a specified ingestion pathway relative to that CEDE by inhalation per annual releases of a radionuclide. Kim & Han (1999) and Liu et al. (2003) assessed the impact of tritium

released from nuclear power plants in China. Both of these studies confirmed that the doses were less than 1% of the regulatory limits. Ziqiang et al. (1996) reported similar results not only for tritium, but for other radionuclides as well.

What is very common in the nuclear power industry is trending and benchmarking of data. This is done to improve plant operations and management. Many organizations that oversee different aspects of nuclear power plants use these methods for comparison. These comparisons may be advantageous or detrimental to a plant. For example, with radiological releases, high activities compared to other plants can lead to lower profits due to higher premiums from American Nuclear Insurers (ANI). It can also lead to scrutiny from the Institute of Nuclear Power Operations (INPO) and greater surveillance from USNRC. Thus, these comparisons are very important. Gilbert (1994) identifies statistical analyses suitable for detecting trends in environmental contamination data. Accurate trend analyses can aid plants in these aforementioned areas. Trend analyses were performed for the data over the 15 year period using the Mann-Kendall non-parametric test. Inspections of release trends over the fifteen year period help identify areas of concern with these releases. Future estimates of release radioactivity and public doses can then be made from these analyses.

3.1 Methodology

The data utilized for the effluent release study were taken from the annual radioactive release reports provided by the nuclear power plants to the USNRC as required in their operating license conditions. These reports were either provided directly to the author from the licensee or taken from the USNRC Agency wide Documents Access and Management System (ADAMS). The reports provide categorical effluent release data, nuclide specific radioactivity, and site specific data needed for dose calculations. Population information not provided by the licensees was taken from appropriate census reports (U.S. Census Bureau, 2010).

Data was analysed for those reactors that have operated for the 15 year period of 1994-2009. This length of time is long enough to allow plants to stabilize in the event of long shutdown periods and allows evaluation of plants for at least seven refuelling cycles. Events that may affect releases, such as power-uprates and failed fuel from defects, will also show up in this period. The beginning of this data set also coincides with the cessation of tracking radiological effluents by the U.S. in 1994. In this time frame, 103 reactors were operating. Browns Ferry Unit 3 began operation in 2006, to become the 104th operating reactor.

Effluent radioactivity was obtained from data reported by the nuclear power plants in their annual radioactive material release reports. The effluent data was compiled for all operating PWR and BWR plants from 1995 - 2005. The completeness of the data was 98%. In keeping with U.S. nuclear power effluent report formatting, data was compiled and analysed using the same categories as those listed in USNRC Regulatory Guide 1.21. The four gaseous effluent categories used were: fission and activation gases (F/A), total iodine (¹³¹I), particulate matter or particulates, and tritium. The three liquid effluent categories used were: fission and activation products, dissolved and entrained gases, and tritium. Because the radioactivity levels of the fission and activation products and dissolved and entrained gases are several orders of magnitude smaller than tritium, those two categories were added together and listed as "F/D". This category replicates the reporting done by UNSCEAR. Gross alpha radioactivity was not included in this study.

Trend analyses were performed for the data over the time period using the Mann-Kendall non-parametric test. This procedure was used since missing values were allowed and the

data need not conform to any particular distribution (Gilbert, 1994). Inspection of trends over the time period identifies the overall direction of industry effluent releases and can roughly be used to predict future releases.

For this updated study, one dose assessment methodology was used. The collective effective doses (CED) were calculated for the U.S. population using the UNSCEAR methodology. For these dose calculations, the effluent data was normalized. This was achieved by taking the amount of radionuclides released per unit of electrical energy generated each year. This method is the most common way to normalize effluent data. The electrical energy generated per year was obtained by multiplying the net electrical energy generated by the capacity factor. Capacity factor is defined as the gross electricity generated divided by the product of the licensed capacity and reference time. Normalizing data in this manner takes into account the operational performance of the nuclear power plant. However, it also assumes that effluent release amounts are a direct consequence of operation time. The author cautions against making simplistic comparisons of radioactive releases with the electrical energy generated because of the many factors which affect the amount of radioactive materials released, including the condition of the fuel, primary system integrity, design of effluent and radioactive waste treatment systems, maintenance activities, operations, and equipment performance.

3.2 Results and discussion

3.2.1 Radiological effluent releases

The annual variation of total nuclear power plant radioactivity released in gaseous effluents in PWRs and BWRs are shown in Figs. 1 and 2, respectively. As expected, the activity from PWR releases is higher than that from BWRs due to the greater number of plants. Regardless of this fact, the average tritium release from PWRs is also higher due to chemistry practices that create more tritium in the plant. Nearly every category from both reactor types is fairly level in terms of activity released for the entire time period. The evaluation of the data over the time period partly eliminates variations in annual values. The advantage of using 15 years of data is that operation anomalies, such as long shutdown times for maintenance, are averaged out. The one notable exception appears in the PWR particulate category. In 2003, one plant experienced an annual release over five orders of magnitude above the mean. This single event was significant enough to skew the entire industry release activity, especially since the annual radioactivity released in particulate matter is so low compared to tritium or fission and activation gases. The increase in 2005 was due to higher activity releases by several plants.

The annual variation of total nuclear power plant radioactivity released in liquid effluents in PWRs and BWRs are shown together in Fig. 3. As expected, and for reasons similar to that of the gaseous releases, PWR liquid radioactivity in releases is higher than in BWRs. Liquid releases have stayed very constant over the 11-year period. The most notable exception is the pronounced decline in BWR non-tritium (F/D) radioactivity from 2003 - 2007.

3.2.2 Radiological effluent trends

U.S. industry effluent trends were evaluated using the Mann-Kendall non-parametric test. The Mann-Kendall test was performed as follows: For any given release category, x , its feature vector consists of the release summation from all plants appearing in a given year i . These release activities are ordered from the first year, 1995, to the final year, 2009, that data was gathered.

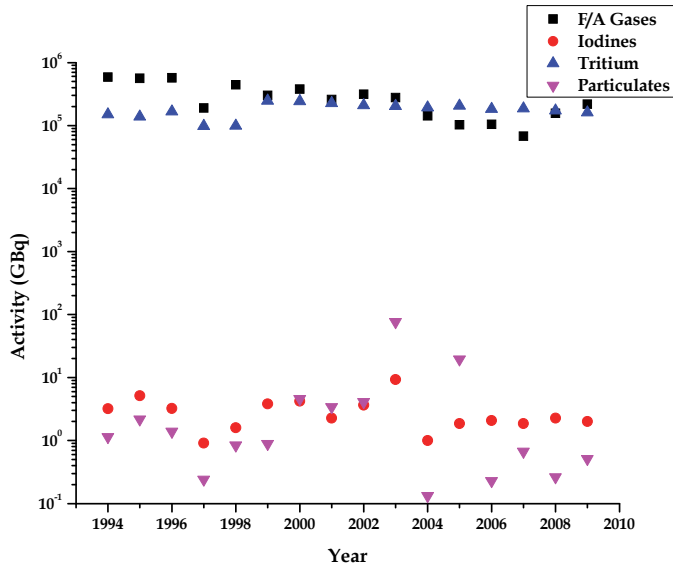


Fig. 1. Variation of total radionuclide activity released in gaseous effluents from PWR plants

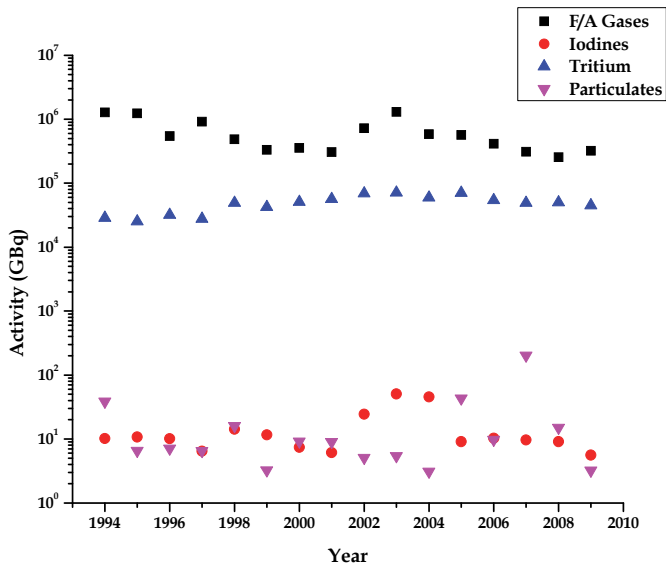


Fig. 2. Variation of total radionuclide activity released in gaseous effluents from BWR plants

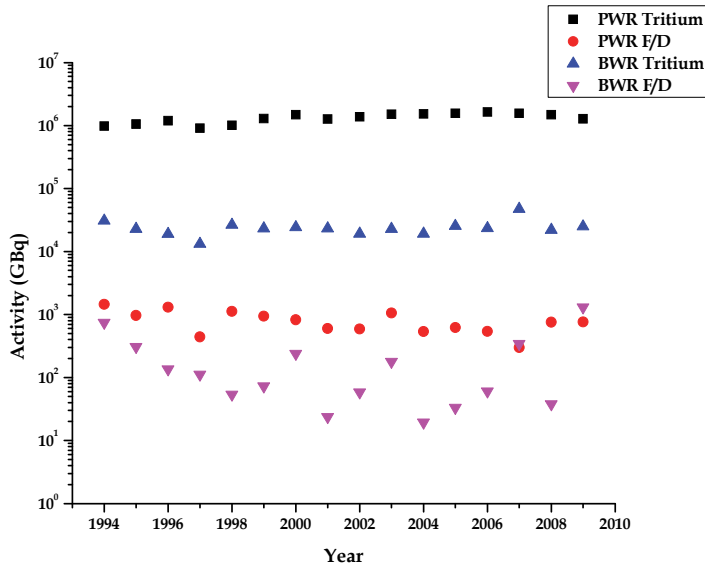


Fig. 3. Variation of total radionuclide activity released in liquid effluents from PWR and BWR plants

The x value for each year is compared to all other years greater than that year, and Kendall's statistic S is calculated as follows:

$$S = \sum_{k=1}^{n-1} \sum_{j=k+1}^n \text{sgn}(x_j - x_k) \tag{1}$$

$$\text{where: } \text{sgn}(x_j - x_k) = \begin{cases} 1, & \text{if } x_j - x_k > 0 \\ 0, & \text{if } x_j - x_k = 0 \\ -1, & \text{if } x_j - x_k < 0 \end{cases}$$

Generally, if a dataset displays a consistently increasing or decreasing trend, S will be positive or negative, respectively, with a larger magnitude indicating the trend is more consistent in its direction. By using the sgn function, the algorithm used was able to detect trends featuring either large or small increase steps from year to year equally. The S statistic is then compared to the corresponding P-value (Hollander & Wolfe, 1999).

Under the null hypothesis, H_0 , that there is no trend displayed by the time series, the distribution of S is then expected to have a zero-mean and variance. The Mann-Kendall test was performed on BWR plant releases, PWR plant releases, and all plant releases (BWR and PWR combined) at a significance level of 0.05.

The results of the trend test are shown in Table 1. Over the past 15 years, it can be seen that for most effluent categories, the releases are level, meaning there is no increasing or decreasing trend. For these categories, improvements in radioactive waste treatment and

reactor operations are offset by increased power production, increased capacity factors, and power up-rates. Looking at PWRs only, gaseous fission and activation products and liquid F/D have decreased while liquid tritium has increased. Reduction in the fission and activation products over the years is probably a direct result of longer holdup times for radioactive decay. In addition lower fission and activation product activities may be due to improved fuel performance from better manufacturing methods. Also, longer operation times in recent years provide stability to the reactor, leading to less fuel shock and defects. The increasing trend for liquid tritium activity is due to an increase in liquid discharges by these plants. Formerly zero-discharge plants have begun to release liquids again to avoid build-up of their tritium inventory. Coupled with this practice, over the last fifteen years many plants have reduced recycling of boron for reactor control. This procedure contributes to increased tritium production.

Release Category	S Statistic	Trend
PWR Gaseous--F/A gases	-61	Decreasing
PWR Gaseous--Iodines	-15	None
PWR Gaseous--Tritium	-3	None
PWR Gaseous--Particulate	-11	None
PWR Liquids--Tritium	57	Increasing
PWR Liquids -- F/D	-35	Decreasing
BWR Gaseous--F/A gases	-41	Decreasing
BWR Gaseous--Iodines	-13	None
BWR Gaseous--Tritium	31	Increasing
BWR Gaseous--Particulate	7	None
BWR Liquids--Tritium	27	Increasing
BWR Liquids -- F/D	-7	None
Total Gaseous--F/A gases	-65	Decreasing
Total Gaseous--Iodines	-21	Decreasing
Total Gaseous--Tritium	-3	None
Total Gaseous--Particulate	13	None
Total Liquids--Tritium	57	Increasing
Total Liquids -- F/D	-13	None

Table 1. Mann-Kendall trend results for U.S. commercial nuclear power plant radiological effluent releases from 1995 - 2009

For BWRs, liquid tritium and gaseous releases have increased and gaseous fission and activation releases have decreased. The increase in gaseous and liquid tritium are relatively new phenomenon and is probably related more to the increased power production and capacity factors over the last several years than anything else. Looking at the entire industry (PWRs and BWRs combined), all effluent releases except gaseous fission and activation products and iodine and liquid tritium are level. Because PWRs make up 66% of the U.S. industry, their releases have a greater impact on the overall release trends, as is evident with the increasing liquid tritium.

3.2.3 Radiological impact of effluent releases

Tracking effluent release quantities is important in determining radioactivity levels in the environment. However, dose determination of the effluents must be performed to estimate the human effects of these radiation sources. The collective effective dose (CED) from radiological effluent releases was obtained using an average collective dose calculation method used by UNSCEAR. UNSCEAR (2000) calculates population dose by first calculating the CED per unit release of radionuclides released from reactors and then normalizes the value with the electrical energy generated. The CED is divided according to type of release (airborne or liquid), radionuclide category (noble gases, tritium, C-14, iodine, and particulate matter), and pathway (immersion, ingestion, inhalation, and external irradiation). The normalized collective effective dose model is given by:

$$D_{CE} = \sum_i \frac{A_i}{E} D_i \quad (2)$$

where: A_i = activity of release category i (GBq); D_{CE} = total CED (person-Sv $\text{GW}^{-1} \text{y}^{-1}$); D_i = collective dose for release category i (person-Sv PBq^{-1}); and E = energy produced by the nuclear reactor (GW y^{-1}).

The dose assessment procedures for this model are applied to a model site with representative environmental conditions. The average population density used is 20 km^{-2} within 2,000 km of the site. Within 50 km of the site, the population density is taken to be 400 km^{-2} . These parameters were obtained from previous UNSCEAR assessments and take into account the transport and dilution of released radionuclides from nuclear installations. The parameters used are assumed to not underestimate dose. Using this model site, the collective effective dose per unit release is obtained for the different release categories. Due to its lack of specificity, this model should be used for general comparisons only. The collective effective doses estimated from commercial nuclear power plant radiological effluent releases are very low especially when compared to other man-made sources of radiation. The doses only represent up to a few percent of the regulatory limits (Harris & Miller, 2008).

From the collective effective doses, effective doses were computed for the entire U.S. population to give average annual doses. This was done by taking the CEDs calculated for each release category, gaseous and liquid, and dividing them by the U.S. population for each year (U.S. Census Bureau, 2010). The effective doses were then summed to give a total dose for each person. The results of these effective doses are given in Table 2. For the 15-year period, total effective doses ranged from $5.42 \times 10^{-8} \text{ mSv}$ ($5.42 \times 10^{-6} \text{ mrem}$) to $1.68 \times 10^{-7} \text{ mSv}$ ($1.68 \times 10^{-5} \text{ mrem}$). The doses to an average person would be expected to be even lower since many do not live near a nuclear power plant. This is just one of several ways to calculate a very general effective dose for the population.

4. U.S. REMF evaluation

An evaluation of all U.S. nuclear power plant radiological environmental monitoring programs (REMP) was conducted from 1995-2007. An attempt was made to assess the significance of the radionuclides detected in the environment compared to natural and other man-made radiation sources. It is important to note that detected concentrations of radionuclides in the local environment as a result of nuclear power radiological releases

are very low. The percentage of plants sampling different pathways, the percent cumulative exposures, and differences between control and indicator measurements were determined.

4.1 Methods

Inspection and analysis of the industry REMP data was taken from the annual summary tables from each nuclear power plant's annual radiological environmental monitoring report. The summary data includes the following parameters: sample medium, type and number of analyses performed, required (LLD), the mean and range of the positive measured values of the indicator locations, the mean, range, and location of the highest indicator annual mean, the mean and range of the positive measured values of the control locations, and the number of non-routine reports sent to the USNRC. In this evaluation, the highest indicator values were compared to the control values.

The following environmental pathways and sample analyses (in parentheses) were investigated: bottom/shoreline sediment (gamma spectral analysis), fish (gamma spectral analysis), edible aquatic invertebrates (gamma spectral analysis), surface water (gamma spectral analysis, gross beta, and ^3H), drinking or potable water (gamma spectral analysis, gross beta, and ^3H), ground water (gamma spectral analysis, gross beta, and ^3H), air particulate filters (gamma spectral analysis and gross beta), airborne radioiodine (^{131}I), milk (^{90}Sr and ^{131}I), food products such as fruits and vegetables (gamma spectral analysis), broadleaf vegetation (gamma spectral analysis), soil (gamma spectral analysis), grass (gamma spectral analysis), and direct radiation using thermoluminescent dosimeters (TLDs). In addition, pathways not normally sampled by most plants, like precipitation, were also studied.

For all data, only positive measured values were used in the statistical calculations. During the study period there were over 1.6×10^6 analyses performed on environmental media collected as part of the required monitoring programs. Broken down, this averages to about 1.27×10^5 analyses y^{-1} and 2.0×10^3 analyses $\text{site}^{-1} \text{y}^{-1}$.

4.2 Results and discussion

4.2.1 Cumulative dose contribution from effluent release pathways

The percent contribution by each pathway to the public was determined using previously compiled effluent data. The calculations provided by each plant from their REMP data identified the most important pathways for their respective sites. Fig. 4 shows the mean results for the seven most frequently sampled pathways or media for all plants. The greatest dose contributor comes from direct radiation released by the plant. This is especially true for BWR plants, which have no secondary loop for the reactor produced steam.

The water, milk, and sediment media, at about the same level, provide the next highest percent contributions to dose. Water media, which includes surface, ground, and drinking types, may contribute to dose to a much larger extent depending on the plant location. Those that are on saltwater sites may not have a known drinking water pathway, or dilution may be so great that submersion doses are low or non-existent. On the other hand, plants on freshwater sites typically have drinking water pathways and less dilution of their effluents (with the exception of sites located on the Great Lakes). All other pathways contribute to a much lesser extent.

Year	Electrical Energy Produced (GW)	U.S. Population ($\times 10^4$)	Annual Effective Dose (mSv GW ⁻¹ person ⁻¹)						
			Gaseous Releases				Liquid Releases		Total
			F/A Gases	Total I-131	Tritium	Particulates	Tritium	F/D Gases	
1995	77.1	266,557	8.36×10^{-8}	1.95×10^{-10}	1.68×10^{-8}	1.28×10^{-9}	2.93×10^{-8}	2.90×10^{-8}	1.60×10^{-7}
1996	77.3	269,667	7.79×10^{-8}	2.75×10^{-10}	1.31×10^{-8}	1.10×10^{-9}	3.18×10^{-8}	2.89×10^{-8}	1.53×10^{-7}
1997	71.9	272,912	1.08×10^{-7}	1.29×10^{-10}	1.90×10^{-8}	1.47×10^{-9}	2.71×10^{-8}	1.22×10^{-8}	1.68×10^{-7}
1998	74.9	276,115	1.38×10^{-8}	2.80×10^{-10}	1.46×10^{-8}	2.66×10^{-9}	2.68×10^{-8}	1.37×10^{-8}	7.19×10^{-8}
1999	82.3	279,295	7.00×10^{-9}	1.75×10^{-10}	1.57×10^{-8}	3.06×10^{-10}	2.83×10^{-8}	1.10×10^{-8}	6.24×10^{-8}
2000	85.2	282,402	7.98×10^{-9}	1.80×10^{-10}	1.48×10^{-8}	1.08×10^{-9}	3.05×10^{-8}	1.07×10^{-8}	6.53×10^{-8}
2001	87.8	285,329	5.58×10^{-9}	9.21×10^{-11}	1.50×10^{-8}	8.57×10^{-10}	2.54×10^{-8}	7.97×10^{-9}	5.49×10^{-8}
2002	88.6	288,173	8.42×10^{-9}	1.95×10^{-10}	1.73×10^{-8}	6.62×10^{-10}	2.70×10^{-8}	1.96×10^{-8}	7.32×10^{-8}
2003	87.0	291,028	1.44×10^{-8}	3.79×10^{-10}	1.51×10^{-8}	3.04×10^{-9}	2.87×10^{-8}	1.15×10^{-8}	7.30×10^{-8}
2004	88.1	293,907	6.94×10^{-9}	2.67×10^{-10}	1.39×10^{-8}	2.07×10^{-10}	2.64×10^{-8}	6.38×10^{-9}	5.42×10^{-8}
2005	88.6	295,753	7.49×10^{-9}	9.78×10^{-11}	1.59×10^{-8}	5.11×10^{-9}	2.77×10^{-8}	5.99×10^{-9}	6.23×10^{-8}
2006	89.3	298,593	5.40×10^{-9}	9.84×10^{-11}	1.28×10^{-8}	4.24×10^{-10}	2.96×10^{-8}	6.18×10^{-9}	5.45×10^{-8}
2007	88.9	301,580	4.82×10^{-9}	1.09×10^{-10}	1.13×10^{-8}	9.48×10^{-9}	2.61×10^{-8}	4.95×10^{-9}	5.67×10^{-8}
2008	88.9	304,375	4.44×10^{-9}	1.03×10^{-10}	1.21×10^{-8}	1.85×10^{-9}	2.82×10^{-8}	1.01×10^{-8}	5.68×10^{-8}
2009	86.8	307,007	5.77×10^{-9}	7.31×10^{-11}	1.14×10^{-8}	3.32×10^{-10}	2.41×10^{-8}	1.41×10^{-8}	5.58×10^{-8}

Table 2. Average effective doses received by members of the public in the U.S. from commercial nuclear power plant radiological effluent releases

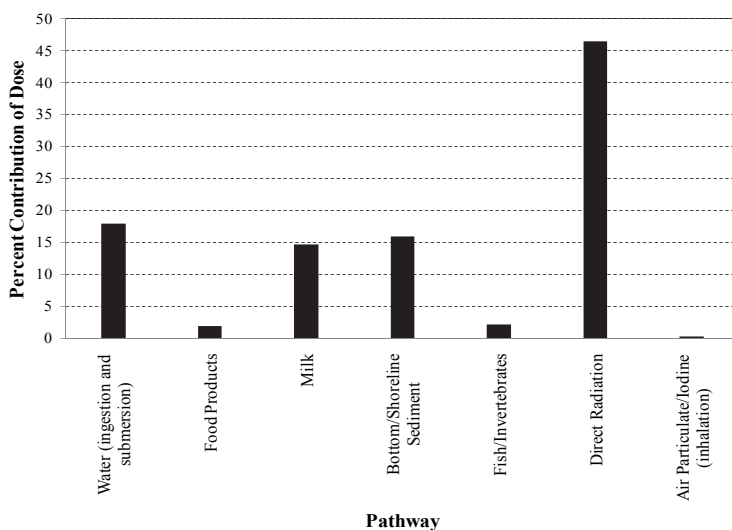


Fig. 4. Percent total cumulative dose contribution of various pathways resulting from U.S. nuclear power plant effluent releases

4.2.2 Plant pathway sampling

The investigation of the number of pathways sampled by each plant is important to gauge the diversity and scope of each plant's REMP in relation to each other. Used in conjunction with the results from Section 4.3.1, omissions of pathways can be reconsidered based on the overall percent contribution of dose. Obviously, programs will vary greatly since the power plant sites themselves also vary greatly. For example, plants may be located on coastal sites, in river valleys, in arid locations, or on small, man-made bodies of water. The level of human activity around the plant will also influence the degree of surveillance. The number of media sampled by plants ranged from five to more than 20, with a mean of 11.

The results of the percentage of plants sampling different media in their REMP are displayed in Fig. 5. As expected, 100% of plants sample for air particulate matter, ^{131}I and direct radiation. Direct radiation is important as it is the greatest dose contributor to members of the public, especially from BWR plants. Milk, once sampled by nearly all plants, is now sampled by only 52% of plants. This is due to the reduction of the milk pathway (from cows or goats) in areas around plants. In lieu of milk sampling, plants may substitute broadleaf vegetation. One important characteristic of the data is that nearly 56% of plants sample groundwater. Recent unplanned tritium releases went unnoticed at several plants due to the lack of groundwater monitoring at those sites. In part due to this study and a national industry initiative, all plants began a groundwater monitoring program starting in 2006. At the time of this research and writing, updated data on nuclear power plant groundwater monitoring was not available. The dose important fish pathway is sampled by 88% of plants. Edible aquatic invertebrates are sampled by only 19% of the plants, mainly due to the lack of the pathway.

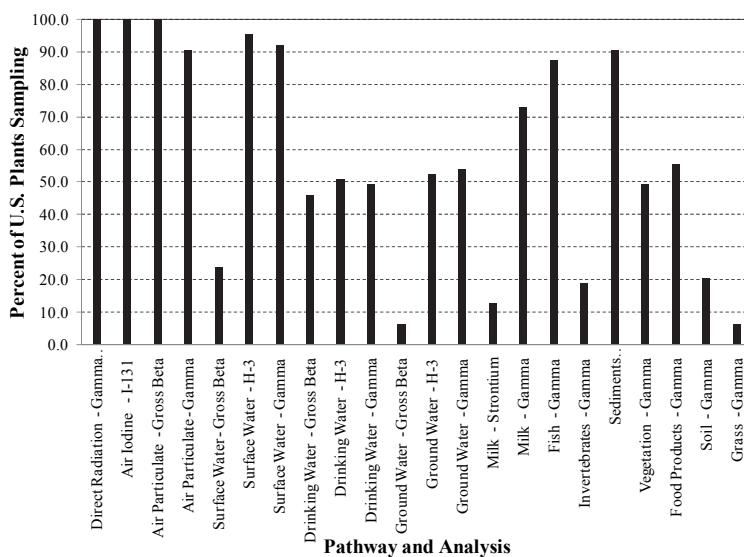


Fig. 5. Percent of U.S. nuclear power plants sampling different REMP pathways and performing specific analyses

4.2.3 REMP summary

Numerical results for the REMP summary are not listed here due to the breath of the study. Comparisons are only made between the control samples and the indicator or test measurements. Direct radiation pathways include radiation from buildings and plant structures, airborne material that might be released from the plant, cosmic radiation, “fallout”, and the naturally occurring radioactive materials in soil, air and water. Analysis of the TLDs, which are used by all plants, indicated that there were no increased radiation levels attributable to plant operations. The mean BWR exposure was slightly higher than that for PWR plants, but the control locations actually gave higher mean values for all plant types.

Airborne pathway measurements include analyses of ^{131}I , gross beta, and gamma spectra. For all ^{131}I measurements, the values were below the LLD. Therefore, the reported mean and median measurements are for half of the LLD values. For the entire 13 years, only one plant reported an indicator value above the LLD. The gross beta and gamma spectral analyses showed no difference between the control and indicator stations. These airborne pathway measurements indicated that there was no increased radioactivity attributable to plant operations.

Terrestrial pathways that include milk, vegetation, grass, and food products, all gave calculated mean indicator measurements that were below that of the controls. Similarly for all waterborne pathways (drinking water, ground water, surface water, fish and invertebrates, and sediments), measurements of the media indicated that there was no adverse radiological impact to the surrounding environment attributed to plant operations for the study period. Individually, several plants have had measurements that resulted in indicator values being significantly higher than those from control stations.

The summary data strongly suggest that for the great majority (>99.9%) of the analyses, the control and indicator concentrations were indistinguishable. Potential plant produced radionuclides were detected in both indicator and control locations. In the past 13 years, the concentration of radionuclides in the environment has stayed nearly level. Prior to this time, radionuclide concentrations showed significant downward trends, mainly due to the decay of “fallout” radionuclides, evidenced in the historical data provided by the plants. The overall trend of the REMP data for these plants is “de minimis” levels of anthropogenic radioactivity with occasional samples showing radioactivity above the LLD. These data also indicate no correlation between total dose and distance from the plants.

The analytical results from the REMP study demonstrate that the routine operation of all facilities had no significant or measurable radiological impact to the environment for the study time period. Also, these environmental surveillance programs continued to demonstrate that the doses to members of the public as a result of nuclear plant operations remained significantly below the federally required dose limits specified in 10 CFR 20 and 40 CFR 190.

5. Tritium recapture study

Tritium is an isotope of hydrogen that decays with a half-life of 12.3 y to helium (^3He), while emitting a low energy beta particle (18.6 keV). In nuclear reactors, tritium is formed in two different ways: by ternary fission of uranium, and by activation (Luykx & Fraser, 1986). Produced tritium that ultimately ends up in the nuclear reactor coolant can then be released into the environment through waste discharge in either gaseous or liquid forms (Kim &

Han, 1999). Because tritium is generated in very large volumes, it is the predominant gaseous and liquid effluent released by these reactors.

Although tritium is not considered to be a particularly toxic radionuclide (Hill and Johnson 1993) and releases by commercial nuclear power plants have traditionally been well below regulatory limits, control and monitoring is important because of sensitive public concerns regarding radioactivity releases (Andersen 1995; Liu et al 2003). This is especially vital at the present time because recent, unplanned tritium releases have occurred at several nuclear power plants in the U.S. These unplanned releases may result in additional dose both to occupational workers and members of the public. This has led to increased scrutiny by plant owners and government agencies. In 2007, Harris also reported that the largest number of non-routine environmental sampling results was from tritium in surface water.

This section describes research conducted at the Cook Nuclear Plant (U.S.) to investigate the behaviour of tritium released in airborne effluents. In addition to studying the behaviour and movement of tritium in the environment, the study has been conducted to help develop a sampling and analysis protocol for other plants to adopt. Methods and results are primarily taken from Hinchcliffe, 2010.

5.1 Background

At the Cook Nuclear Plant, a site consisting of two PWRs, an event in 2007 set off an investigation into tritium release on the site. The plant is located in the state of Michigan along the eastern shore of Lake Michigan. In May of that year sampling began on the site as a result of a leak containing tritium found outside the auxiliary building. This sampling resulted in elevated tritium levels being discovered in the north storm drain outfall, which drains into Lake Michigan. This outfall had previously been sampled on a semi-annual basis with no previous indication of elevated tritium levels (Harris et al., 2008). The investigation concluded that tritium originating in the spent fuel pool was leaving the monitored vents on top of the containment buildings of both units and contributing to the elevated levels. Findings led to increased sampling of precipitation, air-conditioning condensate, surface and well water, and frost formed in refrigerators/freezers (Harris et al. 2008). The importance of precipitation was noted in the form of washout in which tritium can be scavenged by falling raindrops and tritium vapour can exchange with ordinary water in the atmosphere (Chamberlain & Eggleton, 1964; Tokuyama & Oonishi, 1997; Harris et al., 2008). In this way, precipitation becomes contaminated with tritium and sampling can be used to calculate a washout coefficient. This coefficient allows for estimation of tritium washout due to the precipitation which can be used to estimate the extent of tritium recapture on site property (Harris et al., 2008).

After an initial study in 2007 it was decided that additional sampling should be performed to determine the variations in recapture on the site as the weather changed through the year, and that snow should be sampled during the winter. Snow was sampled to determine if there was a difference in washout between rain and snow and to determine if recapture of tritium occurred differently with snow than it did with rain.

5.2 Methodology

The investigation of tritium washout was performed by taking samples at pre-determined site locations and analysing the collected samples for tritium. For rain collection, gauges

with a surface area of $7.85 \times 10^4 \text{ m}^2$ were placed 0.25 m above the ground surface. Thirty two (32) rain gauges were placed in each land-based 22.5° sector of the plant site. Additional gauges were located in the predominant seasonal wind directions; SW in the summer and N and NE in the winter. The rain samples from this investigation were collected between 22 October 2007 and 21 October 2008 during 13 rain events. Snow was collected on 28 March 2008, 11 February 2009 through 16 February 2009, and 5 January 2010 through 10 March 2010.

Samples were taken both inside and outside the plant Protected Area, as shown in Fig. 6 and 7. The sample locations varied in distance from the containment stacks, ranging from 5 m (location 12) to 1.5 km (location 32). For control purposes, location 16 was placed 24 km from the release point. Snow was collected immediately after snow fall events, sampled from the surface of existing snow piles, and sampled with cores to evaluate depth differences from existing piles. Surface snow samples were obtained using 20 mL collection cups. Core samples yielded four to six, 10 cm sections, depending on pile depth. Ground level concentrations of tritium were also determined for calculation of a new washout coefficient. Sample analysis was done using a liquid scintillation counter (Model 2910TR, PerkinElmer). The samples were prepared by mixing 5 mL to 10 mL of the sample with 10 mL of scintillation cocktail in 20 mL vials and counting for 30 minutes. The tritium counting efficiency was 60%, and the lower limit of detection (LLD) was 30 Bq (819 pCi).

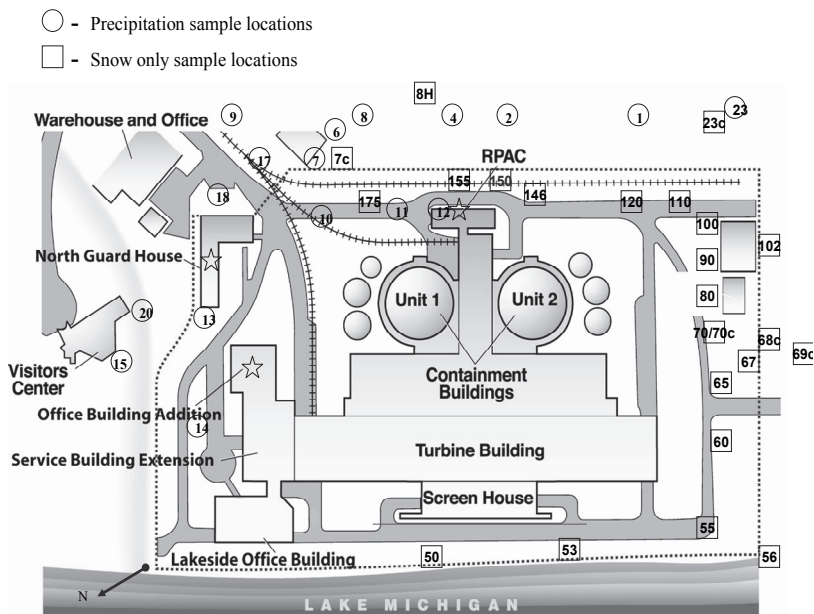


Fig. 6. Rain and snow sample locations located outside the Cook Nuclear Plant protected area

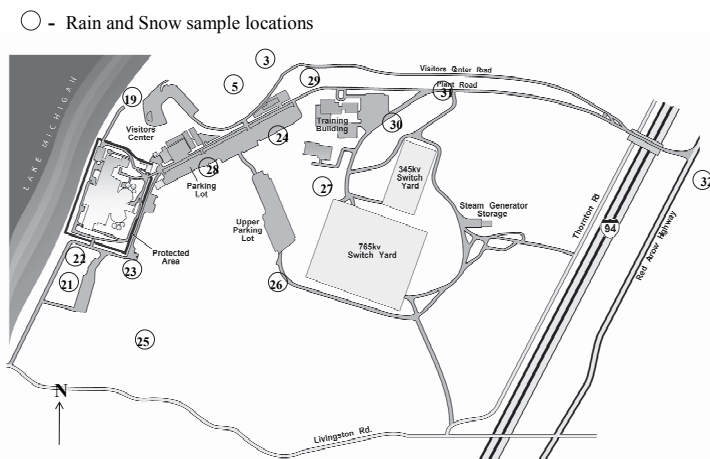


Fig. 7. Sample locations for rain and snow within and immediately outside the Cook Nuclear Plant protected area

5.3 Results

5.3.1 Tritium concentrations

In total, 23 of the 32 rain locations had a positive result for tritium at some point in the study. With the snow, 44 of 56 sample locations resulted in a tritium concentration above the LLD. The highest rain concentration was 514 Bq L^{-1} ($13,900 \text{ pCi L}^{-1}$), and occurred at location 18, 130 m NE of the Unit 1 containment vent. The highest snow concentration was $1,014 \text{ Bq L}^{-1}$ ($27,400 \text{ pCi L}^{-1}$), and occurred at snow sample location 110, 140 m SSE of the Unit 1 containment vent. The highest concentrations of tritium in the snow occurred in the old snow that had accumulated in piles on site. The positive results were found to match well with the meteorological data, with positive samples collected in the predominant wind direction. There were a total of five core samples taken and all indicated the presence of tritium in at least one core piece. Four of the five core samples showed an increasing concentration of tritium closer to the surface of the snow pile. The only core sample that did not show this pattern was core sample V which was taken from the visitor's parking lot, 200 m NNE from the Unit 1 containment vent. All core pieces in this sample were below LLD, with the exception of core piece "2" (second piece from the bottom of the core).

5.3.2 Washout

A rain washout coefficient was calculated from the measured tritium concentrations found in the samples, the atmospheric tritium level, and the meteorological data gathered at the Cook Nuclear Plant. The washout coefficient is calculated by:

$$\Lambda = \frac{\omega}{X_0 \times H_{\text{eff}}} \quad (3)$$

where: Λ = washout coefficient (s^{-1}); ω = tritium deposition rate ($Bq\ m^{-2}\ s^{-1}$); χ_0 = atmospheric tritium concentration at ground-level ($Bq\ m^{-3}$); and H_{eff} = effective height (m). The effective height is calculated using the dispersion equation (Chamberlain & Eggleton, 1964):

$$H_{eff} = \frac{\sum_s \frac{Q}{\sqrt{2\pi}\sigma_{ys}U_s}}{X_{0,cal}} \quad (4)$$

where: Q = tritium emission rate ($Bq\ m^{-2}\ s^{-1}$); σ_{ys} = standard deviation of distribution of concentration in the y direction (m); U_s = mean wind speed ($m\ s^{-1}$); $X_{0,cal}$ = mean concentration for the ground-level atmospheric concentration (m). The subscript S refers to the atmospheric stability. Using the local meteorological conditions, the deposition rate is given as:

$$\omega = \frac{C \times I_R}{3600} \quad (5)$$

where: C = tritium concentration in rainwater ($Bq\ L^{-1}$); and I_R = mean rainfall intensity ($mm\ h^{-1}$).

The emission rates were calculated using the continuous tritium release rates from the Cook Nuclear Plant Annual Radioactive Effluent Release Reports (ARERR) for the periods on which the precipitation events occurred. The precipitation intensities were calculated for each precipitation event, with an average value of $3.1\ mm\ h^{-1}$ for rain, and $1.1\ mm\ h^{-1}$ for the snow. For the rain samples the washout coefficient values ranged from $7.84 \times 10^{-7}\ s^{-1}$ to $1.13 \times 10^{-4}\ s^{-1}$ with an average washout coefficient of $(2.04 \pm 1.85) \times 10^{-5}\ s^{-1}$. Washout coefficients were only calculated for the fresh snow. The reason for this is that as the snow sits, it accumulates tritium from the atmosphere, and thus skews the value of the washout coefficient. The fresh snow was analysed shortly after the snow event. The calculated washout coefficients for the fresh snow ranged from $2.21 \times 10^{-6}\ s^{-1}$ to $2.33 \times 10^{-5}\ s^{-1}$ with an average value of $(1.30 \pm 0.75) \times 10^{-5}\ s^{-1}$. Upon comparing the rain and snow washout coefficient sample populations using a two sample t-test, it was determined that there was a significant difference between the washout coefficients in the snow and rain at the 0.05 decision rule level.

5.4 Discussion

Several other studies have reported values of washout coefficients in the literature. A theoretical washout coefficient based on the rate of exchange of tritiated water (HTO) vapour by rain, was calculated to be $10^{-4}\ s^{-1}$ (Chamberlain & Eggleton, 1964). In Japan, Tokuyama & Oonishi (1997) used a mean rainfall intensity of $2\ mm\ h^{-1}$ and calculated a washout coefficient from releases at a nuclear plant to be $(7.3 \pm 4.1) \times 10^{-5}\ s^{-1}$. The previous study at Cook Nuclear Plant calculated a washout coefficient of $(9.70 \pm 8.40) \times 10^{-5}\ s^{-1}$, based on a rainfall intensity of $6.2\ mm\ h^{-1}$ (Harris et al., 2008). The rain washout coefficient in this study is smaller than those previously listed, but on the same order of magnitude as Tokuyama & Oonishi and Harris et al. The release rates used for this study were monthly averages rather than instantaneous rates used in several of the other studies. In addition, the calculated effective heights were calculated higher in this study than the other studies that listed the effective height used.

Annual fluctuations of weather have multiple effects on the process of tritium recapture at nuclear sites. The locations of greatest recapture vary between seasons and even within

particular seasons. Snow recapture at the Cook Nuclear Plant occurred in locations of the site that previously were not known for rain recapture, thus presenting new pathways of tritium movement needing to be studied. Snow also presents a unique problem, as it is not removed from the site at the same rate that rain would be removed, thus allowing for tritium to be absorbed into snow piles that accumulate around the site. This allows for snow piles to obtain tritium concentrations far above what simple washout can cause in precipitation alone. The piles also appear to accumulate a higher concentration of tritium on and near the surface of the pile where the snow is exposed to the atmosphere.

The results here suggest that individual sites will have to come up with their own sampling methods based on individual site characteristics such as annual fluctuations in wind and precipitation. Variables will change from site to site, and long term annual studies will need to be performed to fully comprehend the behaviour of tritium recapture. A single industry model would be unable to account for the many individual variables that would change between sites. Studies are on-going at Cook Nuclear Plant to better understand tritium behaviour.

6. Future research

Although the research presented here provided important insights into commercial nuclear power plant discharges, more studies are needed to truly understand effluent trends and nuclear power plant radioactivity. As long as commercial nuclear power plants continue to operate and release radioactivity into the environment, there will always be a need to monitor, track, and evaluate these releases. This is especially true as new power plants are constructed and existing plants make operational changes. Evolutions in standards, recommendations, and regulations may also warrant studies to address the potential impact. One expansive area of research that is developing comes from recommendations made by the ICRP in Publications 103 and 108 (2007, 2009). Specifically there is mention of radiological protection of the environment and the development of reference plants and animals. If nations adopt these recommendations, large scale studies at nuclear power plants may need to be undertaken.

In the U.S., a number of potential new areas of research involving nuclear power radiological releases are being investigated. First, revisions in 2009 of USNRC Regulatory Guides 1.21 and 4.1 have prompted plants to begin monitoring their ^{14}C emissions. Only a few plants had done this prior to the release of these revisions and now several organizations are evaluating methods and procedures to best accomplish this. Other countries are also evaluating this scenario, if they are not already monitoring for ^{14}C . In conjunction with the tritium washout study presented in Section 5, several plants are conducting their own studies on tritium releases and movement. The majority of plants in the U.S. are now monitoring groundwater and studying its movement and transport of radionuclides. Finally, with the construction and operation of new plants, studies on effluent fate and transport, dose assessment and environmental impact are sure to be conducted.

7. Conclusion

In conclusion, the research presented here will hopefully provide stakeholders with some additional insights on assessing nuclear power plant radiological releases and

environmental monitoring programs. Evaluation of radionuclide impacts in terms of potential increased dose to people, in relation to natural background, is necessary to determine the true significance of any detection. Maintained effluent tracking and analysis will continue to be important for the future of the commercial nuclear power industry. Effluent trending may also reveal insight into the effect of increased reactor lifetime operation on radioactivity releases. Currently, many plants have been approved for, or are applying for, operating license extensions. Tracking data for siting of new nuclear power plants may also be used to determine environmental radionuclide build-up and long-term nuclear power health effects.

Although the research presented here showed that normal nuclear power operations have no significant effect on the environment, continued surveillance is important. The potential development of new pathways may require changes in monitoring techniques. Doses to members of the general public, and even occupational workers, may increase because of these pathways. Finally, continued industry analysis of radiological effluent releases and environmental monitoring are important for maintaining favourable public opinion about nuclear power. The more accurate, scientifically based information that citizens can be provided with, the more likely they are to make informed, non-emotional judgments about nuclear power.

8. Acknowledgment

This chapter was written from research results and material developed by the author over the last decade. I wish to thank the many friends, family, and colleagues, too numerous to mention by name, for their contributions. Special appreciation goes out to Dr. David Miller, Dr. Richard Brey, Dr. Thomas Gesell, Dr. George Sandison, Dr. George Miley, and the late Dr. Herman Cember. Their guidance and support have truly helped shape not only my career, but my life as well. I would also like to thank Dr. Kenneth Sejkora for sharing his knowledge in nuclear reactor aspects of environmental monitoring and effluents. I am also indebted to my students, especially William Hinchcliffe, Gavin Hawkey, and Peter Lee, for their assistance in many parts of the research presented in this chapter. Lastly, and most importantly, I would like to thank my wife, Dr. Maria Okuniewski. If it were not for her constant support, encouragement, and love, I would not be where I am today.

9. References

- Andersen R. (1995). Criteria for radiological releases, In: *Radiation Protection at Nuclear Reactors*, C. Maletskos, (Ed.), 21-44, MPP, ISBN 978-094-4838-55-6, Madison, USA
- Chamberlain, A. & Eggleton, A. (1964). Washout of tritiated water vapour by rain. *J Air Wat Poll*, Vol.8, pp. 135-149
- Eisenbud, M. & Gesell, T. (1997). *Environmental Radioactivity* (4th), Academic Press, ISBN 978-012-2351-54-9, San Diego, USA
- Electric Power Research Institute (2003). *Strategies for managing liquid effluents-options, actions, and results*, EPRI, Palo Alto, USA
- Glasstone, S. & Jordan, W. (1980). *Nuclear Power and its Environmental Effects*, American Nuclear Society, ISBN 978-089-4480-22-5, La Grange Park, USA
- Gilbert, R. (1994). *Statistical Methods for Environmental Pollution Monitoring*, Van Nostrand Reinhold, ISBN 978-0471288787, New York, USA

- Harris, J. (2002). *Comparative Study of Commercial Nuclear Power Plant Radiological Effluents*, University of Illinois, Urbana, USA
- Harris, J. (2007). *Public Health Analysis Resulting from Commercial Nuclear Power Plant Radiological Emissions*, Purdue University, West Lafayette, USA
- Harris, J. & Miller, D. (2008). Radiological effluents released by U.S. commercial nuclear power plants from 1995-2005. *Health Phys*, Vol.96, pp. 734-743
- Harris, J.; Miller, D.& Foster, D (2008). Tritium behavior at a nuclear power reactor due to airborne releases. *Health Phys*, Vol.95, pp. 203-212
- Hill, R. & Johnson, J. (1993). Metabolism and dosimetry of tritium. *Health Phys* Vol.65, pp. 628-647
- Hinchcliffe, W. (2010). *Investigation of Tritium Recapture at Cook Nuclear Power Plant from Airborne Effluent Releases*, Idaho State University, Pocatello, USA
- Hollander, M. & Wolfe, D. (1999). *Nonparametric Statistical Methods*, Wiley, ISBN 978-047-1190-45-5, New York, USA
- IAEA (2010). *Nuclear Power Reactors in the World (2010)*, IAEA, ISBN 978-92-0-105610-8, Vienna, Austria
- IAEA (2011). Nuclear Power Plant Information, In: *IAEA PRIS Database*, 10.03.2011, Available from: <http://www.iaea.org/cgi-bin/db.page.pl/pris.charts.htm>
- ICRP (1977). *Recommendations of the ICRP - ICRP Publication 26*, Pergamon Press, ISBN 978-085-951-080-6, Oxford, England
- ICRP (1978). *Radionuclide Release into the Environment: Assessment of Doses to Man - ICRP Publication 29*, Pergamon Press, ISBN 978-008-0323-35-0, Oxford, England
- ICRP (1991). *1990 Recommendations of the ICRP -ICRP Publication 60*, Pergamon Press, ISBN 978-008-0411-44-6, Oxford, England
- ICRP (2007). *2007 Recommendations of the ICRP - ICRP Publication 103*, Pergamon Press, ISBN 978-070-2030-48-2, Oxford, England
- ICRP (2009). *Environmental Protection: the Concept and use of Reference Animals and Plants - ICRP Publication 108*, Pergamon Press, ISBN 978-044-4529-34-3, Oxford, England
- Jablon, S. et al. (1991). Cancer in populations living near nuclear facilities, a survey of mortality nationwide and incidence in two states. *J Am Med Assoc* Vol.265, pp. 1403-1408
- Kahn, B. (1980). Composition and measurement of radionuclides in liquid effluent from nuclear power stations, In: *Effluent and Environmental Radiation Surveillance*, J. Kelly, (Ed.), 63-74, American Society for Testing and Materials, Johnson, USA
- Kim, C. & Han, M. (1999). Dose assessment and behavior of tritium in environmental samples around Wolsong nuclear power plant. *Appl Radiat Isot*, Vol.50, pp. 783-791
- Liu, C.; Chao, J. & Lin, C. (2003). Tritium release from nuclear power plants in Taiwan. *Health Phys*, Vol.84, pp. 361-367
- Lopez-Abente, G. et al. (1999). Leukemia, lymphomas, and myeloma mortality in the vicinity of nuclear power plants and nuclear fuel facilities in Spain. *Cancer Epidemiology, Biomarkers & Prevention*, Vol8, pp.925-934
- Luykx, F. & Fraser, G. (1986). Tritium releases from nuclear power plants and nuclear fuel processing plants. *Radiat Prot Dosim* Vol16, pp. 31-36
- NCRP (1985). *Carbon-14 in the environment - NCRP Report No. 81*, NCRP, ISBN , Bethesda, USA

- NCRP (1987). Public radiation exposure from nuclear power generation in the United States - NCRP Report No. 92, NCRP, ISBN , Bethesda, USA
- Nedveckaite, T. et al. (2000). Environmental releases of radioactivity and the incidence of thyroid disease at the Ignalina NPP. *Health Phys*, Vol.79, pp. 666-674
- Patrick, C. (1977). Trends in public health in the population near nuclear facilities: a critical assessment. *Nucl Saf*, Vol.18, pp. 647-662
- Quindos Poncela, L. et al. (2003). Natural radiation exposure in the vicinity of Spanish nuclear power stations. *Health Phys*, Vol.85, pp. 594-598
- Shleien, B.; Rutenber, A. & Sage, M. (1991). Epidemiologic studies of cancer in populations near nuclear facilities. *Health Phys*, Vol.61, pp. 699-713
- Tokuyama, H. & Oonishi, M. (1997). Precipitation washout of tritiated water vapor from a nuclear reactor. *J Environ Radioact*, Vol.34, pp. 59-68
- United Nations Scientific Committee on the Effects of Atomic Radiation (2000). *Sources and Effects of Ionizing Radiation*, UN, ISBN 978-921-1422-39-9, New York, USA
- United States Census Bureau (2010). *Statistical abstract of the United States: 2010*, GPO, Washington, D.C., USA
- USEPA (1977). *Environmental radiation protection standards for nuclear power operations. 40 CFR 190, 42 FR 2860, January 13, 1977*, GPO, Washington, D.C., USA
- USNRC (1975). *Programs for monitoring radioactivity in the environs of nuclear power plants. Regulatory Guide 4.1, rev. 2*, GPO, Washington, D.C., USA
- USNRC (1976a). *Calculation of releases of radioactive materials in gaseous and liquid effluents from boiling water reactors, NUREG-0016*, GPO, Washington, D.C., USA
- USNRC (1976b). *Calculation of releases of radioactive materials in gaseous and liquid effluents from pressurized water reactors, NUREG-0017*, GPO, Washington, D.C., USA
- USNRC (1978). *Preparation of radiological effluent technical specifications for nuclear power plants, NUREG -0133*, GPO, Washington, D.C., USA
- USNRC (1991). *Standards for protection against radiation. 10 CFR 20, 56 FR 23361, May 21, 1991*, GPO, Washington, D.C., USA
- USNRC (1995). *Dose commitments due to radioactive releases from nuclear power plant sites in 1991, NUREG/CR-2850*, GPO, Washington, D.C., USA
- USNRC (1996). *Technical specifications on effluents from nuclear power reactors. 10 CFR 50.36a, 61 FR 39299, July 29, 1996*, GPO, Washington, D.C., USA
- Vold, E. (1983). Ingestion pathway factor in dose assessment for annual airborne releases of radioactivity. *Health Phys*, Vol.47, pp. 429-441
- Walmsley, A. et al. (1991). The distribution of doses to members of the public around UK civil nuclear sites. *Radia Protect Dosimetry*, Vol.36, pp. 215-218
- Ziqiang, P. et al. (1996). Radiological environmental impact of the nuclear industry in China. *Health Phys*, Vol.71, pp. 847-862

Radiological and Environmental Effects in Ignalina Nuclear Power Plant Cooling Pond – Lake Druksiai: From Plant put in Operation to Shut Down Period of Time

Tatjana Nedveckaite¹, Danute Marciulioniene²,
Jonas Mazeika² and Ricardas Paskauskas^{2,3}

¹*Centre of Physical Science and Technology*

²*Nature Research Centre*

³*Costal Research and Planning Institute, Klaipeda university
Lithuania*

1. Introduction

Ignalina Nuclear Power Plant (INPP) is situated in the Northeastern part of Lithuania close to the borders with Latvia and Belarus at a Lake Druksiai utilized as cooling pond (Fig. 1). The two RBMK-1500 reactor units, Unit 1 and Unit 2, were put into operation in December 1983 and August 1987, respectively. Like Chernobyl NPP, the INPP was equipped by RBMK type reactors, i.e. channel-type, graphite moderated pressure tube boiling water nuclear reactors. The RBMK reactors belong to the thermal neutron reactor category each of a design capacity of 1500 MW(e). Unit 1 was shut down on December 31, 2004 and Unit 2 on December 31, 2009 (<http://www.iaea.it>).

Lake Druksiai is the largest lake in Lithuania and has its eastern margin in Belarus, where the lake is called Drisvyaty. The total volume of water is about 369×10^6 m³ (water level altitude of 141.6 m). The total area of the lake, including nine islands, is 49 km² (6.7 km² in Belarus, 42.3 km² in Lithuania). The greatest depth of the lake is 33.3 m and the average is 7.6 m. The length of the lake is 14.3 km, the maximum width 5.3 km and the perimeter 60.5 km. Drainage area of the lake is only 613 km².

The water regime of Lake Druksiai is formed by interaction of natural and anthropogenic factors. The main natural factors are the climatic conditions of the region which determine the amount of precipitations onto the surface of the water reservoir and natural evaporation from the lake surface and watershed. The anthropogenic factors, which are mainly related with INPP operation, are water discharges by the hydro-engineering complex. The yearly amount of water discharged from INPP is 9 times the volume of the lake and 27 times the natural annual influx of water to the lake.

The aim of this study was to evaluate radiological and environmental effects of radioactive, chemical and thermal pollution in cooling pond of INPP (Lake Druksiai). Main efforts were given to assess the presumptive radioactive impact on the lake non-human biota, with special emphasize on macrophytes and fish communities. Macrophytes were selected as

appropriate biological indicators of changes in radioecological situation which comprise one of the largest biomass and able to intensive accumulate radioactive and other substances.

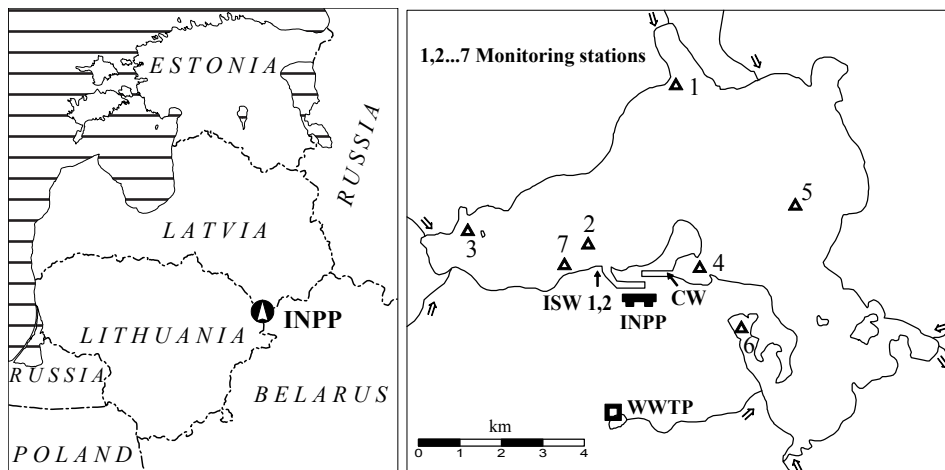


Fig. 1. The location of INPP (left) and permanent sampling (monitoring) stations, industrial storm water (ISW 1.2), cooling water (CW) and waste water treatment plant (WWTP) channels in Lake Druksiai (right)

The need for a systematic approach to the radiological assessment of non-human biota is now accepted by a number of international and national bodies (US DOE, 2002; ICRP, 2008). This requires the development and testing of an integrated approach where decision making can be guided by scientific judgments. The assessment of nuclear sites in context of comparison of non-human biota exposure due to discharged anthropogenic radionuclides with that due to background radiation is required and presented in this study.

2. Materials and methods

2.1 Lithuanian State research and academic institutions INPP environment investigations

The purpose of the environment investigation programmes (Lithuanian State Scientific Research Programme, 1998) was to detect INPP impacts, as they occur, to estimate their magnitude and ensure that they are the consequence of a well identified activity. The INPP environment investigation programs include all environmental exposure pathways that may exhibit long term concentration effects, such as in the case of the Lake Druksiai sediments. This investigation allows also the assessment of the effectiveness and mitigation of remedial measures and includes the follow-up of impacts and their verification against predictions. Samples of lake water, bottom sediments and non-human biota were collected and measured from the very beginning of INPP operation up to shut down period of time.

2.2 Anthropogenic radioactive pollution and natural-background radionuclides

The first stage in the distribution of radionuclides in freshwater ecosystem is quick and intense processes of accumulation of radionuclides in the bottom sediments. That stipulates the rather rapid decrease of the amounts of radionuclides in water. Therefore, data of

radionuclide activity concentrations in the water are insufficient in the assessment of the pollution of the freshwater ecosystem by radionuclides. Bottom sediments reflect the long-term pollution of Lake Druksiai by anthropogenic radionuclides.

This investigation amongst others presents the comparison of freshwater macrophytes and fish exposure due to discharged anthropogenic radionuclides (^{54}Mn , ^{60}Co , ^{90}Sr , $^{134,137}\text{Cs}$) with that due to semi-natural and background radionuclides (^3H , ^{14}C , ^{40}K , ^{210}Pb , ^{210}Po , ^{238}U , ^{226}Ra , ^{232}Th) mostly based on bottom sediments activity data accumulated during Lake Druksiai radiogeochimical mapping and other measurements, as presented in Fig. 2-4.

An assumption in the calculations was that the spatial distribution of investigated radionuclides in the INPP cooling-pond bottom sediments was uniformly distributed. However, the largest amounts of activated corrosion product radionuclides (^{54}Mn and ^{90}Co) coming from the INPP enter the lake with cooling waters (CW) and industrial stormwater discharge (ISW-1,2) outflows. The specific activity of activated corrosion products remains generally low in much of the lake and is concentrated especially close to the outflows (Fig. 3).

Frequency histograms depicting activity concentrations of some primary anthropogenic and naturally-occurring radionuclides in Lake Druksiai sediments are presented in Fig. 4.

Long-term radioecological investigations of Lake Druksiai showed that during the period of 1988–2008 the highest values of ^{137}Cs , ^{90}Sr , ^{60}Co and ^{54}Mn activity concentration in bottom sediments was estimated in 1988–1993 when both Units of INPP were operating. The tendency of decrease of the activity concentration of these most important radionuclides in the bottom sediments was observed from the beginning of 1996 (Fig. 5).

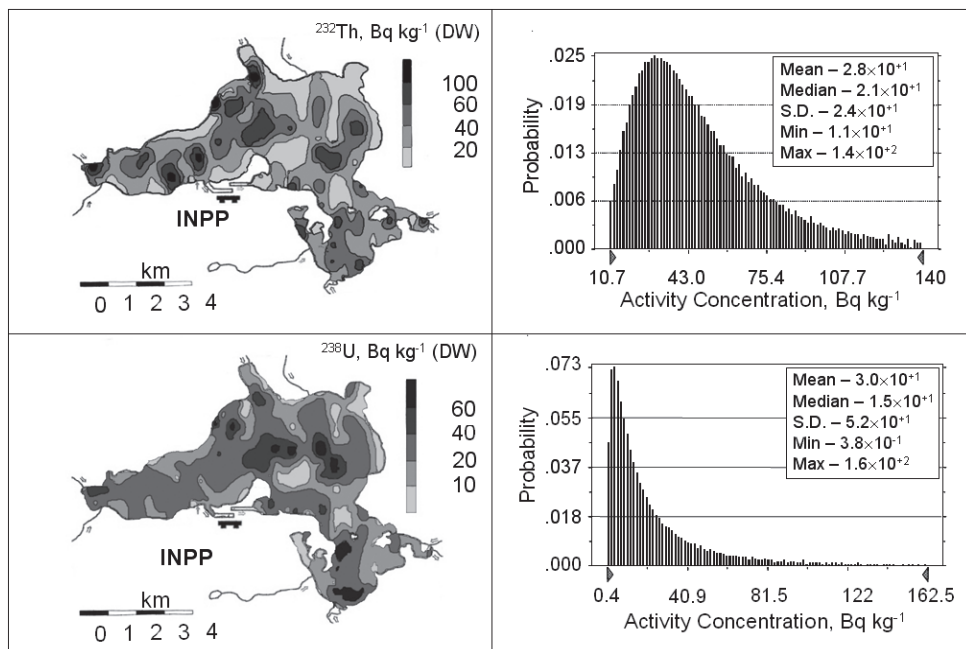


Fig. 2. The maps of spatial distributions (left) and frequency histograms (right) depicting activity concentrations of naturally-occurring background ^{232}Th and ^{238}U in Lake Druksiai sediments

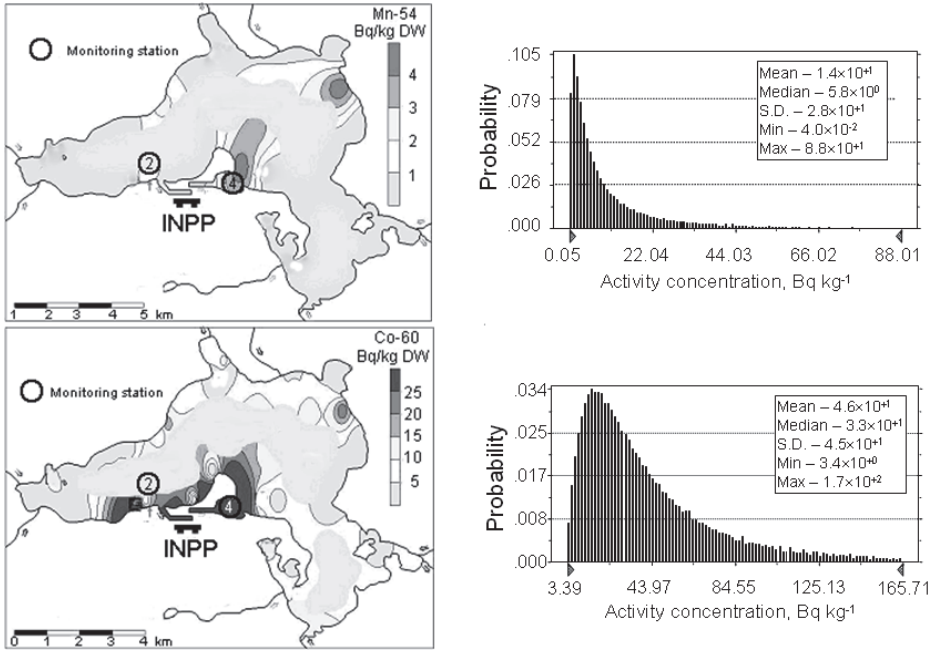


Fig. 3. The spatial pattern of activated corrosion products ⁵⁴Mn and ⁹⁰Co in bottom sediments (left) and frequency histograms (right) of Lake Druksiai. The highest activity concentrations corresponded the ISW-1,2 and CW sampling points

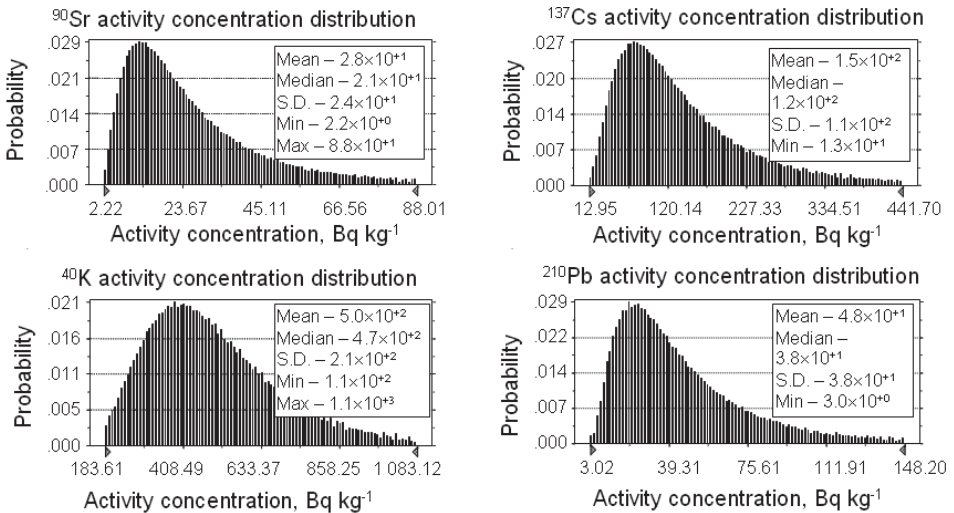


Fig. 4. Frequency histograms depicting activity concentrations of some anthropogenic and naturally occurring radionuclides in Lake Druksiai bottom sediment

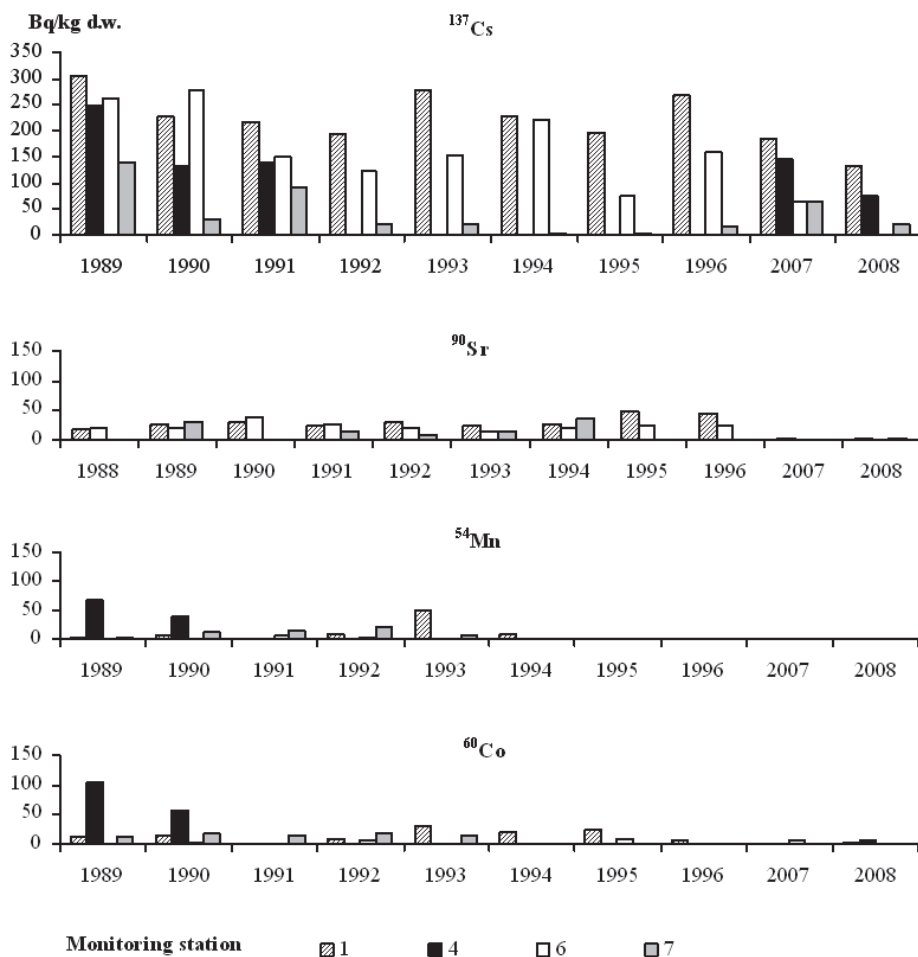


Fig. 5. Time-dependent activity concentration of anthropogenic radionuclides in bottom sediment of Lake Druksiai

Traces of ^3H and ^{14}C originating from the INPP are found in the surface water (Fig. 6). For the period of 1980-2008 the highest ^3H activity concentration in Lake Druksiai was in 2003 year and reached 24 Bq/l. During this period ^3H activity concentration in the background water bodies was 2-3 Bq/l, so approximately 20 Bq/l was originated from INPP releases. ^{14}C activity concentration in background water bodies in Lithuania well fits with the international data for Northern Hemisphere. The excess of ^{14}C originated from thermonuclear weapon tests declines almost to the ^{14}C level of cosmogenic origin for all studied surface water bodies in Lithuania. From period of 1992-1993 in the atmosphere and in the surface water all over the world predominates ^{14}C of cosmogenic origin. Almost for all period of ^{14}C observation in surface water influence of INPP has been hardly estimated. Only from 2002 the ^{14}C excess in water influenced by INPP was observed. Very insignificant

fraction of ^{14}C originated from INPP in surface water bodies can be observed in channels and in Lake Druksiai. In 2005 ^{14}C activity in water from outlet channel compared to background level has increased about 30%. But in 2007 ^{14}C activity already did not differ from background level (Mazeika, 2010).

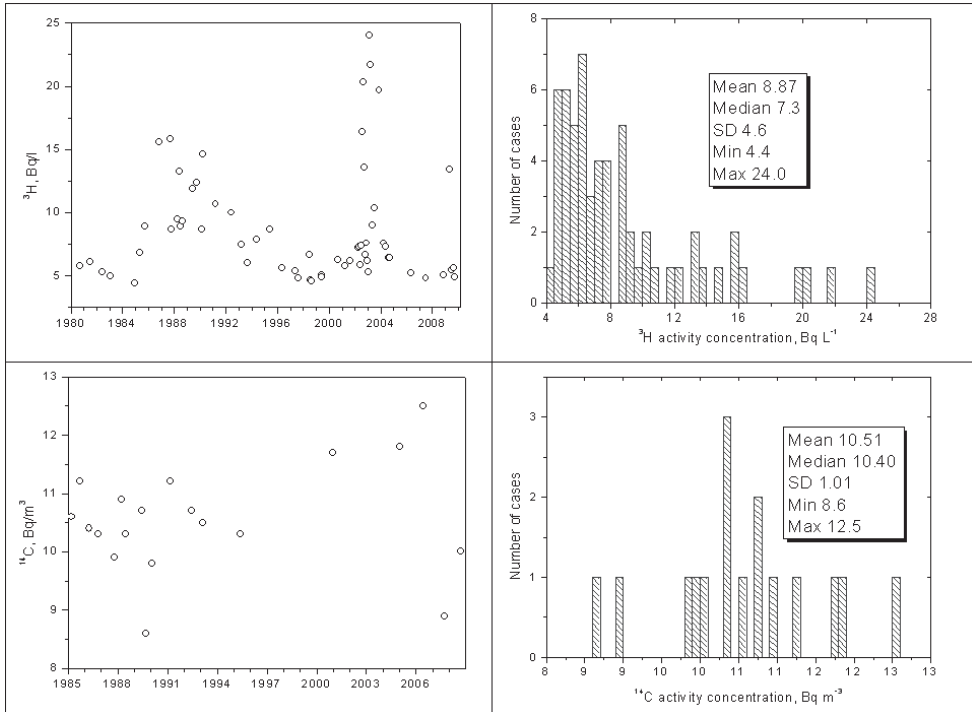


Fig. 6. Time-dependent activity concentrations of ^3H and ^{14}C in Lake Druksiai water (left) and frequency histograms (right)

2.2 Chemical and thermal pollution

The Lake Druksiai was impacted not only by radionuclide pollutions, but also by chemical and thermal pollution. Ignalina NPP discharges into the Lake Druksiai various waste water, which are mainly multicomponent mixtures of chemicals substances (biogenic elements, diluted weak organic acids, heavy metals, petrolic hydrocarbons and so on (Joksas, 1998)). The main pollution source of Lake Druksiai is the treated waste water used for household needs in settlements, Visaginas town and INPP industrial storm water sewers. The wastewater treatment plant is designed for biological treatment and complementary cleaning with sand filters. The treated waste water is discharged into Lake Druksiai through the tertiary treatment pond. However, these facilities can nowadays be considered as a secondary source of organic pollution since the settled biomass or superior plants have not been removed and the accumulation of the produced biomass leads to a secondary eutrophication process. Around 5.5×10^6 – 8.5×10^6 m³ of water enters Lake Druksiai annually from the wastewater treatment plant.

Actually the household waste water discharges from Visaginas town and the INPP are major contributors of nutrients into the lake. (Fig. 7). Up to 1000 tons of organic carbon, 700 tons of nitrogen and 50 tons of phosphorus has been entering the lake annually with maximum values before the year 1991 (Mazeika et al., 2006).

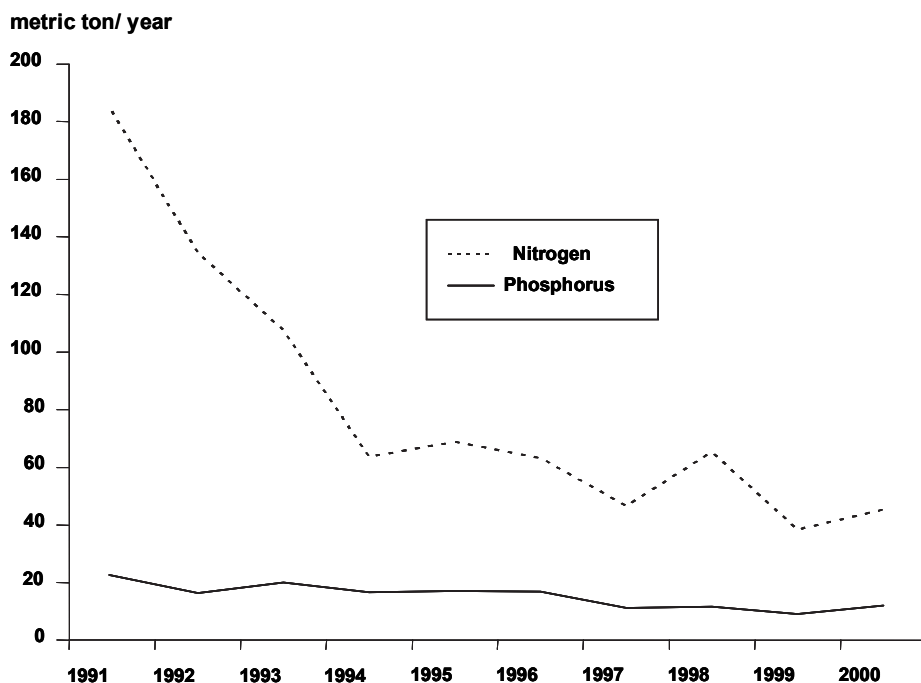


Fig. 7. Nitrogen and phosphorus load into Lake Druksiai

It was evaluated that mean annual concentrations of nitrogen and phosphorus in treated effluents even after the pond of additional purification at that time were 37.7 mg N/l and 3.5 mg P/l accordingly. These figures considerably decreased in the last few decades due to improvement of the purification facility of household effluent. Still this source supplies 55% of nitrogen and 80 % of phosphorus of total annual amount to the lake (Table 1) (Mazeika et al., 2006).

A slightly increasing tendency of total dissolved salts in the water has been observed recently. Waters of Lake Druksiai are dominantly bicarbonate-calcium with medium total dissolved solids (TDS) content. Evaporation from the surface of a lake was expected to become the most important push to increase the concentration of salts in the remaining water. However, it did not have a noticeable effect during several decades of operation of the INPP mainly due to the decrease of HCO_3^- and Ca^{2+} concentration despite the fact (Table 2) that the content of chlorides, sodium, potassium, sulphates, magnesium increased (Salickaite-Bunikiene & Kirkutyte, 2003; Paskauskas et al., 2009).

Sources	N_t metric tons year ⁻¹	P_t metric tons year ⁻¹
Domestic and urban runoff	85.53	15.291
stormwater drainage of INPP site 1,2	1.663	0.244
stormwater drainage of INPP site 3	0.335	0.081
treated household effluents of INPP and Visaginas	81.625	14.720
stormwater drainage of Visaginas town 2	0.617	0.046
stormwater drainage of Visaginas town 1	0.416	0.04
stormwater drainage of site of spent nuclear fuel storage facility	0.870	0.16
Natural runoff	62.02	3.88
Total input	147.54	19.17
Prorva river (output)	98	14.11

Table 1. Long-term balance (1991-2000) of total nitrogen (N_t) and total phosphorus (P_t) load to Lake Druksiai

Parameters	Periods				
	1979–1983	1984–1988	1989–1993	1994–1997	2001–2006
Cl ⁻ , mg/l	8.8	9.9	10.7	9.8	12.9
SO ₄ ²⁻ , mg/l	8.9	12.6	18.6	19.3	18.0
HCO ₃ ⁻ , mg/l	160.5	150.4	157.6	159.4	169.5
Ca ²⁺ , mg/l	39.3	35.8	36.8	35.8	37.9
Mg ²⁺ , mg/l	10.0	10.9	12.9	13.8	15.9
Na ⁺ , mg/l	4.6	6.3	7.0	6.9	7.5
K ⁺ , mg/l	1.8	2.7	3.0	2.9	3.2
TDS, mg/l	233.9	228.6	246.6	247.9	264.3

Table 2. Average long-term main ion concentrations and TDS values in Lake Druksiai

Direct contamination on Lake Druksiai emanate from the industrial areas and the town via storm water release systems, supplying the lake ecosystem with many contaminants and inhibitors of biological processes. However, the concentration of copper, lead, chrome, cadmium and nickel has not exceeded the allowable values for the water quality (Marciulioniene et al. 1998)

Concentrations of heavy metals (HM) in the waste water of the INPP and Lake Druksiai during the INPP operation time was higher in comparison with concentrations measured before the plant had been launched. Maximal concentrations of HM (soluble and suspended forms) discharged into the lake from the ISW-1,2 and WWTP channels (Table 3). The largest amount of Fe, Mn and Co got into the lake and migrated together with suspended particles. The main part of these metals deposited in the bottom sediments (Table 4) and the other part of them were involved into biological processes.

Sampling station No.	Year	Cd	Cr	Cu	Ni	Mn	Zn	Pb
		µg/l						
1	1996	-	0.2	3.7	1.3	15.1	4.5	0.25
	1997	-	0.05	4.8	1.1	2.0	6.0	1.4
	1999	<0.1	<0.2	4.6	0.57	1.0	0.2	0.3
2	1996	-	0.7	4.1	0.6	15.1	2.9	0.3
	1997	-	0.01	3.7	<1	0.6	<2.0	<1
	1999	<0.1	0.3	6.0	0.22	38.0	1.8	3.1
6	1996	-	0.7	3.9	1.4	29.6	4.0	0.3
	1997	-	<0.01	3.3	1.0	0.7	1.0	<1
	1999	<0.1	0.6	6.4	0.58	125.0	29.0	2.9

Table 3. Average midsummer heavy metals concentrations in water of Lake Druksiai

It has been estimated that heavy metal contaminated sediments (from intermediate to high level of contamination) cover 27.5 % of the lake bottom sediment area, slightly polluted area covers 41%, and non-polluted area covers about 32% (Joksas et al., 1998). Pollution with oil products was identified in 3.9 % of the bottom sediment area but major part of this has a natural origin since the natural hydrocarbons dominate. Concentration of hydrocarbons in the water was not high and varied from 2 to 44 µg/l. Their concentration in the surface layer of bottom sediments was from 1.12 to 127 mg/kg dry weight (DW) (Joksas et al., 1998).

Sampling station No.	Pb	Cd	Cr	Zn	Cu
	mg/kg, DW				
1	39.8	1.4	8.4	80.0	74.0
4	10.4	0.2	3.3	23.1	111.3
6	21.8	0.7	5.8	46.0	55.1
7	1.8	0.1	0.8	4.6	4.9

Table 4. Heavy metals concentrations in bottom sediments of Lake Druksiai

Thermal aspects together with chemical and radioactive pollution must be taken into account considered ecological risk. Lake Druksiai has been used as the source of cooling water already since 1983 when first unit was put into operation. When passing through the cooling system of the INPP, the quality of cooling water does not normally change in any other way than that the temperature raises approximately 9–11 °C. Heated water discharge led to changes in the hydrological conditions of the lake: the surface temperatures increased, the natural vertical thermal stratification altered and evaporation rates increased. The increased temperature of the lake and the subsequent decrease of the cold water volume (Fig. 8) did not only stimulate the acceleration of eutrophication of the lake but also changed the prevailing conditions unfavorably for stenothermal cryophilic species. In Druksiai water temperature at 10 m depth has risen by 4°C and at 30 m depth by nearly 2°C (Balkuviene & Parnaraviciute, 1994).

Due to the complex (thermal and chemical) anthropogenic impact the following ecological zones, as presented in Table 5, have developed in Lake Druksiai:

- Zone A: The most eutrophicated south-eastern part of the lake, where the main source of eutrophication is the household effluents of the INPP and Visaginas town with an elevated amount of nutrients (N, P). Increased amount of plankton as well as enhanced activity of production-decomposition processes are observed in this area.
- Zone B: The cooling water outflow zone is the area of the greatest thermal impact, where water temperature in many cases exceeds 28 °C. The lowest abundance and variety of most planktonic organisms (phytoplankton and zooplankton) as well as lower rates of primary production and more intensive decomposition processes of organic matter are observed in this area;
- Zone C: The rest of the lake, including the deep and mediate deep zones, where the various impact factors affect the ecosystem occasionally, depending on the INPP operation, wind direction, waves, etc.

In conclusion, eutrophication, the increase of salts content and warming of the lake water, interact to influence the habitats and ecosystems of the lake. Despite these changes in the lake ecosystem, the parameters examined still meet the requirements and range within the guide values.

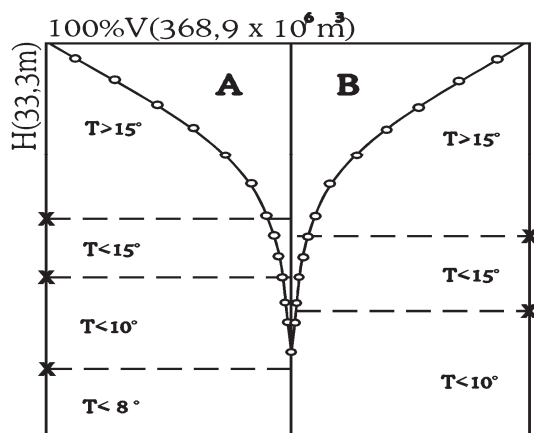


Fig. 8. The distribution of thermal zones during summer stratification in Lake Druksiai, 1977–1983 – A and 1984–1997 – B (Balkuviene & Parnaraviciute, 1994)

Parameter	Zone A	Zone B	Zone C
Secchi depth, m	1.0–2.8	3.0–3.9	1.2–6.5
Chlorophyll a, µg/l	6.6–113.5	0.88–16.5	0.99–70.0
Zooplankton biomass, mg/m ³	2 046–7 180	431–1 863	596–1 153
Phytoplankton primary production, mg C/m ³ d ⁻¹	330–2 800	44–440	2–1 500
C _{org} total in bottom sediments, %	11.7–12.4	3.5–3.7	7.6–12.6
Organic matter mineralization in bottom sediments, mg C/m ² d ⁻¹	1 127–1 590	915–939	513–720

Table 5. Fluctuation range of some parameters in different zones of Lake Druksiai

3. Radioactive pollution and non-human biota exposure

Concerning dose calculations to non-human biota the data of radiological investigations and radionuclide transport pathway must be taken into account.

Radionuclide transfer modeling in various ecosystems using differential equations and transfer factors is desirable. For radiation doses to freshwater biota evaluation ERICA assessment tool (Environmental Risk of Ionizing Contaminants Assessment and Management - <http://project.facilia.se/erica/>) and site specific LIETDOS-BIO code (Nedveckaite et al., 2010) has been used.

3.1 ERICA biota exposure dose rates assessment approach

The ERICA project (the European Community 6th Framework programme at a European level) was carried out between 2004 and 2007. The final outcome of the project is the delivery of the ERICA Integrated Approach. The use of Integrated Approach is facilitated by ERICA Tool which is a software code that keeps records and communicates with a number of purpose-built databases.

The Community research in radiation protection underpins European policy and has already contributed to the high level of environmental protection. To put assessment of nuclear sites into context a comparison of biota exposure due to discharged anthropogenic radionuclides with that of background radionuclides is required. This investigation presents the comparison of freshwater Lake Druksiai reference biota (the reference organisms are the default organisms included in the ERICA code Tool) exposure due to discharged anthropogenic radionuclides with that due to natural background radionuclides using ERICA approaches. The data presented enlarge knowledge about the concentrations of radionuclide in European freshwater ecosystems in order to understand the exposure dose rates of freshwater organisms due to major discharged radionuclides and natural series contributors.

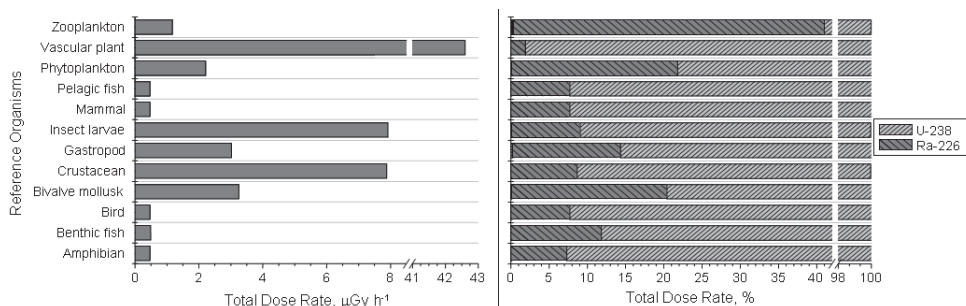


Fig. 9. The comparison of dose rates to freshwater reference organisms from natural background radionuclides (left) and the corresponding percentage due to separate radionuclides (right) in Lake Druksiai. The percentage of ²¹⁰Pb and ²³²Th are less than 1%

In the case of INPP cooling pond Lake Druksiai the estimated exposure of freshwater ecosystem reference organisms is determined mostly by natural background radionuclides and arises from internally incorporated alpha emitters, with ²¹⁰Po, ²²⁶Ra and ²³⁸U being the major contributors (Fig. 9). The contribution of anthropogenic radionuclides exposure composes about 5% of this dose rates (Fig. 10). The exposure of reference organisms due to

the natural background exposure stands out above anthropogenic discharged radionuclides exposure.

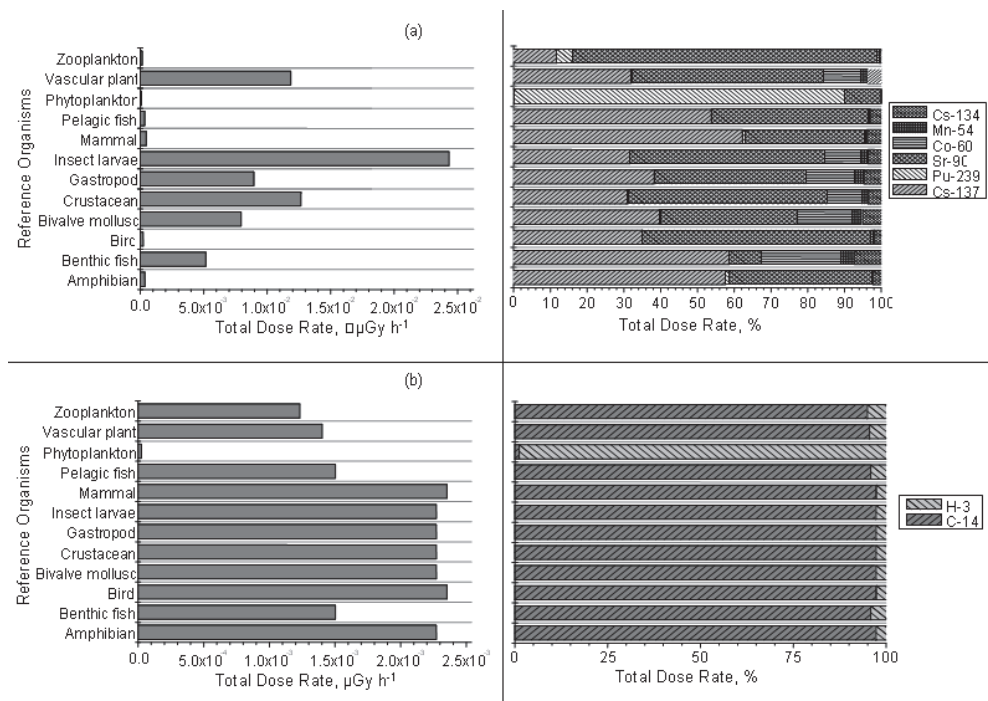


Fig. 10. The comparison of total dose rates derived by freshwater reference organisms inhabiting Lake Druksiai from anthropogenic (a) and natural-anthropogenic (b) radionuclides (left) and the corresponding percentage due to separate radionuclides (right)

3.2 Site-specific LIETDOS-BIO computer code designed for non-human biota exposure assessment approach

The site-specific LIETDOS-BIO assessment approach to non-human biota exposure protection from ionizing radiation is being developed to address contamination issues associated with nuclear power production and radioactive waste repository in Lithuania. LIETDOS-BIO model and computer code for biota exposure dose rate calculation was validated during IAEA EMRAS (Environmental Modeling for Radiation Safety) Working Group designated for model validation for biota dose assessment (Vives-i-Batlle et al., 2007; Beresford et al., 2008a; Beresford et al., 2008b; Beresford et al., 2009; Yankovich et al., 2010). The user is the Centre of Physical Science and Technology and Nature Research Centre. LIETDOS-BIO code was designed to be consistent with MCNPX (general purpose Monte Carlo radiation transport code that can be used for neutron, photon, electron, or coupled neutron/photon/electron transport) (MCNPX, 2002) as well as Crystal Ball software (www.oracle.com/crystalball/index.html) for uncertainty analyses.

3.2.1 Preparing MCNPX input file for dose conversion coefficients (DCC) calculations

The MCNPX code is widely used for radiation transport simulation with relatively high flexibility and is now applied to many fields including radiation safety management, health physics, medical physics and reactor design. Based on information about the organism geometry specification, description of materials, specification of the particle source, the type of answers desired (energy deposited in a given volume) LIETDOS-BIO automatically creates an input file (specially designed to LIETDOS-BIO) that is sub sequentially read by MCNPX and calculates dose conversion coefficients for non-human biota. Examples of geometry specification model for dose conversion coefficient of external exposure calculation by MCNPX code is presented in Fig. 11.

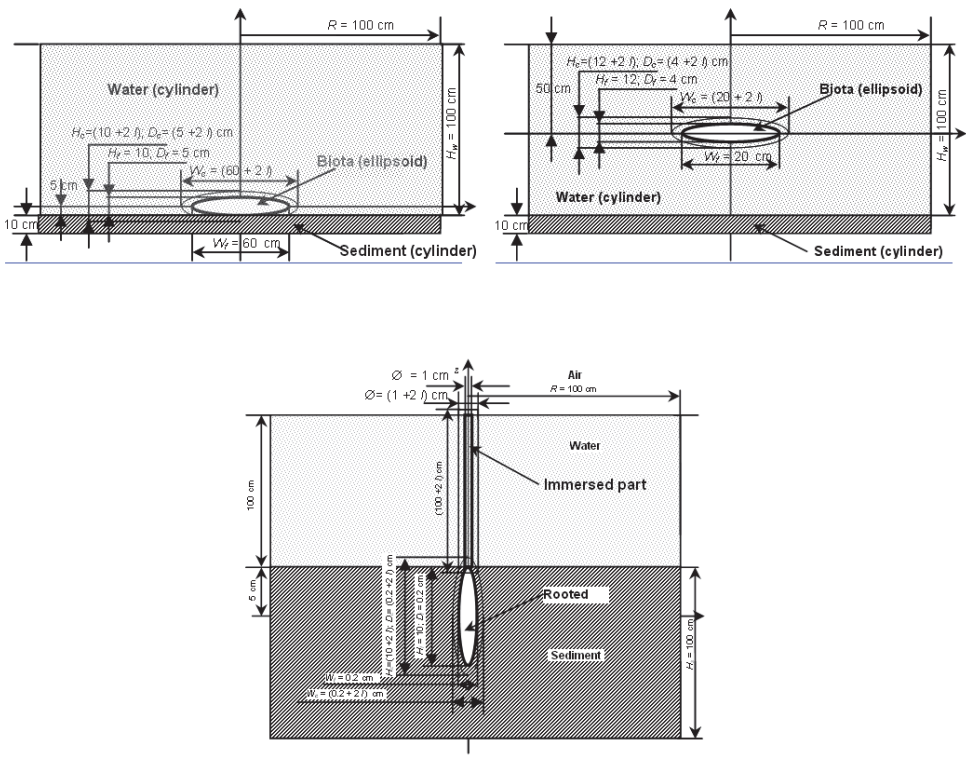


Fig. 11. Geometry specification model for non-human biota DCC of external exposure calculation by MCNPX code: organism on the bottom of water layer (left), organism in the middle of water layer (right), rooted submerged hydrophytes (below)

3.2.2 Method used for deriving uncertainty and accuracy estimates

Like any complex environmental problem, the evaluation of ionizing radiation impact is confounded by uncertainty. In radioecology stochastic calculations are used to an increasing extent. At all stages, from problem formulation up to exposure evaluation, the assessments

depend on models, scenarios, assumptions and extrapolations as well as technical uncertainties related to the data used. Uncertainties can be categorized as follows:

- Knowledge uncertainties defined as a lack of scientific knowledge about parameters and factors or models. It includes measurement errors as well as model misrepresentation and can be reduced through further study. It may be possible to represent some of these uncertainties by probability distributions.
- Variability is defined as a natural variability due to changes in a data set. Variability is easier to represent quantifiable through simple standard deviation or a frequency distribution or through probability density function.

To estimate the uncertainty of the endpoints of the exposure assessment, uncertainties in the inputs and parameters must be propagated through the model using Monte-Carlo analysis. Point estimates in a model equation are replaced with probability distributions, samples are randomly taken from each distribution, and the results are combined, usually in the form of a probability density function, in order to obtain 95% confidence interval. The uncertainties in LIETDOS-BIO model has been determined by Crystal Ball code statistical technique with 10 000 number of trials and the Latin Hypercube sampling method. An example of external dose rate evaluation is presented in Fig. 12. Sensitivity analysis is used to identify the relative quantitative contribution of uncertainty associated with each input and parameter value to the endpoint interested.

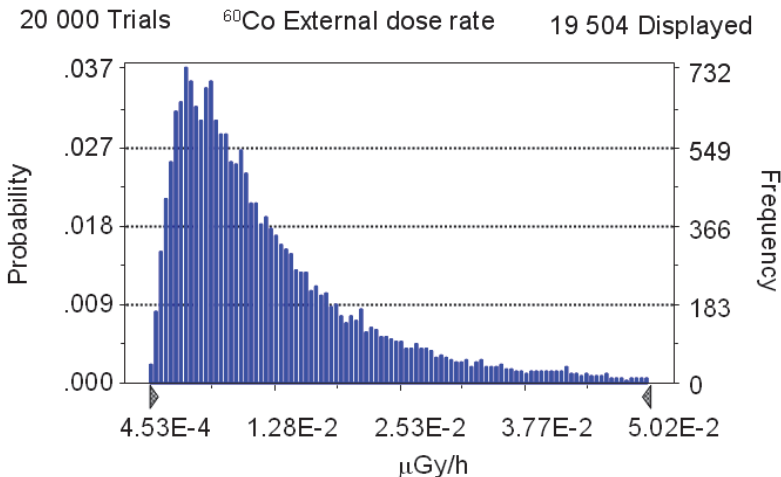


Fig. 12. An example of Druksiai Lake macrophytes external dose rate evaluation (Crystal Ball statistical techniques was used with 20 000 number of trials and Latin Hypercube sampling)

3.2.3 LIETDOS-BIO libraries and data bases

LIETDOS-BIO contains Nuclide library (ICRP, 1983) and site-specific parameters library (terrestrial and freshwater ecosystems). An example of site-specific freshwater ecosystem macrophytes ⁹⁰Sr concentration factor (CF) evaluation is presented in Fig. 13. Various species of macrophyte forming a greatest phytomass in water were investigated

(Marciulioniene et al., 1992). An amount of stable Sr and Ca as well as many biological and physical processes plays the main role among the factors determining ⁹⁰Sr concentration levels of the investigated species. The frequency of ⁹⁰Sr CF distribution based on 250 samples of 19 macrophyte species evaluation in Lithuanian lakes is presented in Fig. 13. The examples of site-specific CF values, based on environmental monitoring of discharged radionuclide activity concentration in the submerged plants and water have been evaluated completing data gaps in freshwater environment. The concentration factors based on submerged hydrophyte and water activity measurements was estimated. Data presented in Table 6.

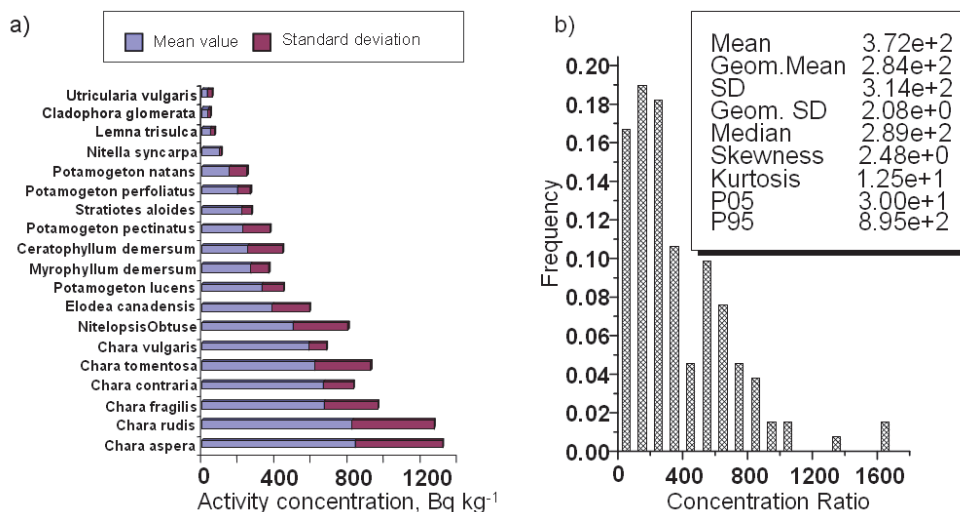


Fig. 13. Site-specific values of ⁹⁰Sr activity concentrations for different types of freshwater ecosystem macrophytes (a) and the distribution of corresponding CF values (b)

Parameters	Concentration factor, m ³ kg ⁻¹				
	⁴⁰ K	⁵⁴ Mn	⁶⁰ Co	⁹⁰ Sr/ ⁹⁰ Y	¹³⁷ Cs/ ^{137m} Ba
Mean	1.5×10 ⁺¹	1.2×10 ⁺¹	8.6×10 ⁺⁰	2.0×10 ⁺⁰	2.5×10 ⁻¹
Median	1.0×10 ⁺¹	2.3×10 ⁺⁰	3.6×10 ⁺⁰	1.1×10 ⁺⁰	1.1×10 ⁻¹
Standard Deviation	1.7×10 ⁺¹	4.5×10 ⁺¹	1.7×10 ⁺¹	2.7×10 ⁺⁰	4.8×10 ⁻¹
Range Minimum	1.4×10 ⁻¹	1.0×10 ⁻³	8.0×10 ⁻³	1.0×10 ⁻²	1.0×10 ⁻³
Range Maximum	3.7×10 ⁺²	2.6×10 ⁺³	5.4×10 ⁺³	6.4×10 ⁺¹	1.3×10 ⁺¹

Table 6. The submerged freshwater hydrophyte site-specific CF values

4. Exposure of biota in the INPP cooling pond Lake Druksiai

On the basis of the long-term studies of the radionuclides in biotic and abiotic components of Lake Druksiai (Marciulioniene et al., 1992; Lithuanian State scientific research programme, 1998) the potential impacts of radioactive pollution on lake non-human biota, with special emphasis on macrophytes were evaluated.

4.1 Submerged macrophytes exposure dose rates assessment

A decline in a hydrophyte population may indicate water quality problems. Such problems may be the result of chemical or thermal lake pollution, as well as exposure by radionuclide ionizing radiation. Internal and external exposures of submerged hydrophytes were estimated by means of LIETDOS-BIO code separately for above-sediment and rooted plant parts. Eighty-five samples of submerged macrophytes (*Myriophyllum spicatum*, *Ceratophyllum demersum*, *Nitellopsis obtusa*) have been measured to determine the activity concentrations of ^{54}Mn , ^{60}Co , ^{137}Cs , ^{90}Sr , ^{40}K , ^{210}Pb .

Based on the knowledge of radionuclide distribution within the freshwater environment a simplified compartmentalization of the ecosystems was used as a basis for selecting suitable target geometries (phantoms) for the macrophyte's above sediment and rooted parts dose rate calculations. The aquatic ecosystem has been considered as two compartments: bed sediment and water column (Fig. 11). It is reasonably safe to suggest that the above-sediment part of submerged rooted plants receive lower external radiation doses as compared with the external exposure of roots in sediments that is in a system which has been receiving radionuclides for a number of years. Consequently, the external and internal exposure of above-sediment and rooted parts of plant must be evaluated separately. An example of DCC values for rooted submerged hydrophyte's parts, calculated by means of LIETDOS-BIO code, are presented in Table 7.

Exposure	DCC, $\mu\text{Gy/h}$ per Bq/kg			
	^{54}Mn	^{60}Co	$^{90}\text{Sr}/^{90}\text{Y}$	$^{137}\text{Cs}/^{137\text{m}}\text{Ba}$
External	2.31E-04	7.63E-04	4.82E-04	2.77E-04
Exposure	DCC, $\mu\text{Gy/h}$ per Bq/kg (FW)			
	^{40}K	^{210}Pb	^{226}Ra	^{232}Th
External	2.41E-04	6.76E-07	2.58E-06	4.41E-08

Table 7. Submerged hydrophyte's rooted part weighted DCC for anthropogenic and background radionuclides (assuming weighting factor of 5 for α -radiation, both β - γ -radiation - 1)

Estimates of exposure were therefore made using two groups of model parameters:

- site-specific data when available - activity concentration in plants, bottom sediments and in most cases water (assuming site-specific equilibrium between two phases);
- generic parameters when site-specific data were lacking, for example CF values were generally needed for ^{232}Th and ^{238}U .

Some examples of submerged hydrophytes root external exposure dose rates evaluation due to discharged anthropogenic and natural background radionuclides are presented in Fig. 14. As presented in (Nedveckaite et al., 2007; Nedveckaite et al., 2011) the ionizing radiation exposure dose rates to submerged hydrophyte roots and above sediment parts due to the anthropogenic radionuclides (^{54}Mn , ^{60}Co , ^{137}Cs , ^{90}Sr) discharged into Lake Druksiai were 0.044 mGy h^{-1} and 0.004 mGy h^{-1} , respectively.

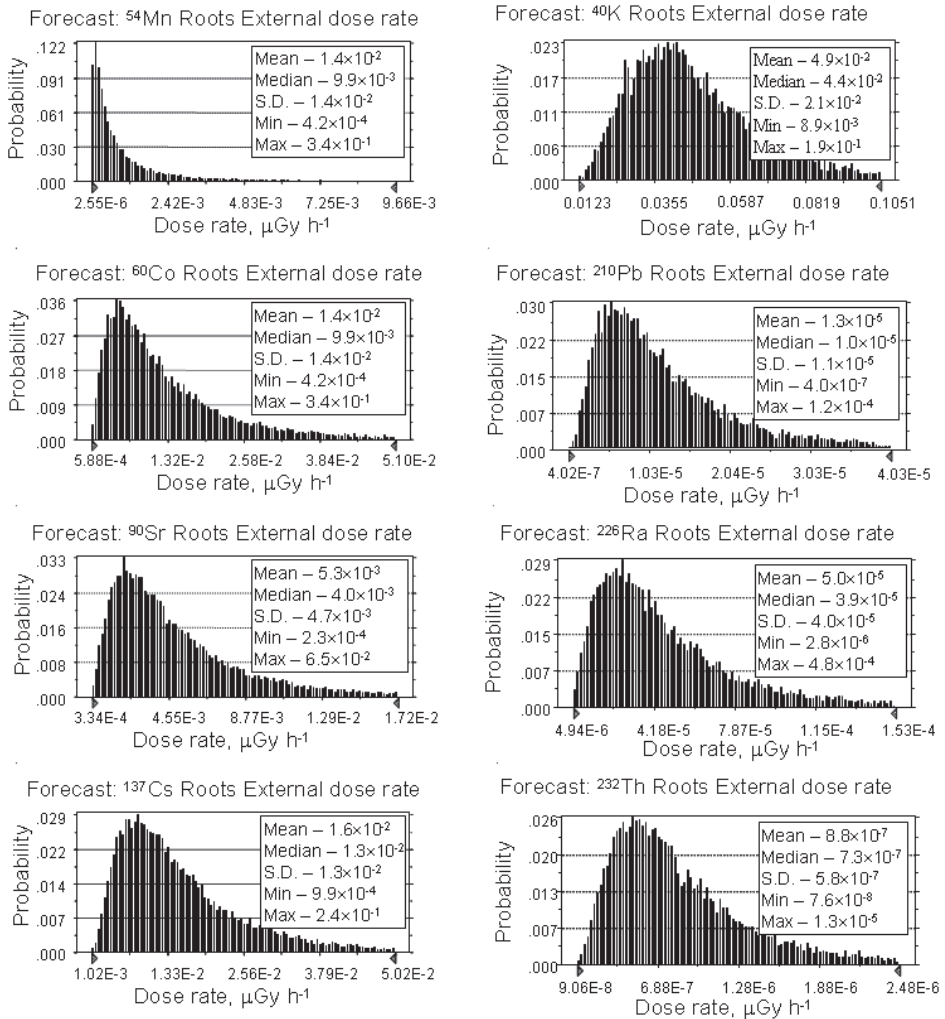


Fig. 14. The examples of submerged hydrophyte's root external exposure dose rates evaluation due to discharged anthropogenic and natural background radionuclides

5. The investigation of radiological, chemical and thermal pollution effects on the lake biota

5.1 Macrophytes

Aquatic plants make up a large biomass and intensively concentrate radionuclide's occurring in the environment in micro amounts by assimilating them both from water and bottom sediments. Therefore, to assess the radioecological state of a hydroecosystem, the plants (bioindicators) are used. Radionuclide activity concentrations in bioindicators are integrated in time (a month, a year or even longer period of time) as well as in space, whereas in the environment they demonstrate fast alteration due to environmental factors. Radionuclide activity concentrations in bioindicators can be established comparatively accurately, even in such cases, when their activity concentrations in other environmental components are under the minimal detectable level (Marciulioniene at al., 2011a). Activity concentration of radionuclides in macrophytes of Lake Druksiai during twenty years period of time is presented in Fig. 15.

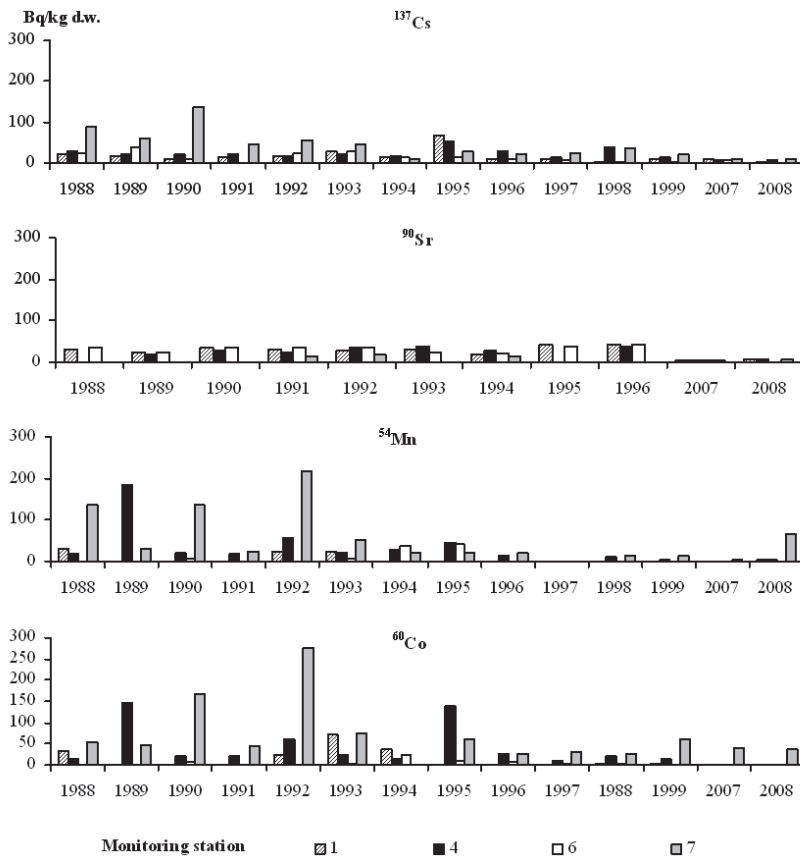


Fig. 15. Time-dependent activity concentration of anthropogenic radionuclides in submerged macrophytes of Lake Druksiai

Macrophytes were collected in the stations of littoral zone at a depth less than 8 m. Ninety-five samples of different submerged macrophytes were measured to determine the radionuclide activity concentrations (Marciulioniene et al., 1992; Mazeika, 2002). In most cases co-located bottom sediment and water samples were also analyzed. It should be stressed that bottom sediment activity which contain radionuclides accumulated over a number of years determined the rooted submerged macrophyte exposure to a greater extent as compared with water activity.

5.1.1 Macrophytes and chemical pollution

Waste water polluted not only with radionuclides, but also with chemical contaminants (acid and alkali solutions, weak organic acids, heavy metals and etc.) were constantly discharged from WWTP and ISW-1,2 channels of INPP into Lake Druksiai, which accumulated in bottom sediments. A tendency of increasing toxicity of INPP WWTP channel discharge and bottom sediments as well as the water of ISW-1,2 channel discharges into Lake Druksiai zone and especially bottom sediments was observed. However, this waste water taking into account the degree of toxicity can be subsumed as low-toxicity waste water.

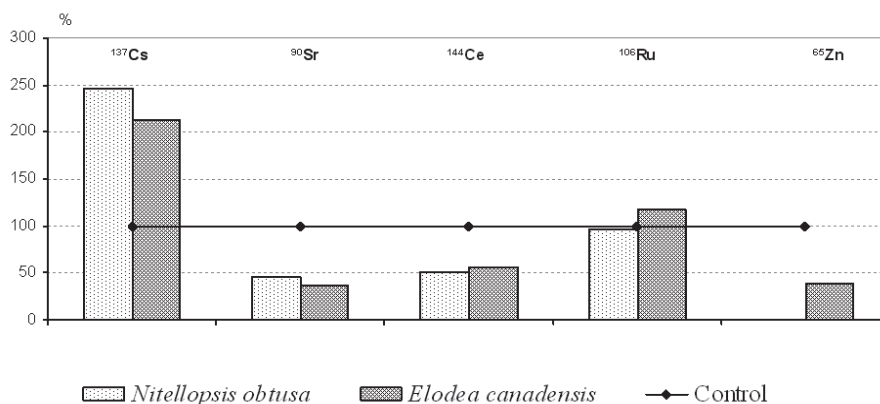


Fig. 16. Impact of INPP industrial storm water discharge channel on radionuclide accumulation (as compared with the control, %) in algae *Nitellopsis obtusa* and higher plant *Elodea canadensis*

The results of INPP industrial storm water discharge channel impact on radionuclide accumulation in algae *Nitellopsis obtusa* and higher plant *Elodea canadensis* are presented in Fig. 16.

5.1.2 Macrophytes and thermal pollution

It is known that stimulation of the growth of aquatic plants under high temperature of water is deviated from the normal functioning of plants. Hence, we may conclude that after the rapid development of the all species of plant of Lake Druksiai (1986–1989), the suppression of species, more sensitive to high temperature, had occurred. Temperature of water is one of the main factors which influence the physiological state of plant and it is strongly related

with the sensitivity of plants to chemical and radioactive matters. Accumulation of radionuclides in the *Nitellopsis obtusa* and *Elodea canadensis* under laboratory conditions showed that the increase in water temperature from 22 to 31°C influenced the accumulation levels of different radionuclides in the tested plant species differently (Fig. 17), accumulation level of ^{134}Ce increased signally.

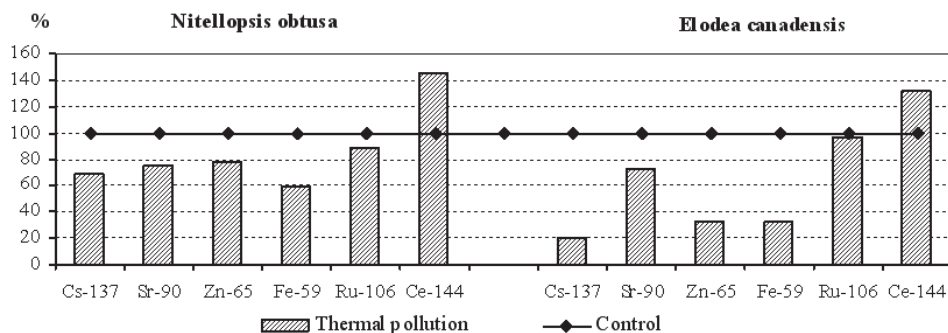


Fig. 17. Impact of thermal pollution (31°C) on radionuclide accumulation (as compared with the control at 22°C, %) in algae *Nitellopsis obtusa* and *Elodea canadensis*

It was found that impact of thermal and chemical pollution on accumulation of ^{137}Cs taking part in the metabolic processes in the aquatic plants may depend more on changes of the functional status of plant. Accumulation of microelement ^{60}Co and ^{54}Mn participating in metabolic processes of the aquatic plants under thermal impact may depend on both the functional status of the plant and changes of physical-chemical properties of these radionuclides.

5.1.3 Macrophytes and complex chemical, thermal and radioactive pollution

The main source of ^{60}Co and ^{54}Mn discharging into the lake was the waste water of the ISW-1,2 and CW channels (Fig. 3). The activity concentration of these radionuclides in the bottom sediments from above mentioned channels were higher than that in Lake Druksiai. The decrease of the activity concentration of ^{60}Co and ^{54}Mn in the bottom sediments of the INPP's discharge channels and the lake was observed since 1994. Since 1996 the activity concentration of ^{54}Mn in the bottom sediments of the INPP's channels and the lake in the most cases was lower than minimal detection limit. It is necessary to stress that values of ^{137}Cs activity concentration in bottom sediments of Lake Druksiai were higher than that in hydrophytes. However, activity concentration of ^{60}Co and ^{54}Mn in bottom sediments were lower than that in hydrophytes (Table 8).

Presumably, high radionuclide activity concentrations in ISW-1,2 channel were induced due to planned maintenance of INPP. It should be indicated that the highest ^{60}Co and ^{54}Mn activity concentrations in macrophytes were established at the outlet of the channel, however, at its end, they markedly decreased: ^{60}Co by 5 times, ^{54}Mn by 43 times. ^{137}Cs and ^{134}Cs activity concentrations in plants differed insignificantly both at the outset of the channel and at its end.

Such differences in radionuclide accumulation in macrophytes can be explained by varying chemical and physical chemical characteristics of these radionuclides, upon which not only

radionuclide accumulation in macrophytes, but also their dispersion in hydroecosystem depends. Although the investigated radionuclide activity concentrations in macrophytes sharply decreased in 2009 in comparison with 2008, however, they were higher than those in 2007 (Table 8).

Nuclides	<i>Ceratophyllum demersum</i>			<i>Myriophyllum spicatum</i>	
	2007	2008	2009	2008	2009
^{137}Cs	20±2**	392±47** 406±54***	22±1.2***	166±33* 271±20***	18±1.6* 13±1.1**
^{60}Co	34±2**	754±51** 634±50***	63±3.0***	2185±108* 463 ±23***	46±1.9* 37±1.6**
^{54}Mn	2±0.6**	2203±147** 1774±129***	75±3.0***	6428±372* 151±88***	44±2.3* 46±2.1**

<mdl – minimal detectable level; ISW-1,2 channel: outset – *, middle – **, end – ***

Table 8. Radionuclides activity concentration (Bq/kg) in macrophytes in INPP industrial storm water discharge channel (ISW-1,2) (2007–2009)

The macrophytes growing in this channel performed the role of cleaning (phytoremediation) of the channel waste water by accumulating large content of radionuclides. The flux of radionuclides discharged from this channel into the lake was low due to low water flow rate in ISW-1,2 channel and large water volume of lake what stipulated activity dilution.

5.2 Ichtiofauna

Lake Druksiai is important for commercial and free-time fisheries. In this connection the corresponding percentage contributions of different radionuclides to the various kinds of fish from key Lake Druksiai radionuclides has been investigated.

The factors that have an effect on the evolution of fish populations are: inputs of sedimentary substance (from the increase of the lake water level due to the construction of a dam and an active erosion of the lake banks), water temperature, in particular the optimum temperature for fish populations, the average biomass of phytoplankton, the average concentration of dissolved nitrogen and phosphorus.

The time-dependent changes in radionuclide activity concentrations in average annual specific activity of radionuclides in fishes are presented in Fig. 18. Corresponding fish muscle activity concentration distributions in Fig. 19.

As regards the fishery and corresponding committed effective human dose assessment as result of fish consumption, Lake Druksiai continues to be a high-productivity water body with intensive angling and possible commercial fishing. The distributions of ingestion doses as a result of fish consumption from the key radionuclides discharged from INPP performed using site-specific consumption data and the LIETDOS computer code demonstrate that adult human annual effective doses would be as small as a few μSv and are mostly attributable to the background radionuclides, for example, ^{40}K .

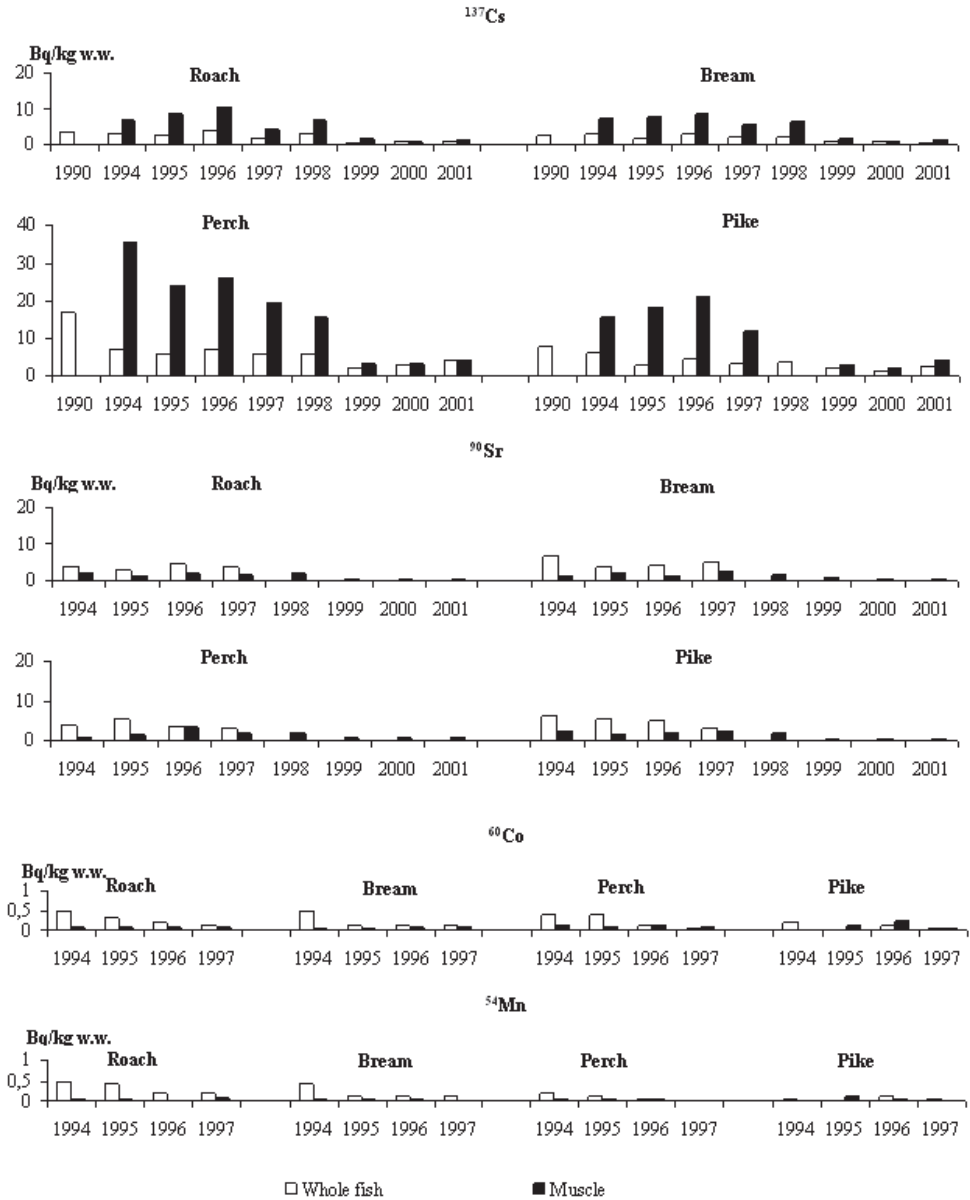


Fig. 18. Time dependent activity concentration of radionuclides in the whole fish and fish muscle from Lake Druksiai

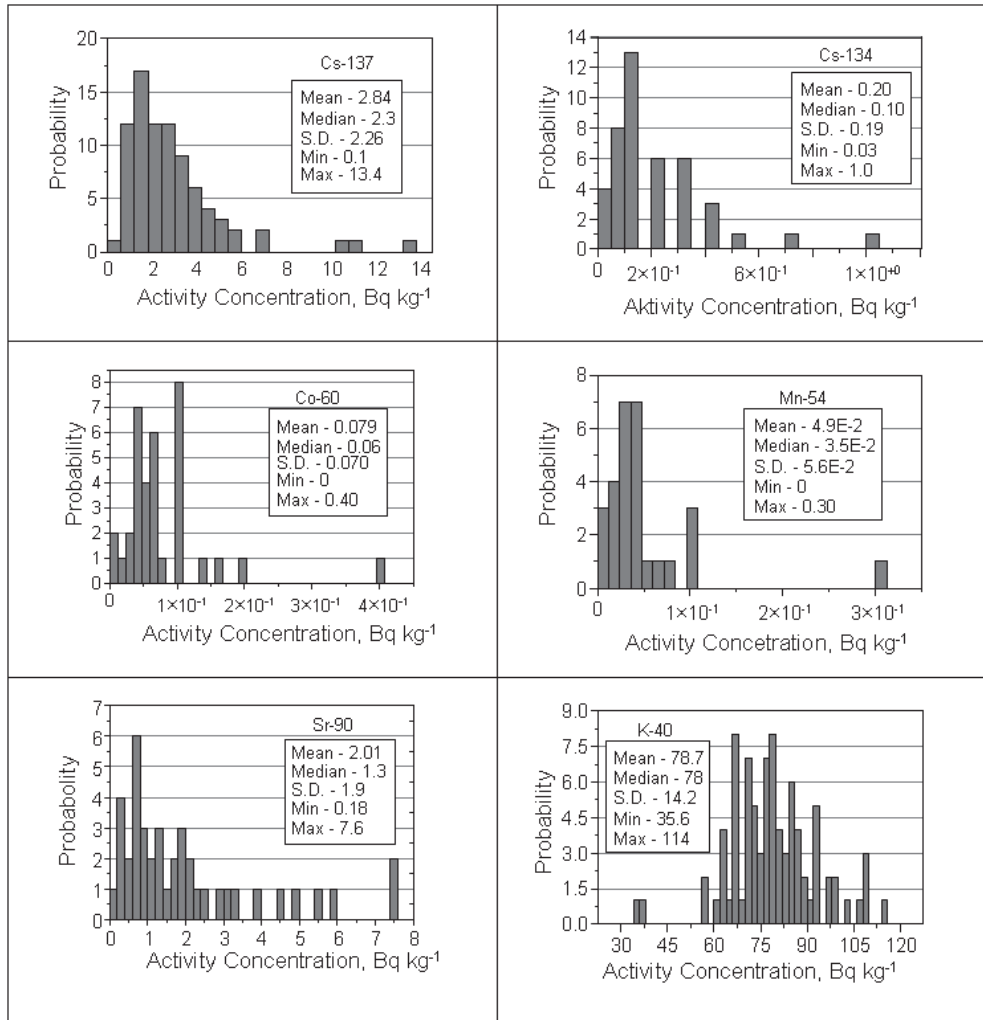


Fig. 19. Pelagic fish muscle activity concentration data (Marcuilioniene et al., 1992) from key radionuclides discharged from the INPP into Lake Druksiai cooling pond and ⁴⁰K

5.3 Macrophytes and fish community changing

73 aquatic macrophyte species were recorded in Lake Druksiai. Among them eight *Charophyta*, two *Bryophyta*, one *Equisetophyta*, and 58 *Magnoliophyta* species. Before operation of the INPP Lake Druksiai was characterized as a typical mesotrophic lake of moderate depth with well developed submerged vegetation (dominant species *Chara rudis*, *C. filiformis*, *Nitellopsis obtusa*, *Potamogeton lucens*, *P. perfoliatus*) and fragmentally developed floating leaved and emerged vegetation (*Potamogeton natans*, *Phragmites australis*) (Marcuilioniene et al., 1992). Maximum depth limit for vegetation varied from 7 to 9 meters.

After 20 years of INPP operation significant changes were observed in all ecological zones of aquatic vegetation. *Charophyta* species have totally become extinct from the submerged plant zone of shallow areas near the INPP. The intensive development of filamentous green algae during a prolonged vegetation period and decrease of water transparency was an important reason for the decline of submerged vegetation. The areas occupied by helophyte communities (*Phragmites australis*, *Schoenoplectus lacustris*) increased significantly in shallow areas up to 2 m.

The fish species diversity in Lake Druksiai significantly decreased from 23–26 fish species to the current list of 14 species mostly due to total anthropogenic pressure and thermal load (Kesminas & Olechnoviciene, 2008). The changes occurred mainly after the first years of INPP operation, and then the successive changes slowed down. During the last years the lake fish community has changed insignificantly. There were also some adaptations among some species populations. *Vendace* (stenothermal fish) population partially adapted to the changed environmental conditions and its abundance in the recent years is quite high and constant. The survival and partial rehabilitation of *Vendace* indicates that some fish species may become acclimated to the disrupted thermal and eutrophic conditions in the lake (Ecosystem, 1992; Institute of Botany, 2008).

6. Conclusions and relevance

Considering the findings of this study, it can be assumed that changes in macrophyte species and fish communities diversity in Lake Druksiai could be induced by the total chemical, predominant thermal and very limited radioactive pollution as anthropogenic pressure which had a negative impact on some aquatic organisms.

The data presented enlarge knowledge about the concentration of radionuclides in European freshwater ecosystems in order to understand the internal and external exposure dose rates of macrophytes and fish communities due to major discharged radionuclides and natural series contributors. In the case of INPP cooling pond - Lake Druksiai the estimation of weighted internal exposure of macrophytes and fish is mostly determined by natural background radionuclides and arises from internally incorporated α -emitters with ^{238}U , ^{226}Ra and ^{210}Po being the major contributors. The total exposure due to anthropogenic discharged radionuclides is substantially lower as compared with the natural background exposure.

The INPP operational history and the routine radiation in environment monitoring data evidenced that INPP was operated safely and helpfully for the society from radiation protection point of view. However environmental changes in Lake Druksiai related mostly to the chemical, thermal and general urbanization pressure are unavoidable and acceptable from society side traces of electric power industry development.

7. References

- Balkuviene, G. & Parnaraviciute, B. (1994). Growth rates of roach (*Rutilus rutilus* L) in cooling water reservoir under different thermal conditions. *Int. Revue ges. Hydrobiol.* Vol. 79, 139-142.
- Beresford, N.A.; Barnett, C.L.; E. Brown, J.; Cheng, J.J.; Coplestone, D.; Filistovic, V.; Hosseini, A.; Howard, B.J.; Jones S.R.; Kamboj, S.; Kryshev, A.; Nedveckaite, T.; Olyslaegers, G.; Saxe'n, R.; Sazykina, T.; Vives i Batlle, J.; Vives-Lynch S;

- Yankovich, T. & Yu, C. (2008a). Inter-comparison of models to estimate radionuclide activity concentrations in non-human biota. *Radiation and Environmental Biophysics*. Vol. 47, 91-514.
- Beresford N. A.; Balonov, M.; Beaugelin-Seiller, K.; Brown, J.; Copplestone, D.; Hingston, J.; Horyna, J.L.; Hosseini, A.; Howard, B.J.; Kamboj, S.; Nedveckaite, T.; Olyslaegers, G.; Sazykina, T.; Vives i Batlle, J.; Yankovich, T.L.; Yu & Ch. (2008b). An international comparison of models and approaches for the estimation of the radiological exposure of non-human biota. *Applied radiation and Isotopes*. Vol. 66, 1745-1749.
- Beresford N.A.; Barnett, C.L.; Beaugelin-Seiller, K.; Brown, J.E.; Cheng, J.J.; Copplestone, D.; Gaschak, S.; Hingston, J.L.; Horyna, J.; Hosseini, A.; Howard, B.J.; Kamboj, S.; Kryshev, A.; Nedveckaite, T.; Olyslaegers, G.; Sazykina, T.; Smith, J.T.; Tellerial, D.; Vives i Batlle, J.; Yankovich, T.L.; Heling, R.; Wood, M.D. & C. Yu. (2009). Findings and recommendations from an international comparison of models and approaches for the estimation of radiological exposure to non-human biota. *Radioprotection*, Vol. 44, 565-570.
- U.S. DOE (Department of Energy). A Graded Approach for Evaluating Radiation Doses to Aquatic and Terrestrial Biota. Technical Standard DOE-STD-1153-2002 (Washington D.C., 2002).
- Ecosystem of the water-cooling reservoir of Ignalina Nuclear Power-Station at the Initial stage of its operation. *Thermal Power Generation and Environment*. 10, Vilnius, Academia Publishers, 1992 (in Russian).
- ICRP (International Commission on Radiological Protection). Radionuclide Transformation Energy and Intensity of Emission. ICRP Publ. 38, Ann. ICRP 11-13 (1983).
- ICRP (International Commission on Radiological Protection). Environmental Protection - the Concept and Use of the Reference Animals and Plants. ICRP Publication 108. Ann ICRP 4-6 (2008).
- Institute of Botany Research Study. (2008) Description of the Aquatic Ecosystem of Lake Druksiai. Institute of Botany, Vilnius Report No.14-193.8.8. Vilnius.
- Joksas, K.; Galkus, A. & Stakeniene, R. (1998). Hydrogeochemical investigation in Lake Drūkšiai – the cooler of Ignalina NPP. *The state and development of the ecosystems in the region of Ignalina Nuclear Power Plant, Final collection of scientific reports*. Vilnius, Vol. 2, 119-225.
- Kesminas, V. & Olechnoviciene, J. (2008). Fish community changes in the cooler of the Ignalina Nuclear Power Plant. *Ekologija*, 54, 124-131.
- Lithuanian State Scientific Research Programme “Ignalina Nuclear Power Plant and the environment (1993-1997)”. (1998). *The state and development of the ecosystems in the region of Ignalina Nuclear Power Plant, Final collection of scientific reports*. Vilnius (in Lithuanian).
- MCNPX User’s Manual Version 2.4.0 (2002) Report LA-CP-02-408, L.S. Waters (ed.). Los Alamos National Laboratory.
- Marciulioniene, D.; Dusauskiene-Duz, R.; Motiejuniene, E. & Svobiene R. (1992). Radiochemoecological situation in Lake Drūkšiai – cooling water reservoir of the Ignalina NPP. Vilnius, Academia Publishers, p. 214.
- Marciulioniene, D.; Lakaciauskiene D. & Montvydiene D. (1998). Assessment of the ecotoxic effect of Ignalina NPP waste water on Lake Drūkšiai ecosystems. *Proceeding of the Latvian Academy of sciences*, section B, Vol. 52 (supplement), 129-139.
- Marciulioniene, D. (2003). Accumulation of technogenic radionuclides in water plants under chemical and thermal pollution. *Ekologija*. No. 4, 28-35.

- Marciulionienė, D.; Montvydiene D. & Paskauskas R. (2011a). Impact of waste water of the Ignalina Nuclear Power Plant on Lake Druksiai before plant Decommissioning (2007–2009). In: P. Hlavivinek et al. (eds.). *Advanced Water Supply and Wastewater Treatment: A road to Safer Society and Environment*. Springer. Science+Business Media B.V.: 277-286
- Marciulioniene, D.; Montvydiene, D.; Kazlauskieni, N. & Kesminas V. (2011b). Changes in Macrophytes and Fish communities Lake Druksiai – cooler of the Ignalina Nuclear Power Plant (1988–2008). *J. of Environmental Engineering and Landscape Management*. (in press).
- Mazeika, J.; Taminskas, J.; Paskauskas, R.; Bodoyan, A.; Baghdassaryan, H.; Tozalakyan, P.; Davtyan, V.; Grillot, J-C. & Travi Y. (2006). Ecohydrological evolution in the catchment of Lake Druksiai, Lithuania, under anthropogenic pressure. *Ekologija*. No. 4. p. 40-50.
- Mazeika, J. (2010). Carbon-14 in Terrestrial and Aquatic Environment of Ignalina Nuclear Power Plant: Sources of Production, Releases and Dose Estimates. *Nuclear Power*, Edited by Pavel V. Tsvetkov, SCIYO, 293-310, ISBN 978-953-307-110-7.
- Nedveckaitė, T.; Filistovic, V.; Marciulioniene, D.; Kiponas, D.; Remeikis, V. & Beresford, N.A. (2007). Exposure of biota in the cooling pond of Ignalina NPP: hydrophytes. *Journal of Environmental Radioactivity*. Vol 132, 137-147
- Nedveckaitė, T.; Filistovic, V.; Marciulioniene, D.; Prokopciuk, N.; Gudelis, A.; Plukiene, R.; Remeikis, V. & Vives I Battle, J. (2010). LIETDOS-BIO assessment approach to the environment non-human biota exposure by ionizing radiation. *Lithuanian Journal of Physics*, Vol. 50, 151-160
- Nedveckaitė, T.; Filistovic, V.; Marciulioniene, D.; Prokoptchuk, N.; Gudelis, A.; Plukiene, R.; Yankovich, T. & Beresford, N. (2011). Background and anthropogenic radionuclide derived dose rates to freshwater ecosystem – Nuclear Power Plant cooling pond reference organisms. *Journal of environmental radioactivity*, doi:10.1016/j.jenvrad.2011.04.012.
- Paskauskas, R.; Mazeika, J. & Kasperoviciene, J. (2009). Impact of nuclear energy objects on lake environment: Lake Druksiai case. *Book of Abstracts of the 2nd International Conference on Environmental Management, Engineering, Planning and Economics (CEMEPE) & Secotox Conference*. Mykonos June 21-26. Greece. p. 70 - 75.
- Salickaite-Bunikiene, L. & Kirkutyte I.(2003). The Investigation of Nutrients of INPP Cooler (Lake Druksiai) in the Period 1998–2002. *Environmental research, engineering and management*, Vol.3, No. 25., 11–15.
- Vives i Battle, J.; Balonov, M.; Beaugelin-Seiller, K.; Beresford, N.A.; Brown, J.; Cheng, J.-J.; Copplestone, D.; Doi, M.; Filistovic, V.; Golikov, S.; Horyna, J.; Hosseini, A.; Howard, B.J.; Jones, S.R.; Kamboj, S.; Kryshev, A.; Nedveckaitė, T.; Olyslaegers, G.; Prohl, G.; Sazykina, T.; Ulanovsky, A.; Vives-Lynch, S.; Yankovich, T. & Yu, C. (2007). Inter-comparison of absorbed dose rates for non-human biota. *Radiation and Environmental Biophysics*. Vol. 46, 349-373.
- Yankovich, T.L.; Vives i Battle, J.; Vives-Lynch, S.; Beresford, N.A.; Barnett, C.L.; Beaugelin, K.; Brown, J.E.; Cheng, J.-J.; Copplestone, D.; Heling, R.; Hosseini, A.; Howard, B.J.; Kryshev, A.I.; Nedveckaitė, T.; Smith, J.T. & Wood, M.D. (2010). International model validation exercise on radionuclide transfer and doses to freshwater biota. *Journal of Radiological Protection*. Vol. 30, 299-341.

Power Uprate Effect on Thermal Effluent of Nuclear Power Plants in Taiwan

Jinn-Jer Peir
*NSTDC, National Tsing Hua University
Hsinchu, 30013
Taiwan, R.O.C.*

1. Introduction

Power uprate is presently being considered by several nuclear power plant (NPP) utilities as a promising way to increase the power generation efficiency of existent power plants with or without increasing nuclear fuel consumption since 1970s. In general there are three types of power uprate: measurement uncertainty recapture power uprate (MURPU, <2%), stretch power uprate (SPU, 2 to 7 %), and extended power uprate (EPU, 7 to 20%) (US NRC, 2011 a). Thorough evaluations of existing plant equipments and environmental impact must be assessed before a final decision and an optimal selection of power uprate are made. Upon a power uprate, the power density and thermal release of a nuclear reactor would increase instantly, followed by the impact due to the waste heat from the thermal effluent to the environment. In Taiwan, two BWR NPPs and one PWR NPP were scheduled for MURPU. These NPPs are all located at the seacoast and using marine water as the coolant due to that fact that there is no rivers can supply enough light water near the site of the NPP in Taiwan. The marine water temperature is high during summer time due to the fact that Taiwan's weather is marine tropical. According to the Effluent Standards of Taiwan's Environmental Law: for effluents discharged directly into marine waters, the temperature at the discharge point shall not exceed 42°C; and the temperature difference should not exceed 4°C for surface water at 500 meters from the discharge point. Hence, the effect from the waste heat is always a very crucial issue to the power uprate of NPPs in Taiwan.

Currently the three operating NPPs of Taiwan are all owned by the Taiwan Power Company (TPC). There are two reactor units setup at each NPP. The technology chosen for the reactors is General Electric (GE) BWR for Chinshan Nuclear Power Plant (NPP1) and Kuosheng Nuclear Power Plant (NPP2), and Westinghouse PWR for Maanshan Nuclear Power Plant (NPP3). Moreover, Lungmen Nuclear Power Plant (NPP4), which is GE ABWR and will to be the largest NPP in Taiwan, is still under construction at present. Fig. 1 shows the locations of NPPs in Taiwan. As can be seen, NPP1 and NPP2 are located in the most northern part of Taiwan in which is a subtropical zone, whereas NPP3 is located in the most southern part of Taiwan where is a tropical zone. They are all located next to the seacoast and using marine water as the coolant due to the fact that there is no any big rivers can

enough supply light water near the site of the NPPs. Table 1 lists the basic operational parameters for one unit of NPP1, NPP2, and NPP3, respectively. The total installed capacity is 5144 MWe which is around 20% of its entire electricity generation in 2007. This makes

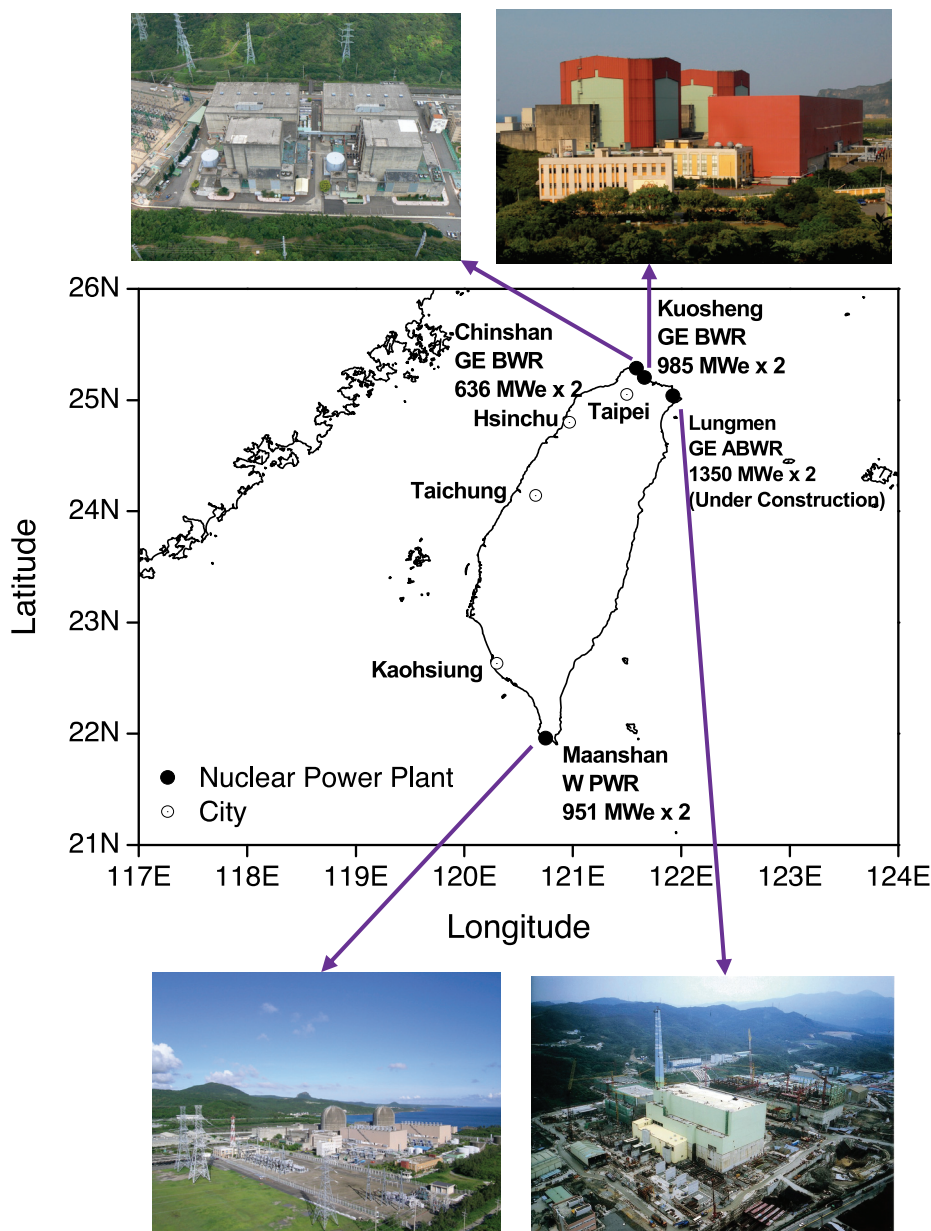


Fig. 1. The locality and outlook of nuclear power plants in Taiwan

Taiwan the 15th largest user of nuclear power in the world. TPC was planned to perform the 1.7% MURPU for all TPC's three operating nuclear power stations by schedule before the end of 2009 (Table 2). Therefore, the impact from the increasing power density and thermal release of a nuclear reactor to the environment from the heated effluent of NPP could enlarge simultaneously. Due to Taiwan's climate is marine tropical, the entire island is hot and humid from June to September. Moreover, the western side of the Pacific Ocean is warmer than the east as a result of the ocean current (WTT, 2011).

The marine water temperature around Taiwan could be more than 30°C during summer time. Therefore the impact from the waste heat of NPP could be severe and is needed to be evaluated when performing the power uprate of NPPs. Furthermore, to comply with the Effluent Standards of Taiwan's Environmental Law, especially in summer, the thermal effluent's problem will cause the reactor must be operated at a reduced power and consequently influence the electricity supply. This paper studies the power uprate effect due to waste heat release from the thermal effluent of Taiwan NPPs. The investigations were based on the thermal equilibrium of 100%, 105%, and 110% rated power, respectively. The long term monitor data of marine water temperature were also used to evaluate the impact level from waste heat during normal operation of NPPs. Moreover, the assessments of some helpful methods to mitigate thermal impact on thermal effluent from NPPs and the feasibility of these methods are also discussed correspondingly.

Parameter	NPP1	NPP2	NPP3
Thermal efficiency	35%	33%	34%
Rated thermal power	1817 MW	2985 MW	2785 MW
Net electric power	636 MW	985 MW	951 MW
Waste thermal power	1181 MW	2000 MW	1834 MW
Cooling water flow rate	34570 kg/sec	43906 kg/sec	47442 kg/sec

Table 1. The operational parameters of each NPP reactor unit in Taiwan

Reactor Unit	NPP1	NPP2	NPP3
Unit 1	2009.02.24	2007.11.30	2009.07.07
Unit 2	2008.07.09	2007.07.07	2008.12.02

Table 2. The MURPU completed date of NPPs in Taiwan

2. Impact of waste heat in Taiwan

In accordance with the second law of thermodynamics of Derive Kelvin Statement which is also called heat engine formulation, it is impossible to convert heat completely into work in a cyclic process (Hyperphysics, 2011). Hence, it is unattainable to extract energy

by heat from a high-temperature energy source and then transfer all of the energy into work. At least some of the energy must be passed on to heat a low-temperature energy sink. Therefore, there is no heat engine with 100% efficiency is possible. Waste heat is always an unavoidably by-product of NPPs. Generally the electrical efficiency of NPP, defined as the ratio between the input and output energy, most of the time amounts up to 33%. So the 67% heat is waste heat and must be released to the environment. Economically the most convenient way is to exchange such heat to water and then discharge them to sea, lake or river. If no sufficient cooling water available, most of the NPPs will equip with cooling towers to reject the waste heat into the atmosphere. In Taiwan, all NPPs are using marine water as the coolant and discharge the thermal water to the nearby sea. Therefore, waste heat impact to the marine environment is very sensitive and monitor by the public rigorously. Much more attention has been paid to workplace ecology for quite a time.

In northern Taiwan, a number of deformed thornfishes (Fig. 2. (a)) were first found since 1993 near the thermal outlet of NPP2. Although there is no clear links between the deformed fishes and the NPP, people directly think that the radiation is from nuclear power plant and therefore resulted in the deformed fishes. Through research studies, high temperature of ocean water had been proved to be the main factor of deformed *Terapon jarbua* and *Liza macrolepis* (Hung et al., 1998; Fang et al., 2004). In southern Taiwan, coral bleaching (Fig. 2. (b)), the whitening of diverse invertebrate taxa, was reported in July 1987 and July 1988 in adjacent marine water of the NPP3 (Fang et al., 2004). High sea surface temperature with high irradiance is assumed to be the primary factor in summer coral bleaching (Huang et al., 1992; Fang et al., 2004; Shiah et al., 2006). The increasing use of marine water for industrial cooling and the global warming might present a potential threat to the ecological environment in the ocean.

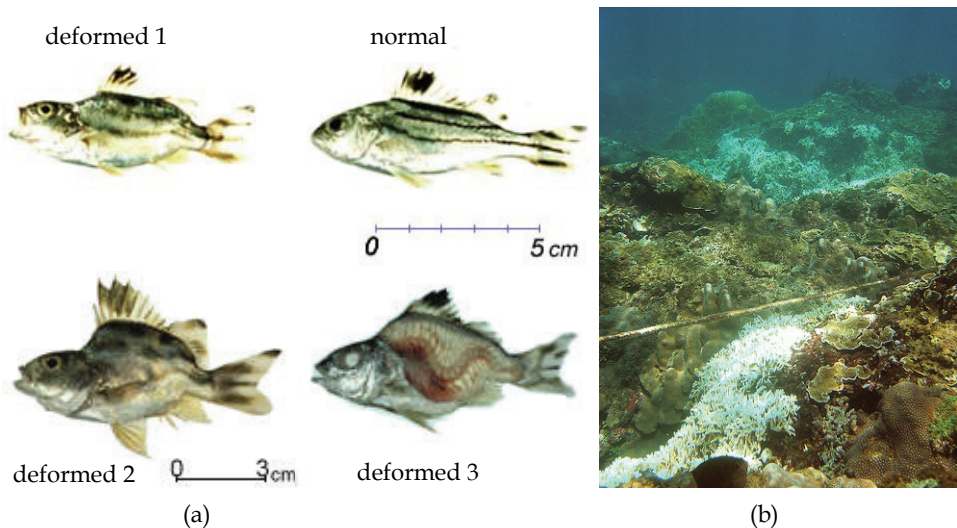


Fig. 2. (a) Deformed thornfishes in northern Taiwan ; (b) Coral bleaching in southern Taiwan (Ching-wai Yuen, 2011)

3. Effluent temperature evaluation

Because the events mentioned above were related to thermal discharge from NPPs, which elevated the marine water temperature and caused the damage, so the Effluent Standards of Taiwan’s Environmental Law: for effluents discharged directly into marine waters, the temperature at the discharge point shall not exceed 42 °C; and the temperature difference should not exceed 4 °C for surface water at 500 meters from the discharge point, are

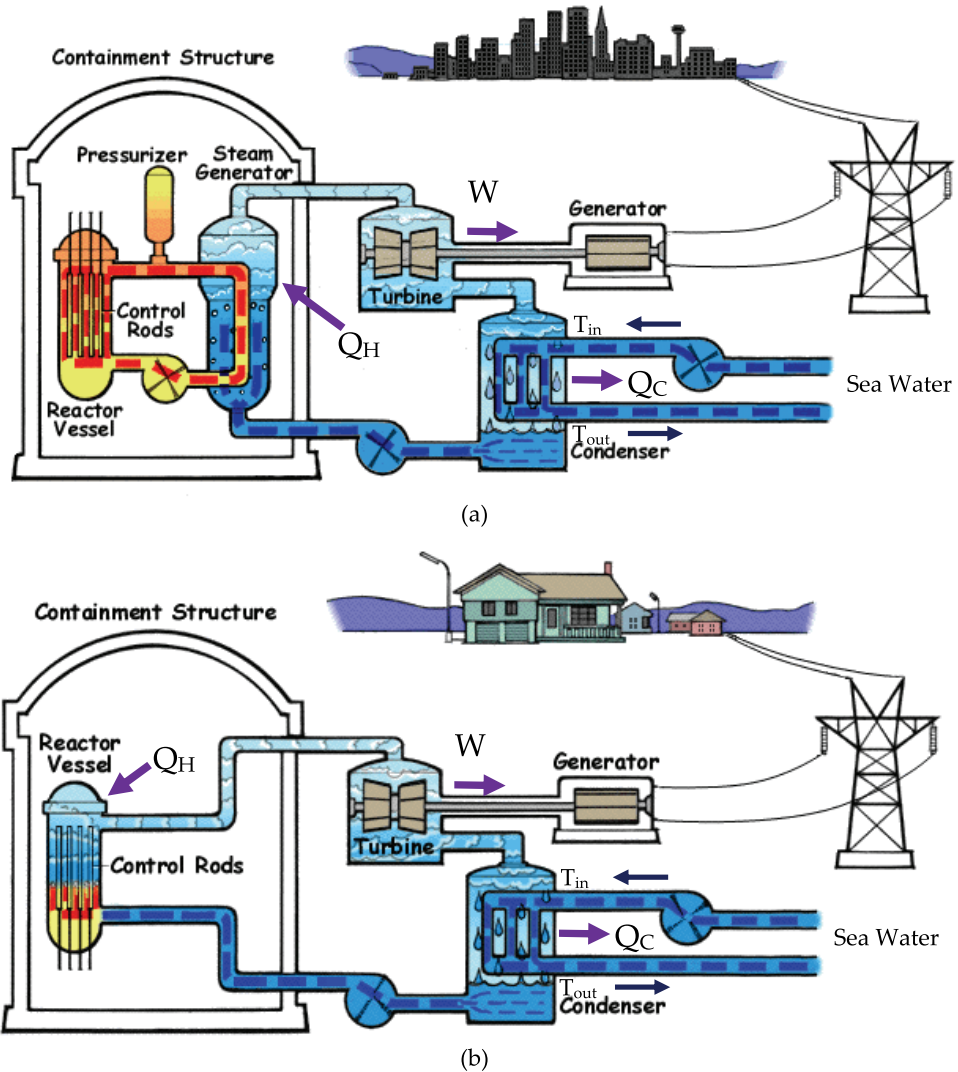


Fig. 3. The schematic diagram of (a) a PWR; (b) a BWR. The heat transfer routes are also depicted, respectively. (background images are taken from USNRC, 2011 b)

formulated to protect the ecological environment in adjacent marine water of NPPs. To assure the feasibility of power uprate in Taiwan's NPPs, based on the Effluent Standards, we conservatively evaluate the temperature difference between the outlet and inlet of condenser at 100%, 105%, and 110% rated power, respectively, by simply using specific heat capacity equation and the basic data in Table 1. Moreover, inlet and outlet temperatures of condenser, the marine water temperatures of 500 from the effluent discharge points, and the background marine water temperatures of 1000~1500 meters from the effluent discharge points, which were all taken from long term temperature monitor setup by TPC's NPPs, are used to assess the impact level of thermal water from June to September, respectively.

Fig. 3 (a) shows the schematic diagram of a PWR system and Fig. 3 (b) is the schematic diagram of a BWR system. As can be seen from the figure, an amount of heat Q_H , which can be derived from the thermal power of NPP, is transferred from the reactor, the net work W is delivered to the electric generator as it is driven by turbine, and the waste heat Q_C is rejected to the cooling water in the condenser and then discharged to the sea which could lead to the thermal pollution problem. To evaluate the elevated temperature of the effluent from NPPs, the waste heat Q_C of the is simply got by the following equation:

$$Q_C = \dot{m} \cdot C \cdot (T_{out} - T_{in}) = \dot{m} \cdot C \cdot \Delta T \quad (1)$$

where \dot{m} is the mass flow rate of cooling water (kg/sec), C is the specific heat of water (4186 joule/kg/°C), T_{out} is the outlet temperature of condenser (°C), T_{in} is the inlet temperature of condenser (°C), and ΔT is the difference between the outlet temperature and of the inlet temperature condenser (°C). Moreover, the waste heat Q_C can also be expressed by

$$Q_C = Q_H(1-\eta) \quad (2)$$

where η is the thermal efficiency and is defined as:

$$\eta = \frac{W}{Q_H} = \frac{Q_H - Q_C}{Q_H} \quad (3)$$

Using (1), (2), and the data listed in Table 1, the elevated temperature can be simply calculated. Furthermore, the ΔT at 100% power is used to predict the average elevated temperature of cooling water at 105%, and 110% power, respectively.

4. Effluent temperature and the reduction of seawater temperature

Table 3 lists the results of calculated temperature difference between inlet and outlet of condenser at 100%, 105%, and 110% rated power of NPP1, NPP2, and NPP3, respectively. The differential temperature from on-line monitor, at 100% normal operation power, and the predicted temperature differences at 105% and 110% rated power, are also shown in the table, correspondingly.

Fig. 4 displays the average water temperature of each NPP at the condenser inlet and outlet from June to September in 2006. Apart from, the corresponding data of 2007 are shown in Fig. 5. The elevated temperatures of cooling water after passing through condenser can also

be seen in the figures. As can be seen, the average inlet temperatures are 27.0, 27.9, and 28.9 °C for NPP1, NPP2, and NPP3; whereas the corresponding outlet temperatures are 36.2, 39.9, and 36.8 °C for NPP1, NPP2, and NPP3 by averaging the values of 2006 and 2007, respectively. Also shown in the figures of the elevated temperatures are calculated to be 8.2, 10.9, and 9.2 °C for NPP1, NPP2, and NPP3; whereas the corresponding monitoring data are 9.2, 12.0, and 7.9 °C for NPP1, NPP2, and NPP3 by averaging the values of 2006 and 2007, respectively. Therefore, the temperature difference between calculated and monitor data are 1.0, 1.1, and -1.3 °C. The different trend between them might be caused by more heat loss into atmosphere during heat exchanging at steam generator of PWR. Notably, the highest elevated temperature of NPP2 is 12 °C. According to the ocean observation of Taiwan, the marine water temperature could be near 30 °C in summer (CWBS 2011), thus the outlet temperature of condenser could be possible over 42 °C. From Fig. 4 and Fig. 5, we can also observe the outlet temperature of condenser is just around 42 °C especially in July. To avoid the effluent temperature exceeding 42 °C which is the limitation temperature of the Environmental Law, TPC cautiously operates NPP in the condition that the outlet temperature of condenser could be under 42 °C. Otherwise the operators of NPPs will operate the reactor from full power to a lower power. This will make TPC in a dilemma especially when the electricity demands are often urgent in summer. Thus for NPP2's power uprate it is better to take feasible engineering actions to lower 0.6~1.1 °C of the elevated temperature.

% Power	Calculated elevated temperature (°C)	Average elevated temperature of cooling water (°C)
NPP1		
100	8.2	9.2
105	8.6	9.6*
110	9.0	10.0*
NPP2		
100	10.9	12.0
105	11.5	12.6*
110	12.0	13.1*
NPP3		
100	9.2	7.9
105	9.6	8.3*
110	10.1	8.8*

*Predicted value

Table 3. Average water temperature differences between condenser inlet and outlet of NPP1, NPP2, and NPP3, respectively

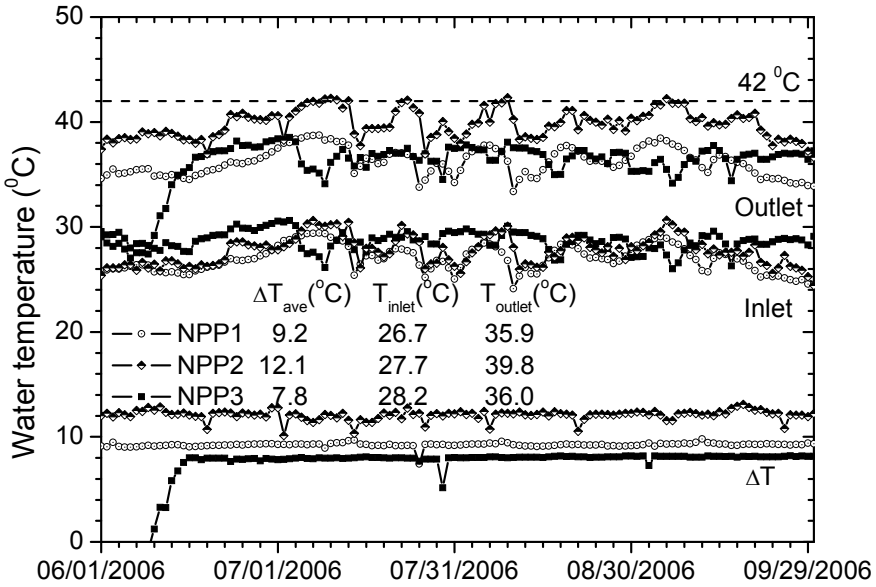


Fig. 4. The average temperature of NPP1, NPP2, and NPP3 at the condenser inlet and outlet from June to September in 2006. ΔT is the elevated temperature of cooling water between the condenser inlet and outlet. NPP3 was not operated in full power before June 15

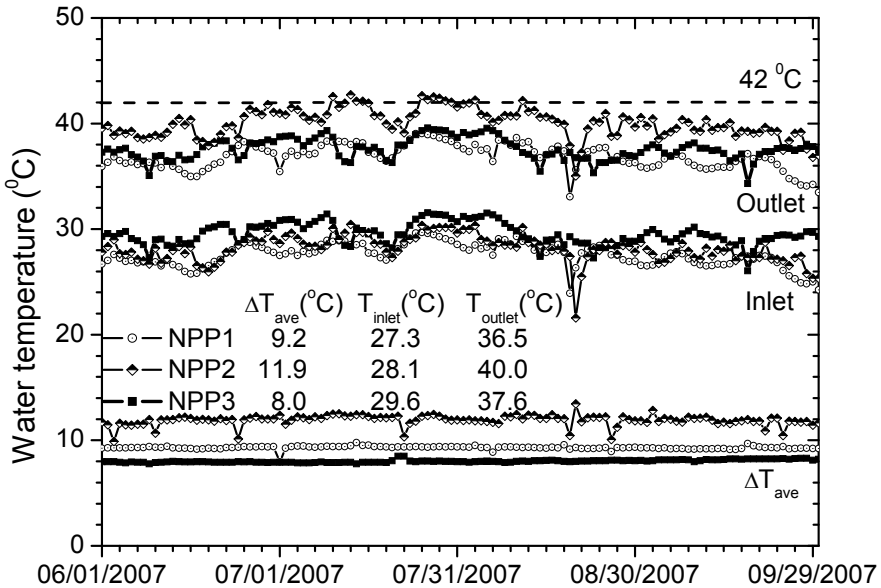


Fig. 5. The average temperature of NPP1, NPP2, and NPP3 at the condenser inlet and outlet from June to September in 2007. ΔT is the elevated temperature of cooling water between the condenser inlet and outlet

To reduce the effect of thermal effluent to the marine water ecology adjacent NPP, some effective methods: for example, prolong the discharge point by extending the path distance of effluent, lower the influent temperature by pumping deep level (deeper than 300 m) marine water, enlarge the transfer area of condenser, increase the flow rate of coolant by using higher power pumps, and improve the heat transfer efficiency by cleaning the pipes or replacing high efficiency pipes, can be used. However, these methods could be difficult to perform because of the huge engineering cost or the induction of side effects, such as water hammer, to the reactor system. Therefore, they are economically impractical or infeasible in solving the thermal effluent problem of NPPs.

Recently, a possible technical solution for increasing the thermoelectrical plant efficiency has been proposed by reducing the cold source temperature (Şerban et al., 2010). The method is originated from the concept of lowering the cooling water temperature by pumping deep level marine water. Approximate 10~20 °C reduction of influent temperature can be achieved by pumping from the 150~500 m ocean depth where the temperature is independent on the season and ranges between 5 ~15 °C. It can effectively reduce the cold source's temperature for open circuit and may increase the rated power of a thermal power plant with 2~4 % without increasing fuel consumption. The method can obviously overcome the problem of large variations of temperature function of the weather conditions and season. Moreover, the surface sea water often contains a lot of microorganisms that can nourish and deposit on the heat transfer pipes. Thus can more or less affect the heat exchange ability and lower the power efficiency. This innovative installation can provide a cold influent to NPPs and circumvent the pumping of polluted sea water. It will be very helpful to the power uprate of NPPs.

In Taiwan, dilution pump, which is currently being used at NPP3 (Fig. 6), of the same level as circulation pump can be employed to pump the background marine water (~30 °C) to mix with thermal effluent (~38 °C) before it is discharged into the ocean. Moreover, there are at least two obvious advantages to install the dilution pump at NPP although additional electricity consumption needed to operate the pump: firstly, it can regulate the thermal effluent temperature of NPP especially in summer time; secondly, it can be also a redundancy of circulation pump.

The idea of dilution pump is originated with the thermal equilibrium concept:

Heat rate lost by thermal water = Heat rate gained by cool water

$$-\dot{Q}_{tw} = \dot{Q}_{cw} \quad (4)$$

and then the following equation can be utilized to calculate the reduced temperature diluted by the marine water,

$$-C\dot{m}_{tw}\Delta T_{tw} = C\dot{m}_{cw}\Delta T_{cw} \quad (5)$$

where \dot{Q}_{tw} is the thermal water heat loss rate (W/sec), \dot{Q}_{cw} the cool water heat gain rate (W/sec), \dot{m}_{tw} the thermal water flow mass (kg/sec), \dot{m}_{cw} the cool water flow mass (kg/sec), C the specific heat of water (4186 joule/kg/°C), ΔT_{tw} the temperature difference of thermal water (°C), ΔT_{cw} the temperature difference of cool water (°C), respectively.

In NPP3, there are four circulation pumps for each unit; the power of dilution pump is 1.07 larger than the circulation pump. Thus 2.1 °C reduction of the outlet coolant for one unit can

be got from equation (5). Similarly, the reduced temperature of the outlet coolant can be 2.4 °C if one dilution pump installed on one unit at NPP2. It is sufficient to compensate the thermal impact causing by the power uprate and make sure that the effluent temperature can be less than 42 °C.

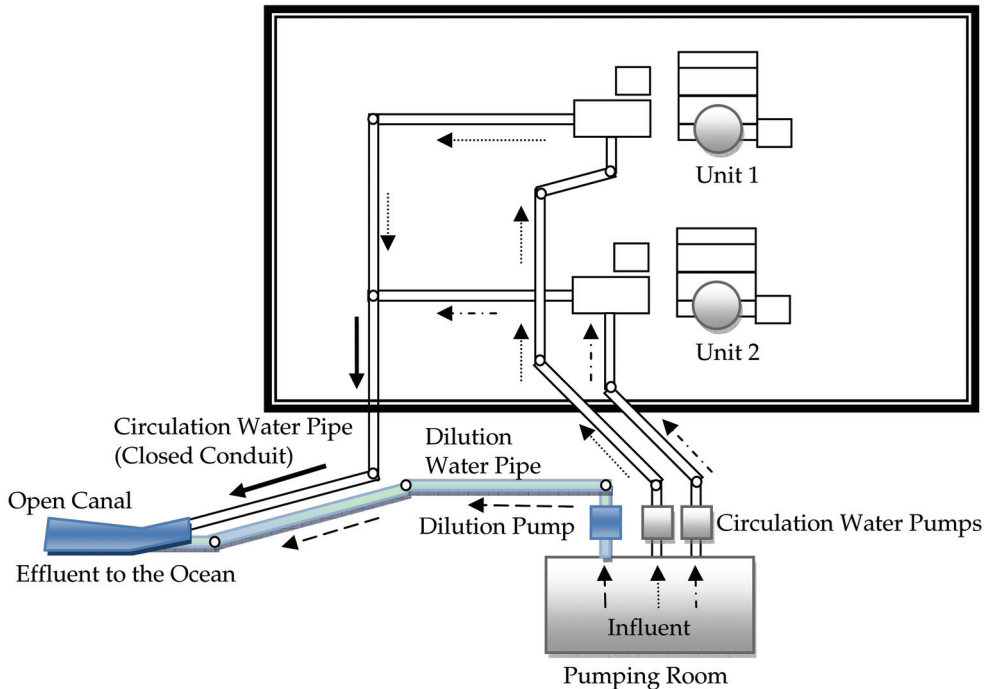


Fig. 6. The schematic flow diagram of dilution pump at NPP3

On the other hand, the Effluent Standards also require that the temperature difference (ΔT) should not exceed 4°C for surface water at 500 meters from the discharge point. Therefore, TPC arranges temperature monitors around the outfall point at each NPP to biweekly inspect the water temperature (Peir et al., 2009). Fig. 7, Fig. 8, and Fig. 9 show the monitor locations of NPP1, NPP2, and NPP3, respectively. As can be seen, there are two monitor groups, group A which is 500 m away from the discharge point, and corresponding group B, which is 1000~1500 m away from the discharge point and is set as the background temperature of marine water. The monitor results showed that the average temperature differences between group A and corresponding group B should be less than 4 °C. The most probable zone for ΔT exceeding 4°C is an area in the range of thermal effluent outfall and group A monitors. Intuitively, the ΔT greater than 4°C should be more frequently observed at the points N1A1, N2A2, N2A3, N3A2, and N3A3 than other points. But the discharged effluent travels in a canal and then mixes with sea water at a distance of 50-500 meters from the discharge point. The travelled distance of the effluent is dependent on the coastal current and littoral drift. Therefore, we observe some of the prompt values of ΔT could not be as expected under the limitation of 4°C (RRTC, 2006, 2007).

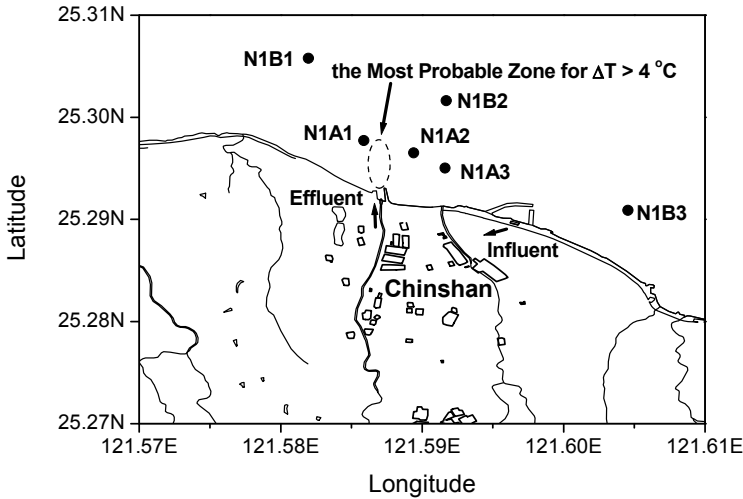


Fig. 7. The locations of water temperature monitors group A, N1A1, N1A2, and N1A3 and corresponding group B, N1B1, N1B2, and N1B3 at NPP1. Group A is 500 m away from the effluent discharge point. Group B is set as the background temperature of marine water

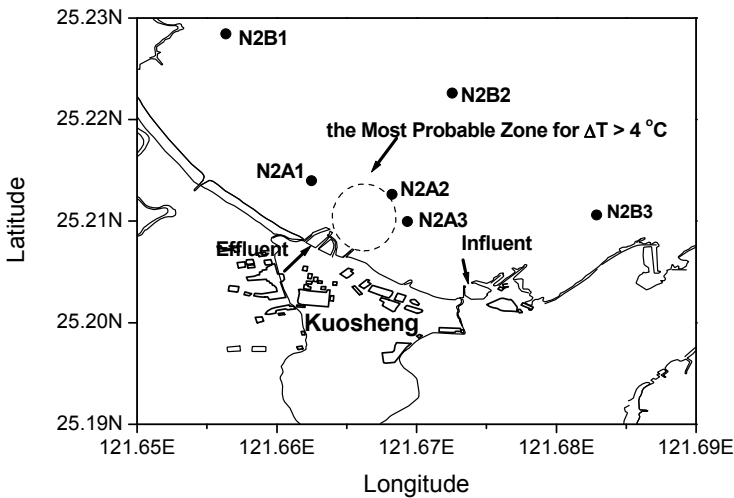


Fig. 8. The locations of water temperature monitors group A, N2A1, N2A2, and N2A3 and corresponding group B, N2B1, N2B2, and N2B3 at NPP2. Group A is 500 m away from the effluent discharge point. Group B is set as the background temperature of marine water

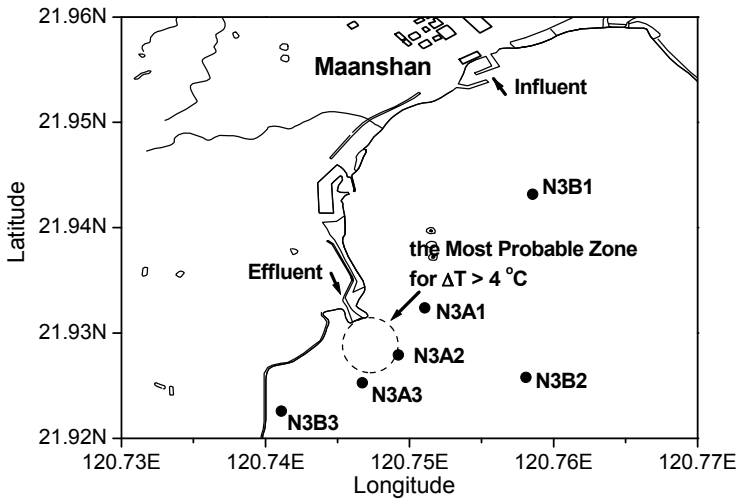


Fig. 9. The locations of water temperature monitors group A, N3A1, N3A2, and N3A3 and corresponding group B, N3B1, N3B2, and N3B3 at NPP3. Group A is 500 m away from the effluent discharge point. Group B is set as the background temperature of marine water

ID No.	2006	2007
NPP1		
N1A1	0	0.49
N1A2	0	0
N1A3	0	0
NPP2		
N2A1	0	1.61
N2A2	0.18	0.62
N2A3	0.85	0.13
NPP3		
N3A1	0.03	0
N3A2	0	0
N3A3	0	0

Table 4. The prompt probability that the temperature difference greater than 4°C between monitor group A and corresponding group B in 2006 and 2007

Table 4 lists the prompt probability of exceeding temperature, which is the data number ratio between exceeding temperature and all measured data, that the temperature difference

is greater than 4 °C between group A and corresponding group B in 2006 and 2007, respectively. As shown, the probability is highest at NPP2; while NPP1 is the second and then is the NPP3. The temperature differences were all less than 4.8 °C and all events were happening in summer (RRTC, 2006, 2007). The probability is apparently dependent on the elevated temperature of effluent and probably on its flow rate, its discharge type, the wind's direction, and coastal current. Current stagnation near the coast, where forming the most probable zone for the temperature difference greater than 4 °C, could also be another possible reason. As shown in Table 5 (the seawater temperatures measured at Longdong buoy which is also set up by Central Weather Bureau located at 120.82280E, 21.90220N near NPP1 and NPP2) and Table 6 (the seawater temperatures measured at Erluanbi buoy which is set up by Central Weather Bureau located at 121.93073E, 25.09348N near NPP3), the average seawater temperatures in adjacent to NPP3 can be 1.0~2.1 °C higher than those of NPP1 and NPP2 during summer, while the prompt probability of exceeding temperature is not correspondingly high. Obviously, by using the dilution pump the heated effluent can be effectively diluted with the background marine water and the discharge flow rate can be increased. The former will directly reduce elevated temperature of effluent; while the latter makes the thermal water be pushed longer away from the seashore. Thus makes the power uprate of NPPs not violating the Environmental Law. Besides, according to the observation data of the seawater temperatures in Table 5 and Table 6, the average seawater temperatures were in the range of 26.1 ~ 27.9 °C near NPP1 and NPP2, and of 28.2 ~ 29.1 °C near NPP3 from

Month	Maximum Seawater Temperature(°C)	Observation Year	Average Seawater Temperature(°C)	Minimum Seawater Temperature(°C)	Observation Year
1	22.8	2001	19.1	15.6	2003
2	23.2	2007	18.7	15.1	2005
3	25.0	2007	19.4	13.8	2000
4	27.9	2002	21.6	14.5	2000
5	28.9	2007	23.9	18.2	2009
6	29.7	2001	26.1	20.0	1999
7	31.5	2001	27.6	16.6	2008
8	31.7	2001	27.9	16.1	2009
9	31.1	2001	26.7	18.6	2008
10	27.4	2000	24.0	19.2	2005
11	26.3	2001	22.2	17.5	2009
12	24.2	2006	20.2	16.8	2004

Table 5. The seawater temperatures measured at Longdong buoy which is set up by the Central Weather Bureau located in the northern Taiwan near NPP1 and NPP2 (CWBS, 2011)

June to September, respectively. In the northern Taiwan near NPP1 and NPP2, the maximum seawater temperature 31.7 °C was observed in August, 2001, and in the southern Taiwan near NPP3, the maximum seawater temperature 36 °C was observed in July, 2005. Notably TPC has performed the 1.7% MURPU for all TPC's operating NPPs during 2007 and 2009. The increasing release of waste heat should directly causing the maximum seawater temperature is observed immediately after 2007. However, based on the observation data of CWBS, the elevation of seawater temperature does not increase correspondingly after the MURPU of NPPs in Taiwan. Although the additional influence of the ecology due to the thermal effluent of MURPU is insignificant at present, TPC has better monitor the seawater temperatures near NPPs continually for further power uprate (SPU or EPU) in the future. Moreover, the installation of dilution pump or innovation of pumping deep level water to effectively reduce the influent temperature could be two feasible options for prevailing over the difficulty of waste heat problem in power uprate.

Month	Maximum Seawater Temperature(°C)	Observation Year	Average Seawater Temperature(°C)	Minimum Seawater Temperature(°C)	Observation Year
1	28.9	2001	24.8	18.7	2006
2	28.4	2001	24.9	20.1	2005
3	30.6	2001	25.5	20.7	2005
4	31.2	2001	27.1	22.4	2005
5	32.5	2001	27.8	19.8	2002
6	32.1	2007	28.2	21.2	2002
7	36.0	2005	29.1	20.8	2002
8	33.7	2007	29.0	23.0	2004
9	32.7	2007	28.9	22.5	2005
10	30.4	2009	28.1	21.0	2001
11	29.4	2002	26.4	21.1	2003
12	29.2	2002	25.1	16.1	2003

Table 6. The seawater temperatures measured at Erluanbi buoy which is set up by the Central Weather Bureau located in the southern Taiwan near NPP3 (CWBS, 2011)

5. Conclusion

In conclusion, the 100%, 105%, and 110% rated power of Taiwan's NPPs are performed to assess the power uprate effect on thermal effluent under normal operation. Based on the long term monitor data of marine water temperature from June to September in 2006 and 2007, the results show that the effluent temperatures of NPP2 could have the opportunity to exceed the limitation 42 °C at the discharge point and the prompt probability of temperature

difference exceeding 4 °C for surface seawater at 500 meters from the discharge point could be higher for each NPP in summer. Feasible engineering actions, such as prolonging the discharge point by extending the path distance of effluent, increasing the flow rate of effluent, or using dilution pump to mix the thermal effluent with the background marine water, could be considered to mitigate the NPP's power uprate effect to the environment. Among others, adding the dilution pump at reactor unit is a very useful method to reduce the elevated temperature of effluent in summer. It can economically and efficiently compensate the power uprate influence of thermal waste heat discharging from NPPs. TPC has accomplished the 1.7% MURPU for its three operating NPPs during 2007 and 2009. The elevation of seawater temperature is currently not significant after the MURPU of NPPs. Long term observation of the additional influence on the ecology due to the thermal effluent of MURPU is needed in the future.

6. Acknowledgment

The author is grateful to Taiwan Power Company for the financial supports. Also the author would like to express his sincere thanks to Prof. Shih C.K. for his encouragement and valuable discussions in this work.

7. References

- Ching-wai Yuen (2011), available on the Internet at <http://vm.nthu.edu.tw/science/shows/nuclear/t-fish/index.html>
- CWBS (Central Weather Bureau Statistics), Taiwan (2011). >Home>Statistics>Marine Statistics>Water Surface Temperature Statistics, available on the Internet at <http://www.cwb.gov.tw/eng/index.htm>
- Fang, T.H., Chen, J.F., Tu, Y.Y., Hwang, J.S., and Lo, W.T. (2004). Hydrographical Studies of Waters Adjacent to Nuclear Power Plant I and II in Northern Taiwan, *J. Mar. Sci. Technol.*, Vol. 12, No. 5, pp. 364-371
- Hung, T.C., Huang, C.C., and Shao, K.T. (1998). Ecological Survey of Coastal Water Adjacent to Nuclear Power Plants in Taiwan, *Chem. Ecol.*, Vol. 15, pp. 129-142
- Huang, C.C., Hung, T.C., and Fan, K.L. (1992). Nonbiological Factors Associated with Coral bleaching in Shallow Water near the Outlet of the Third Nuclear Power Plant, Southern Taiwan, *UNEP Reg. Seas Rep. Stud.*, Vol. 147, pp. 205-224, Taipei, Taiwan
- Hyperphysics (2011), available on the Internet at <http://hyperphysics.phy-astr.gsu.edu/hbase/hframe.html>
- Peir, J.J., Shih, C.K., Pei, B.S., Ferng, Y.M., and Hsu, W.S. (2009). Power Uprate Impact Evaluations on Waste Heat of Nuclear Power Plants in Taiwan, Brussels, Belgium ICONE17: Proceedings of the 17th International Conference on Nuclear Engineering, Vol. 1, pp. 201-207
- RRTC (Research Report of Taipower Company), Taipower Company (2006, 2007). The Survey of Thermal Effluent of the Nuclear Power Plants
- Șerban V., Panait A., Țenescu M., Mingiuc C., Niță I., Androne M., Ciocan G.A., and Zamfir A.M. (2010). Possible Solutions for Increasing the Thermoelectrical Plant Efficiency

and for Pollution Decreasing, Neptun, Romanian, Proceedings of the WEC Regional Energy Forum – FOREN 2010

Shiah, F.K., Wu, T.H., Li, K.Y., Kao, S.J., Tseng, Y.F., Chung, J.L., and Jan, S. (2006). Thermal effects on heterotrophic processes in a coastal ecosystem adjacent to a nuclear power plant, *Mar. Ecol. Prog. Ser.*, Vol. 309, pp. 55–65

USNRC (2011 a). >Home>Nuclear Reactors>Operating Reactors>Licensing>Power Uprates> Types of Power Uprates, available on the Internet at <http://www.nrc.gov/reactors/operating/licensing/power-uprates/type-power.html>

USNRC (2011 b). >Home>Nuclear Reactors>Operating Reactors>Licensing>Power Uprates> Types of Power Uprates, available on the Internet at <http://www.nrc.gov/reading-rm/basic-ref/students/reactors.html>

WTT (Windows to Universe), (2011). Available on the Internet at http://www.windows2universe.org/earth/Water/images/ocean_temp.html

Part 3

Radiation Effects

Long-Term Effects of Exposure to Low-Levels of Radioactivity: a Retrospective Study of ^{239}Pu and ^{90}Sr from Nuclear Bomb Tests on the Swiss Population

Pascal Froidevaux¹, Max Haldimann² and François Bochud¹

¹*Institute of Radiation Physics, University Hospital Center and University of Lausanne*

²*Consumer Protection, Chemical Risks, Federal Office of Public Health
Switzerland*

1. Introduction

The production of nuclear energy may be a source of exposure to ionizing radiations, either for nuclear workers or the general population. Ionizing radiations are one of the most studied and ubiquitous carcinogens in our environment. The main basis for estimating the carcinogenic risk to humans are studies conducted on survivors of the Japanese atomic bomb, a population essentially exposed to acute high dose rates (Cardis et al., 2005b). Epidemiological studies of nuclear workers, who have been chronically exposed to much lower radiation doses show evidences that the classic approach of radiation protection based on the linear non threshold (LNT) model is valid: an excess relative risk (ERR) of cancers other than leukemia of 0.97 per Sv was found among a cohort of more than 400,000 nuclear workers in 15 different countries, all individually monitored for external exposure. Additionally, the study showed an ERR of 1.93 per Sv for leukemia, a disease that may be associated with radiation exposure (Cardis et al., 2005b). Nevertheless, these findings were not confirmed in a later study of workers from the French National Electricity Company (Rogel et al., 2005), and neither in the study of the United Kingdom Atomic Energy Authority (Atkinson et al., 2004). Conversely, both studies showed a strong healthy worker effect (HWE). Higher cancer rates are related to a significant cumulative radiation dose (Hunter and Muirhead, 2009). Besides, an adverse effect on the pulmonary function when exposed to ^{137}Cs has also been recently demonstrated for children living near the Chernobyl exclusion zone (Svendsen et al., 2010). Currently, there is a tremendous interest in the study of the Techa River cohort (TRC), a population which was exposed to low to moderate radiation doses at low-dose rates from radioactive releases from the Mayak plutonium production facilities into the Techa river between 1950 and 1956 (Degteva et al., 2000; Tolstykh et al., 2001; Krestinina et al., 2010). At total body doses as high as 10 Gy, 30% of cancer deaths have been attributed to plutonium exposure among the Mayak workers (Sokolnikov et al., 2008). In that particular case of worker exposure to high doses of radiation, the ERR due to plutonium exposure was 7.1 per Gy for males at age 60.

While numerous studies of the effect of ionizing radiation on nuclear workers exist, there are only a few studies which extend their research to the general population. Among any

given population, children are considered at higher risk (BEIR7, 2006) and several studies have focused on the risk of leukemia for children living in the proximity of a nuclear power plant (NPP) (Roman et al., 1999; Doyle et al., 2000; Cardis et al., 2005a; Kaatsch et al., 2008; Nussbaum, 2009). Laurier et al. (Laurier et al., 2008) have reviewed studies dealing with as much as 198 nuclear installations, three of them showing a significant excess of leukemia among children under 18 years of age (on the order of 5 cases detected for less than one expected). While the statistics tend to support the excess risk, the radioecological studies carried out on these sites failed to correlate the ERR with a significant increase of radioactivity burden in the environment or in food (Heasman et al., 1986; Black et al. 1994; Bithell et al., 1994; Hoffmann et al., 1997). The most recent study concerning the adverse effects of living in the proximity of a NPP revealed an odd ratio (OR) of 2.19 (with lower one-sided 95% confidence limit of 1.51) for leukemia in young children living in the vicinity of German NPP (Kaatsch et al., 2008). This study gave rise to new questions about the relationship existing between ERR and the distance to a NPP and the way to demonstrate the role, if any, of ionizing radiation in the observed ERR.

Most epidemiological studies on the effect of NPP on a general population, especially children, link leukemia statistics with the proximity to a NPP. No clear evidence came out of these studies and by their nature, these studies are subject to bias. There have been very few attempts to correlate leukemia cases with radiation dose because this latter is mostly unknown with respect to the general population, or considered much lower than the natural radiation background. In this respect, some authors have introduced a measure of doubt regarding the validity of the dose factors used for the fetus and newborn (Nussbaum, 2009; Shore, 2009); ERR of leukemia among children under 5 years of age living in the vicinity of a NPP may be the consequence of the father's exposure to radiation or direct fetus exposure, with a possibility that dose factors have been largely underestimated. While this assumption may be valid, Doyle et al. (Doyle et al., 2000) found no evidence of a link between exposure to low-level ionizing radiation before conception and an increased risk of adverse reproductive outcomes in men working in the nuclear industry. Nevertheless, the authors state that a possible link between a woman's exposure to radiation before conception and an increased risk of fetal death requires further investigation.

In addition to the lack of knowledge about the exposure dose to the population, dose rates due to in-vivo alpha-emitters, particularly transuranic elements, have been totally overlooked, mainly because of measuring difficulties (Schmitz-Feuerhake et al., 2005). Our opinion is that there is a lack of data on the radioactivity body burden of the general population, and in particular children. This information would facilitate the interpretation of leukemia statistics in terms of radiation dose rather than in terms of the distance to a radiation emission source (e.g. a NPP).

The determination of the external radiation dose in the vicinity of a NPP is obviously mandatory but may be of little use in the case of the risk related to very low doses of ingested or inhaled radionuclides. In this respect, the main challenge of national authorities is to survey diet and, possibly, the population body burden. While radioactivity surveys of food and the environment are a dedicated task of every laboratory dealing with environmental radioactivity surveys (Froidevaux et al., 2006a), the determination of very low-levels of radioactivity in the body is another challenge; whole body counting may provide data on ^{137}Cs (or other γ -emitters) contamination (Hodgson et al., 2004), but previous studies show that ^{90}Sr and plutonium could be the most radiotoxic isotopes that

should be searched for (Atkinson et al., 2004). Over the last ten years, mass-spectrometry has been applied as an alternative detection method for measuring actinides, especially plutonium. Using ICP-MS, the detection limit is lowered by a factor of ten compared to alpha-spectrometry. The detection limits at the femtogram-level needed for some particular environmental samples, are typically obtained by double focusing sector-field ICP-MS instruments or TIMS (Kim et al., 2000; Becker, 2003; Boulyga et al., 2003; Agarande et al., 2004; Baglan et al., 2004; Lindahl et al., 2010; Qiao et al., 2010). Using sf-ICP-MS, we were recently able to determine ^{239}Pu and $^{239}\text{Pu}/^{240}\text{Pu}$ ratio in the milk teeth of children born in Switzerland between 1951 and 1995 (Froidevaux and Haldimann, 2008) and in the vertebrae of individuals who died between 1962 and 2004 (Froidevaux et al., 2010).

Bones and teeth are both the main targets of plutonium and ^{90}Sr entering the blood stream. Approximately 100% of ^{90}Sr and 50% of the plutonium incorporated in humans is located in the skeleton. Another 30% of the plutonium burden is located in the liver (ICRP (International Commission on Radiological Protection), 1986). In this respect, the analysis of teeth and bones may be of great help to investigate low dose and low dose-rate exposure to radionuclides potentially emitted throughout the process of nuclear energy production (Culot et al., 1997). Among teeth, milk teeth (deciduous teeth) are very precious indicators of bone-seeking radionuclides that can be transferred from the mother's blood plasma to the fetus. Because deciduous enamel forms between week 13 in utero up to 9 months postnatally (thereafter essentially becoming inert), the analysis of milk teeth allows for the retrospective measurement of prenatal and early postnatal trace-element uptake during a critical period of child development (Dolphin et al., 2005). Another advantage of milk teeth as a tool for retrospective studies of bone-seeking radionuclide contamination is the fact that they are naturally shed at ages 6-12 years old. Conversely, there exists no other possibility of bone sampling except for collection at autopsy. Unfortunately, due to legal difficulties in obtaining samples for analysis, there are only limited data available worldwide, mostly concerning ^{90}Sr (Hodgson et al., 2004). The USTUR (United States Transuranium and Uranium Registries) is a source of very valuable information for human tissue studies, including bones, biokinetics, bioeffects and the dosimetry of uranium and transuranium in human. However, this database contains mainly tissues from workers exposed to radionuclides. As an example, USTUR studies show that, in addition to skeleton and liver, muscle is an appreciable reservoir for both plutonium and americium (Kathren, 1995).

We propose to use the ^{90}Sr and plutonium fallout of the nuclear bomb tests (NBT) of the sixties as a proxy to determine the radioactivity body burden that the population has received as a consequence of the tests. We used the Swiss databases on ^{90}Sr and ^{239}Pu in milk teeth and bones because this latter is the most complete that is currently available worldwide and covers a range of years from 1952-2002 (milk teeth) and 1960 to 2009 (vertebrae). We compared our results with other studies carried out worldwide. We hypothesized that the level of both radionuclides incorporated in the skeleton has been very low but significant as well as measurable using careful radiochemical and analytical procedures. We put the incentive on the analysis of ^{239}Pu and ^{90}Sr in milk teeth of children born from 1953 to 2005 to demonstrate the danger that these radionuclides may create if transferred to the fetus across the placental barrier. In addition, we collected vertebrae of deceased individuals (1960-2005) to measure the incorporation of very low-levels of bone-seeking ^{239}Pu and ^{90}Sr in the body.

2. Experimental

^{90}Sr analysis in milk teeth and bones is a very dedicated task and must be carried out with particular care to avoid bias due to other radionuclides that will be present in the sample, such as uranium isotopes, radium isotopes and their daughter products. As a consequence, a careful radiochemical separation of ^{90}Sr (or ^{90}Y) from the matrix and other radioisotopes is compulsory, because ^{90}Sr is a β -emitter whose counting, either by LSC or proportional counting, will be submitted to bias if other β -emitters are still present. In this respect, the analytical method used by the Radiation and Public Health project (RPHP, see www.radiation.org) for the determination of ^{90}Sr in milk teeth appears not satisfactory for the purpose of the authors and the conclusions that they draw from their studies. This is because the RPHP method does not use any chemical separation, except for a carbonate precipitation that will hardly remove ^{90}Y , radium isotopes, ^{210}Pb isotopes and its daughter ^{210}Bi , as well as thorium isotopes and many others (see for instance Mangano and Sherman, 2011). Thus, we propose below a method that is an alternative to the classical method using Eichrom Sr.spec resin in the analysis of ^{90}Sr , particularly for large sample sizes containing significant amounts of Ca, such as teeth, milk and bone. For ^{239}Pu determination, the main problem resides in the purification of plutonium from uranium, because the $^{238}\text{U}^{+}$ hydride will interfere with the determination of ^{239}Pu ; our methodological procedure is addressed in the corresponding sub-chapter.

2.1 Sampling

The vertebrae have been collected by pathologists over the last 45 years all over Switzerland. They were taken during autopsy from different adults ($n=1200$), of whom 80% were older than 60 and none younger than 8 at the date of death. 90% were older than 20 years in 1960. Thus our database represents the impact of nuclear bomb tests fallout on a population of adults, minimizing the problem of age-dependency in modelling. Milk teeth were collected by dentists (mainly school dentists). Both vertebrae and milk teeth were collected as part of the Sampling Program of the Swiss Federal Office of Public Health for environmental radioactivity survey, from the beginning of the nuclear era. The whole program is currently ongoing for ^{90}Sr determination in vertebrae and milk teeth. ^{90}Sr determination in vertebrae was carried out on individual cases as early as 1960 and required at least 5 g of bone ash; this study reports on the data set obtained during the last 50 years. ^{90}Sr analysis of milk teeth requires also at least 5 g of teeth ash, which necessitates about 10 milk teeth of children born during the same year in the same region. ^{239}Pu determination by mass spectrometry was carried out only after 2005, when adequate technology became available (see below). The samples for ^{239}Pu analyses are sub-samples of the vertebrae and milk teeth samples set used for ^{90}Sr determination that were preserved for further analyses. In this respect, the plutonium data set represents a retrospective study. To reach a satisfactory detection level and to minimize the effect of inter-individual variability, we pooled the samples of several individuals deceased in the same year to obtain at least 30 g of vertebrae ash per analysis. For milk teeth, we also used about 30 g of teeth ash, which required pooling about 50 teeth of children born the same year in Switzerland (Froidevaux et al., 2006b; Froidevaux and Haldimann, 2008; Froidevaux et al., 2010).

2.1 Radiochemistry

2.1.1 Plutonium analysis

Teeth ash was spiked with 10 ± 0.5 mBq of ^{242}Pu and submitted to microwave digestion in a Milestone MLS Ethos Plus digester (MLS GmbH, Leutkirch, Germany) for 40 minutes at

170°C in 8 M nitric acid (100 ml). After filtration plutonium was extracted on a Bio-Rad (Bio-Rad, Reinach, Switzerland) ionic exchanger (100-200 mesh, 25 ml in 1 cm diameter chromatography column) and purified on a micro-column (100 mg) of Eichrom® TEVA resin (Eichrom Environment, Bruz, France) while taking care to use Ultrapur® reagents (Merck, VWR International, Dietikon, Switzerland) to minimize the uranium content (plutonium was extracted in 5 ml of HNO_3 8 M, the column was washed with 10 ml of HNO_3 3M, 3 ml of HCl 9 M and once again with 3 ml of HNO_3 3 M). Plutonium was measured in 5% HNO_3 by SF-ICP-MS (see below). The same analytical procedure was used for the vertebrae. Calcium was measured on all samples by AA with a Perkin Elmer 4100 apparatus (Perkin Elmer AG, Schwerzenbach, Switzerland) and results of plutonium isotopes activity are given as Bq g Ca^{-1} (Froidevaux and Haldimann, 2008).

2.1.2 ^{90}Sr analysis

From 1963 to 1971, milk teeth and bones were analysed using the nitric acid fuming method (Froidevaux et al., 2006b). After 1974 and until now, we used a method using two cation exchange chromatography columns (AG 50w-x8, 50 and 8 ml) and specific complexing agents such as EDTA and CyDTA (*trans*-1,2-cyclohexylen-dinitrilo tetraacetic acid) to purify ^{90}Sr . After ingrown into ^{90}Sr , ^{90}Y daughter product was purified using a cationic exchanger (AG 50w-x8, 8 ml) and a malonate eluting solution. After precipitation of ^{90}Y as oxalate, the micro-precipitated source was counted in a low-level (0.3 dpm) proportional counter (Tennelec LB 4100w). For details of the procedure, see (Froidevaux et al., 2006b)

2.2 Mass spectrometry

Determining ^{239}Pu levels in most samples is hampered by the ubiquity and abundant presence of uranium. Consequently, peak tailing from $^{238}\text{U}^+$ and the formation of $^{238}\text{U}^1\text{H}^+$ molecular interference isobaric to ^{239}Pu are the limiting factors of plutonium analysis. The hydrogen originates from the water solvent (Zoriy et al., 2004). Because the degrees of ionization of uranium and hydrogen atoms in argon plasma are 100 % and about 0.1 %, respectively, uranium hydride UH^+ is formed in the plasma, most probably through reaction:



To minimize the formation of $^{238}\text{U}^1\text{H}^+$ ions, the chemical separation of uranium and plutonium using a TEVA resin prior to analysis did not yield sufficient removal of uranium. Therefore, it is essential to further reduce the formation of uranium hydride interference and correct for the residual signal contribution at m/z 239 in order to obtain unbiased plutonium measurements at ultra trace levels. The reduction of hydride formation of uranium requires special sample introduction systems, such as a micronebulizer with a desolvator. In this study, we equipped the instrument with an APEX Q desolvation device (Elemental Scientific, Scientific, Omaha, NE, USA) in combination with an ACM membrane unit (Elemental Scientific) that was effective in removing the solvent from liquid samples, thereby greatly reducing the formation of $^{238}\text{U}^1\text{H}^+$ while retaining plutonium for transport to the plasma ion source in the form of a dry aerosol. Additionally, this special configuration improved the signal-to-noise ratio by a factor of about 10, which was necessary to reach the very low plutonium concentrations. The $^{238}\text{U}^1\text{H}^+ / ^{238}\text{U}$ ratio was determined experimentally and a correction factor was applied to calculate the net ^{239}Pu response. The measured

$^{238}\text{U}^{1}\text{H}^+ / ^{238}\text{U}$ ratio of $1.4 \times 10^{-5} \pm 1 \times 10^{-6}$ was constant under the selected experimental conditions and falls well into the range of $1.2 \times 10^{-4} - 5.0 \times 10^{-6}$ reported in the literature (Becker et al., 1999; Kim et al., 2000; Boulyga and Becker, 2001; Taylor et al., 2001; Wyse et al., 2001). We used a double focusing SF-ICP-MS (Element2; Thermo, Bremen, Germany) for measuring the ^{239}Pu , ^{240}Pu , and ^{242}Pu isotopes. Furthermore, we monitored the ^{238}U isotope to correct for residual background contributions to the ^{239}Pu signal as a result of variable uranium concentrations in the actual sample solutions. Moreover, ^{199}Hg was measured to check for potential $^{199}\text{Hg}^{40}\text{Ar}$ interference. We performed 36 consecutive scans on each sample. The total measurement time per sample was 94 s. We applied the low-resolution mode ($m/\Delta m = 300$) to obtain maximum ion transmission. Optimum argon flow conditions in the PFA-100-1036 nebulizer (Elemental Scientific) were in the range of 0.9–1.1 l/min at a sample uptake rate of 235 $\mu\text{L}/\text{min}$. All other parameters of the ICP-MS corresponded to normal operating conditions. We conducted quality controls of the chemical separation and ICP-MS measurements by spiking 100 mL of 8 M HNO_3 with a reference solution of ^{239}Pu and subjected it to the overall ^{239}Pu determination process. The measured value of 2.7 ± 0.1 mBq ($n = 7$) agreed well with the reference value of 2.8 ± 0.3 mBq.

3. ^{90}Sr in milk teeth

The level of ^{90}Sr in milk teeth has been recorded in several countries since the beginning of the nuclear weapon tests. Data show that there are two peaks in the concentration of ^{90}Sr in milk teeth versus the year of birth, in 1958 and in 1965, followed by an exponential decrease after the entry into force of the Nuclear Test Ban Treaty (Rosenthal et al., 1964; Aarkrog, 1971; Rytomaa, 1972). There were several further studies on teeth, including permanent teeth, initiated punctually to answer specific questions, such as how much radiation the population received following the Chernobyl NPP accident (Kulev et al., 1994; Stamoulis et al., 1999), the contamination from the Sellafield reprocessing plant (ODonnell et al., 1997) or the contamination of the Techa river (Tolstykh et al., 2003; Tolstykh et al., 2008). In Switzerland, a monitoring program of ^{90}Sr in milk teeth was initiated by the Federal Office of Public Health in the late fifties and is still ongoing (Froidevaux et al., 2006b). Figure 1 displays the features of the ^{90}Sr content of milk teeth monitored in Switzerland (1951–2002, (Froidevaux et al., 2006b)), Denmark (1953–1963, (Aarkrog, 1971)), United-Kingdom (1960–1971, (Hodgson et al., 2004)), Germany and Northern Ukraine (1982–1986, (Schmitz et al., 2004)) and shows the maximum value determined in Norway (1965) and Finland (1963) and, between 1976 and 1979, in French Polynesia (Badie et al., 1987). Dates must be understood as the birth year of the children. For the United-Kingdom, the data represent activities found in premolar roots of milk teeth from children aged 10 (Hodgson et al., 2004). In this respect, and because the roots of teeth have a bone-like structure (Gulson and Gillings, 1997), these data correspond better to the activities that can be found in trabecular bones, rather than in the enamel of milk teeth. Figure 1 shows that ^{90}Sr (Bq/gCa) activities found in Switzerland are situated between the maximum values found in Norway and Finland and the activities determined in Denmark. Activities of premolar roots from the UK are significantly lower, showing that milk teeth may actually accumulate ^{90}Sr to a larger extent than bones. ^{90}Sr originating from the Chernobyl disaster (1986) has not significantly impacted Switzerland and Germany, but possibly the slightly higher values found in milk teeth of children from northern Ukraine may reflect the contamination of foodstuff with ^{90}Sr of Chernobyl or other origins in this region. Current values found in Switzerland are close to 25 mBq/gCa.

^{90}Sr is mostly incorporated through ingestion of contaminated food, a situation which may last for decades after fallout deposition on soil. Worldwide studies on milk teeth contamination demonstrate that NBTs fallout from the sixties has significantly increased the ^{90}Sr activity of food, especially milk, so that a very significant increase in ^{90}Sr (up to a value of 0.3 Bq/gCa in 1963 in Switzerland) is observed in milk teeth. Figure 2 shows the results of ^{90}Sr analysis of milk for Switzerland (1954-2009) and Norway (1953-1972, (Christensen et al., 1975)). Additionally, data for milk from New-Zealand are added for comparison of both Northern and Southern hemispheres (Badie et al., 1987). While several large NBTs were conducted in the Southern hemisphere, this latter presents an overall contamination several times less than the Northern hemisphere. This fact is reflected by the very low activity (average 14 mBq/gCa) determined in the milk teeth collected in French Polynesia, 4 times less than in Switzerland for the same date of birth. For Switzerland, the data presented in Figure 2 are issued from the analysis of milk collected in the Swiss lowlands. As a matter of fact, milk activities considerably differ if the milk is sampled from cows who grazed in Alpine pastures, with a ten times increase in activity for grazing land located at 2000 m above sea level (Pourcelot et al., 2007).

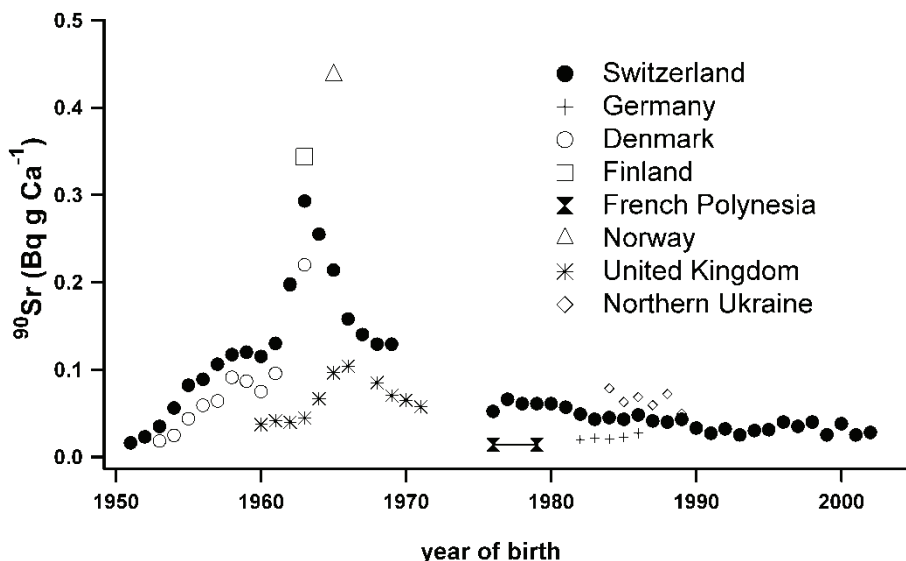


Fig. 1. ^{90}Sr activities (Bq/gCa) in milk teeth as a function of the year of birth of the children.

Activities in milk samples display essentially the same features as milk teeth, with a maximum activity observed in 1963, just before the entry into force of the Partial Nuclear Test Ban Treaty that ended American, British and former Soviet Union atmospheric nuclear weapon tests. Accordingly, we can conclude that the food (milk)-mother-fetus-milk teeth pathway is the most important mechanism of milk teeth contamination. A very significant correlation is observed between milk contamination and milk teeth contamination in Switzerland (Pearson correlation coefficient of 0.92) with a milk-to-milk teeth transfer factor of 0.2. In this respect, milk contamination by ^{90}Sr is a very good proxy of milk teeth contamination.

3.1 Influence of the Swiss nuclear power plants on ^{90}Sr activities of milk teeth

The Swiss database on ^{90}Sr contamination of milk teeth contains information concerning three distinct regions of Switzerland; the first region includes the canton of Zürich and a large part of the Swiss German lowlands. The Gösgen, Beznau and Leibstadt nuclear power plants (NPPs) are included in this region. The second region is the French-speaking part of Switzerland, mainly the canton of Vaud. There is a potential influence of the Mühleberg NPP in the Eastern part of this region. The third region is the Italian-speaking part of Switzerland, which is shielded from the Swiss NPPs by the Alps and borders Italy which has no active nuclear program (Froidevaux et al., 2006b).

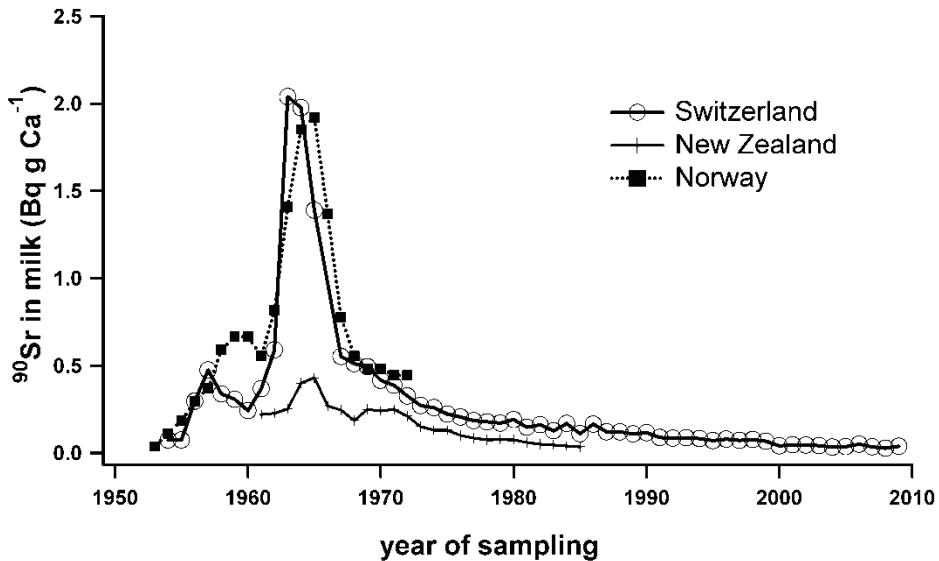


Fig. 2. ^{90}Sr activities (Bq/gCa) in milk sampled in Switzerland, Norway and New-Zealand.

Figure 3 shows the results of an analysis of the ^{90}Sr activities of the cantons of Tessin and Zürich as a function of the ^{90}Sr activities measured in the canton of Vaud, for the same years of birth. Both correlations are very strong (Pearson coefficient = 0.99), which means that the contamination of milk teeth originated from the same event, e.g. the NBT fallout of ^{90}Sr . Nevertheless, both slopes differ from unity (0.84 for Zürich and 0.82 for Tessin). This fact may reflect a difference in consumption habits in the canton of Vaud compared to the cantons of Tessin and Zürich. Additionally, the canton of Vaud includes large areas of the Jura mountains and pre-alpine mountains that possibly contribute to a higher contamination of milk (Pourcelot et al., 2007). The canton of Zürich, which is potentially under the influence of 4 among the 5 nuclear reactors located in Switzerland, presents no statistical differences compared with the canton of Tessin county, which is shielded from these same reactors by the Alps. This indicates that the Swiss NNPs have had no significant impact on the ^{90}Sr activities of milk teeth and that the ^{90}Sr in these human samples arises only from the NBT fallout of the sixties that contaminated foodstuff and the mother-to-fetus contamination across the placental barrier.

4. Plutonium in milk teeth

There exist only a few studies on teeth contamination by plutonium. The lack of data on plutonium in teeth is a result of the difficulty of the analysis, which requires a large sample size to yield results above the detection limit. This is because the plutonium activity is so low that a classical alpha-spectrometry technique is barely satisfactory to produce activities and uncertainties that could be used to demonstrate the potential influence of NPP on the plutonium body burden.

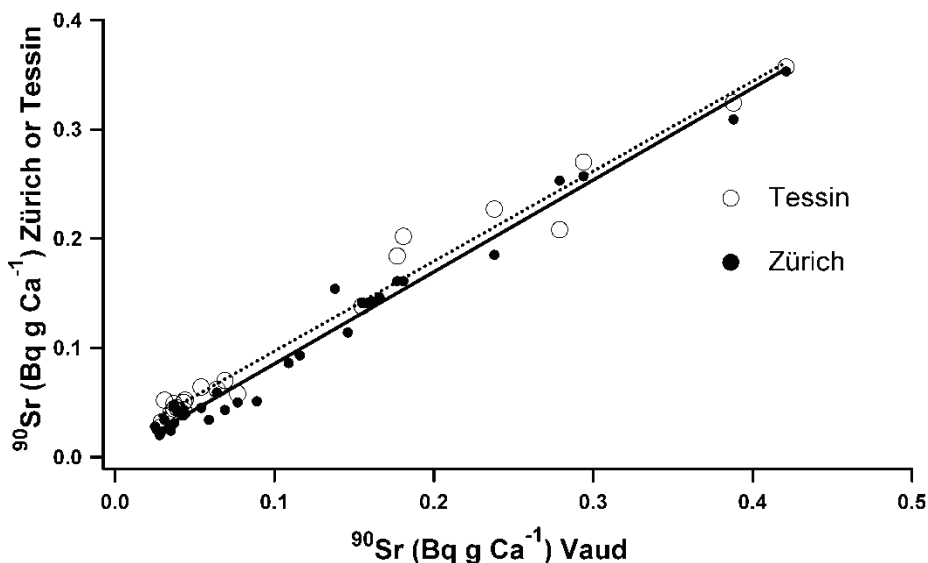


Fig. 3. ^{90}Sr activities (Bq/gCa) of milk teeth of the cantons of Tessin and Zürich as a function of the ^{90}Sr activities of milk teeth of the canton of Vaud, for the same years of birth (1953-1996).

Long et al. (1991) have determined the activity of $^{239+240}\text{Pu}$ in milk teeth of 35 different geographically located child populations in the United Kingdom. The average concentration was 5.2 mBq/kg of teeth ash. They concluded that there was no correlation with mean annual rainfall, that can be used as a proxy for the intensity of the radionuclide deposition (Renaud et al., 2003; Pourcelot et al., 2007), or with the distance from the Sellafield reprocessing plant. In contrast, O'Donnell et al. (1997) found a significant correlation between the plutonium content of milk teeth and the distance to the Sellafield plant, with activities near the plant close to 6 mBq/kg ash. At a distance above 150 miles from Sellafield, the activity drops to 3.0 mBq/kg ash.

The use of sf-ICP-MS allows us to analyse our set of milk teeth sampled from 1951 to 1995 for ^{239}Pu content and $^{239}\text{Pu}/^{240}\text{Pu}$ ratio (Froidevaux and Haldimann, 2008). In fact, we used the ^{239}Pu activity in milk teeth to probe for the potential of plutonium, a highly radiotoxic nuclide, to cross the placental barrier. We hypothesized that the plutonium inhaled by the mother will possibly cross the placental barrier, leading to a similar activity profile as observed for ^{90}Sr in milk teeth. Surprisingly, results show a very different situation, with

^{239}Pu activity peaking for the years of birth 1954-1956, some 9 to 10 years earlier than the ^{90}Sr peak (Figure 4). Nevertheless, the $^{240}\text{Pu}/^{239}\text{Pu}$ isotopic ratio is 0.21 ± 0.06 ($n=23$) from which we infer that the plutonium source is indeed the NBT fallout (Kelley et al., 1999; Warneke et al., 2002).

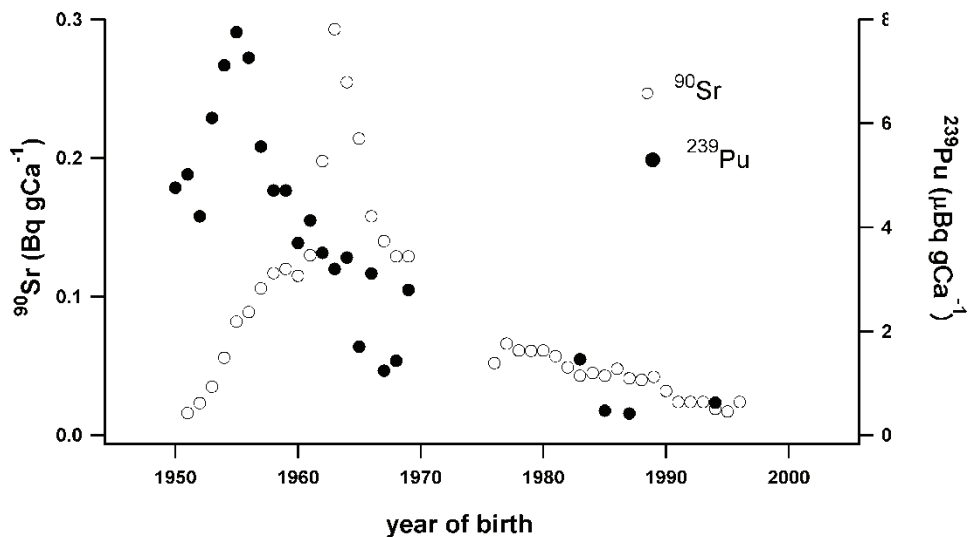


Fig. 4. ^{239}Pu (mBq/gCa) and ^{90}Sr (Bq/gCa) activities in milk teeth of children born in Switzerland 1950-1996.

A careful analysis of the year at which children shed their teeth shows that most of the milk teeth collected in the Swiss study are coming from children about 9 to 11 years old. This is because the teeth are collected by dentists, usually by school dentists. Most of the teeth sampled in this way are thus larger teeth (e.g. premolar or molar) that are shed at an older age compared to other teeth e.g. incisors. The offset between the highest activities of plutonium found in milk teeth and the maximum highest activities that were measured in air during the sixties represents exactly the time necessary to shed the teeth. Thus we interpret this offset as a proof that plutonium has not crossed the placental barrier, otherwise the plutonium activities in the milk teeth would have peaked for the same year of birth than ^{90}Sr . Instead, the plutonium activities that we measured in the teeth reflect the plutonium concentration in the air during the year or so before tooth shedding, which takes place on average 10 years after birth according to our study (Froidevaux and Haldimann, 2008). Because our study used whole teeth, we measured plutonium that was present in the root and cementum structures of the teeth, both remodelling at the same rate as the trabecular bone socket (Gulson and Gillings, 1997). To confirm this hypothesis, we roughly separated the roots of milk teeth from the rest of the teeth for two samples (born 1954 and 1965, 30 teeth) before measurement and found that ^{239}Pu in the roots has activities up to 9 times higher than the rest of teeth (mainly enamel). It is likely that the low residual ^{239}Pu activity found in the enamel represents a contamination by residual root and dentine structures still present in the enamel sample. Therefore, it is highly probable that the enamel laid down in utero is virtually free of ^{239}Pu . Consequently, neonates were probably born free

of plutonium, even when the environmental plutonium was at its highest, in the early 1960s. Our interpretation of the plutonium activity in deciduous teeth as a function of the year of birth is that neonates start to incorporate plutonium through inhalation of contaminated air after birth, until they shed their milk teeth. Because of the exchange of the bone-like structure of the teeth with the blood plasma, a higher concentration in milk teeth will show up for children shedding their whole teeth when the plutonium concentration in the air was at its highest, i.e. 1963. Thus ^{239}Pu activity will peak in milk teeth of children born circa 1953, as observed in Figure 4.

To compare our results with the results from the literature, we used a conversion factor of 0.35 g Ca/g ash (Swiss database, $n=182$, $\text{mean}=0.35\pm 0.04$) because results were given as mBq/kg ash in the former literature. We also used a multiplication factor of 1.68 of our ^{239}Pu value because the literature data concern the activity of both ^{239}Pu and ^{240}Pu isotopes as given by alpha-spectrometry. O'Donnell (O'Donnell et al., 1997), found a mean activity of 5 mBq/kg ash in permanent teeth sampled in 1990 in the UK to compare with our value of 0.6 mBq/kg ash. Long et al. found similar values in a study of 35 different regions of the UK, with a mean value of 5.2 mBq/kg ash. The factor of 9 found between milk teeth in our study and permanent teeth in the UK studies confirms that plutonium does not cross the placental barrier and does not contaminate the enamel of the deciduous teeth that was laid down during pregnancy. In this respect, the activity of the permanent teeth possibly represents a proxy for the activity that might be found in bone. We did not discover any potential influence of the 5 Swiss NPPs on the ^{239}Pu contamination of milk teeth, as demonstrated by the $^{240}\text{Pu}/^{239}\text{Pu}$ isotopic ratio of 0.21 ± 0.06 , close to the reference value of 0.187 for NBT fallout (Kelley et al., 1999; Warneke et al., 2002; Froidevaux and Haldimann, 2008). A significant decrease of this ratio would have supported the hypothesis that some of the plutonium arises from other sources, e.g. burnt nuclear fuel (Ketterer et al., 2004a), while a significant impact of the Chernobyl accident would have increased it up to 0.35 (Ketterer et al., 2004b).

5. ^{90}Sr in bones

Similarly to milk teeth, several countries have initiated a program of measuring the ^{90}Sr body burden through analysis of bones sampled at autopsy (Aarkrog, 1971; Christensen et al., 1975; Bauman et al., 1977; Dehos and Kistner, 1980; Kalmykov et al., 1997; Stamoulis et al., 1999; Hodgson et al., 2004; Froidevaux et al., 2010). In the particular case of bones analysis, the choice of the type of bones sampled is very critical. The strontium levels in bone vary according to the bone structure, and higher amounts of strontium are found in cancellous bone than in cortical bone after stable strontium ingestion. However, strontium levels at different skeletal sites are strongly correlated, and the strontium content of the lumbar vertebra may be estimated from iliac crest bone biopsies in the monkey (Dahl et al., 2001). Usually cancellous bone such as vertebrae, ribs or the iliac crest are used for a ^{90}Sr survey because the remodeling rate is higher compared to compact bones (Martin and Seeman, 2008; Zebaze et al., 2010). In this way, a better evaluation of the radioecological situation in a given location is obtained using cancellous bones because the activity found in the bone will reflect more accurately the current contamination of foodstuff. Nevertheless, the use of cortical bone such as the tibia may be of help when an archive of contamination is needed.

In Switzerland, the Federal Office of Public Health initiated a ^{90}Sr survey program using an analysis of ^{90}Sr in vertebrae of individuals deceased between 1960 and now. To our

knowledge, the Swiss database is the only one reflecting the ^{90}Sr contamination of the human skeleton for the last 50 years and which is still ongoing. Results are presented in Figure 6, in which data from several other studies from the literature are also given for comparison; the ^{90}Sr activities for Switzerland are situated between the average activities found worldwide in adults and activities found in Denmark for children deceased before their first year. Higher values were also found in children less than 5 years in Norway (highest activity=0.52 Bq/gCa for the year of death 1965) with a children/adults (>20y) activity ratio of 2.5 for children less than one year, of 3.3 for children less than 5 years and 1.7 for children between 5 and 20 years at the time of death (Christensen et al., 1975). Current activities are in the order of 0.028 Bq/gCa, a value that is typically found elsewhere (Stamoulis et al., 1999).

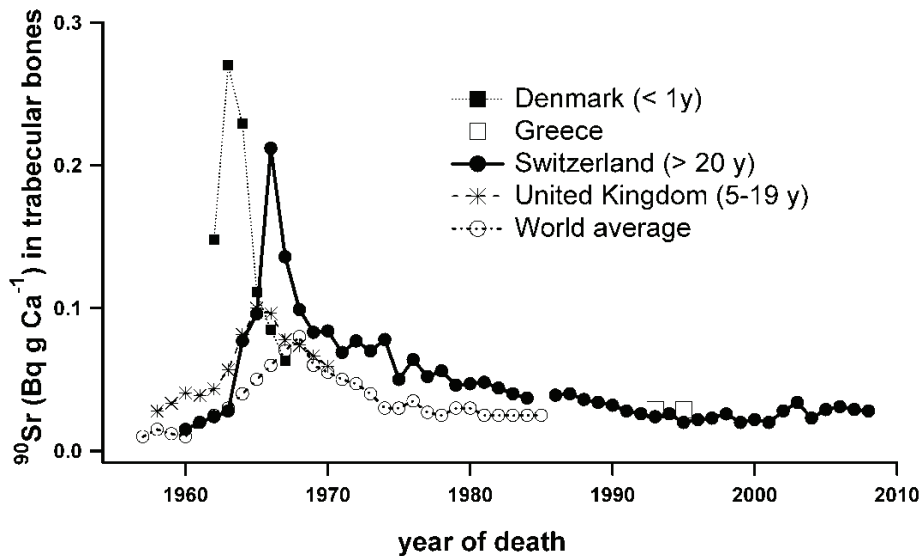


Fig. 6. ^{90}Sr (Bq/gCa) in cancellous (trabecular) bones sampled at autopsy as a function of the year of death.

Swiss data are significantly above the world average data or United Kingdom data, which is most likely a reflection of the Swiss population's high consumption of dairy products. The highest activity is found for the year 1965-1967 in adults in Switzerland and worldwide and in children 5-19 years in UK, but significantly earlier in children less than one year old in Denmark and Norway (1963-1965; (Aarkrog, 1971; Christensen et al., 1975)). This observation is supported by the higher remodeling rate of bones and bone growth measured in younger children. As a consequence, the incorporation of ^{90}Sr in bones is faster (and higher) for young children than for adults (see also (Papworth and Vennart, 1984) for a discussion on the uptake and turnover of ^{90}Sr in the human skeleton). In this way, ^{90}Sr contamination of the environment and foodstuff will have a greater negative impact on children than on adults, leading to an absorbed dose in the marrow to age 70 about 30 times higher if ^{90}Sr is incorporated when less than one year old, compared to a similar ingestion at the age of 20 years (Papworth and Vennart, 1984). No effect of the Chernobyl accident was

observed on the vertebrae activities in Switzerland, the pre-Chernobyl activities being somewhat higher (0.044 Bq/gCa, 1980-1985) before the accident than after (0.037 Bq/gCa, 1986-1989). Vertebrae were collected in different regions of Switzerland, and two regions are still currently being sampled; for the same year of death, the activities in vertebrae sampled in the canton of Vaud are strongly correlated with the activities in vertebrae collected in the canton of Tessin (Pearson=0.98), in the Basel area (Pearson=0.96), and in the St-Gallen area (Pearson=0.99). Nevertheless, the slopes differ from unity for all correlations, showing that vertebrae collected in the canton of Vaud contain 18% more ^{90}Sr than vertebrae collected in the Basel area, 2% more than in vertebrae from the St-Gallen region and 25% less than in the canton of Tessin. These data confirm that the contamination of the skeleton is coming from the same event (the NBT fallout) and that the canton of Tessin, which has received more deposition from the NBT fallout because of a higher average rainfall rate, shows a slightly higher ^{90}Sr body burden. Our results do not support the assumption that the Swiss NPPs have a potential influence on the ^{90}Sr body burden of the population living within range of the NPPs emission (mostly the Basel region here). Conversely, a higher ^{90}Sr skeleton burden is found in the canton of Tessin, an area which is shielded from the Swiss NPPs by the Alps.

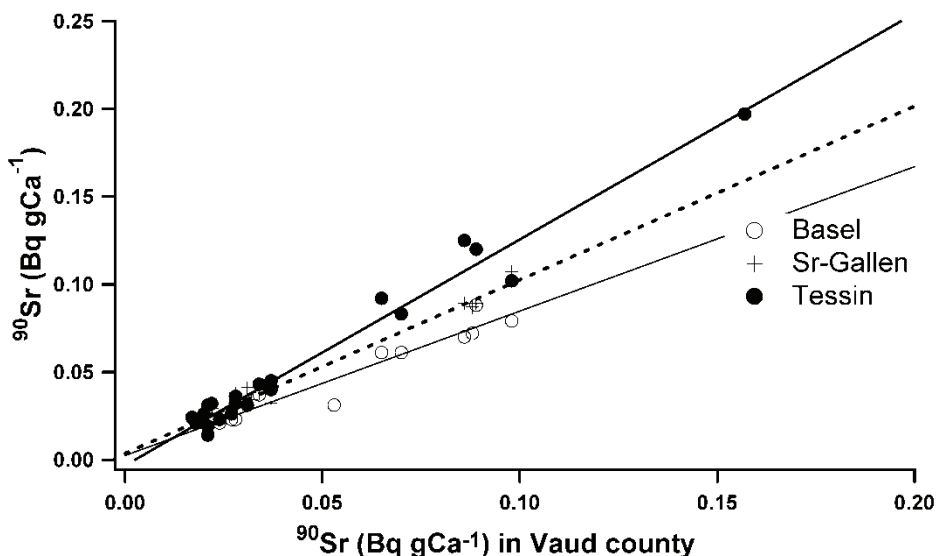


Fig. 7. ^{90}Sr activities (Bq/gCa) in vertebrae of the Basel area, of the St-Gall region and of the canton of Tessin as a function of the ^{90}Sr activities in vertebrae of the canton of Vaud, for the same year of death.

6. Plutonium in bones

If human data for ^{90}Sr are widely available, they are rather scarce for plutonium. USTUR represents probably the most important database for biokinetic modelling of actinides (Kathren, 1995). A review of contributions of human autopsies to the dosimetry of plutonium in man has been further proposed by Kathren (Kathren, 2004). Nevertheless, most of the data concern individuals that have been previously exposed to plutonium

because of their activities in the nuclear industry. Only few studies concern the effect of the NBT fallout on the general population (Taylor, 1995; O'Donnell et al., 1997; Takizawa et al., 2000; Froidevaux and Haldimann, 2008); the most extensive is probably McInroy's work on plutonium in autopsy tissues which contains data on more than 260 people, both from the general public in the US as well as workers from the nuclear industry (McInroy et al., 1979). Nevertheless, all these studies were carried out using alpha-spectrometry, which is a less sensitive technique for plutonium determination than mass spectrometry. Moreover, alpha-spectrometry cannot separate ^{239}Pu and ^{240}Pu signals while the $^{240}\text{Pu}/^{239}\text{Pu}$ is a very good signature of the origin of the plutonium contamination.

In our work, we determined the ^{239}Pu and ^{240}Pu activities in vertebrae of individual who were mostly older than 20 years at the time of the highest fallout rate of plutonium, using high sensitivity sf-ICP-MS. Data contain results for people who died between 1962 and 2004 in Switzerland. In this respect, our database is probably the most complete database covering the last 40 years for a given population. This allows us to determine, with a significant confidence level, how long plutonium is retained in the skeleton, a very important data in dose assessment that was not previously ascertained (Froidevaux et al., 2010). Results are presented in Figure 8, in which a comparison with published data is included. Because published data usually are given as mBq per kg of wet weight in the former literature, we apply a factor of 4.8% Ca per kg of wet weight and a factor of 1.68 to take into account the $^{240}\text{Pu}/^{239}\text{Pu}$ isotopic ratio of the NBT fallout to recalculate the activity in mBq/gCa.

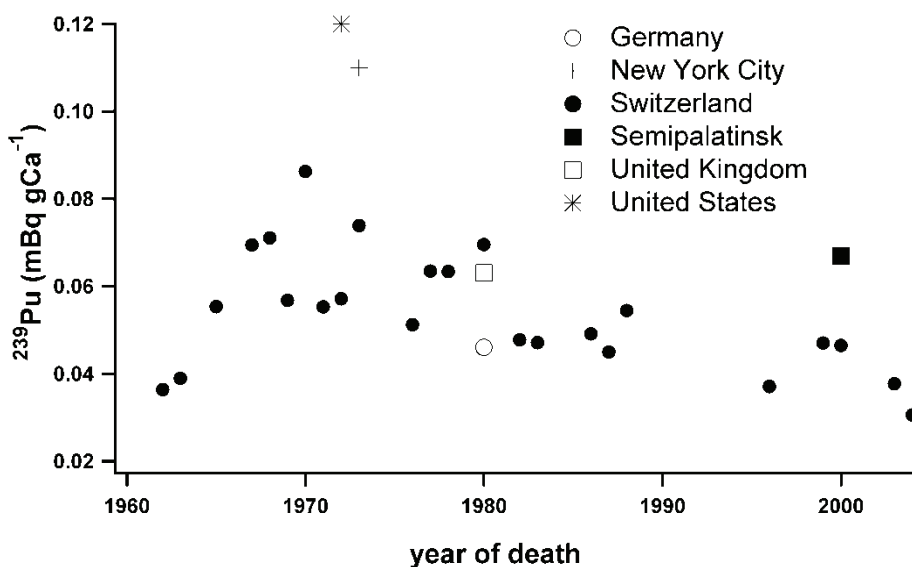


Fig. 8. ^{239}Pu activity (mBq/gCa) as a function of the year of death.

Figure 8 shows that the activities of ^{239}Pu in vertebrae in Switzerland increased similarly to ^{90}Sr , peaking in 1970 at a value of 0.086 mBq/gCa. The $^{240}\text{Pu}/^{239}\text{Pu}$ isotopic ratio is 0.18 ± 0.01 ($n=48$), from which we infer that plutonium measured in this study originated only from the fallout of the atomic bomb tests (Froidevaux et al., 2010). Significantly higher values were found in the US (McInroy et al., 1979) and in New York City (Fisenne et al., 1980), possibly

because these databases contain autopsy tissues from both the general public and workers of the nuclear industry. Similar values to Switzerland were determined in Germany (Bunzl and Kracke, 1983) and in the UK (Popplewell et al., 1985) for the years around 1980. Higher values were obtained at the Semipalatinsk test site (STS) during the 2000's, indicating an effect of the test site fallout in the plutonium body burden of the population (Yamamoto et al., 2006). Using ICP-MS, (Yamamoto et al., 2008) found a significantly lower $^{240}\text{Pu}/^{239}\text{Pu}$ isotopic ratio of 0.125 in autopsy tissues (bone) of individuals from the STS, confirming the influence of the STS fallout on plutonium incorporation.

There were too few bone ash samples in our study to separate individuals from different regions, especially the ones potentially affected by the Swiss NPPs. Accordingly, our data represent a pool of bone samples from all over Switzerland. Nevertheless, the $^{240}\text{Pu}/^{239}\text{Pu}$ isotopic ratio of 0.18 indicates, beyond any reasonable doubts, that the plutonium inhaled by the Swiss population comes from the fallout of the NBTs of the sixties.

7. Retention half-times in the skeleton of ^{90}Sr and plutonium

The retention half-time in the skeleton of bone-seeking radionuclides such as ^{90}Sr and plutonium is a key parameter used for their dosimetry in humans. Currently, only a partial answer is given to the question of how long plutonium will stay in the body. Values found in the literature are situated between 15 to 100 years, with a proposed value by ICRP 56 or Kathren (1995) of 50 y. Our long-term study of ^{90}Sr and plutonium in the vertebrae allowed us to determine, with a high statistical significance, the retention half-time of both radionuclides in cancellous bones. It is of 40 ± 15 y (95% confidence) for plutonium and 13.5 ± 1.5 for ^{90}Sr (Figure 9). Meanwhile, the retention time of ^{90}Sr is very close to the retention time found in milk teeth, milk, grass and soil (0-5 cm, Table 1).

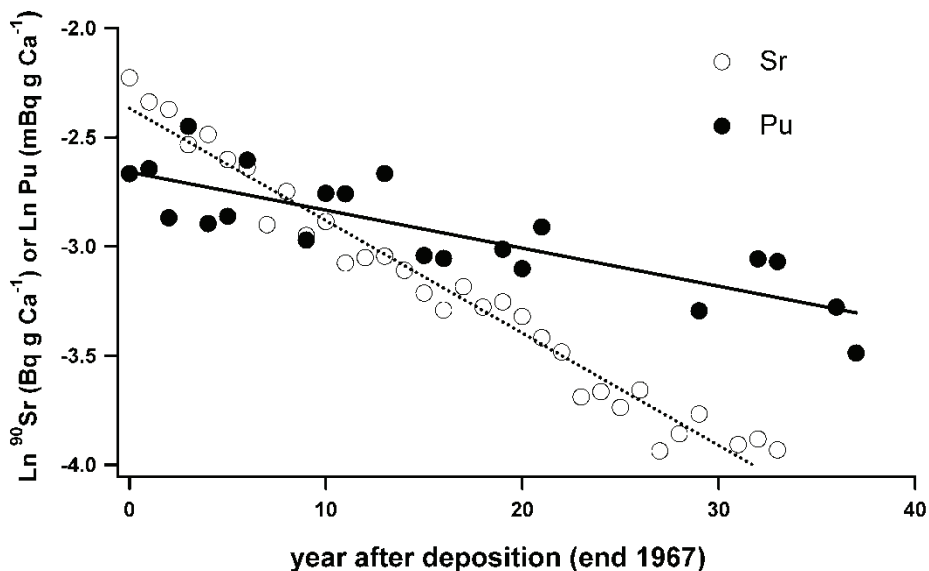


Fig. 9. The use of the data from our long-term study for the determination of the retention time of ^{90}Sr and plutonium in cancellous bones.

Site	Soil (0-5 cm)	Grass	Milk	milk teeth	Vertebrae
Grangeneuve	12.3±3.6	11.6 ±3.9	14.8 ±2.3		
Mühleberg	9.0 ±1.3	7.6 ±1.3	14.5 ±2.6		
Gösgen	7.8 ±0.9	6.7 ±1.1	10.1 ±2.7		
Leibstadt	8.9 ±1.5	12.3 ±3.9	12.5 ±2.5		
Switzerland	9.5±2	9.5±3	13±2	10.0 ±3	13.0 ±1

Table 1. Retention half-time of ^{90}Sr in different compartments of the environment, food and human for different locations in Switzerland.

These results demonstrate that the calculated retention half-time for ^{90}Sr is in fact an apparent retention half-time because ^{90}Sr is still incorporated in bones after the Nuclear Test Ban Treaty, due to ingestion of contaminated food, especially milk. In this respect, the ^{90}Sr activity in vertebrae is a better reflection of the contamination of the food chain and the environment rather than any mechanism of ^{90}Sr excretion. Consequently, bones remain contaminated by ^{90}Sr as long as environmental contamination lasts (Froidevaux et al., 2010).

8. Conclusion

In this work we show that plutonium and ^{90}Sr from NBTs fallout have contaminated the Swiss population. The level of the contamination is very low and the potential effect of this contamination can be classified within the very low dose effects. In this respect, the NBTs contamination can be viewed as a surrogate for the potential effect that a NPP could have on a nearby population in case of accidental release of low intensity. Compared to other studies conducted worldwide on the same problem, we see that the Swiss population received NBTs fallout similar to other Northern Hemisphere regions but that the incorporation of ^{90}Sr might have been slightly higher because the diet of the Swiss population includes a significant portion of dairy products. The determination of plutonium in milk teeth at a very low-level using sensitive sf-ICP-MS technique allowed us to demonstrate that plutonium does not cross the placental barrier and that the babies were probably born free of plutonium. Nevertheless, the determination of significant amounts of plutonium in bones of adults shows that the incorporation of NBT plutonium in the skeleton of the babies starts as soon as they begin to breathe and continues as long as the plutonium is present in air. ^{90}Sr has been incorporated as a consequence of food contamination, as demonstrated by the strong correlation between the milk activity and the milk teeth activity, and ^{90}Sr in the body will stay in equilibrium with the ^{90}Sr present in the environment. We also show that the analytical part of such a study has to be handled with great care because the levels measured are so low that contamination of the samples by other radionuclides easily happens. In this respect, careful radiochemical work must be carried out on the samples, either for ^{90}Sr or plutonium analyses, otherwise results are submitted to significant bias. In addition, our long-time study allowed us to determine the retention half-time of plutonium and ^{90}Sr in the skeleton. We think that this kind of study forms a very good basis for epidemiological studies involving the effects of a low dose of radiation (Wakeford et al., 2010). We thus conclude that a survey of the population by yearly sampling of milk teeth and vertebrae is very useful to demonstrate an increase in the population body burden that may be attributed to air and/or environmental contamination. In view of the presence of 5 NPPs in Switzerland, this program helps to determine any potential negative effect of the NPPs on the population in case of accidental release. This survey program is well accepted

by the population and offers reassurance that people are not submitted to unacceptable doses of radiation.

9. Acknowledgment

Research funding was provided by the Swiss Federal Office of Public Health for PF and MH and by the University of Lausanne (PF and FBo). We thank J.-J. Geering for his long-term collection of vertebrae and milk teeth, in collaboration with pathologists and dentists from different regions of Switzerland, and for ^{90}Sr analyses from 1960 to 2001. F. Barraud is acknowledged for her careful work in the ^{90}Sr analyses of teeth and bones samples. We thank A. Alt for instrumental assistance with the sf ICP-MS.

10. References

- Aarkrog, A. (1971) Prediction Models for Sr-90 in Shed Deciduous Teeth and Infant Bone. *Health Physics*, Vol.21, No.6, pp. 803-&, ISSN 0017-9078.
- Agarande, M., Benzoubir, S., Neiva-Marques, A. M., & Bouisset, P. (2004) Sector field inductively coupled plasma mass spectrometry, another tool for plutonium isotopes and plutonium isotope ratios determination in environmental matrices. *Journal of Environmental Radioactivity*, Vol.72, No.1-2, pp. 169-176, ISSN 0265-931X.
- Atkinson, W. D., Law, D. V., Bromley, K. J., & Inskip, H. M. (2004) Mortality of employees of the United Kingdom atomic energy authority, 1946-97. *Occupational and Environmental Medicine*, Vol.61, No.7, pp. 577-585, ISSN 1351-0711.
- Badie, C., Arnould, C., Sarbach, J., Arnaud, M., Lemercier, R., Bernard, C., Howell, P., & Texier, T. (1987) Sr-90 Levels in Human-Teeth Collected in French-Polynesia. *Radioprotection*, Vol.22, No.4, pp. 325-332, ISSN 0033-8451.
- Baglan, N., Hemet, P., Pointurier, F., & Chiappini, R. (2004) Evaluation of a single collector, double focusing sector field inductively coupled plasma mass spectrometer for the determination of U and Pu concentrations and isotopic compositions at trace level. *Journal of Radioanalytical and Nuclear Chemistry*, Vol.261, No.3, pp. 609-617, ISSN 0236-5731.
- Bauman, A., Franic, N., Baumstark, M., & Popovic, V. (1977) Sr-90 in Human Bone. *Health Physics*, Vol.32, No.4, pp. 318-321, ISSN 0017-9078.
- Becker, J. S. (2003) Mass spectrometry of long-lived radionuclides. *Spectrochimica Acta Part B-Atomic Spectroscopy*, Vol.58, No.10, pp. 1757-1784, ISSN 0584-8547.
- Becker, J. S., Soman, R. S., Sutton, K. L., Caruso, J. A., & Dietze, H. J. (1999) Determination of long-lived radionuclides by inductively coupled plasma quadrupole mass spectrometry using different nebulizers. *Journal of Analytical Atomic Spectrometry*, Vol.14, No.6, pp. 933-937, ISSN 0267-9477.
- BEIR7 (2006) Health Risks from Exposure to Low Levels of Ionizing Radiation: BEIR VII - Phase 2. National research council of the national academies, the national academies press, Washington DC, ISBN 10-309-53040-7 (2006).
- Black, R.J., Sharp, L., Harkness, E.F., & McKinney, P.A. (1994) Leukaemia and non-Hodgkin's lymphoma: incidence in children and young adults resident in the Dounreay area of Caithness, Scotland in 1968-91. *J Epidemiology and Community Health*, Vol.48, pp. 232-236, ISSN 0143-005X.

- Bithell, J. F., Dutton, S. J., Draper, G. J., & Neary, N. M. (1994) Distribution of Childhood Leukemias and Non-Hodgkins-Lymphomas Near Nuclear Installations in England and Wales. *British Medical Journal*, Vol.309, No.6953, pp. 501-505, ISSN 0959-8138.
- Boulyga, S. F. & Becker, J. S. (2001) Determination of uranium isotopic composition and U-236 content of soil samples and hot particles using inductively coupled plasma mass spectrometry. *Fresenius Journal of Analytical Chemistry*, Vol.370, No.5, pp. 612-617, ISSN 0937-0633.
- Boulyga, S. F., Desideri, D., Meli, M. A., Testa, C., & Becker, J. S. (2003) Plutonium and americium determination in mosses by laser ablation ICP-MS combined with isotope dilution technique. *International Journal of Mass Spectrometry*, Vol.226, No.3, pp. 329-339, ISSN 1387-3806.
- Bunzl, K. & Kracke, W. (1983) Fallout Pu-239-240 and Pu-238 in Human-Tissues from the Federal-Republic of Germany. *Health Physics*, Vol.44, No.pp. 441-449, ISSN 0017-9078.
- Cardis, E., Kesminiene, A., Ivanov, V., Malakhova, I., Shibata, Y., Khrouch, V., Drozdovitch, V., Maceika, E., Zvonova, I., Vlassov, O., Bouville, A., Goulko, G., Hoshi, M., Abrosimov, A., Anoshko, J., Astakhova, L., Chekin, S., Demidchik, E., Galanti, R., Ito, M., Korobova, E., Lushnikov, E., Maksioutov, M. A., Masyakin, V., Nerovnia, A., Parshin, V., Parshkov, E., Piliptsevich, N., Pinchera, A., Polyakov, S., Shabeka, N., Suonio, E., Tenet, V., Tsyb, A., Yamashita, S., & Williams, D. (2005a) Risk of thyroid cancer after exposure to I-131 in childhood. *Journal of the National Cancer Institute*, Vol.97, No.10, pp. 724-732, ISSN 0027-8874.
- Cardis, E., Vrijheid, M., Blettner, M., Gilbert, E., Hakama, M., Hill, C., Howe, G., Kaldor, J., Muirhead, C. R., Schubauer-Berigan, M., & Yoshimura, T. (2005b) Risk of cancer after low doses of ionising radiation - retrospective cohort study in 15 countries. *British Medical Journal*, Vol.331, No.7508, pp. 77-80B, ISSN 0959-8146.
- Christensen, G. C., Alstad, J., Kvale, E., & Pappas, A. C. (1975) Strontium-90 in Human Bone in Norway 1956-1972. *Health Physics*, Vol.28, No.6, pp. 677-684, ISSN 0017-9078.
- Culot, J. P., Blommaert, W., Hurtgen, C., & Minon, J. P. (1997) Radioactivity of teeth in the follow-up of old contamination cases. *Journal of Radioanalytical and Nuclear Chemistry*, Vol.226, No.1-2, pp. 139-143, ISSN 0236-5731.
- Dahl, S. G., Allain, P., Marie, P. J., Mauras, Y., Boivin, G., Ammann, P., Tsouderos, Y., Delmas, P. D., & Christiansen, C. (2001) Incorporation and distribution of strontium in bone. *Bone*, Vol.28, No.4, pp. 446-453, ISSN 8756-3282.
- Degteva, M. O., Kozheurov, V. P., Tolstykh, E. I., Vorobiova, M. I., Anspaugh, L. R., Napier, B. A., & Kovtun, A. N. (2000) The Techa River Dosimetry System: Methods for the reconstruction of internal dose. *Health Physics*, Vol.79, No.1, pp. 24-35, ISSN 0017-9078.
- Dehos, R. & Kistner, G. (1980) Sr-90 Content in Human-Bone of West-German Residents. *Health Physics*, Vol.39, No.4, pp. 682-683, ISSN 0017-9078.
- Dolphin, A. E., Goodman, A. H., & Amarasiriwardena, D. D. (2005) Variation in elemental intensities among teeth and between pre- and postnatal regions of enamel. *American Journal of Physical Anthropology*, Vol.128, No.4, pp. 878-888, ISSN 0002-9483.
- Doyle, P., Maconochie, N., Roman, E., Davies, G., Smith, P. G., & Beral, V. (2000) Fetal death and congenital malformation in babies born to nuclear industry employees: report from the nuclear industry family study. *Lancet*, Vol.356, No.9238, pp. 1293-1299, ISSN 0140-6736.

- Fisenne, I. M., Cohen, N., Neton, J. W., & Perry, P. (1980) Fallout Plutonium in Human-Tissues from New-York-City. *Radiation Research*, Vol.83, No.1, pp. 162-168, ISSN 0033-7587.
- Froidevaux, P., Bochud, F., & Haldimann, M. (2010) Retention half times in the skeleton of plutonium and Sr-90 from above-ground nuclear tests: A retrospective study of the Swiss population. *Chemosphere*, Vol.80, No.5, pp. 519-524, ISSN 0045-6535.
- Froidevaux, P., Dell, T., & Tossel, P. (2006a) Radionuclides in Food and Foodstuff, In *Radionuclide concentrations in food and the Environment*, Pöschl and Nollet ed, pp 225-268, Taylor and Francis, ISBN 0-8493-3594-9, Boca Raton.
- Froidevaux, P., Geering, J. J., & Valley, J. F. (2006b) Sr-90 in deciduous teeth from 1950 to 2002: The Swiss experience. *Science of the Total Environment*, Vol.367, No.2-3, pp. 596-605, ISSN 0048-9697.
- Froidevaux, P. & Haldimann, M. (2008) Plutonium from Above-Ground Nuclear Tests in Milk Teeth: Investigation of Placental Transfer in Children Born between 1951 and 1995 in Switzerland. *Environmental Health Perspectives*, Vol.116, No.12, pp. 1731-1734, ISSN 0091-6765.
- Gulson, B. L. & Gillings, B. R. (1997) Lead exchange in teeth and bone - A pilot study using stable lead isotopes. *Environmental Health Perspectives*, Vol.105, No.8, pp. 820-824, ISSN 0091-6765.
- Heasman, M. A., Kemp, I. W., Urquhart, J. D., & Black, R. (1986) Childhood Leukemia in Northern Scotland. *Lancet*, Vol.1, No.8475, pp. 266-266, ISSN 0140-6736.
- Hodgson, S. A., Ham, G. J., Youngman, M. J., Etherington, G., & Stradling, G. N. (2004) A review of measurements of radionuclides in members of the public in the UK. *Journal of Radiological Protection*, Vol.24, No.4, pp. 369-389, ISSN 0952-4746.
- Hoffmann, W., Dieckmann, H., Dieckmann, H., & SchmitzFeuerhake, I. (1997) A cluster of childhood leukemia near a nuclear reactor in northern Germany. *Archives of Environmental Health*, Vol.52, No.4, pp. 275-280, ISSN 0003-9896.
- Hunter, N. & Muirhead, C. R. (2009) Review of relative biological effectiveness dependence on linear energy transfer for low-LET radiations. *Journal of Radiological Protection*, Vol.29, No.1, pp. 5-21, ISSN 0952-4746.
- ICRP (International Commission on Radiological Protection) (1986) The Metabolism of Plutonium and Related Elements.
- Kaatsch, P., Spix, C., Schulze-Rath, R., Schmiedel, S., & Blettner, M. (2008) Leukaemia in young children living in the vicinity of German nuclear power plants. *International Journal of Cancer*, Vol.122, No.4, pp. 721-726, ISSN 0020-7136.
- Kalmykov, L., Paschenko, G., & Gur, E. (1997) Sr-90 internal irradiation of population residing in the north-east region of Ukraine. *Radiation Protection Dosimetry*, Vol.71, No.1, pp. 57-60, ISSN 0144-8420.
- Kathren, R. L. (1995) The United-States Transuranium and Uranium Registries - 1968-1993. *Radiation Protection Dosimetry*, Vol.60, No.4, pp. 349-354, ISSN 0144-8420.
- Kathren, R. L. (2004) A review of contributions of human tissue studies to biokinetics, bioeffects and dosimetry of plutonium in man. *Radiation Protection Dosimetry*, Vol.109, No.4, pp. 399-407, ISSN 0144-8420.
- Kelley, J. M., Bond, L. A., & Beasley, T. M. (1999) Global distribution of Pu isotopes and Np-237. *Science of the Total Environment*, Vol.238, No.pp. 483-500, ISSN 0048-9697.
- Ketterer, M. E., Hafer, K. M., Link, C. L., Kolwaite, D., Wilson, J., & Mietelski, J. W. (2004a) Resolving global versus local/regional Pu sources in the environment using sector

- ICP-MS. *Journal of Analytical Atomic Spectrometry*, Vol.19, No.2, pp. 241-245, ISSN 0267-9477.
- Ketterer, M. E., Hafer, K. M., & Mietelski, J. W. (2004b) Resolving Chernobyl vs. global fallout contributions in soils from Poland using Plutonium atom ratios measured by inductively coupled plasma mass spectrometry. *Journal of Environmental Radioactivity*, Vol.73, No.2, pp. 183-201, ISSN 0265-931X.
- Kim, C. S., Kim, C. K., Lee, J. I., & Lee, K. J. (2000) Rapid determination of Pu isotopes and atom ratios in small amounts of environmental samples by an on-line sample pre-treatment system and isotope dilution high resolution inductively coupled plasma mass spectrometry. *Journal of Analytical Atomic Spectrometry*, Vol.15, No.3, pp. 247-255, ISSN 0267-9477.
- Krestinina, L., Preston, D. L., Davis, F. G., Epifanova, S., Ostroumova, E., Ron, E., & Akleyev, A. (2010) Leukemia incidence among people exposed to chronic radiation from the contaminated Techa River, 1953-2005. *Radiation and Environmental Biophysics*, Vol.49, No.2, pp. 195-201, ISSN 0301-634X.
- Kulev, Y. D., Polikarpov, G. G., Prigodey, E. V., & Assimakopoulos, P. A. (1994) Sr-90 Concentrations in Human Teeth in South Ukraine, 5 Years After the Chernobyl Accident. *Science of the Total Environment*, Vol.155, No.3, pp. 215-219, ISSN 0048-9697.
- Laurier, D., Jacob, S., Bernier, M. O., Leuraud, K., Metz, C., Samson, E., & Laloi, P. (2008) Epidemiological studies of leukaemia in children and young adults around nuclear facilities: a critical review. *Radiation Protection Dosimetry*, Vol.132, No.2, pp. 182-190, ISSN 0144-8420.
- Lindahl, P., Keith-Roach, M., Worsfold, P., Choi, M. S., Shin, H. S., & Lee, S. H. (2010) Ultra-trace determination of plutonium in marine samples using multi-collector inductively coupled plasma mass spectrometry. *Analytica Chimica Acta*, Vol.671, No.1-2, pp. 61-69, ISSN 0003-2670.
- Mangano, J.J & Sherman, J. D. (2011) Elevated In Vivo Strontium-90 From Nuclear Weapons Test Fallout Among Cancer Decedents: A Case-control Study Of Deciduous Teeth. *International Journal of Health Sciences*, Vol. 41, No. 1, pp 137-158.
- Martin, T. J. & Seeman, E. (2008) Bone remodelling: its local regulation and the emergence of bone fragility. *Best Practice & Research Clinical Endocrinology & Metabolism*, Vol.22, No.5, pp. 701-722, ISSN 1521-690X.
- McInroy, J. F., Campbell, E. E., Moss, W. D., Tietjen, G. L., Eutsler, B. C., & Boyd, H. A. (1979) Plutonium in Autopsy Tissue - Revision and Updating of Data Reported in La-4875. *Health Physics*, Vol.37, No.1, pp. 1-136, ISSN 0017-9078.
- Nussbaum, R. H. (2009) Childhood Leukemia and Cancers Near German Nuclear Reactors: Significance, Context, and Ramifications of Recent Studies. *International Journal of Occupational and Environmental Health*, Vol.15, No.3, pp. 318-323, ISSN 1077-3525.
- ODonnell, R. G., Mitchell, P. I., Priest, N. D., Strange, L., Fox, A., Henshaw, D. L., & Long, S. C. (1997) Variations in the concentration of plutonium, strontium-90 and total alpha-emitters in human teeth collected within the British Isles. *Science of the Total Environment*, Vol.201, No.3, pp. 235-243, ISSN 0048-9697.
- Papworth, D. G. & Vennart, J. (1984) The Uptake and Turnover of Sr-90 in the Human Skeleton. *Physics in Medicine and Biology*, Vol.29, No.9, pp. 1045-1061, ISSN 0031-9155.
- Popplewell, D. S., Ham, G. J., Johnson, T. E., & Barry, S. F. (1985) Plutonium in Autopsy Tissues in Great-Britain. *Health Physics*, Vol.49, No.2, pp. 304-309, ISSN 0017-9078.

- Pourcelot, L., Steinmann, P., & Froidevaux, P. (2007) Lower variability of radionuclide activities in upland dairy products compared to soils and vegetation: Implication for environmental survey. *Chemosphere*, Vol.66, No.8, pp. 1571-1579, ISSN 0045-6535.
- Qiao, J. X., Hou, X. L., Roos, P., & Miro, M. (2010) Rapid and simultaneous determination of neptunium and plutonium isotopes in environmental samples by extraction chromatography using sequential injection analysis and ICP-MS. *Journal of Analytical Atomic Spectrometry*, Vol.25, No.11, pp. 1769-1779, ISSN 0267-9477.
- Renaud, P., Pourcelot, L., Metivier, J. M., & Morello, M. (2003) Mapping of Cs-137 deposition over eastern France 16 years after the Chernobyl accident. *Science of the Total Environment*, Vol.309, No.1-3, pp. 257-264, ISSN 0048-9697.
- Rogel, A., Carre, N., Amoros, E., Bonnet-Belfais, M., Goldberg, M., Imbernon, E., Calvez, T., & Hill, C. (2005) Mortality of workers exposed to ionizing radiation at the French National Electricity company. *American Journal of Industrial Medicine*, Vol.47, No.1, pp. 72-82, ISSN 0271-3586.
- Roman, E., Doyle, P., Maconochie, N., Davies, G., Smith, P. G., & Beral, V. (1999) Cancer in children of nuclear industry employees: report on children aged under 25 years from nuclear industry family study. *British Medical Journal*, Vol.318, No.7196, pp. 1443-1450, ISSN 0959-8138.
- Rosenthal, H. L., Austin, S., Oneill, S., Takeuchi, K., Bird, J. T., & Gilster, J. E. (1964) Incorporation of Fall-Out Strontium-90 in Deciduous Incisors + Foetal Bone. *Nature*, Vol.203, No.494, pp. 615-&, ISSN 0028-0836.
- Rytomaa, I. (1972) Sr-90 in Deciduous Teeth Collected in Northern Finland from Children Born in 1952-1964. *Acta Odontologica Scandinavica*, Vol.30, No.2, pp. 219-&, ISSN 0001-6357.
- Schmitz, M., Schmitz, K., & Aumann, D. C. (2004) A simple radiochemical method for determining bone-seeking radionuclides in bone and teeth: Sr-90 in teeth of children from Ukraine and Germany. *Journal of Radioanalytical and Nuclear Chemistry*, Vol.260, No.3, pp. 451-457, ISSN 0236-5731.
- Schmitz-Feuerhake, I., Dieckmann, H., Hoffmann, W., Lengfelder, E., Pflugbeil, S., & Stevenson, A. (2005) The Elbmarsch leukemia cluster: Are there conceptual limitations in controlling immission from nuclear establishments in Germany? *Archives of Environmental Contamination and Toxicology*, Vol.49, No.4, pp. 589-600, ISSN 0090-4341.
- Shore, R. E. (2009) Low-Dose Radiation Epidemiology Studies: Status and Issues. *Health Physics*, Vol.97, No.5, pp. 481-486, ISSN 0017-9078.
- Sokolnikov, M. E., Gilbert, E. S., Preston, D. L., Ron, E., Shilnikova, N. S., Khokhryakov, V. V., Vasilenko, E. K., & Koshurnikova, N. A. (2008) Lung, liver and bone cancer mortality in Mayak workers. *International Journal of Cancer*, Vol.123, No.4, pp. 905-911, ISSN 0020-7136.
- Stamoulis, K. C., Assimakopoulos, P. A., Ioannides, K. G., Johnson, E., & Soucacos, P. N. (1999) Strontium-90 concentration measurements in human bones and teeth in Greece. *Science of the Total Environment*, Vol.229, No.3, pp. 165-182, ISSN 0048-9697.
- Svendsen, E. R., Kolpakov, I. E., Stepanova, Y. I., Vdovenko, V. Y., Naboka, M. V., Mousseau, T. A., Mohr, L. C., Hoel, D. G., & Karmaus, W. J. J. (2010) (137)Cesium Exposure and Spirometry Measures in Ukrainian Children Affected by the Chernobyl Nuclear Incident. *Environmental Health Perspectives*, Vol.118, No.5, pp. 720-725, ISSN 0091-6765.
- Takizawa, Y., Hisamatsu, S., Abe, T., & Yamashita, J. (2000) Actinides and long-lived radionuclides in tissues of the Japanese population: Summary of the past 20-year

- studies. *Journal of Radioanalytical and Nuclear Chemistry*, Vol.243, No.2, pp. 305-312, ISSN 0236-5731.
- Taylor, D. M. (1995) Environmental Plutonium in Humans. *Applied Radiation and Isotopes*, Vol.46, No.11, pp. 1245-1252, ISSN 0969-8043.
- Taylor, R. N., Warneke, T., Milton, J. A., Croudace, I. W., Warwick, P. E., & Nesbitt, R. W. (2001) Plutonium isotope ratio analysis at femtogram to nanogram levels by multicollector ICP-MS. *Journal of Analytical Atomic Spectrometry*, Vol.16, No.3, pp. 279-284, ISSN 0267-9477.
- Tolstykh, E. I., Degteva, M. O., Vorobiova, M. I., & Kozheurov, V. P. (2001) Fetal dose assessment for the offspring of the Techa Riverside residents. *Radiation and Environmental Biophysics*, Vol.40, No.4, pp. 279-286, ISSN 0301-634X.
- Tolstykh, E. I., Shagina, N. B., Peremyslova, L. M., Degteva, M. O., Phipps, A. W., Harrison, J. D., & Fell, T. P. (2008) Reconstruction of Sr-90 intake for breast-fed infants in the Techa riverside settlements. *Radiation and Environmental Biophysics*, Vol.47, No.3, pp. 349-357, ISSN 0301-634X.
- Tolstykh, E. I., Shishkina, E. A., Degteva, M. O., Ivanov, D. V., Shved, V. A., Bayankin, S. N., Anspaugh, L. R., Napier, B. A., Wieser, A., & Jacob, P. (2003) Age dependencies of Sr-90 incorporation in dental tissues: Comparative analysis and interpretation of different kinds of measurements obtained for residents on the Techa River. *Health Physics*, Vol.85, No.4, pp. 409-419, ISSN 0017-9078.
- Wakeford, R., Darby, S. C., & Murphy, M. F. G. (2010) Temporal trends in childhood leukaemia incidence following exposure to radioactive fallout from atmospheric nuclear weapons testing. *Radiation and Environmental Biophysics*, Vol.49, No.2, pp. 213-227, ISSN 0301-634X.
- Warneke, T., Croudace, I. W., Warwick, P. E., & Taylor, R. N. (2002) A new ground-level fallout record of uranium and plutonium isotopes for northern temperate latitudes. *Earth and Planetary Science Letters*, Vol.203, No.3-4, pp. 1047-1057, ISSN 0012-821X.
- Wyse, E. J., Lee, S. H., La Rosa, J., Povinec, P., & de Mora, S. J. (2001) ICP-sector field mass spectrometry analysis of plutonium isotopes: recognizing and resolving potential interferences. *Journal of Analytical Atomic Spectrometry*, Vol.16, No.9, pp. 1107-1111, ISSN 0267-9477.
- Yamamoto, M., Hoshi, M., Sakaguchi, A., Shinohara, K., Kurihara, O., Apsalikov, K. N., & Gusev, B. I. (2006) Plutonium and uranium in human bones from areas surrounding the Semipalatinsk nuclear test site. *Journal of Radiation Research*, Vol.47, No.pp. A85-A94, ISSN 0449-3060.
- Yamamoto, M., Oikawa, S., Sakaguchi, A., Tomita, J., Hoshi, M., & Apsalikov, K. N. (2008) Determination of Pu-240/Pu-239 isotopic ratios in human tissues collected from areas around the Semipalatinsk nuclear test site by sector-field high resolution ICP-MS. *Health Physics*, Vol.95, No.3, pp. 291-299, ISSN 0017-9078.
- Zebaze, R. M. D., Ghasem-Zadeh, A., Bohte, A., Iuliano-Burns, S., Mirams, M., Price, R. I., Mackie, E. J., & Seeman, E. (2010) Intracortical remodelling and porosity in the distal radius and post-mortem femurs of women: a cross-sectional study. *Lancet*, Vol.375, No.9727, pp. 1729-1736, ISSN 0140-6736.
- Zoriy, M. V., Halicz, L., Ketterer, M. E., Pickhardt, C., Ostapczuk, P., & Becker, J. S. (2004) Reduction of UH⁺ formation for U-236/U-238 isotope ratio measurements at ultratrace level in double focusing sector field ICP-MS using D₂O as solvent. *Journal of Analytical Atomic Spectrometry*, Vol.19, No.3, pp. 362-367, ISSN 0267-9477.

The Biliprotein C-Phycocyanin Modulates the DNA Damage Response in Lymphocytes from Nuclear Power Plant Workers

K. Stankova¹, K. Ivanova¹, V. Nikolov¹, K. Minkova²,
L. Gigova², R. Georgieva¹ and R. Boteva¹

¹National Center of Radiobiology and Radiation Protection

²Institute of Plant Physiology and Genetics
Bulgaria

1. Introduction

The biliprotein C-phycoerythrin (C-PE) is a light-harvesting photoreceptor in cyanobacteria and in red algae (Rhodophyta and Cryptophyta) with applications as a natural colorant in nutritional industry and cosmetics (Prasanna et al., 2007) and as a fluorescent marker in medical and biological studies (Glazer, 1994; Sun et al., 2003). The protein is composed of two homologous subunits - α and β (Stec et al., 1999; Contreras-Martel et al., 2007), respectively with one and two phycocyanobilin chromophores, covalently attached to cysteine residues. The subunits form $\alpha\beta$ complexes which aggregate into $\alpha\beta\beta$ trimers and $\alpha\beta\beta\beta$ hexamers, the latter being the functional unit of the protein. C-PE has been shown to display a variety of pharmacological activities, related to the antioxidant, anti-inflammatory, neuro- and hepato-protective, anti-tumour and wound-healing mechanisms (Romay et al., 2003; Ge et al., 2006; Li et al., 2005; Madhyastha et al., 2008). These properties have attracted attention to the compound as a possible radio-protective agent. It has been demonstrated that rats exposed to 5 Gy of X-rays and fed phycocyanin normalized their antioxidant system within 4 weeks after exposure (Karpov et al., 2000).

Recently, we studied the effects of C-PE in combination with ionizing radiation on lymphocytes, isolated from nuclear power plant workers, exposed to low doses of ionizing radiation (IR), and compared them with the effects on lymphocytes from nonexposed controls (Ivanova et al., 2010). We found that the biliprotein stimulated the expression of the antioxidant enzymes manganese superoxide dismutase (MnSOD), catalase and glutathione-S-transferase (GST) during the early radiation response of lymphocytes from workers, but not from controls. Since the biliprotein positively affects the antioxidant defense pathways, it might be of interest for the radioprotection of occupationally exposed people.

In this study we have further characterized the effects of C-PE on the early radiation response of lymphocytes from unexposed controls and from workers, exposed to low doses of radiation. We quantified the level of persisting radiation-induced DNA double-strand breaks (DSBs) in the presence and absence of C-PE. DSBs are the most dangerous type of DNA lesions, induced by several genotoxic agents, including gamma IR (γ -IR). The ability of cells to readily process DSBs is of vital importance for genomic integrity, as failure to repair these lesions results in

chromosomal breakage, fragmentation and translocation. Moreover, impaired or defective rejoining of radiation-induced DNA strand breaks usually correlates strongly with the individual susceptibility to cancer (Alapetite et al., 1999; Berwick & Vineis, 2000).

The amount of persisting DSBs in cells was determined by the comet assay (CA), a quick, simple and reliable method for analyzing DNA damage and repair that requires a small number of cells and can be performed on both freshly isolated and cryopreserved cells (Decordier et al., 2010). Due to its sensitivity, the method is preferred in human epidemiological studies related to biomonitoring (Möller et al., 2000; Touil et al., 2002). Additionally, the CA is able to provide information on different types of DNA damage/repair and detect cellular damage in a wide dose range of exposures from 0.05 to 10 Gy (Kalthur et al., 2008; Mohseni-Meybodi et al., 2009; Palyvoda et al., 2003). The experiments were performed on human lymphocytes, which, due to their radiosensitivity and circulation throughout the body, reflect the overall state of the organism and are the cellular type most frequently used for assessment of the systematic radiation response (Collins et al., 2008; Decordier et al., 2010). A major problem with CA is that its sensitivity often leads to detection of a high variation within a single individual. A reliable methodology should be able to detect differences between individuals, but should show a minimal intra-individual variation. Therefore, prior to the epidemiological experiment, in an attempt to achieve minimal intra-individual variation and a linear dose-response curve, we carefully tested a number of conditions. We attained a stable linear dose-response dependence of DNA lesions, persisting 2h after exposure in the dose range from 0.5 to 8 Gy gamma rays.

Our data indicated that C-PC might stimulate the repair of radiation-induced DNA lesions in lymphocytes from both occupationally exposed subjects and non-exposed controls. Moreover, the biliprotein seems to limit the manifestations of high radiosensitivity. Interestingly, we registered a pronounced lower genotoxicity of C-PC in lymphocytes from workers with cumulative doses higher than 20 mSv. Additionally, the effects of C-PC were age-dependent.

2. Experimental procedures

2.1 Subjects and sampling

The exposed group consisted of 44 workers aged between 26 and 62 years, employed at the “Kozloduy” Nuclear Power Plant (NPP), Bulgaria. Cumulative exposure to ionizing radiation (IR), estimated from personal dosimeter records, ranged from 0.32 to 330.77 mSv and represented the sum of the doses collected for the whole period of occupation in the “strictly controlled area”. The control group included 12 non-exposed subjects from the NPP administrative staff, aged between 42 and 58 years. In order to exclude external effect on the results of this study, we recorded information on the smoking habits, alcohol consumption, use of medications and previous diagnostic exposure to X-rays. The studied groups were homogenous on the aforementioned criteria and the statistical analysis found no significant effects due to any factor. The study was performed under the National Program “Genomics” of the Ministry of Health and Ministry of Education, Youth and Science of Bulgaria. Informed consent was obtained from all participants.

Blood (2 ml) drawn by venipuncture and collected in EDTA-coated tubes (Vakutainer, Benton Dickinson, Oxford, UK) was delivered to the laboratory and stored at 4°C for up to 24h before processing. The samples from the control and exposed subjects were handled concurrently and the assays were run on coded samples.

2.2 Isolation, treatment with C-PC and irradiation of lymphocytes from human peripheral blood

C-PC was extracted, purified and concentration-adjusted as previously described (Ivanova et al., 2010).

Peripheral blood mononuclear cells were isolated by density-gradient centrifugation (Lymphoflot, Biotest, Dreieich, Germany), suspended in 1 ml RPMI 1640 supplemented with 10% fetal calf serum (RPMI, Sigma, St Louis, MO, USA) and counted on haemocytometer. The lymphocytes from each subject were then split and subjected to four different treatments, using the conditions, described by Ivanova (Ivanova et al., 2010) as shown in Fig. 1a: (A) 4 hours of incubation with RPMI before lysis; (B) 2 hours of incubation in RPMI, followed by irradiation with 2 Gy (^{137}Cs gamma source, dose rate 2.07 Gy/min), incubation for another 2 hours and lysis; (C) 4 hours of incubation in RPMI, supplemented with 5 μM C-PC (RPMI-C-PC) before lysis; (D) 2 hours of incubation in RPMI supplemented with 5 μM C-PC, followed by irradiation (as described), incubation for another 2 hours and lysis. All above procedures were carried out at room temperature.

2.3 Single Cell Gel Electrophoresis (Comet assay)

The neutral comet assay was applied for analysis of radiation- and/or C-PC-induced strand breaks in DNA. Three comet test slides were prepared from each treatment, described in Section 2.2 and Fig. 1a. Lymphocytes (5×10^5 cells/ml) were suspended in low melting point agarose (final concentration 0.7% in phosphate buffered saline), dropped onto frosted glass slides which had been precoated with 0.5% normal melting point agarose, then refrigerated (4°C) for 15 min. To dissolve cellular proteins and lipids, the slides were immersed in lysis buffer (10 mM Tris, 100 mM EDTA, 2.5 M NaCl, 1% Triton X-100, pH 8.0) for 40 min at 4°C, and washed 3 times for 5 min in pre-cooled TBE buffer, pH 8.0. Electrophoresis was performed in TBE for 20 min at 0.5 V/cm². Finally, the slides were washed in ethanol and air-dried, stained with ethidium bromide (5 $\mu\text{g}/\text{ml}$) and analyzed under a fluorescence microscope (Olympus BX41). Double-strand breaks were analyzed by the parameter “tail moment” (TM), determined by the Comet Score 1.5 Software for fifty cells per slide. This parameter is the product of tail length and % DNA in the tail and is considered most informative when low levels of damage are present (Collins et al., 2008).

2.4 Statistical analysis

Distributions of variables were determined using Kolmogorov-Smirnoff test (Marques de Sá & Frias, 2007). Lilefors and Levene tests were used to determine the homogeneity of variance. The effects of different treatments (such as exposure to IR, C-PC treatment or the combination of C-PC treatment plus irradiation) were analyzed using one way ANOVA. Student t-test for dependent variables was carried out in order to compare every factor pair in each group. Results showing $p < 0.05$ were considered significant. As a null hypothesis it was presumed that there is no difference between groups.

3. Results

3.1 C-PC induces changes in DNA response to irradiation in non-irradiated subjects included in the control group

First we wanted to analyze whether the cells of each individual responded with an increase in DNA lesions to the different treatments. For this we determined the standard deviation

for the TM values which we had calculated from each triplet of comet test slides. Average TM values which increased for different treatments with more than two standard deviations, were considered elevated. Thus, as evident from Table 1, *in vitro* irradiation alone generates elevated levels of persisting DNA lesions in the lymphocytes from all (100%) of the non-exposed subjects included in the control group. 5 μM C-PC by itself also causes an increase in the lesions in more than half (67%) of the cases suggesting that treatment with C-PC is toxic for more than half of the subjects, included in the control group. Notably, when incubated with C-PC prior to irradiation, the samples from only half of the subjects show levels of DNA lesions, higher than those of the non-treated samples. This means that C-PC treated cells do not accumulate additional lesions upon radiation exposure. Thus, despite the fact that C-PC shows some toxicity, it also seems to protect cells from additional radiation damage.

There was a significant increase in the median value of the parameter TM, upon irradiation of cells which were grown in the absence of C-PC (Fig. 1b, **B** vs. **A**, $t_{11}=6.4$). In contrast, for cells grown in C-PC supplemented medium, the median value slightly decreased upon irradiation (Fig. 1b, **D** vs. **C**, $t_{11}=2.36$). The lower median TM value, calculated for the combined treatment, C-PC plus irradiation (**D**), in comparison to the separate treatments with C-PC (**C**) or irradiation (**B**), suggested that the biliprotein exerted radio-protection. Residual damage calculations (**B** minus **A** vs. **D** minus **C**) confirmed these findings (data not shown).

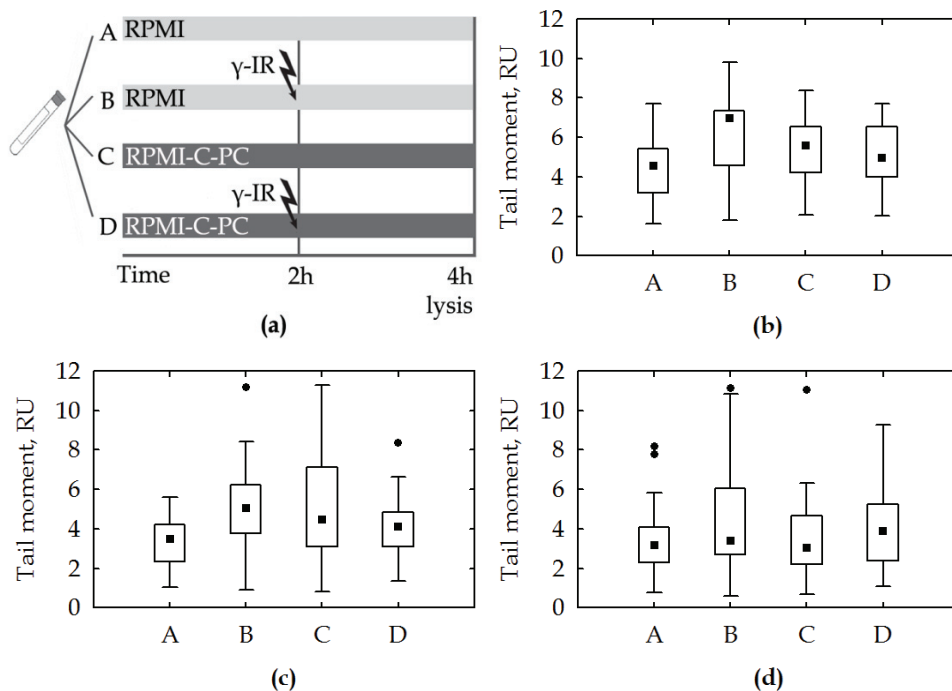
The relatively high levels of data dispersion (wide confidence intervals), observed in all conditions (Fig. 1b) are consistent with high inter-individual variations in the cellular response of the control subjects. Notably, the cells irradiated after treatment with C-PC (**D**) showed a lower level of data scattering than that of treatments (**B**) or (**C**), which was comparable to the dispersion range of values found for the non-treated samples (**A**). This is evidently due to a reduction of the maximal TM values in (**D**). This observation suggests that the biliprotein limits the manifestations of high radiosensitivity.

3.2 C-PC induces changes in the DNA response of lymphocytes from workers with very low cumulative doses of radiation

The average annual exposure of 17 subjects with very low cumulative doses, ranging from 0.32 to 12.12 mSv, did not exceed 1 mSv/year - the public dose limit, mandated by ICRP (ICRP 60, 1990), and these workers were unified in a group with very low dose occupational exposure. Cumulative doses and data on the levels of DNA damage in the workers are summarized in Table 2. Similar to the non-exposed control group, the additional, *in vitro* irradiation of the cells generated a significant increase in the levels of persisting lesions (Fig. 1c, **B** vs. **A**, $t_{16}=3.63$) in the majority of cases (76%). Treatment of the cells with C-PC also generated elevated levels of unrepaired DNA strand breaks in the majority (82%) of the subjects (Fig. 1c, **C** vs. **A**, $t_{16}=3.11$). Notably, after irradiation, samples, which had been pre-incubated with C-PC, showed lower median levels of DNA breaks as well as a reduction in the number of the subjects with higher levels of persisting DNA lesions (59% of the subjects) when compared with the samples which were irradiated only (Fig. 1c, **D** vs. **B**, $t_{16}=2.68$) or incubated with C-PC without *in vitro* irradiation (Fig. 1c, **D** vs. **C**, $t_{16}=2.77$). This result was similar to the effect of the protein on the non-exposed control group and demonstrated its radio-protective effect on the subjects with a very low dose occupational exposure.

As seen in Fig. 1c, the exposure of the cells only to C-PC or to IR (**B** and **C**) elevated the median values of TM and extended the range of the data dispersion. This is consistent with the cellular toxicity of the two agents. The data dispersion towards the higher break

extremes was more drastic with C-PC (C) than with irradiation alone (B), although the median values of damage levels in C-PC treated cells (C) was lower than that of irradiated cells (B). Notably, in combination, C-PC and radiation (D) induced a well pronounced decrease in the median values of TM, which were brought down almost to the levels of the controls (A). Additionally, the combination of the two agents (D) narrowed the range of data dispersion, again bringing it close to that of controls (A). In conclusion, for this group we observed a beneficial effect of C-PC on lymphocytes treated prior to radiation exposure, despite the toxicity of the protein. This conclusion was further confirmed by residual damage calculations (B minus A vs. D minus C).



(a) Lymphocytes from each subject were treated as follows: **A** - 4 hours of incubation with RPMI before lysis (controls); **B** - 2 hours of incubation in RPMI, followed by irradiation, incubation for another 2 hours and lysis; **C** - 4 hours of incubation in RPMI, supplemented with 5μM C-PC; **D** - 2 hours of incubation in RPMI supplemented with 5μM C-PC, followed by irradiation, incubation for another 2 hours and lysis.

(b) TM for the different treatments of lymphocytes from non-exposed subjects

(c) TM for the different treatments of lymphocytes from workers with cumulative doses, ranging from 0.32 to 12.12 mSv

(d) TM for the different treatments of lymphocytes from workers with cumulative doses, ranging from 26.77 to 330.77 mSv

Whiskers represent non-outlier range, boxes: 25-75% confidence intervals (CI), (■) median value and (●) outlier values.

Fig. 1. Treatment patterns and their effects on subjects from different exposure groups

3.3 C-PC induces changes in the DNA response of lymphocytes from workers with higher cumulative doses of radiation

This group included 27 professionals with cumulative doses, ranging from 26.77 to 330.77 mSv. Data, summarized in Table 3, showed, that in this group, in comparison with the two previous groups (non-exposed controls and exposed to very low doses of radiation), which were characterized by high levels of radiation-induced DNA lesions in the majority of samples (100 and 76%, respectively), the number of workers with persisting DNA lesions, induced after the *in vitro* exposure of the cells to 2 Gy gamma rays or treatment with C-PC was reduced by half to 48% and 44%, respectively. This is consistent with improved repair capacity of the subjects included in this group, which is probably relevant to their chronic low dose radiation exposure, which may have acted as *in vivo* adaptive dose. C-PC showed the lowest cytotoxicity in this group of workers since the median TM values and the range of data scattering were similar to those in untreated samples (Fig. 1d, C vs. A). This is also consistent with a general robustness of the cellular DNA repair capacity of this group of subjects, which is evident from the similar TM median of treatments A and B (Fig. 1d) - a sign of possible protective adaptation to toxic exposures, developed in subjects with higher cumulative doses of radiation. Significant differences in the levels of persisting lesions were detected only between the cells, irradiated *in vitro* and those treated with C-PC (Fig. 1d, C vs. B, $t_{24}=2.44$). It is important to note, however, that regardless of the similarity of TM median values of B and A (Fig. 1d), irradiation of cells caused a definite increase in the data scattering towards the higher TM values, as compared to non-irradiated cells. Such an increase was not evident in the cells treated with C-PC only (Fig. 1d, C vs. A), rendering the C-PC treatment in this group less toxic to DNA than in the previous two groups (Fig. 1b and 1c). However, in contrast to the other two groups of subjects, C-PC treatment in this case did not cause a decrease in the amount of radiation-induced DSBs (Fig. 1d, D) - a finding that was confirmed by residual damage calculations (B minus A vs. D minus C).

3.4 The magnitude of the C-PC effect depends on the cumulative doses of exposure

We compared the TM values for each treatment among the three subject groups. As seen in Fig. 2, the only significant differences found were for treatment of cells with C-PC only (C), which showed that the protein was less toxic for workers with cumulative doses higher than 20 mSv (Fig. 2, group 3) and this effect contrasted with the toxicity registered for the controls and the group of professionals with very low dose radiation exposure (Fig. 2, groups 1 and 2). This indicates that chronic occupational exposure might stimulate the cellular defense mechanisms and induce resistance to DNA damage, caused by agents, such as C-PC. The workers with higher cumulative doses might also be more resistant to radiation-induced toxicity since in the same group (Fig. 1d, B) we registered lower median values of TM in the lymphocytes irradiated with 2 Gy gamma rays as compared to the TM values in the other two groups (Fig. 1b, B and 1c, B).

It is worth noting the differences between the control (Fig. 1b) and the two groups of workers (Fig. 1c and 1d) regarding the median values of the parameter TM. For both groups of professionals, we found lower median values of TM upon each of the exposures (C-PC, 2 Gy or the combination of the two agents) in comparison with the median TM values of the non-exposed controls (Group 1). This result suggests that workers possess lower levels of persisting DNA lesions than the controls, which is probably due to improved DNA repair capacity induced by the low dose professional exposure. This may also be relevant to radio-adaptive phenomena, mobilizing and activating repair of DNA damage in the groups of the professionals.

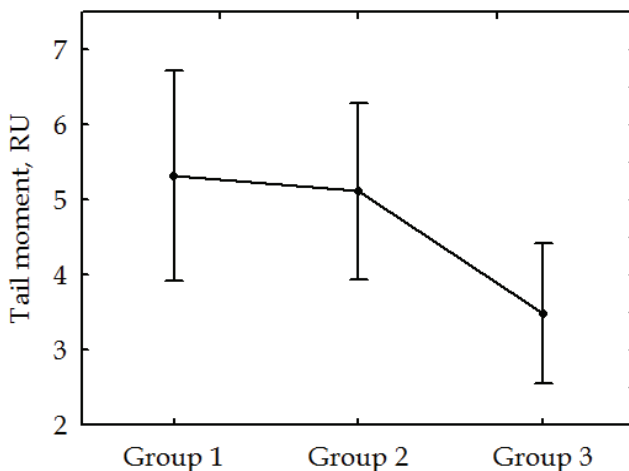


Fig. 2. TM in non-exposed controls (Group 1) and in subjects with cumulative doses, ranging from 0.32 to 12.12 mSv (Group 2) or from 26.77 to 330.77 mSv (Group 3) treated with 5 μ M C-PC. Vertical bars represent 95% CI.

3.5 Age dependence of the DNA response of lymphocytes treated with C-PC and/or irradiated with 2 Gy gamma rays

All individuals, non-exposed controls and occupationally irradiated workers, were divided into two groups. The first one included 24 subjects (3 controls and 21 occupationally exposed) of the age from 26 to 46 years. The second group consisted of 32 subjects, all of them older than 46 years (9 controls and 23 occupationally exposed). Comparison of all mean TM values in the first group showed significant differences between the levels of DNA damage in the non-treated samples and the *in vitro* irradiated lymphocytes in the presence and absence of C-PC (Fig. 3a, **A** vs. **B** and **D**, $t_{23}=2.35$ and $t_{23}=2.03$, respectively). We also observed a significant narrowing of the dispersion of the TM values for the cells, irradiated after pre-treatment with C-PC (Fig. 3a, **D**), indicating reduction of the inter-individual variability and unification of the radiation responses by C-PC. Notably, the dispersion was narrowed predominantly by reducing the non-outlier range from the top - indicating that C-PC, combined with radiation, selectively improves the repair capacity of cells which, in all other conditions (**A**, **B** and **C**) demonstrate impaired DNA repair mechanisms. The last observation suggested that the protein stimulated better the repair of the radiation-induced DNA lesions in lymphocytes of the susceptible individuals. This observation may be important for the maintenance of genomic integrity in this high-risk subgroup of the population.

Comparison of the TM values obtained for the older group (age 46-62 years, Fig. 3b) showed increased levels of persisting DNA lesions ($p=0.05$) in the cells irradiated *in vitro* (**B**, $t_{31}=3.54$), incubated with C-PC (**C**, $t_{31}=2.26$), or incubated with C-PC prior to radiation exposure (**D**, $t_{31}=2.93$), when compared to the control setting in this group (**A**). As with the younger group, the median values of the TM for treatment **B**, **C** and **D** were similar. However, the significant top-down reduction in the TM value scattering, described for the younger group after irradiation of the cells, pre-treated with C-PC (Fig.3a, **D**), was not evident in this group of subjects.

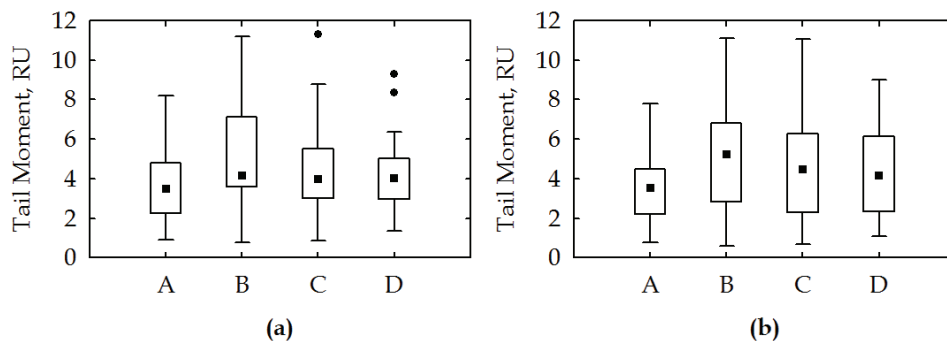


Fig. 3. Effect of different treatment patterns on subjects, grouped according to age: (a) from 26 to 46 years and (b) from 47 to 62 years. Note that both groups included exposed subjects and non-exposed controls. Whiskers represent non-outlier range, boxes: 25-75% confidence intervals (CI), (■) median value and (●) outlier values.

No.	Age	TM (Ctrl.)	TM (2Gy)	TM (C-PC)	TM (C-PC + 2Gy)
1	50	1.85 ± 0.21	3.41 ± 0.32	6.16 ± 0.11	3.88 ± 0.19
2	48	3.10 ± 0.22	6.80 ± 0.10	6.86 ± 0.07	7.15 ± 0.16
3	50	3.86 ± 0.13	5.38 ± 0.18	2.38 ± 0.51	4.91 ± 0.29
4	45	7.71 ± 0.15	9.82 ± 0.13	6.65 ± 0.24	6.24 ± 0.10
5	58	7.23 ± 0.17	8.24 ± 0.13	8.36 ± 0.08	6.80 ± 0.16
6	50	3.23 ± 0.04	3.78 ± 0.09	3.93 ± 0.04	4.13 ± 0.04
7	47	5.38 ± 0.01	7.45 ± 0.04	4.52 ± 0.14	4.12 ± 0.06
8	53	4.44 ± 0.09	7.28 ± 0.05	5.84 ± 0.01	3.91 ± 0.05
9	49	1.61 ± 0.09	1.79 ± 0.02	2.07 ± 0.03	2.02 ± 0.09
10	42	5.21 ± 0.04	7.10 ± 0.12	5.32 ± 0.07	5.13 ± 0.07
11	54	4.62 ± 0.02	6.68 ± 0.04	6.39 ± 0.05	7.70 ± 0.05
12	42	5.46 ± 0.02	7.13 ± 0.41	5.28 ± 0.03	5.00 ± 0.26

Table 1. Levels of persisting DNA strand breaks determined by TM in lymphocytes of non-exposed controls treated like in Fig. 1a.

No.	Age	Cumulative dose (mSv)	TM (Ctrl.)	TM (2Gy)	TM (C-PC)	TM (C-PC + 2Gy)
1	33	0.32	3.32 ± 0.28	8.44 ± 0.17	11.29 ± 0.48	4.77 ± 0.51
2	32	1.15	2.82 ± 0.02	3.75 ± 0.08	3.08 ± 0.04	2.08 ± 0.10
3	37	1.33	4.36 ± 0.03	11.19 ± 0.13	8.78 ± 0.16	8.34 ± 0.05
4	35	1.67	4.15 ± 0.03	5.29 ± 0.08	4.45 ± 0.08	4.11 ± 0.17
5	32	1.79	3.46 ± 0.02	3.98 ± 0.07	3.69 ± 0.02	3.78 ± 0.05
6	38	1.80	2.35 ± 0.09	2.30 ± 0.04	2.97 ± 0.04	3.08 ± 0.08
7	55	2.29	4.22 ± 0.14	5.05 ± 0.44	7.77 ± 0.39	4.64 ± 0.18
8	55	2.29	3.62 ± 0.16	7.35 ± 0.12	7.96 ± 0.13	6.62 ± 0.08
9	55	2.59	1.24 ± 0.45	1.01 ± 0.18	1.16 ± 0.42	1.69 ± 0.73
10	55	3.50	5.47 ± 0.02	6.18 ± 0.04	6.58 ± 0.10	4.84 ± 0.03
11	26	4.71	3.62 ± 0.53	3.90 ± 0.31	5.67 ± 0.09	4.55 ± 0.15
12	46	6.55	4.50 ± 0.07	6.21 ± 0.09	6.15 ± 0.04	6.38 ± 0.04
13	52	8.37	4.14 ± 0.03	5.82 ± 0.06	4.39 ± 0.05	3.80 ± 0.10
14	26	9.32	5.57 ± 0.02	7.07 ± 0.03	7.11 ± 0.04	6.36 ± 0.06
15	44	9.71	2.14 ± 0.10	4.16 ± 0.09	4.21 ± 0.04	3.56 ± 0.08
16	30	10.06	1.86 ± 0.27	3.72 ± 0.26	0.86 ± 0.16	1.77 ± 0.09
17	49	12.12	1.08 ± 0.12	0.91 ± 0.20	0.82 ± 0.02	1.33 ± 0.27

Table 2. Levels of persisting DNA strand breaks (TM) in lymphocytes of workers with very low cumulative doses (0.32-12.12 mSv) treated like in Fig. 1a.

4. Discussion

Our study has addressed three main questions: (i) are there significant differences in the DNA strand break repair in lymphocytes of workers, chronically exposed to low doses of IR and of non-exposed controls; (ii) can the biliprotein C-PC modify the DNA repair capacity of lymphocytes and the early cellular radiation response; (iii) is the level of the chronic exposure of significance for the impact of the biliprotein on the repair of DNA lesions. To answer the questions we assessed the amount of unrepaired DNA lesions in lymphocytes by the neutral comet assay 2h after irradiation of the cells in the presence or absence of C-PC.

The experiments were performed with freshly drawn human G₀ phase lymphocytes (Kaczmarek et al., 1987), which are known to utilize the NHEJ pathway for the repair of DSBs in DNA, supposedly the main lesions, detected by the neutral CA. NHEJ is a relatively fast process, which is completed within 2h after the exposure (Lankoff et al., 2006; Palyvoda et al., 2003). This was also confirmed by kinetics, utilizing the comet test in our laboratory (data not shown). With our setup we have detected changes in the cellular capacity to mend breaks in DNA generated after exposure to toxic agents, but not the differences in initial IR-induced lesions.

No.	Age	Cumulative dose (mSv)	TM (Ctrl.)	TM (2Gy)	TM (C-PC)	TM (C-PC + 2Gy)
1	38	26.77	0.90 ± 0.05	0.78 ± 0.11	3.46 ± 0.08	3.82 ± 0.04
2	44	28.47	2.05 ± 0.06	4.10 ± 0.10	1.79 ± 0.06	2.80 ± 0.15
3	53	31.14	4.65 ± 0.18	2.92 ± 0.09	2.44 ± 0.07	4.14 ± 0.28
4	54	31.43	7.82 ± 0.09	8.54 ± 0.09	6.23 ± 0.05	7.73 ± 0.18
5	48	36.39	3.47 ± 0.17	2.63 ± 0.20	0.94 ± 0.11	2.27 ± 0.11
6	56	37.06	1.61 ± 0.15	0.58 ± 0.05	0.76 ± 0.13	1.06 ± 0.06
7	48	38.05	5.76 ± 0.08	6.84 ± 0.12	6.33 ± 0.03	5.25 ± 0.16
8	32	38.72	3.74 ± 0.18	5.64 ± 0.26	4.11 ± 0.19	3.90 ± 0.05
9	45	44.66	1.44 ± 0.20	1.09 ± 0.08	1.30 ± 0.23	1.33 ± 0.30
10	50	53.19	0.81 ± 0.20	0.58 ± 0.12	0.67 ± 0.10	1.07 ± 0.01
11	36	56.07	3.97 ± 0.02	3.47 ± 0.16	2.90 ± 0.06	2.39 ± 0.10
12	49	67.76	4.06 ± 0.02	5.36 ± 0.07	5.17 ± 0.07	5.36 ± 0.03
13	41	70.46	5.36 ± 0.11	4.05 ± 0.13	3.88 ± 0.15	3.56 ± 0.06
14	50	73.21	2.54 ± 0.03	3.40 ± 0.12	3.04 ± 0.08	3.24 ± 0.05
15	45	84.57	4.34 ± 0.45	10.16 ± 0.54	6.16 ± 0.33	4.10 ± 0.15
16	54	85.80	1.04 ± 0.22	3.21 ± 0.14	1.43 ± 0.08	1.76 ± 0.08
17	48	87.48	3.95 ± 0.10	6.05 ± 0.03	4.66 ± 0.04	5.88 ± 0.07
18	56	88.28	3.60 ± 0.05	2.89 ± 0.09	5.00 ± 0.14	7.41 ± 0.05
19	50	95.02	2.35 ± 0.10	2.76 ± 0.17	2.19 ± 0.18	2.38 ± 0.12
20	52	95.14	2.10 ± 0.35	10.85 ± 0.96	11.05 ± 1.11	9.01 ± 1.64
21	62	116.82	2.95 ± 0.12	3.03 ± 0.09	2.98 ± 0.05	2.88 ± 0.17
22	42	125.17	2.82 ± 0.03	1.65 ± 0.21	0.91 ± 0.07	2.48 ± 0.32
23	48	126.39	2.55 ± 0.28	11.12 ± 0.41	2.76 ± 0.22	5.06 ± 0.11
24	41	130.23	1.22 ± 0.80	1.61 ± 0.38	3.45 ± 0.24	4.26 ± 0.32
25	41	180.61	3.37 ± 0.39	7.97 ± 0.34	4.03 ± 0.43	9.29 ± 0.37
26	40	246.94	8.21 ± 0.13	4.82 ± 0.14	3.79 ± 0.08	5.02 ± 0.02
27	48	330.77	2.42 ± 0.16	2.68 ± 0.15	2.52 ± 0.02	2.22 ± 0.11

Table 3. Levels of persisting DNA strand breaks (TM) in lymphocytes of workers with cumulative doses ranging from 26.77 to 330.77 mSv treated like in Fig. 1a.

The comet assay which we have used is an approach, applied in a number of studies to assess the repair capacity of occupationally exposed populations and recently reviewed by Decordier (Decordier et al. 2010). The CA method has also been applied in several small pilot studies, comparing the DNA repair capacity between cancer patients and healthy subjects (Alapetite et al., 1999; Leprat et al., 1998; Djuzenova, et al., 2006; Zhang et al., 2006). In these studies, the CA has demonstrated an impaired DNA lesion repair capacity in the lymphocytes of cancer

patients, when compared to that of the healthy controls. It has also been shown that CA could be a useful approach to study the radiosensitivity and individual risk of radiation therapy induced toxicity in cancer patients after *in vitro* challenging of the cells with ionizing radiation. The results of our work have indicated large inter-individual variations in the baseline endogenous levels of DNA lesions in lymphocytes from workers and non-exposed controls. Notably, the data dispersion covered a relatively large range of values and was registered in all three experimental groups, including the non-exposed control group. In the control group we observed the highest variation in persisting baseline levels of DNA lesions (Fig. 1b, A). *In vitro* irradiation with 2 Gy γ -rays or treatment with C-PC of the cells additionally enlarged the range of data dispersion, indicating significant differences in the individual susceptibility of the subjects to toxic exposures. Exposure to 2 Gy gamma rays exerted the strongest effects on data scattering in the group of professionals with cumulative doses higher than 20 mSv (Fig. 1d, B) whereas C-PC generated highest level of data dispersion in samples from the group of workers, exposed to very low doses of occupational IR (Fig. 1c, C).

The biliprotein elevated the number of persisting, unrepaired DNA lesions in the group of subjects with lower professional irradiation and in the control group. Such toxicity was not observed in the group of professionals with higher doses of occupational radiation exposure (Fig. 2). This effect might be attributed to induction of adaptive processes, due to the chronic exposure to low doses of radiation of the subjects in the last group. Studies of other laboratories on the repair capacity of nuclear power plant workers (Toili et al., 2002) or workers exposed to xenobiotics, lead or pesticides (Restrepo et al., 2000; Vodicka et al., 2004; Piperakis et al., 2009) have shown, similar to our results, that workers repair DNA damage more efficiently than the non-exposed controls. The authors attributed this phenomenon to adaptive response by the sub-chronic genotoxic exposures. The adaptive protection, shown in this study is also consistent with the conclusion of our previous study (Ivanova et al., 2010).

Notably, in combination with radiation exposure, C-PC exerted protective effects on lymphocytes of controls and of workers exposed to very low doses of radiation. For these groups, the lymphocytes, treated with C-PC and exposed to gamma rays, showed reduced levels of DNA lesions (in comparison to C-PC treatment alone), which suggested that the protein neutralized the genotoxic effects of IR and exerted radio-protection. It seems that the biliprotein selectively improved the DNA repair capacity of the individuals with higher radiosensitivity, which could be of particular interest for the radio-protection of high-risk subgroups of the population and workers.

The toxic effect of C-PC, registered in this study, is probably linked to the photosensitizing properties of the protein (Padula & Boiteaux, 1999; Zhang et al., 1999; Paul et al., 2006). It has been shown that visible light, absorbed by the tetrapyrrolic chromophores of phycobiliproteins, can generate reactive oxygen species (ROS), such as hydroxyl radical and singlet oxygen, which induce oxidative damage to DNA. The photosensitizing properties of C-PC may also contribute to the apoptotic effects of the protein in cancerogenic cell lines (Roy et al., 2007; Subhashini et al., 2004) and macrophages (Reddi et al., 2003). Apoptotic activity, however, is evident only for higher protein concentrations (>20 μ M) and longer incubation times of the cells with the protein (>24h). The trends in DNA damage, induced by C-PC, were found quite similar to those, induced by ionizing radiation or by hydrogen peroxide in the presence of transition metals (Epe, 1995; Padula & Boiteaux, 1999). Notably, for subjects with low cumulative doses of IR and for those from the control group, we registered higher levels of unrepaired DNA lesions both in cells, treated with C-PC and in those, irradiated with 2 Gy.

5. Conclusion

The data from this and from a previous study, carried out in our laboratory, which was focused on the effects of C-PC on the enzymatic anti-oxidant defense system of lymphocytes (Ivanova et al., 2010), suggest that C-phycoyanin can affect the anti-oxidant and repair mechanisms in lymphocytes, and modulate the early radiation response. They showed that the protein impacts the repair of deleterious forms of DNA damage, generated upon exposure of the cells to γ -rays, which is essential for the preservation of genomic integrity. Notably, the biliprotein might selectively improve the DNA repair capacity of the individuals with higher radiosensitivity, which could be of particular interest for the radio-protection of the high-risk subgroups of population and workers. The protein induced significantly less persisting DNA lesions in the group of workers with higher doses (>20 mSv, Fig. 2, group 3) in comparison with the other two groups, which is relevant to adaptive phenomena induced by the chronic occupational exposure of the subjects. However, the present study should be considered a pilot one and additional experiments are needed to decide whether the protein could be applied for the protection of occupationally exposed individuals (such as nuclear power plant workers, miners, some medical doctors and pilots), and subgroups of the population with higher susceptibility to the toxic effect of ionizing radiation.

6. Acknowledgement

This study was carried out as part of the National Program “Genomics” of the Republic of Bulgaria and is partially financed by the Bulgarian Ministry for Education, Youth and Science (Grant G-3-10/05). We would like to thank Savina Stoitsova for her critical reading of the text.

7. References

- Alapetite, C., Thirion, P., De La Rochefordiere, A., Cosset, J.M. & Moustacchi, E. (1999). Analysis by Alkaline Comet Assay of Cancer Patients with Severe Reactions to Radiotherapy: Defective Rejoining of Radioinduced DNA Strand Breaks in Lymphocytes of Breast Cancer Patients. *Int J Cancer*, Vol. 83, No. 1, (Sep 24), pp. (83-90)
- Berwick, M. & Vineis, P. (2000). Markers of DNA Repair and Susceptibility to Cancer in Humans: An Epidemiologic Review. *J Natl Cancer Inst*, Vol. 92, No. 11, (Jun 7), pp. (874-897)
- Collins, A.R., Oscoz, A.A., Brunborg, G., Gaivao, I., Giovannelli, L., Kruszewski, M., Smith, C.C. & Stetina, R. (2008). The Comet Assay: Topical Issues. *Mutagenesis*, Vol. 23, No. 3, (May), pp. (143-151)
- Contreras-Martel, C., Matamala, A., Bruna, C., Poo-Caamano, G., Almonacid, D., Figueroa, M., Martinez-Oyanedel, J. & Bunster, M. (2007). The Structure at 2 Å Resolution of Phycocyanin from *Gracilaria Chilensis* and the Energy Transfer Network in a Pc-Pc Complex. *Biophys Chem*, Vol. 125, No. 2-3, (Feb), pp. (388-396)
- Decordier, I., Looock, K.V. & Kirsch-Volders, M. (2010). Phenotyping for DNA Repair Capacity. *Mutat Res*, Vol. 705, No. 2, (Oct), pp. (107-129)
- Epe, B. (1995). DNA Damage Profile Induced by Oxidizing Agents *Rev Phys Bioch Pharm*, Vol. 127, pp. (223-249)

- Ge, B., Qin, S., Han, L., Lin, F. & Ren, Y. (2006). Antioxidant Properties of Recombinant Allophycocyanin Expressed in *Escherichia Coli*. *J Photochem Photobiol B*, Vol. 84, No. 3, (Sep 1), pp. (175-180)
- Glazer, A.N. (1994). Phycobiliproteins - a Family of Valuable, Widely Used Fluorophores. *J of Appl Phycol*, Vol. 6, pp. (105-112)
- ICRP (1991). 1990 Recommendations of the International Commission on Radiological Protection. ICRP Publication 60. *Ann ICRP* 21 (1-3)
- Ivanova, K.G., Stankova, K.G., Nikolov, V.N., Georgieva, R.T., Minkova, K.M., Gigova, L.G., Rupova, I.T. & Boteva, R.N. (2010). The Biliprotein C-Phycocyanin Modulates the Early Radiation Response: A Pilot Study. *Mutat Res*, Vol. 695, No. 1-2, (Jan), pp. (40-45)
- Kaczmarek, L., Calabretta, B., Elfenbein, I.B. & Mercer, W.E. (1987). Cell Cycle Analysis of Human Peripheral Blood T Lymphocytes in Long-Term Culture. *Exp Cell Res*, Vol. 173, No. 1, (Nov), pp. (70-79)
- Kalthur, G., Kumar, P., Devi, U., Ali, S., Upadhyay, R., Pillai, S. & Rao, A. (2008). Susceptibility of Peripheral Lymphocytes of Brain Tumour Patients to in Vitro Radiation-Induced DNA Damage, a Preliminary Study. *Clin Exp Med*, Vol. 8, No. 3, (Sep), pp. (147-150)
- Karpov, L.M., Brown, I., Poltavtseva, N.V., Ershova, O.N., Karakis, S.G., Vasil'eva, T.V. & Chaban Iu, L. (2000). The Postradiation Use of Vitamin-Containing Complexes and a Phycocyanin Extract in a Radiation Lesion in Rats]. *Radiats Biol Radioecol*, Vol. 40, No. 3, (May-Jun), pp. (310-314)
- Lankoff, A., Bialczyk, J., Dziga, D., Carmichael, W.W., Gradzka, I., Lisowska, H., Kuszewski, T., Gozdz, S., Piorun, I. & Wojcik, A. (2006). The Repair of Gamma-Radiation-Induced DNA Damage Is Inhibited by Microcystin-Lr, the Pp1 and Pp2a Phosphatase Inhibitor. *Mutagenesis*, Vol. 21, No. 1, (Jan), pp. (83-90)
- Leprat, F., Alapetite, C., Rosselli, F., Ridet, A., Schlumberger, M., Sarasin, A., Suarez, H.G. & Moustacchi, E. (1998). Impaired DNA Repair as Assessed by the "Comet" Assay in Patients with Thyroid Tumors after a History of Radiation Therapy: A Preliminary Study. *Int J Radiat Oncol Biol Phys*, Vol. 40, No. 5, (Mar 15), pp. (1019-1026)
- Li, B., Zhang, X., Gao, M. & Chu, X. (2005). Effects of Cd59 on Antitumoral Activities of Phycocyanin from *Spirulina Platensis*. *Biomed Pharmacother*, Vol. 59, No. 10, (Dec), pp. (551-560)
- Madhyastha, H.K., Radha, K.S., Nakajima, Y., Omura, S. & Maruyama, M. (2008). Upa Dependent and Independent Mechanisms of Wound Healing by C-Phycocyanin. *J Cell Mol Med*, Vol. 12, No. 6B, (Dec), pp. (2691-2703)
- Marques De Sa, J.P. & Frias, R. (2007). *Applied Statistics* (2), Springer-Verlag, 978-3-540-71971-7, Berlin-Heidelberg
- Mohseni-Meybodi, A., Mozdarani, H. & Mozdarani, S. (2009). DNA Damage and Repair of Leukocytes from Fanconi Anaemia Patients, Carriers and Healthy Individuals as Measured by the Alkaline Comet Assay. *Mutagenesis*, Vol. 24, No. 1, (Jan), pp. (67-73)
- Moller, P., Knudsen, L.E., Loft, S. & Wallin, H. (2000). The Comet Assay as a Rapid Test in Biomonitoring Occupational Exposure to DNA-Damaging Agents and Effect of Confounding Factors. *Cancer Epidemiol Biomarkers Prev*, Vol. 9, No. 10, (Oct), pp. (1005-1015)
- Padula, M. & Boiteaux, S. (1999). Photodynamic DNA Damage Induced by Phycocyanin and Its Repair in *Saccharomyces Cerevisiae*. *Braz J Med Biol Res*, Vol. 32, No. 9, (Sep), pp. (1063-1071)

- Palyvoda, O., Polanska, J., Wygoda, A. & Rzeszowska-Wolny, J. (2003). DNA Damage and Repair in Lymphocytes of Normal Individuals and Cancer Patients: Studies by the Comet Assay and Micronucleus Tests. *Acta Biochim Pol*, Vol. 50, No. 1, pp. (181-190)
- Paul, B.T., Patel, A., Selvam, G.S., Mishra, S., Ghosh, P.K. & Murugesan, R. (2006). Photodynamic Action of C-Pcs Obtained from Marine and Fresh Water Cyanobacterial Cultures: A Comparative Study Using Epr Spin Trapping Technique. *Free Radical Res.*, Vol. 40, No.8, (Aug) pp. (821-825)
- Piperakis, S.M., Kontogianni, K., Karanastasi, G., Iakovidou-Kritsi, Z., Cebulska-Wasilewska, A. & Piperakis, M.M. (2009). Investigation of the Genotoxic Effect of Pesticides on Greenhouse Workers' Lymphocytes. *Environ Mol Mutagen*, Vol. 50, No. 2, (Mar), pp. (121-126)
- Prasanna, R., Sood, A., Suresh, A. & Kaushik, B.D. (2007). Potentials and Applications of Algal Pigments in Biology and Industry. *Acta Bot Hung*, Vol. 49, pp. (131-156)
- Reddy, M.C., Subhashini, J., Mahipal, S.V., Bhat, V.B., Srinivas Reddy, P., Kiranmai, G., Madyastha, K.M. & Reddanna, P. (2003). C-Phycocyanin, a Selective Cyclooxygenase-2 Inhibitor, Induces Apoptosis in Lipopolysaccharide-Stimulated Raw 264.7 Macrophages. *Biochem Biophys Res Commun*, Vol. 304, No. 2, (May 2), pp. (385-392)
- Restrepo, H.G., Sicard, D. & Torres, M.M. (2000). DNA Damage and Repair in Cells of Lead Exposed People. *Am J Ind Med*, Vol. 38, No. 3, (Sep), pp. (330-334)
- Romay, C., Gonzalez, R., Ledon, N., Ramirez, D. & Rimbau, V. (2003). C-Phycocyanin: A Biliprotein with Antioxidant, Anti-Inflammatory and Neuroprotective Effects. *Curr Protein Pept Sci*, Vol. 4, No. 3, (Jun), pp. (207-216)
- Roy, K.R., Arunasree, K.M., Reddy, N.P., Dheeraj, B., Reddy, G.V. & Reddanna, P. (2007). Alteration in Mitochondrial Membrane Potential by Spirulina Platensis C-Phycocyanin Induces Apoptosis in the Doxorubicin-Resistant Human Hepatocellular-Carcinoma Cell Line Hepg2. *Biotechnol Appl Biochem*, Vol. 47, No.3, (Jul). pp. (159-167)
- Stec, B., Troxler, R.F. & Teeter, M.M. (1999). Crystal Structure of C-Phycocyanin from Cyanidium Caldarium Provides a New Perspective on Phycobilisome Assembly. *Biophys J*, Vol. 76, No. 6, (Jun), pp. (2912-2921)
- Subhashini, J., Mahipal, S.V., Reddy, M.C., Mallikarjuna Reddy, M., Rachamalla, A. & Reddanna, P. (2004). Molecular Mechanisms in C-Phycocyanin Induced Apoptosis in Human Chronic Myeloid Leukemia Cell Line-K562. *Biochem Pharmacol*, Vol. 68, No. 3, (Aug 1), pp. (453-462)
- Sun, L., Wang, S., Chen, L. & Gong, X. (2003). Promising Fluorescent Probes from Phycobiliproteins. *IEEE J. Cel Top Quantum Electron*, Vol. 9, pp. (177-188)
- Touil, N., Aka, P.V., Buchet, J.P., Thierens, H. & Kirsch-Volders, M. (2002). Assessment of Genotoxic Effects Related to Chronic Low Level Exposure to Ionizing Radiation Using Biomarkers for DNA Damage and Repair. *Mutagenesis*, Vol. 17, No. 3, (May), pp. (223-232)
- Vodicka, P., Kumar, R., Stetina, R., Musak, L., Soucek, P., Haufroid, V., Sasiadek, M., Vodickova, L., Naccarati, A., Sedikova, J., Sanyal, S., Kuricova, M., Brsiak, V., Norppa, H., Buchancova, J. & Hemminki, K. (2004). Markers of Individual Susceptibility and DNA Repair Rate in Workers Exposed to Xenobiotics in a Tire Plant. *Environ Mol Mutagen*, Vol. 44, No. 4, pp. (283-292)
- Zhang, C., Naftalis, E. & Euhus, D. (2006). Carcinogen-Induced DNA Double Strand Break Repair in Sporadic Breast Cancer. *J Surg Res*, Vol. 135, No. 1, (Sep), pp. (120-128)

Effects of Gamma-Ray Irradiation on Tracking Failure of Polymer Insulating Materials

Boxue Du, Yu Gao and Yong Liu
Tianjin University
China

1. Introduction

Electrical insulation and dielectrics play a key role in the performance and reliability of most electrical systems, where a single-point system failure may prove catastrophic or even fatal to the electrical equipment. Polymers are the most commonly used dielectrics because of their reliability, availability, ease of fabrication and low cost. The selection of the proper polymer dielectric for a desired application depends on the requirements and operating conditions of the system. Voltage surges are known to be one of the factors leading to tracking failure, which often appear in lighting, switching and circuit breaker operation. Tracking failure is a dielectric breakdown phenomenon occurring on polymer surfaces comprising carbonized conductive paths. When a sufficiently intense discharge lasts for a considerable time, the decomposed carbon products, with some parts of the channel carbonized, are progressive and rapidly form on the sample surface. When the carbonized deposits bridge the interval between electrodes, a sudden decrease in the insulating resistance occurs. The importance of this information has been revealed for preventing fires, short-circuit and insulation failure in electrical appliances and devices, and especially the tracking and ignition of polymers have been examined.

Polymer materials are widely used in radiation environments, such as scientific research fields and nuclear power stations, where the high safety and reliability are demanded. The polymer insulating materials are inevitably exposed to various kinds of radiation. The changes in their physical and chemical properties could prematurely terminate the useful life of the dielectric. Outside and inside of the secondary shield in the containment vessel of nuclear power plants, the maximum dose rates of irradiation are 0.01 Gy/h and 1 Gy/h. The dose rate in nuclear power plants varies widely from 10 μ Gy/h to 10 kGy/h with a potential of total exposure 1000 kGy or greater. The high reliability is based on construction safety and system safety during the use of electrical equipment. Accordingly, it is important to investigate the influence of radiation on polymeric insulating materials used in the radioactive environments. Presently, the researches on irradiation aging are mostly concentrated on electrical and mechanical performance, but the effect of radiation, especially the radiation aging theory is rarely studied. Kuriyama et al have measured the physical and electrical properties of gamma-ray irradiated PVC jacketed cable and concluded that the electrical receptivity of PVC is reduced obviously. We have investigated the tracking resistance of gamma-ray irradiated polyethylene and modified

polycarbonate materials, and the results reveal that the tracking resistance is improved by irradiation for cross-linking type materials, but the conclusions for degradation type materials are opposite.

The polymers used in the field of electrical and electronic engineering are not only subject to an electric field alone, quite often they operate under the influence of both electric and magnetic fields. In addition to shielding effects against space plasma flux, magnetic field changes the electron kinematics and the gas desorption rate, and hence the flashover potential. The effect of a magnetic field parallel to an applied electric field has been considered and reported that a magnetic field can shorten the formative time lag of breakdown. Magnetic field might influence dielectric breakdown in different ways. The basic mechanisms and physical phenomena providing magnetic insulation have been investigated in the past mainly for vacuum-insulator interfaces in high-power transmission lines and vacuum diodes. The influence of magnetic field on the sparking voltage has been examined for a slightly non-uniform electric field applied perpendicularly to a magnetic field, including its effects on the formative time lag and on the cycloidal movement of electrons. Low energy non-disruptive discharge carbonized “track” marks have been identified by a number of users on gas insulating switchgear (GIS) insulating surfaces and the cause of this phenomenon has not yet been identified. However, there have been very few investigations concerning the influence of magnetic field on the tracking failure of polymer materials used in electrical equipments. Therefore, it is necessary to study how their electrical characteristics change under magnetic field.

Polymers are used on space equipment with the examples of these devices working at high dc voltage on satellites such as ionic propulsion systems, photomultiplier tubes, scientific electronic instruments, communication systems and solar cell power supply systems. Energetic electromagnetic radiation and low pressure are two main factors in the space environment. We have reported that surface discharge occurs earlier at low pressures than atmospheric pressure. In fact, surface discharge is one of the principal causes for premature failure in electronic equipments used in low pressure regions. The dielectric properties of the polymers under the environments of low pressure and radiation may change. It is necessary to study the way how their electrical characteristics change under the combined environments.

As technology advances, increasing demands on the reliable operation under various operating and environmental conditions are made on materials and components. Therefore, it is necessary to study how their electrical characteristics change with consideration of radiation, low pressure and magnetic field. However, knowledge of influence of irradiation under combined conditions of radiation, low pressure and magnetic field is limited, and systematic study is desirable.

Polymer materials are widely used in electrical insulation because of their high breakdown strength, high resistivity and low dielectric loss. Polybutylene naphthalate is widely used in aerospace electronics, electric engineering, chemical, metallurgy and medical equipment. Polybutylene terephthalate is usually used for electric coupler, blind plug, switch and insulating cover. Polyethylene terephthalate is one of the most widely used polymers for electrical and electronic industries. Whether the dielectric property of the polymers is changed by irradiation and magnetic field or not are worth investigating. In this chapter, effects of total dose of gamma-ray irradiation on tracking failure of polymer materials are described. The results reveal that the tracking failure properties are greatly changed by gamma-ray irradiation.

2. Experiment setup and procedure

2.1 Test samples

Polybutylene naphthalate (PBN) and polybutylene terephthalate (PBT) are produced with butanediol by reaction with 2, 6-naphthalic acid and dimethyl terephthalate, respectively. Polyethylene terephthalate (PET) is produced with ethylene glycol by reaction with purified terephthalic acid. For comparison, both polycarbonates mixed with 3% polyethylene (M-PC) and polyethylene (PE) samples are also tested.

The samples are irradiated in air up to 100 kGy and then up to 1000 kGy with a dose rate of 10 kGy/h by using a ^{60}Co gamma-source. The thickness and dimensions are 3 mm and 20 mm \times 20 mm. The sample surface is cleaned with ethyl alcohol and dried in a desiccator in air at room temperature for 24 h or longer before the testing.

2.2 Experimental apparatus and procedure for pulse voltage application

Schematic diagram of experimental set-up is shown in Fig. 1. Test sample is stressed electrically under a HV pulse voltage at the level of 30 kV and the pulse width is 1 ms. The pulse interval is adjusted from 5 ms to 10 ms. The electrode geometry is needle-plate electrode pattern, where the needle electrode is connected to the HV voltage and the plate electrode is grounded through the discharge detecting circuit. The length of each stainless steel electrode is 45 mm, the radius of the semicircle plate electrode is 5 mm and the thickness is 0.5 mm. The diameter of the needle electrode is 0.65 mm and the interval between the electrodes is 3 mm. The magnetic environment is produced by the electromagnet (PEM-50). The magnetic flux density (MFD) is 495 mT and the direction of $E \times B$ is 0, 90 and 270 degrees with respect to the sample surface. The vacuum chamber is made from a glass tube with two sheets of acrylic board for the cover and bottom.

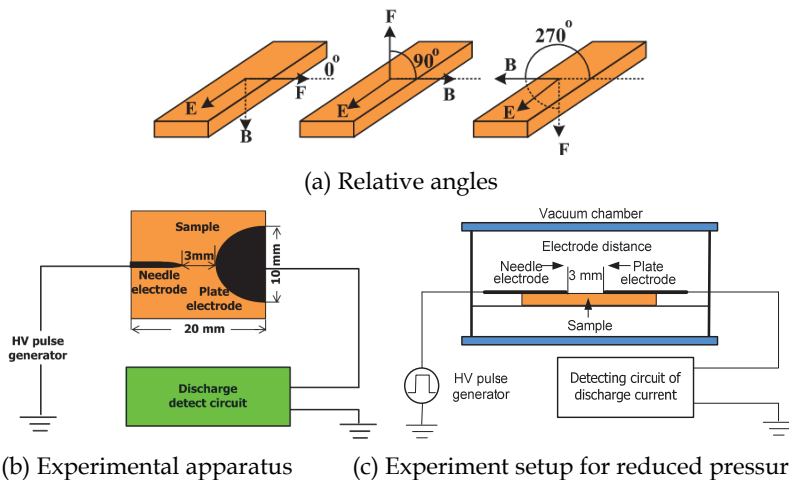


Fig. 1. Schematic diagram of test system for pulse voltage

Tracking failure is defined as the insulation failure under electric field with consequent lack of dielectric properties, which is determined when the surface is burning or short-circuit of the electrodes has persisted for 2s. The tracking failure is caused by decomposed carbon on the sample surface due to heat generated by the discharge, which starts locally across the

electrodes and forms on the sample surface. A high-speed general purpose AD conversion module (DRF2A) is connected with the experimental circuit in order to measure the discharge current. The sampling time used by this method is 25 μ s. The test is repeated 10 times, thus each datum is an average of ten measurements. A monocular-video-zoom microscope with the magnification of 420 is used to acquire the pictures of tracking failure for the detailed analysis to identify the tracking failure phenomenon.

2.3 Experimental apparatus and procedure for IEC 60112 tracking test

The experimental set-up of tracking failure is constructed according to the specifications given in IEC 60112 as shown in Fig. 2. The thickness of each electrode is 2 mm, the length 45 mm, the width 5 mm, and the interval distance between the two electrodes 4 mm. The solution is 0.1% NH_4Cl in de-ionized water, giving a resistivity of approximate 395 Ω cm at the temperature of 23 $^\circ\text{C}$. Droplets are applied at the intervals to keep up the discharge between the electrodes on the sample surface. The droplet size of the electrolyte is 20 mm^3 and the time interval between each added droplet is 30 s. Tracking failure is defined as when the sample burns or the current exceeds 0.5 A and persists for 2 s. But because some of the samples do not track evenly at the highest test voltage, repeated discharges gradually cause the erosion of the sample surface between the electrodes. The erosion depth and weight loss are measured after adding 100 droplets.

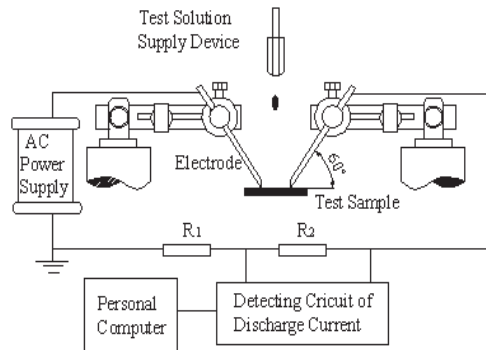


Fig. 2. Experimental set-up for IEC 60112 test

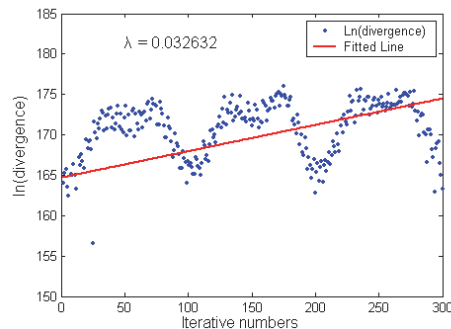


Fig. 3. Estimate of largest Lyapunov exponent

3. Methods of data-processing

3.1 The proof for chaos in the discharge process

Detecting the presence of chaos in the discharge process is a precondition for applying the non-linear method to analyze discharge currents. Lyapunov exponents characterize the exponential divergence of neighbor embedding vectors $X(i)$ and $X(j)$ in phase space and one or more positive Lyapunov exponents can provide a necessary and sufficient proof for a dynamic system to be chaotic. By calculating the largest Lyapunov exponent of an experimental time series, the discharge process is proved chaotic. Fig. 3 shows an estimation of the largest Lyapunov exponent by the algorithm given by Rosenstein. The data are sampled at the middle state of the tracking test with unirradiated PBT at 375 V. Here, the largest Lyapunov exponent is calculated as 0.032632 indicating that the process is chaotic.

3.2 Recurrence plot method

Recurrence plots (RPs), which are used to characterize the degree of aperiodicity of time series, are first introduced by Eckmann. The RP method provides a useful graphical framework for extracting information from time series. By using the RP method, the non-linear characteristics of dynamical systems can be illustrated. The RP method is constructed as follows:

First, according to Takens' embedding theorem, vector $X(i)$ can be reconstructed from a time series $x(i)$:

$$X_{(i)} = [x(i), x(i + \tau), \dots, x(i + (m - 1)\tau)], i = 1, 2, 3, \dots \quad (1)$$

Where $X(i)$ is the embedding vector, m is the embedding dimension, and τ is the delay time; $x(i)$ is the time series which stands for the discharge current series in this paper. The embedding dimension m and delay time τ can be chosen by the C-C method. For a given time series $x(i)$, the estimation of τ assures that the coordinates $x(i)$ and $x(i+t)$ are somewhat independent but not completely uncorrelated. The C-C method provides a good criterion for the choice of m and τ and also works well in the presence of noise, especially for noise levels below 30%.

Then the RP can be drawn based on the following matrix:

$$R_{ij} = H(\varepsilon - \|X_{(i)} - X_{(j)}\|_2), X_{(i)}, X_{(j)} \in R^m, i, j \in (1, M) \quad (2)$$

where ε is a predefined threshold, $H(x)$ is the Heaviside function, and M is the number of $X(i)$ vectors constructed from the time series. The value one in this matrix is plotted in black in the RP. The choice of ε is the critical, if it is too big, it will produce irrelevant points, and if it is too small, useful information will be lost. In the investigation, ε is chosen as 0.25σ . Where, σ is the standard deviation of the time series.

The discharge currents sampled directly from the tracking test of IEC 60112 have power frequency components of leakage currents, which have negative effects on non-linear analysis. To filter the power frequency components, wavelet transform of discharge currents are applied and the Morlet wavelet db8 is chosen as the mother wavelet.

Fig. 4 shows an RP example of discharge current with unirradiated PBT at 325 V. Fig. 4a shows an original discharge current and the related RP. It can be concluded that the discharge occurs frequently at the positive and negative peaks of the waveform. Due to the ac voltage, the current waveform has power frequency components. Reflected in the RP, recurrence points are mainly parallel to the diagonal. The distribution of recurrence points of sinusoidal series in RP is determined by the RP method. The periodic characteristic of RP

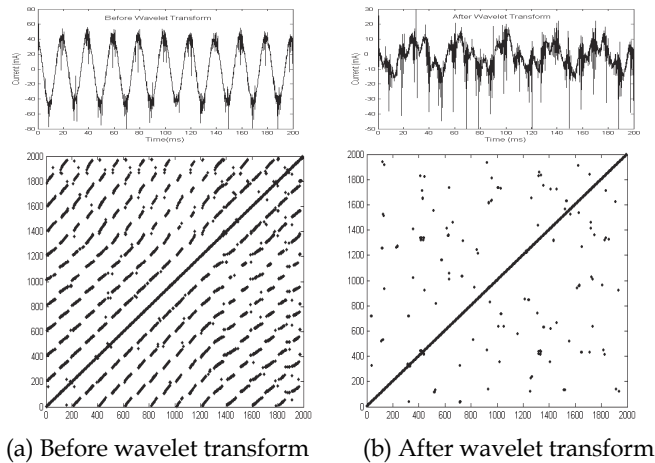


Fig. 4. Examples of recurrence plots of discharge current

covers non-linear features and acts as adverse factor for non-linear analysis. Fig. 4b shows the treated discharging sequence by wavelet transform and its reconstructed RP. After the data preprocessing, the recurrence points are randomly distributed in the picture and the topological structure can actually reflect the non-linear characteristics. The effects of dosages of gamma-ray irradiation on the resistance to tracking for both PBT and PET are presented by comparing the RP structure, as the above description.

4. Dielectric breakdown and tracking resistance

4.1 Dielectric breakdown by HV pulse voltage application

Fig. 5 shows the photographs of sample surface after the discharge for 20 s at the discharge interval of 10 ms. The color of sample surfaces in both PBN and PBT are gradually dark as the total dose of gamma-ray irradiation increases. The noticeable changes of sample surface in the breakdown process are evidently observed. The repetitive discharges occur before the dielectric breakdown and the quantity of decomposition carbon increases in the area close to the electrodes. As shown in Fig. 5, a carbonization conducting path forms on the surface between the electrodes. The surface is carbonized by the heat energy from the discharge. With the high repetition rate of discharges, there is a high increase of discharge quantity which affects the carbonization progress and the situation of carbon deposition. When the intensive discharge lasts for a certain time, the surface is carbonized first to the area close to the electrodes. Due to the conductive nature of carbonization products, they act as the extension of the electrodes. After a sufficiently long time, the carbonized conduction path finally forms between the electrodes. By comparing Fig. 5a and 5b, the features of dielectric breakdown phenomenon are significantly different between PBN and PBT. The carbonized area decreases with increasing the total dose of irradiation with PBN, but increases with PBT. The difference indicates that the thermal properties are improved with PBN, but worsened with PBT.

Fig. 6 shows the relation between the time to dielectric breakdown and the total dose of the irradiation. For the investigated range of the irradiation, the time to dielectric breakdown

increases with the increase of the total dose with PBN, but decreases with increasing the total dose with PBT. The time to dielectric breakdown of both PBN and PBT decreases with

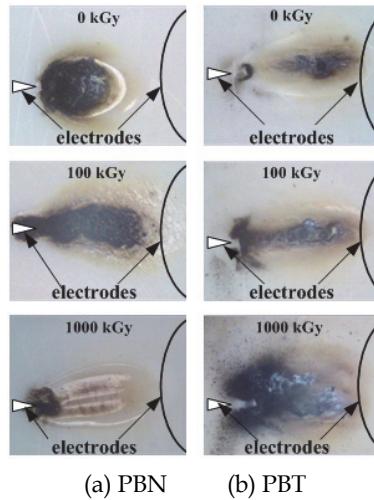


Fig. 5. Sample surface after carbonization

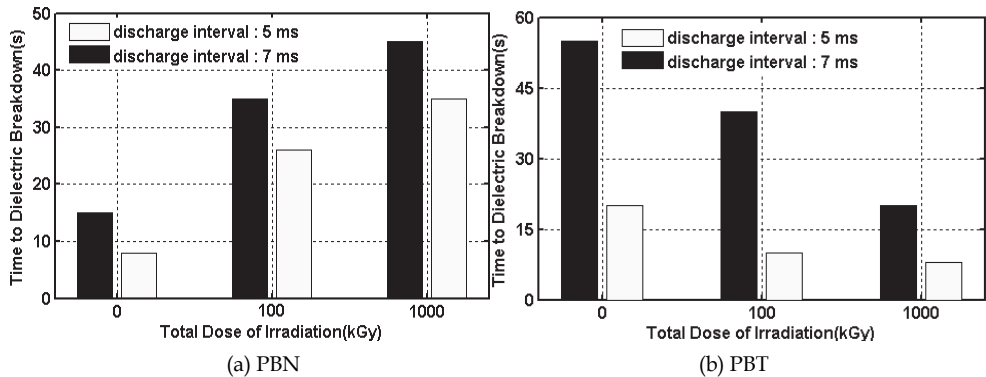


Fig. 6. Relation between the time to dielectric breakdown and the total dose of irradiation

the decrease of the discharge interval. With the increase of the total dose of irradiation, the time to dielectric breakdown of PBN increases, which indicates that the thermal properties are improved. However, the time to dielectric breakdown of PBT decreases with the increase of the total dose, which indicates that the thermal properties are worsened. The atoms that make up a polymer are bounded together by weak covalent bonds that are disrupted easily by gamma-ray radiation, and as bonds are broken new ones are formed and the structure of the polymer is altered. In practice, cross-linking and degradation reaction often occur simultaneously, the reaction result is determined by the one that is dominant. For PBN, it is supposed that the cross-linking reaction exceeds the degradation reaction and the combination between the molecules extends the three-dimensional networks. For PBT, it is

supposed that the degradation reaction exceeds the cross-linking reaction and the scission of the main chain bonds results in the formation of low-molecular-weight chain fragments. With the decrease of the discharge interval, the tendency of the time to dielectric breakdown decreases. When the discharge interval decreases, electron emission from the electrode becomes more frequent, the heat caused by the discharge energy which makes the carbon chain of the molecules broken increases, and the carbon conductive path of polymer surface forms more steadily. As a result, the time to dielectric breakdown decreased. By the way, at the discharge interval of 10 ms, the accurate time to dielectric breakdown of the test results does not show in the figure as the dielectric breakdown did not occur until 200 s under the same condition at discharge intervals of 7 ms and 5 ms.

Fig. 7 shows the relation between the discharge quantity and the total dose of irradiation after the discharge for 600 times. The dielectric breakdown is mainly dependent upon the thermal energy formed by the discharge. The discharge quantity is the total integrated charge of the discharge current during the dielectric breakdown period, which is the degree of the heat-durability. If the discharge quantity is smaller, it suggests that the carbon chain is harder to be broken. In other words, the heat-durability of the material is better. With the increase of the total dose, the discharge quantity decreases with PBN, which suggests that the thermal property is improved and the dielectric breakdown becomes not easy. As mentioned in Fig. 6a, the time to dielectric breakdown is delayed with the increase of the total dose. This fact may be due to the occurrence of the cross-linking reaction. With the increase of the total dose of irradiation, the discharge quantity increases with PBT, which suggests that the thermal properties are worsened and the dielectric breakdown becomes faster. As mentioned in Fig. 6b, the time to dielectric breakdown decreases with the increase of the total dose. The reason for this may be due to the degradation reaction by irradiation.

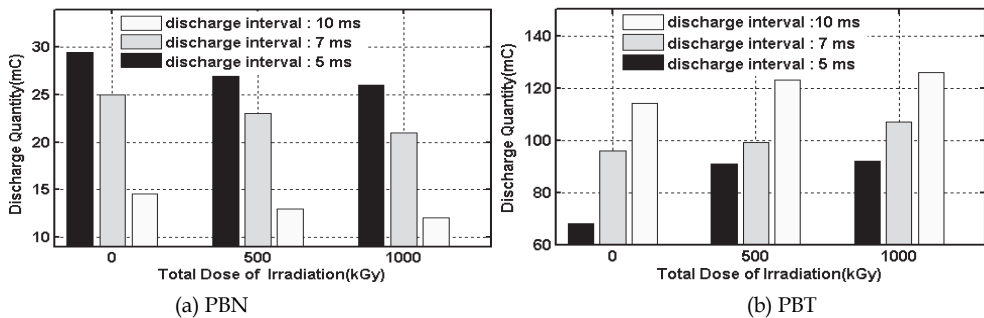


Fig. 7. Relation between the discharge quantity and the total dose of irradiation

From Fig. 7a and 7b, the discharge quantity increases with the decrease of discharge interval for PBN, but the tendency is opposite for PBT. The discharge is much more intensive in the shorter discharge interval because the accumulative energy of consecutive discharge is higher, and the dielectric breakdown occurs more quickly. For PBN, the dielectric breakdown is not easy due to the inherent property and the discharge was continuous. The formation of carbon conductive path is gradual, and the discharge quantity is bigger at the shorter discharge interval. For PBT, the carbonization and dielectric breakdown are faster. The discharge is discontinuous from the visual observation. At the shorter discharge

interval, the carbonization forms more quickly and the brief short circuit occurs more frequently, and the discharges could not completely take place, so the total discharge quantity is smaller as shown in Fig. 7b.

The dielectric properties are improved for PBN but worsened for PBT by gamma-ray irradiation. This difference is attributed to the radiation-induced cross-linking and degradation. The effect of the total dose on electrical properties is markedly different, depending on the chemical structure of the base polymer. The radiation adds a particular dimension to the aging problem, because it interacts strongly with materials in general and brings about structural changes that alter their properties. This is because that it can alter the macroscopic properties of polymeric materials through mechanisms like chain scission, cross linking and oxidation. Comparing the molecule formulas, there are two phenyls in the main chain of PBN but one for PBT. The amount of phenyl in the main chain plays a main role on the result of the radiation reaction. In another word, the dielectric properties of polybutylene polymers are improved for PBN which contains more combined phenyls in the main chain. It is known that to disrupt the two combined phenyls needs more energy than one phenyl. It is supposed that the disruption of the bonds is harder for PBN than PBT after the same dosage of the irradiation. The formation of new bonds does not seem to have much difference because of the same fringe structure. The new main chain is bigger for PBN because of more phenyls. For PBN, it is considered that the effects of the new bonds exceed the disruptive ones. For PBT, it is considered to be opposite to PBN. Therefore, PBN represents cross-linking type results and PBT represents scission type results.

4.2 Effects of tracking resistance by use of IEC60112 method

To estimate the resistance to tracking of polymer material, there are many traditional methods including recording the time to dielectric breakdown, calculating the discharge quantity, measuring the dielectric loss angle and testing the CTI value. Among the methods, the CTI value is extremely important and also considered as an index mark to select insulating materials. The minimal voltage, which could cause tracking failure with the application of 50 drops of electrolyte, is used as a measure of the susceptibility of the material to tracking and is defined as the CTI value according to IEC60112. The example of discharge events is shown in Fig. 8. The test solution is evaporated by Joule heat caused by leakage current which flows between the electrodes across the sample surface. A discharge appears at the dry band. After the appearance of the discharge, the sample surface is eventually dried between the electrodes. The initiation of a carbon deposit is



(a) Scintillation discharge (b) Arc discharge (c) Discharge and carbonization (d) Intense discharge
Fig. 8. Example of discharge events with 100 kGy irradiated M-PC.

closely related to the location where a dry band is formed in the evaporation of solution due to Joule heat, and to heat degradation of the sample surface caused by scintillation discharge across the dry band. With further application of the test solution, the erosion of the sample surface occurs as a result of the tracking test. Fig.9 shows the relation between dosage of the irradiation and the CTI value for both PET and PBT with ac voltage application. As total dosage increases, the CTI value of PET increases, but the CTI of PBT decreases.

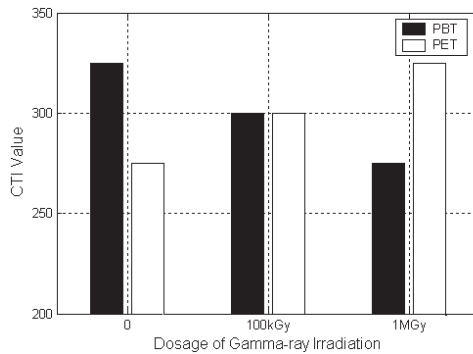


Fig. 9. Relation between the CTI value and the dosage of gamma-ray irradiation

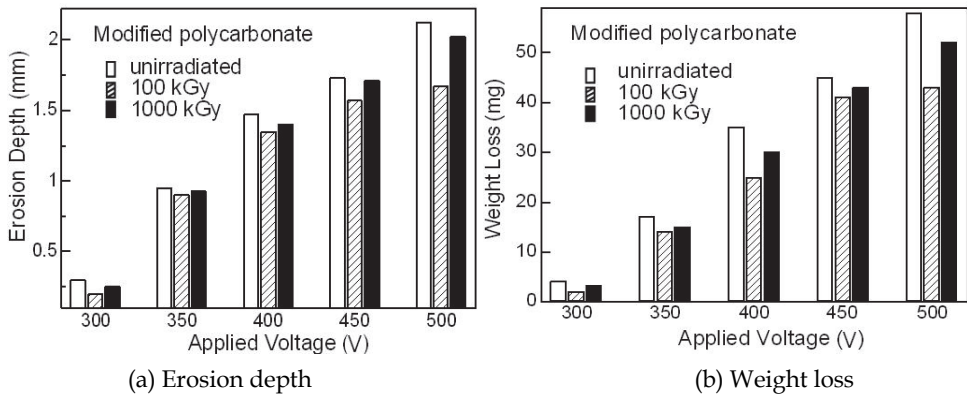


Fig. 10. The changes of tracking resistance on M-PC

Fig. 10 shows the relationship between the biggest erosion depths, weight loss and test voltage with M-PC. For the range of irradiation, both the erosion depths and weight loss are smaller than that of unirradiated samples. It indicated that after the irradiation, the tracking resistance was improved. A cross-linking reaction of an organic material is one main factor for improving tracking resistance and conversely a degradation reaction is conceivable as a factor for decreasing tracking resistance. It is believed that the improvement is due to the result of the cross-linking reaction. However, both the erosion depths and weight loss decreases with increasing the total dose from 0 kGy to 100 kGy, but increases from 100 kGy to 1000 kGy. It indicates that there is a threshold value for the tracking resistance of M-PC

around 100 kGy. When the total dose exceeds the threshold value, the tracking resistance begins to decrease. The decrease might be attributed to the result of the degradation reaction.

The M-PC is mixed with 3% PE. It is known that gamma-ray irradiation caused degradation reaction with PC. Therefore, the mixing of PE maybe one main reason for the improvement of the tracking resistance with irradiated M-PC. In order to confirm the judgment, the tracking resistance of PE after gamma-ray irradiation was investigated.

Fig. 11 shows the relationship between the biggest erosion depths, weight loss and test voltage with PE. For the range of the irradiation, both the erosion depths and weight loss decreased with the increase of the total dose. Accordingly, the trend that the tracking resistance improves through gamma-ray irradiation is assumed. It is also supposed that the heat from irradiation causes the formation of 3-dimensional structures, which strengthens the PE by cross-linking reaction. Therefore, the mixing of PE is probably one main reason for the improvement of the tracking resistance with irradiated M-PC.

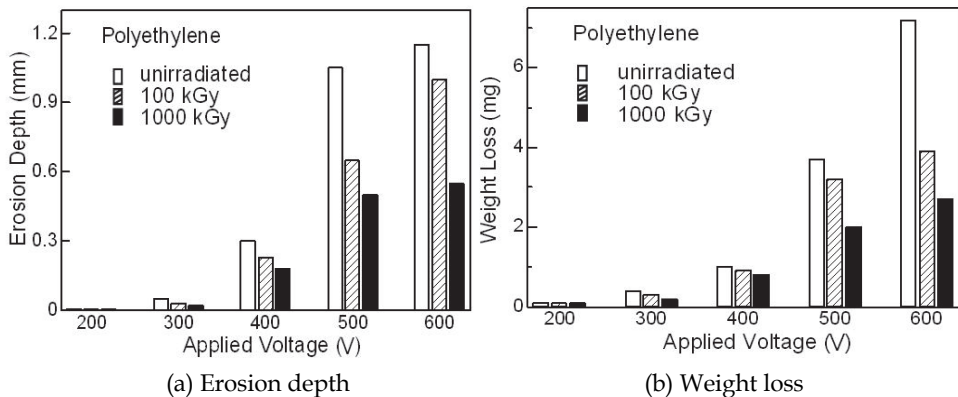


Fig. 11. The changes of tracking resistance on PE

5. Effect of gamma-ray irradiation on tracking resistance under reduced pressure

The relation between the time to tracking failure and the total dose of the irradiation under 100 kPa and 1 kPa are shown in Figs. 12, 13 and 14. With increasing the total dose of irradiation, the time to tracking failure increases with PBN and PET, but decreases with PBT for the investigated range of the irradiation. With the decrease of the atmospheric pressure, the time to tracking failure of all samples increases. With decreasing the pulse interval, the time to tracking failure of all samples decreases.

With the increase of the total dose, the time to tracking failure of PBN and PET increase, which indicates the thermal properties of tracking resistance are improved. However, the time to tracking failure of PBT decreases with the increase of the total dose, which indicates that the thermal properties of tracking resistance are worsened. Evidently, the total dose has different effects on the polymers. A cross-linking reaction is one main factor for improving tracking resistance and conversely a degradation reaction is conceivable as a factor for decreasing tracking resistance. The atoms that make up a polymer are

bounded together by weak covalent bonds that are disrupted easily by gamma-ray radiation, and as bonds are broken, new ones are formed and the structure of the polymer is altered. In practice, cross-linking and degradation reaction often occur simultaneously, and the reaction result is determined by the one that is dominant. For PBN and PET, it is supposed that the cross- linking reaction is superior to the degradation reaction and the combination between the molecules extends the three-dimensional networks. For PBT, it is supposed that the degradation reaction is superior to the cross-linking reaction and the scission of the main chain bonds results in the formation of low-molecular-weight chain fragments.

The time to tracking failure of all samples increases with the decrease of the atmospheric pressure. Under the reduced pressure, the supply of oxygen is not sufficient. The probability of the oxidation reaction on sample surface and the cracked gas decreases with the decrease of the oxygen content. The burning becomes more difficult and the complete carbonized conductive path becomes hard to form. Therefore, the time to tracking failure increases with the decrease of the atmospheric pressure.

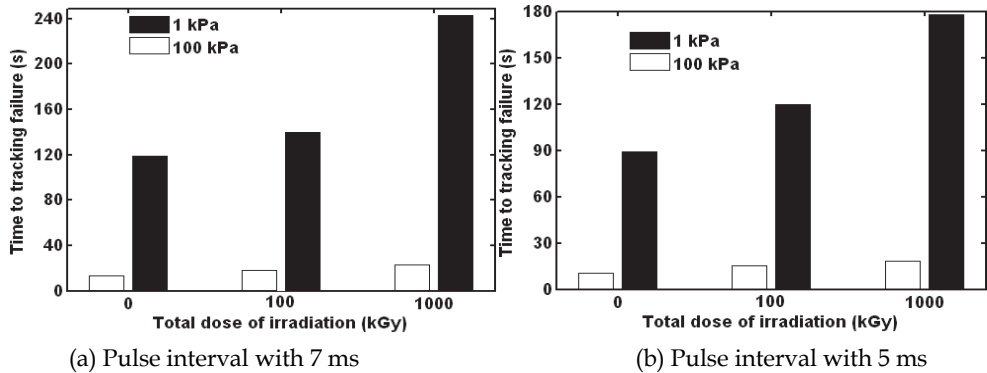


Fig. 12. Relation between the time to tracking failure and the total dose of irradiation for PBN

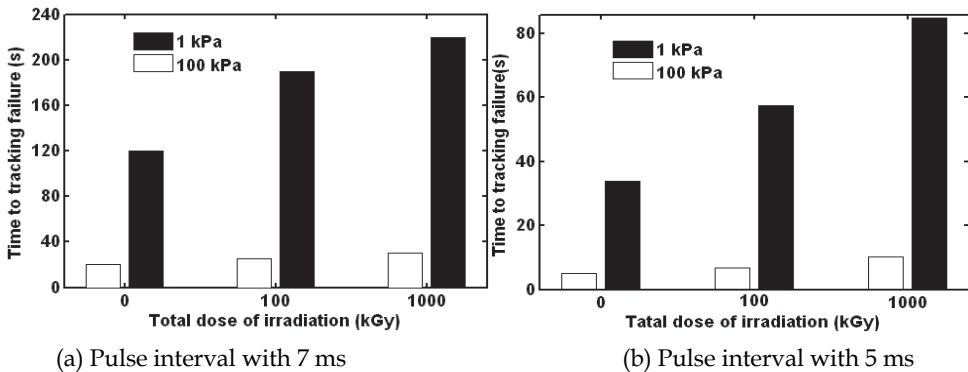


Fig. 13. Relation between the time to tracking failure and the total dose of irradiation for PET

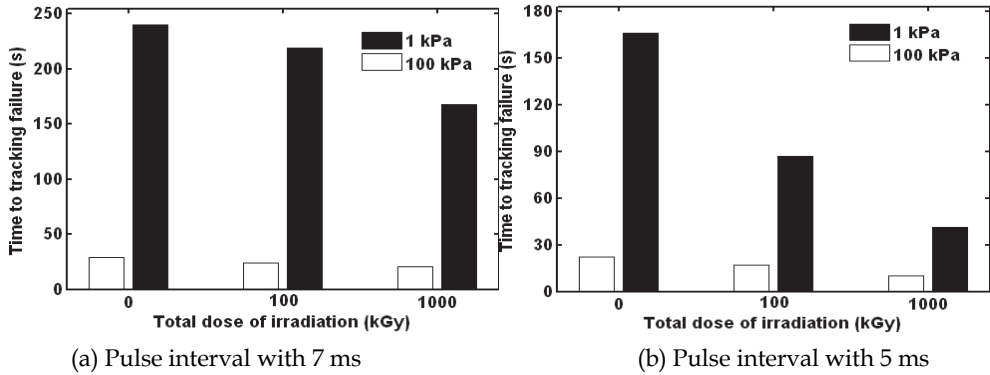


Fig. 14. Relation between the time to tracking failure and the total dose of irradiation for PBT

The time to tracking failure of all samples decreases with the decrease of the pulse interval. When the pulse interval decreases, electron emission from the electrode becomes more frequent, the heat caused by the discharge energy makes the carbon chain of the molecules broken increases, and the carbon conductive path of polymer surface forms more steadily. As a result, the time to tracking failure decreases. In addition, at the pulse interval of 10 ms, the accurate time to tracking failure is not shown from Figs. 12 to 14 as the tracking failure does not occur until 300 s under the same condition as pulse intervals of 7 ms and 5 ms.

The discharge quantity is a token of the heat-durability. The tracking failure mainly depends upon the heat energy formed by the discharge. If discharge quantity is smaller, it suggests that the carbon chain is more difficult to be broken. The relationship between the discharge quantity and the total dose of irradiation before tracking failure for 600 discharges under 100 kPa and 1 kPa are shown in Figs 15, 16 and 17. The discharge quantity decreases with PBN and PET, but increases with PBT with increasing the total dose of irradiation. From Figs. 15 to 17, with the decrease of the atmospheric pressure, the discharge quantity of PBN and PET increase, but decrease with PBT.

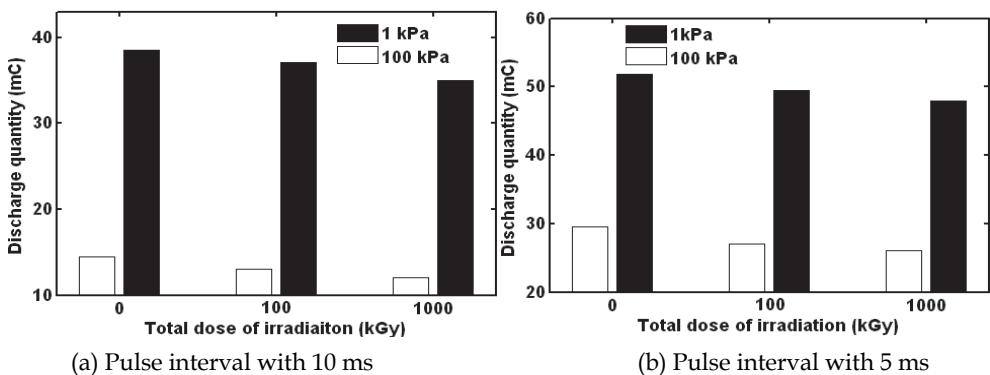


Fig. 15. Relation between the discharge quantity and the total dose of irradiation for PBN.

The discharge quantity of PBN and PET decrease with the increase of the total dose, which suggests that the thermal properties of tracking resistance are improved and the tracking

failure becomes more difficult. This fact is due to the occurrence of the cross-linking reaction. With the increase of the total dose of irradiation, the discharge quantity increase with PBT, which suggests that the thermal properties are worsened and the tracking failure becomes easier. The reason for this is due to the degradation reaction by irradiation.

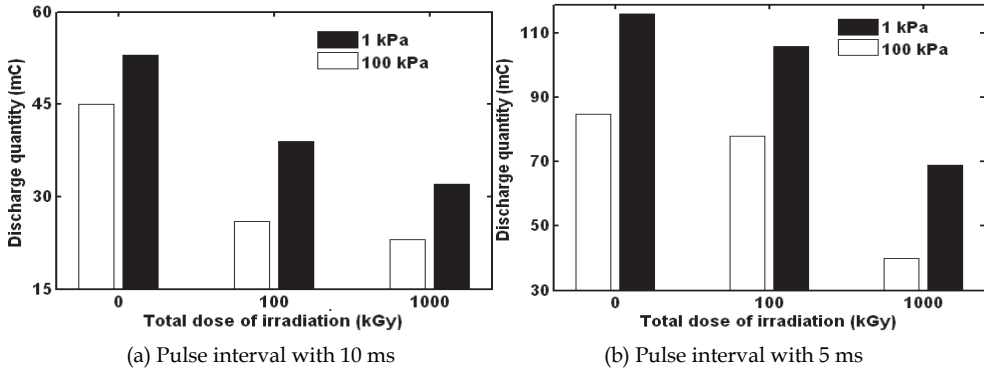


Fig. 16. Relation between the discharge quantity and the total dose of irradiation for PET

The discharge quantity of PBN and PET increase with decreasing the atmospheric pressure. Under the reduced atmospheric pressure, the density of the gases is decreased, the speed of electron becomes fast, and the surface more readily causes the discharging. As a result, the discharge quantity increases with the decrease of the atmospheric pressure. The discharge quantity decreases with decreasing the atmospheric pressure for PBT. It is because under the reduced atmospheric pressure, the probability of the oxidation reaction of PBT surface and the cracked gas decrease with the decrease in the oxygen content. The carbon deposition of PBT by the ignition to the surface increases, and the discharges can not completely take place due to the decomposed carbon, so the total discharge quantity of PBT under the reduced atmospheric pressure is smaller.

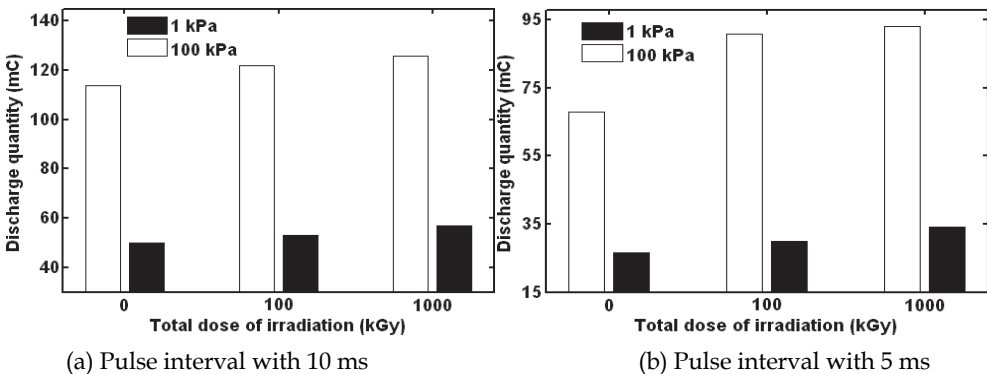


Fig. 17. Relation between the discharge quantity and the total dose of irradiation for PBT

From Figs. 15 to 17, discharge quantity of PBN and PET increased with the decreasing the pulse interval, but the tendency is opposite for PBT. The discharge quantity is bigger in

shorter pulse interval because the higher accumulative heat quantity of consecutive discharge is, the more quickly tracking failure occurred. For PBN and PET, tracking failure is more difficult due to the inherent carbonization property and the discharge is continuous. The formation of carbon conductive path is gradual, and the discharge quantity is bigger at the shorter pulse interval. For PBT, the formation of carbonization and tracking failure are easier. It is observed that short-circuit forms in a very short time, and the discharge is discontinuous. At the shorter pulse interval, the carbonization forms more quickly and the brief short-circuit occurs more frequently, which causes the discharges cannot completely take place, so the total discharge quantity is smaller.

The photographs of sample surface after the discharge for 20 s with the pulse interval of 10 ms under 100 kPa and 1 kPa are shown Tables 1, 2 and 3. The color of sample surfaces is gradually dark according to the total dose of gamma-ray irradiation. The noticeable changes of sample surface in the tracking failure process are observed. The repetitive discharge occurs before tracking failure and the quantity of decomposition carbon increases in the area close to the electrodes. The features of tracking failure phenomenon are different between PBN, PET and PBT. The carbonized area decreases with PBN and PET, but increases with PBT with increasing the total dose of irradiation. The difference indicates that the thermal properties of tracking resistance are improved with PBN and PET, but worsened with PBT.

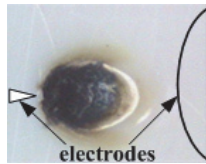
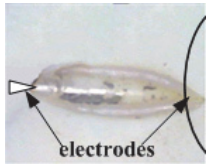
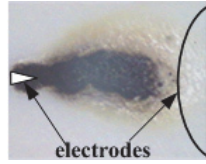
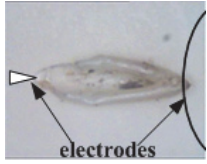
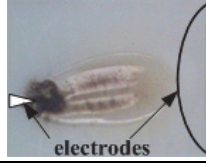
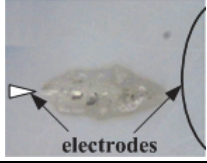
Total dose	100 kPa	1 kPa
0 kGy		
100 kGy		
1000 kGy		

Table 1. Sample surface after the carbonization with PBN

By comparison with the case of 1 kPa, the features of tracking failure phenomenon are different in the case of 100 kPa. The oxidation reaction, which took place on the electrodes, is an exothermic reaction initiated by scintillation discharge and increases the intensity of the discharge. In the case of 100 kPa, there is enough aerial oxygen for the samples to be oxidized completely, which shows more carbonization area in the second columns of Tables 1, 2 and 3. In the case of 1 kPa, there is not enough aerial oxygen for the samples to be

oxidized completely and the oxidation product is largely decreased, which shows less carbonization points in the third columns of Tables 1, 2 and 3. The differences of shape and area of carbonized resultants are independent of the carbonization process with reducing the atmospheric pressure.

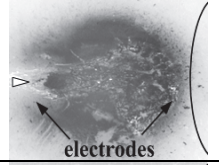
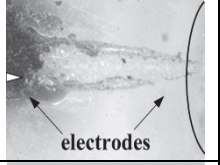
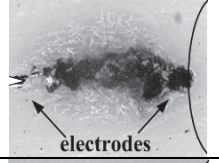
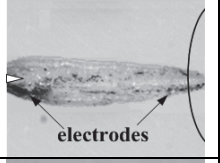
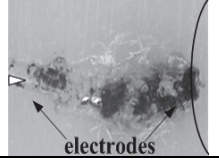
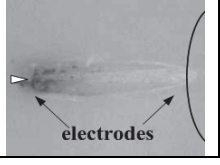
Total dose	100 kPa	1 kPa
0 kGy		
100 kGy		
1000 kGy		

Table 2. Sample surface after the carbonization with PET

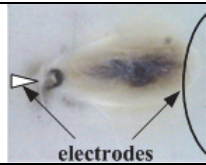
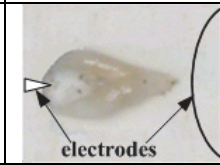
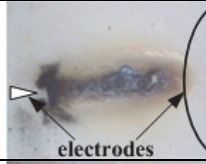
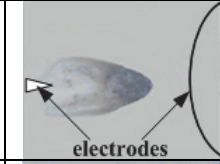
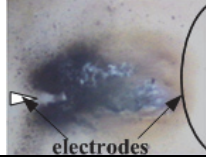
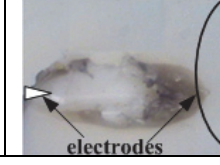
Total dose	100 kPa	1 kPa
0 kGy		
100 kGy		
1000 kGy		

Table 3. Sample surface after the carbonization with PBT

The tracking failure properties are improved for PBN and PET but worsened for PBT by gamma-ray irradiation. This difference is attributed to the radiation-induced cross-linking

and degradation. The effect of the total dose on electrical properties is markedly different, depending on the chemical structure of the base polymer. The radiation adds a particular dimension to the aging problem, because it interacts strongly with materials in general and brings about structural changes that alter their properties. This is because that it can alter the macroscopic properties of polymeric materials through mechanisms like chain scission, cross-linking and oxidation. By the comparison of the molecule formulas of PBN and PBT, there are two phenyls in the main chain of PBN but one for PBT. The amount of phenyl in the main chain plays a main role in the result of the radiation reaction. In another word, the resistance to the tracking failure of polybutylene polymers is improved for PBN which contains more combined phenyls in the main chain. Comparing the molecular structures of PET and PBT, there are four methylene groups in the chain of PBT but two for PET. The four methylenes increase the length of the thinner, less bulky, portion of the molecular chain, resulting in easier bending.

6. Effects of gamma-ray irradiation on tracking failure under magnetic field

Figs. 18, 19 and 20 show the relation between the time to tracking failure and the total dose of irradiation with and without magnetic field. The time to tracking failure increases with increasing the total dose with PBN and PET, but decreases with PBT. Under the magnetic field, the time to tracking failure of all the samples increases with the relative angles of 0 and 90 degrees, but decreases with the relative angle of 270 degrees.

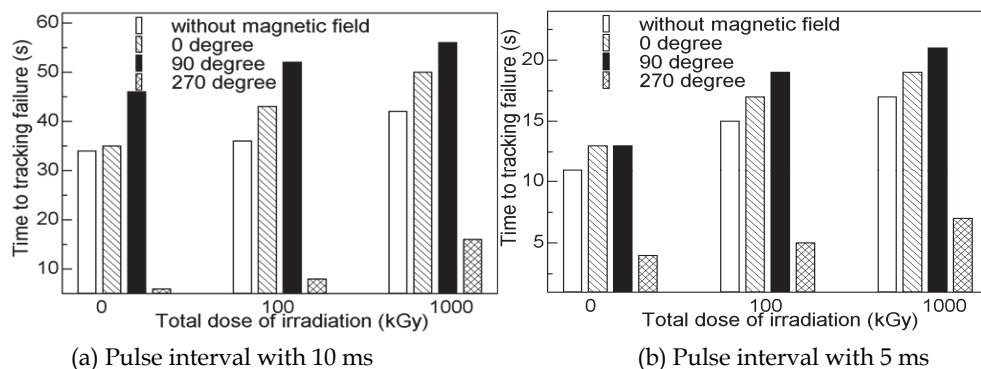


Fig. 18. Relation between the time to tracking failure and the irradiation with PBN

With increasing the total dose, the time to tracking failure of PBN and PET increases, which indicates the properties of tracking resistance are improved. However, the time to tracking failure of PBT decreases with increasing the total dose, which indicates that the properties of tracking resistance are worsened.

Under the magnetic field, the time to tracking failure of the three samples are delayed with the relative angles of 0 and 90 degrees, but shortened with the relative angle of 270 degrees. The tracking failure is caused by the decomposed carbon on the sample surface, which is precipitated due to heat generated by the discharge between the electrodes. Free electrons which are emitted from electrode dissociate polymer molecules by the rupture of C-H bond. When magnetic field is applied, an electromagnetic force, the direction of which is decided by the direction of $E \times B$, will affect the frequency of electron collision and the formation of

decomposed carbon. As a result, the dielectric performance is changed by the magnetic field. With the relative angles of 0 and 90 degrees, the charge carriers are deflected to one side and upward away from the surface, respectively. As a result, there is a decrease in collision frequency and the time to tracking failure increases. When the relative angle is 270 degrees, the electrons are deflected towards the sample surface because of the electromagnetic force. The C-H bonds are ruptured and the carbon is separated more readily. Therefore, the time to tracking failure is shortened with the relative angle of 270 degrees.

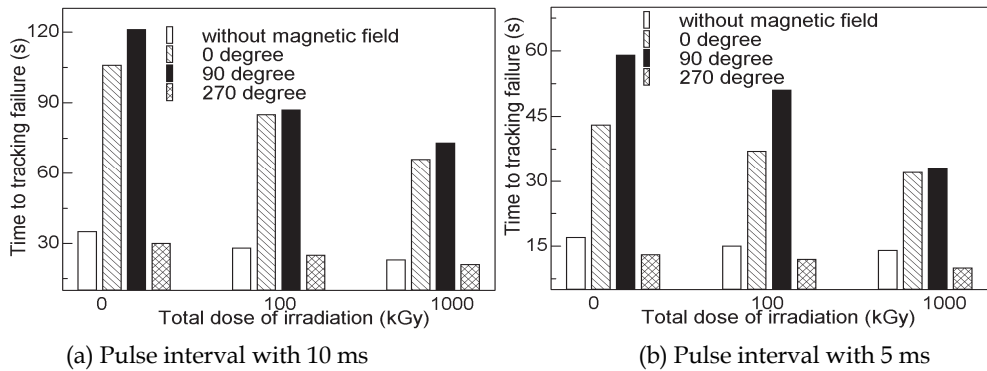


Fig. 19. Relation between the time to tracking failure and the irradiation with PBT

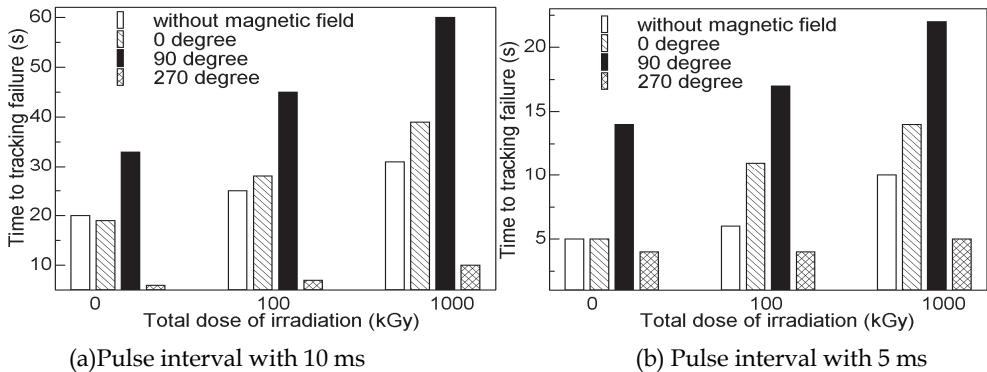


Fig. 20. Relation between the time to tracking failure and the irradiation with PET

Figs. 21, 22 and 23 show the relation between the discharge quantity and the total dose of irradiation. With the increase of the total dose of irradiation, the discharge quantity decreases with PBN and PET, but increases with PBT. Under magnetic field, the discharge quantity of the samples increases with the relative angles of 90 and 270 degrees, but decreases with the relative angle of 0 degree. The discharge quantity increases with the relative angles of 90 and 270 degrees, but decreases with the relative angle of 0 degree. In addition, it decreases with the relative angle of 90 degrees for PBT. When the relative angle is 0 degree, the electromagnetic force is parallel to the sample surface, which makes the electrons deviate to the surface. The tracking failure is suppressed, since the probability of the electron collision is decreased. Therefore, the discharge quantity is smaller.

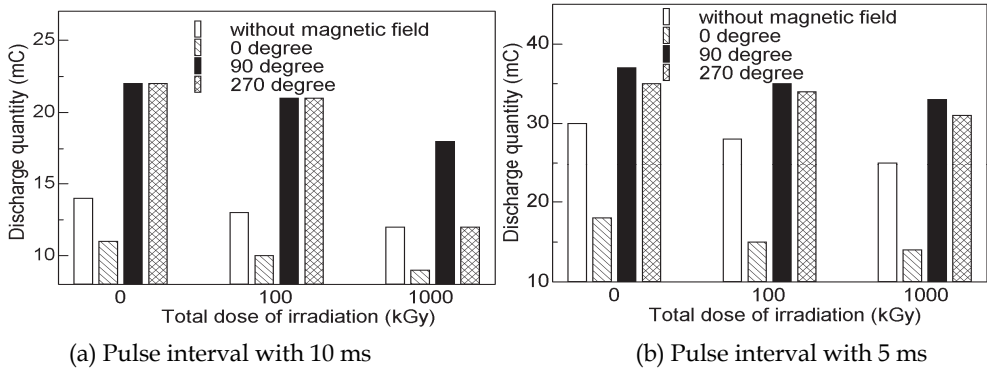


Fig. 21. Relation between the discharge quantity and the total dose of irradiation with PBN

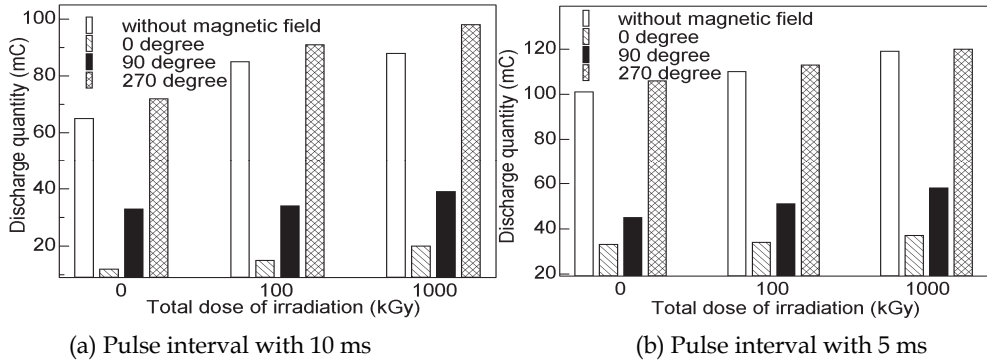


Fig. 22. Relation between the discharge quantity and the total dose of irradiation with PBT

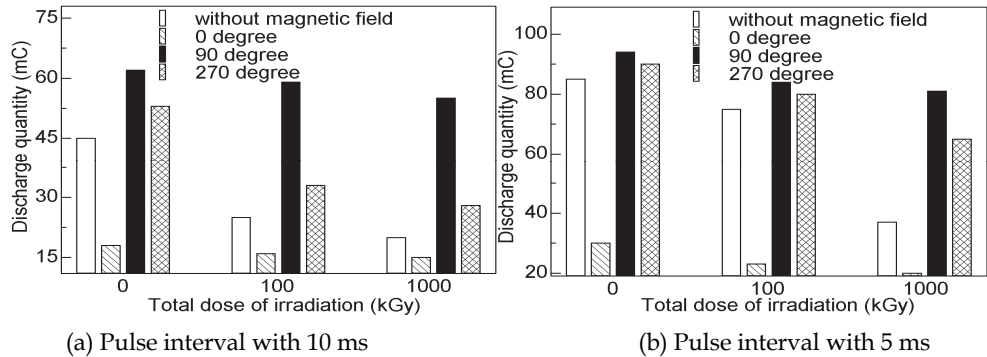


Fig. 23. Relation between the discharge quantity and the total dose of irradiation with PET

Conversely, with the relative angle of 270 degrees, the electromagnetic force is downward to the sample surface, the electron collision is increased on the sample surface and the discharge quantity increases. The electromagnetic force is upward to the sample surface

with the relative angle of 90 degrees, which makes the electrons pass the sample surface more easily. As a result, the electromagnetic force is upward to the sample surface and the discharge quantity is larger for PBN and PET. For PBT, the tracking failure is mostly decided by the carbonization. The electrons upward to the sample surface inhibit the carbonization process, and the discharge quantity decreases.

The photographs of sample surface after tracking failure with the pulse interval of 10 ms at the relative angles of 0, 90 and 270 degrees are shown in Tables 4, 5 and 6. The color of sample surface is gradually dark according to the total dose of gamma-ray irradiation. The repetitive discharge occurs before tracking failure and the quantity of decomposition carbon increases in the area close to the electrodes. As shown in the Tables, the surface is carbonized by the heat energy from the discharge. With the high repetition rate of discharges, there is a high increase of discharge quantity that affects the carbonization progress and the situation of carbon deposition. When the intensive discharge lasts for a period of time, the surface is carbonized first to the area close to the electrodes. Due to the conductive nature of carbonization products, they act as the extension of the electrodes. After a sufficiently long time, the carbonized conduction path is finally formed over the short-circuited path.

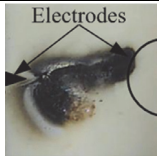
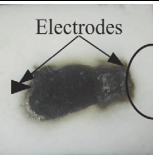
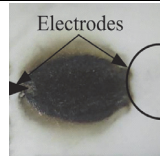
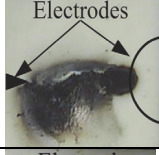
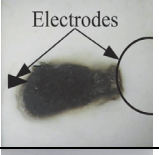
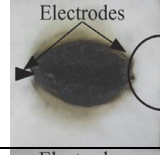
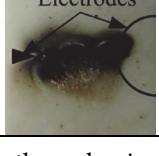
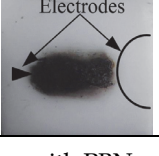
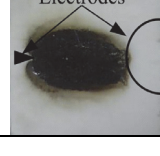
Dosage	0	90	270
0kGy			
100kGy			
1000kGy			

Table 4. Sample surface after the carbonization with PBN

The features of tracking failure phenomenon are different among PBN, PET and PBT. The carbonized area decreases with PBN and PET, but increases with PBT with increasing the total dose of irradiation. By comparing the cases of 0, 90 and 270 degrees, the features of tracking failure phenomenon are different. The carbonization path is downside to the sample surface with the relative angle of 0 degree. The carbonization path of 90 degrees is narrow and the carbonization path of 270 degrees was almost circular.

The oxidation reaction, which takes place on the electrodes, is an exothermic reaction initiated by scintillation discharge and enhanced the intensity of the discharge. When the relative angle is 0 degree, the electromagnetic force is parallel to the sample surface, which makes the electrons deviate to the surface of the samples. The decomposition carbon separates out by the energy of electrons. As a result, the carbonization path is downside to the sample surface. When the relative angle is 90 degrees, the electromagnetic force is

upward to the sample surface. There is a decrease in collision frequency of the electrons and the sample surface. The discharge energy is smaller and the carbonization progress is difficult. As a result, the growth of carbonization path is inhibited. The shape is narrow and the carbonized area decreases. When the relative angle is 270 degrees, the electromagnetic force is downward to the sample surface. The electron collision is increased on the sample surface and the discharge energy increases. The carbonization growth is easier and the carbonization paths extend more easily. Accordingly, the carbonization path of 90 degrees is almost circular and the carbonized area increases. The carbonized area of 0 degree is biggest and that of 90 degrees is smallest for PBT and PET, but that of 270 degrees is biggest for PBN. For PBN, the development of carbonization is not complete.

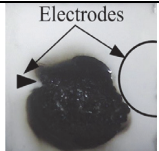
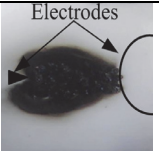
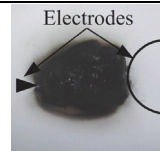
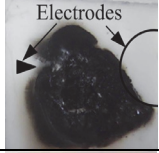
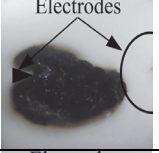
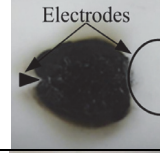
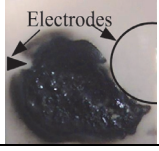
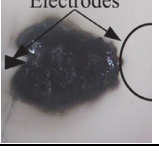
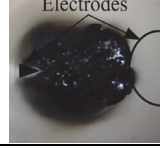
Dosage	0	90	270
0kGy			
100kGy			
1000kGy			

Table 5. Sample surface after the carbonization with PBT

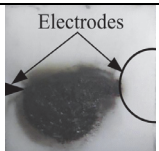
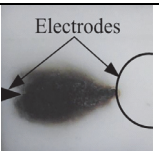
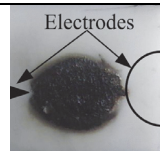
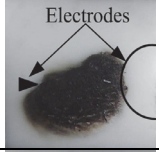
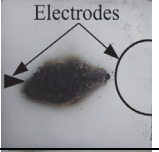
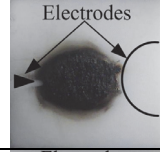
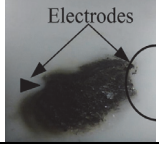
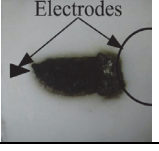
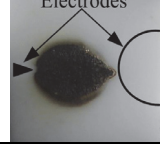
Dosage	0	90	270
0kGy			
100kGy			
1000kGy			

Table 6. Sample surface after the carbonization with PET

7. Recurrence plots of discharge current in tracking test

Fig. 24 shows the variation of RP topological structure at different states of discharge process for PBT with 100 kGy dosage at 350 V. Fig. 24a shows the initial state of the test. The sparse recurrence point density indicates a low correlation between embedding vectors $X(i)$ and $X(j)$ in m -dimension space. It also shows that the beginning of the tracking test is an unstable state due to incomplete evolution of the solution on the sample surface, which results in leakage currents and the occurrence of discharge between tiny droplets. Fig. 24b shows the middle state of discharge process. It shows a stationary state which is manifested in a comparatively regular and dense recurrence point distribution. This indicates that some embedding vectors are the same or very similar to other embedding vectors in m -dimension phase space. It can also be considered to correspond to the state of the discharge process when the discharge mainly occurs between the deposited carbon patches and the process is in a comparatively stationary state. Fig. 24c shows the state of the discharge process just before tracking failure. The topological structure is completely different from that shown in Fig. 24a or Fig. 24b. From vector $X(0)$ to $X(4500)$, the main segments of the map indicates a stationary state with an exception of a short unstable one that produced the white cross blank area between vector $X(4500)$ to $X(5000)$. This also indicates that the discharge state will switch to the next state which indicates the imminence of the breakdown.

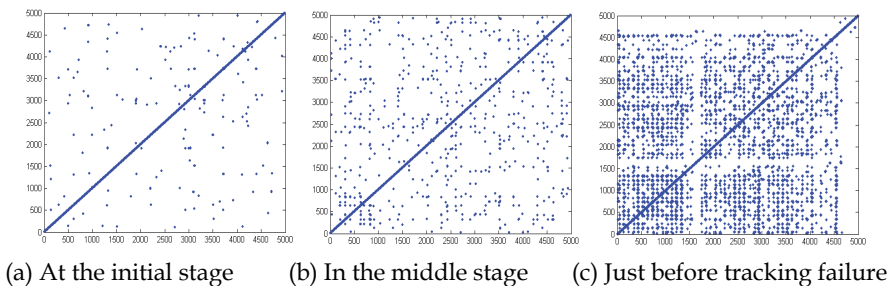


Fig. 24. Recurrence plots for three different stages in the discharge

The variations of topological structures for PBT at 375 V and for PET at 450 V with the increase of irradiation dosage are shown in Fig. 25. In Fig. 25a, the point density of PBT decreases with the increase of the irradiation dosage. By contrast, in Fig. 25b, the point density of PET increases with the increase of irradiation dosage. The two opposite tendencies of recurrence point density indicate that gamma-ray irradiation has completely different effects on the resistance to tracking for PBT and PET.

In order to understand the underlying mechanism of the confusing discharge process, the RP has been made to evaluate the tracking resistance. Fig. 26 shows the RPs of the discharge resulting from the application of 400V with M-PC. The structures of the irradiated samples are different from that of the unirradiated ones and there are bigger white space segments in the plot of the unirradiated sample. The white space segments stand for inflation processes due to the high amplitude transients, which indicate that there are high amplitude changes in the discharge currents of unirradiated sample and the fluctuation is more strenuous than that of the total dose at 100 kGy and 1000 kGy. The discharge processes change due to the

increase of the irradiation. There is almost no obvious difference in the white space, but the point density increases with the irradiation dosage from 100 kGy to 1000 kGy, which indicates that the embedding vectors are very similar to the neighbor vectors. It is suggested that the discharge process at 1000 kGy is more intensive than that at 100 kGy. This results of is related to the phenomenon in which as total dose increases, the tracking resistance of M-PC is improved compared with unirradiated samples and the tracking resistance decreases with the total dose from 100 kGy to 1000 kGy.

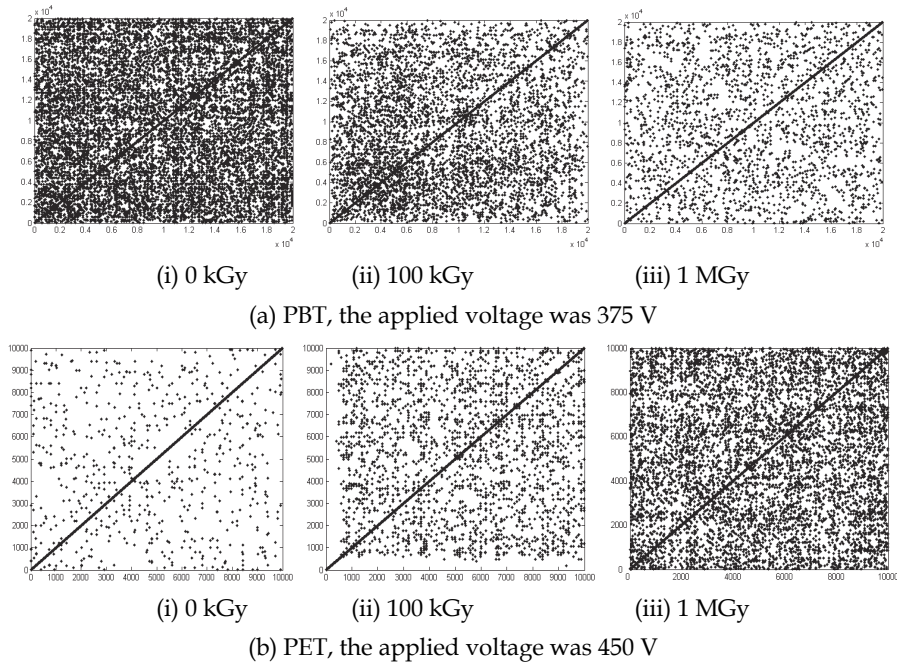


Fig. 25. Relation between the RP and the dosage of gamma-ray irradiation

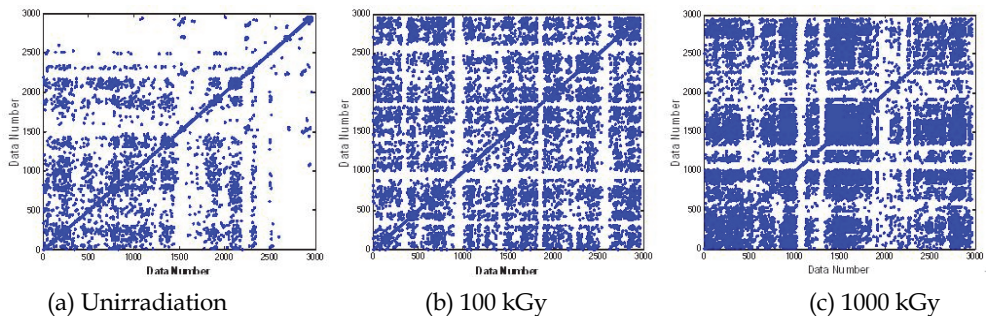


Fig. 26. RPs of discharge currents with M-PC

Fig. 27 shows the recurrence plots of the discharge currents with PE at 400V. The point density and the white spaces all decrease with the increase of the irradiation dosage, which

indicates the intensity and the high amplitude transients of the discharge currents decrease. These results are related to the phenomenon where as total dose increases the tracking resistance of PE is improved. It is also confirmed that the point density and the white space are directly related to the features of the discharge process.

Fig. 28 shows the relationship between the quantitative indicators and the gamma-ray radiation. The RR increases for M-PC but decreases for PE with the increase of the radiation dosage, while the DET of PE increases. The DET of M-PC increases with the total dose from 0 kGy to 100 kGy and decreases from 100 kGy to 1000 kGy. For M-PC, the increasing of RR indicates that the intensity of the discharge currents increases. The DET increases first and then decreases indicate that the deterministic ingredients of the discharge currents increases first and then decreases with increasing the radiation dosage. For PE, the decreasing of RR and the decreasing of DET indicate that the discharge is more stable and regular.

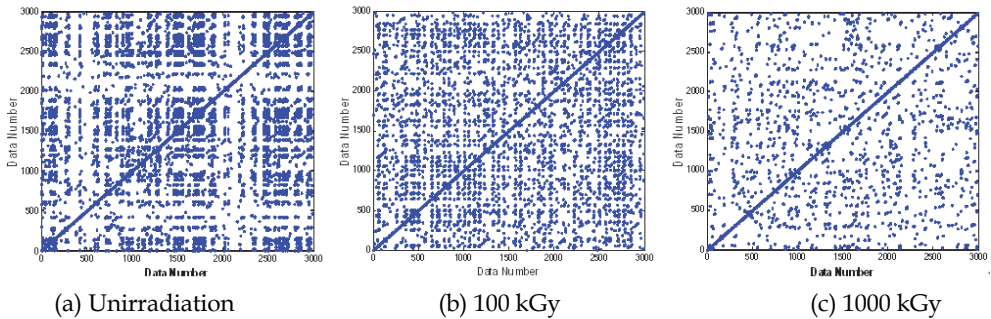


Fig. 27. RPs of discharge currents with PE

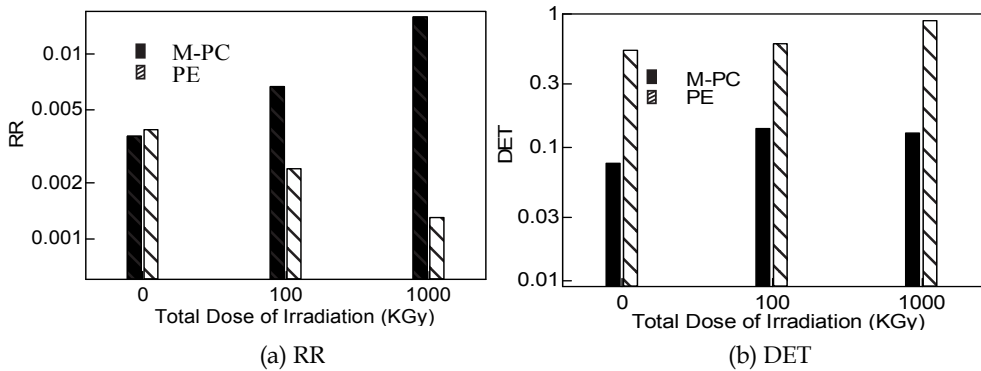


Fig. 28. Relationship between the quantitative indicators and the gamma-ray radiation

8. Conclusions

The effects of gamma-ray irradiation on dielectric breakdown have been studied by applying a dc pulse voltage. The experiments reveal that the dielectric properties of polybutylene polymers are obviously changed by the gamma-ray irradiation. With the

increase of the total dose of irradiation, the time to dielectric breakdown increases with PBN, but decreases with PBT, the discharge quantity decreases with PBN, but increases with PBT. It indicates that the total dose of irradiation has a converse effect on the discharge quantities. The discharge quantity increases with the decrease of the discharge interval with PBN, but the tendency is opposite with PBT. Time to dielectric breakdown for both PBN and PBT all decreases with the decrease of the discharge interval. The dielectric properties of PBN are improved, but worsened for PBT by gamma-ray irradiation. Dielectric properties are improved by irradiation for polybutylene polymers which contain more combined phenyls in the main chain.

The tracking resistance of gamma-ray irradiated polycarbonate mixed with polyethylene by use of IEC 60112 is studied. With the increase of the total dose of Gamma-ray irradiation, both the erosion depth and weight loss are smaller than that of unirradiated samples, which show the tracking resistance is improved. Both the erosion depth and weight loss decrease with the total dose increasing from 0 kGy to 100 kGy, but increase from 100 kGy to 1000 kGy. There is a threshold value for the tracking resistance near 100 kGy. When the total dose exceeds the threshold value, the tracking resistance begins to decrease.

The effect of gamma-ray irradiation on tracking failure of PBN, PBT and PET by applying a dc pulse voltage under reduce atmospheric pressure is studied. With the decrease of the atmospheric pressure, the time to tracking failure and the discharge quantity all increase with PBN and PET. The time to tracking failure is delayed with PBT, and the discharge quantity decreases with decreasing the atmospheric pressure. It is found that the irradiation and reduced pressure stress response of PBN, PET and PBT are variable: the resistance to tracking failure of PBN and PET are improved, but worsened for PBT by gamma-ray irradiation and the resistance to tracking failure of all them are influenced obviously by the reduced atmospheric pressure.

The effects of gamma-ray irradiation and magnetic field on tracking failure of PBN, PBT and PET by applying a HV pulse voltage are studied. Under the magnetic field, the time to tracking failure of all the samples are delayed with the relative angles of 0 and 90 degrees, but decrease with the relative angle of 270 degrees, the discharge quantity of the samples increase with the relative angles of 90 and 270 degrees, but decrease with the relative angle of 0 degree. In addition, it decreases with the relative angle of 90 degrees for PBT. The carbonization path is downside to the sample surface with the relative angle of 0 degree. The carbonization path of 90 degrees is narrow and the carbonization path of 270 degrees is almost circular. The carbonized area decreases from 0 to 90 degrees and then increases from 90 to 270 degrees for all the samples. The carbonized area of 0 degree is biggest and that of 90 degrees is smallest for PBT and PET, but that of 270 degrees is biggest for PBN.

Recurrence plots are employed to evaluate the resistance to tracking of polymer samples with gamma-ray irradiation. The results obtained show that it is useful to visualize the state of discharge process. The recurrence plots confirmed by the CTI can successfully indicate the resistance to tracking of polymer material with gamma-ray irradiation. Recurrence plots can serve as a visual method to identify different dynamic systems and reveal time-domain features of the discharge. The recurrence point density decreases with the increase of the dosage of irradiation for PBT. This can be explained by the resistance to tracking of PBT decreasing by increasing the dosage of gamma-ray irradiation. On the other hand, with the increase of the dosage of gamma-ray irradiation, the recurrence point density increases for PET, indicating less complex discharge process. This can be explained due to cross-linking

being the predominant process through irradiation. The improvement in mechanical and thermal performance through irradiation leads to less easy carbonization. In the dc tracking test of gamma-ray irradiated polycarbonate, the topological structures of the recurrence plots with the irradiated samples are different from that of the unirradiated sample. There are bigger white space segments, which indicate that there are high amplitude transients in the discharge currents of unirradiated sample. The recurrence point density increases from 100 kGy to 1000 kGy, which suggests that the discharge processes of the total dose at 1000 kGy irradiated samples is more intensive than that at 100 kGy.

9. References

- N. Yoshimura, S. Kumagai & B. X. Du. Research in Japan on the Tracking Phenomenon of Electrical Insulating Materials. *IEEE Electrical Insulation Magazine*, Vol.13, No.5, (October 1997), pp.8-19, ISSN 0883-7554.
- B. X. Du, Yong Liu & H. J. Liu. Effects of Low Pressure on Tracking Failure of Printed Circuit Boards. *IEEE Transactions on Dielectrics and Electrical Insulation*, Vol.15, No. 5, (October 2008), pp.1379-1384, ISSN 1070-9878.
- G. C. Stone, R. G. Van Heeswijk & R. Bartnikas. Electrical Aging and Electroluminescence in Epoxy under Repetitive Voltage Surges. *IEEE Transactions on Electrical Insulation*, (April 1992), Vol. 27, No. 2, pp. 233-244, ISSN 0018-9367.
- B. X. Du. Discharge Energy and dc Tracking Resistance of Organic Insulating Materials. *IEEE Transactions on Dielectrics and Electrical Insulation*, (December 2001), Vol.8, No.6, pp. 897-901, ISSN 1070-9878.
- B. X. Du, L. Gu & Yong Liu. Application of Nonlinear Methods in Tracking Failure Test of Printed Circuit Boards under Reduced Pressure. *IEEE Transactions on Dielectrics and Electrical Insulation*, (April 2010), Vol.17, No.2, pp. 548-554, ISSN 1070-9878.
- B. X. Du, L. Gu & Yong Liu. Luminescence in Tracking Test of Polymer Insulating Materials, *International Symposium on Electrical Insulating Materials*, pp. 408-411, ISBN 978-4-88686-005-7, Yokkaichi, Japan, September 7-11, 2008.
- T. Zaharescu, F. Ciuprina & P. Notinghe. Electrical Properties of Polyolefin Blends under γ -Radiation Exposure. *Proceedings of the 2004 IEEE International Conference on Solid Dielectrics*, pp.367-369, ISBN 0-7803-8348-6, Toulouse, France, July 5-9, 2004.
- B. X. Du & Y. Gao. Gamma-ray Irradiation Inhibiting Surface Charge Accumulation on Polyethylene. *IEEE Transactions on Dielectrics and Electrical Insulation*, (June 2009), Vol.16, No.3, pp.876-881, ISSN 1070-9878.
- A. F. Fernandez, B. Brichard, H. Ooms & F. Berghmans. High-Vacuum Gamma Irradiation Facilities for Synergistic Effects Testing on Optoelectronic Components and Materials. *IEEE Transactions on Nuclear Science*, (December 2006), Vol.53, No.6, pp.3726-3730, ISSN 0018-9499.
- A. K. Pikaev, S. A. Kabakchi & G. F. Egorov. Some Radiation Chemical Aspects of Nuclear Engineering. *International Journal of Radiation Applications and Instrumentation. Part C. Radiation Physics and Chemistry*, (August 1988), Vol. 31, No. 4-6, pp. 789-803, ISSN 0969-806X.
- A. Singh. Irradiation of Polymer Blends Containing a Polyolefin. *Radiation Physics and Chemistry*, (March 2001), Vol.60, No.4-5, pp. 453-459, ISSN 0969-806X.

- V. K. Agarwal, H. M. Banford, B. S. Bernstein, E. L. Brancato, R. A. Fouracre, G. C. Montanari, J. L. Parpal, J. N. Seguin, D. M. Ryder & J. Tanaka. The Mysteries of Multifactor Ageing. *IEEE Electrical Insulation Magazine*, (June 1995), Vol.11, No.3, pp. 37-43, ISSN: 0883-7554.
- Y. Ohki. Radiation Effects on Polymers. *IEEE Transactions on Electrical Insulation*, (December 1986), Vol. 21, No. 6, pp. 919-922, ISSN 0018-9367.
- Y. Ohki, K. Matsumoto, M. Ikeda, Y. Kusama, M. Harashige & F. Yazaki. Radiation Resistance of Ethylene-Styrene Copolymers. *Proceedings of Second International Conference on Properties and Applications of Dielectric Materials*, pp. 391-395, ISBN 3462357, Beijing, China, September 12-16, 1988.
- M. Kyoto, Y. Chigusa, M.Ohe, H. Go, M. Watanabe, T. Matsubara, T. Yamamoto & S. Okamoto. Gamma-ray Radiation Hardened Properties of Pure Silica Core Single-mode Fiber and its Data Link System in Radioactive Environments. *Journal of Lightwave Technology*, (March 1992), Vol. 10, No. 3, pp. 289-294, ISSN 0733-8724.
- E. J. Kim, G. Kato, T. Ohara, Y. Ohki & S. T. Li. Effect of Gamma-Ray Irradiation on the TSC in Polyethersulfone. *IEEE Transactions on Dielectrics and Electrical Insulation*, (December 1997), Vol. 4, No.6, pp. 732-737, ISSN 1070-9878.
- G. Chen, H. M. Banford & A. E. Davies. Space Charge Formation in γ -Irradiated Low Density Polyethylene. *IEEE Transactions on Dielectrics and Electrical Insulation*, (February 1998), Vol. 5, No.1, pp. 51-57, ISSN 1070-9878.
- V. Rajini & K. Udayakumar. Degradation of Silicone Rubber under AC or DC Voltages in Radiation Environment. *IEEE Transactions on Dielectrics and Electrical Insulation*, (June 2009), Vol. 16, No.3, pp. 834-841, ISSN 1070-9878.
- K. Anandakumaran, S. Barreca, N. Seidl & P. V. Castaldo. Nuclear Qualification of PVC Insulated Cables. *IEEE Transactions on Dielectrics and Electrical Insulation*, (October 2001), Vol. 8, No.5, pp. 818-825, ISSN 1070-9878.
- K. Shiyama & S. Fujita. Dielectric and Thermal Properties of Irradiated Polyetheretherketone. *IEEE Transactions on Dielectrics and Electrical Insulation*, (June 2001), Vol. 8, No.3, pp. 538-542, ISSN 1070-9878.
- I. Kuriyama, N. Hayakawa, Y. Nakase, S. Kawawata, J. Ogura, K. Kasai & T. Onishi. Radiation Resistance of Cable Insulating Materials for Nuclear Power Generating Stations. *IEEE Transactions on Electrical Insulation*, (June 1978), Vol. 13, No.3, pp. 164-171, ISSN 0018-9367.
- B. X. Du & S. Kobayashi. Wavelet Analysis of Scintillation Discharge Current on dc Tracking Resistance of Gamma-Ray Irradiation Polyethylene and Polycarbonate. *Radioisotopes*, (March 2001), Vol. 50, No.1, pp. 1-11, ISSN 0033-8303.
- B. X. Du & H. J. Liu. The Application of Recurrence Plot in DC Tracking Test of Gamma-Ray Irradiated Polycarbonate. *IEEE Transactions on Dielectrics and Electrical Insulation*, (February 2009), Vol. 16, No.1, pp. 17-23, ISSN 1070-9878.
- B. X. Du & H. J. Liu. Effects of Atmospheric Pressure on Tracking Failure of Gamma-Ray Irradiated Polymer Insulating Materials. *IEEE Transactions on Dielectrics and Electrical Insulation*, (April 2010), Vol. 17, No.2, pp.541-547, ISSN 1070-9878.

- B. X. Du & D. S. Dong. Recurrence Plot Analysis of Discharge Currents in Tracking Tests of Gamma-Ray Irradiated Polymers. *IEEE Transactions on Dielectrics and Electrical Insulation*, (August 2008), Vol. 15, No.4, pp. 974-981, ISSN 1070-9878.
- B. X. Du, A. Suzuki & S. Kobayashi. Effects of Gamma-rays Irradiation Tracking Resistance of Organic Insulating Material. *IEEJ Transactions on Fundamentals and Materials*, (April 1996), Vol. 116, No.5, pp. 461-467, ISSN 0385-4205.
- B. X. Du & S. Kobayashi. Effects of Gamma-ray Irradiation on Discharge Characteristics of Organic Insulating Materials. *Radioisotopes*, (January 2002), Vol. 51, No. 1, pp. 1-9, ISSN 0033-8303.
- B. X. Du and S. Kobayashi, "Environmental Factors Affecting dc Resistance to Tracking of Polyethylene", *IEEE Trans. Dielectr. Electr. Insul.*, (April 2003), Vol. 10, No.2, pp.271-277, ISSN 1070-9878
- B. X. Du, A. Suzuki, and S. Kobayashi, "Effects of Gamma-rays Irradiation and Atmospheric Pressure on Tracking Resistance of Polyethylene", *Trans. IEE Japan*, (February 1996), Vol.116-A, No.2, pp. 170-176, ISSN 0385-4205
- B. X. Du and H. J. Liu, "Effects of Magnetic Field on Tracking Failure of Gamma-ray Irradiated Polymer Insulating", *IEEE Transactions on Dielectrics and Electrical Insulation*, (February 2011), Vol.18, No.1, pp.140-148, ISSN 1070-9878.
- B. X. Du and S. Kobayashi, "Wavelet Analysis of Scintillation Discharge Current in DC Tracking Resistance of Gamma-rays Irradiated Organic Insulating Materials", *Trans. IEE Japan*, (July/August 1998), Vol.118-A, No.7/8, pp. 780-784, ISSN 0385-4205
- B. X. Du, "Effects of Gamma-ray Irradiation on Erosion Depth of Polybutylene Naphthalate under Decreased Pressure" , *Radioisotopes*, (July 2002), Vol. 51, No.7, pp. 256-560, ISSN 0033-8303
- B. X. Du, "Effects of Atmospheric Pressure on Discharge Characteristics of Gamma-ray irradiated Polybutylene Terephthalate" , *Radioisotopes*, (May 2002), Vol. 51, No.5, pp. 197-203, ISSN 0033-8303
- B. X. Du, "Effects of Atmospheric Pressure on Insulation Breakdown of Gamma-ray Irradiated Polyphenylene Oxide", *IEEJ Trans. Fundamentals and Materials*, (March 2004), Vol.124, No.3, pp. 271-276, ISSN 0385-4205